MEASUREMENT OF THE FIDUCIAL DIFFERENTIAL CROSS-SECTION OF TOP QUARK PAIR PRODUCTION IN THE DILEPTON FINAL STATE AT 8 TEV

Umar Gul

School of Physics and Astronomy

University of Glasgow

A thesis submitted in fulfilment of the requirements for the award of the degree of Doctor of Philosophy

January 2017

To my late parents for all their love and support and putting me through the best education I could ever have, I appreciate their great sacrifices and I wouldn't have been able to get to this stage without their love and prayers.

To my supervisor, Professor Doctor Craig Buttar for his unending support and encouragement, I wouldn't have gotten through this doctorate without his consistent support.

To my wife, Sahida, for putting up with me throughout the course of my PhD.

Declaration

The work presented in this thesis is in many respects the culmination of decades of preparation by many thousands of physicists working on the LHC and ATLAS experiment. I hereby declare that except where specific reference is made to the work of others, the contents of this dissertation are original and have not been submitted in whole or in part for consideration for any other degree or qualification in this, or any other university. I declare that, except where explicit reference is made to the contribution of others, that this dissertation is the result of my own research work in the Experimental Particle Physics group of the school of Physics and Astronomy at the University of Glasgow. The thesis is structured in the following way:

- Chapter 1 is a brief introduction of particle physics;
- Chapter 2 gives a very quick and brief overview of the theory relevant to the measurement and describes the properties of the top quark along with a brief overview of previous measurements;
- Chapter 3 describes the ATLAS experimental set-up and different components needed to reconstruct objects of interest;
- Chapter 4 describes my authorship qualification, the non-collision background studies done using the semi-conductor tracker. This study plays an important role to understand more about the performance of the subdetectors, non-collision background contributions from various sources. The most significant non-collision background for physics searches arises from sources including beam-induced backgrounds. Muons can be emitted from the particle showers initiated by beam-gas interactions or scattering of beam-halo protons hitting collimators. Such beam-induced background (BIB) muons, with energies that can reach the TeV range, may enter the ATLAS calorimeters and can deposit energy which is then reconstructed as a fake jet. The rate of these fake jets is very small but they still contribute in searches for rare physics processes;
- Chapter 5 is the first chapter dedicated to my main analysis work on selecting the objects from the 8 TeV collision data. This chapter describes the data and simulation

samples, event selection criteria and reconstruction. The latter part of this chapter describes the details of the objects like electrons, muons, jets, b-tag jets, and missing transverse momentum. This chapter finishes with the description of reconstruction efficiencies;

- Chapter 6 describes the control plots, migration matrices, resolution plots and analysis method and measurement;
- Chapter 7 describes the statistical and systematic uncertainties;
- Chapter 8 describes the cross-section results and discussion; and
- Chapter 9 concludes this measurement and some future prospects are discussed at the end of this chapter.

The thesis ends with two appendices: A and B. Appendix A contains a complete list of detector related systematics. Appendix B contains the results of the *ee* and $\mu\mu$ channels.

Umar Gul

January 2017

Acknowledgements

Throughout my PhD, there have been many people who have fully supported me and helped me bring it to its end. I am especially grateful to my supervisor Professor Craig Buttar who has given me excellent advice throughout my PhD and without his incredible support and help, the completion of this thesis would not have been possible. He encouraged and motivated me in my hardest times. He has been a great mentor and shown a great deal of patience over the course of my PhD. He has also taught me many complicated concepts of Particle Physics along with technical details of the ATLAS experiment at LHC CERN. I would also like to thank my second Supervisor, Professor Tony Doyle, who gave me a chance to involve myself in the ATLAS experiment at the LHC, CERN and not only did he give me a chance to work with a great university but also to work with top scientists of the world. He has been very supportive and has been encouraging me throughout my PhD and I am thankful for him for giving me an opportunity to do such a thing especially since I had left education 15 years ago and was married and a father of young children. I don't think I could ever repay the help, support and encouragement given to me by my supervisors.

I would also like to acknowledge my experimental group who have all, in one way or another, helped me at some point. I would like to thank the Scotgrid team of Glasgow University who have been helpful regarding technical issues and grid software. And I would like to thank Dr Andrew Pickford, David, Gordon, Gareth and Sam who helped me with my grid certificate and other computer related issues.

During my stay at CERN I had the chance to meet with Dr Saverio D'Auria, Dr Jie, Dr Samir, Dr Simon and Dr Richard Hawkings. All of whom have provided me with excellent support and guidance and have been very encouraging. Another person I would like to mention is Valerie Flood who has been very supportive of me and very helpful in regards with my admission and my travel schedule. I would like to specially mention Dr Ki Lie and Dr Saleem who have been extremely helpful and encouraging.

I am thankful to Dr Chris Pollard for providing regular feedback on my analysis. I am also thankful to Dr Adrian Buzatu for helping me write a better code and automate it. I am also thankful for the help given to install different packages by my PhD colleague, William

Breaden Madden. I am also thankful to Dr Kenneth Wraight for always being very helpful and willing to help.

I wish to express my sincere thanks to the faculty for providing me with all the necessary facilities for the research. I take this opportunity to express my gratitude to all of the Department faculty members for their help and support. I would also like to express my gratitude towards all my teachers throughout my life.

I am thankful to my brothers and sisters for their love and support and I am grateful to my wife for her immense support, and my children for their patience during my studies.

I would specially like to mention my beloved mother who is not here with me right now. My mother was the most supportive and encouraging person in my life and after her death last year, I was grieve stricken and emotionally unable to cope. She did a lot for me to gain primary education and then encouraged me to go further and built a love for gaining knowledge within me. Without her I wouldn't have been able to stand on my feet and do everything that I've done and for this I will forever remain indebted to her as she remains in my heart forever.

Last but certainly not the least, I would like to mention my late father who passed away at a very early age and was not with me throughout many stages of my life. He wished for me to stand on my own two feet and build a life for myself. Although he passed away at a young age, he taught me many things before leaving.

Abstract

The top quark is the most massive fundamental particle of the Standard Model of particle physics and being the only quark which decays before hadronization gives a unique opportunity for studying Quantum Chromodynamics (QCD). This dissertation presents a measurement of differential cross-sections of top quark pairs decaying in a purely leptonic mode as a function of the dilepton invariant mass, transverse momentum, difference in the pseudorapidity and azimuthal angle between two leptons in the same event at 8 TeV proton-proton collision data collected by the ATLAS detector at the Large Hadron Collider. This data corresponds to an integrated luminosity of 20.3 fb^{-1}. Events with top quark pair signatures are selected in the dilepton channel in the ATLAS acceptance (two leptons with $p_T > 25$ GeV and $|\eta| < 2.5$). The measured cross-sections are compared to the Standard Model predictions generated using current Monte Carlo generators. All the measurements are found to be in agreement with the SM.

Table of contents

List of figures

List of tables

Chapter 1

Introduction

‘A science is any discipline in which the fool of the generation can go beyond the point reached by the genius of the last generation’- Max Gluckman

Science is all about asking questions and looking for a systematic and logically consistent approach to discovering how things in the universe work. The word "science" is derived from the Latin word "scientia", which is knowledge based on demonstrable and reproducible data. It aims for measurable results through testing and analysis. Physics is an experimental science that needs theory frameworks to elucidate results and render the data meaningful. The theoretical interpretations have led physicists to relate results from distinct experiments and make predictions for new experiments. The long history of physics is full of "signals" that, upon further review, "disappeared" but it has been seen that in the end experiment always trumps theory.

Given science is concerned with asking questions, let us search for the smallest thing that can be seen by our unaided eye. A dot (.) is certainly visible but what about something that has size much less than that, say, one-tenth the size of the dot, this would be out of the scope of eyesight. For the naked human eye, therefore, the limit of smallness is of the order of 0.05 mm. The atom and many subatomic structures are all entirely invisible to our naked eye but yet their existence has been confirmed by science, they are real entities with measurable characteristics. The power of the scientific quest lies far beyond the human ability to sense. The smallest size meaningful for a physicist, by which it is meant that known physical theories use it, is that of the Planck length (1.6×10^{-35} m). The Planck length is the fundamental scale below which physics is no longer applicable. The Greek philosophers and scientists initiated the long struggle to tease from nature a rational understanding of its properties that has turned into modern science. For over more than three decades, particle physics has been dominated by a theory that describes the way that particles interact with

one another known as the Standard Model (SM). The Standard Model (SM) is presently the best theoretical description of how matter behaves and interacts at very small distances and high energies and it is consistent with all available high energy experimental data as of 2016. The Standard Model is described by the quantum field theory (particles of the theory are quanta of fields) which unifies the two interactions of particle physics: the electroweak interaction - interactions via the electromagnetic and weak forces unified into a single force - and the theory of the strong nuclear force, which describes the interaction of quarks via the force carriers gluons, also known as quantum chromodynamics (QCD). In the quantum field theoretical description of the SM there are 6 leptons and 6 quarks, 4 vector bosons and 1 spin zero boson, known as elementary particles, and gauge fields introduced by gauge-symmetry requirements in the gauge group $(SU(3)_C \otimes SU(2)_L \otimes U(1)_Y)$ produce interactions between the particles. Hundreds of predictions of this theoretical framework have been confirmed with greater precision in dozens of experiments. Many past high energy accelerators have played their role to test the Standard Model at an astonishing level of precision, most notably the Tevatron at Fermilab, LEP (The Large Electron Positron Collider) at CERN, SLC (The Stanford Linear Collider) at SLAC, HERA at DESY (Deutsches Elektron-Synchroton). The Standard Model of particle physics is our current best answer to the question 'What are material things made of if they decomposed into their constituents?' With a bit of energy, the electrons can be knocked out from atoms. With more energy still, the nucleus can be decomposed into protons and neutrons, with still more energy and a big collider, quarks can be observed inside protons and neutrons. We have never managed to break a quark to see anything inside it. Electrons are an example of particles called leptons. Muons and taus are just heavier versions of electrons. The only other leptons are neutrinos which are of three types. Like six leptons there are six quarks, which are called up, down, strange, charm, bottom and top.

In the SM, there are 12 point-like particles, described by fermionic quantum fields, that make up the basic constituents of matter. They all have anti-particles and they all interact with each other via forces, which are carried by another type of particle called vector bosons. The electromagnetic force is carried by quanta of light known as photons. This force is experienced by all electrically charged particles. The particles responsible for the strong force are gluons; this force is experienced by quarks and gluons. The particles responsible for the weak force are W and Z bosons; all particles experience this force. The Higgs boson (or Higgs particle) is a particle that gives mass to other particles. On the fourth of July, 2012, this long-awaited particle, the Higgs boson, was discovered. This was one of the most significant discoveries in the history of particle physics. This discovery has enabled us to validate the remaining missing piece of the Standard Model. The mass of an elementary particle

is determined by its interaction with the Higgs field. Many properties of the fundamental particles have been accurately known; many new particles have been predicted and confirmed by experiments, and three of the four known fundamental forces (electromagnetic force, weak force and strong force) are formulated in the framework of the SM. The SM is an impressive achievement but it is not the whole story. Still many questions within and outside the Standard Model are left unanswered; it fails to explain the following features of nature:

- gravity;
- neutrino oscillations;
- dark matter;
- hierarchy problem;
- too many parameters;
- strong CP[1] issues;
- inflation; and
- grand unification.

According to the electroweak theory, when the universe was very hot in the beginning, the electromagnetic and weak nuclear forces were merged into a single force called the electroweak force that was believed to exist at that time. The particles that carried the electroweak force were basically very similar. As the temperature of the universe decreased, the electroweak force split into the electromagnetic force carried by massless particles (photons) and the weak nuclear force carried by W and Z bosons. Unlike the photon, the W and Z have mass, which means that some kind of event took place that has caused the splitting due to which mass was obtained by W and Z bosons. This is known as spontaneous symmetry breaking. The discovery of the Higgs boson has validated this theory. The Higgs field is believed to have caused the spontaneous symmetry breaking [1].

The electron is lighter than the top quark since the top quark interacts more strongly with the Higgs field than does the electron. The heaviest particle of the standard model is the top quark. The top quark's extremely large mass (relative to the other fermions) has led to

[1]CP is the combination of two fundamental symmetries; Charge conjugation and Parity. C is the symmetry between the positive and negative charge and P is the symmetry of spatial coordinates. CP violation is at the origin of asymmetry between matter and anti-matter. The long lived K_L^0 normally decays into three pions (CP=-1). It could, from time to time, decay into two pions (CP=1). This result represents the source of CP symmetry violation.

speculation that it might have played a significant role in the electroweak symmetry breaking, or that it might be a window to the physics beyond the SM (essential to know, for example, the origin of dark matter). Along with these speculations, the top quark is interesting as a probe of the SM theory of the strong force, Quantum Chromodynamics (QCD).

The top quark was discovered in 1995, using the CDF detector at Fermilab's Tevatron Collider [2, 3]. Each of the beams had a maximum energy of 1 TeV. At these energies, pairs of top quarks can be produced. The top quark can decay to a real W boson plus a quark that can be a d, s or b quark. The most significant decay of the top quark is into a W and a bottom quark. The bottom quark produces a jet of hadrons. The W boson from the top quark decays to either pairs of lighter quarks and anti-quarks, or to leptons. The anti-top quark, $\bar{t}$ also decays in a similar fashion. The decays of a $t\bar{t}$ pair can therefore be classified according to the following three channels:

The dilepton channel Both W bosons decay to leptons and neutrinos, i.e. $t\bar{t} \to \ell\ell\nu\nu bb$

The semileptonic channel One W boson decays to a lepton and a neutrino, while the second decays hadronically, i.e. $t\bar{t} \to \ell\nu bbjj$

The fully hadronic channel Both W bosons decay to hadrons, i.e. $t\bar{t} \to bbjjjj$

These decay modes are further discussed in Section 2.4.6.

Chapter 2

The top quark in the Standard Model

2.1 Introduction

The Standard Model (SM) of particle physics is the most established and well-tested theory to represent the elementary particles and their fundamental interactions since the early 1970s. The detailed theoretical framework about this theory is explained elsewhere [4–7]. This chapter presents only some aspects of the SM that are relevant to the top quark. The focus is to understand the implications of top quark measurements within the framework of the SM. According to the SM, matter is composed of fermions[1] and their antiparticles, with the same mass and spin, but opposite charges. Fermions are divided into leptons and quarks, which are both organized into three generations, as shown in Figure 2.1. The SM describes the forces between the fermions through the exchange of gauge particles with integer spin, called bosons[2], which correspond to quantised gauge fields. The basis of the model is a set of fields corresponding to the known fermions and the gauge symmetries $SU(3)_C \times SU(2)_L \times U(1)_Y$.

[1] A fermion is any particle that has an odd half-integer spin. Quarks and leptons, as well as most composite particles, like protons and neutrons, are fermions. The fermions obey the rules of Fermi-Dirac statistics, namely the Pauli Exclusion Principle (one fermion can exist in a given quantum state) and therefore cannot co-exist in the same state at the same location at the same time. Any particle which is comprised of an odd number of fermions is a fermion.

[2] Can put as many bosons into the same quantum state. This allows the creation of very special bosonic states known as Bose-Einstein condensates. Any particle which consists of an even number of fermions is a boson.

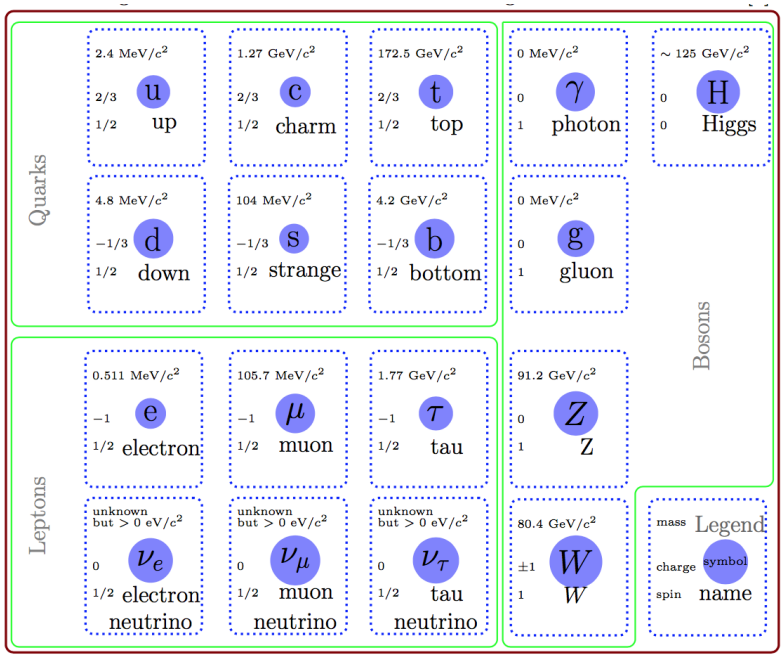

Fig. 2.1 A pictorial view of the Standard Model of particles [8]. Particle's masses are rounded to show their order of magnitude. Latest measurements can be found in [8].

2.2 Fundamental forces

Forces can be defined in simple words as something which change the motion of objects. The forces can attract or repel, and can even cause the phenomenon of radioactivity. In order to generalise the word, the word "interaction" should be used instead of force. Gravity[3] has been the most mysterious in the particle physics realm. The electromagnetic force is much stronger than gravity and it unifies electric and magnetic forces. The strong force is responsible for holding the nucleons together, while the weak force manifests itself in some kinds of radioactivity. Because the forces are different in behaviour, their strengths cannot be explained by a single number. When two quarks are pulled apart, it causes hadronisation, due to strong force. The quarks still experience gravity and electromagnetism. When two particles are brought closer than the size of the nucleus, strong and weak forces disappear and play no significant role. If we take the strong force as a standard then all other forces can be expressed using powers of 10. The electromagnetic force is 100 times weaker than the strong force. The weak force is about a hundred thousand times smaller than the strong force. Gravity is 10^{-40} weaker than the strong force. Each force has been described by a characteristic particle associated with it. The heavier the exchanged particle, the shorter the range of the interaction. Because the electromagnetic force carriers, photons, have no mass,

[3]Gravity is neglected at the mass scale of the high energy physics.

the range of the electromagnetic interaction is infinite. The strong interaction, responsible for the forces that bind quarks, is defined by the gauge theory of Quantum Chromodynamics (QCD) [9]. This theory is based on the gauge group $SU(3)_C$ which couples three different colour charges (red, green, blue), caused by quarks and eight massless gauge bosons called gluons (which carry both a colour and anti-colour charge).
The carriers of the strong force are gluons, because they "glue" the nucleons together. There are eight different gluons, with different colour-anticolour combinations. They come in eight different species of colour-anticolour pairs. The quarks come in three different colours: blue, red and green. The distinctive feature of the strong force is that as the quarks are pulled apart from each other, the force becomes stronger. Here the use of colours is just an attribute picked by physicists to describe another form of charge. The colour can be thought of as the charge of the strong force. The strength of strong interactions is described by the coupling constant α_S, which depends on the interaction momentum transfer Q^2 (to a first approximation as $\frac{Q^2}{\lambda^2}$). The strong coupling constant can be written as

$$\alpha_S(Q^2) = \frac{12\pi}{(33-2f)\ln\frac{Q^2}{\lambda^2}} \tag{2.1}$$

where f is the number of different flavoured quarks with a mass lower than Q^2, and λ is the phenomenological scale constant which is set around 200 MeV. This leads to the asymptotic freedom for a large transferred momentum compared to λ. At increasingly short distance compared to $\frac{hc}{\lambda}$, the strong interaction becomes weak, making possible perturbative calculations.
The electromagnetic interaction is mediated by photons, while the weak interaction, responsible for β decay is mediated by three massive bosons W^+, W^- and Z, with mass $m_W = (80.425 \pm 0.038)$ and $m_Z = (91.1876 \pm 0.0021)$ GeV [10]. The Glashow-Salam-Weinberg (GSW) gauge theory of electroweak interactions [11–13] provides an explanation which unifies weak and electromagnetic forces. This theory is based on the $SU(2)_L \times U(1)_Y$ gauge group of the weak left handed isospin T and hyper charge Y. The weak interaction takes the (V-A) form, coupling only to left-handed particles (the direction of the particle spin is opposite to the direction of its motion) and right-handed antiparticles (particles spin and motion have the same direction), explaining in this way its parity violation. So, the fermion fields of the theory are split up into left-handed and right-handed fields arranged in weak

isospin T = $\frac{1}{2}$ doublets and T = 0 singlets

$$\begin{array}{lcccccccccc} \text{Leptons:} & \begin{pmatrix} \nu_e \\ e \end{pmatrix}_L & \begin{pmatrix} \nu_\mu \\ \mu \end{pmatrix}_L & \begin{pmatrix} \nu_\tau \\ \tau \end{pmatrix}_L & & e_R & & \mu_R & & \tau_R \\ \text{Quarks:} & \begin{pmatrix} u \\ d \end{pmatrix}_L & \begin{pmatrix} c \\ s \end{pmatrix}_L & \begin{pmatrix} t \\ b \end{pmatrix}_L & u_R & d_R & c_R & s_R & t_R & b_R \end{array} \tag{2.2}$$

In the doublets, the weak isospin T_3 has the value $+\frac{1}{2}$ for neutrinos and up-type quarks (u, c, t) and $-\frac{1}{2}$ for the charged leptons and the down type quarks (d, s, b). Using the electric charge and weak isospin it is possible to define the weak hypercharge as $Y = 2Q - 2T_3$, where Q is the electric charge in units of the fundamental electron charge $|q_e|$. So, within the doublets every lepton carries the same hypercharge $Y = 1$ and every quark has $Y = \frac{1}{3}$.

Mass terms for the gauge bosons or fermions are not permitted in a gauge group like $SU(2_L) \times U(1)_Y$ without violating the gauge invariance. The most convincing origin of the mass of the particles seems to be the introduction of a mechanism for spontaneous symmetry breaking, known as the Higgs mechanism [14].

When the neutral component of the doublet obtains a non-zero vacuum expectation value, the $SU(2)_L \times U(1)_Y$ symmetry is broken to $U(1)_{QED}$, giving mass to the W and Z bosons, while the electromagnetic symmetry $U(1)_{QED}$ remains unbroken and the photon remain massless. According to the Higgs mechanism, the mass of elementary particles would be the result of their interaction with an $SU(2)$ doublet of complex scalar fields $\phi = (\phi^+, \phi^0)^T$ mediated by a spin 0 particle known as the Higgs boson. When the neutral component of the doublet obtains a non-zero vacuum expectation value, the $SU(2)_L \times U(1)_Y$ symmetry $U(1)_{QED}$ remains unbroken and the photon is massless.

In July 2012, the ATLAS and CMS experiments announced the discovery of a new particle, with a mass about 125 GeV, compatible with the Standard Model Higgs boson. The masses of the new boson measured by ATLAS ($125.5 \pm 0.2 \pm^{0.5}_{0.6}$) GeV [15] and CMS ($125.7 \pm 0.3 \pm 0.3$) GeV [16] are compatible with each other and agree with electroweak precision data.

2.2.1 CKM mixing matrix and W boson mass

In order to explain the suppression of the strangeness-changing decays, in 1963 Nicola Cabibbo assumed that, for the d and s quarks, the pure flavour eigenstates were obtained by the mixing of two mass eigenstates. The experimental evidence is that a certain mixing angle of $\theta_C \sim 13.1°$ [17] is present in down type quarks and that the weak interaction is sensitive to a (u, d,cos θ_C + s, sin θ_C) quark doublet. In 1970 Cabibbo's model was extended by Glashow, lliopoulos and Maiani by postulating the existence of a fourth quark, the charm quark, to

explain the suppression of the flavour changing current processes [18].
To explain the small CP violation observed by Cronin and Fitch in some kaon decays [19] and to include it in the electroweak theory, in 1973 Kobayashi and Maskawa assumed the existence of a third generation of quarks (the top and bottom quark), at a time when the charm quark was yet to be discovered [20]. In this model, the weak eigenstates of the down type quarks d', s' and b' have to be considered as a combination of the corresponding mass eigenstates d, s and b. This mixing of eigenstates is described by the Cabibbo-Kobayashi-Maskawa (CKM) matrix:

$$\begin{pmatrix} d \\ s \\ b \end{pmatrix}_{\text{weak}} = \begin{pmatrix} V_{ud} & V_{us} & V_{ub} \\ V_{cd} & V_{cs} & V_{cb} \\ V_{td} & V_{ts} & V_{tb} \end{pmatrix} = \begin{pmatrix} 0.97427 & 0.22534 & 0.00351 \\ 0.22520 & 0.97344 & 0.04120 \\ 0.00867 & 0.04040 & 0.99915 \end{pmatrix} \begin{pmatrix} d \\ s \\ b \end{pmatrix}_{\text{mass}} \tag{2.3}$$

Since the matrix is not diagonal, it is evident that there could be transitions between quark generations. By convention, only a mixing between down-type quarks is considered. The W boson couples with up-type and the mixed down-type quarks of every doublet.
The CKM matrix is unitary, and its diagonal entries are very close to unity, while the other elements are very small. Indeed, the other terms are of the order of ~ 0.2 between the first and the second generation and ~ 0.04 between the second and third generation and even smaller between the first and the third generation [10]. All these terms are measured experimentally, except $|V_{tb}|$ which is expected to exceed 0.999 at 90% of confidence level. The experimental measurements are in good agreement with the theoretical constraints, although they are affected by large uncertainties.

2.3 Pre-history of the top quark

In the 1940s and 1950s, physicists analysed the cosmic ray data and discovered particles that did not fit into the already existing classification scheme: neutrons, protons, electrons and atoms. Just like the spinning and orbital motion of electrons in an atom give rise to the excited states of the atoms, the spinning and orbital motion of the constituent quarks will give rise to excited hadronic states. The resonances or excited states are short-lived particles which have the lifetimes of the order of 10^{-23} seconds. By application of the uncertainty principle, the uncertainty in energy is interpreted as the width of the resonance. As more and more particles and resonances were discovered, recurring patterns started emerging. The observation of these patterns among the 30 or so hadrons known in the early 1960s was an indication to the probability of a more fundamental class of matter. In order to be able to describe the hadronic resonances, the quark model was proposed in the 1960s. Deep inelastic scattering (a process to understand the internal structure of the hadron) was used in 1960 to

probe the constituents of the proton [21, 22]. By the late 1960s more than 100 varieties of hadrons had been listed. The code was ultimately cracked by two scientists, Gell-Mann and Zweig, in 1964. They proposed that hadrons were made of three fundamental particles: up, down and strange quarks. Quarks are "confined," which means they exist in clusters so there are no isolated quarks. Some years later, Sheldon Glashow, John Iliopoulos, and Luciano Maiani started working hard to make sense of an unexpected property in the interaction of the Z particle with the quarks. The Eightfold way explained the structure of hadrons in terms of up, down and strange quarks. They realised that in order to be able to understand interactions with the Z, a fourth quark, the charm quark [23, 24] must exist.

Two experimental groups in the USA, one at SLAC and one at Brookhaven National Laboratory, had accumulated data that showed a huge enhancement in the production of electron-positron pairs at 3090 MeV/c^2 to discover a particle [25, 26], which had a clumsy notation of J/ψ (Ting called it J and Richter called it psi (ψ)). It discovered the existence of charm, the lowest lying $c\bar{c}$ state in 1974. It also convinced physicists that the quark model of hadrons was not a mathematical construct but a truthful description of reality. From the mass of J/ψ, the calculated mass of the c quark was about 1500 MeV/c^2. It not only proved the existence of charm but also confirmed QCD, because the properties of the J/ψ could only be described by asymptotic freedom. Two more quarks were yet to come. After the discovery of the tau lepton in 1975 [27], theorists suggested the existence of the third generation of quarks to restore the symmetry between quarks and leptons. Fermilab's 400 GeV proton–nucleus collider observed a strong dimuon excess around 9.5 GeV in 1977 [28] which was later found to be due to two mass peaks Υ and Υ' (the epsilon resonances at 9.44 GeV and 10.17 GeV) [29]. The upsilon was the first of a series of $b\bar{b}$ states to be observed.

2.3.1 The race for the discovery of the top quark

After the discovery of the b-quark in 1977 at Fermilab, the existence of a weak isospin partner of the b-quark, the top, was anticipated and the race to find the top quark started. Since a priori, no preference was given to its mass, a low mass (15 GeV) was considered to observe the resonance states. The e^+e^- colliders at PETRA, DESY, collected data between 1979 and 1984 at the centre-of-mass energies between 12 - 46.8 GeV and was used to start searching for the top quark as an increase in the ratio of reaction events with the final state hadrons and muons. This ratio would increase after the energy exceeded the threshold of the mass of the top quark. No excess was seen for the available energy, the experiment excluded the top quark mass below 23.3 GeV [30, 31]. The TRISTAN e^+e^- collider, at KEK (Japan), also collected data from 1987 to 1990, searching up to 61.4 GeV, and excluded the mass below 30.2 GeV [32]. In 1989 -1990, experiments at SLAC (Stanford, USA) and LEP at CERN in

Geneva, increased the limit to 46 GeV [33–36]. After some indication of the production of the top quark at the $Sp\bar{p}S$ experiment UA1, the hint of mass 40 GeV came in 1984 [37, 38]. After more data and better analyses, the UA2 experiment on the same ring proved this limit to be a fluctuation due to mismodelling of the background [39]. The UA2 experiment increased the top quark mass limit in 1989 to greater than 69 GeV [40].

The Tevatron Collider at Fermilab was a proton-antiproton ($p\bar{p}$) collider designed in the 1970s with the aim of colliding p and $\bar{p}$ with a centre-of-mass energy at or above 1 TeV. In 1985, the Tevatron collided proton and antiproton beams for the first time at an energy of 1.6 TeV. The newly commissioned Collider Detector at Fermilab (CDF) detector pushed the lower limit on the top quark mass to 77 GeV. In 1992, the energy of the Tevatron was increased to 1.8 TeV, and a second detector, DZero (D0), commissioned. In 1994, CDF published the first evidence for the observation of the top quark [41], which was discovered in 1995 jointly by the CDF [42] and D0 [43] experiments. History on the limits of the top quark mass with time is shown in Figure 2.2. To understand how the top quark was discovered using a hadron collider, the next section gives a brief overview of the physics involved in hadron colliders.

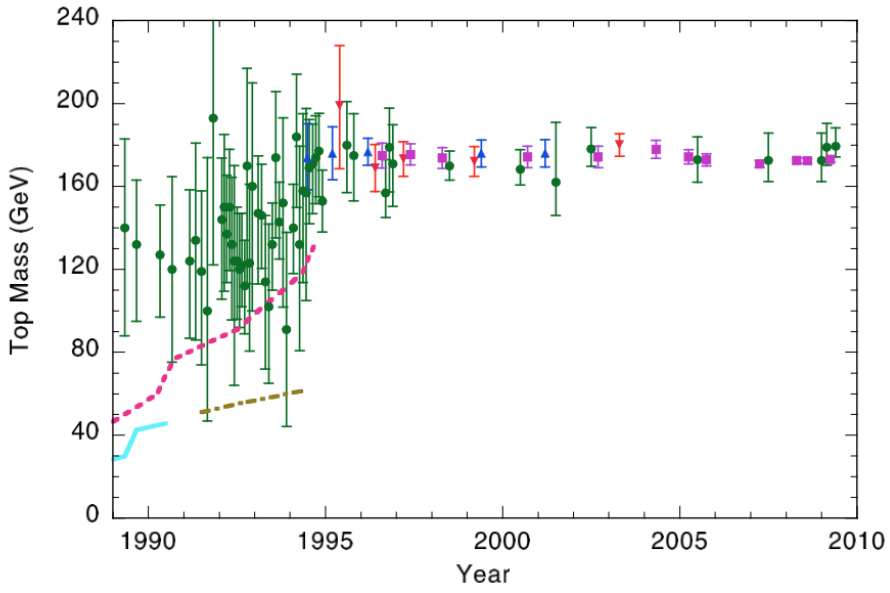

Fig. 2.2 History on the limits of the top quark mass with time. This includes fits to electroweak observables (green dots), 95% confidence limit lower bounds from e^+e^- colliders (PETRA,TRISTAN, LEP and SLAC) shown as a solid line and $p\bar{p}$ collisions as a broken line, indirect lower bounds from the W boson width (dot dash line) and direct measurement from CDF (blue triangles) and D0 (red triangles). The Tevatron average has been shown in magenta [44].

2.3.2 Physics at hadron colliders

Theoretical analyses of hadron collisions follow along a similar path as for e^-e^+. The e^- and e^+ are point-like but the LHC collides protons, which are made of quarks and gluons. The quarks bind to each other by the strong force carriers, the gluons. The quarks exchange gluons between them in order to be able to keep themselves bound together. It may well be true that quarks are not fundamental particles. The structure of the quarks will be one of the exciting questions which can be addressed by the LHC. When hadrons interact with each other then the interactions can be modelled by partons, which are valence quarks, sea quarks (produced due to vacuum fluctuations) and gluons. These partons carry a fraction[4] of the momenta of their interacting hadrons. Any collision with hadrons involves both long and short distance scales that are separated from each other. A hadronic collision can be factorised into perturbative cross-section weighted by a parton distribution function PDF. The PDF of the parton is different for different partons, for example, the PDF of valence quarks is peaked at around 1/3. The cross-section measured in a hard-scattered process can be expressed as

$$\sigma = \sum_{i,j} \int dx_1 dx_2 F_i^1(x_1, \mu_F) F_j^2(x_2, \mu_F) \hat{\sigma}_{ij}(s; \mu_F, \mu_R) \tag{2.4}$$

where the sum runs over gluons and quarks (both the valence and the sea ones) of the interacting hadrons. In this formula, σ_{ij} is the perturbative cross section for collisions of partons i and j. The parton distribution functions (PDFs) $F_i^1(x_1, \mu_F)$ and $F_i^2(x_2, \mu_F)$, on the other hand, explain the long-distance effects that are related to the hadron structure. Here μ_R is the renormalisation scale which describes the size of strong coupling constant, and μ_F is the factorization scale which is a free parameter that dictates the proton structure if it is analysed by a virtual photon or gluon with $q^2 = -\mu_F^2$.

The cross-sections of interesting processes in hadron collider are shown in Figure 2.3. This diagram shows that the total scattering cross-section is $\sigma_{tot} \sim 0.1$ nb while the cross-section scale shows that for the *b*-quark production it is 2-3 orders of magnitude lower. The cross-section for W and Z production is of the order of 10-100 nb, which means that one electroweak boson is produced per 1-10 million pure-QCD events. Looking further down the scale, the top quark pair-production cross-section is a few pb at the Tevatron while it is close to a nb at the LHC [45, 46]. The sudden rise with the centre-of-mass energy can be interpreted on the basis of the fact that top quark pairs are typically produced by interacting partons which have a different fraction of hadron momentum (x $\sim$ 0.2 at the Tevatron and x

[4]Varies with the energy of the collider, it is $\sim 1/10$ at the LHC at 14 TeV.

~ 0.02 at the LHC). At a low x there is a higher parton density, especially for gluons, which in turn increases the cross-section. The LHC produces approximately 10^7 top quark pairs anually at design luminosity, which enables for more in depth studies of the properties of the top quark and also serves as a background for many new physics searches.

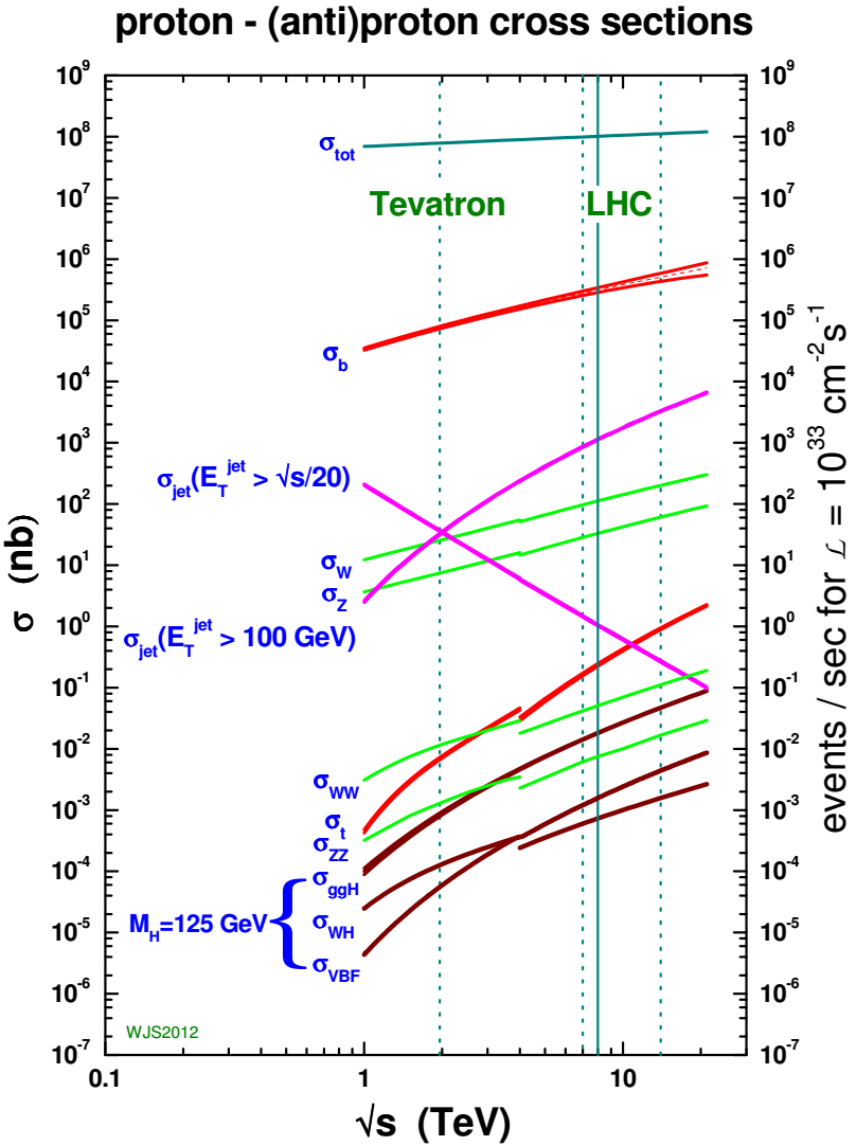

Fig. 2.3 Summary of the cross-sections of various physics processes at the Tevatron and the LHC. The cross-sections are plotted with respect to the centre-of-mass energy of the hadron collision and are shown for $p\bar{p}$ collisions below 3 TeV and for pp collisions above 3 TeV [46].

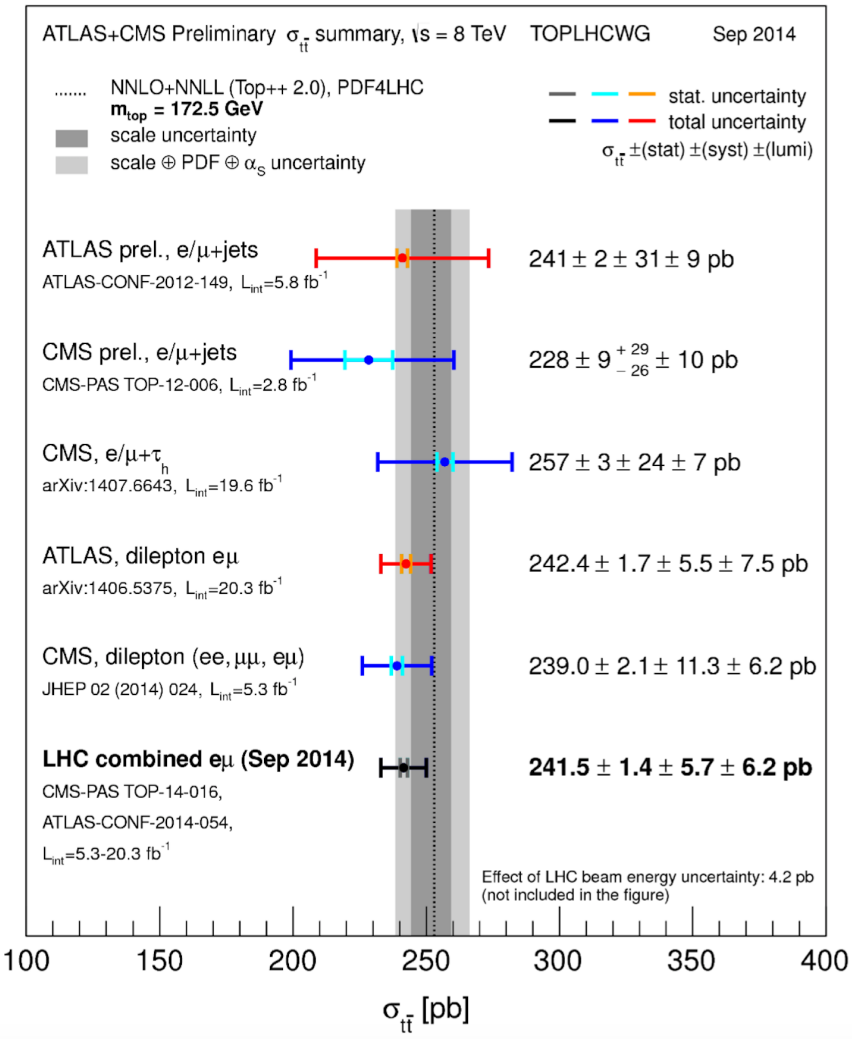

Fig. 2.4 Summary of measurements of the $t\bar{t}$ production cross-section at 8 TeV compared to the exact NNLO QCD calculations with m_{top} =172 GeV [48].

Feynman diagrams for $t\bar{t}$ production at leading order QCD are shown in Figure 2.5. Depending on the type of particle beams (proton-antiproton, $p\bar{p}$, or proton-proton, pp) and centre-of-mass energy, the top quark pair production is described by two processes: at the LHC energy, the top quark pairs are mainly produced through gluon fusion or gluon scattering ($\sim$ 80 - 90% for $\sqrt{s}$ = 7 - 14 TeV) and quark-antiquark annihilation at the Tevatron ($\sim$ 85% for $\sqrt{s}$ = 1.8 - 1.96 TeV). The $t\bar{t}$ production cross-section varies from $7.16^{+0.20}_{-0.23}$ pb at the Tevatron, to $172.0^{+6.4}_{-7.5}$ pb ($\sqrt{s}$ = 7 TeV), $245.8^{+8.8}_{-10.6}$ pb ($\sqrt{s}$ = 8 TeV) and $953.6^{+27.9}_{-38.3}$ pb ($\sqrt{s}$ = 14 TeV) at the LHC [47]. A summary of the measurements of the $t\bar{t}$ production cross-section at 8 TeV is shown in Figure 2.4.

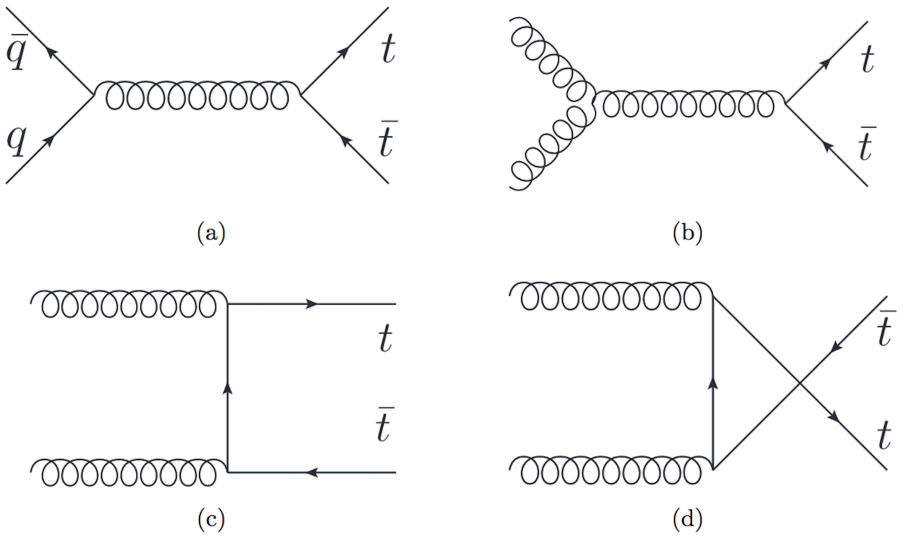

Fig. 2.5 $t\bar{t}$ production via $q\bar{q}$ annihilation (a) and gluon-gluon fusion ((b), (c) and (d)).

2.4 Top quark properties

This section describes some important properties of the top quark.

2.4.1 Mass

Since the top quark decays before hadronisation, its mass can be directly measured from the products it decays to, resulting in the most precise measurement of mass among the other quarks (under 2%). A better knowledge of the mass of the top quark (m_{top}) and W boson imposes indirect constraints on the Higgs boson mass. The value of m_{top} has an effect on theory predictions of particle production cross-sections required for searching for new physics (NP) phenomena and exploring Higgs boson properties. Theoretical preditions for many physics observables are modified due to top-quark induced quantum-loop corrections. To test the overall consistency of the SM and constrain the NP models, the precise determination of m_{top} is necessary. For the determination of the m_{top} and W boson mass (m_W), the 68% and 95% confidence level (CL) contours are shown in Figure 2.6, from Ref. [49]. The blue areas display the fit results when including (excluding) the direct Higgs boson mass [16, 15]. These contours are compared with the direct measurements of m_{top} and m_W. Recently the CMS collaboration has published [50] their results of the measurement of the top quark mass in the semileptonic decay channel at $\sqrt{s}$ = 8 TeV using data of integrated luminosity 19.7 fb^{-1}, quoting a measured top quark mass of $m_t = 171.83 \pm 0.26$ GeV in the μ+jets channel and $m_t = 172.27 \pm 0.27$ GeV in the e+jets channel. A combined fit for these channels gives:

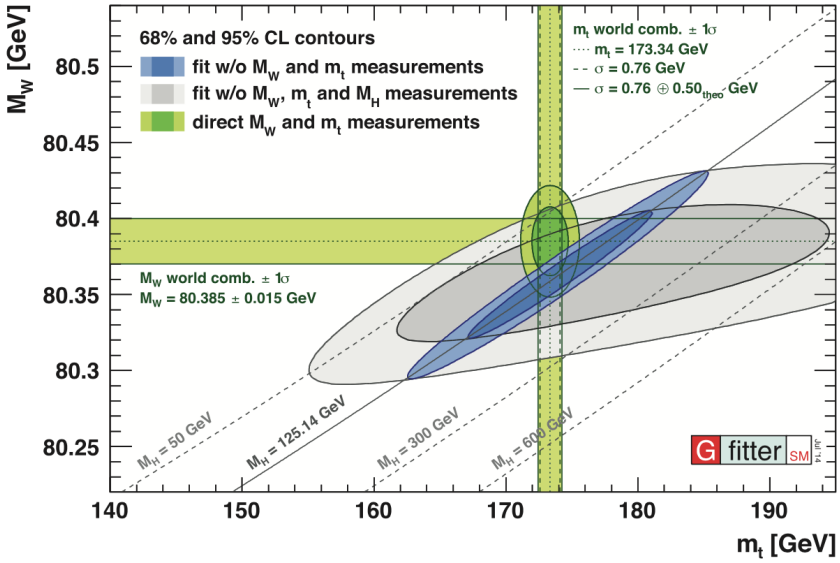

Fig. 2.6 The 68% and 95% CL contours for the indirect determination of m_{top} and m_W from global SM fits to electroweak precision data [49].

$m_t = 172.04 \pm 0.19 \pm 0.75$ GeV. The world combination (2014) [50] is $m_t = 173.3 \pm 0.3 \pm 0.7$ GeV.

The top mass measurements are shown in Figure 2.7.

2.4.2 Electric charge

The electric charge of the top quark predicted by the SM is $\frac{2}{3}e$. A recent measurement of the top quark electric charge was carried out in the ATLAS experiment at the Large Hadron Collider using 2.05 fb^{-1} of data at a centre-of-mass energy of 7 TeV. In units of the elementary electric charge, the top quark charge is determined to be $0.64 \pm 0.02(stat.) \pm 0.08(syst.)$ [51]. This excludes models that propose a heavy quark of electric charge $\pm\frac{4}{3}e$.

2.4.3 Coupling to the Z boson

Constraining the coupling of top quarks to the Z boson in $t\bar{t}$ + Z has been determined in the SM [52] as

$$Vector \text{ coupling} = C_V = \frac{1/2 - 2q_t sin^2\theta_w}{2sin\theta_w.cos\theta_w} \approx 0.24 \tag{2.5}$$

$$Axial \text{ coupling} = C_A = \frac{1/2}{2sin\theta_w.cos\theta_w} \approx -0.60 \tag{2.6}$$

The top quark pair production in association with the Z boson has been studied to investigate the properties of measuring the coupling of top quarks to the Z boson at the LHC [53].

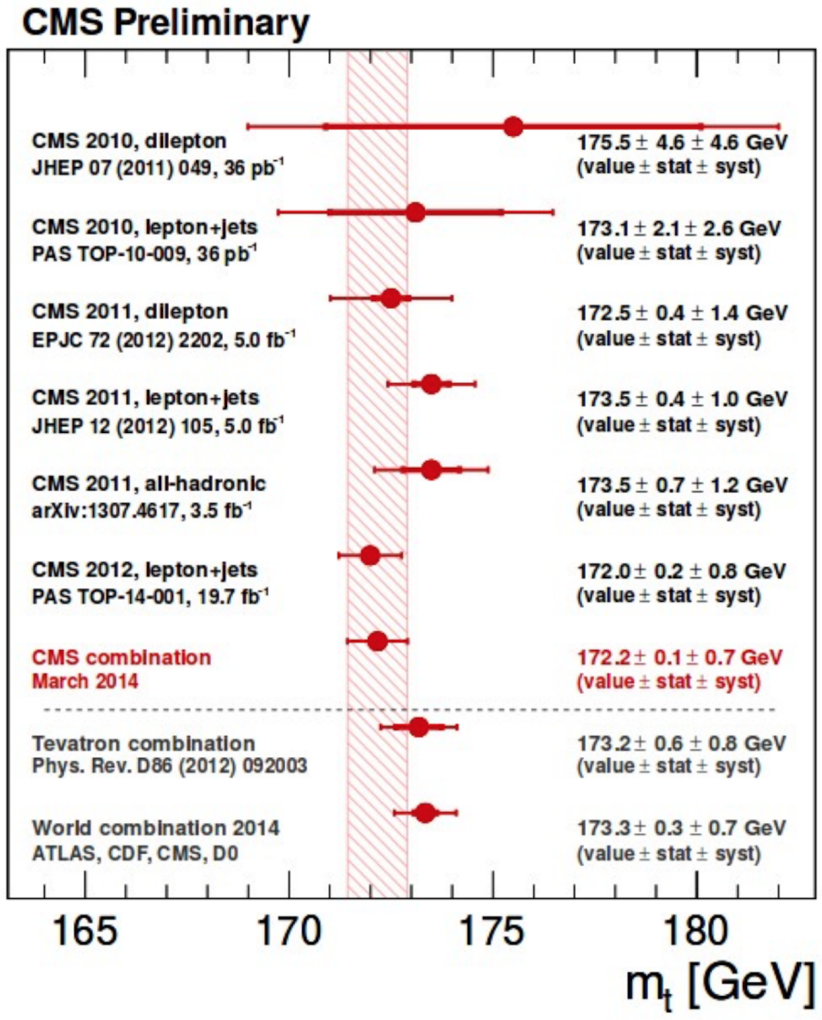

Fig. 2.7 Overview of the top quark mass measurements presented by the CMS, their combination, the Tevatron average and the world combination [50].

Yukawa coupling

In the SM the Higgs boson couples to the top quark through a Yukawa coupling of strength.

$$y_t = \frac{\sqrt{2}m_t}{v} \tag{2.7}$$

here v is the vacuum expectation value which is ≈ 246 GeV. The SM predicts a value of Yukawa coupling close to one. The Yukawa coupling obtained from quite recent measurements with ATLAS [54] at 7 and 8 TeV is:

$$y_t = 1.35 \pm 0.30$$

For CMS [55], it is

$$y_t = 1.6 \pm 0.30$$

Many theories beyond the Standard Model predict different Yukawa coupling theoretical values for the top quark. A precise experimental constraint on its value represents a good test for the SM.

2.4.4 Spin correlations

Detailed studies of the correlation of the spin of the top and anti-top quarks in $t\bar{t}$ production at hadron colliders have been a topic of great interest; they provide important precision tests of the predictions of the SM and are sensitive to many new physics scenarios. Since the top quark decays before it can hadronize, the information of orientations of the top and anti-top quark spins are transferred to the decay products and can be measured directly via their angular distributions. The correlation between the top and anti-top quark spins is extracted with the ATLAS detector from dilepton events at 8 TeV by using the difference in the azimuthal angle between the two charged leptons in the laboratory frame. In the helicity basis, the measured degree of correlation corresponds to $A_{helicity} = 0.38 \pm 0.04$ [56], in agreement with the Standard Model prediction.

2.4.5 Charge symmetry

The SM predicts an asymmetry in top and anti-top production in quark-quark annihilation. Although the dominant $t\bar{t}$ production mechanism in pp collisions at the LHC is gluon-gluon fusion, QCD predicts a small excess of top quarks produced at higher absolute rapidities than anti-tops. The measurement of the top quark charge asymmetry is therefore an important test of QCD and is also sensitive to new physics [57]. The recent experimental value is:

$A_c^{t\bar{t}} = 0.029 \pm 0.018 \pm 0.014$. This value is comparable with the Standard Model predictions and shows no hint of new physics.

2.4.6 $t\bar{t}$ final states

As top quark decays are almost exclusively to a W boson and a b-quark, for $t\bar{t}$ events the final state is determined by the decay of the two W bosons from t and $\bar{t}$, since b-quarks become B-hadrons. In Figures 2.8, 2.9 and 2.10, the Feynman diagrams for the three main decays are drawn. The W boson either decays into a pair of quarks ($u\bar{d}$ or $c\bar{s}$) or into a lepton and its corresponding neutrino. Taking into account both decay modes of the W, there are a total 9 final states W can decay to. The three are described as follows:

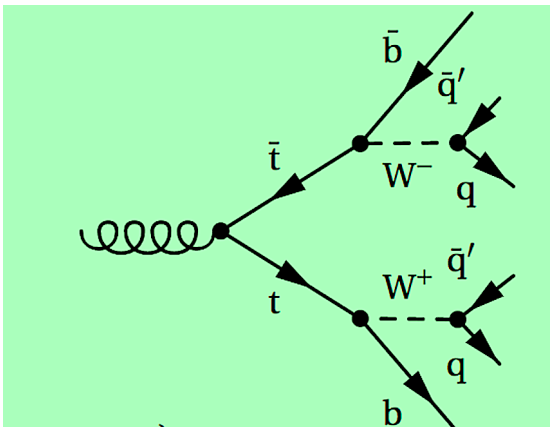

Fig. 2.8 Fully hadronic final state.

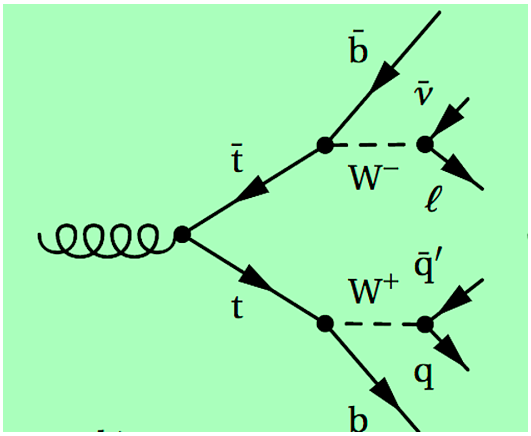

Fig. 2.9 Semileptonic final state.

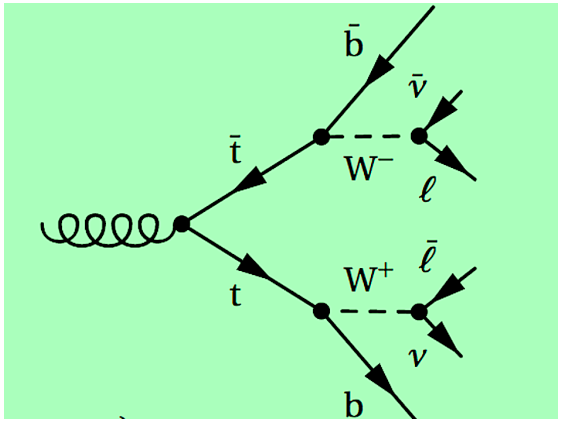

Fig. 2.10 Dileptonic final state.

- Dilepton channel: In this channel both W bosons decay leptonically and thus events consist of two opposite sign leptons, two b-quarks and a large missing transverse energy due to the presence of two neutrinos in the final state that leave the detector without any appreciable interactions. This is the cleanest channel from the background

contamination point of view but the presence of two neutrinos makes the kinematic reconstruction extremely challenging as the longitudinal components of neutrino momenta stay undetermined. There are not many SM processes with two high transverse momentum leptons in the final state and significant missing transverse momentum. The two high transverse energy leptons allow an efficient discrimination of the signal events with a small background contamination. The branching ratio [5] of the process is relatively small compared to other channels. It is only 10.3% in total which is seen in Figure 2.10. Experimentally, only two leptons, electron and muon, out of three can be directly observed. Due to its short lifetime and high mass, only the decay products of the tau lepton can be observed. If the tau lepton decays into an electron or a muon the process is considered as a dilepton. This is the decay channel which has been used for the analysis discussed in this thesis.

- Semileptonic channel: Here one W boson decays into leptons and the other decays into quarks. The final state is characterised by one lepton, two b-quarks, two light quarks from the hadronic W decay and relatively large missing transverse energy. This is the favourite channel to analyse the properties of the top quark. Compared to the dilepton channel, the branching ratio of this channel is quite high (43.5%), which does make the full reconstruction possible, however at the same time the signal to background ratio is not so high as compared to the dilepton channel. In spite of the presence of one high transverse momentum lepton, processes such as QCD or W boson production also contribute to this final state.

- Fully hadronic channel: In this channel both W bosons decay into $q\bar{q}$ pairs (hadronically). The channel is characterised by the presence of two high-p_T b-quarks and four light quarks in the final state. This decay channel has the highest branching ratio, at 46.2%. This is the only channel where all the final state constituents are available to be observed by the detector, but the lack of any high-p_T lepton in the final state makes it difficult to suppress the contamination from background processes from multi-jet production due to the strong interaction, which do not produce top quarks and are called multi-jet QCD production. All decay modes are summarised in Figure 2.11.

2.5 Overview of previous $t\bar{t}$ cross-section measurements

The precise experimental verifications of the theory and quests for new phenomena beyond the SM are in progress to further develop particle physics. In particular, a precise measurement

[5] The ratio of the number of particles which decay via a specific decay mode with respect to the total number of particles which decay via all decay modes.

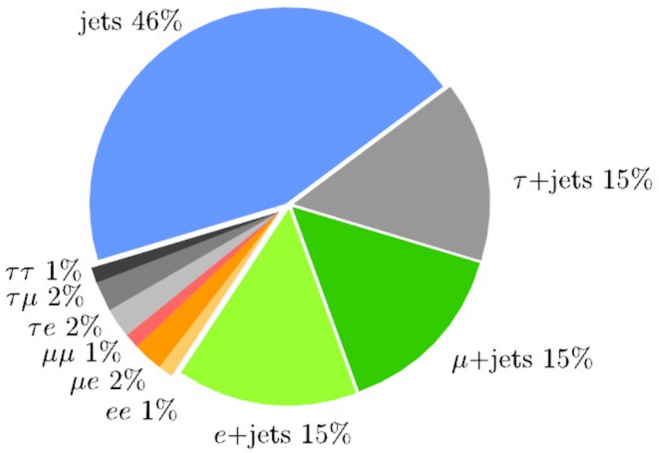

Fig. 2.11 Branching fractions for all possible $t\bar{t}$ decay final states.

in the high energy frontier is one of the most important approaches since the higher energy particle collider data can probe new quantum effects, such as new heavy particle pair-productions. The Large Hadron Collider (LHC) which started operating in 2009, is the energy frontier collider experiment where protons (p) collide at the centre-of-mass energy[6] $\sqrt{s} = 8$ TeV and now (as of 2016) is at the centre-of-mass energy $\sqrt{s} = 13$ TeV.

This thesis focuses on the top quark pair-production fiducial differential cross-section measurements as a function of the dilepton mass (m_{ll}), transverse momentum (p_T), difference of azimuthal angle ($\Delta\phi_{ll}$) and difference of pseudorapidity ($\Delta\eta_{ll}$), using data recorded by the ATLAS detector at the LHC. The top quark is a special particle that can provide many interesting tests of present particle physics theories. It is the heaviest particle of all known particles in the SM, and its mass has been measured to be 173.29 ± 0.23 (stat.) ± 0.92 (syst.) GeV [58]. Due to its large mass, there are several theoretical models that predict new phenomena in the $t\bar{t}$ production and decay. The inclusive cross-section for $t\bar{t}$ production $\sigma_{t\bar{t}}$ in pp collisions at a centre-of-mass energy $\sqrt{s} = 7$ TeV has been measured by both the ATLAS and CMS experiments with increasing precision in a variety of channels [59–65].

[6]The centre-of-mass energy is is the total energy of the colliding system and is represented as $\sqrt{s}$. The four-momenta of the colliding protons is p_1 = (E, 0, 0, E) = (4.0 TeV, 0, 0, 4.0 TeV), p_2 = (E, 0, 0, -E) = (4.0 TeV, 0, 0, -4.0 TeV). The four-momentum of the centre-of-mass system is p_1+p_2 = (8 TeV, 0, 0, 0) = $2E_p = \sqrt{s}$.

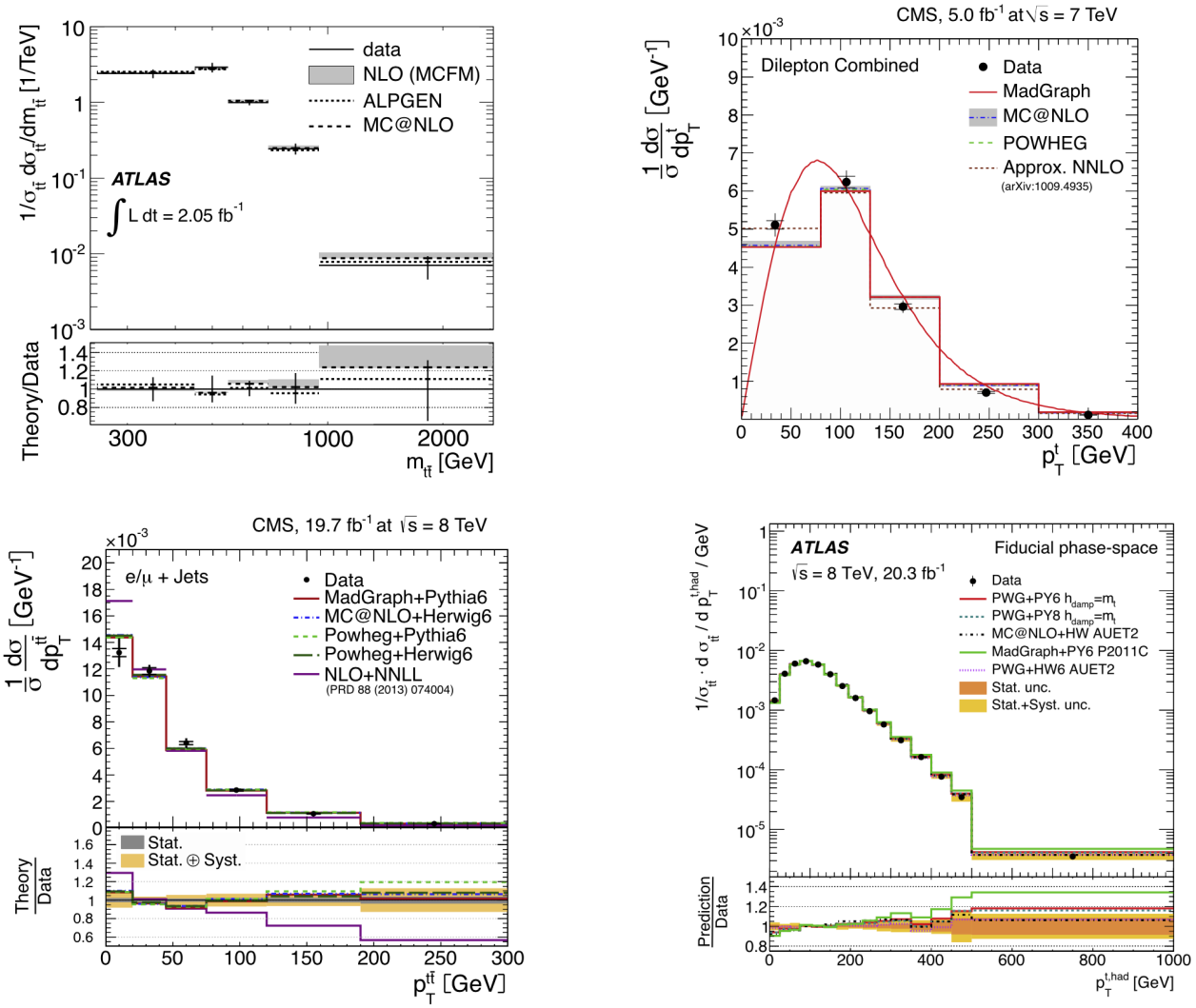

Fig. 2.12 First normalised $t\bar{t}$ differential production cross-section measurements: the invariant mass of the $t\bar{t}$ system in the single-lepton channel, measured by ATLAS [66] (top left) and the transverse momentum of the top quark in dilepton events as measured by CMS [67] (top right). Normalised differential $t\bar{t}$ production cross-section in single-lepton channel as a function of the transverse momentum of the $t\bar{t}$ system [68] (bottom left). Normalised differential $t\bar{t}$ production cross-section as a function of the top $p_{T,t}$ distribution in a fiducial phase-space [69] (bottom right).

The ATLAS and CMS collaborations have published differential cross-sections, using the dataset collected in 2011 at 7 TeV [60, 70], as a function of the mass ($m_{t\bar{t}}$), the transverse momentum ($p_{T,t\bar{t}}$), and the rapidity ($y_{t\bar{t}}$) of the $t\bar{t}$ system. This research leads to statistically precise measurements over the previous ATLAS results by including the full 2012 datasets (10 fb^{-1}) at pp collisions with $\sqrt{s} = 8$ TeV. Furthermore, improved reconstruction algorithms and calibrations are used in this research, thereby significantly reducing the systematic

uncertainties affecting the measurements. The rapidity distribution is symmetrized and presented as $|y_{t\bar{t}}|$ and in addition to the variables previously shown, this paper also presents a measurement of the cross-section as a function of the top quark transverse momentum ($p_{T,t}$).

The LHC is not only the energy frontier accelerator but also the intense frontier hadron collider owing to a high frequency of pp crossings and intensive proton beams. It is expected that multiple collisions occur per bunch crossing, and they can affect the detector performance significantly. Therefore, the correct understanding of the detector performance in the LHC environment is a basic requirement for the precise measurement of the above differential cross-sections. The optimized analysis for the experimental environment enables to identify more than 3000 $t\bar{t}$ candidate events from pp collisions of 10 fb^{-1} with a high purity ($\approx 80\,\%$) in the dilepton final states that are characterized by a pair of isolated leptons (electrons or muons). This $t\bar{t}$ sample is used for the $t\bar{t}$ production cross-section measurement and the study of kinematic properties of top quark pair production. The large top quark samples available at the LHC after Run-1 have made it possible to study differential distributions in depth. Firstly, this enables more thorough tests of perturbative QCD, to constrain the parameters of the MC's simulation and the proton distribution functions. It also allows for a greater understanding of a significant background in the sector of Higgs boson physics, rare physics processes and searches for beyond the Standard Model physics effects. The approach for differential measurements is to begin with a tight event selection to acquire a high purity of $t\bar{t}$ sample by applying tighter cuts. This purity further depends upon the number of b-tag jets in the analysis and can be more than 96% if 2 b-tagged jets are required in the process of $t\bar{t}$ decaying to two leptons. The signal is obtained by subtracting backgrounds from the data. The procedure of unfolding is applied to account for the detector effects like acceptance and resolution. The differential distribution of various kinematic variables are then presented at parton or particle level. The comparison of measured differential cross-section is made with various MC simulations or perturbative QCD calculations. ATLAS made a measurement of $t\bar{t}$ differential cross-section using 2.05 fb^{-1} of 7 TeV data [66] and results were presented as a function of $t\bar{t}$ system kinematic variables, namely the invariant mass, $m_{t\bar{t}}$ (Figure 2.12, top left). Differential measurements using the full 7 TeV dataset were performed by CMS in the single-lepton and dilepton channels [67] (Figure 2.12, top right). Normalised differential $t\bar{t}$ production cross-section in single-lepton channel as a function of the transverse momentum of the $t\bar{t}$ system [68] (Figure 2.12, bottom left). Normalised differential $t\bar{t}$ production cross-section as a function of the top p_T distribution in a fiducial phase-space [69] (Figure 2.12, bottom right). Figure 2.13 shows comparisons of some differential distributions obtained by ATLAS and CMS to the full NNLO calculation [71]. ATLAS data appear to be well modelled by the full NNLO calculation, while the CMS data show a small residual difference.

This thesis uses 2012 collision data collected by the ATLAS to measure the differential cross-section of top pairs as a function of lepton kinematic variables. The details will be discussed in Chapter 6.

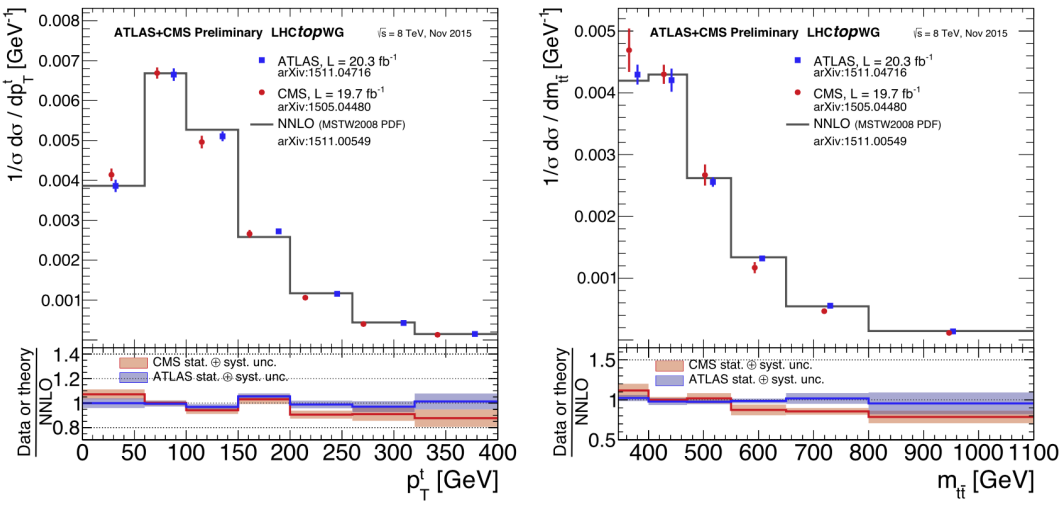

Fig. 2.13 Full phase-space normalised differential $t\bar{t}$ cross-section as a function of the transverse momentum of the top quark (left) and the invariant mass of the $t\bar{t}$ (right). The CMS and ATLAS results are compared to the NNLO calculation. The shaded bands show the total uncertainty on the data measurements in each bin [71].

Chapter 3

The ATLAS detector at the LHC

Studying the constituents of matter and describing the important questions in particle physics are marvellous objectives, but without the development and understanding of the equipment involved, it is not possible to be able to answer these questions to make discoveries. The Large Hadron Collider (LHC) is often known as the discovery machine by scientists and it has been designed to discover new elementary particles. Higher and higher collision energies and greater and greater luminosity enable researchers to reproduce the physical conditions that were present at the birth of our universe a long time before the elementary particles and forces we observe today had come into play. The LHC allows us to run the clock backwards almost to the time less than one hundred-billionth of a second after the Big Bang. The discovery of the Higgs Boson at the LHC is believed to underpin the Standard Model of Particle Physics and is hypothesized by that model to give mass to all elementary particles. This chapter gives a brief overview of the LHC and the ATLAS (A Toroidal LHC ApparatuS) detector followed by some details on its subsystems. The cross-section measurement presented in this thesis was performed using the data collected by the ATLAS experiment [72].

3.1 The Large Hadron Collider

The Large Hadron Collider (LHC) [73] is the most powerful and complicated particle accelerator in the world, operating at CERN[1]. It represents an extraordinary and unprecedented adventure in information technology, with a flux of data of the order of millions of gigabytes per second. It is a fantastic intellectual venture because it explores spaces where no previous experiment has been able to probe. The LHC is a journey inside the deepest structure of matter towards the unknown. This gigantic microscope is able to peer at a depth less than 1000 zeptometres (billionth of a billionth of a millimetre). The LHC is vital to test current

[1] Conseil Européen pour la Recherche Nucléaire.

physics theories and to investigate what lies beyond them. In order to be able to achieve it, the LHC needs to accelerate protons or heavier ions such as lead in opposite directions and then make them collide into each other at higher energies. To achieve the desired energies, the longer the path, the better. The LHC is a ring-shaped proton-proton accelerator, 27 kilometres in circumference and is comprised of 1,232 primary magnets that required 6,900 km of wire to make and were installed in a tunnel 100 m underground. In order to study and analyse the extremely small particle explosions called events, the LHC needs instruments which are called detectors. They register the event by measuring the properties of the particles produced in the collisions, such as momentum, energy, mass and by reconstructing the tracks[2]. Seven experiments at the LHC use detectors to analyse the myriad of particles produced by collisions in the accelerator. At the LHC, new caverns were dug, with the largest, at interaction "point 1", housing the very large ATLAS detector. The other detectors are: CMS (Compact Muon Solenoid), ALICE (A Large Ion Collider Experiment) and LHCb (Large Hadron Collider beauty). They are at another three interaction points around the ring. The CMS [74] is the other general purpose detector, built with the same objectives as ATLAS; it uses different technical solutions and a different magnet-system design. It has been built around a big magnetic solenoid magnet that produces a magnetic field of strength 4 T. This detector is 21 metres long, 15 metres wide and 15 metres high and involves 4300 scientists from 182 institutions in 42 countries (February 2014). The LHCb [75] experiment will shed light on why we live in a universe that appears to be made almost entirely of matter, but no antimatter. It investigates the slight differences between matter and antimatter by studying hadrons containing *b* quarks. It works in the forward region since it is made up of a single forward spectrometer. It is 21 metres long, 10 metres high and 13 metres wide and involves 700 scientists from 66 different institutes (October 2013).

ALICE [76] is a heavy ion (Pb) experiment focused on studying a new phase of matter called the quark-gluon plasma, thought to have been produced just after the Big Bang. The existence of such a state and its related properties are central issues in the theory of quantum chromodynamics (QCD). It is 26 metres long, 16 metres high, and 16 metres wide and engages almost 1000 scientists from 100 institutes from 30 countries. The smallest experiments on the LHC are LHCf[3] [77], MoEDAL[4] [78] and TOTEM[5] [79]. During 2011 proton proton run the LHC was operated at a centre-of-mass energy of 7 TeV and integrated luminosity 4.6 fb^{-1}. In 2012 its centre-of-mass energy was increased to 8 TeV

[2]The trajectory of a charged particle through the magnetic field of the inner detector (or muon spectrometer) is referred to as track.

[3]LHC forward.

[4]Monopole and Exotics Detector At the LHC.

[5]TOTal Elastic and diffractive cross-section Measurement.

that corresponded to an integrated luminosity of 20.3 fb^{-1}. The LHC was shut down for 27 months for re-commissioning and its centre-of-mass energy has been increased to 13 TeV, almost double the collision energy of its first run [80].

3.1.1 Accelerator complex

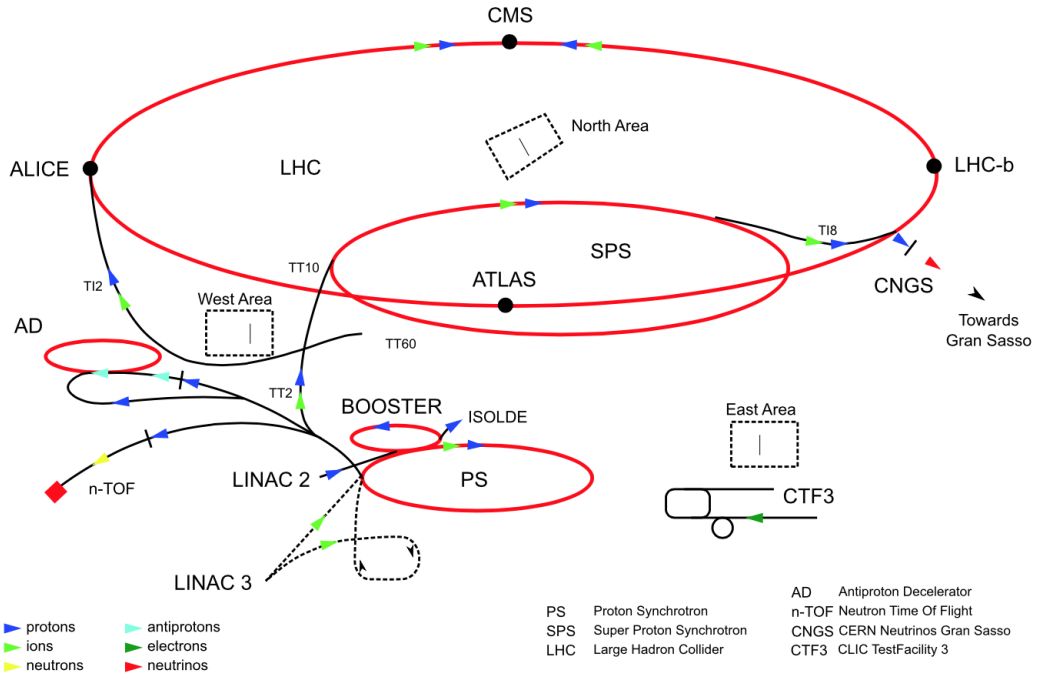

Fig. 3.1 Schematic view of the LHC accelerator complex. Protons are accelerated by various accelerators before being injected to the LHC. The ATLAS, ALICE, CMS, and LHC-b detectors are located at four points along the ring, as shown [81].

The accelerator complex consisting of a chain of accelerators has been shown in Figure 3.1. Each accelerator boosts the energy of the beam, before it enters into the next machine in the chain. The protons are obtained from hydrogen gas which is surrounded with an electric field that can decompose the gas into its constituent protons and electrons. This process gives about 70% protons. The first accelerator in the sequence is the Linear Particle Accelerator (LINAC 2), which accelerates the protons to the energy of 50 MeV. The beam is then injected into the next machine, Proton Synchrotron Booster (PSB), which accelerates the protons to 1.4 GeV, followed by the next machine, Proton Synchrotron (PS), which can operate to 25 GeV. Protons are then injected into the Super Proton Synchrotron (SPS) where they receive their final energy kick to 450 GeV before they enter the LHC rings. These highly accelerated protons are finally transferred to the two beam pipes, which are tubes at ultrahigh vacuum.

The beam in one pipe starts circulating clockwise while the beam in the other pipe starts circulating anticlockwise. It takes 4 minutes and 20 seconds to fill each LHC ring, and 20 minutes to accelerate each beam to its final energy of 4 TeV. Beams are kept circulating for many hours inside the LHC beam pipes under normal operating conditions. The two beams are then brought into collision inside four detectors - ALICE, ATLAS, CMS and LHCb.

3.1.2 Delivered and recorded luminosities

The rate of physics processes at the colliders depend on the cross-section of the process and the luminosity of the collider. The instantaneous luminosity describes the event rate for unit cross-section and it depends on the number of particles in the beam and the overlap integral of the beams. The importance of luminosity will be presented in Section 6.2. Due to the Radio Frequency (RF) fields in the accelerating cavities, the proton beams are segmented into groups of protons called bunches. The main role of the RF cavities is to keep the proton bunches tightly bunched to ensure a high luminosity at the collision points and hence maximize the number of collisions (luminosity). Each beam contains 2808 bunches and each bunch consists of 1.7×10^7 protons. The instantaneous luminosity of two equal bunches

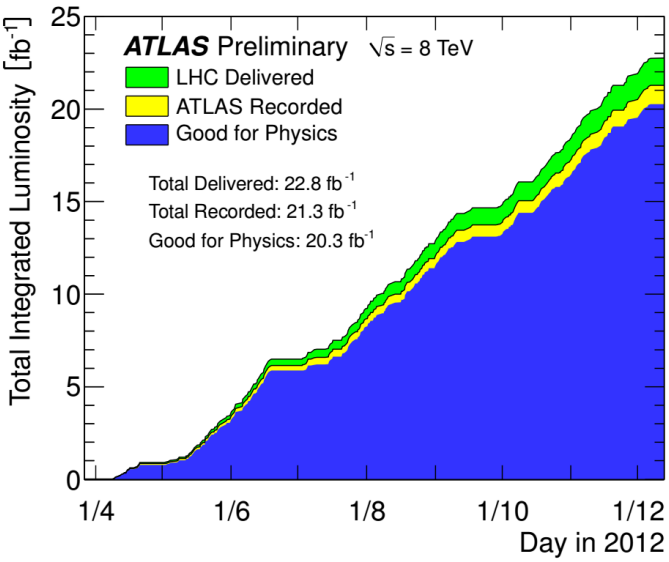

Fig. 3.2 Plot showing the integrated luminosity delivered and accumulated by the ATLAS detector during 2012 data taking [82].

beams is given as

$$L = f \frac{n_1 n_2}{4\pi\sigma_x\sigma_y} \tag{3.1}$$

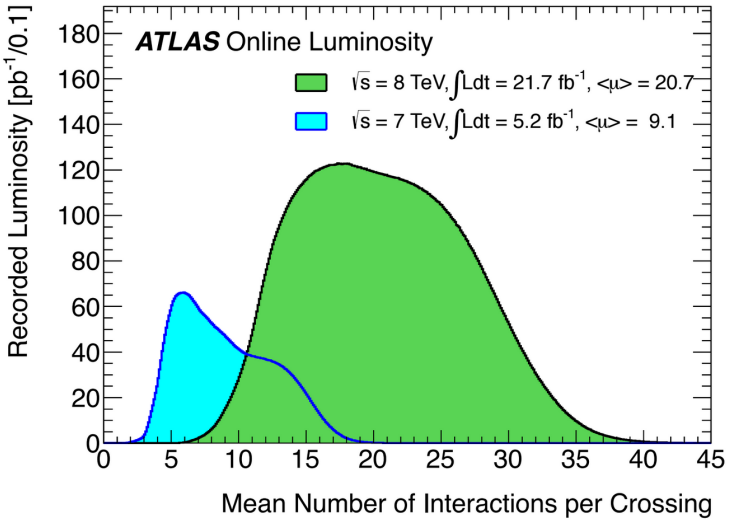

Fig. 3.3 Plot showing the distribution of the mean number of proton–proton interactions taking place per bunch-crossing in 2011 and 2012 data taking [82].

where f = 11245.5 Hz is the collision frequency of the beams; n_1 and n_2 are the number of protons in each beam and σ_x and σ_y are RMS beam widths in the horizontal and vertical directions. The peak instantaneous luminosity of the LHC in 2012 was 7.7×10^{33} cm^{-2}s^{-1}. The integrated luminosity is obtained by integrating the instantaneous luminosity over a certain time. If N is the number of events for a given process and σ is the cross-section of the process then

$$N = \sigma \times \int L(t)dt \tag{3.2}$$

The integrated luminosity delivered and cumulated by the ATLAS detector during 2012 is shown in Figure 3.2. In the first seven months of 2012, the LHC had delivered more than twice as many collisions to the ATLAS experiment as it did in all of 2011. The delivered integrated luminosity refers to the integrated luminosity which the LHC has delivered to an experiment, and recorded integrated luminosity refers to the amount of data that has actually been stored to a disk by the experiments.

The beam conditions determine the number of proton-proton interactions that occur in a single bunch-crossing. When a single bunch-crossing produces multiple separate proton-proton collisions, these events are referred to as pile-up. During 2011, the number of proton-proton collisions per bunch-crossing increased from 5 to 15, and during 2012 the number increased from 10 to almost 35. Figure 3.3 shows the mean number of interactions per bunch-crossing for 2011 and 2012, demonstrating the substantial increase of pile-up events in the latter. It has a significant impact on the analysis. The extra particles produced

in the final state due to pile-up could be confused as coming from the interaction. The MC simulations cannot perfectly model the shape of the mean number of proton–proton interactions ($< \mu >$) in the data, which can be fixed by applying a pile-up weight to each MC event.

3.1.3 Worldwide LHC computing grid

The Worldwide LHC Computing Grid (WLCG) is a global computing infrastructure consisting of more than 170 computing centres in 42 countries. It makes it possible to store a huge amount of data produced by the LHC, but it also makes data accessible to thousands of research centres, universities and laboratories established all over the world. This computing grid allows over 6000 scientists to run their physics analyses simultaneously. The WLCG consists of four levels, or "Tiers", called 0, 1, 2 and 3. Each Tier is composed of several computer centres and provides a specific set of services.

Tier 0: Tier 0 is the CERN Data Centre, which is responsible for the safe-keeping of the data produced by the LHC. It is capable of storing 20% of all the grid data and distributes the raw data and the reconstructed output to Tier 1. It is used to reprocess data when the LHC is not running.

Tier 1: Tier 1 consists of 13 computer centres to store the LHC data (see Table 3.1).

List of Tier 1 Grid sites	
Country Name	Grid 1 Site
Canada	TRIUMF
Germany	KIT
Spain	PIC
France	IN2P3
Italy	INFN
Nordic countries	Nordic Datagrid Facility
Netherlands	NIKHEF / SARA
Republic of Korea	GSDC at KISTI
Russian Federation	RRC-KI and JINR
Taipei	ASGC
United Kingdom	GridPP
US	Fermilab-CMS
US	BNL ATLAS

Table 3.1 Tier 1 sites.

Tier 2: Tier 2 includes 160 sites typically universities and other scientific centres, which provide computing power to produce and keep a share of simulated events.

Tier 3: Individual scientists and researchers can access the Grid through local (or Tier 3) computing resources, which consist of local clusters e.g. in a university department.

3.1.4 The ATLAS detector

The ATLAS detector shown in Figure 3.4 is a multi-purpose apparatus operating at the Large Hadron Collider (LHC) [73], designed to study the widest possible range of physics processes. It records the complete information about the events by identifying almost all the produced particles and reconstructing their trajectories - can take a complete snapshot of every event. The interested particles are produced over a wide range of all possible energies. Since the identification of different particles have to meet different requirements, the detectors have to fulfil strict requirements that produce difficult technological challenges. First and foremost, the response from the electronic components has to be quick, because the time lag between the bunches is very small. Secondly, components should offer very high resistance to radiation since they are exposed to a large flux of very energetic particles. Finally, no repair is possible during operation so they have to be reliable. In order to be able to analyse the results, it is aimed to have the information of almost all the particles. Therefore, the detectors are designed to cover any direction around the collision point i.e. they have to be "hermetic". ATLAS consists of several layers of sub-detectors - from the interaction point outwards: the inner detector tracking system, the electromagnetic and hadronic calorimeters, and the muon system. The most important dimensions of the ATLAS sub-detectors are summarised in Table 3.2. The inner detector is immersed in a 2 T magnetic field generated by the central solenoid. It is designed to provide high-precision tracking information for charged particles and consists of three sub-systems, the Pixel detector, the Semi-Conductor Tracker (SCT), and the Transition Radiation Tracker (TRT). The first two subsystems cover a pseudo-rapidity (defined below in Equation 3.4) region of $|\eta| < 2.5$, while the TRT reaches up to $|\eta| = 2.0$. A track in the barrel region typically produces 11 hits in the Pixel and SCT detectors and 36 hits in the TRT. The electromagnetic (EM) and hadronic calorimeters cover the range $|\eta| < 4.9$, with the η region matched to the inner detector having a finer granularity in the EM section, needed for precision measurements of electrons and photons. The EM calorimeter uses lead as an absorber and liquid argon (LAr) as the active material. The hadronic calorimeter uses steel and scintillating tiles in the barrel region, while the end-caps use LAr as the active material and copper as the absorber. The forward calorimeter also uses LAr as the active medium with copper and tungsten absorbers. The muon spectrometer relies on the deflection of muons as they pass through the magnetic field of the large superconducting air-core toroid

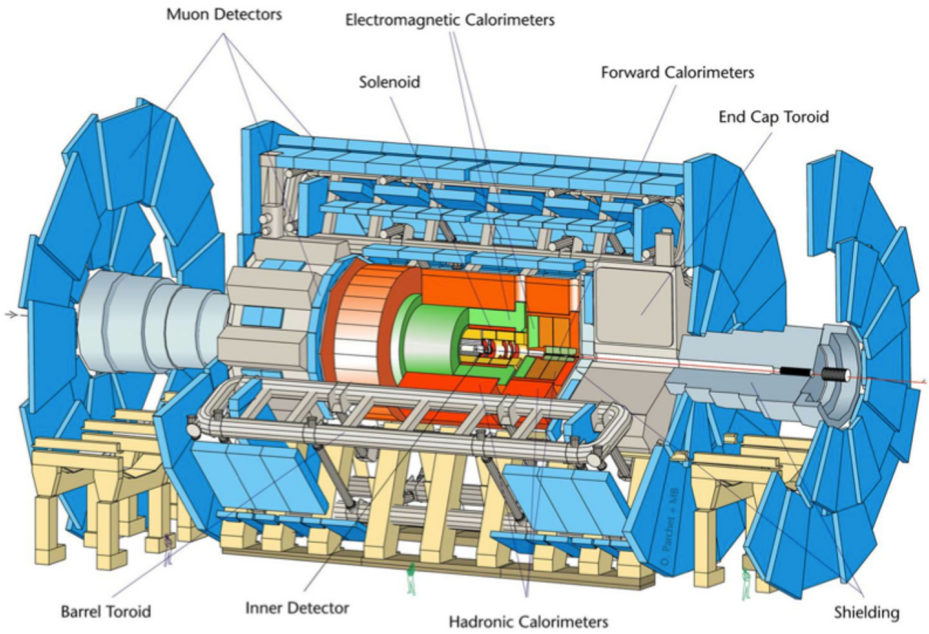

Fig. 3.4 Schematic view of the ATLAS detector showing the main detector components.

component	radius [m]	length [m]	η-coverage
barrel muon spectrometer	11	26	$\|\eta\| < 1.4$
end-cap muon spectrometer	11	2.8	$1.1 < \|\eta\| < 2.8$
barrel hadronic calorimeter	4.25	12.2	$\|\eta\| < 1.0$
end-cap hadronic calorimeter	2.25	2.25	$1.5 < \|\eta\| < 3.2$
barrel em-calorimeter	2.25	6.42	$\|\eta\| < 1.4$
end-cap em-calorimeter	2.25	0.63	$1.4 < \|\eta\| < 3.2$
forward/backward calorimeter	integrated in end-cap		$3.1 < \|\eta\| < 4.9$
barrel + end-cap inner detector	1.15	6.8	$\|\eta\| < 2.4$

Table 3.2 Dimensions of the ATLAS sub-detectors.

magnets. The precision measurement of muon track coordinates in the bending direction of the magnetic field is provided, over most of the η-range, by Monitored Drift Tubes (MDT). Cathode Strip Chambers (CSC) are used in the innermost plane for $2.0 < |\eta| < 2.7$ due to the high particle rate in that region. The muon trigger, as well as the coordinate in the direction orthogonal to the bending plane, are provided by Resistive Plate Chambers (RPC) in the barrel and Thin Gap Chambers (TGC) in the end-caps. The ATLAS detector has a three-level trigger system consisting of Level-1 (L1), Level-2 (L2), and the Event Filter (EF). At design

Components	Resolution	η coverage	
		Measurements	Trigger
Tracking	$\sigma_{p_T}/p_T = 0.05\% p_T \oplus 1\%$	$\|\eta\| < 2.5$	-
EM calorimetry	$\sigma_E/E = 10\%/\sqrt{E} \oplus 0.7\%$	$\|\eta\| < 3.2$	$\|\eta\| < 2.5$
Hadron calorimetry			
barrel and end-cap	$\sigma_E/E = 50\%/\sqrt{E} \oplus 3\%$	$\|\eta\| < 3.2$	
forward	$\sigma_E/E = 100\%/\sqrt{E} \oplus 10\%$	$3.1 < \|\eta\| < 4.9$	
Muon spectrometer	$\sigma_{p_T}/p_T = 10\%$ at p_T=1 TeV	$\|\eta\| < 2.7$	$\|\eta\| < 2.4$

Table 3.3 Resolution and η coverage of different components of the ATLAS detector.

luminosity the L1 trigger rate is approximately 75 kHz. The L2 and EF triggers reduce the event rate to approximately 200-400 Hz before data transfer to mass storage. Figure 3.5 shows an example of $t\bar{t}$ event decaying to dilepton final state, illustrating the response of the ATLAS detector to these events. In particular, it illustrates the way the different components of the ATLAS detector respond to the various particles produced in these events. The general performance features of the detector have been listed in Table 3.3. The ATLAS sub-detector can be divided into the Inner Detector, Calorimetry System and the Muon Spectrometer. They will be briefly described in the next sections. Different particles interact differently so this difference distinguish one type of particle from another. A transverse plane profile of the ATLAS detector is shown in Figure 3.6 in order to illustrate different layers and the passage of different particle types through the layers. Muons are the only particles that reach (and are detected by) the outermost layers of the detector. Electrons are very light and therefore lose their energy quickly, while protons pass further through the layers of the detector. Photons themselves leave no track, but in the calorimeters, each photon is converted into one electron and one positron, the energies of which are then measured.

3.1.5 ATLAS coordinate systems

The ATLAS detector is housed at interaction point 1 on the LHC ring, close to the CERN main site. The vector that points from the interaction point to the centre of the LHC ring defines the x-axis and the y-axis points upwards. The z-direction known as the A-side, is along the beam axis and the $-z$ side is known as the C-side for the naming conventions in the pit. Besides the standard Cartesian coordinate system, especially for physics analyses, a coordinate system with (r, ϕ, θ) is useful. Here, r is the transverse radius from the beam-pipe and ϕ the azimuthal angle, measured from the x-axis. θ can be used to directly measure the angle away from the beam-pipe. For describing tracks of particles in a detector, rapidity,

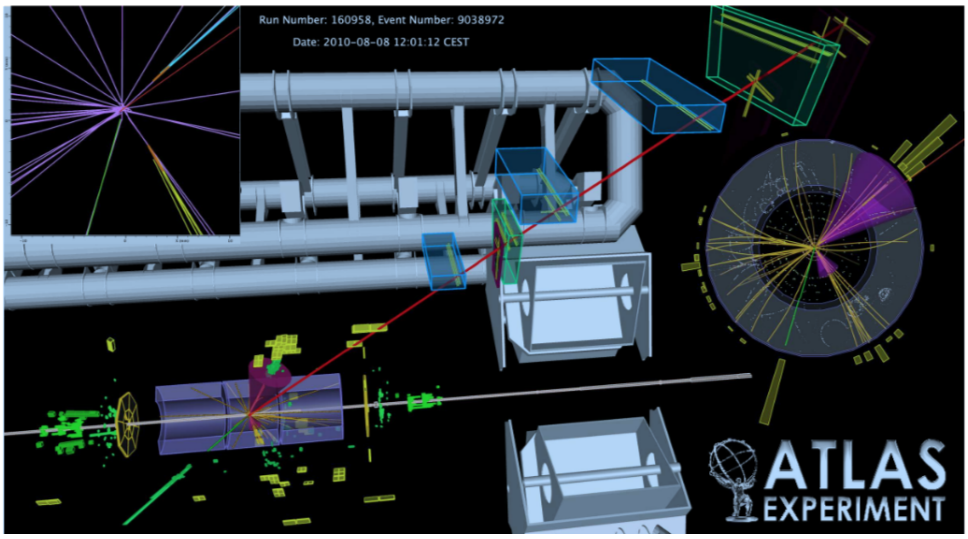

Fig. 3.5 A typical event display of a top pair decaying into $e\mu$ (dilepton) with two b-tagged jets. The electron has been shown by the green track while the muon is shown by the red track which is long enough to reach the muon chambers. The two b-tagged jets have been shown by the purple cones whose sizes are correlated with the jet energies [83].

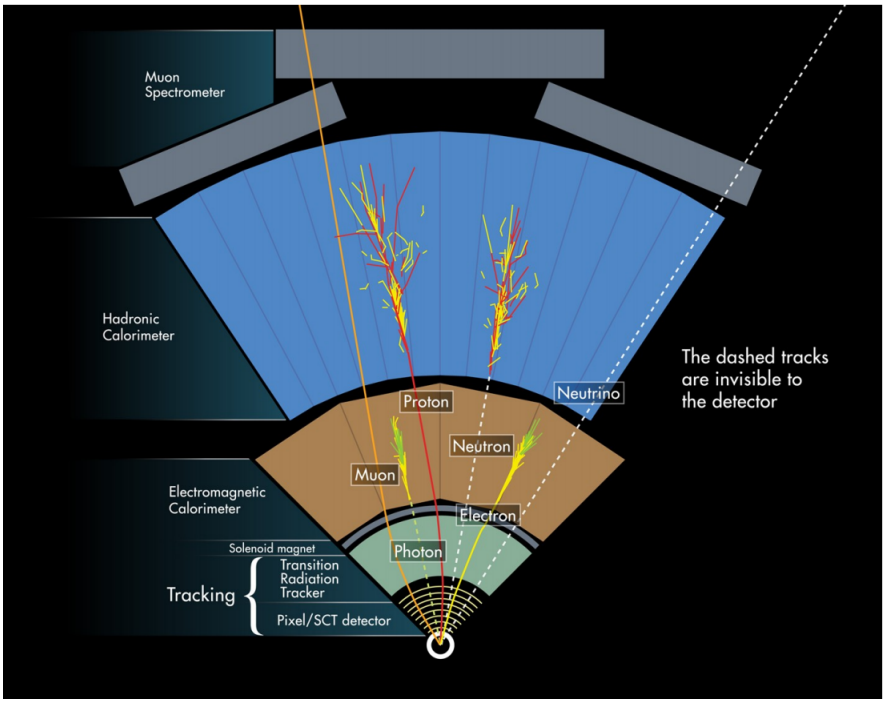

Fig. 3.6 A computer generated diagram showing the paths of different particles passing through the ATLAS detector [84].

y, is especially useful because it is invariant under longitudinal (in z) Lorentz boosts and in hadron collisions, the original longitudinal momentum of the interacting partons is not known. Rapidity is defined as:

$$y = \frac{1}{2} \ln \frac{E + p_L}{E - p_L}, \tag{3.3}$$

where E is the energy of the particle and p_L is the longitudinal component of the momentum of the particle. For a particle with zero rest mass, this equation is reduced to:

$$\eta = -\ln \tan \frac{\theta}{2}, \tag{3.4}$$

where η is the pseudo-rapidity. η is a good approximation for y in the relativistic limit. This parameter is convenient for describing the coverage of a detector. A high η coverage, meaning $\eta \gg 1$, means that a detector has good coverage in the forward regions. It is also useful to define ΔR as the angular distance between two points (η_1, ϕ_1) and (η_2, ϕ_2):

$$\Delta R = \sqrt{(\Delta\eta)^2 + (\Delta\phi)^2}, \tag{3.5}$$

where $\Delta\eta = \eta_2 - \eta_1$ and $\Delta\phi = \phi_2 - \phi_1$.
Along the z-axis the detector is divided in five parts: a central part called the barrel region, the two lateral parts called the end-caps and the two parts close to the beam axis called forward regions. The helical trajectories of tracks are parametrised in the ATLAS software as five dimensional vectors with the following parameters:

$$\tau = (d_0, z_0, \phi_0, \theta, q/p), \tag{3.6}$$

where d_0 and z_0 are the transverse and longitudinal impact parameter respectively, measured with respect to the origin. The ratio q/p is the inverse of the particle momentum multiplied by its charge. The momentum projected in x-y plane is referred to as transverse momentum and is often represented as p_T, while the magnitude of three-momentum is denoted by p. The transverse momentum, p_T, is computed as $p_T = p \sin\theta$.

The energy of the particle is referred to as E. The transverse momentum can be obtained from three-momentum as

$$p_T = \frac{p}{\cosh(\eta)} \tag{3.7}$$

A "transverse energy" can be written mathematically as

$$E_T = \frac{E}{\cosh(\eta)} \tag{3.8}$$

The integral over time of the instantaneous luminosity gives the total luminosity. The LHC design instantaneous luminosity is 10^{34} cm^{-2}s^{-1}. The analysis done in this thesis uses the 2012 dataset with integrated luminosity 20.3 fb^{-1} after applying requirements on the quality of data.

3.2 Inner Detector Trackers

Approximately 1000 particles emerge from the LHC collision points every 25 ns, creating a very large flux in the detector. This is the innermost subdetector of ATLAS [85, 86] which is divided into the Pixel Detector with incredibly fine resolution, the Semi-Conductor Tracker made of silicon strips, and the Transition Radiation Tracker made of gold-plated tungsten wire inside thin tubes known as "straws" (see Figures 3.7 and 3.8). The role of the inner detector is to measure the tracks made by the charged particles during their interaction with the sub-detectors. The job of the inner detector is to record the trajectories of the particles as precisely as possible, allowing to reconstruct the interaction points from which these particles originate. The point where the interaction takes place in the inner detector is called a "hit". The Pixel Detector has three layers, including one of them at a radius of 4 cm, the B-layer, which is vital for good vertexing. The SCT is a charged particle tracking device for the precise measurement of momentum, collision point and secondary vertex measurements with pixel and TRT detectors in a 2 Tesla magnetic field. The basic readout unit of the SCT is a module. The SCT modules are built from two pairs of single-sided silicon micro-strip sensors. Each silicon wafer is 6 cm long. Two wafers are daisy chained together on each side of the module, resulting in a 12 cm long module. Each pair of sensors is glued back-to-back with a relative stereo angle of 40 mrad. A total of 4088 SCT modules are used to form four concentric barrel layers (2112 modules) and 2×9 end-cap disks (1976 modules). Each module has 768 readout channels per side. All barrel modules are identical [87, 88], whilst there are 3 types of end-cap modules. The inner end-cap modules are shorter (6-cm-long) as they are formed just by two back-to-back sensors. The barrel modules have a rectangular shape with a constant strip pitch of 80 µm. The end-cap silicon wafers and their strips have a wedge shape with a constant inter-strip angle which results in an average strip pitch of 80 µm. The resolution of the SCT modules in the $r\phi$ (direction across the strips) is $\sim$417 µm. The module is read out by 12 ABCD3TA ASICs mounted on a hybrid circuit. Each chip provides binary readout of 128 detector channels. The ID sub-detector with the biggest radius is the Transition Radiation Tracker, which consists of 36 layers each of 4 mm diameter straw drift tubes. It is a combination of tracking and transition radiation detector. It covers the region of $|\eta| < 2.0$. with a gap for the readout at $|\eta| < 0.1$. The straw tubes have been aligned parallel to the beam pipe which limit on the resolution in $|\eta|$. Particles that traverse

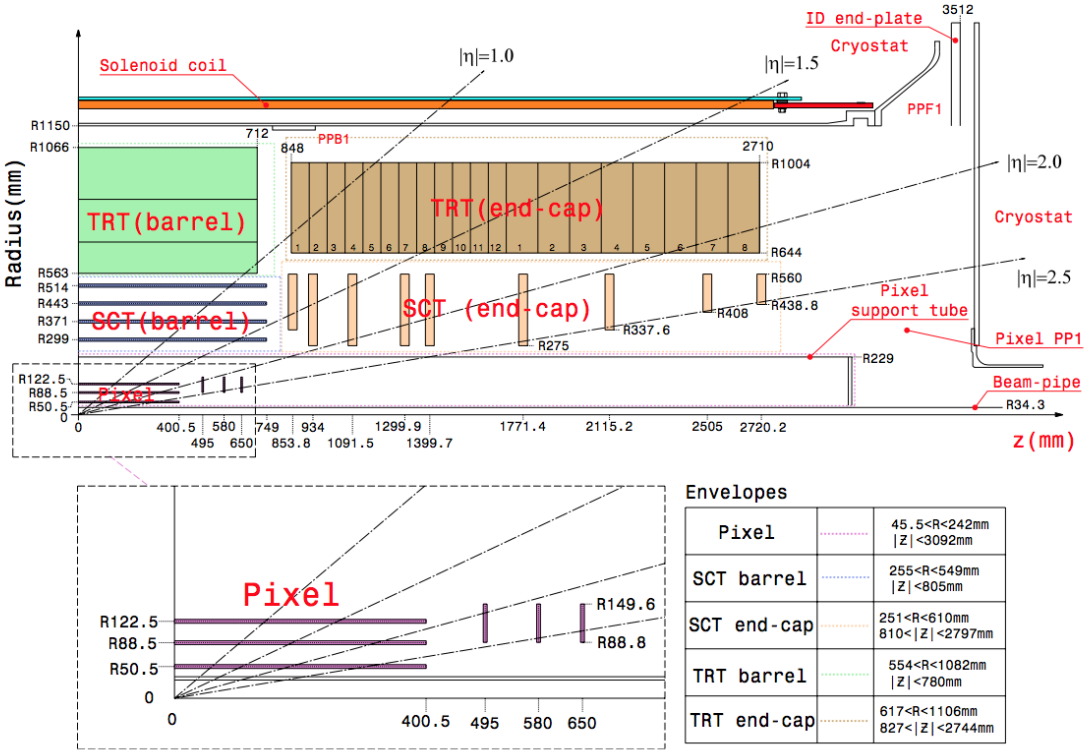

Fig. 3.7 Sketch of the inner detector [85].

the inner detector interact with the material in the detector. This leads to the deviation of charge particle trajectories through the process of multiple Coulomb scatterings and, in the case of electrons, highly fluctuating energy losses due to Bremsstrahlung. Figure 3.9 shows the amount of material expressed in number of radiation lengths[6] as a function of absolute value of pseudo-rapidity contributed by the sub-detectors and the various services[7] essential to operate the detector.

3.3 Tracking

The process of sampling a particle's trajectory that are bursting out from the collisions and determining its parameters such as momenta, direction, decay points is carried out by the tracking detectors. The trackers consist of several different sub-detectors in the innermost part of the detectors and they are the first set of apparatus being hit by the particles coming from the proton collisions. They are the most elaborate component of the detector and is comprised

[6] One radiation length X_o is defined as the mean distance over which a high-energy electron loses all but $\frac{1}{e}$ of its energy by Bremsstrahlung.

[7] Detector elements like cables, cooling pipes, support structures etc. are referred to as services.

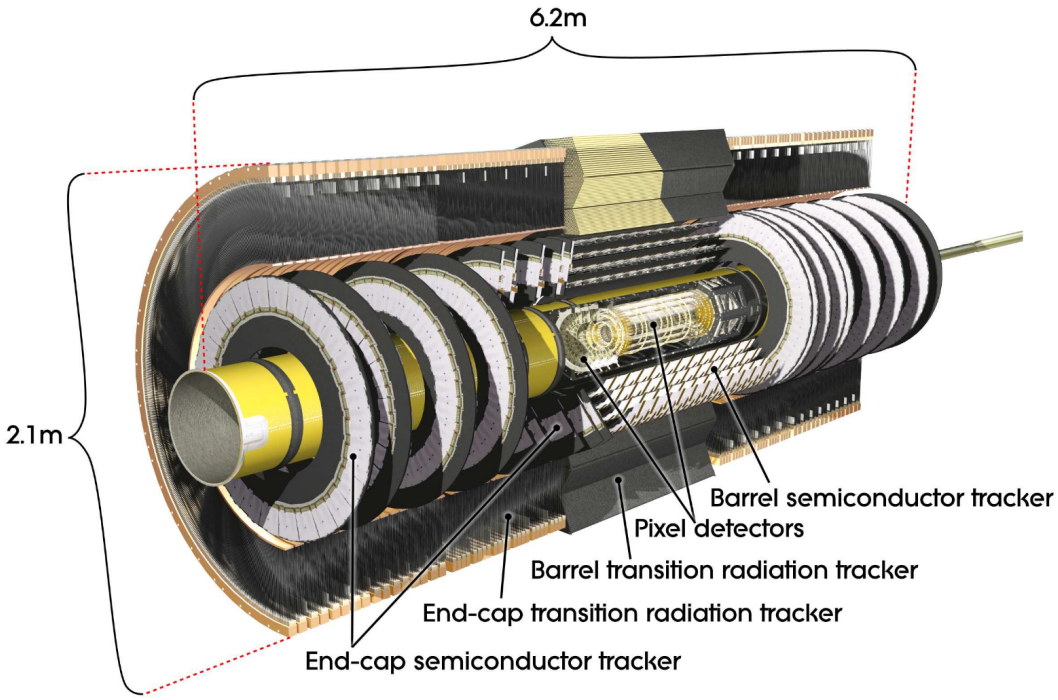

Fig. 3.8 The entire inner detector system [85].

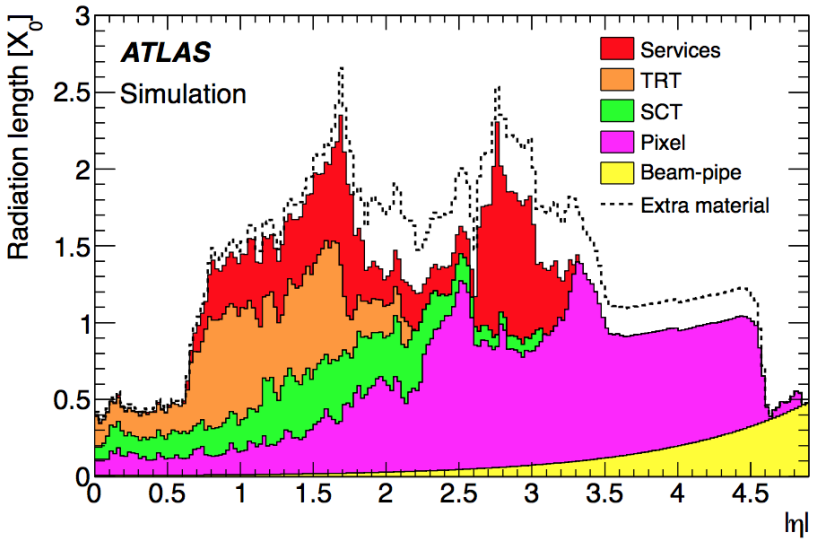

Fig. 3.9 Material in the inner detectors in term of radiation length X_0 as a function of η [89].

of a very large number of sensors and millions of electronic channels. Charged particles ionize matter along their path, which is the basic detecting principle of the tracking. The trackers are mostly made of thin layers of silicon that are connected to electronic channels. The motion of the charged particles through the silicon layer liberates electron-hole pairs which are detected by electronics as a current and they are then turned into digital signals. This gives the precise position at which the silicon is being hit by the particles. To reconstruct the trajectory (track) of the particle, the information from different layers is joined together. This detection is based on electromagnetic interactions and it is not sensitive to neutral particles like neutrons and photons which are invisible to trackers. The tracks only provide some preliminary information on the nature of the interacting particle but it is not sufficient to know about the exact identity of the particle. Most tracking devices do not make particle tracks directly visible, but only record tiny electrical signals that particles trigger as they pass through the device. A computer algorithm then reconstructs the tracks from the pattern of hits recorded in the detectors.

3.4 Calorimeters

The next layers are the calorimeters, electromagnetic and hadronic. Calorimeter is an "instrument that measures energy". Calorimeters have been designed to measure the energy a particle loses as it passes through. After the Inner Detector, the detectors with larger radius are, respectively, the Liquid Argon Calorimeter and the Tile Calorimeter [90]. The calorimeters stop entirely or “absorb” most of the particles coming from a collision, forcing them to deposit all of their energy within the detector. They typically consist of layers of “passive” or “absorbing” high-density material like lead – interleaved with layers of an “active” medium such as solid lead-glass or liquid argon. Schematic drawing of the ATLAS calorimeter system has been shown in Figure 3.10. In the middle, the barrel cryostat hosts two electromagnetic wheels, at each end the end-cap cryostats host two concentric electromagnetic wheels, two hadronic wheels and three forward calorimeter wheels. Electromagnetic calorimeters measure the energy of electrons and photons as they interact with nuclei and electrons in the calorimeter itself. Strongly interacting particles pass through the electromagnetic calorimeter, only to be stopped by the hadronic calorimeter. Hadronic calorimeters sample the energy of hadrons (particles containing quarks, such as protons and neutrons) as they interact with atomic nuclei. They can stop most known particles except muons and neutrinos.

3.4.1 Electromagnetic calorimeters

After interacting with the inner detector, the electromagnetic calorimeters are the next set of detectors traversed by the particles coming from the collisions. They stop electrons and

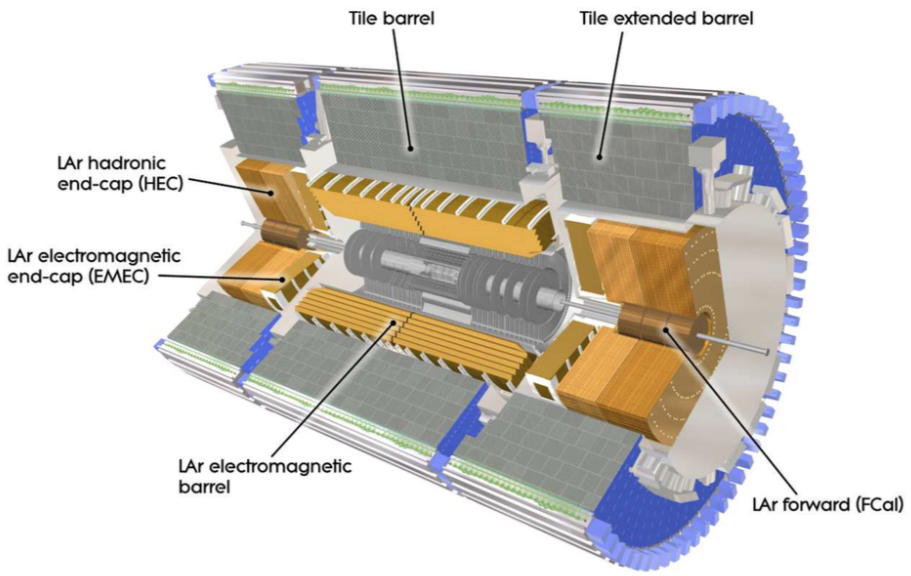

Fig. 3.10 View of the ATLAS calorimeter cross-section. The LAr and Tile parts are shown along with their segmentation in barrel and end-cap calorimeters [85].

photons by releasing their energy into the material. They promptly measure the energy contained by a photon or electron. Although both of these particles are stopped here, the electrons can be distinguished from the photons, the former leave a trace in the trackers, while the latter do not. Indeed, the electrons and the photons are completely identified. The ATLAS detector makes use of lead arranged in the shape of an accordion that is filled with Argon at temperature -186°C. Argon is a noble gas that is suitable as a detector medium because it does not react with other elements. Krypton is another gas which gives a better energy resolution and is suitable as a calorimeter but is much more expensive. The mechanism is that a high energy particle produced in the proton collision hits the metal layers and produces showers[8] of relatively low energy particles. These particles interact with the Argon and liberate electrons from their atoms. The total charge freed in this process provides information on the energy of the initial particle. The Liquid Argon Calorimeters [91] have been in use to measure the energy of electromagnetic showers in the barrel and end-cap regions and also for measurements of energy in hadronic showers in the end-caps. The liquid argon calorimeter has 175,000 data readout channels. The electromagnetic calorimeter [92] also contains a pre-sampler detector that is installed in front of the electromagnetic calorimeter, followed by three lengthwise layers of the EM calorimeter, named strip, middle

[8] A shower is defined as the cascade production of electrons, photons (electromagnetic shower) and hadrons (for hadron showers).

and back layers. Most of the higher energy electromagnetic showers have energy that is detected in the middle layer. The strip layers being small in cell size have good discrimination against multiple photon showers. The back layer only absorbs the energy of high energy electromagnetic showers. The electromagnetic calorimeter covers the pseudo-rapidity region $|\eta| < 3.2$, forward calorimeters cover a region with $3.1 < \eta < 4.9$ and the pre-sampler covers a region $|\eta| < 1.8$. Because of the special interest in electrons the resolution of the electromagnetic calorimeter is of vital importance. The design goal energy resolution for photons and electrons is [93]:

$$\frac{\sigma_E}{E} = \frac{0.1}{\sqrt{E}} \oplus 0.01 \oplus \frac{0.3}{E}. \tag{3.9}$$

3.4.2 Hadron calorimeter

Hadrons can easily penetrate through the electromagnetic calorimeter and reach the next stage of the detector, called the hadron calorimeter, where they come to a halt. The metal absorbers stop the hadron here and their energies are measured by tiles of plastic scintillators. These absorbers radiate light when they are exposed to charged particles. The intensity of light can measure the energy carried by these hadrons. The hadron calorimeter surrounds the electromagnetic calorimeter and works in conjunction with it in order to measure the energy and direction of jets and give hermetic coverage for making a good measurement of missing energy. The active elements of the hadron calorimeter are made up of plastic scintillator tiles with a wavelength-shifting fibre readout system. To make it into a sampling calorimeter, layers of tiles alternate with layers of copper. After $|\eta| = 3$, the forward calorimeter at 11.2 m from the interaction point brings $|\eta|$ to 5.2 using a Cherenkov-base, radiation technology. The Tile Calorimeter [90, 92] is a sampling hadronic calorimeter that surrounds the Liquid Argon Calorimeter in the barrel region. The hadrons produced in collisions travel tightly together in a cascade of particles, like the drops of water bursting in the jet from a hose. While analysing the data from the LHC, all hadrons streaming closely are combined into a single quantity called the jet. The jet is just a spray of hadrons flying like a dense flock of birds. A jet is treated as a signal for the production of quarks or gluons though it is not easy to distinguish between them. Research is in progress to retrieve this information from the jets. The hadron calorimeters are less accurate, which is also partly due to the nature of hadronic showers in the calorimeter. The design goal energy resolution for hadrons is:

$$\frac{\sigma_E}{E} = \frac{0.5}{\sqrt{E}} \oplus 0.03. \tag{3.10}$$

3.4.3 Forward calorimeter

Since the forward region experiences the highest particle fluxes in the ATLAS calorimeter system it was necessary to design a detector that has to be extremely radiation hard to cope with the situation and has been called the Forward Calorimeter (FCal). It is desired to be located as far from the interaction point (IP) as possible. The original ATLAS design [94] placed the FCal at about 15 m from the IP. But further study [95] showed there were many advantages to locating the FCal at roughly the same distance as the end-cap calorimeters. The distance of the ATLAS FCal from the IP is now about 5 m where the density of particles is approximately 9 times greater. It has been split into three components, the forward electromagnetic calorimeter (FCal1), which uses liquid argon as the active material and copper as the passive material, followed by two hadronic calorimeters (FCal2 and FCal3) which use tungsten as an absorber with argon filled between the rods.

Behind the FCal3 module at each end, a "plug" of passive brass (Plug3) is deployed to help shield the muon system. The three modules and plug at one end of ATLAS have been shown in their support tube in Figure 3.11. The FCal is a liquid argon, ionisation, sampling calorimeter [96]. Because liquid argon and the absorber metals are radiation hard it is anticipated that the FCal performance will be stable over the life of the detector. The liquid argon electrodes (the ionisation chambers) for the forward calorimeters have been designed with a different geometry from the other liquid argon calorimeters. The forward calorimeter performance requirements are driven by events with missing transverse energy and tagging jets. The FCal extends the coverage to the high pseudo-rapidity region $3.1 < \eta < 4.9$.

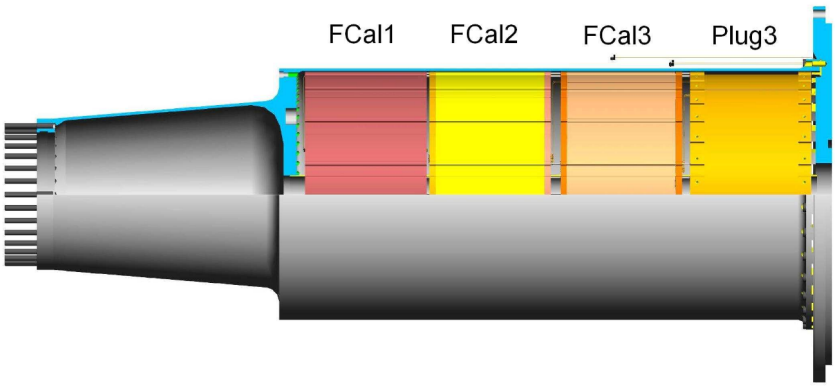

Fig. 3.11 Cut-away side-view of the FCal assembly in the cryostat support tube. From left to right are FCal1, FCal2, FCal3, and Plug3 [97].

3.5 Muon spectrometer

The fourth and final layer of the experiment is the muon detectors. Muons are the only charged particles which are not stopped by the inner detector components. Instead, they continue their path through the hadron calorimeter and reach the outermost part of ATLAS, known as the muon spectrometer. The ATLAS muon spectrometer (MS) [85, 86] is based on the magnetic bending of the muon tracks in large superconducting air-core toroid magnets. The MS has been shown in Figure 3.12.

It surrounds the calorimeters and precise determination of muons trajectories, their electric charge, their direction, and their momentum. The events reconstructed with muons are of interest for many analyses including the analysis presented in this thesis where the top pair decays into electron and muon. Also, the high transverse momentum muons can be a signature of new and interesting physics. The muon spectrometer is a tracking instrument embedded in a toroidal magnetic field generated by a system of air-core toroid coils; it measures the charge to momentum ratio of the muons escaping the calorimeters. The ATLAS detector uses several different techniques in order to be able to analyse muons. The detection elements (the muon chambers) consist of small tubes equipped with a central wire and filled with gas. When muons pass through them, they leave a trail of electrically charged particles that either drift towards a central filament or the side of the tube. The position of a muon can be determined with good accuracy from the time taken by the drifting charge. The muon chambers enable the measurement of the trajectories down to hundredths of a millimetre. The muon spectrometer has been optimized to provide a momentum measurement with a relative resolution designed to be better than 3% over a wide range of transverse momentum (from 3 GeV up to 1 TeV) and 10% at p_T= 1 TeV. The strong magnetic fields are needed to bend the trajectories of the charged particles. The way particles are bending make it possible to extract useful information. For instance, if the positively charged particle bends one way, the negatively charged particle bends other way. It helps to construct the opposite sign leptons which is the requirement of this analysis and will be discussed in Chapter 5. Also, faster particles show less bending than the slower ones which makes the momentum measurement from the curvature of their trajectories possible. The stronger the magnetic field, the more accurate the measurement of the momentum. The toroidal magnetic field has been achieved by eight coils assembled around the beam pipe outside the main barrel components. The central barrel toroid covers $0 < |\eta| < 1.4$, while the two end-cap toroids can cover $1.6 < |\eta| < 2.7$. The non-toroid region ($1.4 < |\eta| < 1.6$) provides much less bending power and so it causes the momentum resolution degradation in this region. Monitored Drift Tube chambers (MDTs) and Cathode-Strip Chambers (CSCs) are used for the tracking and determination of momentum while Resistive Plate Chambers (RPCs) and Thin Gap

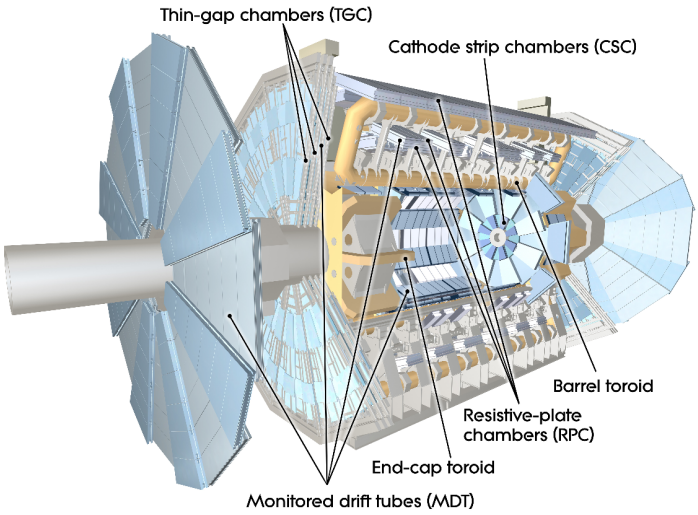

Fig. 3.12 View and illustration of Muon Spectrometer with its components [98].

Chambers (TGCs) are used for bunch-crossing identification and triggering. A study of the 2012 collision data at the $Z \to \mu\mu$ mass peak shows that the muon momentum resolution modelled in the ATLAS detector simulation is in good agreement with the data [99].

3.6 The ATLAS trigger system

At the LHC, bunches of protons collide about 40 million times per second. So processing and selecting events within the 25 ns time between successive bunches is not possible. On average about 20 to 40 collide during each bunch-crossing; the rate of individual proton-proton collisions at the LHC is very high (about one billion collisions every second). The total amount of data produced at the LHC would be about a million gigabytes per second. The amount of data would be enough to saturate all the hard disks on Earth in one day. The data produced by the LHC over many years is tremendously large. Not all the produced collisions are of interest. Occasionally, quarks and gluons have direct head-on collisions; these collisions are referred to as "hard-scattering", or hard events for short. The vast majority of interactions are through low energy QCD processes and are of limited experimental interest (soft events). Also, the time required to analyse this data is extremely large. Physicists have to collect a large number of hard events for physics analyses. In order to be able to select the events that have the right characteristics (interesting events), a trigger system has been developed. The ATLAS Trigger System [101] has been developed in a very modular and flexible way, so that events that are most relevant to a set of studies are accepted, while most background events can be rejected. The trigger system has been implemented in three

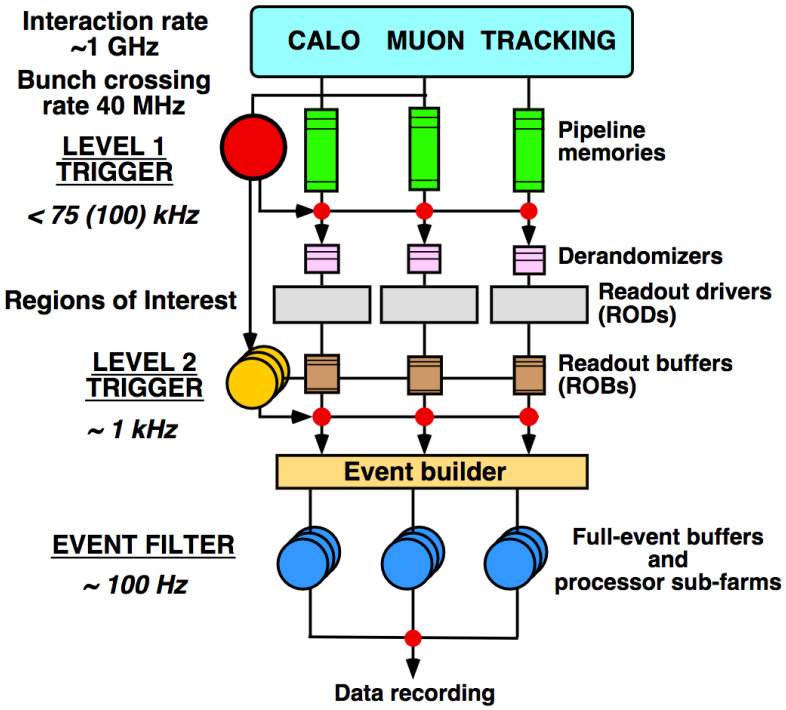

Fig. 3.13 A schematic view of the ATLAS three level trigger system [100].

layers which progressively refine the decision to accept or reject events for storage: the Level 1 (L1), Level 2 (L2) and the Event Filter (EF). Each stage of triggering refines the selections previously made and, where needed, additional selection criteria are applied. The first level trigger makes a selection decision in less than 2.5 µs, reducing the data flow to about 75 kHz. The first layer is hardware-based while the other two are software-based. The hardware-based first level of trigger uses a subset of the detectors to perform an initial search for high-transverse momentum electrons, muons, taus, photons and jets, as well as large missing and total transverse energy. The first level trigger calculations themselves need to be efficient to identify physics objects and signatures. A schematic view of the ATLAS Trigger is shown in Figure 3.13, with the expected event rate at each level. The first level of triggering, as far as the calorimetry system is concerned, only has access to $\Delta\eta \times \Delta\phi$ regions of 0.1×0.1, which are referred to as trigger towers. The two higher levels of the trigger further reduce the data flow to 200 Hz.

3.7 LUCID

Luminosity can be measured by several detectors in ATLAS, but LUCID (LUminosity measurement using Cerenkov Integrating Detector) is the only detector which is primarily

dedicated to online luminosity monitoring. It consists of two stations that are located at a distance of $\pm$ 17 m [102] from the interaction point, as shown in Figure 3.14, near the TAS (Target Absorber Secondaries) collimator. Each station consists of 20 aluminium tubes that are placed along the beam line. The tubes are 1.5 m long and have a diameter of 15 mm.

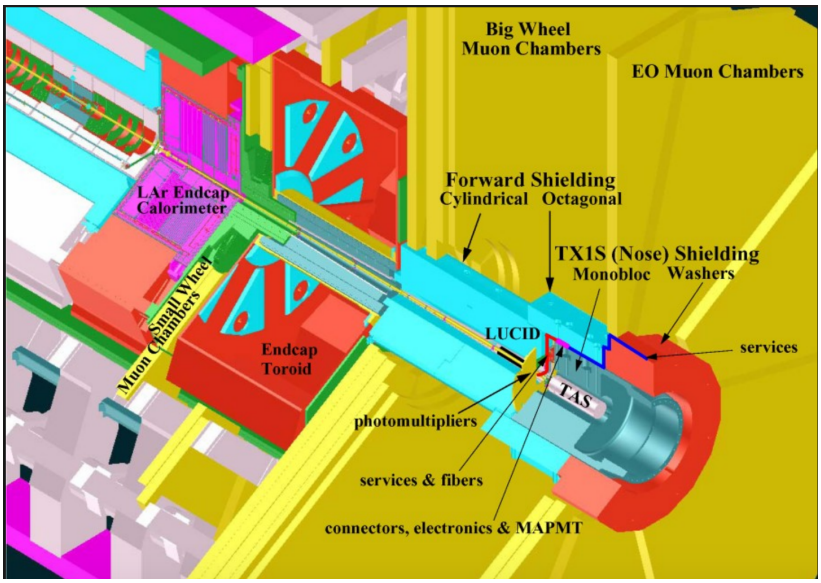

Fig. 3.14 LUCID location scheme inside ATLAS [102].

They are filled with a low refractive index gas (C_4F_{10}). Charged particles entering a tube with a momentum larger than the Cherenkov threshold in the gas, emit light at an angle of about 3° with respect to their flight direction, resulting in an average number of 2.8 of reflections of the produced photons on the tube walls [103]. The produced photons get reflected from the inner tube walls until they reach the end of the vessel, where they are registered by a photomultiplier (PMT). A hit is registered by the tube if the PMT signal is above a certain threshold. The customised LUMAT card applies prompt online luminosity algorithms for each bunch to the readout system where the signals of all tubes are sent.

The contribution of two types of particles; primary and secondary, gives the signal from a pp collision. Primary particles are produced from a prompt decay of a primary particle or at the IP directly in the pp collisions. They follow a straight path until they reach the LUCID detector. Primary particles interact with any other material (beam pipe, detector, machine elements, etc.) to produce secondary particles. They travel along scattered trajectories before reaching LUCID. A primary particle is expected to release a greater amount of Cherenkov light than a secondary particle since light is emitted continuously over the tube length.

The benefits of the LUCID design are that the detector is made of light material, which is naturally radiation hard, and the detector response is fast, within a few nanoseconds from the

moment a particle passes the detector. The band-width of the electronics allow to keep the FWHM of the PMT signals at a level of 10 ns. These characteristics ensure the capability to differentiate collisions coming from different bunch-crossings (separated by 25 ns) and make LUCID appropriate for the online monitoring of the LHC bunch structure.

Chapter 4

Non-collision background studies for the ATLAS SCT

4.1 Introduction

This chapter is about my authorship task on non-collision background or beam-induced background (BIB) studies in the Semi Conductor Tracker (SCT) of ATLAS. The term non-collision background refers to the signals in the detector, which have not been produced in the normal collisions of the Large Hadron Collider. Particles are lost from the beam by various processes such as beam-gas scattering, which takes place all around the accelerator, and becomes a source of background in the detector. Most of these backgrounds have been reduced by shielding but the background very close to the beam-pipe increases the detector occupancy and can introduce spurious clusters that can affect track reconstruction. The occupancy in extreme cases can increase the dead time which in turn can decrease the data-taking efficiency. Also, highly energetic muons are not affected by the shielding and can cause large energy deposits in the calorimeters where this energy can be identified as a jet. These fake jets are removed from the physics analyses. An algorithm has been developed based on the asymmetry of early clusters to study and identify the events containing beam-induced background hits from unpaired isolated bunch-crossing identification (BCID). The first section disscusses BCIDs.

4.2 Using BCIDs to identify beam backgrounds

This section will present an overview of the LHC filling scheme. The LHC has a Radio Frequency (RF) of 400.79 MHz and the protons have a revolution frequency of 11.245 kHz. This constitutes a chain of 35460 RF-buckets which could potentially contain a bunch in every tenth RF-bucket. Bunches are spaced by 25 ns in the standard filling scheme. This

creates 3564 potential "slots", each of which is labeled by an integer BCID. The injections from the Super Proton Synchrotron (SPS) have a bunch train structure, i.e. a certain number of equally spaced bunches. Between the trains, short gaps for the injection kicker magnets are left. In addition, a 3 μs abort gap is kept free, in order to allow for a safe abort of the LHC beam. The first BCID after the abort gap is numbered as 1 by definition. In practice, the LHC is flexible to run with several different filling schemes designed for various purposes.

In addition to the nominal 25 ns spacing, the bunch-splitting in the Proton Synchrotron (PS) allows different bunch spacings: 50 ns, 75 ns and 150 ns. For several reasons, in 2011, the LHC was running with a 50 ns bunch spacing for protons, allowing 1782 potential slots and 1380 nominal bunches that can be filled. The BCIDs are organised in bunch groups by the Central Trigger Processor (CTP) [104] which has been designed to give the Level 1 trigger decision. In general, not all bunches are paired, i.e. colliding. BCIDs can be divided into different bunch groups according to their characteristics:
Filled: These are colliding BCIDS (each LHC fill contains bunches colliding in ATLAS/CMS). Both beams have a BCID with the same identifier filled with a proton bunch.
Empty: Any BCID without a bunch in either beam.
Unpaired: Only one beam has the corresponding BCID filled with a bunch.
Unpaired isolated: No bunch in the other beam within 75 ns or within three BCIDs.
Unpaired non-isolated: A bunch in only one LHC beam with a nearby (within 3 BCIDs) bunch in the other beam.

Unpaired isolated and unpaired non-isolated BCIDs are of particular importance to study beam backgrounds. More bunch groups are defined in the CTP, but they are not relevant for this study. This discussion of BCIDs will be widely used in the rest of this chapter.

4.3 Previous studies of beam background levels

The methodical study of the machine induced background in the LHC was estimated in 2001 [105]. The effect of the machine induced background was studied for the low luminosity insertion of the LHC and estimations for the secondary particle fluxes (induced by protons losses) were presented for several running conditions of the colliders. The beam-induced flux is proportional to the beam current. The protons lost from the beam interact with the residual gas nuclei, giving rise to multiple productions of secondary particles. These interactions have been divided into two groups: inelastic and elastic. The momenta of the secondaries from inelastic interactions is smaller than the momenta from the beam particles so they cannot traverse through the machine and are stopped close to the point of interaction due to the curvature of the machine. The elastic collisions of the lost beam particles with the residual gas produce protons with a momenta much closer to the initial one. These quasi-

beam-particles can travel a long distance and interact with different parts of the machine [106]. The level of non-collision background and their properties were also studied during

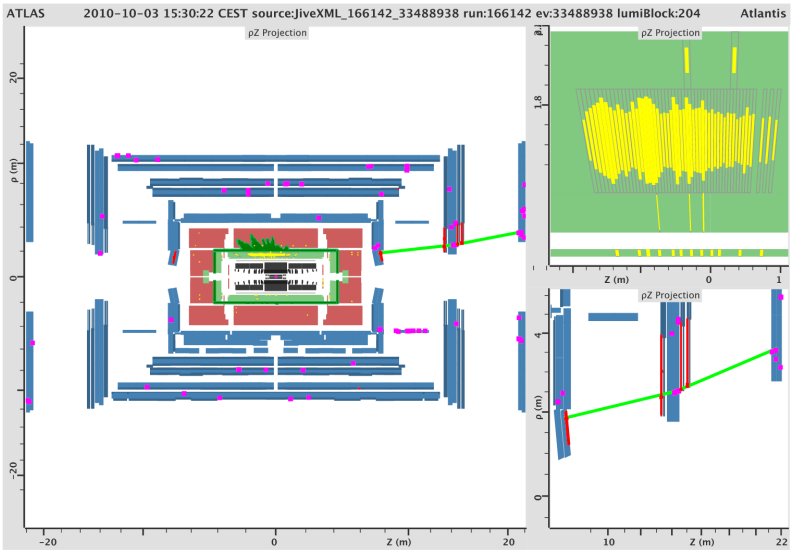

Fig. 4.1 Event display of a typical beam-induced background event, where a muon travelling almost parallel to the beam axis leaves a huge energy deposit in the LAr calorimeter [107].

the 2010 proton-proton run at a centre-of-mass energy of 7 TeV [107]. This study was to identify, estimate and reject the non-collision backgrounds in the physics analyses. The main focus of this study was beam-induced backgrounds and cosmic ray showers. During the 2010 proton-proton run, the BIBs in ATLAS were monitored online via selected Level 1 trigger. The beam backgrounds were studied using the observable $\Delta t = \frac{\Delta z}{c}$.

The time measurements were obtained by using the Beam Condition Monitor (BCM). Studies indicate that the BCM is sensitive to beam-loss events taking place rather close to the ATLAS detector, while large energy deposits in the Liquid Argon calorimeter are likely to be caused from events that happen far from the Interaction Point (IP), allowing enough distance for muons to reach the radial coverage of the calorimeters. Since the BCM is situated very close to the beam line, it is not reasonable to assume that it would be sensitive to the same BIB event which can cause a large energy deposit in the calorimeter. The BCM modules use very small diamond sensors so their efficiency is not large enough to trigger on halo events. A single muon produced in beam-gas interactions can traverse through the entire ATLAS detector and deposit a large amount of energy at the calorimeter. The BCM is discussed briefly in Section 4.3. These muons can be identified by combining the information from calorimeters and the muon spectrometer. These energetic muons can be produced

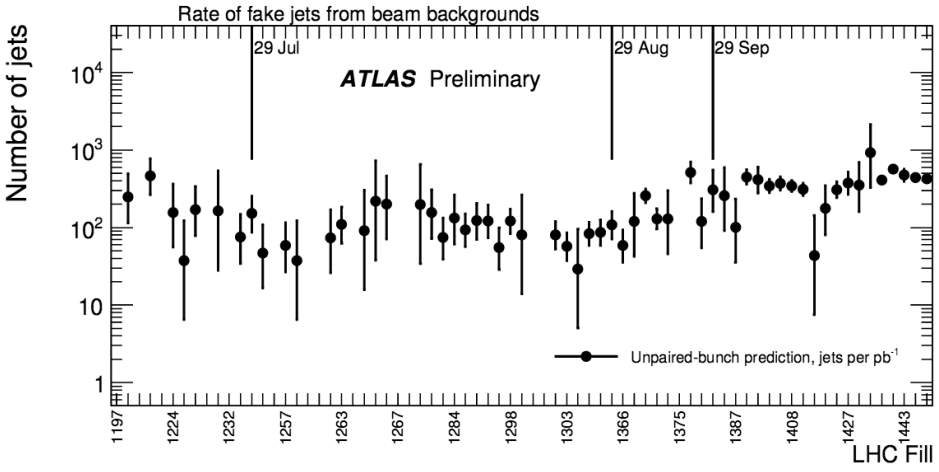

Fig. 4.2 The estimated number of jets due to beam-induced backgrounds. The rate is estimated from a control sample of events in the unpaired BCIDs and scaled according to the number of bunches and integrated luminosity [107].

with an energy of the order of the LHC beam energy and can deposit substantial energy via bremsstrahlung in the electromagnetic and hadronic calorimeters.

The 2010 data taken with unpaired bunch groups was analysed to flag the events containing these background muons by developing three methods. These methods were based on matching high energy calorimeter clusters with the muon spectrometer hits for muons with a path parallel to the beam-pipe. The clusters in the calorimeter end-caps with a radius less than 1 m have not been taken into account since this region does not overlap with the muon detectors. To reject these muons faking jets, calorimeter based cuts, labelled as "loose" and "tight" were defined in 2010 to reject the jets produced due to these non-collision backgrounds. The analyses that need to reconstruct events with large missing transverse energy, like exotic and supersymmetric particles, make use of this tight selection to reduce these backgrounds. The fraction of selected events originating from cosmic-ray muons crossing the ATLAS calorimeter was estimated using a sample triggered by a jet in the empty BCIDs and it has been found to be about 10%. Figure 4.1 depicts the beam-induced events containing a muon in unpaired Bunch Crossing Identifier (BCID) hits. The muon goes parallel to the beam pipe and eventually deposits a huge amount of energy in the Liquid Argon calorimeter. The fake jet rate due to non-collision background was also estimated in the paired BCIDs data during 2010 data-taking periods as shown in Figure 4.2. The estimated fake jet rate shows large fluctuations from one data period to another. The number of jets estimated due

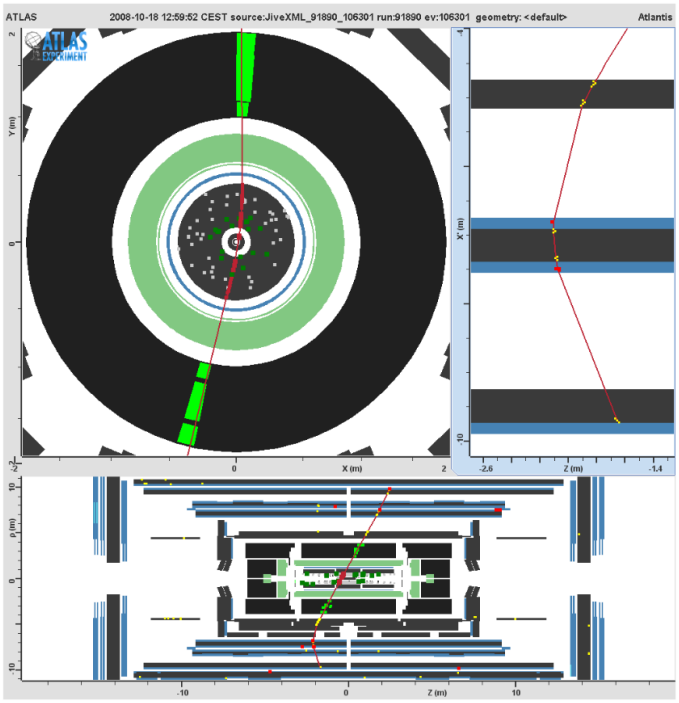

Fig. 4.3 Event display of a cosmic-ray muon coming from above and crossing the entire ATLAS detector, close to the nominal IP, leaving hits in all tracking subsystems and substantial energy deposits in the calorimeter [108].

to beam-induced backgrounds was about 13000 for the entire 2010 dataset, corresponding to an integrated luminosity of 36 pb^{-1}.

The other source of non-collision background is cosmic ray muon backgrounds [108] which can penetrate the cavern and deposit energy in all detector subsystems. The cosmic ray events have been important since the start of the installation phase in 2005. Their analyses have played an important role for the detector performance before the arrival of LHC beams. An analysis has been made to tag them during dedicated data-taking periods to reject the cosmic ray background in physics analyses. The cosmic ray muons passing through the entire ATLAS detector have been reconstructed in the muon spectrometer as two independent back-to-back tracks. One track is reconstructed in the top portion of the Muon Spectrometer and the other in the bottom sector. Event display of a cosmic-ray muon passing the entire ATLAS detector and leaving hits in all tracking subsystems is shown in Figure 4.3, it deposits considerable amount of energy in the calorimeter. The reconstruction of cosmic muons has been divided into two distinct cases:

•**"single–leg" track:** the cosmic-ray muon track is reconstructed in either hemisphere.

•**"double–leg" track:** the cosmic-ray track is reconstructed in upper and lower hemispheres.

The beam-induced and cosmic backgrounds were studied during 2010 with their additional jet-like signatures.

4.4 Beam Condition Monitor

In 2011, the LHC was operated at the energy of 3.5 TeV for both beams. The Radio-Frequency (RF) cavities are metallic chambers that have an electromagnetic field which can accelerate the beam particles. These cavities are structured like beads on a string, where the beads are cavities and the string is the beam line. On the LHC, each RF cavity is tuned to oscillate at 400 MHz. This corresponds to a "bucket" every 2.5 ns. The bucket is just a virtual position on the LHC circumference that can hold a bunch of protons or can be empty. The nominal bunch spacing during the proton-proton run in 2011 was 50 ns. Another ATLAS sub-detector extensively used to monitor beam-related losses is the Beam Conditions Monitor (BCM) [109]. Its basic function is to monitor the beam-conditions that can damage

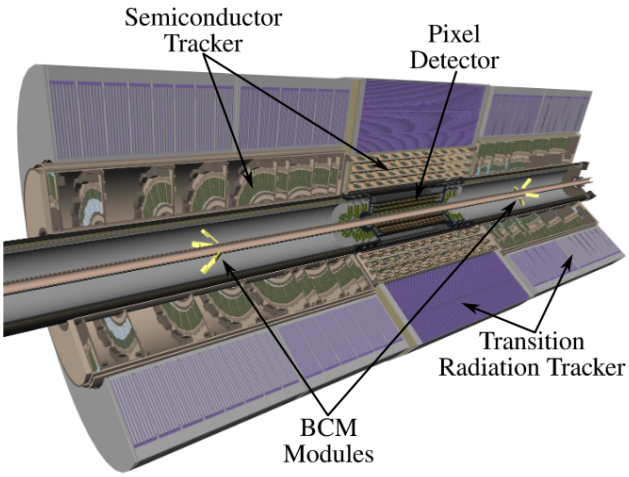

Fig. 4.4 The BCM detector modules inside the ATLAS Inner Detector positioned at $z = 1.84$ metre [109].

the detector. It has been in use to measure the bunch-by-bunch luminosity and beam-induced background levels. In order to be able to distinguish between normal and abnormal collisions, two BCM detectors are positioned symmetrically on both sides of the interaction point at $z = \pm 184$ cm as shown in Figure 4.4, corresponding to a time delay of $\frac{z}{c} = 6.13$ ns. Each side has four BCM modules at ϕ = 0°, 90°, 180°, 270°. They are inclined at an angle of 45° with respect to the beam pipe. Each module has two diamond sensors of $1 \times 1\text{cm}^2$ surface area

and 500 μm thickness. The 1 ns signal rise time allows discrimination of particle hits due to collisions (in-time) from background (out-of-time). Background rates for the two circulating beams can be measured separately, and are used to assess the conditions before ramping up the high voltage on the SCT modules. Normal collisions occur every 50 ns and hit the BCM

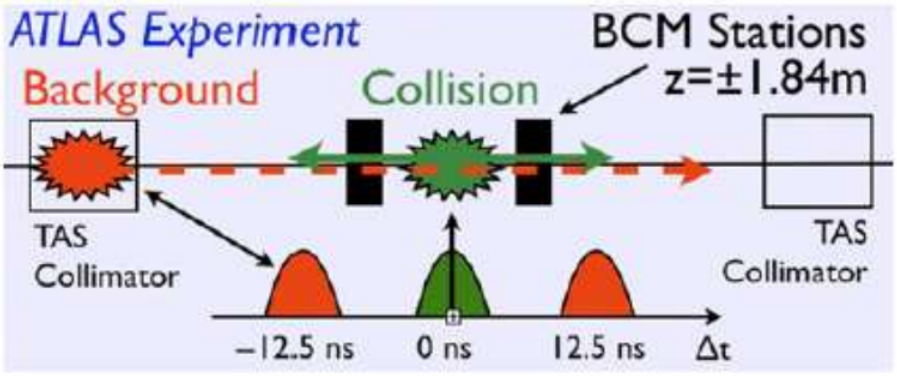

Fig. 4.5 Schematics of out-of-time hits shown in red (beam protons hitting the Target Absorber Secondaries (TAS) collimator) and in-time-hits shown in green [110].

detectors simultaneously (see Figure 4.5) whereas the events occurring upstream ($z > 1.84$ m), hit the closest BCM detector at $\Delta t = \frac{2z}{c}$ before the other. The nominal separation between the BCMs is $\Delta t = 12.5$ ns. The detector closes to the collision point receives a signal 6.25 ns before the normal proton-proton collision at the interaction point. In normal collision events, both BCM detectors will receive signals at the same time, after 6.25 ns [111]. The former case is referred to as "out-of-time" hits, whereas the latter will be "in-time" hits.

A description of BCM background-like and collision-like trigger rates for a BCID range with a bunch pattern of 13177 colliding bunches is shown in Figure 4.6. Many ATLAS runs which have the same bunch-pattern have been averaged to produce this plot. The first train of a batch is shown with part of the second train in this plot. The rates of stable beam collisions for the first $\sim$ 15 minutes are shown in the histograms, while the trigger rates of both beams before they collide are shown in the symbols. Since the rates are not normalised by the intensity, and longer periods would have influenced the histograms due to the intensity decay, the restriction applied at the start of the collisions is essential. The unpaired bunches can be seen between BCID 1700 and 1780 in front of the beam 2 trains, while they are visible at around BCID 1770 after the beam 1 train. The collision rate in paired BCIDs is seen to increase when the beams collide. The background rate also rises by around an order of magnitude. This rise is caused by accidental background-like happenings from afterglow[1].

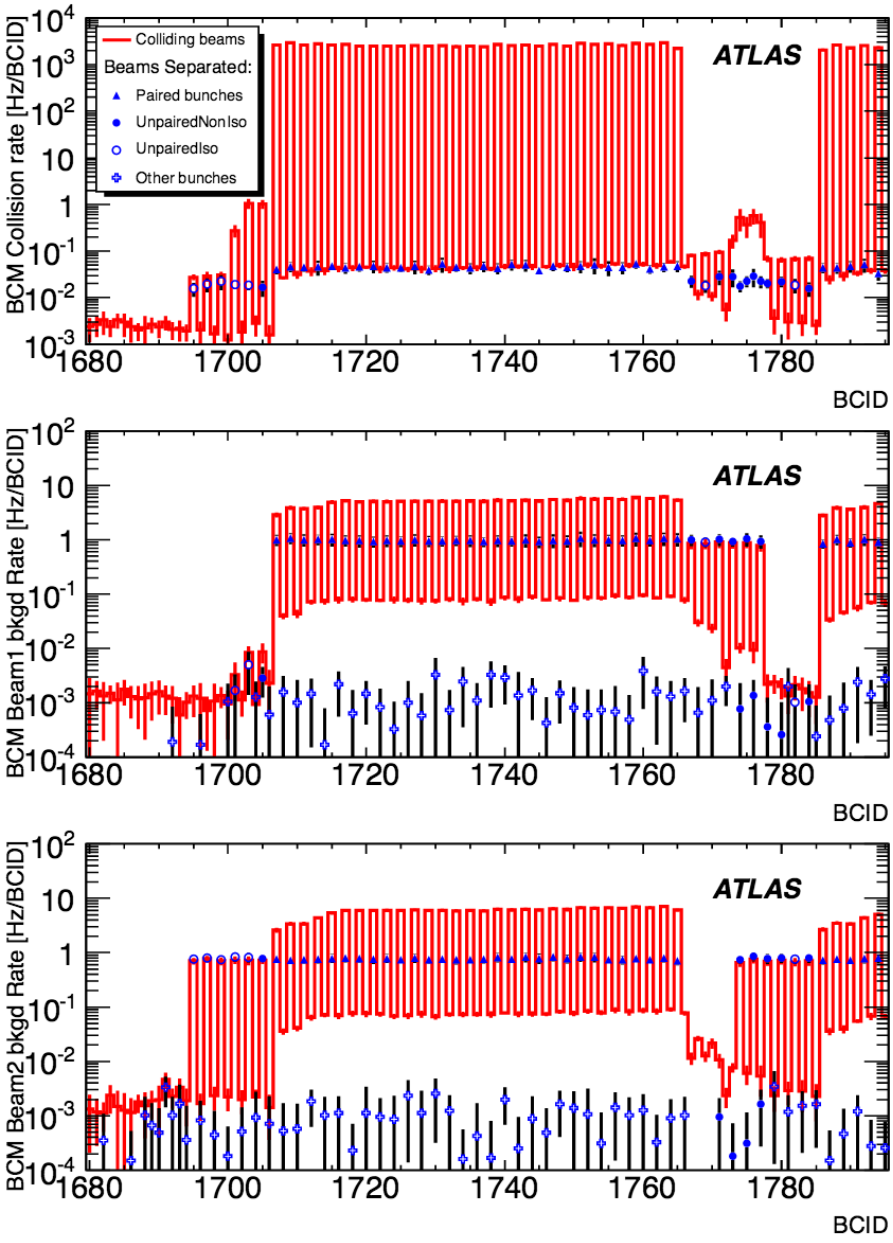

Fig. 4.6 BCM collision rate (top) and background rates for beam 1 (middle) and beam 2 (bottom) per BCID before and during collisions [112].

The topmost plot in Figure 4.6, which shows the collision rate, displays two interesting

[1]Collision debris activates the silicon detectors and decays via photon emission to leave spotlike clusters in the innermost layer of the ATLAS detector. A significant background is created by this collision "afterglow". The afterglow level is seen to be proportional to the luminosity in the colliding-bunch slots for a given bunch pattern.

features:

- In BCIDs 1701, 1703 and 1705, collision activity can be evidently seen in front of the train. This relates to the relatively small increase seen in the background for beam 1 (middle plot) for the same BCIDs. This slight increase in the background seen before and during collisions is an indication of ghost charge. Genuine collisions occur since beam 2 contains nominal unpaired bunches in the matching BCIDs. A similar rise is not seen in front of the second train of the batch (seen on the very right of the plots).
- Another interesting feature is seen around BCID 1775, where a small peak is seen in the collision rate. This peak correlates with a BCID range where beam 1 bunches are in odd BCIDs and beam 2 in even BCIDs. Thus, the bunches are interleaved with only 25 ns spacing. Therefore this peak is almost certainly due to ghost charge in the neighbouring BCID, colliding with the nominal bunch in the other beam.

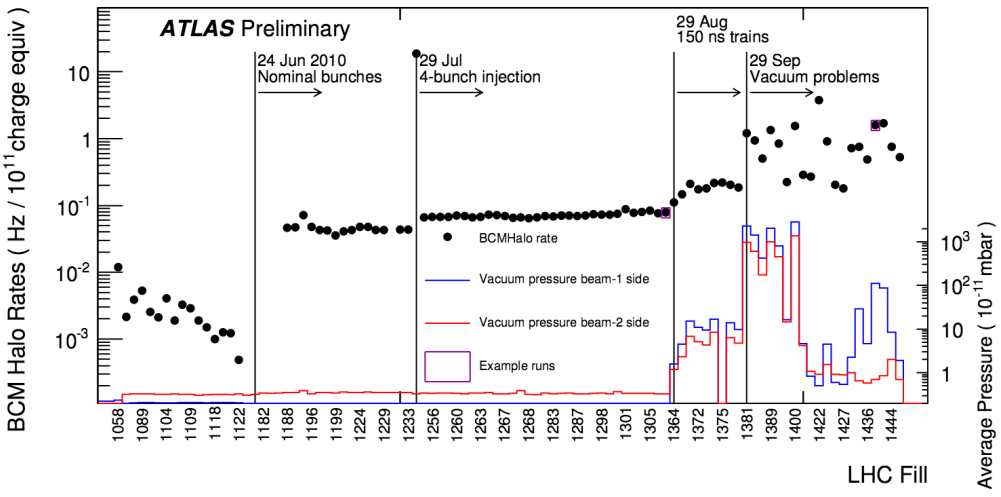

Fig. 4.7 BCM specific beam-induced background trigger rate (normalised to 10^{11} protons), for the whole 2010 proton-proton run. The first jump in background is seen at the end of June (the LHC moves from low to nominal bunches (10^{11} protons/bunch). Another small variation for multi-bunch and finally a significant change when the LHC operates at 150 ns bunch-trains. These cause the deposit of electron clouds that badly affect the vacuum [107].

The BCM specific beam-induced background over the entire 2010 proton running period with the P22 average residual pressure (the pressure at 22 m from the IP) is shown in Figure 4.7. A significant change of background characteristics appears when the LHC moved to 150 ns bunch-trains as shown in the right end of Figure 4.7.

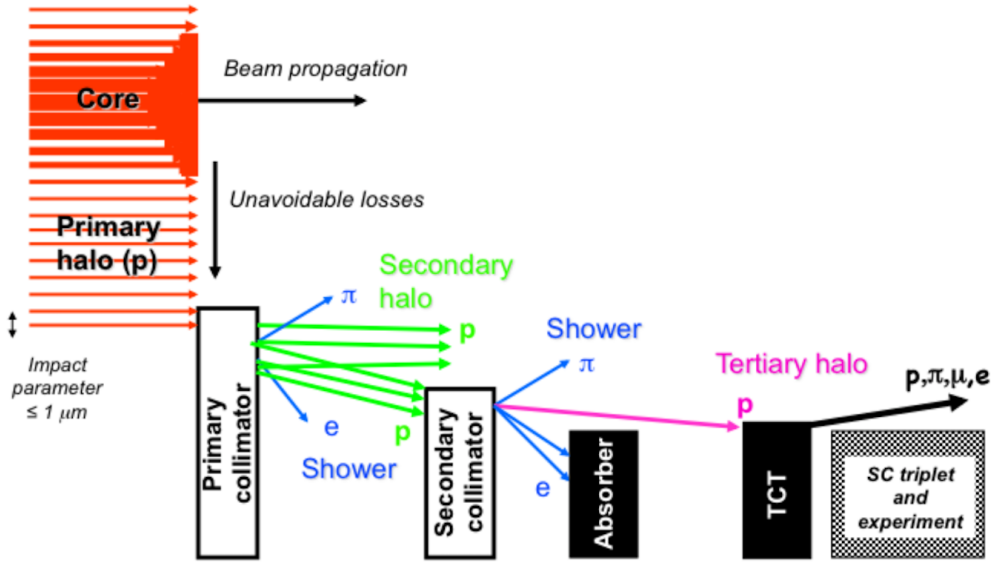

Fig. 4.8 Schematic sketch of the LHC cleaning system showing primary and secondary collimators and absorbers in the cleaning insertions which remove most of the halo. It shows tertiary halo that can escape and intercept close to the experimental physics experiments by the tertiary collimators (TCT) [113].

4.5 Aim of the analysis

The aim of the analysis is to develop an algorithm to find the number of hits on the silicon which is not associated with tracks. These hits are not a part of the reconstructed tracks and are generally divided into the following four categories:

1. Noise hits:
    - Also present without beam circulating.
2. Hits from cosmic rays [114]:
    - Typically included in noise hit;
    - Hit pattern not pointing to the beamline; and
    - The electron showers fall into a category of noise. They are also present when there is no beam.
3. Hits from collisions:
    - Hits from low momentum particles, which are not part of reconstructed tracks.

4. Beam-Induced Backgrounds (BIB):

    - Beam-induced backgrounds appear in ATLAS due to proton losses upstream of the interaction point.

The beam-induced backgrounds are classified as:

- Tertiary halos, which are protons lost on limiting apertures near the experiment (typically the tertiary collimator located at $z = 150$ m from the interaction point) are shown in Figure 4.8.

- Inelastic beam-gas, which are inelastic interactions of protons with the residual gas inside the beam-pipe or also due to beam-gas interactions.

- Elastic beam-gas scattering, which can result in small angular deflections of the protons.

The rate of beam-induced backgrounds is proportional to the beam current and depends on the operational conditions of the LHC (machine optics, collimator settings, residual gas densities and filling scheme). The main concern of this analysis is to focus on beam-induced backgrounds using early hits in both the end-caps. Furthermore, the early hits on the outermost disks are flagged to identify the events contaminated with the beam-induced backgrounds.

4.5.1 Distinct features of non-collision backgrounds

The distinct features of non-collision backgrounds are:

- To be almost parallel to the beam pipe and perpendicular to the end-cap disks.

- For non-collision backgrounds one side of the SCT sees the early hits while the other side sees hits "in-time" with the collision hits.

- The particle trajectories are not pointing to the interaction point and, therefore, are not part of the reconstructed tracks.

4.5.2 Read-out system and timing

The SCT readout system was designed to operate with 0.2 - 0.5% occupancy in the 6.3 million sampled strips, for the original expectations for the LHC luminosity of 1×10^{34} $\mathrm{cm}^{-2}\mathrm{s}^{-1}$ and pile-up of up to 23 interactions per bunch crossing. The strips are read out by radiation-hard front-end ABCD chips [115] mounted on copper-polyimide flexible circuits termed the readout hybrids. Each of the 128 channels of the ABCD has a preamplifier and

shaper stage; the output has a shaping time of ∼20 ns and is then discriminated to provide a binary output.

In order to facilitate the read-out of these channels as efficiently as possible with a bunch crossing frequency of 40 MHz, three different read-out architectures were investigated by the ATLAS collaboration; analogue, digital and binary. In the binary read-out system, the strips transmit only hits or no hits information. Any strip that collects an amount of charge greater than an externally set threshold fires the strip discriminator. Hence, direct information about pulse height is not recorded. The SCT read-out system consists of front-end electronics, links, cables, power supplies, detector control systems and monitoring [116]. The front-end electronics are mounted onto hybrid assemblies that are a part of the actual detector modules. These components perform the initial signal processing before the data are transmitted off detector by optical data links. Other optical links distribute clock and control signals to the detector. The cable system provides all power and DC control signals to detector modules from power supplies located off detector. A binary scheme has been adopted as the ATLAS read-out architecture. The binary system was also deemed to be the most cost effective read-out scheme. The SCT read-out system reads three time bins with the central bin synchronised

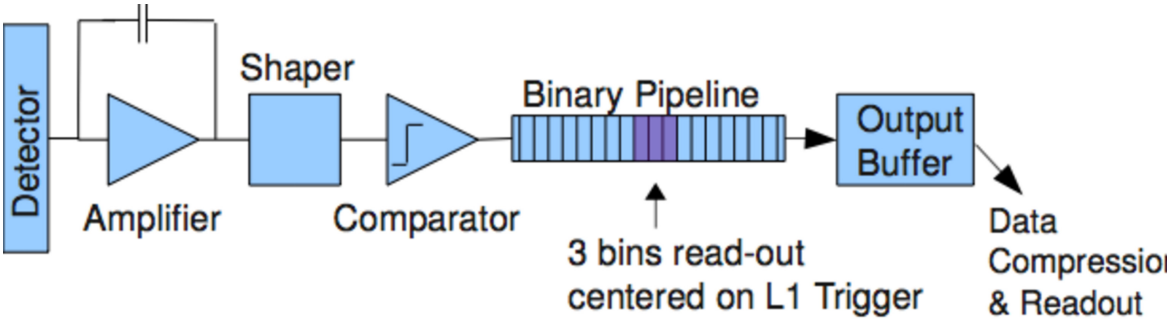

Fig. 4.9 SCT binary read-out circuits with important components.

with the Level 1 trigger. A brief review of the time bin in the SCT is discussed in this section. One time bin = 25 ns (40 MHz LHC clock). Three 25 ns time bins are read out around the Level 1 trigger. The threshold for a hit or signal is 1 fC. If the hit is above threshold, it is shown by 1 and if the hit is below the threshold, it is shown by 0. Say, for example, if 110 is taken as the three time bin readout of the SCT then the first bit means a hit above threshold at Level 1-25 (25 ns before triggering) and 1 in the middle means a hit above threshold at Level 1. The last bit means no hit above threshold at Level 1+25 (25 ns after triggering). The pulse shape is determined by the output of the electronics, i.e. the amplifier and shaper. The pulse shape for one of the bin patterns is shown in Figure 4.10.

Setting the binary threshold to its optimal value is the challenge of the binary read-out. The binary threshold minimizes the noise and maximizes the efficiency for each channel. In

order for an optimal threshold to be set, the noise generation and signal deposition has to be well understood and the charge-injecting mechanism should be accurate. The specific number chosen to maximise the efficiency is 1 fC[2], which corresponds to the noise occupancy ($< 5 \times 10^{-4}$). The binary read-out of the SCT with important components is shown in Figure 4.9. The discriminator compares the level of the signal with what is the equivalent signal level from a 1 fC charge deposition. There are two modes of latching this signal to the clock: "edge-detect" mode and "level" mode. Both of these modes discriminate the signal at 1 fC. Initially they produce binary pulses that have a duration a few ns more than the time over threshold and do not latch to the clock cycle. The level mode samples at the rising edge of the clock, giving rise to a signal latched to the clock with the same number of clock-cycles as the length of the initial signal. On the other hand, the edge-detect mode is designed to detect a high to low transition in the data, producing a signal of duration of 1 clock-cycle irregardless of the length of the incoming signal. A threshold of 1 fC was established to be the optimal

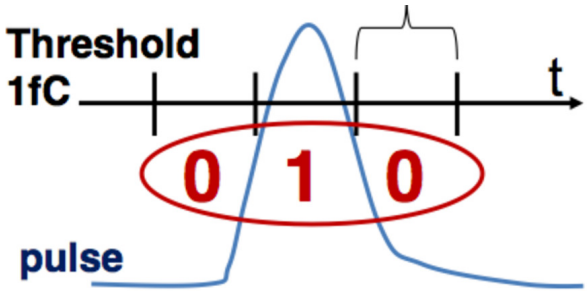

Fig. 4.10 The SCT bin pattern.

working point for the SCT. The most likely value deposited by a minimizing ionizing particle (MPI) is 3.6 fC, the 1 fC working point is >99% efficient with Landau fluctuations even with ≈ 50% of the charge collected on a single strip due to charge sharing between strips. Setting the 1 fC threshold evenly across all channels is one of the most significant tasks of the calibration electronics and software. To avoid the offline tracking algorithm from being biased, a technique is required to calibrate out the channel to channel variations in response to the same deposited charge. To design a well-calibrated SCT, channel to channel variations as well as module to module variations need to be kept mimimum.

[2] 1 fC is equivalent to $\approx 6250\bar{e}$.

4.6 Operational modes of the SCT for different data-taking periods

When the event is dequeued out of the read-out buffer, it needs to be compressed to reduce the event size in the mode stated by the configuration. The compression logic is assembled to cut off channels with specific hits patterns [115]. There are four compression modes available:

· Hit-mode, also known as XXX, returns a hit in any of the 3 time-bins and suppresses only those channels with no hits in any of the 3 time-bins. This mode is used when hits outside of the central bunch crossing need to be recorded, for example to record cosmic-ray data.

· Level-mode, also known as X1X, returns only those channels with a hit in the central time-bin. This is the default mode used to record data in 2011–2013, when the LHC bunch spacing was 50 ns, and was used for all data presented in this thesis unless otherwise stated.

· Edge-mode, not to be confused with edge-detect mode, also known as 01X, matches a central hit following a no-hit time-bin. This mode is designed for 25 ns LHC bunch spacing, to remove hits from interactions occurring in the preceding bunch crossing.

· Test-mode returns all hit patterns and provides no compression.

The time bin histogram for level-mode (X1X) is shown in Figure 4.11. This mode shows an excess of fractions of 010, 011, 110, 111 time bins, which represent bin numbers 2, 3, 6 and 7 (see Table 4.1) in decimal notation. The fractions for these bin patterns are in greater proportion. The bin 101 (5 in decimal notation) is supressed, although not zero, for this configuration as seen from the time bin histogram.

Time bin 7 means	111
Time bin 6 means	110
Time bin 5 means	101
Time bin 4 means	100
Time bin 3 means	011
Time bin 2 means	010
Time bin 1 means	001

Table 4.1 Conversion of time bin from binary to decimal form.

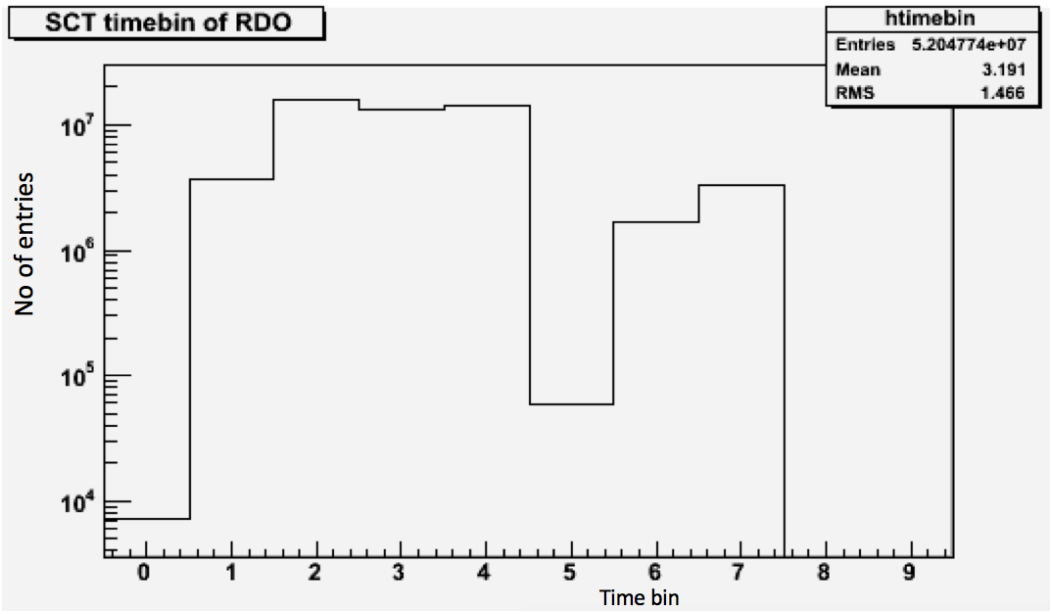

Fig. 4.11 Time bin distribution for run 186729 with operational mode X1X.

Hit-mode provides a good measurement of noise in patterns such as 100 or 001, if there is no hit on the other side of the module then the hit is not due to a particle. However, the read-out of the hit-mode takes longer as the information to be transfered off-detector is larger. For commissioning and low occupancy running, hit mode is ideal to debug the detector, but for high luminosity running, level-mode and edge-mode will be used. Edge-mode ensures that the hit in the central bin is not due to a hit that spilled over from the previous bin and further reduces the event size. Further compression is provided by the “clustering” of hits. Quite often, the deposited charge from a particle will be spread over several channels. The information from such a cluster of such hits is read out by identifying the first hit channel and then giving the number of consecutive channels and then the hit patterns for each of them.

The SCT hit information for each strip is stored in a series of 25 ns time bins (hit patterns are stored as a binary number). If the charge collected in the strips is above threshold within one of these 25 ns bins, a hit is registered in that bin. The threshold is the charge above which the pulse must be if it is to be recorded in that time bin. On Level 1 trigger three of these time bins are read out: a central bin corresponding to the expected time of arrival for a particle from the collision, along with the preceding time bin (the ‘early’ bin); and the following time bin (the ‘late’ bin). The contents of these three bins is known as the ‘hit pattern’ and can be expressed in binary. 010, for example, represents an "in-time" hit in the central time bin, whilst 100 means a pulse that was over threshold 25 ns before the bunch crossing of interest, and then dropped back under threshold for the following two i.e. the pulse would

be measured too early (an "early hit"). To reduce the read-out data size some hit patterns can be suppressed, and in 2011 the SCT was typically run in 'X1X' mode. This places a requirement that a hit is registered in the central time bin, with no requirement placed on the other bins. For this study, an 'early hit' is defined as having the hit pattern 1XX, i.e. a hit in the first time bin with no requirements on the other bins. In X1X mode, however, the only early hit patterns available are 110 and 111 (the 100 pattern is suppressed and the 101 pattern is illegal). We could also look at 4 consecutive bunch crossings or even 5 (XXXX and XXXXX), but this would be too demanding on the read out system.

4.7 Dataset used for beam-induced background

The beam-induced background studies were not possible using the standard datasets available during 2011, rather background streams are needed. For around forty runs in 2011, full datasets were available for these kind of studies. The number of runs that have been flagged as interesting by other ATLAS sub-detectors within the non-collision background working group in 2011, fall into three categories:

- Available runs flagged as having a large beam-halo rate;
- Available runs flagged as having a small beam-halo rate; and
- Available runs flagged as having a large vacuum pressure difference between 22 m and 58 m.

In order to understand the origin of the background seen by the BCM, the evolution of the rates and residual pressure in various parts of the beam pipe at the beginning of an LHC fill were studied. The vacuum gauges providing data for this study were located at 58 m, 22 m and 18 m from the IP. The pressures from these locations are referred to as P58, P22 and P18, respectively. Information about these runs along with the background rate is shown in Tables 4.2, 4.3 and 4.4.

Run No.	Date	No. Colliding Bunches	Integrated Luminosity (pb^{-1})	22 m Pressure (10^{-12}bar)	58 m Pressure (10^{-12}bar)	Halo Rate Hz/(10^{11} protons)
82454	22nd May	874	11.50	6.70	0.43	5.21
187196	12th Aug	1317	21.90	1.24	1.79	1.08
187219	12th Aug	1317	51.40	2.58	2.30	2.17
191513	23rd Oct	1331	16.20	1.46	2.06	1.63

Table 4.2 Available runs flagged as having a large beam-halo rate in 2011.

Run No.	Date	No. Colliding Bunches	Integrated Luminosity (pb^{-1})	22 m Pressure (10^{-12}bar)	58 m Pressure (10^{-12}bar)	Halo Rate Hz/(10^{11} protons)
187763	21st Aug	1317	42.90	0.29	1.00	0.27
188921	7th Sep	423	15.46	0.20	0.39	0.16
190300	4th Oct	1331	71.20	0.35	0.42	0.27
191426	22nd Oct	1331	106.00	0.27	0.84	0.32

Table 4.3 Available runs flagged as having a small beam-halo rate in 2011.

Run No.	Date	No. Colliding Bunches	Integrated Luminosity (pb^{-1})	22 m Pressure (10^{-12}bar)	58 m Pressure (10^{-12}bar)	Halo Rate Hz/(10^{11} protons)
182516	24th May	874	11.13	2.44	0.63	2.20
182747	28th May	874	29.90	1.34	0.43	1.36
185761	18th Jul	1041	18.40	0.24	6.25	0.55
186049	20th Jul	1317	45.46	0.71	3.07	0.49

Table 4.4 Available runs flagged as having a large vacuume pressure difference in 2011.

4.8 Beam-induced events and unpaired isolated BCIDs

Different BCID groups have been discussed in Section 4.2. This section describes the beam-induced background studies on the basis of one of the important categories of BCIDS: unpaired isolated. In some runs, ATLAS triggers on events with unpaired isolated BCIDs that could be used to identify beam backgrounds. These are well separated with almost zero or very little contamination from the collision. In Figure 4.12, events have been selected with low track-to-hits ratio requiring only unpaired BCIDs. There are no triggers in other runs for unpaired isolated BCIDs. The track-to-hits ratio for nominal collisions is different than the beam-induced background events. Because the beam-induced events have more hits than tracks, this ratio can be plotted against the beam crossing ID to get an idea of the early hits. The collision-like activity for the range of unpaired isolated BCIDs is between 1767 and 2542 for beam 1 and beam 2 for the early hits in the barrel and end-caps, and is clearly shown in Figure 4.12. Because the events are unpaired isolated, they should be empty but the excess of entries in this range shown by the spikes give evidence of non-collision backgrounds. The low track-to-hits ratio does help to investigate beam-backgrounds but a more robust method based on the asymmetry of end-caps on both sides is discussed in the next section.

To get these contaminated events, asymmetry of early clusters for end-caps (barrel is excluded for this study) was considered a good candidate. Furthermore, to flag the

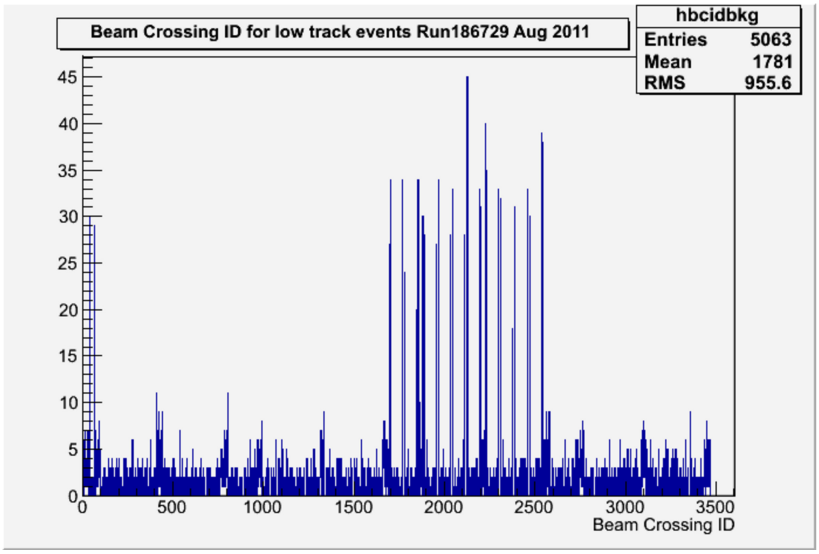

Fig. 4.12 The beam crossing ID for early hits in the barrel and end-caps for unpaired isolated bunches requiring low track-to-hit ratio in the minimum bias stream.

contaminated events coming from each of the two beams, a positive and negative asymmetry has been used.

4.9 Asymmetry for identifying BIB hits

The beam-induced background hits in the SCT will be more easily identifiable in the end-caps, as the BIB hits will be earlier in the end-cap than the beam with which they are associated, and in-time on the other side. The time by which a BIB hit is early is approximately:

$$\Delta t \simeq \frac{2z}{c} \tag{4.1}$$

where z is the distance from the collision point of the end-cap disk that is hit and c is the speed of light ($\simeq$ the speed of particle). $2z$ is then the distance by which a hit is early (particles resulting from collisions must first reach the collision point as a proton bunch and then return back to the disk, whereas BIB particles hit the disk as soon as the beam first passes it). In the SCT end-caps 0.85 m $\leq z \leq$ 2.72 m leading to 6 ns $\leq \Delta t \leq$ 18 ns. As Δt is largest for the outermost end-cap disks, Disks 8 and 9, it is most likely that a BIB hit will be registered as early in these layers. However, Disk 9 of side "C" is not completely functional because a cooling loop (see Figure 4.22 right hand side plot), corresponding to an entire quadrant, has leaks and cannot be operated. Therefore, it was decided to use Disks 7 and 8, which have full beampipe coverage. Events triggered in unpaired isolated BCIDs, i.e. with only one bunch

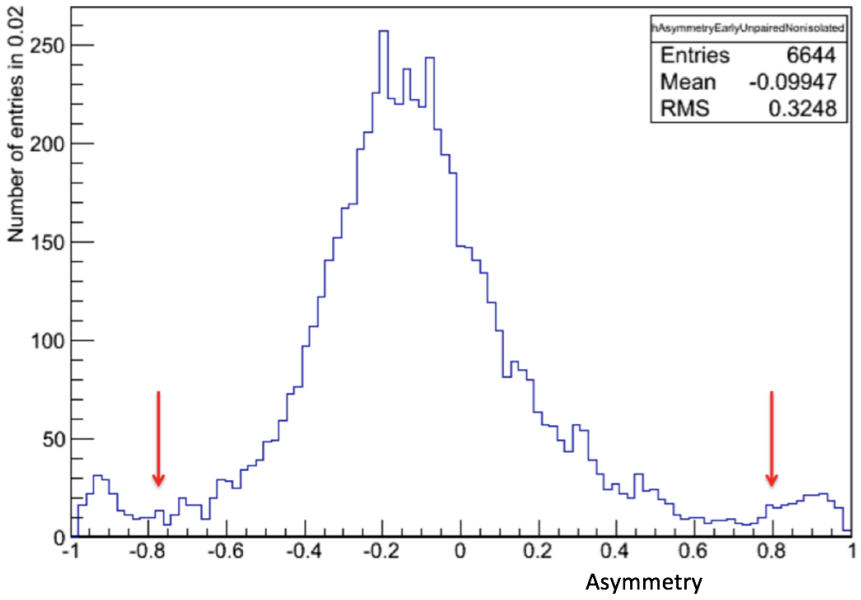

Fig. 4.13 Asymmetry of early clusters for background stream run 180636 (no triggers on unpaired isolated BCID).

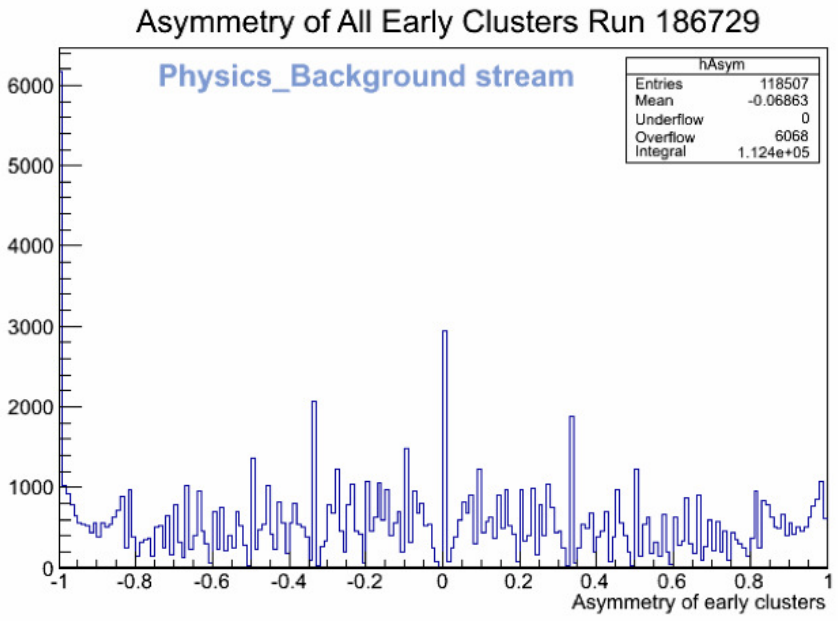

Fig. 4.14 Asymmetry of all early clusters for background stream run 186729.

traversing the ATLAS detector are particularly interesting: in case of an upstream beam-gas interaction or beam-halo one would expect a large number of early-hits in one end-cap and mostly in-time hits in the other end-cap. As such, the difference in the number of early hits in both end-caps in an unpaired isolated event could be a useful tool for identifying BIB hits in the SCT. To measure this, the z-asymmetry is defined as follows:

$$\text{asymmetry} = \frac{N_{early}(z>0) - N_{early}(z<0)}{N_{early}(z>0) + N_{early}(z<0)} \tag{4.2}$$

where $N_{early}(z>0)$ is the number of early hits with $z>0$, number of early hits in end-cap "A" and $N_{early}(z<0)$ is the number of early hits with $z<0$, number of early hits in end-cap "C". The asymmetry has a value of -1 if there are only early hits in end-cap "C", and +1 if there are only early hits in the end-cap "A". The asymmetry for two background data streams from two runs 180636 and 186729 collected in 2011 is shown in Figures 4.13 and 4.14.

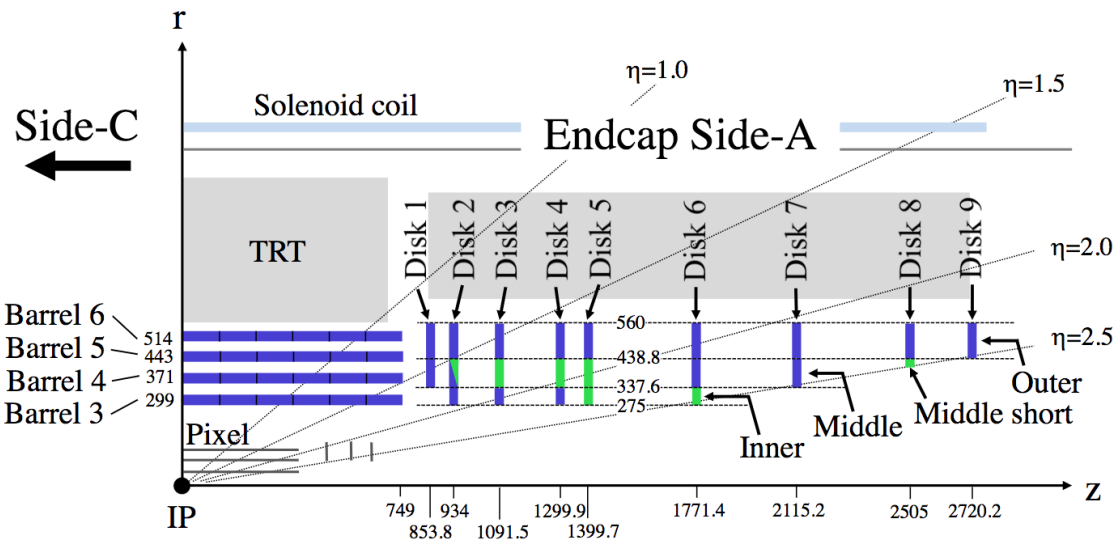

Fig. 4.15 Schematic view of the SCT end-cap disks layout. The distance to the interaction point (z) and the distance to the beam (R) are indicated [117].

The positions of all disks in the SCT end-cap are shown in Figure 4.15 and their longitudinal distance with the number of modules are shown in Table 4.5.

Disk	1	2	3	4	5	6	7	8	9	Total
|z| (mm)	847	934	1084	1262	1377	1747	2072	2462	2727	
Modules	92	132	132	132	132	132	92	92	52	988

Table 4.5 Longitudinal distance and number of modules for the nine disks on each SCT end-cap.

4.10 Beam halo rates

The overall asymmetry of out-of-time clusters for both end-caps for unpaired isolated BCIDs is shown in Figure 4.17. The distribution is not centered around zero due to the cooling loop on Disk 9 that has missing modules on it. This can be seen from the two dimensional plot in the bottom right plot in Figure 4.22. Careful inspection of the asymmetry clearly indicates highly asymmetric regions ($|\text{asymmetry}| > 0.8$) for one of the background streams. The highly asymmetric events containing early clusters are plotted in Figure 4.17 for background stream 186729 that have also been triggered on unpaired isolated BCIDs. To get the threshold of early clusters in Disks 8 and 9, a plot in Figure 4.16 is shown where the threshold of early hits in the two outermost disks, Disks 8 and 9 (in both end-caps), across all events can be seen. Based on this figure, it was decided that a requirement of at least 30 early hits across Disks 8 and 9 is appropriate.

Using this threshold of 30 early Disk 8 and 9 hits, the end-cap asymmetry in early hits in unpaired isolated BCID events was investigated, as shown in Figure 4.17. It can be seen that for all hits in all events (blue), which is dominated by collision hits, the hits are highly symmetric whereas for early hits in unpaired isolated BCID events, two peaks are seen at high positive and negative z-asymmetry. This is exactly what was expected for BIB events in Section 4.5; in an unpaired isolated event one end-cap sees a large number of early hits, whereas hits on the other are predominantly in-time, leading to a large asymmetry in early hits. Although this simple selection appears to be successful, in order to select the purest sample of good BIB candidates, only events with an end-cap asymmetry with magnitude greater than 0.8 in both Disks 7 and 8 are flagged.

As a final cross-check, the BCID of the events flagged as passing all the previous criteria broken down into events with positive and negative z-asymmetry is shown in Figure 4.18. By comparing the BCID of the flagged events with the available ATLAS run information [3], it can be seen that the flagged events with positive z-asymmetry come from the unpaired isolated bunch crossings, in which the LHC beam labeled beam 1 is passing through the detector. Alternatively, flagged events with negative z-asymmetry are associated with beam 2. Beam 1 travels in the direction that passes end-cap A first, whereas Beam 2 passes end-cap

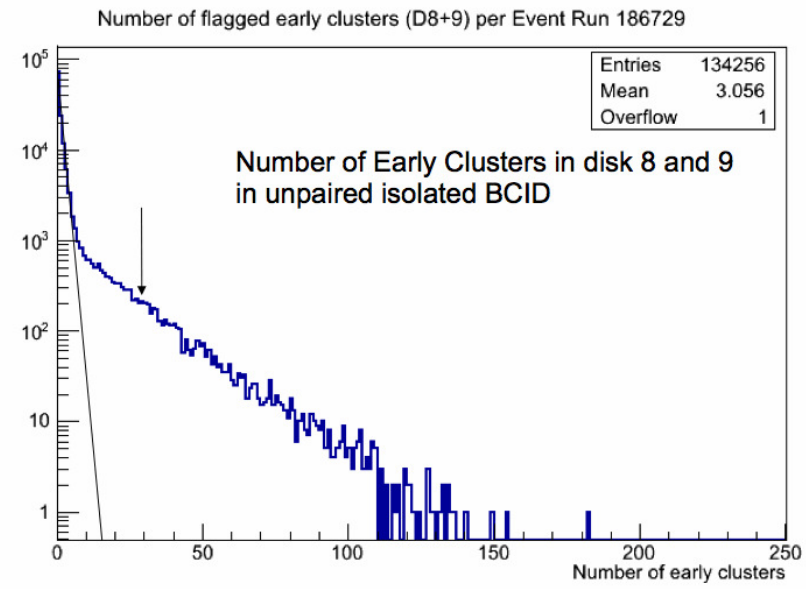

Fig. 4.16 The flagged early clusters in end-cap Disks 8 and 9 in unpaired isolated BCID. The sensible threshold (early clusters > 30) can be determined from this plot. All early clusters with no cut on the asymmetry.

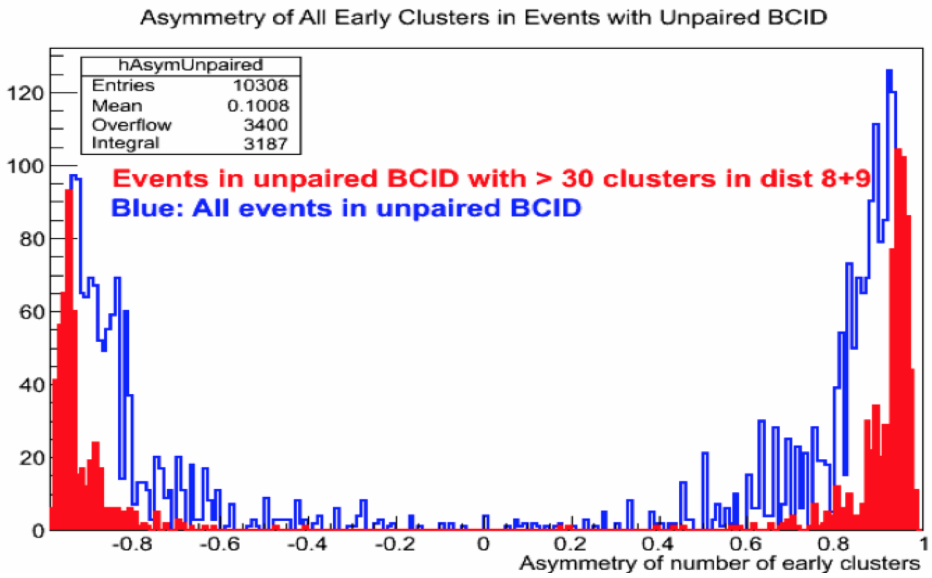

Fig. 4.17 Events contaminated with more than 30 early clusters in unpaired isolated BCID (red) and events containing all early clusters for unpaired isolated BCID (blue). There is an additional cut on the asymmetry (> 0.8).

C first. As a result, it is expected that beam 1 unpaired isolated events should have a large number of early hits in side A, whereas for beam 2 the same can be said for side C. This is exactly what is observed in Figure 4.18 and provides confidence that the selection process is working correctly. Figure 4.19 shows a specific region of unpaired BCID for flagged events by zooming into Figure 4.18. The range of unpaired isolated BCIDs are obtained from Run Query tool and have been shown with red and blue colours in Figure 4.19.

The fraction of unpaired isolated events in Disks 8 and 9 that have high asymmetry and also contain more than 30 early clusters are plotted in Figure 4.17. The total number of events passing these two cuts is 2943. The total number of events tested is 340853 and therefore the fraction of events is 0.008%. These events can be treated as high background events. The number of highly asymmetric events in Disks 8 and 9 with less than 30 early clusters is found to be 131029. The fraction of these low background events is 3.84%. The list of unpaired bunches is already known from ATLAS run query [118] and therefore the backgrounds coming from either of the two beams can be identified. To relate the beam backgrounds with either of the two beams, the flagged events are further divided into two categories: positive asymmetry events and negative asymmetry events. The BCID of positive and negative asymmetric events for flagged events is plotted in Figure 4.18. The unpaired bunches get selected for both positive and negative asymmetric events. The beam 1 passes side A first which gives a positive asymmetry and beam 2 passes side C first, giving a negative asymmetry. It is clearly seen from Figure 4.19 that the positive asymmetry events are mostly coming from beam 1 and negative asymmetry events are mostly coming from beam 2. The plot of asymmetry vs. BCID verifies this expected behaviour. A plot of ϕ against z of early clusters in the flagged events in run 186729 is shown in Figure 4.20.

4.11 Conclusion

The number of colliding bunches were increased from a few hundred to 1331 during 2011, with almost 50 unpaired (non-colliding) bunches. These non-colliding bunches play a significant role to monitor the beam-induced backgrounds. The events in these bunches were triggered by dedicated triggers and have been stored in SCT background streams for around forty runs in 2011. The triggers on unpaired isolated bunches were not in place at the start of 2011, the first available run (180636), containing events triggered on those bunches, was available on 30th April 2011 (no detailed study has been carried out on these early runs). After some initial studies of beam-induced backgrounds, it has been seen that the results are highly sensitive to minor defects in the detector. These defects are a source of fake asymmetries in the flagged events, showing interesting results that are not related to BIB. This effect can be seen from the ϕ distribution of early hits for disks on both sides. Several

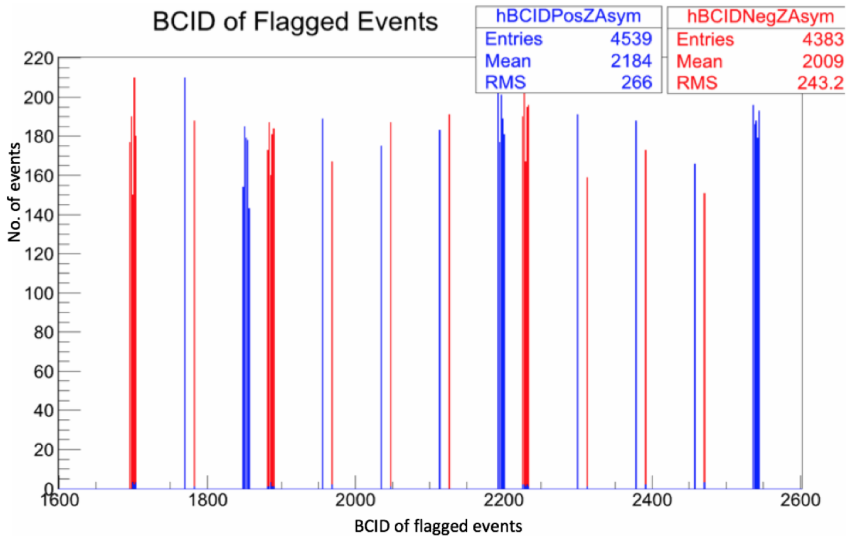

Fig. 4.18 Unpaired BCIDs of flagged events for both positive asymmetry events and negative asymmetry events for background stream run 186729.

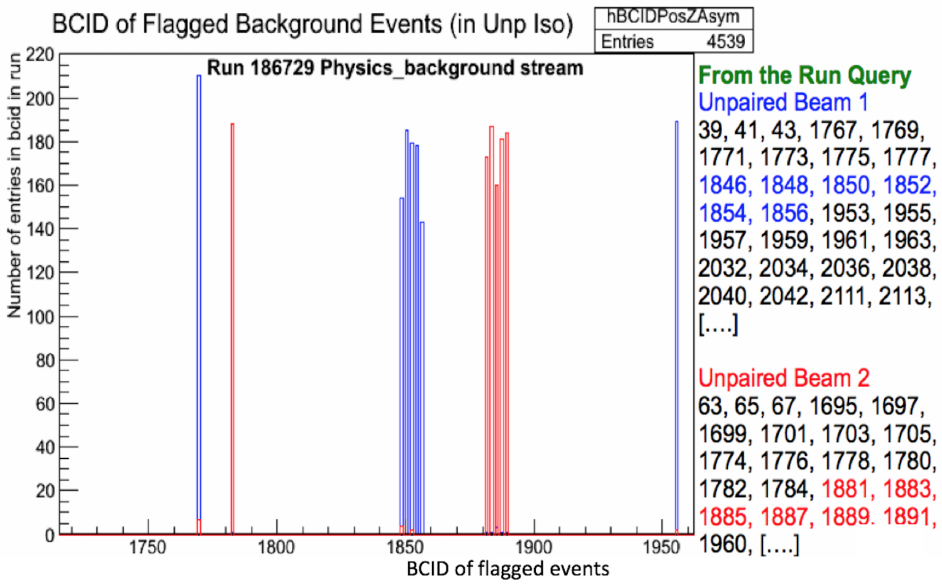

Fig. 4.19 Zooming in the specific region of the unpaired BCID for the flagged events in the previous Figure 4.18.

sharp peaks, known as ϕ spikes, are seen in the ϕ distribution in Figures 4.21 and 4.22. They are due to noisy chips in the detector. These chips are unable to register the hits correctly and should be removed from background streams that have been used here. To get rid of these

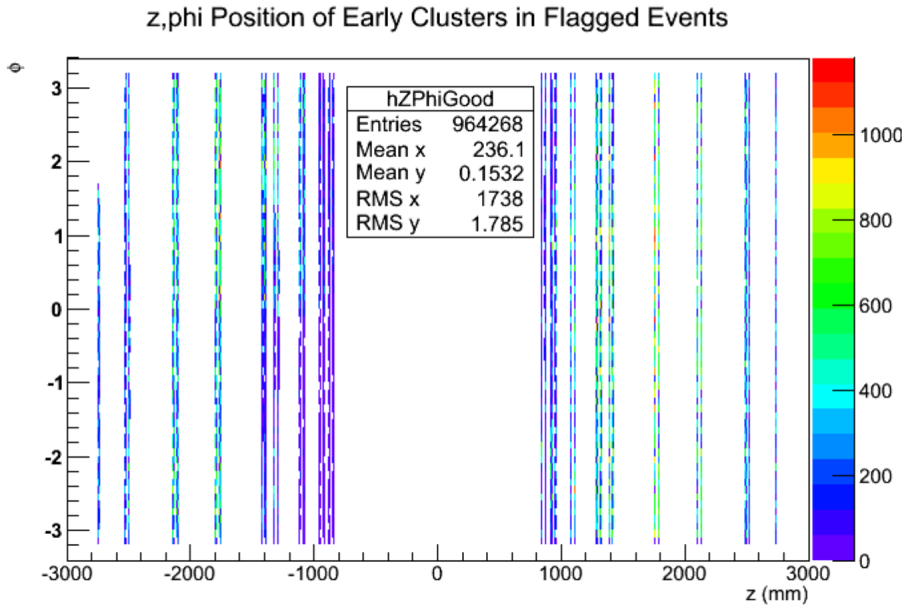

Fig. 4.20 A plot of ϕ against z of early clusters in the flagged events in run 186729.

spikes, the regions of the distribution are excluded from this study. An algorithm has been developed that identifies a sample of events containing beam-induced background hits in the SCT for events with unpaired isolated BCIDs. The flagged events have high z-asymmetry in early end-cap hits, and events originating from beam 1 have positive z-asymmetry and vice versa for beam 2, as expected. It has been planned to include a BIB event flag, based on the selection criteria developed here in the online SCT monitoring algorithm (i.e. in the monitoring that occurs during data-taking, rather than after). This would allow BIB rates in the SCT to be compared with other ATLAS sub-detectors in real time and could be used to identify times at which large rates of BIB may impact physics analyses. More details can be found from the ATLAS internal note [119] for which the author has contributed.

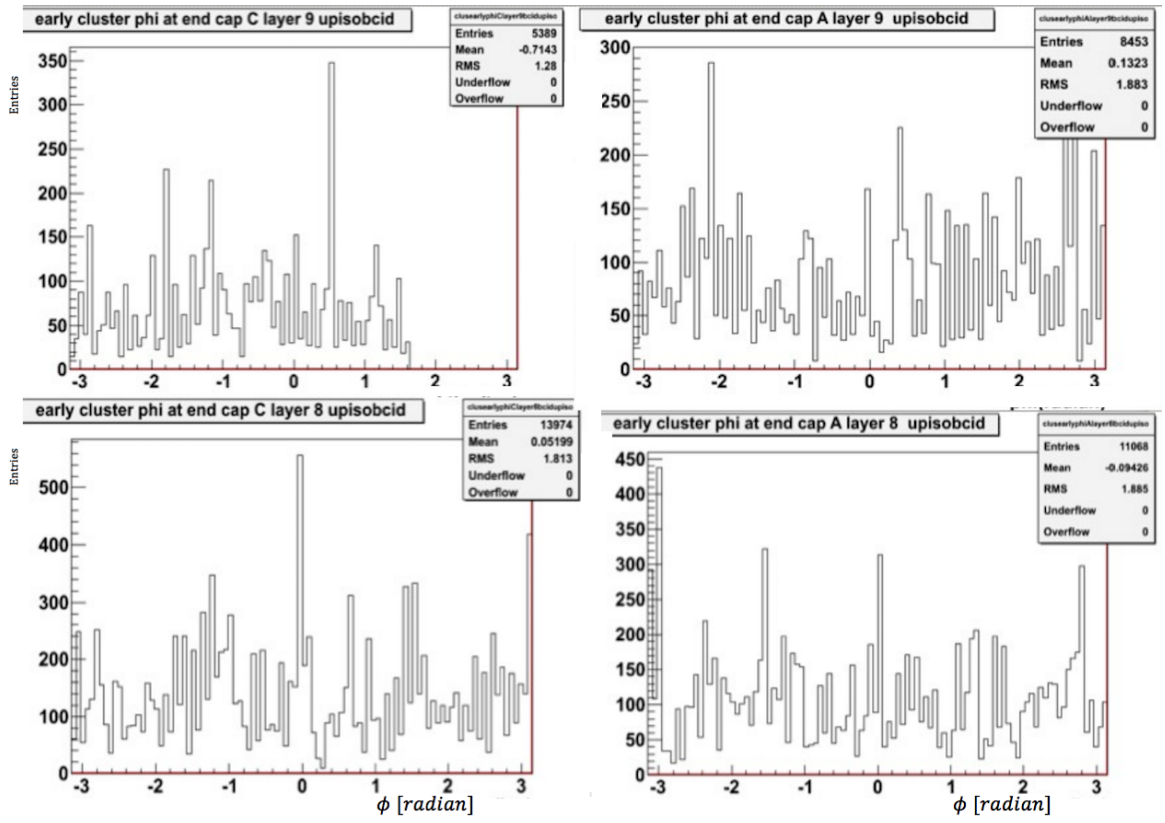

Fig. 4.21 ϕ spikes of early hits in Disks 8 and 9 of the end-caps A and C. Disk 9 of side C is not completely functional due to a cooling loop and can be seen in the top left hand side plot.

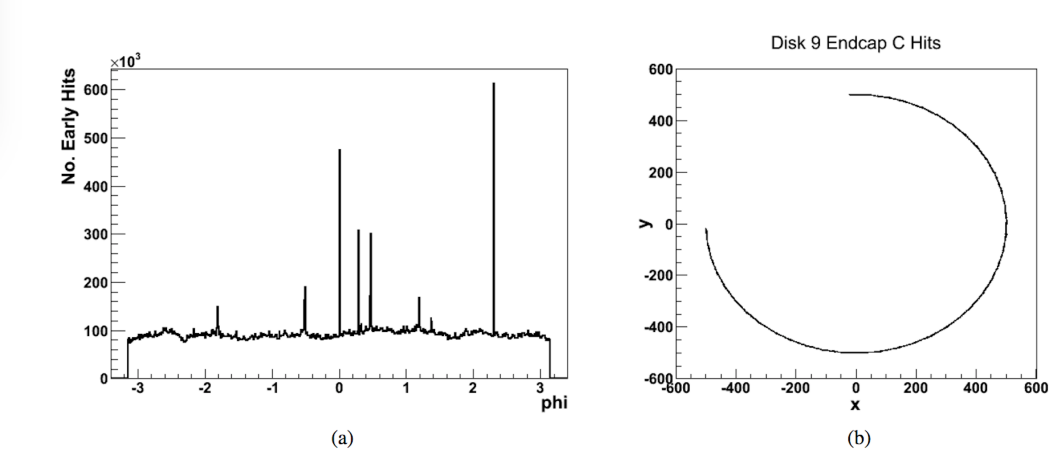

(a) (b)

Fig. 4.22 The problems caused by noisy chips in creating '*phi* spikes' (a) and the missing segment in Disk 9 end-cap C (b).

Chapter 5

Object reconstruction and event selection

5.1 Introduction

As discussed in Chapter 2, the dilepton channel is characterised by two leptons, the large missing transverse energy (E_T^{miss}) corresponding to undetected neutrinos from the leptonic decay of W and two jets with large p_T corresponding to two b-quarks from a $t\bar{t}$ decay. Other processes that have similar event topologies include multijets, W+jets, Z/γ^*+jets, dibosons (WW, WZ, ZZ) and single top (t-channel, s-channel and W_t channel). The two measured lepton requirements suppress multijet background processes (dominated by QCD, W+jets, $t\bar{t}$ single lepton and hadronic channels), while the ≥ 1 b-tagged jet requirement further rejects the Z boson production in association with jets. The single top t-channel and s-channel, W+jets and multi-jet samples do not contribute for two isolated leptons so they are treated as a source of fake background. On real date, semileptonic events can still pass all the cuts, and is briefly discussed in Section 5.13. This chapter discusses the objects of interest: electrons, muons, jets, b-tagging, E_T^{miss} and samples used to model signal and background.

The background processes mimicking $t\bar{t}$ dilepton signatures are significantly suppressed by the two isolated lepton requirements and at least one b-tagged jet requirement.

5.2 Object and event selection

From the detector components detailed in Chapter 3, the physics objects of interest may be reconstructed. This section discusses the objects, events, and samples that will be used for the analysis described in Chapter 8. The work presented in this chapter summarises the work of the ATLAS top reconstruction and top background groups, for the 2012 data analysis. These groups aim to provide the common starting point for the ATLAS top analyses to produce the results needed to go from the detector output to top quark events, including background estimates [120]. Hadron colliders like the LHC collide protons together at high

energies so that the point-like interactions that take place are between quarks and gluons. Before these quarks and gluons scatter into the different components of the detectors, they "dress" themselves into hadronic bound states due to the phenomenon of confinement. At these colliders, physics objects can be described at different stages, starting from the collision point as the hard interaction process which is described by leading order (referred to as the parton level). The next stage is parton showering, which means partons can radiate more low energy partons as quarks and gluons emit other quarks/gluons and increase in number; this then reduces their energy so that eventually the quarks and gluons must confine into hadrons. The formation of hadrons is called hadronization. These bound states can be detected, i.e. they can leave their signatures at the detector level. The process of event reconstruction links the signatures of the objects reconstructed at detector level with the objects at the parton level. The physics of "interesting" particle production is distinguished from that of the "background" contribution in such collisions. While the former is typically a single parton-parton scattering process at a very high p_T, the latter involves the remnants of the two protons that did not take part in the hard-scatter, including the products of any additional soft, multiple-parton interactions. This soft-physics component in almost every pp collision is referred to as the "underlying event".

Different stages of the process comprising hard-scattering, parton showering, hadronization and interaction with the detector are shown in Figure 5.1. This chapter describes the objects observed in the detector. Figure 5.2 shows a $t\bar{t}$ candidate event containing two leptons, two jets and missing transverse energy.

5.3 Monte Carlo generators

Both experimental and theoretical high-energy physics make use of Monte Carlo event generators to generate the sets of simulated events needed to characterize the detector response, estimate the detector efficiency, make predictions about the new physics processes of interest and understand what certain backgrounds will look like. pp collisions are very complex so a MC generator has to describe and simulate all of the sub-processes starting from hard process and then parton showering, hadronization, underlying events and unstable particle decays. The last component of the event generation addresses the fact that the hadrons produced are not stable particles but heavy resonances which have to decay. As an example of the importance of MC, a vast majority of the Higgs discoveries strongly rely on MC predictions to be able to set limits on Higgs in certain parameter space regions. This example shows the vital importance of the event generators to make discoveries in various physics sectors. Although some features differ, the process of hard-scattering to

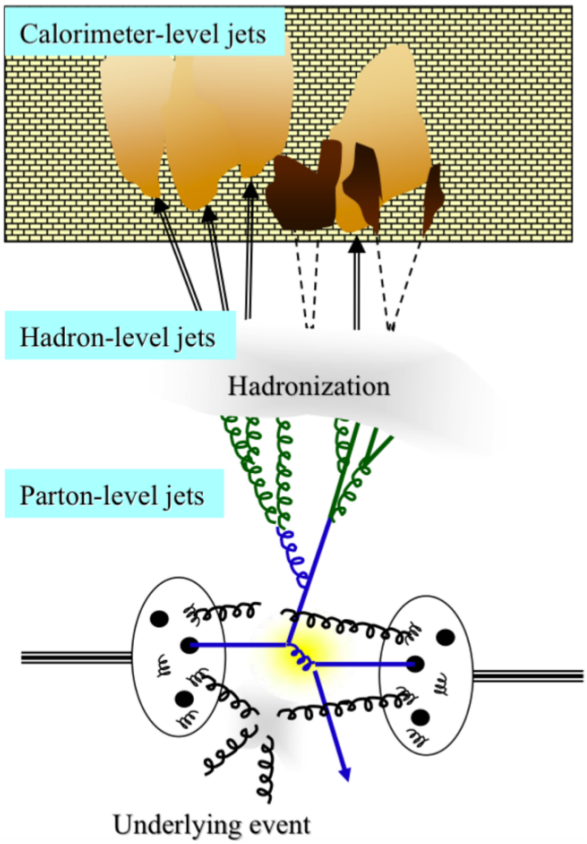

Fig. 5.1 Schematic depiction of the different stages of the process comprising hard-scattering, parton showering, hadronization and interaction with the detector [121].

stable hadrons for all current general purpose event generators[1] like HERWIG, PYTHIA and SHERPA is the same. Some of the available event generators provide software for each of the steps needed to generate an event at the LHC, while others can only take care of some of the steps. Other generators such as MC@NLO [122] and POWHEG [123–126] only generate a fixed order calculation of the hard processes and need to be interfaced to another generator, e.g. PYTHIA or HERWIG, for the parton shower and hadronisation. The classical textbook on this subject is [127]. A detailed description can be obtained from [128]. Different features of important event generators are summarized below:

- PYTHIA [129] is a standard tool for the generation of high-energy physics events to provide a complete description of event properties within and beyond the Standard Model, comprising a coherent set of models to produce multihadronic final states. It

[1] A general purpose generator can handle the entire process, starting from matrix element to parton showers and hadronization.

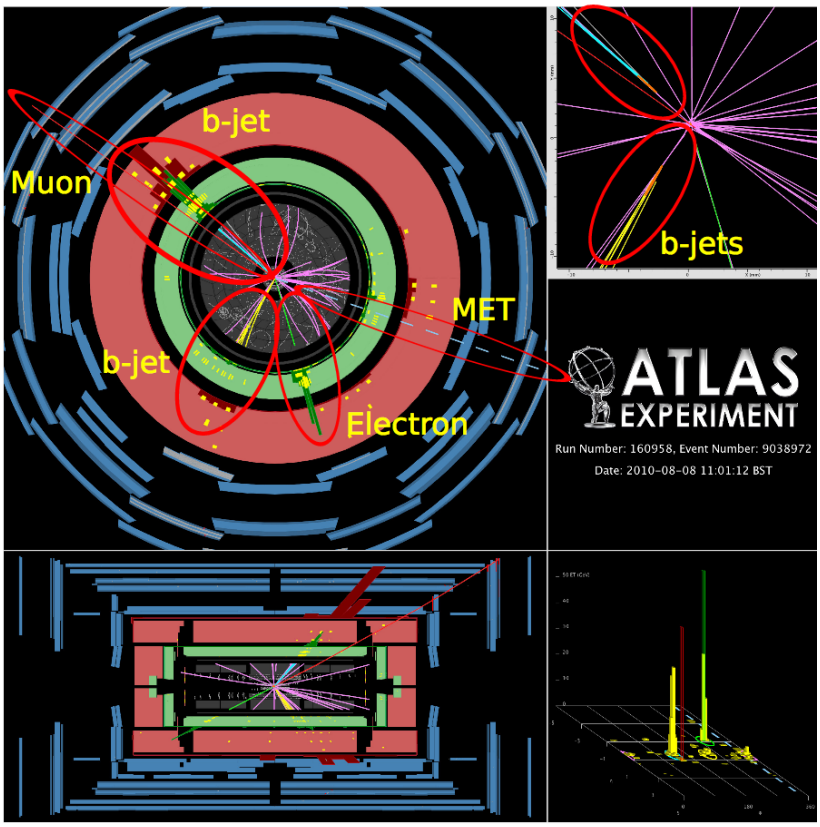

Fig. 5.2 Example of a candidate data $t\bar{t}$ event decaying to electron and muon (dilepton) with both jets tagged as b-jets [121].

contains a library of hard processes which model initial and final-state parton showers[2], multiple parton-parton interactions[3], beam remnants, string fragmentation and particle decays. PYTHIA makes use of the string method, where the confinement is modelled as a string stretched between each colour charge and its anti-colour charge. The string is then stretched until it breaks and produces a new pair. This process continues until the string energy is low enough to produce primary hadrons. Its main features are:

- generation of hard-processes having $\sqrt{s} > 10$ GeV;
- built-in pdf sets can be used with or without LHAPDF[4];
- parton showers are ordered with respect to p_T;

[2]Radiation emitted by the partons before the collision is called Initial State Radiation (ISR), while the radiation emitted after the collision is called Final State Radiation (FSR).

[3]A proton contains many partons, further partons may collide within a single pp collision. This process is called multiparton interaction (MPI).

[4]The Les Houches Accord PDF interface.

  - both hard and soft interactions in the underlying event are simulated using multiple parton interaction (MPI); and
  - in spite of the fact that it lacks NLO corrections, PYTHIA is still used because it describes a broad spectrum of physics processes (including supersymmetric or more exotic models) and an advanced hadronisation procedure.

- HERWIG [130] is another general purpose Monte Carlo event generator. It makes use of a cluster model to group quark pairs into colourless clusters, which decay into other colourless clusters or Standard Model hadrons. It provides simulation of high-energy collisions with the following special features:
  - uses an angular-ordered parton shower;
  - a space-time picture of event simulation from parton showers to decay of hadrons;
  - uses the external JIMMY[5] package [131]; and
  - the underlying events are modelled using hard and soft partonic interactions.

- MC@NLO [122] simulates hard-scattering events at Next-to-Leading Order matrix elements for the scattering process, giving a better description of the transverse momentum distribution than HERWIG. As this generator only deals with hard interactions, it needs to be interfaced to a general purpose generator such as PYTHIA or HERWIG to handle parton showers and hadronisation processes. MC@NLO always generates some events with negative weights [132]. The correct distributions are obtained by summing weights with their signs (i.e. the absolute values of the weights are not used to fill the histograms).

- ALPGEN [133] is designed to provide a better description of the final states consisting of a large number of partons initiated from the hard-scattering, for which the fixed order QCD matrix element can provide a better approximation than the one obtained using HERWIG or PYTHIA. ALPGEN is interfaced to HERWIG/PYTHIA for the evolution of the partonic final state through parton shower.

- SHERPA [134] is a general-purpose generator which matches fixed-order QCD matrix elements to QCD showers using the Catani-Krauss-Kuhn-Webber duplicate removal prescription. Unlike PYTHIA and HERWIG, it was developed from the beginning in C++. It is interfaced to PYTHIA's hadronization model and produces complete events which give better approximations for the final states with a large number of

[5] JIMMY is a model of multiple parton interactions which can be combined with HERWIG to enhance the "underlying event" thereby improving the agreement with data.

isolated jets than other generators based on pure QCD showering, such as PYTHIA and HERWIG.

There are many other generators available, but only those which are used for this analysis have been briefly discussed in this discussion.

5.4 Data and simulation samples

The dataset used in the analysis described in Chapter 8 was collected at $\sqrt{s}$ = 8 TeV with the ATLAS detector at the LHC in 2012. The recorded datasets are not always good for physics analyses. To define a good dataset, we have to know the data quality (DQ) information. The DQ group is responsible for making use of dedicated lists of runs and luminosity blocks, known as a Good Run List (GRL). Data in ATLAS is recorded over a period of time and split into periods. A luminosity block is the unit of time for data-taking that only lasts about 2 minutes. The physics DQ status couples with other run information, such as range, number of events and beam energy to determine a GRL. Different physics groups determine which final states are relevant for their analysis and publication and recommend a GRL. The GRL used for this analysis follows recommendations from the top working group. Data in ATLAS is recorded over a period of time. Consequently they are grouped in periods. The data periods A to L inclusive (excluding periods F and K which are not standard runs) have been used for this analysis and are listed in Table 5.1.

Events are required to pass a single electron or muon trigger chain, with the thresholds fully efficient for leptons passing an offline selection requirement of $p_T > 25$ *GeV*. For electrons, the OR of trigger chains EF_24vh_medium and $EF\_e60\_medium1$ has been used. For muons, the OR of EF_mu24i_tight and EF_mu36_tight has been used. The single electron trigger has a threshold of $p_T \geq 24$ GeV for isolated electrons and $p_T \geq 60$ GeV for the non-isolated ones, while the single muon trigger has a threshold of $p_T \geq 24$ GeV for isolated muons and $p_T \geq 36$ GeV for non-isolated ones. To avoid an overlap of events coming from both streams, the egamma stream and the muon stream, the events passing electron triggers have been accepted from the egamma stream i.e. the muon stream has been used for events selected from muon triggers. The single electron trigger is fully described in Ref. [135]. The single muon trigger has been fully described in Ref. [136].

The total integrated luminosity of the analysed sample is (20.3$\pm$0.6) fb^{-1}. In order to analyse the complex processes at the LHC, a software that can virtually produce the conditions of physics experiments is relied upon. Monte Carlo (MC) methods have been developed to simulate the experimental conditions, making use of pseudo-random number generators. In the real experiment, collisions are produced and stored for offline processing. In the simulation, event generators such as HERWIG [130] and PYTHIA [129] are used to

produce final state particles. GEANT4 (for GEometry ANd Tracking) is a software toolkit for "the simulation of the passage of particles through matter", using MC methods.

Standard ATLAS top group recommended MC12 simulated samples [137] have been used to develop the analysis, make a direct comparison to the data, evaluate signal and background efficiencies, estimate background rates, derive correction factors and response matrices, and to evaluate uncertainties for the signal and background. The main $t\bar{t}$ and background samples have been processed through the full ATLAS detector simulation [138], based on GEANT4. The samples used to estimate signal systematic uncertainties were processed through a faster simulation using the Atlfast2 (a fast simulation package for ATLAS) framework [139]. All samples had additional overlaid minimum bias events produced with PYTHIA8 [140] to simulate pile-up background, and have been reconstructed using the same algorithms as the data. Since pile-up events can have an impact on the reconstructed event topology, such as jet multiplicity or E_T^{miss}, the simulated samples have been re-weighted such that distributions of μ, which is the mean number of interactions per bunch crossing, matches with the data. The MC events have been re-weighted to have the same lepton efficiency as in the data by deriving multiplicative event-by-event scale factors[6]. These corrections or scale factors take into account the mismodelling of lepton identification, reconstruction and efficiency of triggers. Further re-weighting is applied for scaling the jet vertex fraction distributions. Data and Monte Carlo samples have been accessed through the standard top group D3PDs [141] which has three production types.

The data samples are processed using a specialised software package, ToprootCore [142].

5.4.1 Simulated signal

The baseline $t\bar{t}$ full simulation samples were produced using POWHEG interfaced to PYTHIA6, with the Perugia 2011C (P2011C) tune [143] and CT10 parton distribution functions (PDFs) [144]. The parton shower and hadronization have been performed with PYTHIA. In order to estimate the signal modelling uncertainties POWHEG+HERWIG with AUET2 tune (DSID =105860) and MC@NLO+HERWIG with AUET2 tune (DSID=105200) are used. These sample were fast simulation versions. The simulation of vector boson production has been made at Leading Order with ALPGEN using the CTEQ6L1 parton distribution function set [145] interfaced to PYTHIA for the parton shower, producing samples with several final state jet multiplicities and enriched with jets from heavy flavours.

The effects due to the modelling of extra radiation in $t\bar{t}$ events are assessed at both the matrix element and parton shower levels. At $\sqrt{s}$ = 7 TeV, the uncertainty due to matrix

[6] A scale factor is the ratio of the efficiency in data to the efficiency in MC i.e. $SF = \frac{\varepsilon_{data}}{\varepsilon_{MC}}$. In ATLAS these weights are often called Scale Factors.

Table 5.1 Luminosity by data period.

Periods	Integrated Luminosity (fb^{-1})
A	0.84
B	5.30
C	1.54
D	3.37
E	2.70
G	1.30
H	1.56
I	1.06
J	2.72
L	0.89
Total	21.28

element renormalization and factorization scales is computed using MC@NLO+HERWIG samples with varied renormalization/factorization scales, and the uncertainty due to parton showering in different initial-state and final-state radiation (ISR/FSR) conditions is estimated using two different ALPGEN+PYTHIA samples with varied radiation settings. At $\sqrt{s}$ = 8 TeV, the treatment of these uncertainties was improved by using POWHEG+PYTHIA samples with tuned parameters to span the variations in radiation compatible with the ATLAS $t\bar{t}$ gap fraction (gap fraction was shown to be a useful variable sensitive to $t\bar{t}$ modelling) measurements at $\sqrt{s}$ = 7 TeV [146] as discussed in detail in Ref. [147]. The samples (DSID[7] = 110407, 110408) have varied renormalization/factorization scales and hdamp parameter values, resulting in either more or less radiation than the nominal signal sample.

5.5 Simulated background

Backgrounds are classified into two types: those with two real prompt leptons arising from decays of W or Z and those where one of the reconstructed leptons is 'fake', i.e. a non-prompt lepton from the decay of heavy flavour quarks (b or c), an electron produced from a photon conversion, a jet misidentified as an electron, or muon arising from an in-flight decay of a pion or kaon. Backgrounds containing two real prompt leptons consist of single top production in association with a W boson (Wt), Z+jets samples and diboson production (WW, WZ and ZZ). The single top quark production is simulated using AcerMC for the t-channel and POWHEG for the s-channel and the W_t production mechanism. In both cases the CTEQ6L1 parton distribution function set and the PYTHIA parton showering has been

[7]The DSID is the ATLAS identification of the data sample.

used. Diboson production is modelled using SHERPA with the CT10 parton distribution function set.

DSID	Brief description	ME+PS	σ [pb]	k-factor
183585	$ZW \to eeqq$ with up to Np3 and massive b,c quarks	Sherpa	1.4622	1.0500
183586	$ZZ \to eeqq$ with up to Np3 and massive b,c quarks	Sherpa	0.24854	1.0500
183587	$ZW \to \mu\mu qq$ with up to Np3 and massive b,c quarks	Sherpa	1.4624	1.0500
183588	$ZZ \to \mu\mu qq$ with up to Np3 and massive b,c quarks	Sherpa	0.24747	1.0500
183589	$ZW \to \tau\tau qq$ with up to Np3 and massive b,c quarks	Sherpa	1.4523	1.0500
183590	$ZZ \to \tau\tau qq$ with up to Np3 and massive b,c quarks	Sherpa	0.24167	1.0500
183734	$WW \to e\nu qq$ with up to Np3 and massive b,c quarks	Sherpa	7.2790	1.0500
183735	$WZ \to e\nu qq$ with up to Np3 and massive b,c quarks	Sherpa	1.9022	1.0500
183736	$WW \to \mu\nu qq$ with up to Np3 and massive b,c quarks	Sherpa	7.2776	1.0500
183737	$WZ \to \mu\nu qq$ with up to Np3 and massive b,c quarks	Sherpa	1.9076	1.0500
183738	$WW \to \tau\nu qq$ with up to Np3 and massive b,c quarks	Sherpa	7.2756	1.0500
183739	$WZ \to \tau\nu qq$ with up to Np3 and massive b,c quarks	Sherpa	1.9086	1.0500

Table 5.2 Diboson samples with up to three partons and massive b and c quarks. Matrix element calculation and parton showering both are done by SHERPA.

In the analysis, every sample is rescaled to the luminosity of the data, taking into account the number of generated events and the cross-section of the processes. Finally, every event is rescaled by a k-factor, which corrects for the recent Next-to-Leading Order calculation from the previous Next-to-Leading Order calculations.

Uncertainties arising from the background estimates are evaluated by repeating the full analysis procedure, varying the background contributions by $\pm\ 1\sigma$ from the nominal values. The differences between the results obtained using the nominal and the varied background estimations are taken as systematic uncertainties.

5.5.1 Single top

Single top W_t associated production has the same dilepton signature as the $t\bar{t}$ dilepton decay channel. It also produces a b-jet that passes the nominal selection cuts with ≥ 1 b-tagged jets. Thus, the W_t channel is the largest background in this analysis. This dominant background was modelled using POWHEG+PYTHIA with the CT10PDF and the Perugia tune, using

the 'diagram removal' scheme (DR) (DSID 110140). The single top samples used for this analysis are given in Table 5.7. Because the dominant background for this analysis is the W_t background, the uncertainties due to the W_t background modelling are estimated by comparing the inclusive "diagram removal" and inclusive "diagram subtraction" samples. Other background related systematics have no significant impact on the analysis so they have not been estimated.

5.5.2 Z+jets

Z+jets light samples (DSID 147105-10, 147113-18, 147121-26) with up to five partons are given in Table 5.3. Z+jets heavy quark flavour samples (DSID 200332-43, 200348-51, 200432-35, 200440-43, 200448-51) are given in Table 5.4. The matrix element calculation for these samples is done with ALPGEN while the parton showering is achieved with PYTHIA. The contribution of these events is very small so no systematic uncertainties have been evaluated from the diboson background samples.

5.5.3 W+jets

W+jets light flavour samples (DSID 147025-38, 147041-46) with up to variable number of partons are given in Table 5.5. W+jets heavy flavour samples (DSID 110801-4, 126601-9) with up to variable number of partons are given in Table 5.6. The matrix element calculation is done with ALPGEN while the parton showering is done with PYTHIA. A W+jets sample is normally called a fake lepton because a jet is needed to 'fake' one more lepton (or two) for it to pass the event selection. There is also a very small contribution from W+jets events with a heavy flavour. These backgrounds are heavily suppressed due two jets (b-tag jets), where both b-quarks produced in the top decays have already produced well-defined b-tagged jets.

5.5.4 Dibosons

The diboson samples (DSID 183585-90, 183734-39) used in this analysis are given in Table 5.2. The diboson production is a small background in this analysis. The WW, WZ and ZZ diboson production are estimated from a fully-fledged event generator, SHERPA, comprising of solutions to all aspects of event simulation. The WW, WZ and ZZ processes are rejected due to the b-tagging requirement. The contribution of these events is very small so no systematic uncertainties have been evaluated from the diboson background samples.

5.6 Object reconstruction and event selection

The analysis presented in this thesis relies on the selection of isolated electrons, muons, jets and the tagging of jets as b-jets. The $t\bar{t}$ signal events are characterised by two leptons, two jets coming from the b-quarks with at least one tagged as a b-jet and missing transverse

DSID	Brief description	ME+PS	σ [pb]	k-factor
147105	$Z \to ee + \mathrm{N}p0$	AlpGen+Pythia	718.97	1.1800
147106	$Z \to ee + \mathrm{N}p1$	AlpGen+Pythia	175.50	1.1800
147107	$Z \to ee + \mathrm{N}p2$	AlpGen+Pythia	58.760	1.1800
147108	$Z \to ee + \mathrm{N}p3$	AlpGen+Pythia	15.636	1.1800
147109	$Z \to ee + \mathrm{N}p4$	AlpGen+Pythia	4.0116	1.1800
147110	$Z \to ee \geq \mathrm{N}p5$	AlpGen+Pythia	1.2592	1.1800
147113	$Z \to \mu\mu + \mathrm{N}p0$	AlpGen+Pythia	719.16	1.1800
147114	$Z \to \mu\mu + \mathrm{N}p1$	AlpGen+Pythia	175.74	1.1800
147115	$Z \to \mu\mu + \mathrm{N}p2$	AlpGen+Pythia	58.795	1.1800
147116	$Z \to \mu\mu + \mathrm{N}p3$	AlpGen+Pythia	15.673	1.1800
147117	$Z \to \mu\mu + \mathrm{N}p4$	AlpGen+Pythia	4.0057	1.1800
147118	$Z \to \mu\mu \geq \mathrm{N}p5$	AlpGen+Pythia	1.2543	1.1800
147121	$Z \to \tau\tau + \mathrm{N}p0$	AlpGen+Pythia	718.87	1.1800
147122	$Z \to \tau\tau + \mathrm{N}p1$	AlpGen+Pythia	175.76	1.1800
147123	$Z \to \tau\tau + \mathrm{N}p2$	AlpGen+Pythia	58.856	1.1800
147124	$Z \to \tau\tau + \mathrm{N}p3$	AlpGen+Pythia	15.667	1.1800
147125	$Z \to \tau\tau + \mathrm{N}p4$	AlpGen+Pythia	4.0121	1.1800
147126	$Z \to \tau\tau \geq \mathrm{N}p5$	AlpGen+Pythia	1.2561	1.1800

Table 5.3 Z+jets light samples with up to five partons. The matrix element claculation is done with ALPGEN while parton showering is done with PYTHIA.

DSID	Brief description	ME+PS	σ [pb]	k-factor
200332	$Z \to ee + bb + \mathrm{N}p0$	AlpGen+Pythia	6.5083	1.1800
200333	$Z \to ee + bb + \mathrm{N}p1$	AlpGen+Pythia	3.2948	1.1800
200334	$Z \to ee + bb + \mathrm{N}p2$	AlpGen+Pythia	1.2546	1.1800
200335	$Z \to ee + bb \geq \mathrm{N}p3$	AlpGen+Pythia	0.61800	1.1800
200340	$Z \to \mu\mu + bb + \mathrm{N}p0$	AlpGen+Pythia	6.5056	1.1800
200341	$Z \to \mu\mu + bb + \mathrm{N}p1$	AlpGen+Pythia	3.2909	1.1800
200342	$Z \to \mu\mu + bb + \mathrm{N}p2$	AlpGen+Pythia	1.2585	1.1800
200343	$Z \to \mu\mu \geq bb + \mathrm{N}p3$	AlpGen+Pythia	0.61808	1.1800
200348	$Z \to \tau\tau + bb + \mathrm{N}p0$	AlpGen+Pythia	6.5062	1.1800
200349	$Z \to \tau\tau + bb + \mathrm{N}p1$	AlpGen+Pythia	3.2935	1.1800
200350	$Z \to \tau\tau + bb + \mathrm{N}p2$	AlpGen+Pythia	1.2485	1.1800
200351	$Z \to \tau\tau \geq bb + \mathrm{N}p3$	AlpGen+Pythia	v0.61363	1.1800
200432	$Z \to ee + cc + \mathrm{N}p0$	AlpGen+Pythia	11.763	1.1800
200433	$Z \to ee + cc + \mathrm{N}p1$	AlpGen+Pythia	7.1249	1.1800
200434	$Z \to ee + cc + \mathrm{N}p2$	AlpGen+Pythia	3.3656	1.1800
200435	$Z \to ee + cc \geq \mathrm{N}p3$	AlpGen+Pythia	1.7010	1.1800
200440	$Z \to \mu\mu + cc + \mathrm{N}p0$	AlpGen+Pythia	11.795	1.1800
200441	$Z \to \mu\mu + cc + \mathrm{N}p1$	AlpGen+Pythia	7.1254	1.1800
200442	$Z \to \mu\mu + cc + \mathrm{N}p2$	AlpGen+Pythia	3.3694	1.1800
200443	$Z \to \mu\mu + cc \geq \mathrm{N}p3$	AlpGen+Pythia	1.7003	1.1800
200448	$Z \to \tau\tau + cc + \mathrm{N}p0$	AlpGen+Pythia	11.760	1.1800
200449	$Z \to \tau\tau + cc + \mathrm{N}p1$	AlpGen+Pythia	7.1410	1.1800
200450	$Z \to \tau\tau + cc + \mathrm{N}p2$	AlpGen+Pythia	3.3582	1.1800
200451	$Z \to \tau\tau + cc \geq \mathrm{N}p3$	AlpGen+Pythia	1.7046	1.1800

Table 5.4 Z+jets heavy quark flavour samples. The matrix element calculation is done with ALPGEN while the parton showering is achieved with PYTHIA.

DSID	Brief description	ME+PS	σ [pb]	k-factor
147025	$W \to e\nu + \mathrm{N}p0$	AlpGen+Pythia	8127.3	330
147026	$W \to e\nu + \mathrm{N}p1$	AlpGen+Pythia	1792.7	330
147027	$W \to e\nu + \mathrm{N}p2$	AlpGen+Pythia	542.18	330
147028	$W \to e\nu + \mathrm{N}p3$	AlpGen+Pythia	147.65	330
147029	$W \to e\nu + \mathrm{N}p4$	AlpGen+Pythia	37.736	330
147030	$W \to e\nu + \mathrm{N}p5$ (incl.)	AlpGen+Pythia	11.962	330
147033	$W \to \mu\nu + \mathrm{N}p0$	AlpGen+Pythia	8127.1	330
147034	$W \to \mu\nu + \mathrm{N}p1$	AlpGen+Pythia	1792.9	330
147035	$W \to \mu\nu + \mathrm{N}p2$	AlpGen+Pythia	542.24	330
147036	$W \to \mu\nu + \mathrm{N}p3$	AlpGen+Pythia	547.66	330
147037	$W \to \mu\nu + \mathrm{N}p4$	AlpGen+Pythia	37.745	330
147038	$W \to \mu\nu + \mathrm{N}p5$ (incl.)	AlpGen+Pythia	11.970	330
147041	$W \to \tau\nu + \mathrm{N}p0$	AlpGen+Pythia	8127.1	330
147042	$W \to \tau\nu + \mathrm{N}p1$	AlpGen+Pythia	1792.2	330
147043	$W \to \tau\nu + \mathrm{N}p2$	AlpGen+Pythia	542.27	330
147044	$W \to \tau\nu + \mathrm{N}p3$	AlpGen+Pythia	147.64	330
147045	$W \to \tau\nu + \mathrm{N}p4$	AlpGen+Pythia	37.781	330
147046	$W \to \tau\nu + \mathrm{N}p5$ (incl.)	AlpGen+Pythia	11.959	330

Table 5.5 W+jets light flavour sample with up to variable number of partons. The matrix element calculation is done with ALPGEN while the parton showering is done with PYTHIA.

DSID	Brief description	ME+PS	σ [pb]	k-factor
110801	$W + bb + \mathrm{N}p0$	AlpGen+Pythia	52.255	330
110802	$W + bb + \mathrm{N}p1$	AlpGen+Pythia	45.540	330
110803	$W + bb + \mathrm{N}p2$	AlpGen+Pythia	23.671	330
110804	$W + bb + \mathrm{N}p3$	AlpGen+Pythia	12.525	330
126601	$W + c + \mathrm{N}p0$	AlpGen+Pythia	758.93	1.5200
126602	$W + c + \mathrm{N}p1$	AlpGen+Pythia	274.24	1.5200
126603	$W + c + \mathrm{N}p2$	AlpGen+Pythia	71.634	1.5200
126604	$W + c + \mathrm{N}p3$	AlpGen+Pythia	16.425	1.5200
126605	$W + c + \mathrm{N}p4$	AlpGen+Pythia	4.7468	1.5200
126606	$W + cc + \mathrm{N}p0$	AlpGen+Pythia	143.07	1.1330
126607	$W + cc + \mathrm{N}p1$	AlpGen+Pythia	143.68	1.1330
126608	$W + cc + \mathrm{N}p2$	AlpGen+Pythia	80.762	1.1330
126609	$W + cc + \mathrm{N}p3$	AlpGen+Pythia	35.932	1.1330

Table 5.6 W+jets heavy flavour sample with up to variable number of partons. The matrix element calculation is done with ALPGEN while the parton showering is done with PYTHIA.

DSID	Process	ME+PS	σ [pb]	k-factor
110101	t-channel (lept.)	AcerMC+Pythia	25.750	1.1042
110119	s-channel (lept.)	POWHEG+PYTHIA	1.6424	1.1067
110140	W_t-channel (incl.)	POWHEG+PYTHIA	20.46	1.0933

Table 5.7 The single top quark production is simulated using AcerMC for the t-channel and POWHEG for the s-channel and the W_t production mechanism. The PYTHIA parton showering has been used for all channels.

momentum due to two neutrinos. The definition of the selected objects followed the top working group recommendation for 2012 data [148, 149].

5.6.1 Primary vertex reconstruction

In the challenging environment of the Large Hadron Collider at CERN, efficient reconstruction of the primary vertex is vital for many physics analyses. The interaction point (IP) is the point where collisions of protons take place. The primary vertex is the spatial location where two particles in a colliding beam interact with each other. It is reconstructed from charged particle tracks that originate from the hard collision event. In 2012, the LHC was operated at $\sqrt{s} = 8$ TeV in a mode with a mean of 40 inelastic pp collisions per bunch crossing (pile-up). The pile-up contribution needs to be disentangled to look at the individual pp collision of interest. While pile-up has no significant impact on tracking or the identification of electrons and muons, it can have a sizeable effect on the reconstruction of jets. The primary vertex of the event is distinguished from the pile-up vertices, which are the vertices from proton–proton collisions in the bunch crossing that are not from the hard interactions, and secondary vertices which are formed from particles in the hard collision which travel a measurable distance away from the primary vertex before they decay. For this analysis, one reconstructed primary vertex with a mean of at least 5 tracks, each with $p_T > 0.4$ GeV is needed.

5.7 Electrons

The energy of the electron is completely deposited in the electromagnetic calorimeter with little or no energy in the hadronic calorimeter. Electrons are reconstructed [89] from the energy deposited in the electromagnetic calorimeter using a sliding window algorithm [150]. The calorimeter has been divided into $\Delta\eta \times \Delta\phi = 0.025 \times 0.025$ patches and any 3×5 window of these patches which has a combined energy greater than 2.5 GeV has been selected as an electron seed cluster. The shape of the clusters in the different layers of the electromagnetic calorimeter is narrow for electrons compared to jets. Three sets of reference selection criteria labelled "loose", "medium" and "tight++" are designed for the selection of electrons. The selection of loose electrons is based on the partial information obtained from the calorimeters. A collection of requirements is implemented on the calorimeter electromagnetic shower shape. These requirements have a high efficiency but poor discrimination between the signal and background. The medium selection needs additional cuts in order to be able to reduce the background from decays like $\pi^0 \to \gamma\gamma$.

In order to be able to distinguish isolated electrons from the jets from the electron candidates that are reconstructed by the above procedure, “tight++” [151] requirements have been imposed. These include stringent selection cuts on the calorimeter, tracking and

combined variables. The tight selection makes full use of the particle identification tools available for the electron identification. In addition to the generally tighter requirements on medium selection discriminating variables, stricter requirements on track quality in the presence of a track extension in the TRT detector, on the ratio of the EM cluster energy to the track momentum, and a veto on reconstructed photon conversion vertices associated with the cluster [152] are applied. Overall, a rejection power higher by a factor of two is achieved with respect to the medium selection. The loose, medium, and tight identification criteria naturally excludes a large fraction of the candidates with additional close-by activity, such as electrons within jets. The electrons are selected with the following requirements:

- The final electron momentum measurement can be made from tracking or calorimeter information (or a combination of both). The electrons are required to have a transverse momentum of at least 25 GeV and $|\eta| < 2.47$, excluding the barrel/end-cap transition region of $1.37 < |\eta_{cl}| < 1.52$, in which the energy of the electron is not well reconstructed.

- The electrons of interest are isolated - require little calorimeter energy or tracks close to the electron. The calorimeter isolation cuts with 90 % efficiency were applied on the energy sum around the direction of each selected electron calculated within a cone of radius ΔR = 0.2 ($E_T$cone20@90)[8] and a track isolation cut with 90 % efficiency was applied at a cone size of Δ R = 0.3 ($p_T$cone30@90)[9]. Absolute $E_T$cone20@90 and Absolute $p_T$cone30@90 were provided by the EisoTool2012 in the package egammaAnalysisUtils-00-03-99 [151].

- To prevent the double counting of jets as electrons, jets within $\Delta R < 0.2$ of the electron axis (electron-jet overlap removal) are removed.

- To clean the electron from the nearby jet activity, reject electrons within $\Delta R(e, jet) < 0.4$ after the electron-jet overlap removal (electron scale factors from egamma are valid for $\Delta R(e, jet) > 0.4$). There are many thousands more jets than electrons, so the rate of jets faking the electrons is required to be very small (10^{-4}).

5.8 Muons

The ATLAS experiment makes use of the information from the muon spectrometer (MS) and from the inner detector (ID) and, to a lower extent, from the calorimeter to fully identify

[8] This is a cut on E_TCone20 (an isolation variable) - the amount of calorimeter cell energy (in GeV) in an η cone of radius $R = 0.2$ around the electron (excluding the deposit from the electron itself). The actual cut varies with electron η and is set such that 90% of genuine electrons from W decays pass - hence the 90% name.

[9] This is cut on $p_T$cone (an isolation variable), this uses tracks in an η cone of R = 0.3 around the electron (excluding the electron track) and the 90% corresponds to a cut which is 90% efficient.

and precisely reconstruct the muons produced in the pp collisions. Muon identification is performed according to several reconstruction criteria (leading to different muon "types"), according to the available information from the ID, the MS, and the calorimeter sub-detector systems. The different types stated in the ATLAS muon reconstruction paper [153] are:

- Stand-Alone (SA) muon: In this type of muon, the trajectory is reconstructed only in the MS, no associated ID tracks. The estimated loss of energy of the muon in the calorimeters is taken into account and the tracks are extrapolated back to the interaction point to determine the parameters of the muon track. In general, a track measurement is provided by the muon after it has passed through at least two layers of the MS chambers. To get the maximal acceptance in the range of $2.5 < |\eta| < 2.47$ in the uncovered region of the ID, SA muons are mainly used;

- Combined (CB) muon: In the ID and MS, track reconstruction is performed separately. The combination of a MS track with an ID track produces a combined track. Their efficiency is driven by the MS geometry. CB muons have the best momentum resolution and are the main type of reconstructed muons;

- Segment-Tagged (ST) muon: Is the ID track identified as a muon if it is matched to at least one segment in the Monitored Drift Tube (MDT) or Cathode Strip Chambers (CSC). In cases where the muon traverses only one layer of the MS chamber, either due to having a low p_T or because it reaches the regions with a lower value of acceptance, then it can be used to increase the efficiency in poorly instrumented regions; and

- Calorimeter-Tagged (CaloTag) muon: If a track in the ID could be associated to a deposit of energy in the calorimeter that is compatible with a minimum ionizing particle then it is classified as a muon. CaloTag muons have the lowest purity however, they are able to recover acceptance in the unintrumented regions of the MS. The identification criteria for these muons is optimized for the muons having a momentum range between 25 and 100 GeV and a region of $|\eta| < 0.1$.

The muon candidates for the current analyses are reconstructed by using combined muons. Following the recent recommendations from the Muon Combined Performance (MCP) group, the selection of muon objects is based on the following requirements:

- The reconstructed muons have tracks in both the muon spectrometer (MS) and inner detector (ID).

- The detector acceptance of the ID and MS is required to have $|\eta| < 2.5$.

- To avoid the trigger turn-on curve, the transverse momentum p_T is > 25 GeV.
- The longitudinal impact parameter with respect to the primary vertex is required to be $z_o < 2$ mm.
- No requirement on the pixel b-layer hits has been made and TRT hit requirements have been made in the regions with $0.1 < |\eta| < 1.9$.
- To reduce the background from muons produced from heavy quark decays inside the jets, muons are required to be isolated by $\Delta R > 0.4$ from the nearest jet.
- The muons are required to satisfy the mini-isolation requirement for the 2012 dataset. This is similar to the fixed cone isolation but it uses a cone size which varies as a function of muon p_T and gives a better rejection of backgrounds from the muons inside jets. They are required to satisfy the mini-isolation requirement $I^l_{mini} < 0.05$, where the mini-isolation variable is the ratio of the sum of p_T of tracks in variable cone size $\Delta R = (10\ GeV)/(p_T(\mu))$ with respect to p_T of the muon, $p_T(\mu)$ [148].

5.9 Jets

High energy partons from hard-scattering processes fragment into hadrons that are collectively called "jets". They leave their energy deposits in the hadronic calorimeters and are grouped together by a jet algorithm. The main types are cone and k_t algorithms. The algorithm that the LHC experiments used is the anti-k_T algorithm [154] with a distance parameter of 0.4. The input energy deposits are "topocluster" (topological clusters) defined from the output of the detector [155]. A topocluster is a collection of neighbouring cells that are grouped together as a way of approximating the energy deposition of such a single particle. In the 2011 data, the energy of the cells in the topoclusters was measured at the electromagnetic scale. The EM scale is the detector response that was corrected assuming that the total energy response is due to electromagnetic showers and no jet area correction was applied. In 2012, jets were calibrated using the local cluster weighting (LCW) method and corrected for the pile-up using the jet area technique [156]. Further details on the jet algorithms are described in [157]. The jets used in this analysis also meet the following requirements:

- Reconstructed jets are removed if within $\Delta R < 0.2$ of a reconstructed electron, as mentioned in the requirements for electrons above.
- A transverse momentum greater than 25 GeV.
- Jet reconstructed efficiently using the calorimeter is required within $|\eta| < 2.5$.

- Another jet quality criteria is to check if the jet has not been produced by a real energy deposit, but instead from beam-gas interactions, cosmic rays or noise bursts in the calorimeter.

- Jets are required to pass quality criteria to reject so-called "bad jets".

Each bunch crossing includes a beam of protons in both the +z and -z directions. More than one interaction takes place that leads to a number of low momentum hadrons. This effect is referred to as pile-up and can have a significant impact in the analyses. Most of them come from “soft“ interactions and will produce minimum bias events. The pile-up can produce extra particles in the final state that could be treated as coming from the interaction of interest. If these low momentum hadrons happen to overlap with a region of interest, a jet can be reconstructed which is not fully or partly coming from the hard collisions of interest. In order to be able to reject these pile-up or low momentum jets [158], the jet vertex fraction (JVF)[10] algorithm has been developed. If all the tracks in the jet are associated with the primary vertex, a value of 1 is assigned to JVF. A value near 0 means that none of the tracks in the jet are associated with the primary vertex and the jet may come from the pile-up. The jets with no associated tracks or with $|\eta| > 2.4$ at the edge of tracker acceptance have a JVF value of -1. For this analysis, the |JVF| > 0.5 only for jets with $p_T \leq 50$ GeV and $|\eta| < 2.4$. It is seen from Figure 5.3 that the fraction of tracks originating from the primary vertex of jet1 is f, which can be calculated for each jet. If f is higher then the jet is correctly signed to that vertex. Cutting on this fraction allows for the soft primary jets to be differentiated from the pile-up or soft jets.

5.10 b-tagging

A b-tagging algorithm is an experimental tool used to identify b-jets. Many Standard Model processes, such as $t\bar{t}$, lead to the production of b-quarks in the final state. The top quark decays almost exclusively to a W boson and a b-quark, while the b-quark always turns into a jet. Identifying a b-jet is, therefore, not only important to select events which contain top quarks, but also separates them from the background due to u, d, c and s quarks. In order to be able to identify if a jet is a b-jet or another type of jet, many algorithms have been developed and used. The other jets are either called "c-jets" or "light-jets". When a c-quark hadronizes into a jet, it is a c-jet, while "light jets" are from the hadronization of u, d, and s quarks. The jets initiated from gluons also fall into the latter type. A b-jet contains B-hadrons. A B-hadron has a long lifetime, approximately 1.6 ps [159], which can

[10] JVF is the ratio of the sum of the transverse momentum of tracks associated to the jet and primary vertex to the sum of transverse momentum of all tracks associated with the jet.

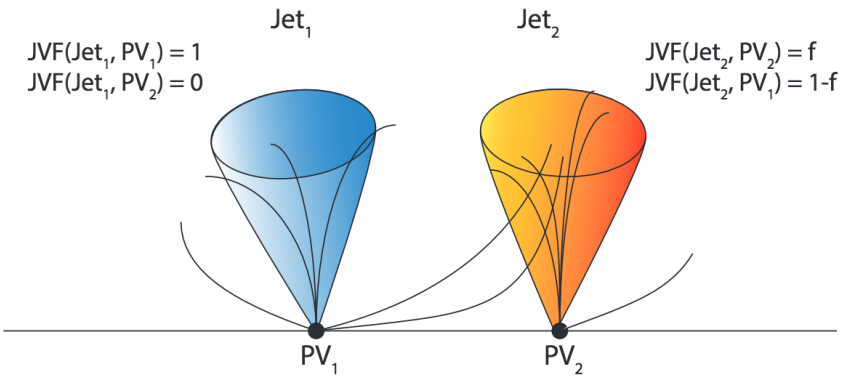

Fig. 5.3 Sketch describing the JVF variable. It shows that for jet1 all the tracks come from its primary vertex (PV1) and no tracks come from the primary vertex (PV2) of jet2. Jet2 shows a fraction f of tracks originated from the PV2 and another fraction 1-f comes from the PV1 [42].

be exploited to discriminate against light jets. The *B*-hadron travels some distance before decaying and can be identified from a reconstructed secondary vertex (SV) or the large impact parameter (the distance of the closest approach of the track to the primary vertex) of the charged tracks it decays into. So a jet which has a secondary vertex is much more likely to be a *b*-jet. The *B*-hadron can also be identified from the large mass ($\sim$5 GeV) and large branching ratio to decay into leptons. Due to their long life-time, a *B*-hadron has a mean lifetime $c\tau$ of approximately 480 - 500 μm.

This analysis contains at least two jets in which at least one is tagged by a *b*-tagging algorithm [160, 161]. The algorithms used to tag *b*-jets have a weight as an output, on which a cut needs to be applied. Several *b*-taggers are available in ATLAS but currently most top analyses use the MV1 algorithm, with 70% efficiency for real *b*-jets. For this analysis, *b*-tagging is performed using the neural network-based algorithm, which combines the outputs of the SV1, IP3D and JetFitterCombNN algorithms [162] into a multivariate discriminant having values between 0 and 1. A value of 1 has been assigned to the *b*-flavoured jets; light quarks and gluons have a value close to 0. For the charm quark it lies between 0 and 1. JetFitter makes use of the topology of the weak decays of the *b*-hadrons and *c*-hadrons in the jet, defining with a Kalman Filter a common line on which the primary vertex and the hadron decay vertices lie. The algorithm also supplies their position on this line, giving an approximated flight path for the *b*-hadron. The IP3D tagger does not construct decay vertices or flight paths, but uses the significance of the tracks' impact parameters in the longitudinal and transverse plane, to calculate a likelihood probability for a jet to originate

from a *b*-quark. The SV1 algorithm looks for secondary vertices due to a *b*-quark decay. The secondary vertex is found by minimizing a χ^2, based on the one-dimensional distribution of the invariant masses of the tracks, on the ratio between the sum of the energies of the vertex tracks and the sum of the energies of the jet. These three taggers are combined and the p_T and η of the jet are also used as input to MV1. The jets are *b*-tagged if the MV1 weight is larger than 0.7892 [163], corresponding to 70% *b*-tagging efficiency for *b*-jets in $t\bar{t}$ events over a wide range of transverse momenta. Scale factors need to be applied to tagged jets in the MC simulations to properly model the data.

5.11 Missing Transverse Energy

Particles which do not leave a signature in the ATLAS detector, such as neutrinos, can be reconstructed indirectly by applying the laws of momentum conservation. Although full momentum conservation cannot be used due to the unknown initial state of pp collisions, the conservation on the transverse plane applies, since the total transverse momentum before the collision is equal to the total transverse momentum after the collision. From this, the momentum imbalance can be evaluated and it is referred to as missing transverse momentum. Missing momentum (energy) is not a good quantity in the regime of the hadron collider as energy from the proton remnants is lost near the beam-pipe.

The dilepton decays are of the ee, eμ and $\mu\mu$ channels. The requirements in each channel follow the recommendation from the ATLAS top group. To suppress the backgrounds from Drell-Yan and multi-jet process in the ee and $\mu\mu$ channels, the missing transverse cut is required.

No requirements were made on the magnitude of the missing transverse momentum ($E_T{}^{miss}$) for the eμ channel; instead a cut on the scalar sum of the two selected leptons and jet transverse momenta (H_T) has been applied. The missing transverse energy is not easy to measure due to a bias caused by electronic noise and particles ending up in cracks and dead calorimeter cells. Corrections are needed for the calorimeter missing transverse energy due to: correction for muons (muons are minimum ionising particles), and known leakage effects like cracks and particle type dependence. Each calorimeter cell contributes to this energy according to the final calibration of the reconstructed objects (electron, muon, jet) and a correction for the impact of pile-up. The E_T^{miss} is evaluated through a clustering approach [164].

$$E_T^{miss} = \sqrt{(E_x^{miss})^2 + (E_y^{miss})^2} \tag{5.1}$$

$$E_x^{miss} = -\sum_{i=1}^{N_{cells}} E_i \sin\theta_i \cos\phi_i \quad \text{and} \quad E_y^{miss} = -\sum_{i=1}^{N_{cells}} E_i \sin\theta_i \sin\phi_i$$

The E_T^{miss} is evaluated using the contribution from the topological clusters, transverse energy corrected for energy losses in the cryostat system, and reconstructed muons:

$$E_{x,y}^{miss} = E_{x,y}^{calo} + E_{x,y}^{cryo} + E_{x,y}^{muon} \tag{5.2}$$

The cryostat term $E_{x,y}^{cryo}$ [164] takes into account the non-negligible loss of energy in x,y hadronic showers due to the cryostat system installed between the Liquid Argon electromagnetic calorimeter and tile hadronic calorimeter, and is computed through the energy correlation between the last Liquid Argon calorimeter layer and the first tile calorimeter layer. $E_{x,y}^{muon}$ is the contribution to E_T^{miss} from the energy lost by muons in the calorimeter. It is calculated from the information on muons extracted from the Inner Detector and Muon spectrometer (according to the muon type used for the calculation).

The calorimeter term $E_{x,y}^{calo}$ is determined using cells belonging to the topological clusters and included in the pseudorapidity range $|\eta| < 4.9$. The values of $E_{x,y}^{calo}$ are obtained after a refined calibration of every topological cluster to the electromagnetic scale. Every calorimeter cell is associated with a parent high-p_T object which has been reconstructed and identified in this order: electrons, photons, muons, hadronically decaying taus, *b*-jets and light jets. The link between cells and reconstructed objects is done through the use of an association map, which is filled starting from the identified objects (in the order which has been mentioned), moving back to their component clusters and back again to their cells. In order to avoid double counting in the E_T^{miss} calculation, if a cell belongs to several kinds of reconstructed objects, only the first association is taken into account in the map i.e. the overlap removal is performed at cell level. If a cell belongs to more than one object of the same kind, all associations are included in the map, but with geometrical weights which detail the shared energy between the topological clusters [165]. The calibrated $E_{x,y}^{calo}$ is then calculated from different calorimeter energy deposits as follows:

$$E_{x,y}^{calo} = -(E_{x,y}^{ele} + E_{x,y}^{photons} + E_{x,y}^{muons} + E_{x,y}^{taus} + E_{x,y}^{bjets} + E_{x,y}^{jets} + E_{x,y}^{cellout}{}^{11} \tag{5.3}$$

where the $E_{x,y}^{cellout}$ term [166, 167] includes the remaining energy from cells which are not associated with high-p_T objects. It is calibrated at the electromagnetic scale. The missing transverse energy is often not due to the presence of a neutrino: there are also effects relevant to the energy resolution (especially in some transition regions between different detectors), the electric noise of the calorimeter and muon spectrometer, which multiplies the value of the missing energy, and errors in the muon reconstruction, due to fake muons and non-detected muon in the region of smaller coverage ($\eta = 0$ and $|\eta| > 2.7$). The main contribution to

[11] Cells outside physics objects.

the fake missing energy is caused due to measurements in the calorimeters, where there are transition regions with lower resolution, in particular for $1.3 < |\eta| < 1.6$ and $3.1 < |\eta| < 3.3$.

5.12 Event-level selection

The dilepton $t\bar{t}$ final state is characterized by two relatively high p_T isolated leptons (ee, $\mu\mu$, eμ), at least two jets and missing transverse momentum arising from the two undetected neutrinos. The taus are not included in the analysis, however, the leptonic decays of taus have been taken into account. To select an event satisfying the signature of dilepton final states in ee, $\mu\mu$ and eμ channels, a series of requirements on the reconstructed objects have to be applied i.e. electrons, muons and jets according to the object definitions on the TopCommonObject page [149]. The event selection criteria are listed below.

C1 - All events: Total number of events in the sample.

C2 - Number of events without corrupted events: Corrupted data events are removed

C3 - After GRL for data/truth MC cut: For real data, this cut ensures that high-quality data for the desired final state is present (i.e. with all sub-detectors required for: reconstruction of electrons, muons, missing energy, b-tagging etc.). On the other hand, a truth MC cut is applied on simulated samples, requiring two true isolated leptons, originating from either an on-shell W or from a tau-lepton decay.

C4 - Pass trigger: The events selected need to pass a single lepton trigger (e or μ). The electron trigger is required for the ee channel, the muon trigger is required for the $\mu\mu$ channel and for the $e\mu$ channel, either of the triggers is required.

C5 - Cosmic rejection: Events containing cosmic muons are discarded. The cosmic muons are identified as pairs satisfying the following requirements:

- $\Delta\phi > 3.10$ radian between the two muons (back-to-back in $\eta - \phi$) plane
- Opposite sign d_0 (the impact parameter d_0 is calculated with respect to the primary vertex)
- Both $|d_0| > 0.5$ mm

C6 - At least one charged lepton: Electron $p_T > 25$ GeV, muon $p_T > 25$ GeV.

C7 - Primary vertex: The events should have at least one good vertex (a vertex through which at least five tracks are passing non-collision background rejection).

C8 - At least two charged leptons: Requires an event with at least one electron and one muon.

C9 - Trigger match: One of the reconstructed offline leptons matches the trigger lepton. To make sure that the event was triggered by the leptons used in the analysis, a match between

the triggered leptons and offline reconstructed leptons is required. The offline reconstructed leptons and triggered leptons have to be within $\Delta R < 0.15$ of one another.

C10 - $e\mu$ overlap:
If the offline reconstructed electrons and muons share the same track then to avoid inconsistencies and double counting, the event is rejected. For the dilepton final state, the leptons must be oppositely charged. The decays of tops are back-to-back and the probability of overlap is very low but due to the possibility of a fake muon in the event, the distance between good electrons and muons in the $\eta - \phi$ plane is determined. This distance is calculated between the selected objects and, if it is less than $\Delta R < 0.005$, the events are discarded from the analysis.

C11 - Jet cleaning (for data only): No bad jets with $p_T > 20$ GeV
In order to avoid double counting, the jets and electron overlap removal is done before the jet cleaning cut. Jets overlapping with the reconstructed electron within $\Delta R < 0.2$ are not considered. Events are discarded if any jet with $p_T > 20$ GeV fails jet quality cuts i.e. jets originating from out-of-time activity (beam backgrounds) or from calorimeter noise. These jets are not physical objects and adversely affect the resolution of the missing transverse energy.

C12 - H_T: H_T ($e\mu$) >130 GeV

In the ee and $\mu\mu$ channel only, $E_T^{miss} > 60$ GeV has been used. The scalar sum of the transverse momenta of the two selected leptons and all selected jets is denoted by H_T. The cut on H_T is $H_T > 130$ GeV for the $e\mu$ channel.

C13 - At least one jet: Requires at least one good jet.

C14 - At least two jets: At least two jets with $p_T > 25$ GeV, $|\eta| < 2.5$ and $|JVF| > 0.5$

C15 - Exactly two leptons: Only keeps the events with have exactly two leptons.

C16 - Opposite sign leptons:
The two leptons in the event must have an opposite charge.

C17 - Invariant mass cut: Low mass cut: $M(ee, \mu\mu) > 15$ GeV
This cut is not applied to the $e\mu$ channel.

C18 - Z mass window cut : $|M(ee, \mu\mu) - 91|$ GeV > 10 GeV
The $e\mu$ channel is not affected by this cut.

C19 - Lepton truth matching: Both leptons match the truth leptons
The reconstructed leptons are matched with the MC truth leptons obtained in the MC truth cut (C3). The C19 truth match cut ensures that the selected leptons at reconstruction level actually match the MC truth leptons, i.e. the correct selection of the leptons has been made. Events lost at C19 are true dilepton events where one of the reconstructed leptons is fake, so, the real true lepton is missed.

C20 - At least one b-tag jet:
At least one b-jet must be identified using the MV1 tagger at the 70% efficiency working point.

These event-level selections are applied on the MC and data samples and after these selections, the cross-sections are measured from various lepton kinematic distributions discussed in Chapter 8.

5.13 Semileptonic events passing the selection

As has been mentioned before, it is not impossible that - in real data - some semileptonic $t\bar{t}$ events with a mis-identified lepton, may pass the dilepton event selection. (Recall that, in the MC, such events are explicitly removed via cuts on truth information; see cuts C3 and C19.) In this section we determine the size of this potential contamination, and justify why it was ignored. The analysis has been re-run to calculate the contribution of semileptonic (fake lepton background) events in the full MC signal sample (containing dilepton and semileptonic $t\bar{t}$ events). It is found that 20 semileptonic events pass the full dilepton selection. If the MC sample is normalised correctly, this will give a prediction for the number of semileptonic events that could pass the full selection on data. The number of events in the full MC signal sample is 40 M. The cross-section for this sample (POWHEG+PYTHIA with DSID 117050) is 252.9 $\times$ 0.543 = 137.3 pb (total $t\bar{t}$ production cross-section at 8 TeV multiplied by the fraction which is not all-hadronic). The effective integrated luminosity of this MC sample is obtained by dividing the size of the sample by the corresponding cross-section: $\frac{40\,\mathrm{M}\,events}{137.3\,\mathrm{pb}} = 291.3\,\mathrm{fb}^{-1}$. This is 14.4 times larger than the integrated luminosity of the data set used (20.3 fb^{-1}). Hence 20 events passing the full selection in MC would correspond to 20/14.4 =1.4 events in data. The number of events relative to the 23194 (see Table 8.1) selected in data is 1.4/23194 = 6 $\times$ 10^{-5}. From this calculation, it is concluded that the contribution from semileptonic events is entirely negligible.

Chapter 6

Data and MC comparison

6.1 Introduction

In the Standard Model, a top quark decays almost exclusively to a W boson and b-quark. Therefore, the final state of $t\bar{t}$ is categorised with the decay of W bosons, as described in Section 2.4.6. The final state is determined by the decay of two W bosons since b-quarks hadronise into B-hadrons. Figure 6.1 shows the decay of a $t\bar{t}$ pair. W bosons decay into a pair of quarks or leptons plus neutrinos. W bosons decay hadronically into $u\bar{d}$ and $c\bar{s}$ i.e.
$W \rightarrow u + \bar{d}$
$W \rightarrow c + \bar{s}$
Because quarks come in three colours, there are three distinct channels corresponding to each decay:
$u(blue)$+$\bar{d}(anti\text{-}blue)$
$u(red)$+$\bar{d}(anti\text{-}red)$
$u(green)$+$\bar{d}(anti\text{-}green)$
$c(blue)$+$\bar{s}(anti\text{-}blue)$
$c(red)$+$\bar{s}(anti\text{-}red)$
$c(green)$+$\bar{s}(anti\text{-}green)$
The final states with other quark combinations are Cabibbo-suppressed. As a result, there are three leptonic (an electron, a muon and tau with corresponding flavours of neutrinos) and six hadronic states (9 in total) for W boson decay. The purely leptonic decay modes are listed below:

- $t\bar{t} \rightarrow W(\rightarrow e\nu)b + W(\rightarrow e\nu)b$

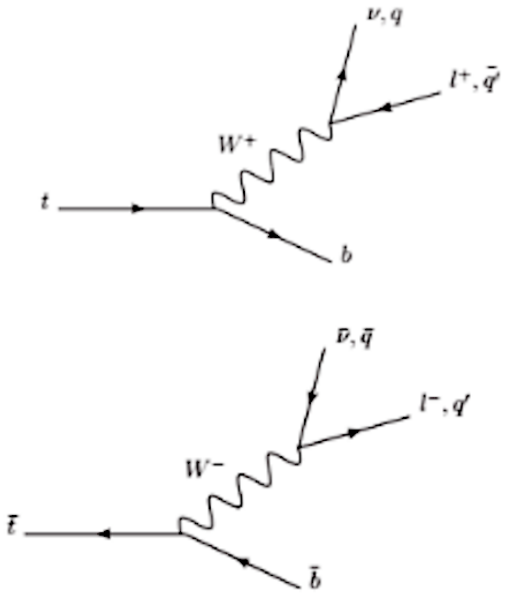

Fig. 6.1 Decay of top and anti-top pair.

- $t\bar{t} \to W(\to \tau(\to e\nu\nu)\nu)b + W(\to e\nu)b$
- $t\bar{t} \to W(\to \tau(\to e\nu\nu)\nu)b + W(\to \tau(\to e\nu\nu)\nu)b$
- $t\bar{t} \to W(\to \mu\nu)b + W(\to \mu\nu)b$
- $t\bar{t} \to W(\to \tau(\to \mu\nu\nu)\nu)b + W(\to \mu\nu)b$
- $t\bar{t} \to W(\to \tau(\to \mu\nu\nu)\nu)b + W(\to \tau(\to \mu\nu\nu)\nu)b$
- $t\bar{t} \to W(\to \mu\nu)b + W(\to e\nu)b$
- $t\bar{t} \to W(\to \tau(\to \mu\nu\nu)\nu)b + W(\to e\nu)b$
- $t\bar{t} \to W(\to \tau(\to e\nu\nu)\nu)b + W(\to \mu\nu)b$

- $t\bar{t} \to W(\to \tau(\to e\nu\nu)\nu)b + W(\to \tau(\to \mu\nu\nu)\nu)b$

The first three decay modes are the *ee* final states, the second three are the $\mu\mu$ final states and the last four decay modes are treated as signal for the $e\mu$ final states. The leptons that are a direct decay of W or leptonic decay of taus are included in the signal definition.

6.2 Cross-section measurement

A cross-section in particle physics, is a measure of the probability of an interaction and it is measured in barns (10^{-24} cm^2) which is a huge cross-section for most particle physics processes. The cross-section is defined by

$$\sigma = \frac{N}{L} \tag{6.1}$$

where N is the number of generated events due to process p, L is the integrated luminosity and σ is the cross-section of the process. The selection procedure applied to the events of process p does not reconstruct all the events of interest due to detector acceptance and inefficiencies. At the LHC, two protons interact to give rise to many processes to produce other types of events as well. The efficiency, ε, is the fraction of all the signal events that are reconstructed

$$\varepsilon = \frac{N_{passed}}{N_{total}} \tag{6.2}$$

where N_{passed} is the total number of events passing the selection and N_{total} is the total number of signal events.
The efficiency will be reduced as:

- It is hard to trigger objects at low p_T.
- It is hard to reconstruct an object at low p_T; and
- Identification and isolation cuts are applied.

In regard to the low p_T objects, while the detector can reconstruct them, the ratio of signal to background gets smaller at a low p_T, so the signal can get overwhelmed. This is particularly important for the trigger, where the trigger rate for a single electron and muon would be too high if the threshold is below 25 GeV or so. When the events are triggered, the reconstruction of electrons and muons with low p_T (down to 5 GeV or so) will mostly be from fakes or from heavy flavour hadrons (B-hadrons or charmed-hadrons) decays rather than from top or W decays. A process might have final state objects at all η, while the detector covers a fixed

range in η e.g. there is a restriction in the angular (η) coverage because most leptons from top quark decays tend to be within $|\eta| < 2$.
The efficiency refers to the detector effectiveness in finding objects which have passed through the detector. The fiducial acceptance refers to the phase space of the detector that is available for observations. It is the ratio of the events passing the fiducial cuts to the total number of events. The efficiency and acceptance are calculated from Monte Carlo and they are discussed in detail in Sections 6.9 and 8.6. The efficiency includes triggers, lepton identification and reconstruction efficiencies. This efficiency can be subdivided into:

1. trigger efficiency; and

2. reconstruction and pre-selection efficiency of objects.

To make a simple measurement of the fiducial cross-section, the equation used is as follows:

$$\sigma = \frac{N_{data} - N_{bkg}}{L\varepsilon} \tag{6.3}$$

where N_{data} is the number of events observed after selection (from the data), N_{bkg} is the number of background events that pass our selection and ε is the reconstruction efficiency which is evaluated and discussed in Section 6.8. The background is normally calculated using Monte Carlos (see Section 5.3.2 and Tables 5.3, 5.4, 5.5 and 5.6) except fake lepton estimation that can also be estimated with data-driven techniques. The fakes do not play a significant role in the backgrounds so they have not been discussed in this thesis. The background events are subtracted from the data sample to extract the signal. The POWHEG+PYTHIA simulated sample is used to find the efficiency and the background modelling is done for the channel of interest. The knowledge of luminosity is essential for the measurement of the cross-section, so the next section briefly discusses it. The fiducial differential cross-section along with the fiducial cuts is discussed further in Section 8.1.

6.3 Luminosity

Luminosity measurements are a necessary part of any experimental beam colliding program, since they provide the frequency of the interactions and are needed for normalization for the physics process under study. It is one of the vital parameters of an accelerator and it measures the capability of a particle accelerator to produce the desired number of interactions. It describes the number of collisions per cm^2 per second. The higher the value of luminosity, the larger the number of collisions. To calculate the number of collisions, the cross-section is required. Multiplying the luminosity of the beam by the cross-section for any process, such as $t\bar{t}$ production, the rate at which the process is going to happen can be determined. When

the luminosity is multiplied by the sum of the cross-sections for all possible processes, the total number of collisions can be obtained. The integrated luminosity of all data periods used for this analysis has been listed in Table 5.1.

6.4 Scale Factors

Before making a comparison between data and MC, the MC needs to be scaled according to the object of interest. This section briefly describes different scale factors/corrections that have already been computed and stored in the MC data format. These scale factors correct the MC to look more like the data, making the MC a better model of the performance of the real detector. Normally the scale factors (SF) are applied to MC, not to the data, so that the efficiencies may be derived from the corrected MC. In order to be able to compare cut-flow with the others, the SFs are always applied on MC. They are typically corrections to efficiencies (e.g. for identifying electrons or muons, or tagging b-jets), so when SFs are applied, it is just a change in the MC event weight. The final scale factor for an event is then the product of all the scale factors for different objects. There exist additional correction factors applied. For example, a change in the jet energy might be required, so the energies of all jets are multiplied by some factor (which perhaps depends on p_T and η), which might change which events pass the cuts. The reconstructed particle energies and resolutions (as opposed to efficiencies) are typically modelled in this way. For the individual scale factors:

- b-tag SF corrects for the efficiency of tagging b-jets, which is typically overestimated by a few percent in the MC compared to the data. The value depends on the number of true b-flavoured jets in the event (i.e. jets initiated by b-quarks) and whether they were tagged or not. There are also related scale factors dealing with the rates of mistagging light quarks, gluons or charm jets as b-jets.

- Electron SFs correct the efficiency to reconstruct and identify electrons, and whether they pass the top group isolation cuts.

- Trigger SFs deal with the modelling of events passing the trigger selections, typically electron and muon triggers. These are similar to the electron and muon SFs, but are applied differently, as it is typically only required that one object passes the trigger (e.g. one electron in a dielectron event), but if two electrons are required in the offline selection then the efficiency for both electrons needs to be corrected.

- Pile-up SF corrects the distribution of interactions per bunch crossing (the μ distribution as shown in Fig. 3.3) in the MC to be like that in the data. Efficiencies normally

depend slightly on the μ of the event, since if there is a higher than average number of additional superimposed pile-up interactions in the same bunch crossing, there will be more energy in the detector, changing some efficiencies such as isolation cuts. The MC is normally generated with an estimate of the data μ distribution, and these SFs correct the μ distribution to that observed in the data, by applying event weights as a function of μ.

- Similarly, the z-vertex SF corrects the distribution of the z-coordinates of the event primary vertex in the MC to be the same as that in the data. The data distribution depends on the LHC running conditions, and the electron efficiency is slightly lower for electrons coming from the edges of the z-vertex distribution (for example $\pm$12 cm from the origin) than those coming from the centre (z = 0), due to geometrical effects in the detector acceptance.

- Finally, the jet calibration refers to the process of correcting the raw jet energies (measured in data or MC) to the best estimates of the energies of jets defined at the truth (particle) level. These calibrations have to be applied to both the data and MC. The MC is processed several times with different calibrations, whose differences reflect the uncertainties in the calibration procedure, leading to a systematic error.

The distributions in data and MC agree very well after applying the scale factors to the objects of interest in this analysis as shown in the next section where control plots for different lepton kinematic variables have been shown.

6.5 Data and MC comparison

Having discussed background estimates and described the signal sample in Chapter 5, the object kinematics will be explored. To verify whether the physics objects and event variables used in this analysis are well defined by the MC simulation, a comparison between data and MC is carried out. In order to be able to compare the detector data with the simulated data, the luminosity of the MC is determined first. This information is used to scale the MC to the data in use. For example, if a real data set of 100 fb^{-1} is needed to be compared with a MC data set of 400 fb^{-1}, the MC has to be rescaled to a factor of $1/4$ to be able to make a direct comparison between them.

The luminosity needed for this purpose is usually an equivalent luminosity. To normalize the MC samples to a value of luminosity, a weight has been applied per event to this analysis using the formula:
$W_{norm} = \frac{L_{data}}{L_{MC}} = \frac{L_{data}}{N_{MC}\sigma_{MC}}$ where L_{data} is the integrated luminosity (20.3 fb^{-1}) of the data sample, N_{MC} is the number of generated events in the MC sample (retrieved from the monitoring

Cut	Description of cut	Number of events
C1	ALL	722298000
C2	CORRUPTEDEVT	722298000
C3	TRUDILEP/GRL	695481000
C4	TRIGGER	305276000
C5	NPV	302022130
C6	COSMICS	301612060
C7	>=1LEPT	90787700
C8	>=2LEPT	103200
C9	TRIGMATCH	57671
C10	E-MU OVER	57742
C11	JET CLEAN	57742
C12	MET/HT	40535
C13	>=1 JETS	38803
C14	>=2 JETS	29874
C15	EXACTLY 2 LEPT	29619
C16	OS	29213
C17	M>15	29200
C18	Z-Veto	29200
C19	TRUTHMATCH	29200
C20	1BTAG JET	23194

Table 6.1 Cut-flow for all data periods using $e\mu$ standard selection.

histogram or from the ATLAS Metadata Interface (AMI)) and σ_{MC} is the cross-section of the specific physics process modelled by the MC sample. The analysis code has the TopDataPreparation package with a file containing the *k*-factor values and the latest cross-sections at 8 TeV of all the samples used for the analysis. The *k*-factor is defined as:

$$k = \frac{\sigma_{t\bar{t}_{NLO}}}{\sigma_{t\bar{t}_{LO}}} \tag{6.4}$$

The MC samples are generated at leading order, with a lower value of cross-section. The cross-section of a process at Next-to-Next leading order is *k* times the cross-section at the leading order. After applying the luminosity normalization and overall event weight (the number obtained after multiplying all the SFs), the data and MC are plotted to make a comparison. The agreement between the data and prediction is shown in Figures 6.2, 6.3, 6.4, 6.5, 6.6, 6.7, they are in good agreement except at large values of H_T, p_T and E_T, in which the MC underestimates the data. All plotted variables have been defined, except for H_T, which is the scalar sum of p_T of electron, muon and jets in an event. The kinematic variables

Cut	Description of cut	Number of events
C1	ALL	4.99733×10^{07}
C2	CORRUPTEDEVT	4.99733×10^{07}
C3	TRUDILEP/GRL	2.98298×10^{06}
C4	TRIGGER	2.31868×10^{06}
C5	NPV	2.31704×10^{06}
C6	COSMICS	2.31704×10^{06}
C7	>=1LEPT	1.97763×10^{06}
C8	>=2LEPT	638667
C9	TRIGMATCH	638604
C10	E-MU OVER	638580
C11	JET CLEAN	637664
C12	MET/HT	612456
C13	>=1 JETS	606960
C14	>=2 JETS	502996
C15	EXACTLY 2 LEPT	502964
C16	OS	500244
C17	M>15	499727
C18	Z-Veto	499727
C19	TRUTHMATCH	499408
C20	1BTAG JET	423781

Table 6.2 Cut-flow for MC using $e\mu$ standard selection.

of selected objects in the $t\bar{t}$ dilepton channel have been studied to validate the modelling of the chosen MC in comparison to the detector data. The details of these objects have been described in Section 5.4 and they include jets, b-tagged jets, missing transverse energy, and leptons.

The lepton kinematic variables: leading lepton p_T, invariant mass of two reconstructed leptons m_{ll}, absolute $\Delta\phi_{ll}$ and absolute $\Delta\eta_{ll}$ have been picked for further analysis in order to measure the differential cross-section in the $e\mu$ channel. The data and MC agreement for these variables is shown in Figure 6.8. All events selected in the plots are in the signal region after all the event selection cuts which have been discussed in Section 5.5. The cut-flow tables for the data and MC are shown in Tables 6.1 and 6.2. These tables show the number of events surviving after each event-level cut described in detail in Section 5.9. From the stack plots, generally good agreement is seen between the data and the estimation within the systematic uncertainties which will be discussed in Chapter 7 and evaluated in Chapter 8.

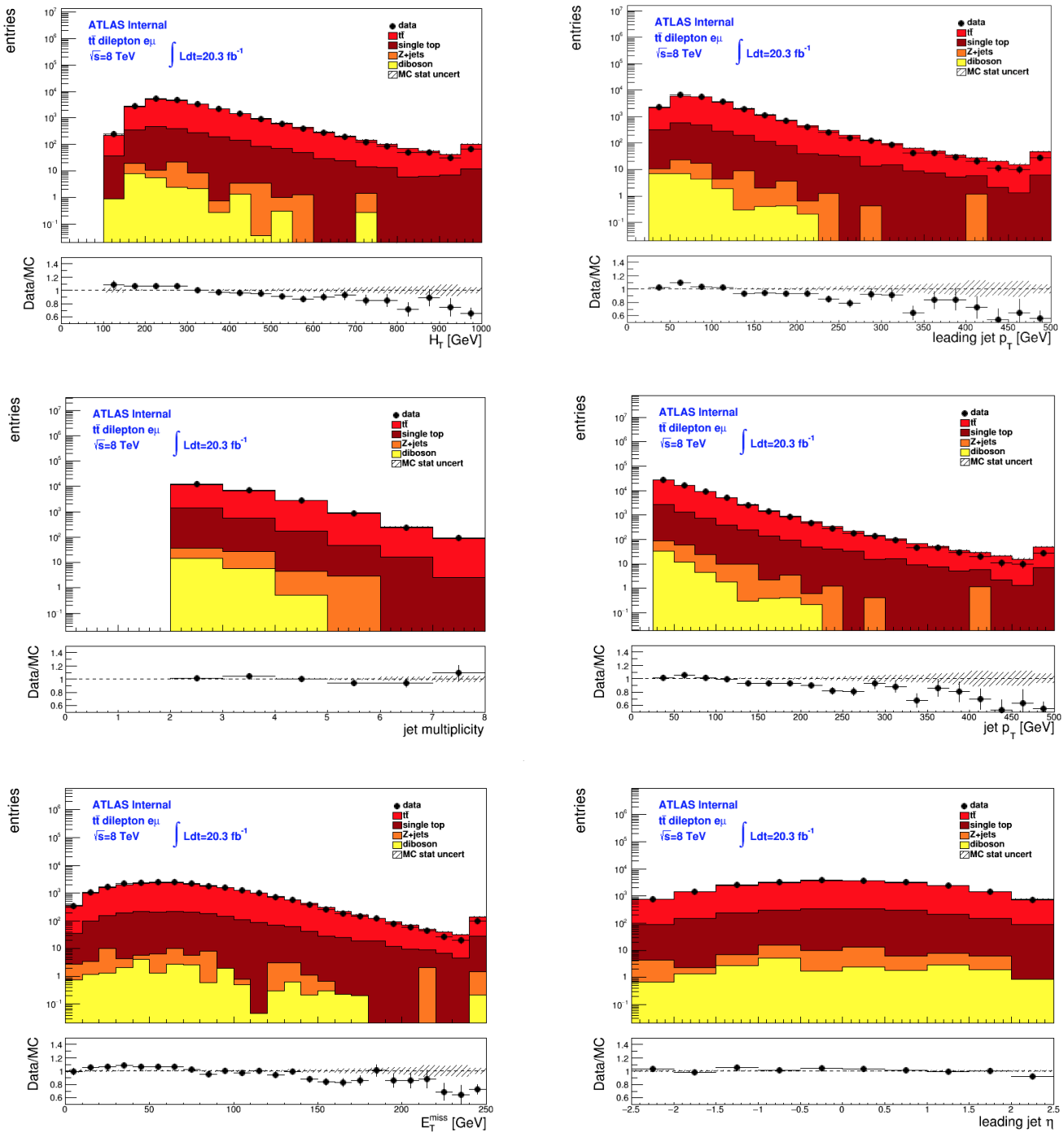

Fig. 6.2 Distribution of H_T, leading jet p_T, the number of jets, the p_T of the jet, missing transverse energy and the leading jet η in opposite sign $e\mu$ events with at least one b-tagged jet. The data is shown compared to the expectation from simulation, split into contributions from $t\bar{t}$, single top, Z+jets and dibosons normalized to the same number of events as in the data. The ratio plot of data to MC is shown in the lower parts, POWHEG+PYTHIA MC is used for the signal expectation and the errors shown here are just statistical. The hashed area in the ratio plot shows the MC statistical uncertainty.

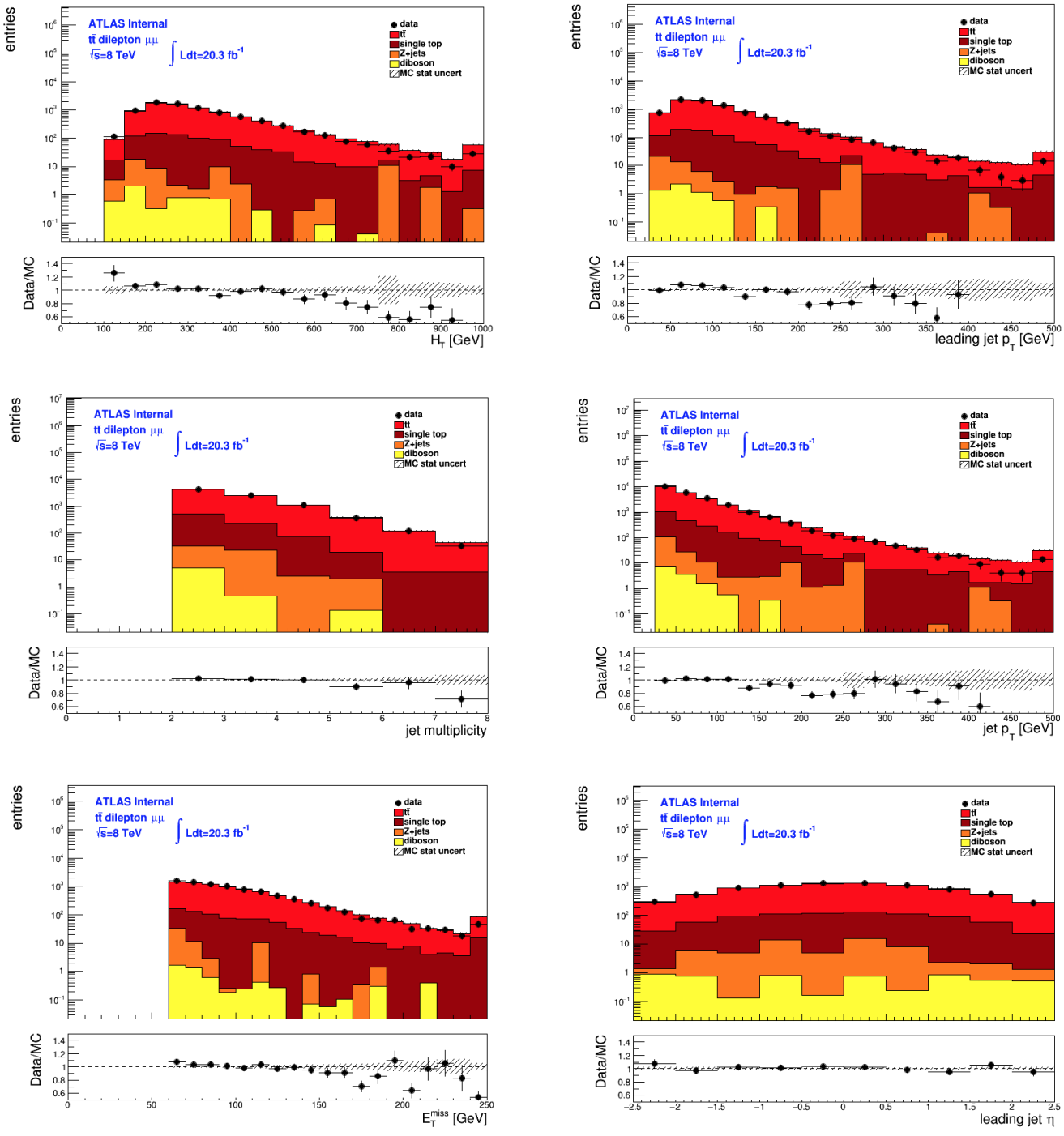

Fig. 6.3 Distribution of H_T, leading jet p_T, the number of jets, the p_T of the jet, missing transverse energy and the leading jet η in opposite sign $\mu\mu$ events with at least one b-tagged jet. The data is shown compared to the expectation from simulation, split into contribution from $t\bar{t}$, single top, Z+jets and dibosons normalized to the same number of events as in the data. The lower part shows the ratio plot of data to MC, POWHEG+PYTHIA MC is used for the signal expectation and the errors shown here are just statistical. The hashed area in the ratio plot shows the MC statistical uncertainty.

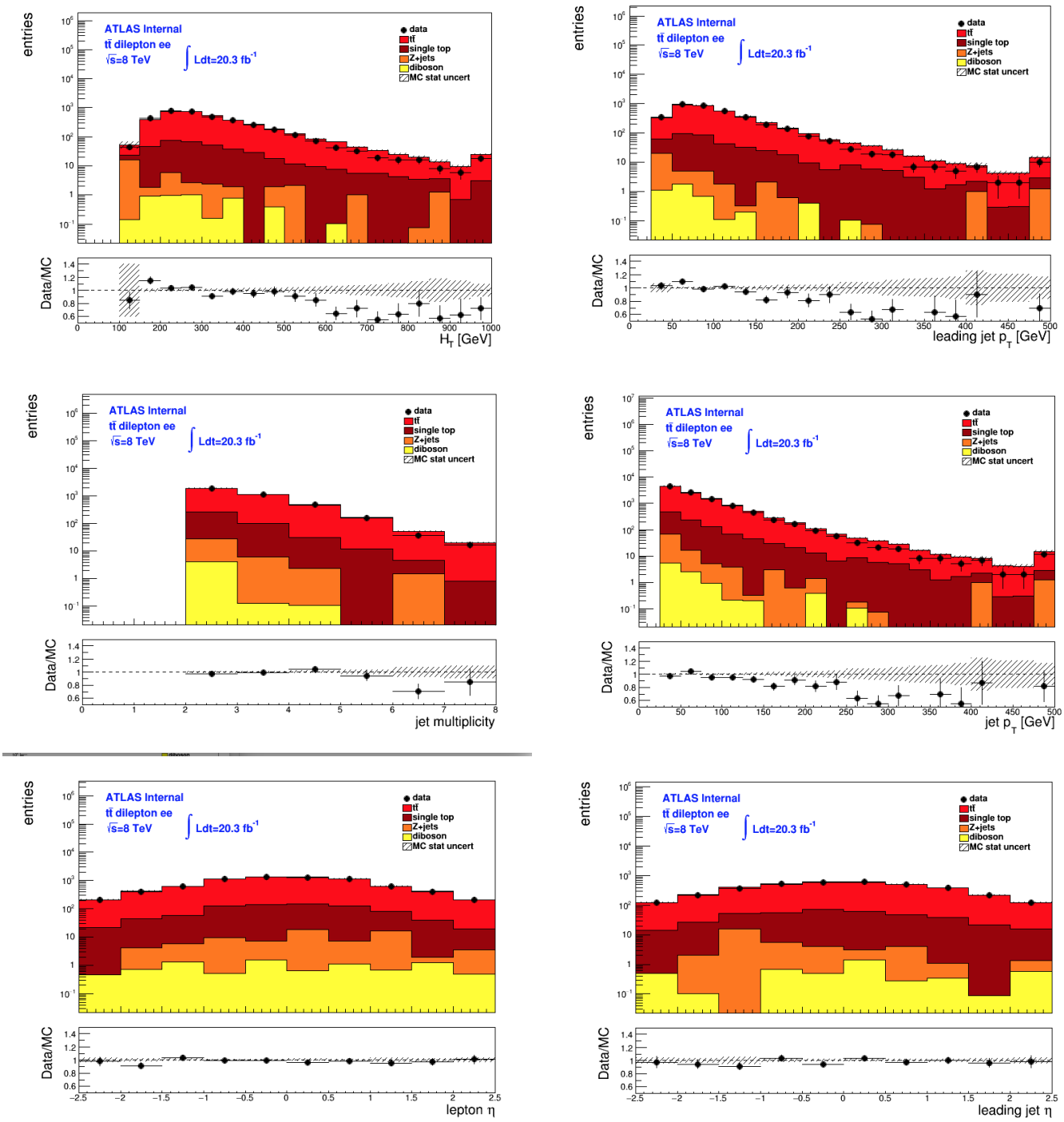

Fig. 6.4 Distribution of H_T, leading jet p_T, the number of jets, the p_T of the jet, lepton η and the leading jet η in opposite sign *ee* events with at least one *b*-tagged jet. The data is shown compared to the expectation from simulation, split into contributions from $t\bar{t}$, single top, Z+jets and dibosons normalized to the same number of events as in the data. The ratio plot of data to MC is shown in the lower parts, POWHEG+PYTHIA MC is used for the signal expectation and the errors shown here are just statistical. The hashed area in the ratio plot shows the MC statistical uncertainty.

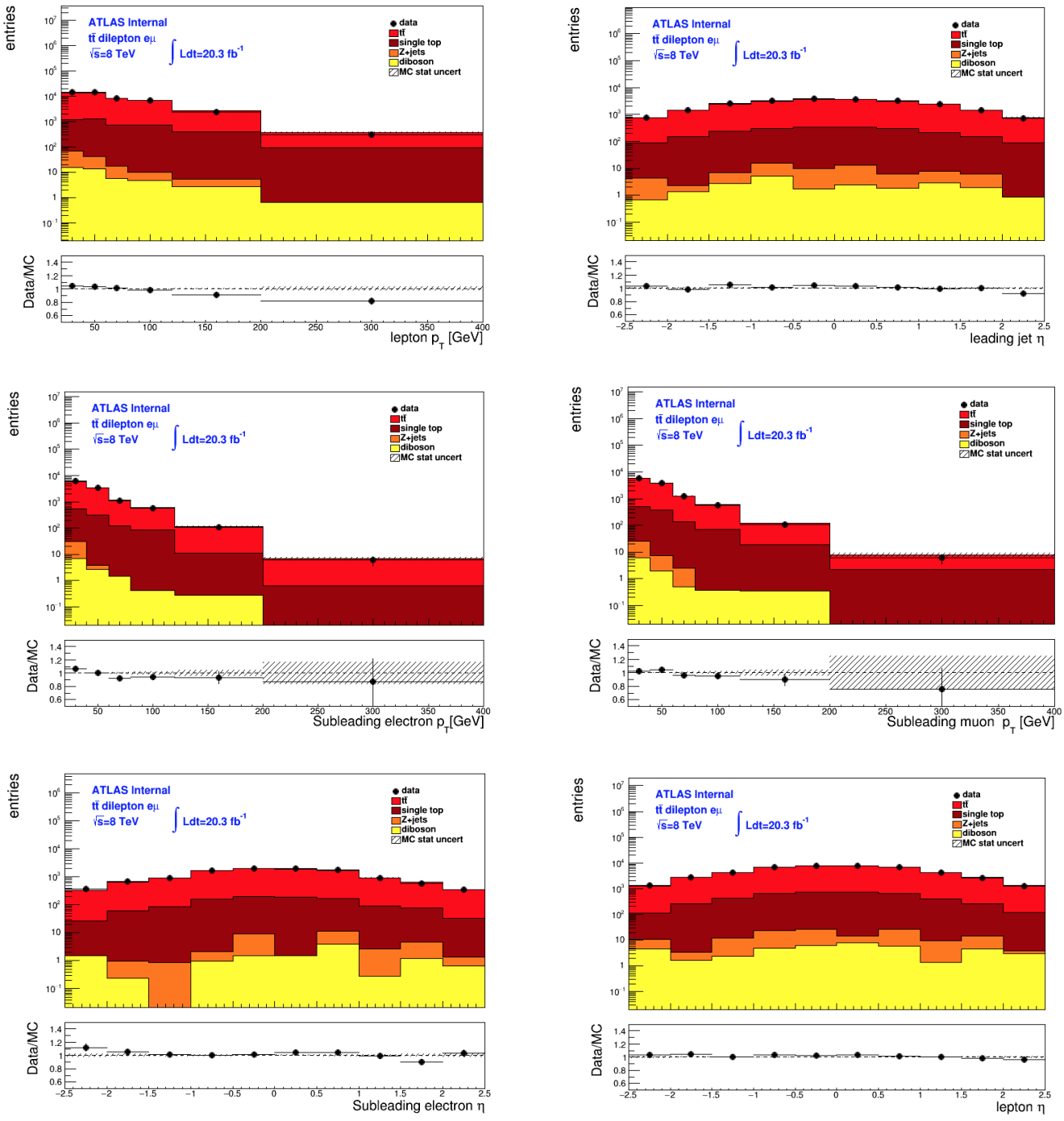

Fig. 6.5 Distribution of lepton p_T, leading jet η, the sub-leading electron p_T, the sub-leading muon p_T, the sub-leading electron η and lepton η in opposite sign $e\mu$ events with at least one b-tagged jet. The data is shown compared to the expectation from simulation, split into contribution from $t\bar{t}$, single top, Z+jets and dibosons normalized to the same number of events as in the data. The ratio plot of data to MC is shown in the lower parts, POWHEG + PYTHIA MC is used for the signal expectation and the errors shown here are just statistical. The hashed area in the ratio plot shows the MC statistical uncertainty.

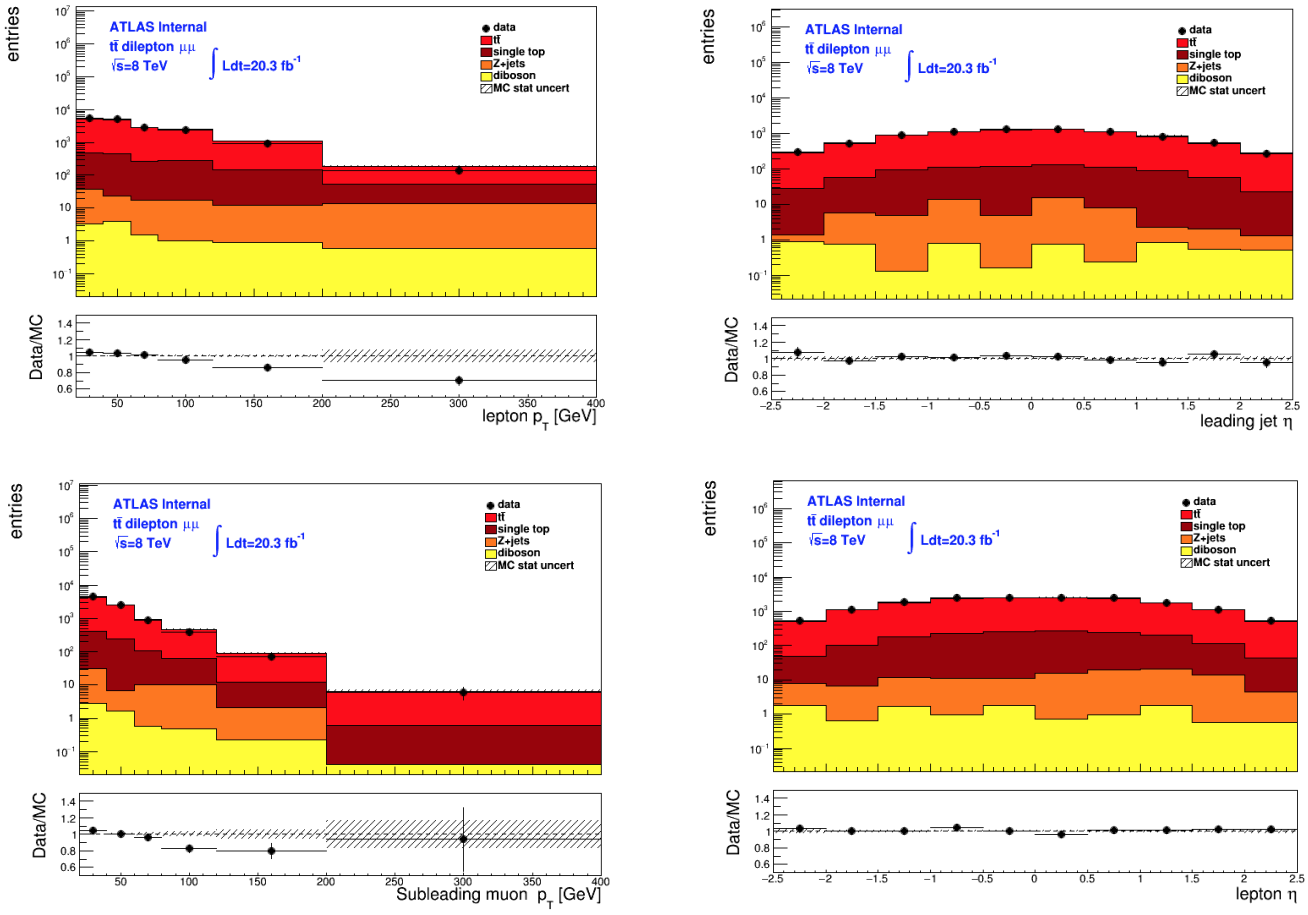

Fig. 6.6 Distribution of lepton p_T, leading jet η, the sub-leading muon p_T and lepton η in opposite sign $\mu\mu$ events with at least one b-tagged jet. The data is shown compared to the expectation from simulation, split into contributions from $t\bar{t}$, single top, Z+jets and dibosons normalized to the same number of events as in the data. The ratio plot of data to MC is shown in the lower parts, POWHEG + PYTHIA MC is used for the signal expectation and the errors shown here are just statistical. The hashed area in the ratio plot shows the MC statistical uncertainty.

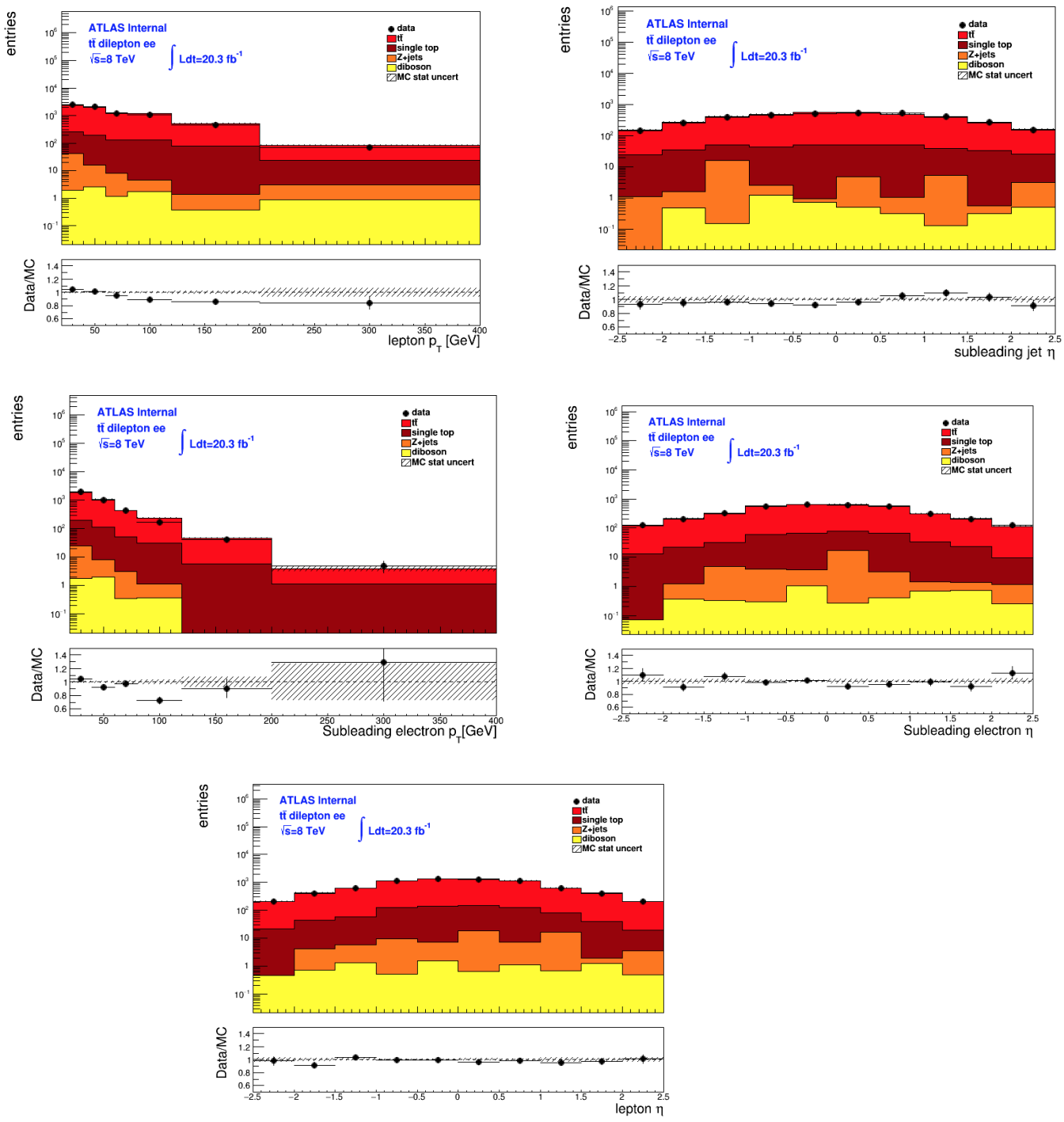

Fig. 6.7 Distribution of lepton p_T, sub-leading jet η, the sub-leading electron p_T, the sub-leading electron η and lepton η in opposite sign ee events with at least one b-tagged jet. The data is shown compared to the expectation from simulation, split into contributions from $t\bar{t}$, single top, Z+jets and dibosons normalized to the same number of events as in the data. The ratio plot of data to MC is shown in the lower parts, POWHEG + PYTHIA MC is used for the signal expectation and the errors shown here are just statistical. The hashed area in the ratio plot shows the MC statistical uncertainty.

6.6 Lepton kinematical variables of interest

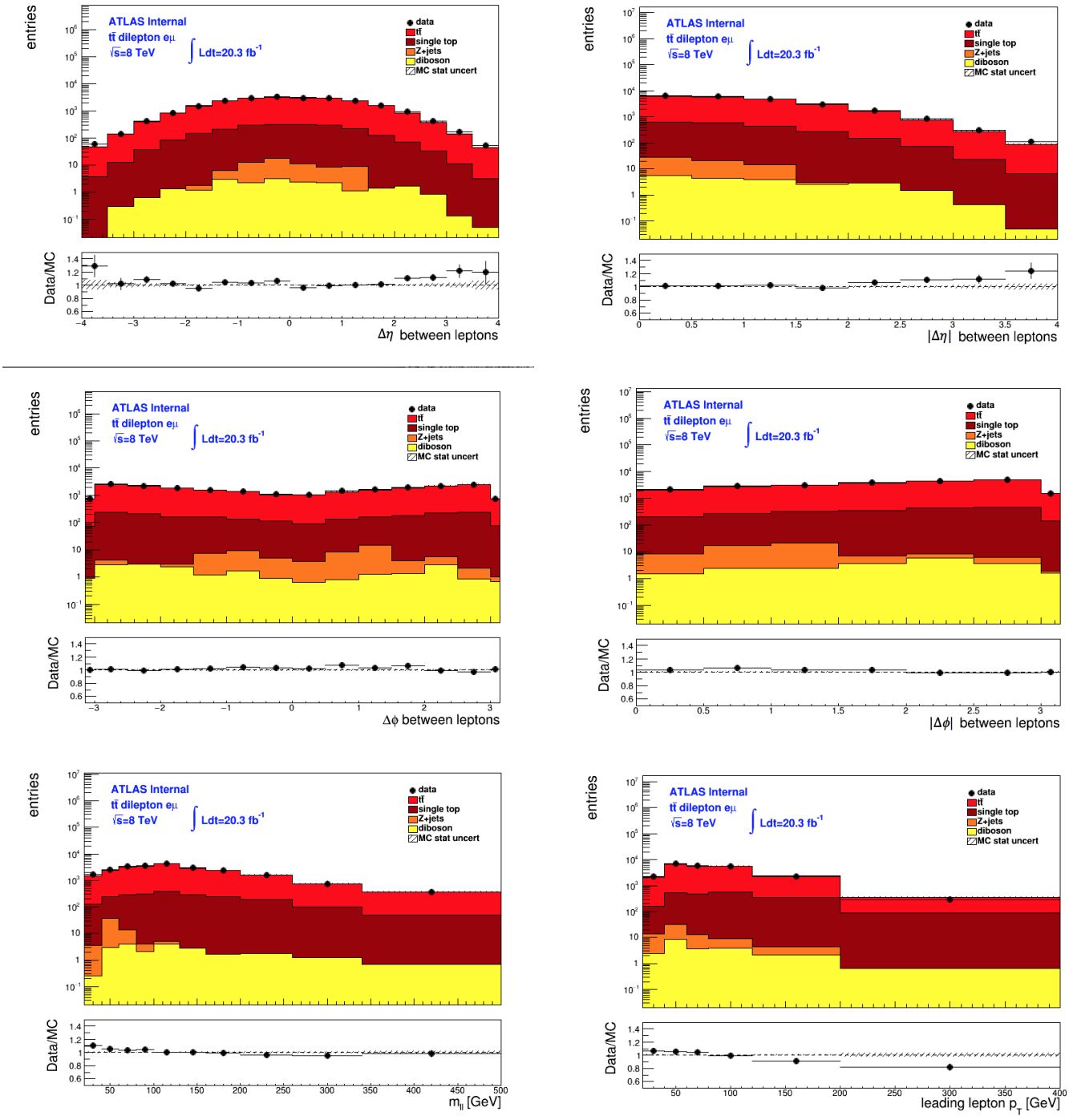

Fig. 6.8 Distribution of $\Delta\eta_{ll}$, the absolute $\Delta\eta_{ll}$, $\Delta\phi_{ll}$, absolute $\Delta\phi_{ll}$, invariant mass of reconstructed leptons m_{ll}, and the leading lepton p_T in opposite sign $e\mu$ events with at least one b-tagged jet. The data is shown compared to the expectation from simulation, split into contributions from $t\bar{t}$, single top, Z+jets and dibosons normalized to the same number of events as in the data. The ratio plot of data to MC is shown in the lower parts, POWHEG + PYTHIA MC is used for the signal expectation and the errors shown here are just statistical. The hashed area in the ratio plot shows the MC statistical uncertainty.

6.7 Resolution studies

The resolution for lepton kinematic variables has been studied and shown in order to be able to understand the quality of measurement as well as to test if it agrees with the resolution determined for the ATLAS detector. The absolute and relative resolutions have been studied for the electron p_T, muon p_T, leading lepton p_T, sub-leading lepton p_T, dilepton mass m_{ll}, signed and absolute azimuthal angle of dilepton and signed and absolute $\Delta\eta$ of the dilepton. To make these histograms, the root mean squared (RMS) of the reconstructed minus the simulated Monte Carlo truth has been taken. The electron (or muon) p_T resolution shown here is propagated from, or mainly determined by the calorimeter/tracking/muon spectrometer resolutions. A comparison of these resolutions is made with the detector

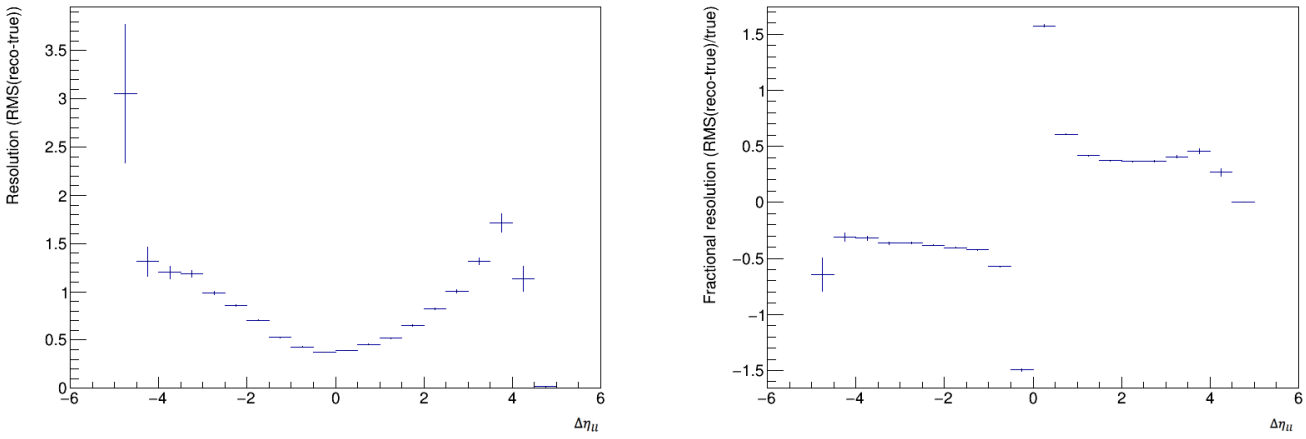

Fig. 6.9 Absolute and relative resolution of the dilepton $\Delta\eta_{ll}$.

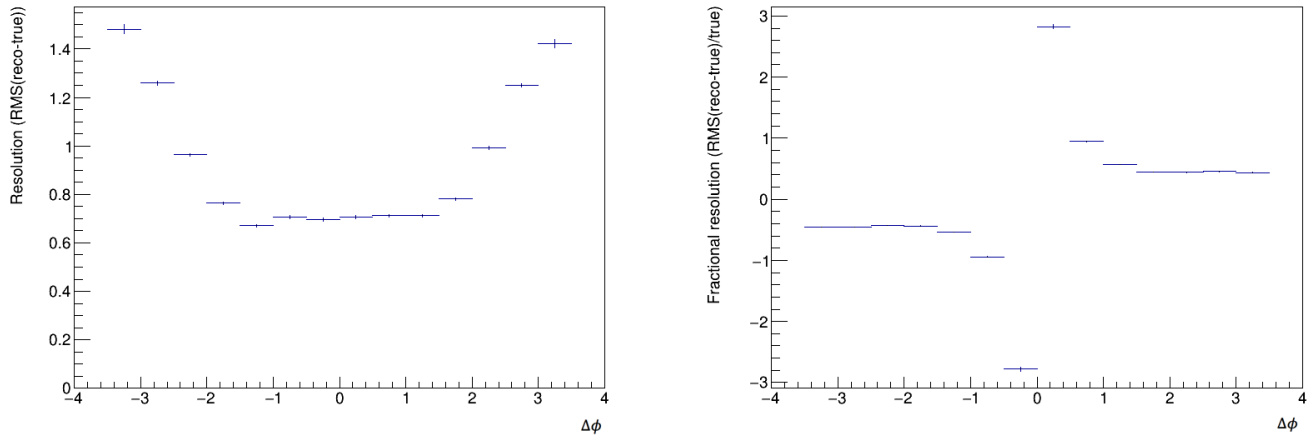

Fig. 6.10 Absolute and relative resolution of the dilepton $\Delta\phi_{ll}$.

documentation, they are in good agreement. The electron and muon under discussion are the decay products of $t\bar{t}$ so the detector resolutions are comparable to the ones here in the $t\bar{t}$ events. The resolution for the electron as a function of energy for electrons at absolute η = 0.1, 1.1, 2.0 has been given in Ref. [168], which is: 3.5% at 20 GeV to $\sim$ 1.5% at 200 GeV. The p_T resolution of the electrons is shown in Figure 6.12 and shows a decreasing trend from 5% at the cut-off p_T of 25 GeV to 1.7% at 200 GeV. For a stand-alone and combined muon (discussed in detail in Section 5.6), the fractional momentum resolution as a function of p_T with $|\eta| < 1.1$ is $\sim$ 2% at 20 GeV to 10% at 1000 GeV [169]. Expected stand-alone and combined fractional momentum resolution as a function of p_T for single muons [170] with absolute $\eta > 1.7$ increases from $\sim$ 4% at 20 GeV to $\sim$ 8% at 1000 GeV. The trends of both electron and muon p_T resolutions in this analysis are confirmed. In general, the resolutions are slightly worse in this analysis than those obtained in reference [171] because these events are from $t\bar{t}$ decays, while those measurements are from the better-known Z or J/ψ events. Absolute and relative resolutions for different kinematic variables of leptons are shown in Figures 6.9, 6.10, 6.11, 6.12, 6.13, 6.14, 6.15, 6.16, 6.17.

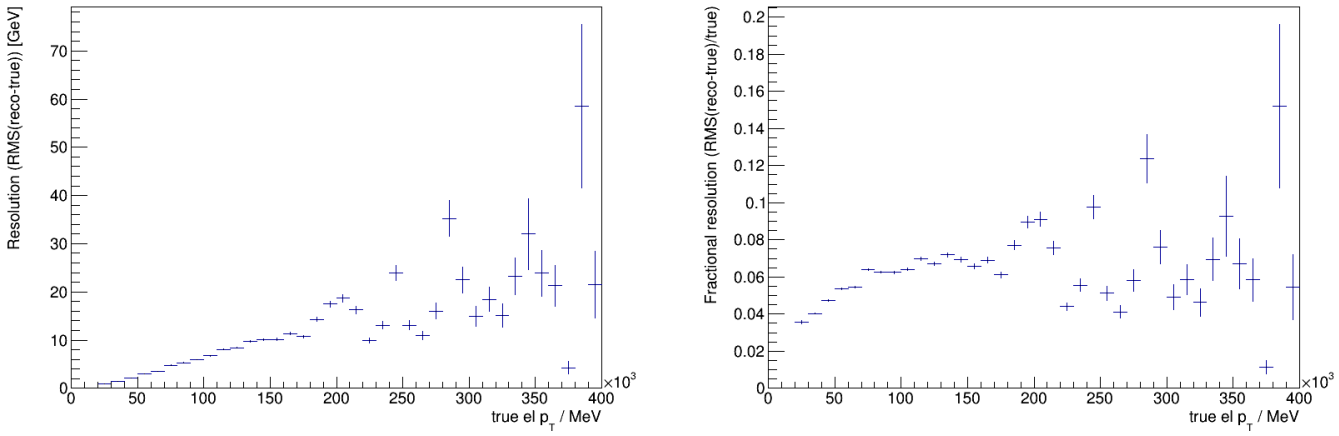

Fig. 6.11 Absolute and relative resolution of the leading lepton p_T.

6.8 Migration matrices

In high energy physics, experiments are usually performed as counting experiments, where events are binned in certain ranges of phase-space. The kinematic properties of each event, such as four-momentum of the particles and quantities derived from them, are measured only at a finite precision due to detector resolution. As a consequence, the events originally with a measured value land into other bins in a different range of values. Furthermore, there is

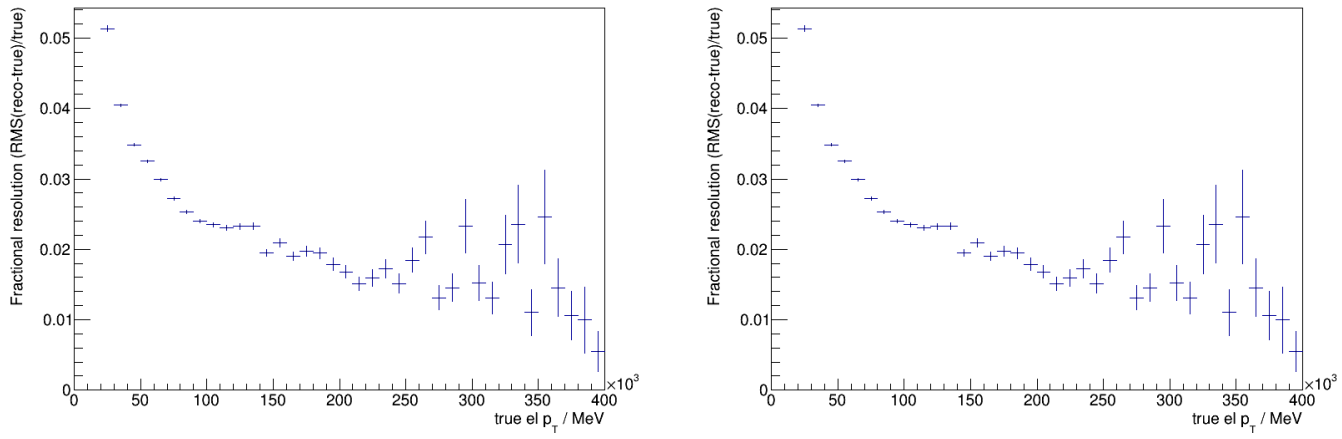

Fig. 6.12 Absolute and relative resolution of electron p_T.

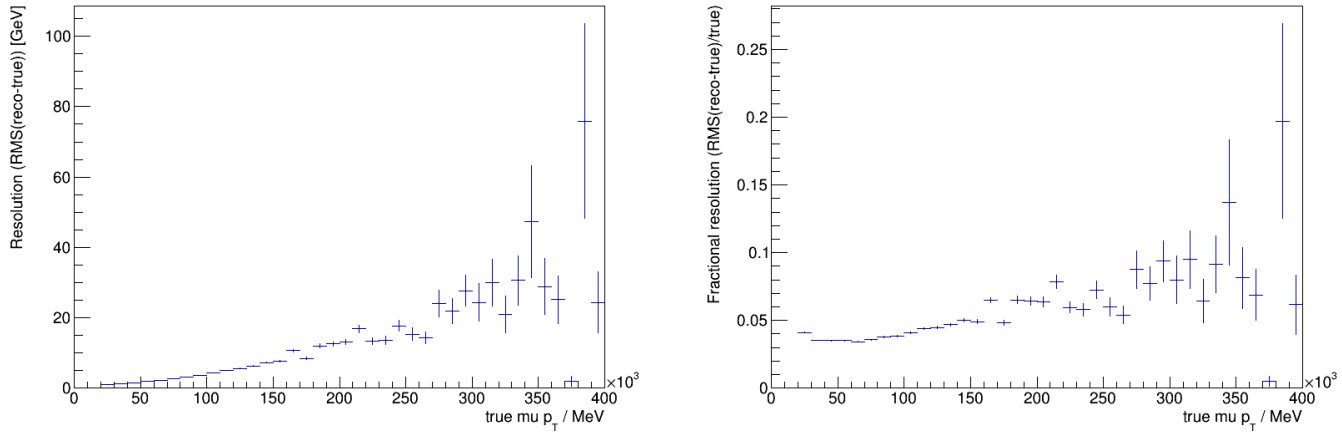

Fig. 6.13 Absolute and relative resolution of muon p_T.

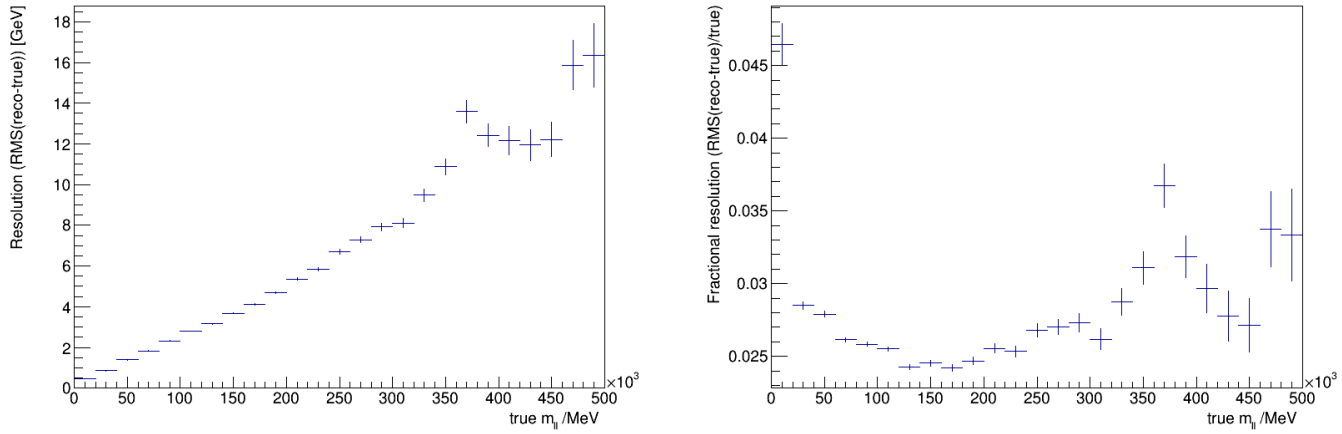

Fig. 6.14 Absolute and relative resolution of the dilepton invariant mass m_{ll}.

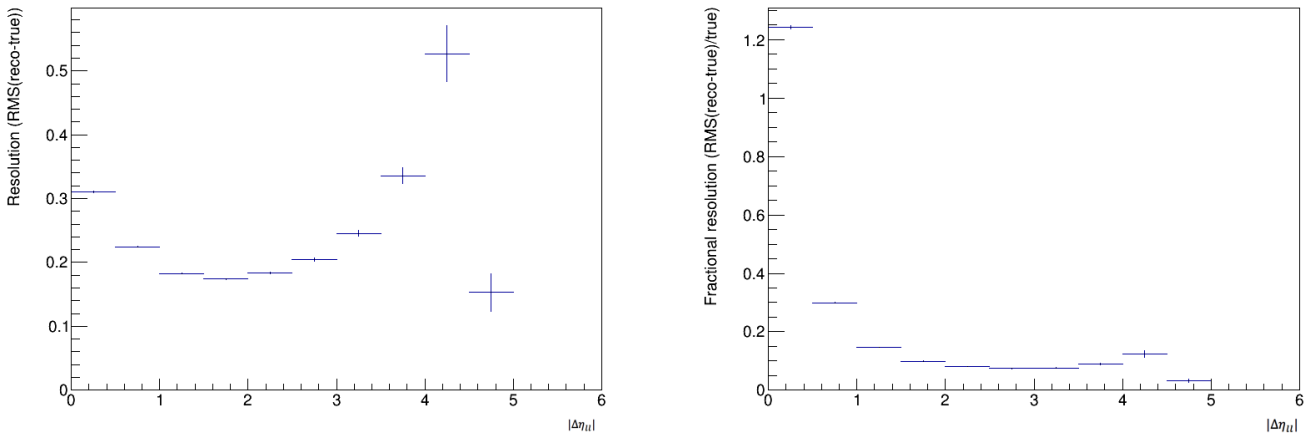

Fig. 6.15 Absolute and relative resolution of the dilepton absolute $\Delta\eta_{ll}$.

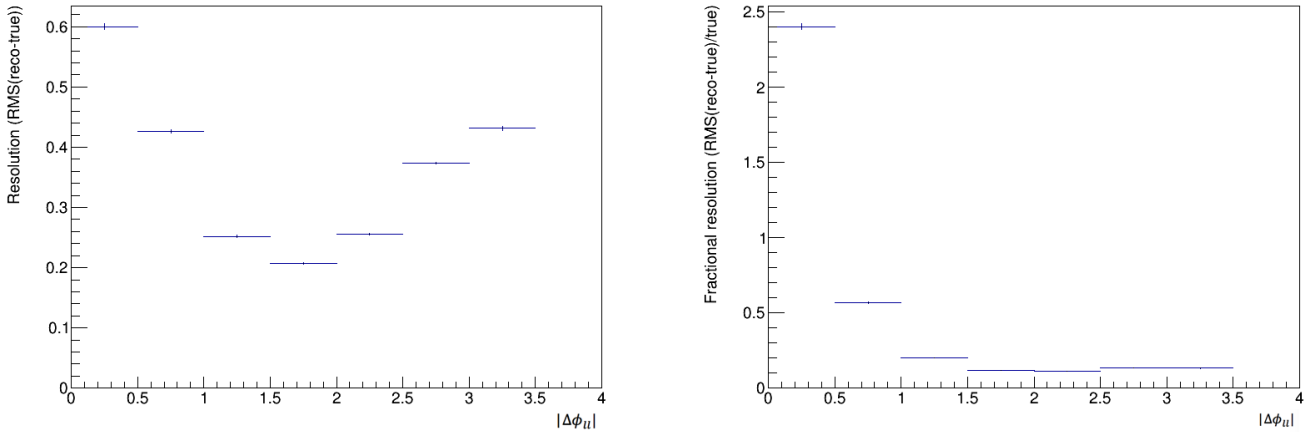

Fig. 6.16 Absolute and relative resolution of the dilepton absolute $\Delta\phi_{ll}$.

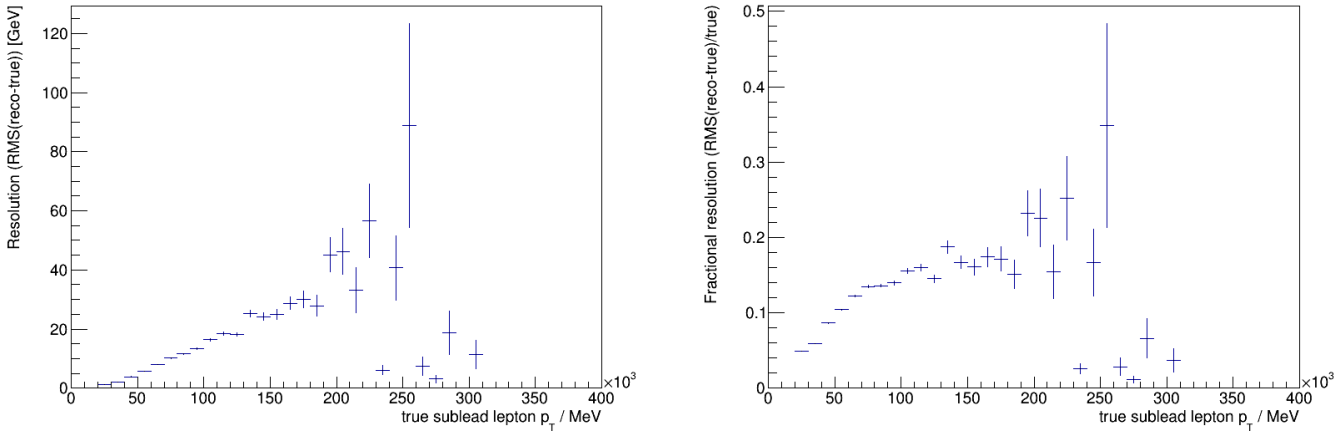

Fig. 6.17 Absolute and relative resolution of the sub-leading lepton p_T.

presence of background so only a fraction of events in a given bin actually originated from the desired process.

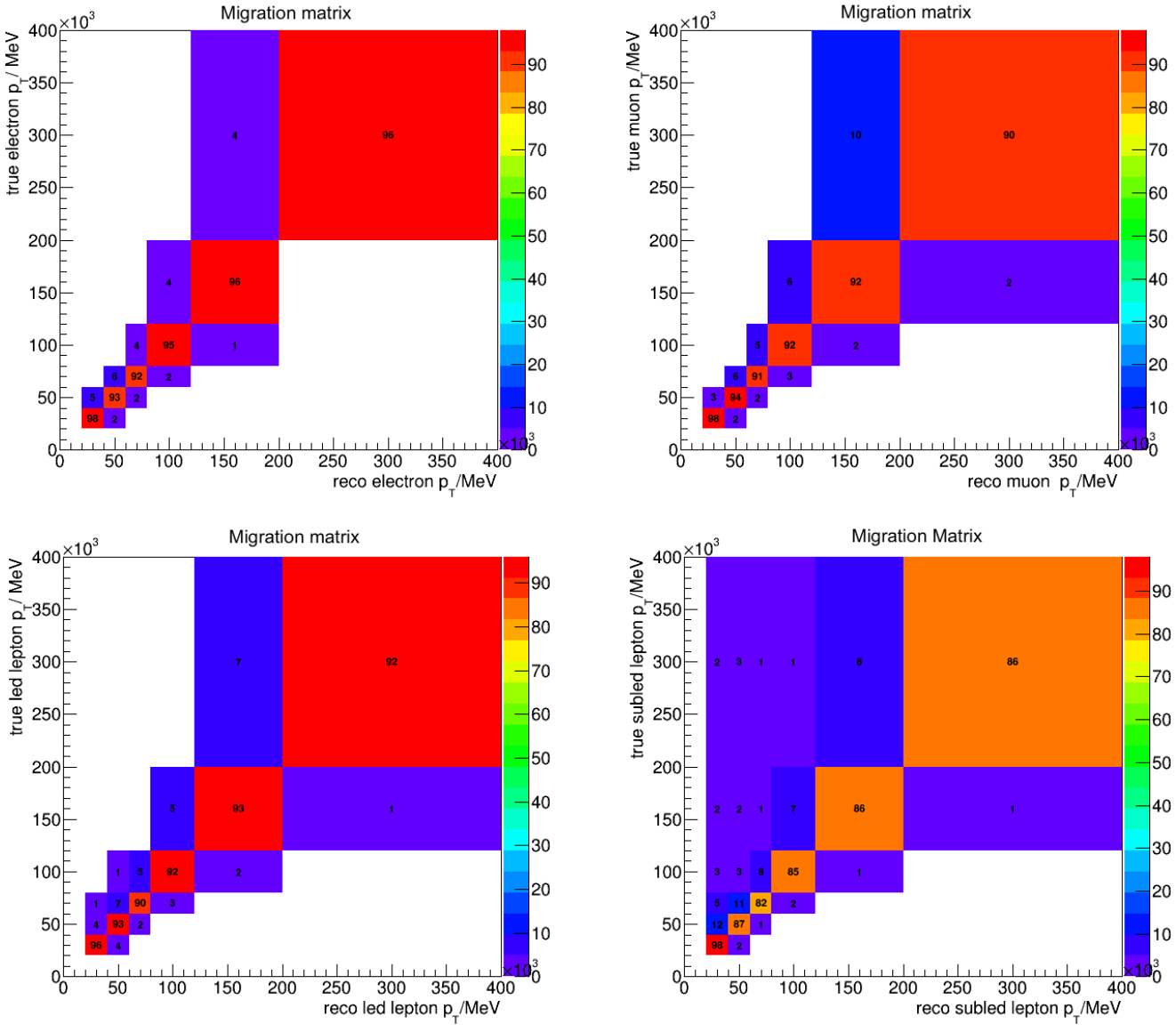

Fig. 6.18 Migration matrix for the electron p_T, muon p_T, the highest p_T lepton and sub-leading lepton p_T for the dilepton $e\mu$ are shown. The percentage probability that the lepton with a given p_T is reconstructed in the given p_T bin is shown in the bins.

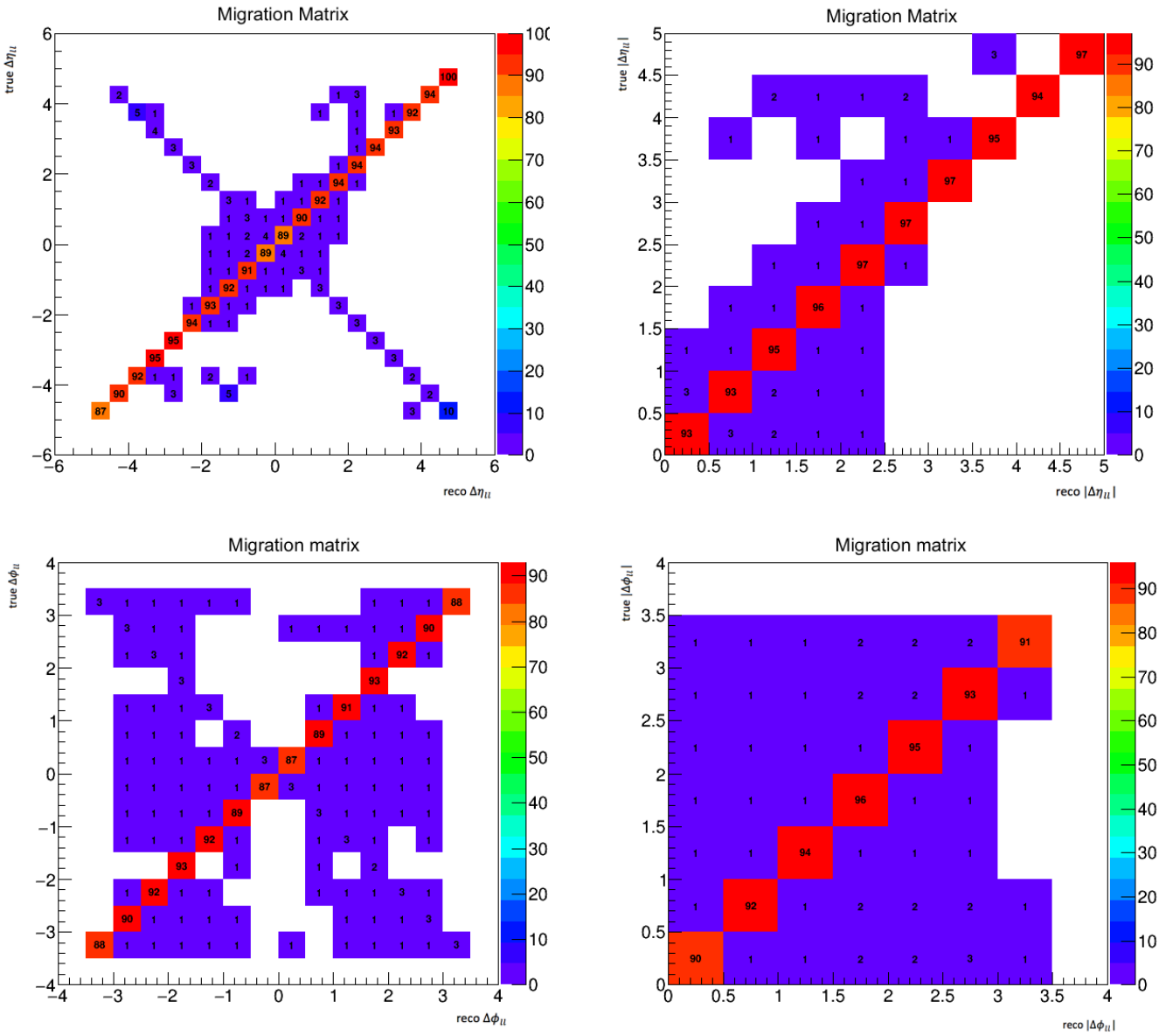

Fig. 6.19 Migration matrix for the dilepton signed $\Delta\eta_{ll}$, absolute $\Delta\eta_{ll}$, azimuthal angle $\Delta\phi_{ll}$ and absolute $\Delta\phi_{ll}$ for the $e\mu$ are shown. The percentage probability that the dilepton variables move from one bin to another is shown in the bins.

In order to be able to check the migration across the bins, a two dimensional matrix between truth versus reconstructed variables is plotted for different lepton kinematic variables. The migration matrices show that all the truth levels do not necessarily fall into the same bins as reconstructed level events. In practice, the lepton kinematic variables show better reconstruction than the top anti-top system variables but migration between bins is still seen. This migration changes the efficiency number and hence some of the systematics as well.

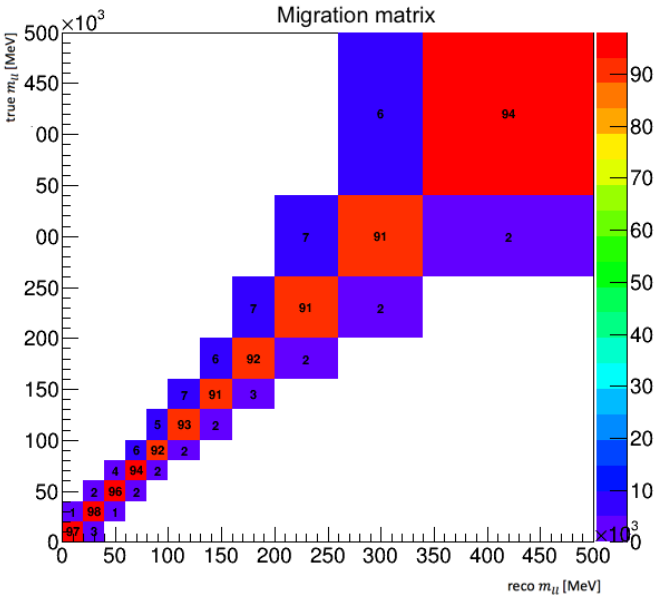

Fig. 6.20 Migration matrix for the dilepton invariant mass.

Ideally, more than 90% of events should land in the correct bin but due to an error in the energy scale, the events are systematically put in a different bin (e.g. if the measured energy was only 95% of the true energy due to calibration error, leptons near the bottom of bin two land in bin one). For the measurements involving jets, diagonal fractions of 60-70% are more common, and then much larger migration takes place, which needs more complex unfolding techniques (with iterations). For the leptons, binning has been constructed to ensure about 90% of events have the same reconstructed and true values. This allows a simple bin-by-bin correction to be used. The migration matrices for different lepton kinematic variables are shown in Figures 6.18, 6.19 and 6.20.

6.9 Differential efficiency measurement

The methodology to extract the efficiency of the event selection as a function of the true Monte Carlo p_T of the lepton, is as follows:

1. Make a histogram of the lepton true p_T for all events passing the basic selection (both leptons have $p_T > 25$ GeV and $|\eta| < 2.5$).

2. Make a histogram of the lepton true p_T for the subset of all events in step one which also pass the reconstructed event selection (i.e. having two reconstructed leptons passing the lepton ID and isolation cuts). Some reconstructed events which do not pass the truth selection in step one are not included in the selection.

The efficiency is calculated by dividing histogram two by histogram one. The information about the truth can be obtained from a software package called top fiducial. To make the efficiency plot, the same quantity has been plotted in both the numerator and denominator of the histogram, if one is the truth p_T, the other should be the same. If truth p_T for the denominator and reconstructed p_T for the numerator are plotted, it mixes up the efficiency and resolution effects, as the same event may appear in different bins for the two histograms. The following two fiducial cuts are applied on the selected electrons and muons:

- p_T and η cuts ($p_T > 25$ GeV and $|\eta| < 2.5$);
- pdgid ==11 (electron) and pdgid ==13 (muon)[1].

p_T (GeV)	Efficiency
20-40	0.64
40-60	0.65
60-80	0.64
80-120	0.63
120-200	0.61
200-400	0.62

Table 6.3 Reconstruction efficiency per bin as a function of the leading lepton p_T.

and muons should be the decay product of top anti-top pairs that decay to Ws which in turn decay to electrons and muons for this analysis. Electrons from other sources, like from the decay of heavy flavour jets, are not considered for this calculation. The electrons and muons from heavy flavour decays and photon conversions are not included in the plots. The fiducial cuts on lepton $|\eta|$ and p_T for this analysis are the same as those chosen at reconstruction level. The reconstruction efficiency as a function of the leading lepton, $|\Delta\phi_{ll}|$, $|\Delta\phi_{ll}|$ and m_{ll} are shown in Figures 6.21 and 6.22. The overlaid reconstruction efficiency for the three MC generators for all four variables shows a good agreement as shown in Figures 6.23, 6.24 and 6.25. The impact on efficiency by changing the MC generator will introduce a systematic uncertainty in the measured cross-section and will be evaluated in Chapter 8. The bin-by-bin efficiency for all four variables are shown in Tables 6.3, 6.4, 6.5 and 6.6.

[1]Monte Carlo particle numbers assigned to electrons and muons.

m_{ll} (GeV)	Efficiency
20-40	0.66
40-60	0.66
60-80	0.66
80-100	0.65
100-130	0.64
130-160	0.63
160-200	0.62
200-260	0.60
260-340	0.60
340-500	0.59

Table 6.4 Reconstruction efficiency per bin as a function of the mass of the dilepton, m_{ll}.

$\|\Delta\phi_{ll}\|$	Efficiency
0.0-0.5	0.67
0.5-1.0	0.67
1.0-1.5	0.65
1.5-2.0	0.64
2.0-2.5	0.63
2.5-3.0	0.61
3.0-3.142	0.61

Table 6.5 Reconstruction efficiency per bin as a function of the absolute azimuthal angle of the dilepton, $|\Delta\phi_{ll}|$.

$\|\Delta\eta_{ll}\|$	Efficiency
0.0- 0.5	0.63
0.5-1.0	0.63
1.0-1.5	0.64
1.5-2.0	0.64
2.0-2.5	0.63
2.5-3.0	0.63
3.0-3.5	0.63
3.5-4.0	0.58

Table 6.6 Reconstruction efficiency per bin as a function of the absolute pseudorapidity of the dilepton, $|\Delta\eta_{ll}|$.

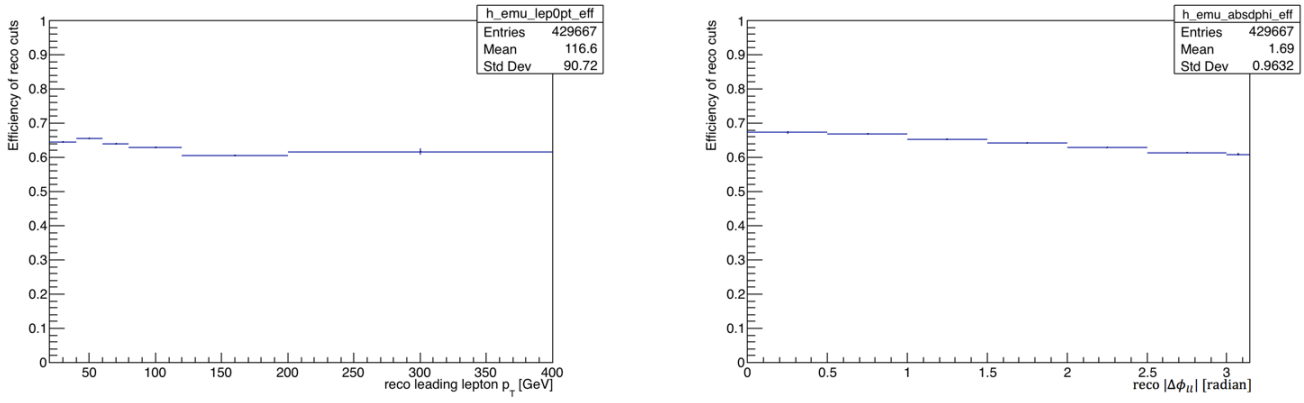

Fig. 6.21 Reconstruction efficiency as a function of the leading lepton p_T (left) and the absolute $\Delta\phi_{ll}$ (right).

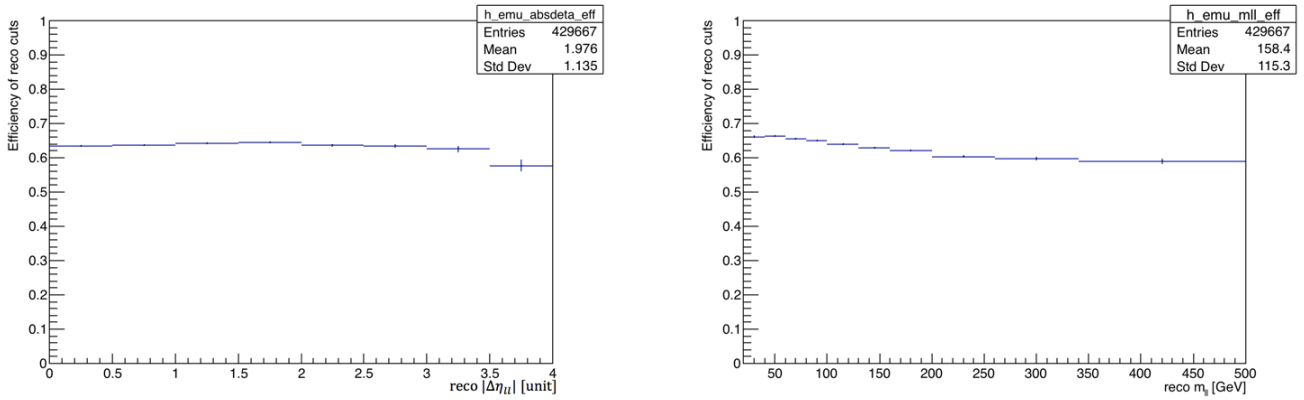

Fig. 6.22 Reconstruction efficiency as a function of the absolute $\Delta\eta_{ll}$ (left) and the dilepton invariant mass (right).

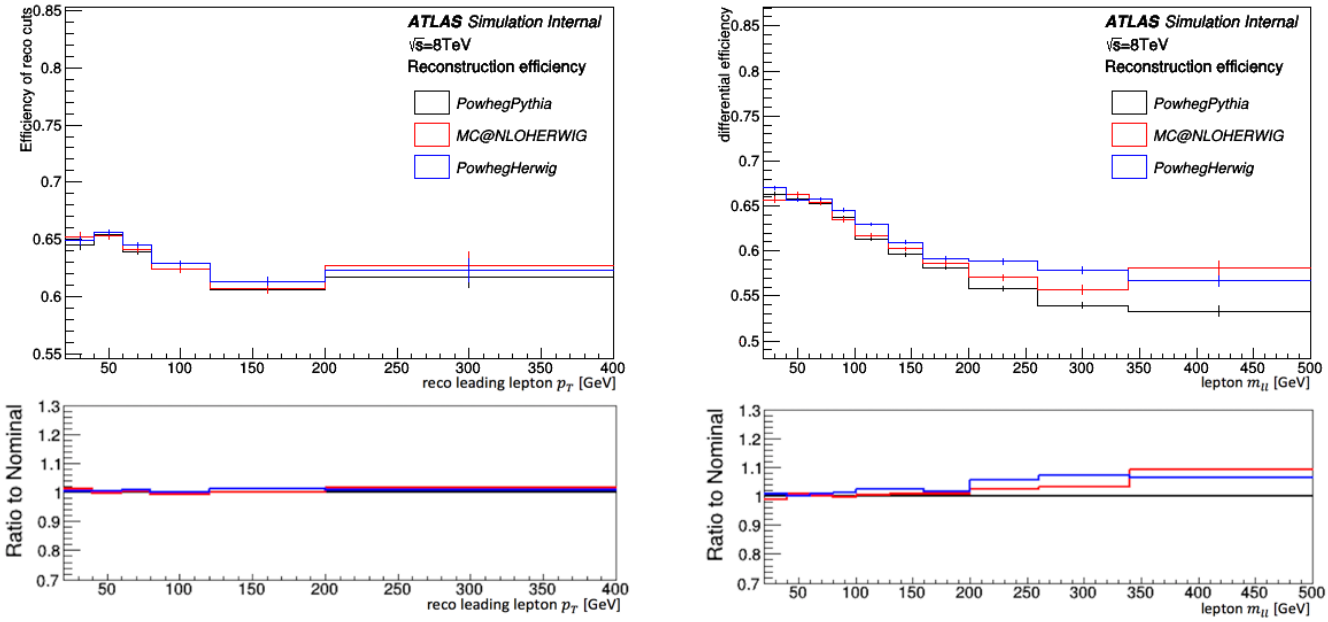

Fig. 6.23 Comparison of the reconstruction efficiency for different MCs as a function of the leading lepton p_T on the left, and the dilepton mass m_{ll} on the right.

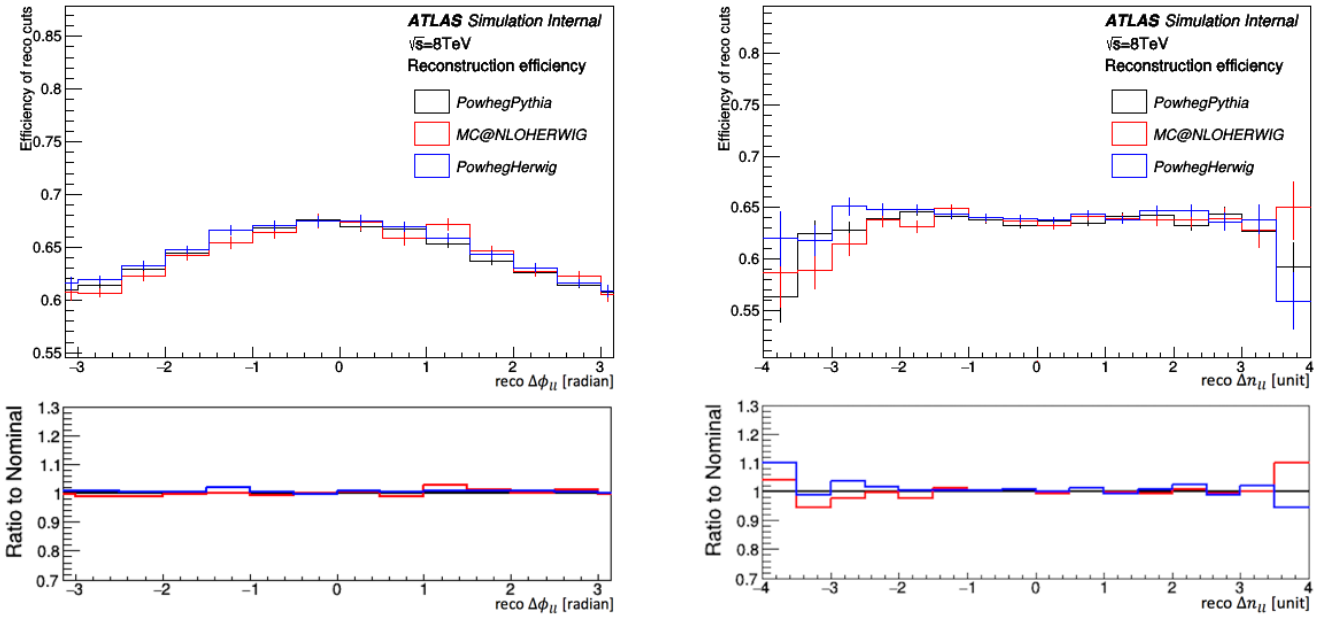

Fig. 6.24 Comparison of the reconstruction efficiency as a function for different MCs of the azimuthal angle of dilepton on the left and the difference of pseudorapidity of the dilepton on the right.

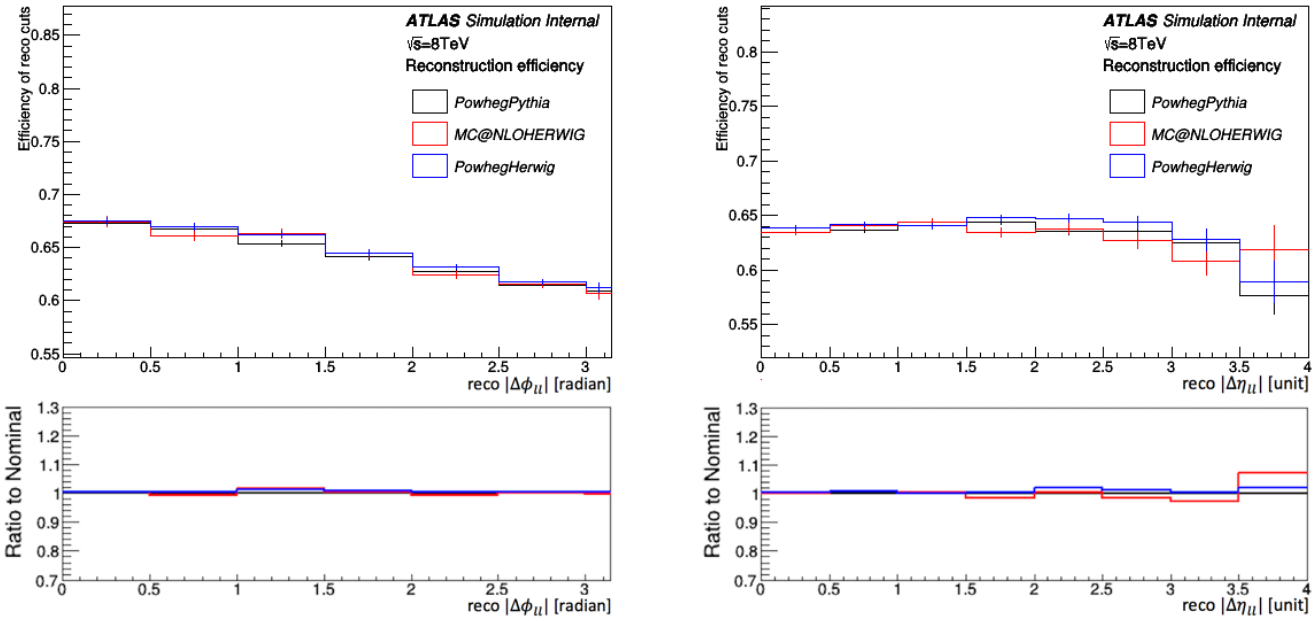

Fig. 6.25 Comparison of the reconstruction efficiency for different MCs as a function of the absolute azimuthal angle of the dilepton on the left, and absolute difference of pseudorapidity of the dilepton on the right.

Chapter 7

Sources of uncertainty

Measurements of a physics quantity of interest in high energy physics require a statistical uncertainty and an additional "systematic" uncertainty. The statistical uncertainty is due to the result of statistical fluctuations owing to the limited number of data events. If the measurement is repeated under the same conditions, the resulting measurement would be different from the previous ones. The statistical uncertainty is associated with the range of variation in the measurement due to a limited number of events. The statistical variations are uncorrelated as the signal and background are not the same events and to estimate them, statistics has well developed tools. The other main sources of uncertainties are:

- detector modelling systematics
- signal modelling systematics
- background modelling systematics
- uncertainty due to luminosity
- uncertainty due to reconstruction efficiency

Systematic uncertainties, however, are those variations in a measurement produced by the measurement itself. The signal modelling systematics arise due to a change in the MC generator and the background modelling systematics arise due to a change in the MC generator of background simulated samples. These are discussed briefly in the following sections.

7.1 Statistical and Monte Carlo uncertainty

The measurement is affected by statistical uncertainties due to the size of the data sample and has been determined for each bin of the lepton kinematic variables. The statistical errors

on the signal and background have been treated as uncorrelated to each other. To evaluate the statistical error on the total data histogram, the nominal value has been set equal to the nominal $\pm$ 1 standard deviation of statistical variation and calculated the new cross-section with the remainder being constant (the background N_{bkg}, efficiency and luminosity), as mentioned in Equation 6.3. The statistical error is much smaller than systematic error. The statistical uncertainty of each bin is the square root of the sum of the square of the number of events filling that bin. Each sample set is filled with a value generated by picking a random value from a Gaussian distribution with the mean as the weighted value of the bin and the width equal to the statistical uncertainty. Each bin of the fiducial distribution contains the fiducial cross-section rather than just a simple data count.

The contributions from these different sources have been shown by the overlaid histograms with a ratio plot at the lower pad as shown in Figures 7.1, 7.2, 7.3, 7.4, 7.5, 7.6, 7.7, 7.8, 7.9. The impact of each variation has been evaluated one at a time for each of the three sources: data, MC signal and MC background.

7.2 Systematic uncertainties

Systematic uncertainties or systematic errors arise due to the nature of the measuring device (particle physics detectors) and due to models used to make corrections for efficiencies and acceptance (MC generator in particle physics). No simulation is expected to describe real data perfectly, the limited knowledge and model used to describe the underlying physics always gives rise to systematic uncertainties. The classical approach to evaluate these uncertainties is to perform ensemble tests which mean that the default template is varied up and down by one standard deviation. If the experiment is repeated under the same conditions, the outcome will not change i.e. repeated measurements of a quantity produce the same result. The systematic error is "any error that is not a statistical error". Common examples include uncertainties due to the poor calibration of the device, the probability to detect any given type of physics process (acceptance) and parameters of the model used to make inference that may have uncertainties associated with them. The fiducial cross-section defined in the previous section has:

- number of data events, N_{data};
- number of background events, N_{bkg};
- efficiency; and
- integrated luminosity.

All of the above factors contribute to the cross-section. For example, the backgrounds for this analysis are single top, WW, WZ, ZZ, fakes etc. Any variation in the background changes the cross-section. Different MC signal samples have different cross-sections. The following sources of systematic uncertainties have been taken into account for this analysis:

- uncertainty due to the modelling of the detector (reconstruction level systematics).
- uncertainty due to the physics modelling including the statistics and parameters used to describe the signal and background.
- uncertainty arising due to the luminosity evaluation.

Each of these systematics will be discussed in the next sections and evaluated in Chapter 8.

7.3 Detector modelling systematics

Detector modelling or performance uncertainties are evaluated from the baseline $t\bar{t}$ simulation sample by varying default scale factors within their systematic uncertainties which have been evaluated by combined performance groups. The evaluation of every systematic uncertainty on a bin is carried out with a variation of the nominal by a standard deviation and then dividing with the efficiency after varying the systematic variation.

The evaluation of the systematic uncertainties in this analysis closely follows the recommendations of the ATLAS top working group. The list of some of the important systematic variations that have been evaluated for this analysis have been discussed in the next section. The full list of all the detector related systematics are given in Appendix A. The electron related uncertainties and scale factors have been taken from a sub-package, ElectronEfficiencyCorrection, with a tag useful for 2012 data. The muon related uncertainties have been taken from another sub-package, MuonEfficiencyCorrection. The tag compatible for the 2012 data has been used. Each bin of the lepton kinematic variable is affected by these systematics, so a bin-by-bin evaluation of all these uncertainties has been made. Each of these have up and down variations that are attached as a prefix with the name of systematic trees. It can be seen from Appendix A that quite a few of the detector modelling systematics have no up and down variation which means that they are a one sided variation. All the one sided variations need to be symmetrised in order to be able to evaluate the net effect of both the up and down variation.

The jet related uncertainties like b-tag and Jet Energy Scale (JES) are the major detector modelling systematics. Many lepton related uncertainties have been carefully evaluated but their contribution is not significant. While evaluating these systematics, it has been seen that a certain upward variation ends up with a negative sign so it is effectively a down type

variation. These need to be added in quadrature with their down type variations in the same bin. The same is for when the down variation is evaluated and certain down variations end up with a positive sign. It has also been noted that certain systematics have the same sign in certain bins. While evaluating the detector modelling systematics, it has been seen that in certain bins, both up and down type variations end up having the same sign. This can only take place if the migration of events takes place from one bin to the next or previous bin. It seems strange but it happens when events migrate from one region to another, especially in differential analyses. This effect causes a huge migration for the $t\bar{t}$ system variables, but it is still present in the lepton case, however it does not contribute heavily and can be corrected using bin-by-bin correction. If the lepton observable is m_{ll}, it has three regions: low, middle and high. If one of the systematics shown in the table moves events to have higher m_{ll}, the m_{ll} low region will move a few events from m_{ll} low to m_{ll} medium. The middle region of m_{ll} will move a few events to m_{ll} high region. A bin-by-bin correction can lead to around 90 % of truth events to fall into reconstructed ones which does not need a complex unfolding.

The Jet energy scale (JES) is a complicated detector modelling systematic. It deals with the jets systematics, it can be ignored if no b-tag requirement is made on the jets. This analysis requires at least one b-tag jet so, all its components must be evaluated. The efficiency changes due to different components of the JES. Due to its complexity, the JES has been broken down into 22 components. This decomposition is called eigenvector decomposition, which decomposes the main quantity into these components just like diagonalising a matrix. These components make a covariance matrix which has been diagonalised to make all the components orthogonal. Being orthogonal (uncorrelated), these components can be added in quadrature. All the detector modelling systematic uncertainties are calculated in Chapter 8 in Tables 8.4, 8.7, 8.10 and 8.13.

7.4 Description of detector modelling systematics

This analysis does not require any jet cuts at the particle level so the reconstruction level uncertainties relating to jets will not be playing a significant role except b-tag related uncertainties. The impact of varying different systematics relating to leptons (uncertainties on electron and muon reconstruction, identification and trigger efficiencies) also do not show much impact on the measurement. A brief description of detector or reconstruction level systematic uncertainties is given below.

- Electron energy scale and resolution: The uncertainties on the electron energy scale and resolution have been studied from well known sources of electrons like Z decaying to ee mass distributions. These studies were also supported by $J/\psi \to ee$ decays.

- Muon momentum scale and resolution: The muon momentum resolution is extracted from the Z width in the samples where Z decays to $\mu\mu$ events. Uncertainties due to the momentum scale are estimated by smearing the muon transverse momentum, p_T in MC by the resolution. This smearing is applied separately to the inner detector and the muon spectrometer. The size of the uncertainty is taken as the shift with respect to the nominal unfolding using the smeared sample. The uncertainty due to resolution is calculated from the quadrature sum of the independent uncertainties in the inner detector and muon spectrometer.

- Electron energy: The energy scale for the electrons is obtained from studying dielectron peaks from the decay of particles of well-known mass, such as the Z boson, and energy over momentum using isolated electrons from the W decay. The correction is applied as a function E_T, ϕ and η and uncertainties from the measurements are treated as systematic uncertainties. To match the energy resolution in data, an energy smearing term is also applied to MC samples. The uncertainty is obtained by rerunning the MC with the resolution smearing used as the extremes of the uncertainty band on the resolution, and the difference between these bands and the nominal gives the uncertainty.

- Electron and muon efficiencies: The electron and muon have reconstruction, identification and trigger efficiencies. For both, there are uncertainties on the difference in efficiency between MC and the data for them to be (1) triggered, (2) reconstructed offline and (3) identified as a good quality lepton. The Z to ee tag and probe method (a tight selection is applied to one electron candidate – tag and analyse how often the other electron candidate with loose selection criteria passes the cuts – tag and probe) is used for the trigger and reconstruction efficiencies of the electron. For the identification efficiency, it is required that the W decays to electron and neutrino and the Z decays to ee. The systematic uncertainty from these factors mostly arises due to the uncertainty in subtracting the backgrounds from these analyses. The muon reconstruction efficiency is measured using the Z tag and probe method (a tight selection is applied to one muon candidate – tag and analyse how often the other muon candidate with loose selection criteria passes the cuts – tag and probe) [172]. The muon identification and trigger efficiencies were also measured using tag and probe methods. To obtain the uncertainty, the nominal sample is run with extreme values of the uncertainty of the measurements, and the difference between these samples and the nominal in the final unfolded distributions gives the uncertainty. Furthermore, additional uncertainties are also evaluated due to top-specific isolation cuts for electron

and muon. The isolation cuts for muons for the 2012 data were called mini-isolation cuts. The lepton efficiencies somehow also weakly relate to the reconstruction of jets due to an overlap removal between them.

- Jet Energy Scale: The reconstructed jets need to be energy corrected to the jet energy scale. The jet energy scale (JES) is a correction from the initial calorimeter calibrated energy based on the electromagnetic response (EM scale) to the energy of the hadronic jets. The JES is derived initially from the MC by reconstructing jets from stable particle level objects to the reconstructed EM scale jet energy. The jets used for this correction are isolated jets from an inclusive MC sample which include pile-up. Then, to account for residual differences between the data and simulation, an in-situ correction technique has been used as a last step of jet reconstruction [173]. The JES is complicated to evaluate, so, it has been broken down into 22 components for the 2012 data, 12 of which describe orthogonal components in the baseline jet energy scale [174]. This decomposition is called eigenvector decomposition, which decomposes the main quantity into these components just like diagonalising a matrix. Being orthogonal (uncorrelated), these components can be added in quadrature. The orthogonal components are divided into categories which describe statistical, modelling, detector or mixed uncertainties. The other 10 components describe the η-intercalibration model and statistics, the single particle response, pile-up offset dependence, jet flavour composition in $t\bar{t}$ events, jet flavour response, additional b-jet energy scale uncertainties [175]. All these components can be seen in Tables 8.4, 8.7, 8.10 and 8.13.

- Jet Energy Resolution (JER): The jet energy resolution in data has been seen to be well modelled in simulation using the bisector method [176]. The measurement shows that the JER in the MC simulation agrees with the observed data distribution. Therefore, by default no extra smearing is applied to reconstructed MC jets but an additional smearing is applied to the simulation to cover the uncertainties in the bi-sector measurement.

- Jet reconstruction efficiency: The efficiency of the calorimeter to reconstruct jets was measured using data by reconstructing jets from tracks and searching for a matching calorimeter jet [177, 178]. The MC simulation efficiency agreed with the data within the uncertainty bands of the measurement. The residual difference between the data and MC has been modelled by randomly discarding jets.

- Jet Vertex Fraction: The systematic uncertainty due to the Jet Vertex Fraction (JVF) cut to discard soft jets is evaluated by varying the scale factors for the hard-scatter jet selection efficiency (the fraction of hard-scatter jets that are classified as hard-scatter

by the JVF selection) and for the pile-up jet rejection efficiency (the fraction of jets from pile-up energy deposits classified as pile-up jets by the JVF selection). The scale factors for the JVF are defined as the ratio of the data efficiency to the MC efficiency, and are applicable to MC. For 2012 data, the uncertainty modelling the JVF cut efficiency has been accessed by varying the value of the cut. The efficiencies are measured using a tag and probe method looking for a Z boson recoiling back-to-back against a single jet [158]. From this sample a hard-scatter enriched region is defined as having a Z boson with $p_T > 30$ GeV and $\Delta\phi(Z, jet) > 2.9$. Very few of the events in this region have pile-up jets, since the p_T requirement implies the Z boson is recoiling off QCD radiation. A pile-up enriched region is defined by requiring the Z boson has $p_T < 10$ GeV, and the jet has $p_T > 20$ GeV, without any requirements on the $\Delta\phi(Z, jet)$. The low p_T requirement on the Z, along with the requirement that only one jet is reconstructed, implies that the Z boson was produced with negligible QCD radiation in this region, and the jet is being constructed from the energy due to pile-up interactions.

7.4.1 Signal modelling systematics

These uncertainties affect the estimate of signal detection efficiency, including the acceptance of the detector. They also have an impact on the detector response due to the change of kinematic properties of the objects. Like the detector performance related systematics, these are also evaluated for all lepton kinematics in all the bins of observables. These systematics have been evaluated by making new signal samples using several MC generators. The effect of initial and final state radiation was evaluated using POWHEG+PYTHIA samples with two combinations: the variation of the factorization and renormalisation scale μ by a factor of 0.5 and 2 and variation of the damping parameter hdamp (between mtop and twice mtop). To evaluate the parton showering POWHEG+fHERWIG and MC@NLO+fHERWIG have been used. The size of this uncertainty is estimated by taking the relative difference between these two samples. The generator modelling systematics have been evaluated using POWHEG+PYTHIA and POWHEG+fHERWIG, the hdamp parameter for both of these samples is hdamp = infinity. The effect of these modelling uncertainties have been shown by the overlaid plots in the upper left plot in Figure 7.2, the right hand side plot in Figure 7.3, the bottom left and right hand plots in Figure 7.5, the bottom left and right hand side plot in Figure 7.6 the upper left hand side plot in Figure 7.7, the bottom left and right hand side plot in Figure 7.8 and the upper left hand side plot in Figure 7.9. The numerical values of all the signal modelling systematics are given in Chapter 8.

7.4.2 Background modelling systematics

Ideally, the systematic uncertainties due to all the backgrounds need to be evaluated for completeness but for the dilepton $e\mu$ signature the main background is the single top W_t channel, which contributes around 10-11%. The other backgrounds like ZZ, WZ, WW, Z+jets and fakes are still present but their contribution is not significant and hence the systematic uncertainties for them have been ignored. The background modelling systematics include the systematics due to single top: s-channel, t-channel and W_t but the s and t-channels play almost no role in the decay to two isolated leptons. The leptons from the other two decay channels of single top fall into the category of fakes. No estimate has been carried out for the s-channel and t-channel. The former has a smaller cross-section than the t-channel. The background modelling has been split into two: the systematic uncertainty due to uncertainty on the cross-section and the systematic uncertainty due to generator interference. The uncertainty on the W_t cross-section is 22.37 ± 1.5 pb so the recommendation from the top working groups is to vary the cross-section of W_t up and down by 1.5 and then calculate the difference in each bin. W_t is special, since $t\bar{t}$ cannot be easily separated from $t\bar{t}$ in the NLO calculation. This would mean, at NLO (or higher), the $t\bar{t}$ and W_t calculations overlap each other. One needs to exclude the overlapped part, otherwise combining the two would overestimate the data.

There are two schemes to exclude this overlap, diagram subtraction (DS) and diagram removal (DR). There is no easy way to say which one is better, so comparing the two gives the uncertainty. In W_t, the nominal sample uses the diagram removal approach to handle the interference between the $t\bar{t}$ and W_t final states starting at NLO. The W_t $t\bar{t}$ pair overlap has been estimated by Diagram Removal (DR) and Diagram Subtraction (DS) schemes. i.e. POWHEG+PYTHIA with DR vs POWHEG+PYTHIA with DS. The differences between the two schemes are not small so the separation in the selected phase space is not well defined and is an indication that an inclusive $WWbb$ sample should be used instead of separate $t\bar{t}$ and W_t samples. This has not been performed for this analysis and the evaluated systematics are relatively high. The $t\bar{t}$ analysis in the dilepton channel with non-negligible W_t channel contribution can be affected by this systematic uncertainty. The single top W_t channel systematics are shown in the bottom left plot in Figure 7.2, the bottom left plot in Figure 7.5, the upper right plot in Figure 7.6 and the upper left plot in Figure 7.8 and the W_t $t\bar{t}$ pair overlap systematics have been shown in the bottom left plot in Figure 7.3, the bottom right plot in Figure 7.5, the upper left plot in Figure 7.6 and the upper right plot in Figure 7.8. The numerical values of these systematic uncertainties are given in Chapter 8.

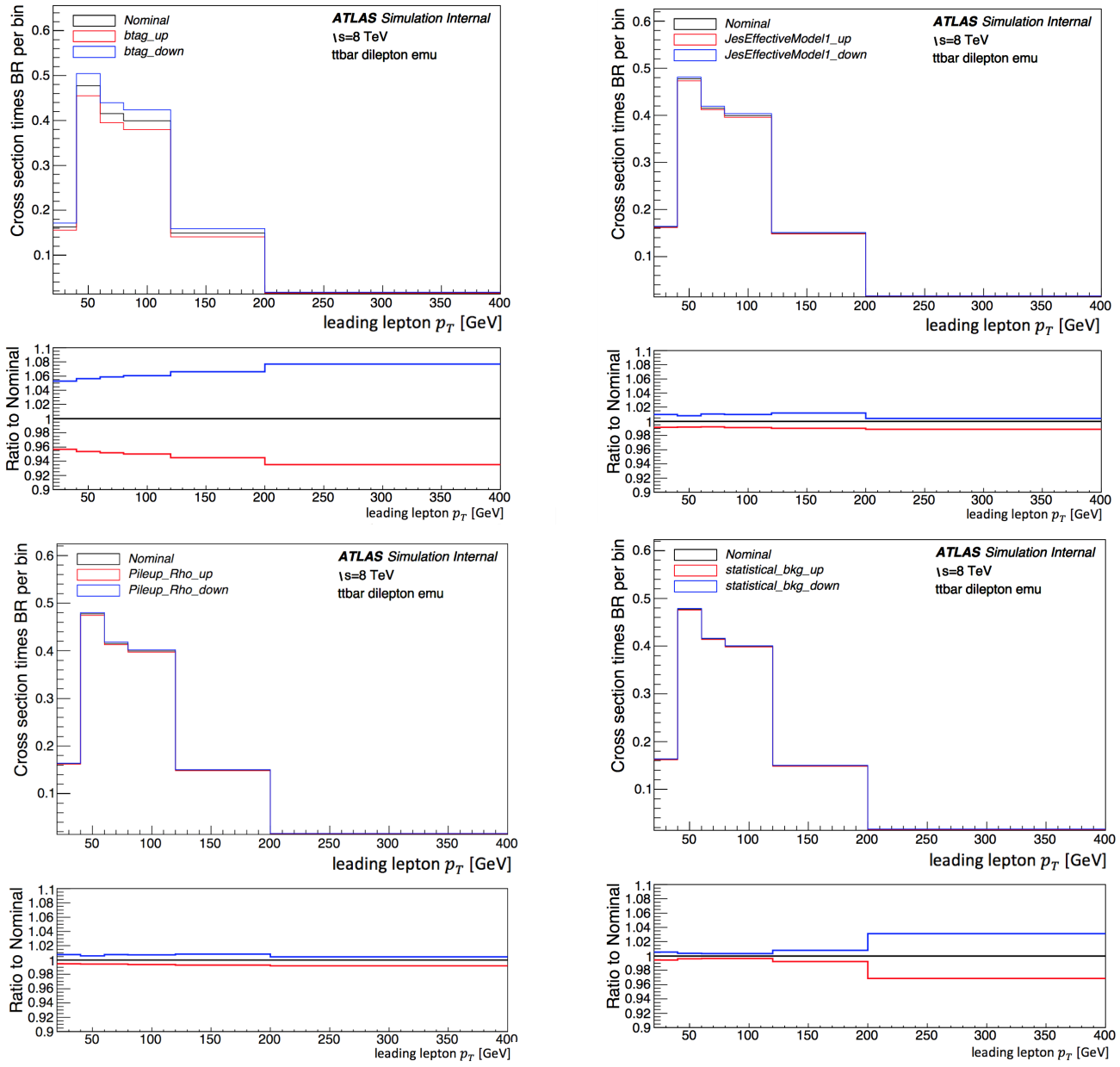

Fig. 7.1 Differential cross-section per bin for the channel $e\mu$ in the variable of p_T of the leading lepton with measured signal overlaid with statistical uncertainties on data and MC (signal and background), as well as various systematics.

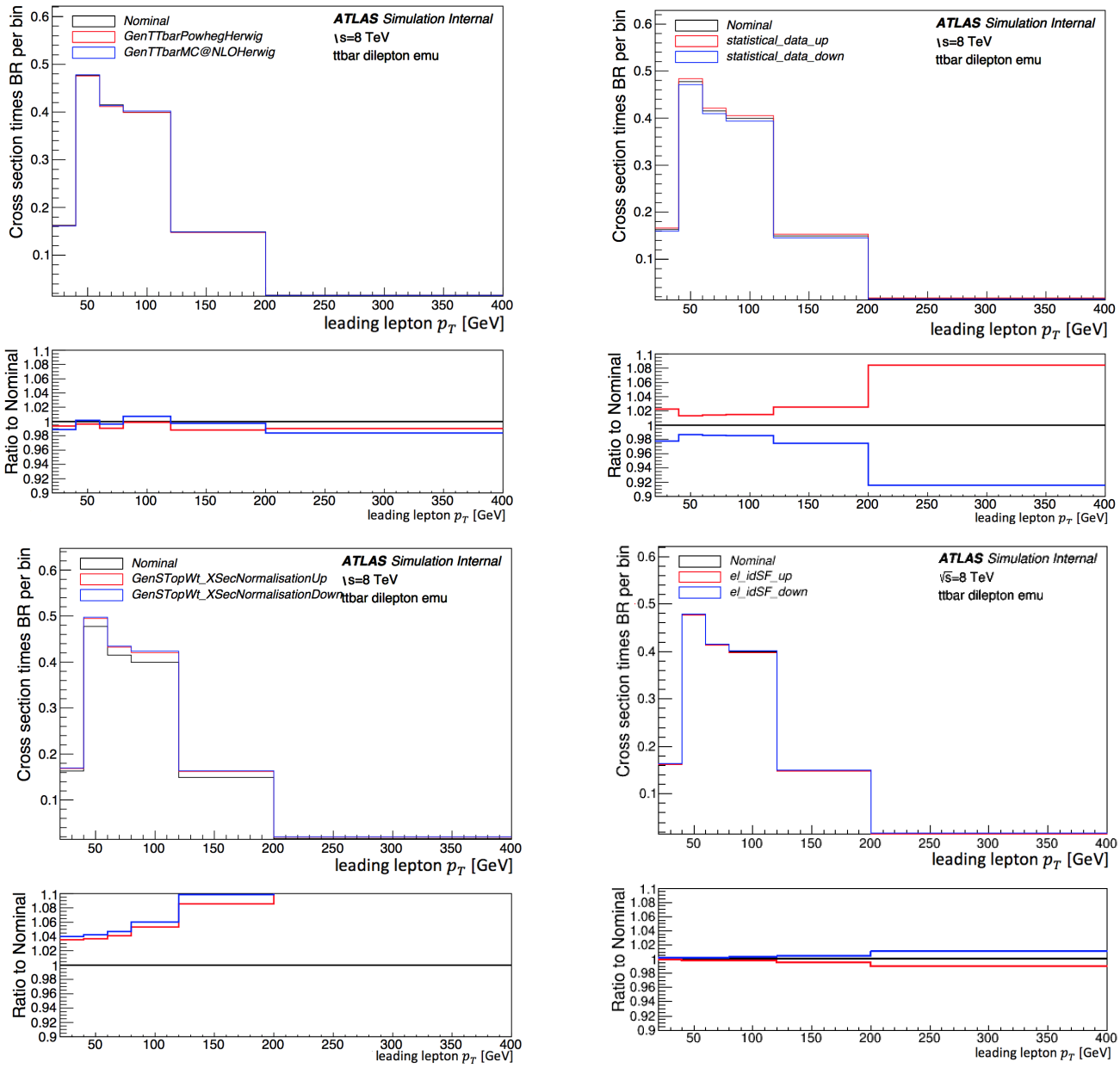

Fig. 7.2 Differential cross-section per bin for the channel $e\mu$ in the variable of p_T of the leading lepton with measured signal overlaid with statistical uncertainties on data and MC (signal and background), as well as various systematics.

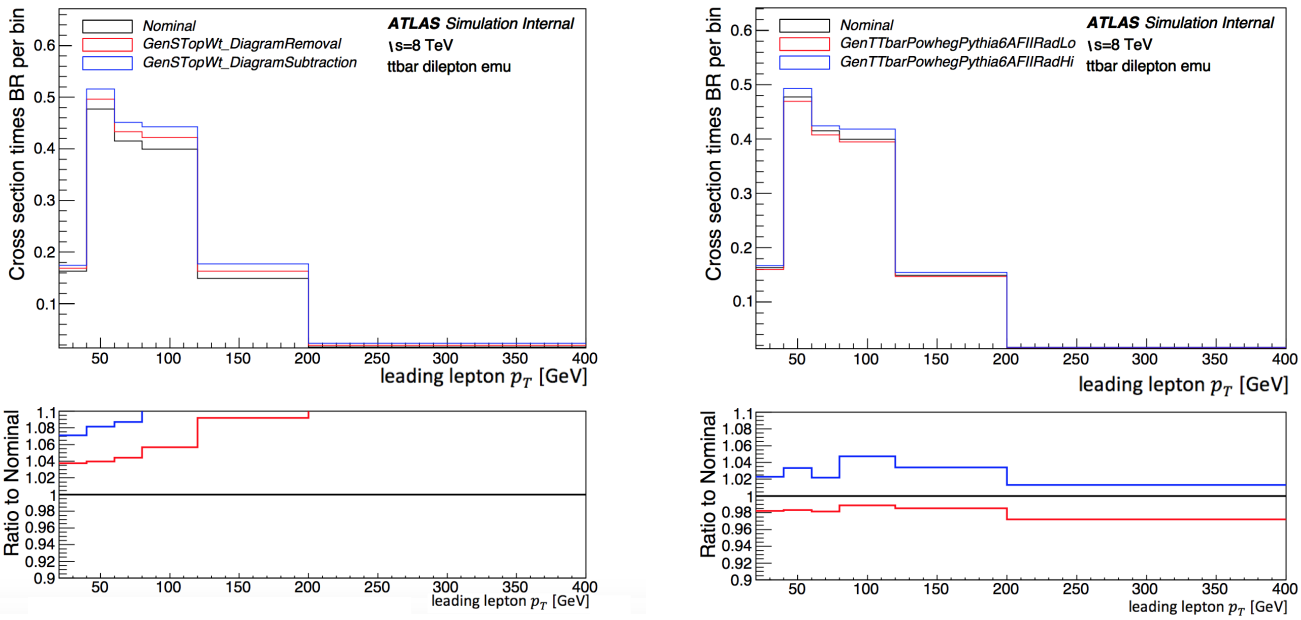

Fig. 7.3 Differential cross-section per bin for the channel $e\mu$ in the variable of p_T of the leading lepton with measured signal overlaid with statistical uncertainties on data and MC (signal and background), as well as various systematics.

7.4.3 Luminosity uncertainty

The luminosity uncertainty for 8 TeV is 2.8% so, according to the definition of fiducial cross-section discussed in Section 6.3:

$$\sigma = \frac{N_{data} - N_{bkg}}{L \times \varepsilon} = \frac{N}{L \times \varepsilon} \tag{7.1}$$

here, L is varied by dL which changes σ to dσ which can then be determined by applying a zeroth order calculation as:

$$\sigma + d\sigma = \frac{N}{((L + dL) \times \varepsilon)} \tag{7.2}$$

$$d\sigma = \frac{N}{((L + dL) \times \varepsilon)} - \sigma \tag{7.3}$$

The uncertainty in the luminosity is:

$$dL = \frac{\frac{1}{20.3} - \frac{1}{20.3+0.6}}{\frac{1}{20.3}} = 3.04\% \tag{7.4}$$

Repeating this for all the bins, the answer is almost the same. The luminosity uncertainty can also be determined by applying other rigorous ways where dL can by applied in all normalisations of MCs and efficiency calculations but the effect is very small.

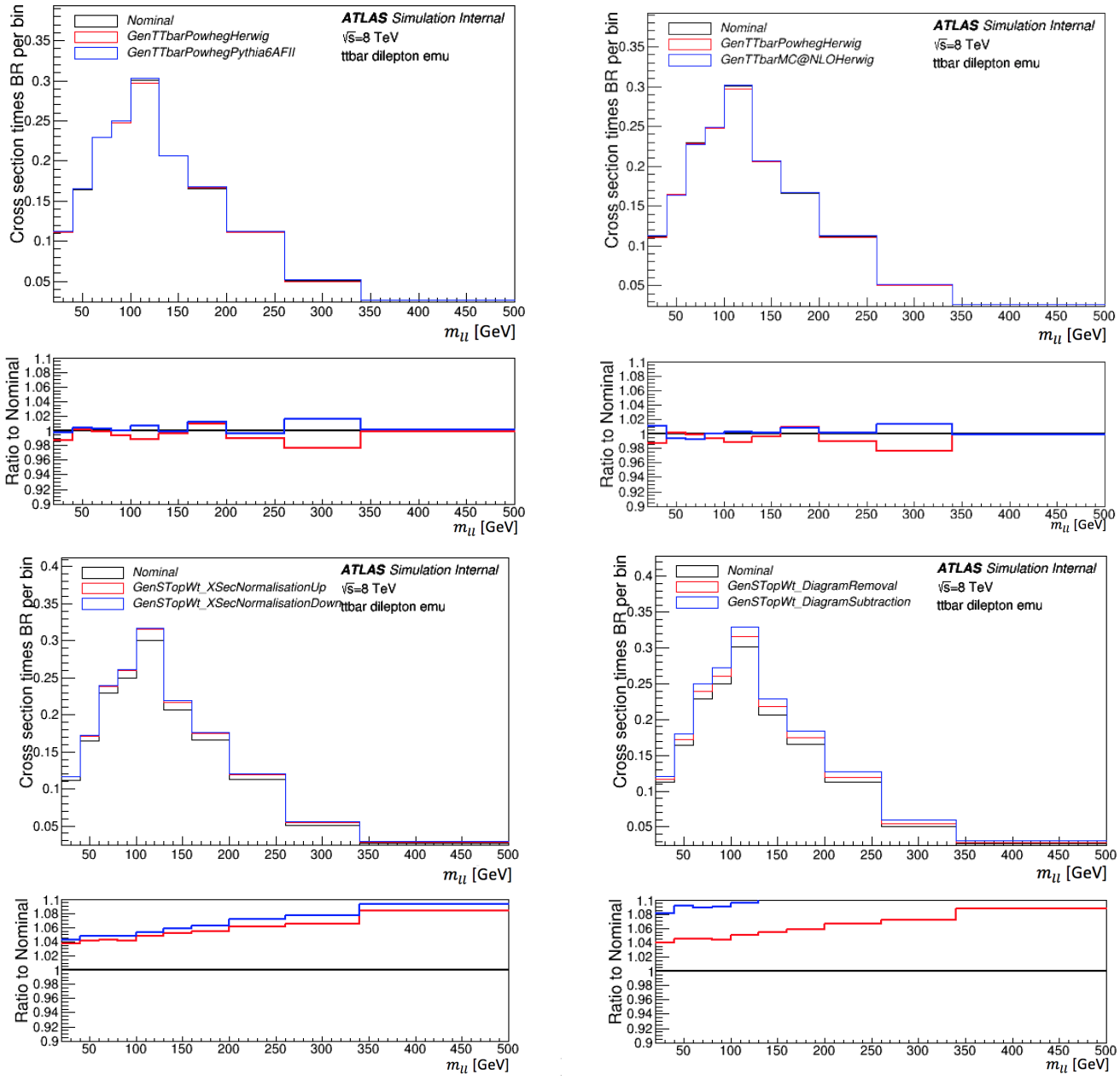

Fig. 7.5 Differential cross-section per bin for the channel $e\mu$ in the variable of m_{ll} of dilepton with measured signal overlaid with statistical uncertainties on the data and MC (signal and background), as well as various systematics.

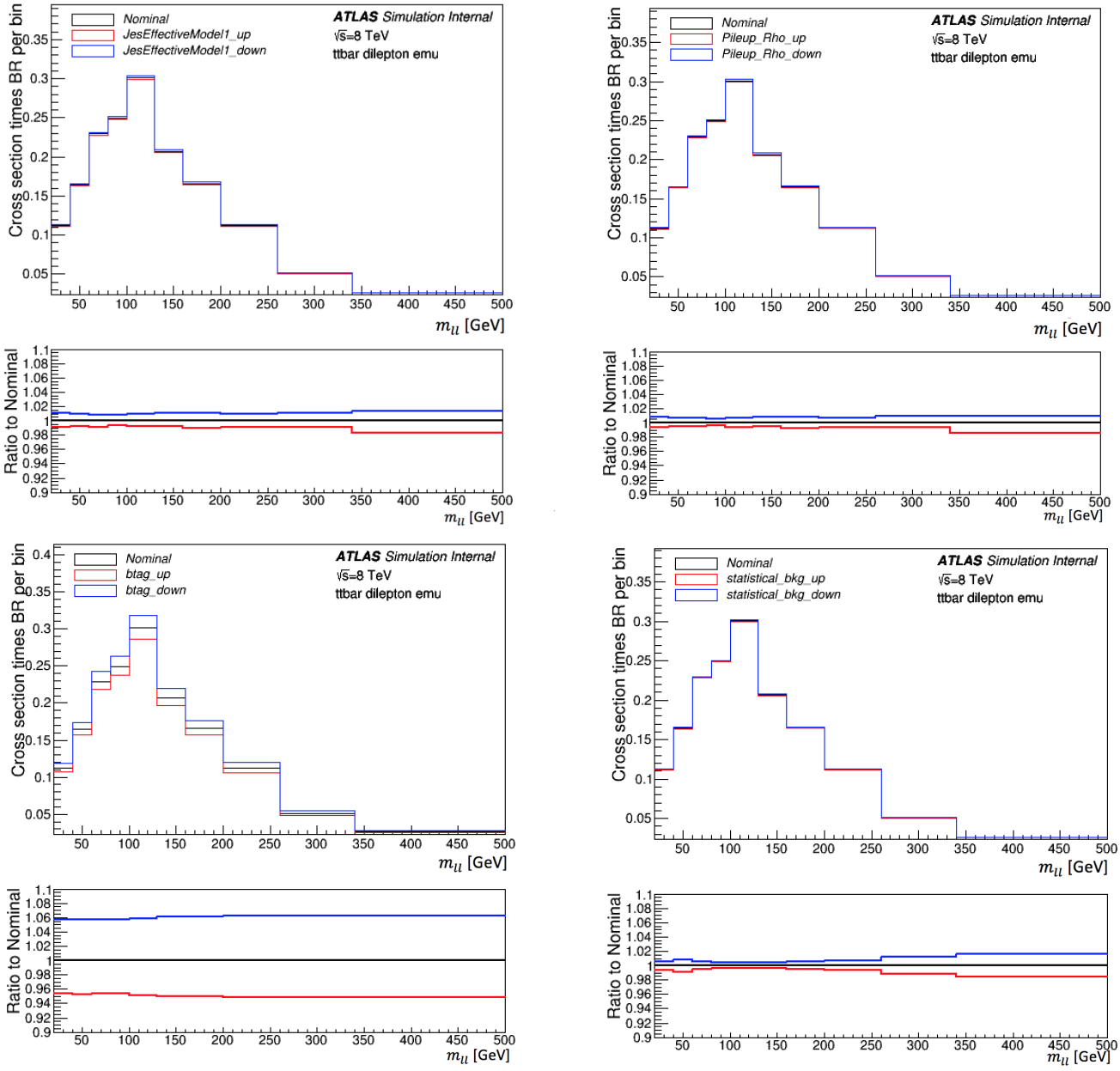

Fig. 7.4 Differential cross-section per bin for the channel $e\mu$ in the variable of the dilepton mass m_{ll} with measured signal overlaid with statistical uncertainties on the data and MC (signal and background), as well as various systematics.

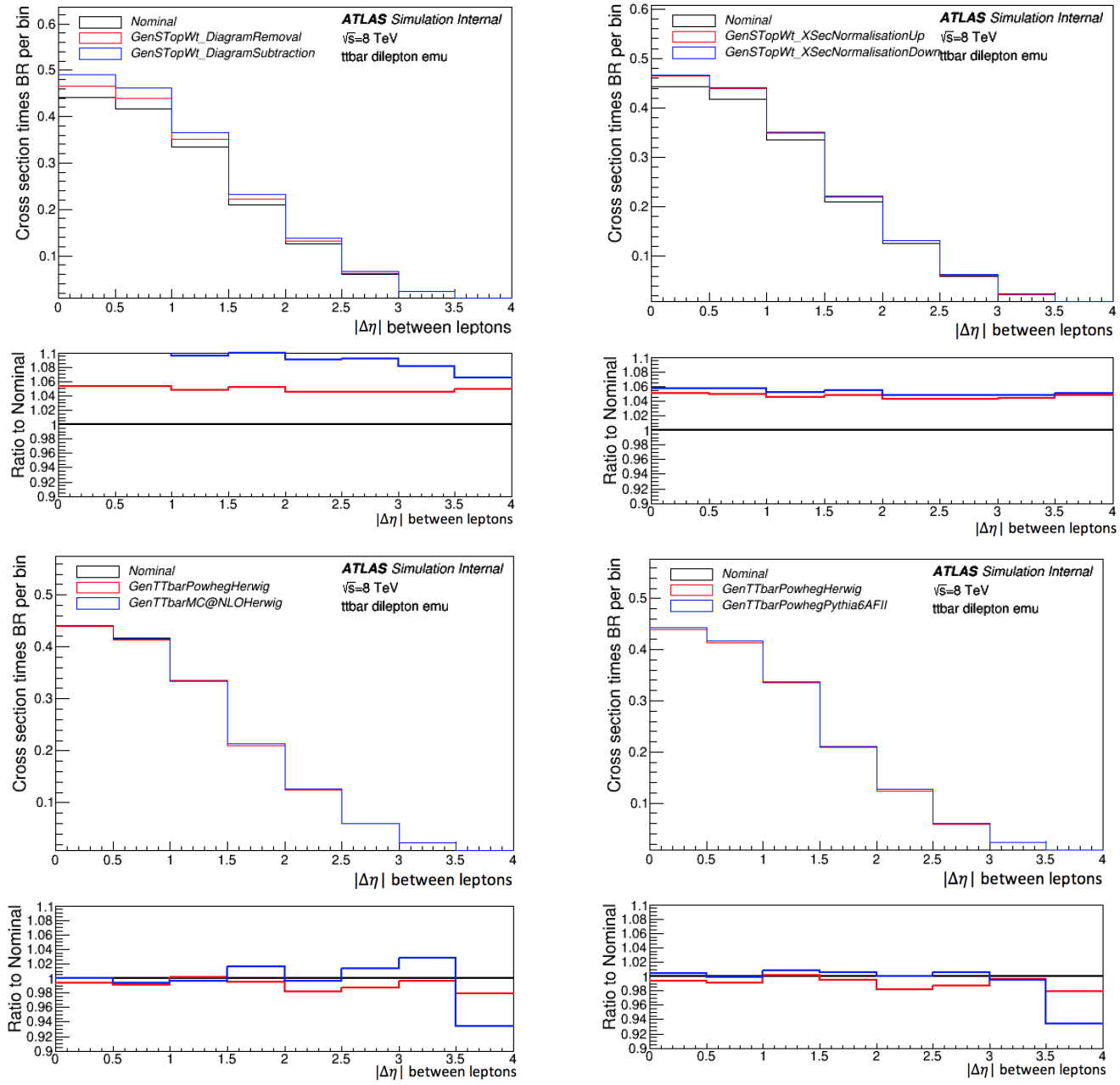

Fig. 7.6 Differential cross-section per bin for the channel $e\mu$ in the variable of the dilepton absolute $\Delta\eta_{ll}$ with measured signal overlaid with statistical uncertainties on the data and MC (signal and background), as well as various systematics.

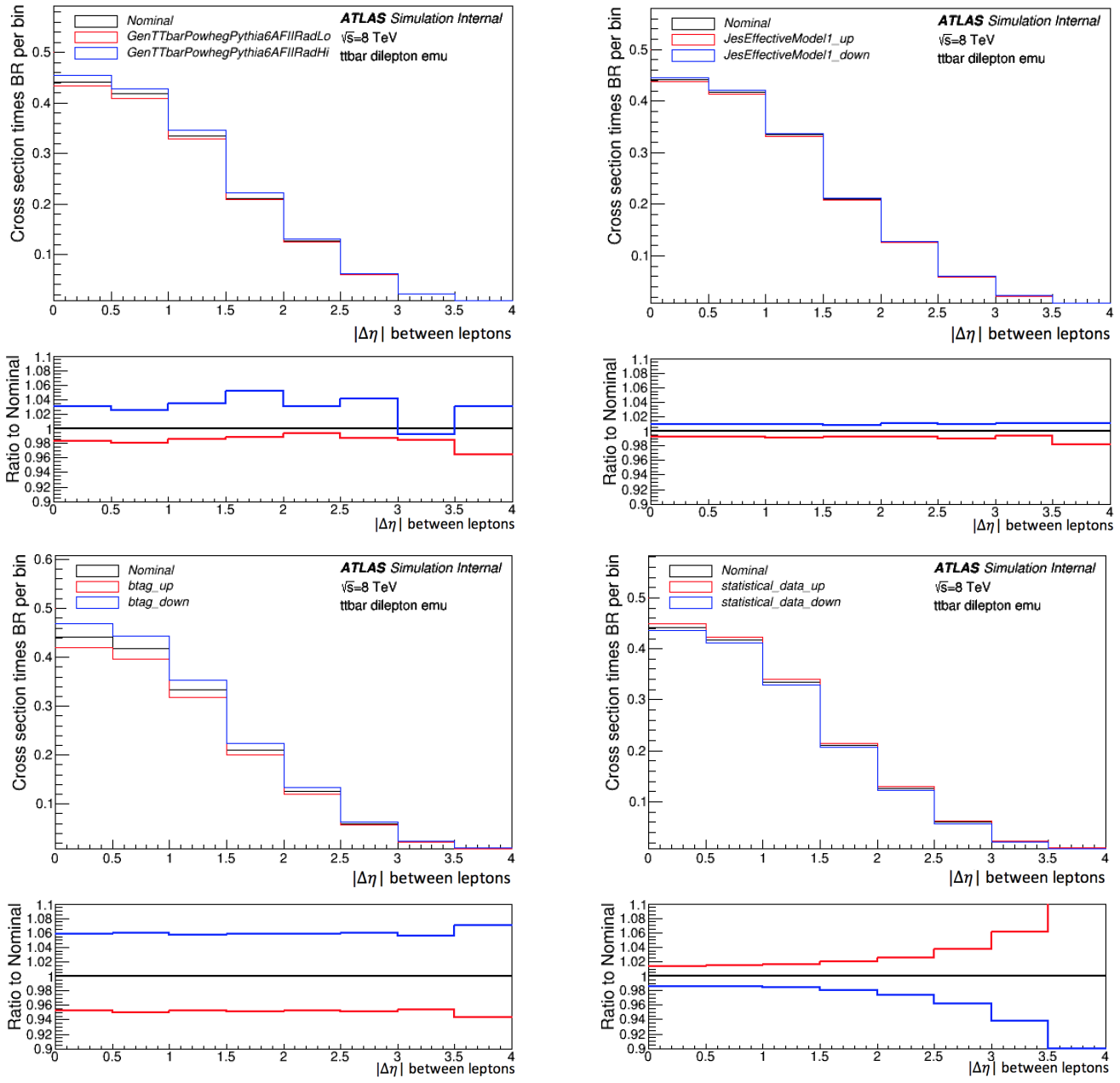

Fig. 7.7 Differential cross-section per bin for the channel $e\mu$ in the variable of the dilepton absolute $\Delta\eta_{ll}$ with measured signal overlaid with statistical uncertainties on the data and MC (signal and background), as well as various systematics.

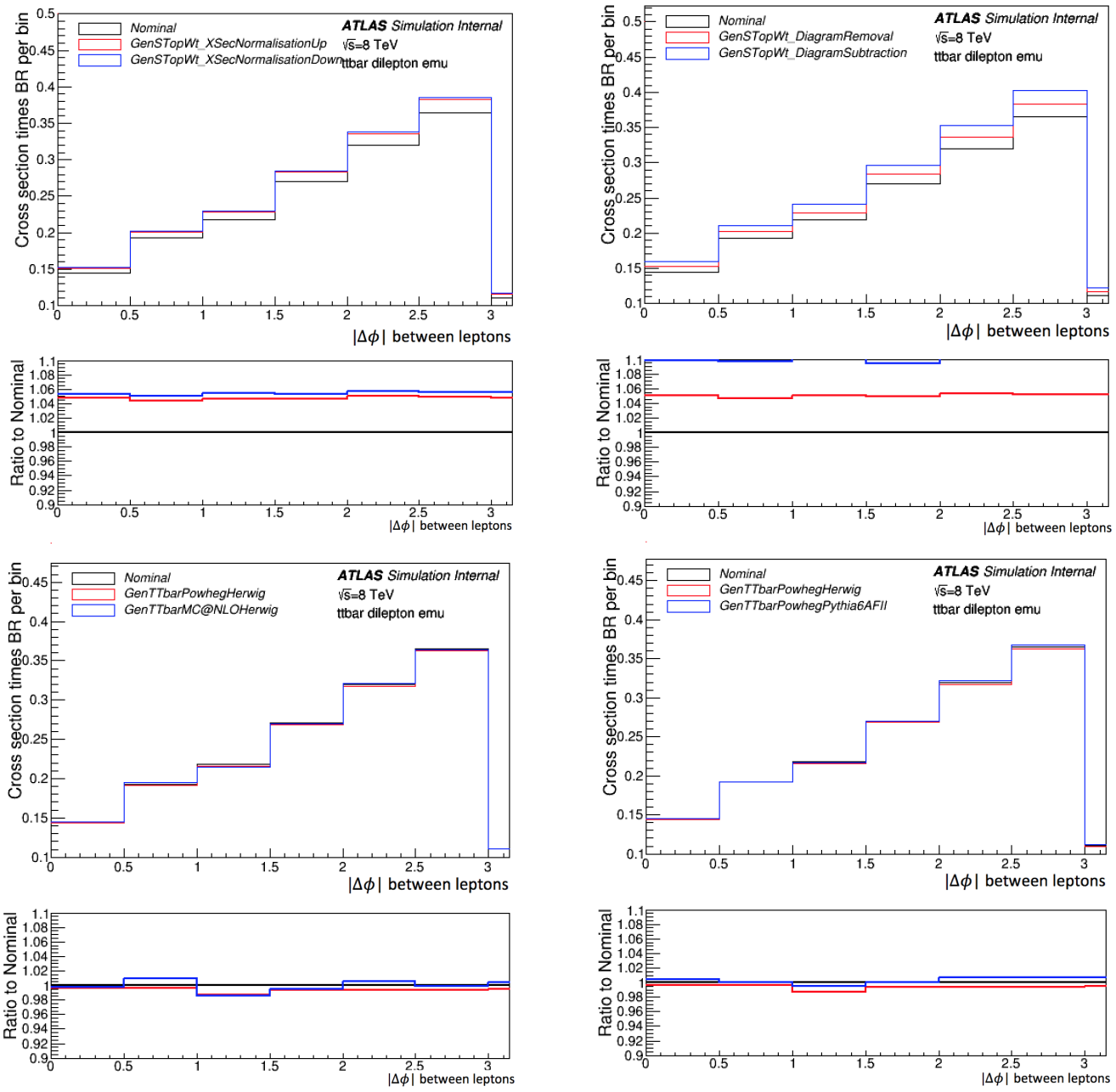

Fig. 7.8 Differential cross-section per bin for the $e\mu$ channel in the variable of the dilepton absolute $\Delta\phi_{ll}$ with measured signal overlaid with statistical uncertainties on the data and MC (signal and background), as well as various systematics.

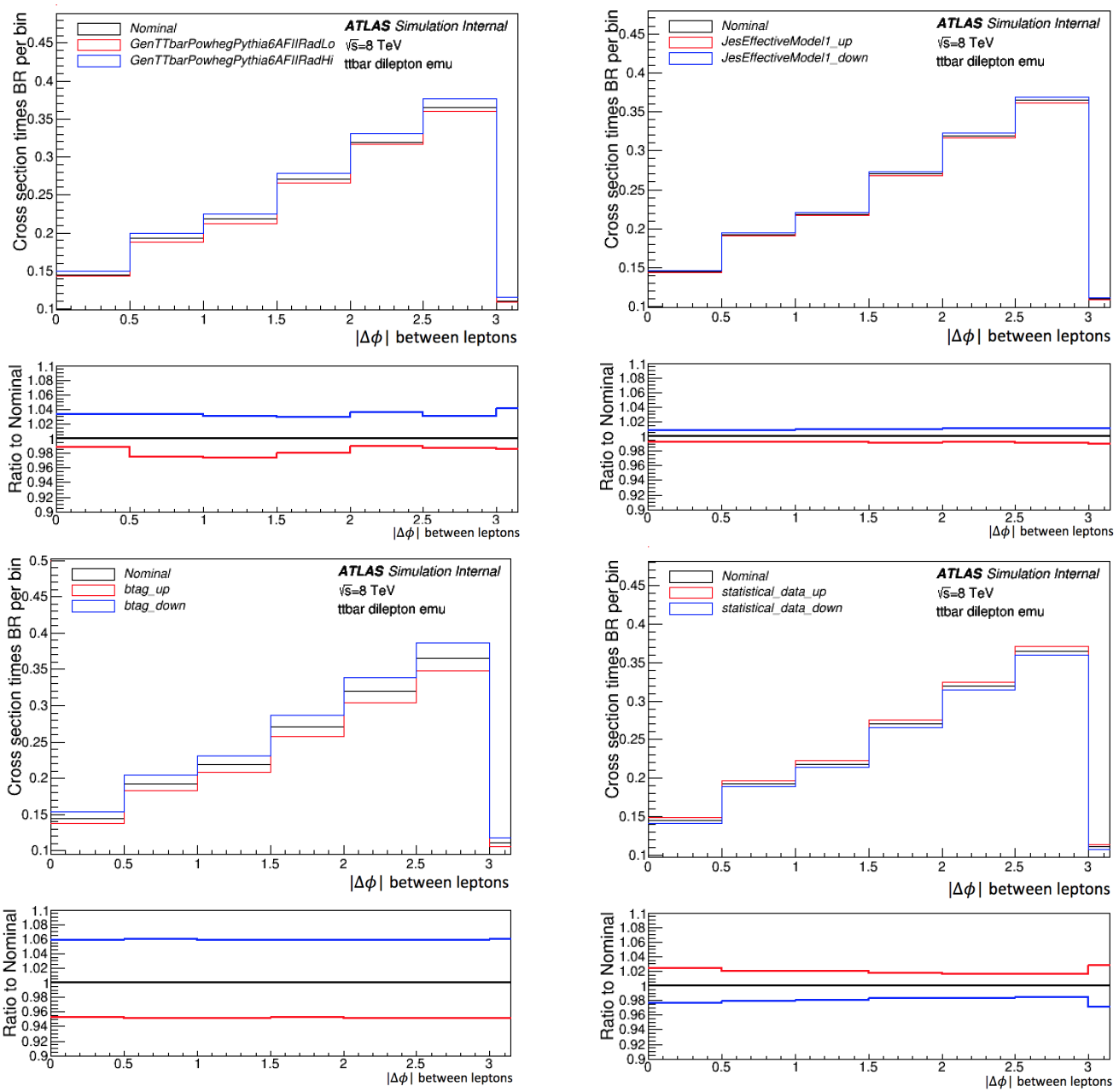

Fig. 7.9 Differential cross-section per bin for the $e\mu$ channel in the variable of the dilepton absolute $\Delta\phi_{ll}$ with measured signal overlaid with statistical uncertainties on the data and MC (signal and background), as well as various systematics.

Most of the detector modelling systematics almost play no role but they have been evaluated for completeness. The most significant contribution arises due to b-tag and Jet Energy Scale. Alternative signal samples have been used to evaluate the systematic uncertainties due to generator, parton showering, initial and final state radiation background.

Modelling systematics have also been evaluated according to the recommendations of the top working group. The most significant contribution comes from the modelling of signal and backgrounds. The cross-sections for different up and down variations have been evaluated and overlaid with respect to the nominal in order to make a direct comparison between them.

Chapter 8

Results

8.1 Differential and fiducial cross-section

In order to be able to describe the scattering-angle distribution, the differential cross-section is defined. From this, it can be determined how many particles on average are produced or scattered in an event at a certain angle. The differential cross-section gives more insight into the underlying physics compared to the inclusive cross-section. The motivation to do differential analysis is to compare with different MC generators bin-by-bin to provide feedback to theorists on their predictions. It is comparatively difficult in the inclusive cross-section to get conclusions for each of the generators.

The top or $t\bar{t}$ system variables like $m_{t\bar{t}}$ or $p_{t\bar{t}}$ are sensitive to new physics in the decays of top quarks, but the lepton channels allow for a more precise measurement than the $t\bar{t}$ system. The differential measurements provide a better understanding of the SM, e.g. the lepton p_T can be well predicted by the SM and compared to data. It depends on the parameters in the SM, which may not be known well, like the top p_T distribution which affects the lepton p_T so it is useful to measure the differential cross-section with respect to the lepton p_T. Certain variables are sensitive to new physics, e.g. the invariant mass of the top-antitop pair or the two leptons are sensitive to a heavy resonance. Experimentally precise measured quantities like lepton p_T or the angles all have low uncertainty. The normalized differential cross-section reduces certain systematic errors e.g. the uncertainty in luminosity is a flat uncertainty whose shifts get cancelled due to normalization by the total cross-section. The ATLAS experiment has no experiment-wide definition of "fiducial". The fiducial volume defines the physical volume where the experiment is sensitive to certain signals and it depends on the analysis. Generally, the fiducial phase space is determined so that the final leptons are produced here within the detector acceptance. This reduces model-related uncertainties

from the extrapolation of the measurement outside the experimentally well-defined region of phase space.

For this analysis, additional fiducial cuts are made on the p_T and η of the leptons. The most natural and standard way carried out by ATLAS to define fiducial volume is the "Cut and Count" method which involves an application of cuts on the most discriminant physical quantities of events, such as p_T, η, H_T etc. The cuts are applied on individual or many variables at the same time. The selection procedure is a sequence of cuts, and is typically well described by yield tables or histograms that are called “Cut-Flows”. The choice of each single cut is motivated by the shape of the MC signal and background distributions in the variables and their cut value is “optimized”. The aim is to have the largest contribution of events from the sample but to minimise the background contamination. A score function is used to define the optimum cut. The fiducial differential measurement presented in this thesis makes use of particle-level objects, charged leptons from the decay of W boson with absolute $\eta < 2.47$ and $p_T > 25$ GeV in the dilepton channel. There are no fiducial cuts on the b-jets in this analysis. A summary of yields for the data, $t\bar{t}$, single top, Z+jets, and diboson samples used in this analysis has been given in Table 8.1. lf N is the number of surviving events at the end of the selection procedure, then it is the number of signal (S) and background (B) events respectively, so that the best estimate of signal is:

$$S = N - B \tag{8.1}$$

with uncertainty

$$\sigma^2(S) = \sigma^2(N) + \sigma^2(B) = N + \sigma^2(B) \tag{8.2}$$

where the number of data events have been characterised by a Poissonian fluctuation and the uncertainty in the estimated mean value of background is $\sigma(B)$. With large MC statistics, the uncertainty on the background becomes very small and hence can be ignored. Under this assumption

$$\frac{S}{\sigma(S)} = \frac{S}{\sqrt{N}} = \frac{S}{\sqrt{S+B}} \tag{8.3}$$

8.2 Measurement of $\frac{d\sigma_{t\bar{t}}}{dp_t}$

This section describes the fiducial differential cross-section of $t\bar{t}$ decaying to dilepton as a function of the leading lepton p_T in the $e\mu$ channel. The sub-leading lepton has also been investigated but its migration matrix is not diagonal, which might need more effort to investigate and unfold. It has been seen that for the bin 600-800 GeV, there is only one

Process	Number of events
$t\bar{t}$	20540.24±143
Single top	2159.70±28.34
Z+jets	50.84±9.78
Dibosons	21.34 ±2.84
Total background	2231.84±47
Data	23194 ±152

Table 8.1 Summary of yields for the data, $t\bar{t}$, single top, Z+jets, and diboson samples used in this analysis. The yields are written with their statistical uncertainty. The $t\bar{t}$ sample is POWHEG+PYTHIA.

event in the MC. As there is no data above 400 GeV the differential cross-section yields zero cross-section for a bin above 400 GeV.

Bin [GeV]	Measured $d\sigma/dx$ [pb/GeV]	Statistical Data [%]	Statistical MC Bkg [%]	Statistical MC Sig [%]	Systematic [%]
[20,40]	0.0081	+/- 2.2	+/- 0.6	+/- 0.5	+5.5/-4.5
[40,60]	0.0239	+/- 1.3	+/- 0.4	+/- 0.3	+5.8/-4.8
[60,80]	0.0208	+/- 1.4	+/- 0.3	+/- 0.3	+6.1/-5.0
[80,120]	0.0100	+/- 1.5	+/- 0.4	+/- 0.3	+6.3/-5.2
[120,200]	0.0019	+/- 2.5	+/- 0.8	+/- 0.5	+6.9/-5.8
[200,400]	0.0001	+/- 8.4	+/- 3.1	+/- 1.5	+8.6/-7.5

Table 8.2 Per-bin total statistical and systematic uncertainties in $e\mu$ for the leading lepton p_T, with only detector modelling systematic uncertainties.

Bin [GeV]	Measured $d\sigma/dx$ [pb/GeV]	Statistical Data [%]	Statistical MC Bkg [%]	Statistical MC Sig [%]	Systematic [%]
[20,40]	0.0081	+/- 2.2	+/- 0.6	+/- 0.5	+7.7/-7.0
[40,60]	0.0239	+/- 1.3	+/- 0.4	+/- 0.3	+8.8/-8.2
[60,80]	0.0208	+/- 1.4	+/- 0.3	+/- 0.3	+8.6/-7.8
[80,120]	0.0100	+/- 1.5	+/- 0.4	+/- 0.3	+10.2/-9.5
[120,200]	0.0019	+/- 2.5	+/- 0.8	+/- 0.5	+13.0/-12.5
[200,400]	0.0001	+/- 8.4	+/- 3.1	+/- 1.5	+24.5/-24.2

Table 8.3 Per-bin total statistical and systematic uncertainties in $e\mu$ for leading lepton p_T, with all systematic uncertainties (detector modelling, signal modelling and background modelling).

A slope is seen in the lepton p_T distribution for the data compared to most of the MCs, which is expected as the lepton spectra in the MC are usually a bit harder than those in the data, which can also be seen in the plots of similar studies. The lepton p_T tails are not modelled well. The statistical uncertainty, systematic uncertainty, signal modelling

systematics, background modelling systematics, MC statistical uncertainty and all detector modelling systematics have been evaluated in each bin of the observable. The individual components in each bin are presented in Table 8.4 but only the final numbers are shown in Tables 8.2 and 8.3. The measured fiducial differential cross-section has been normalised to the unit area in order to be able to make a direct comparison between different particle level predictions. The unfolded cross-section agrees well in shape with the predictions. A normalised version of the fiducial differential distribution is shown in Figure 8.6. The systematic bands become barely visible for the case of detector modelling systematics but are still significant if the systematic uncertainty includes all the modelling systematics. The normalised distributions show that at a high p_T, the lepton p_T is not well described by the modelling even allowing for systematic effects in the modelling.

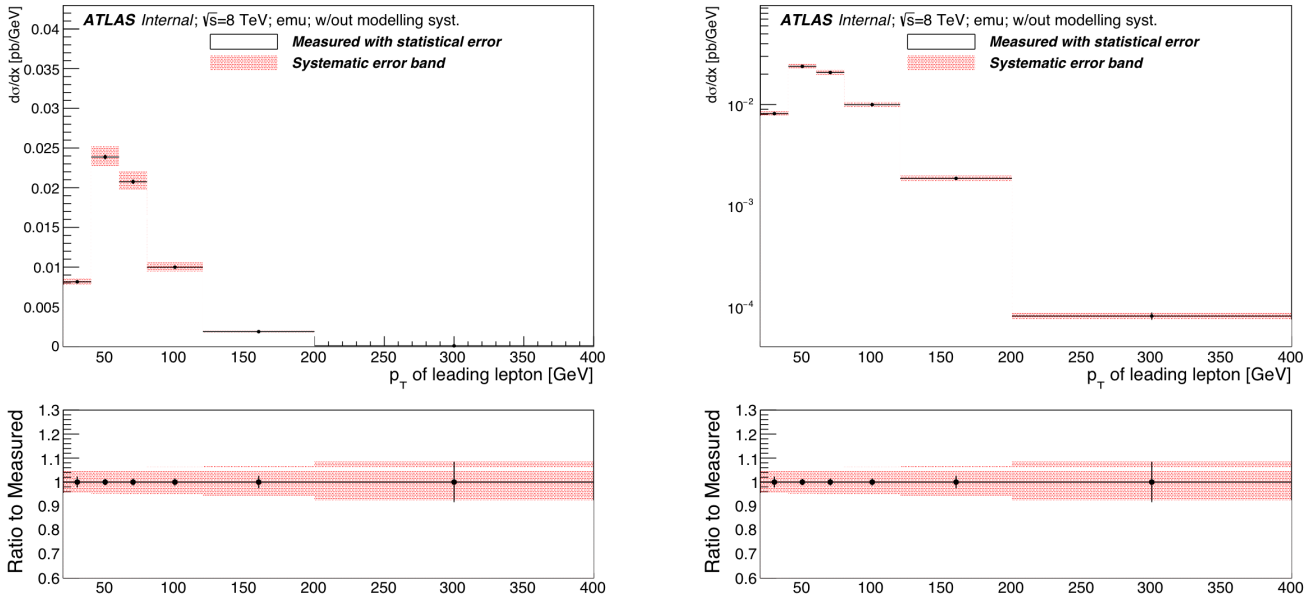

Fig. 8.1 Fiducial differential distribution as a function of the leading lepton p_T. The left hand side plot is linear while the right hand side is semi-log, only the detector modelling systematics have been shown by the systematic error band.

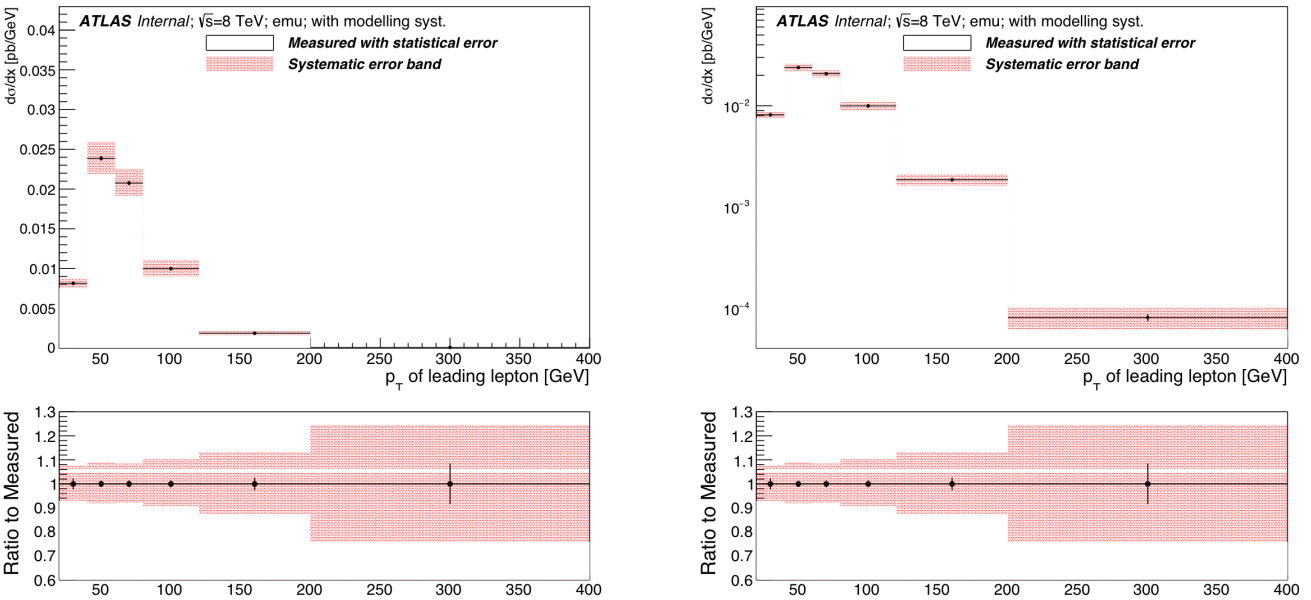

Fig. 8.2 Fiducial differential distribution as a function of the leading lepton p_T. The left hand side plot is linear while the right hand side is semi-log, the detector modelling, signal modelling and background modelling systematics have been shown by the systematic error band.

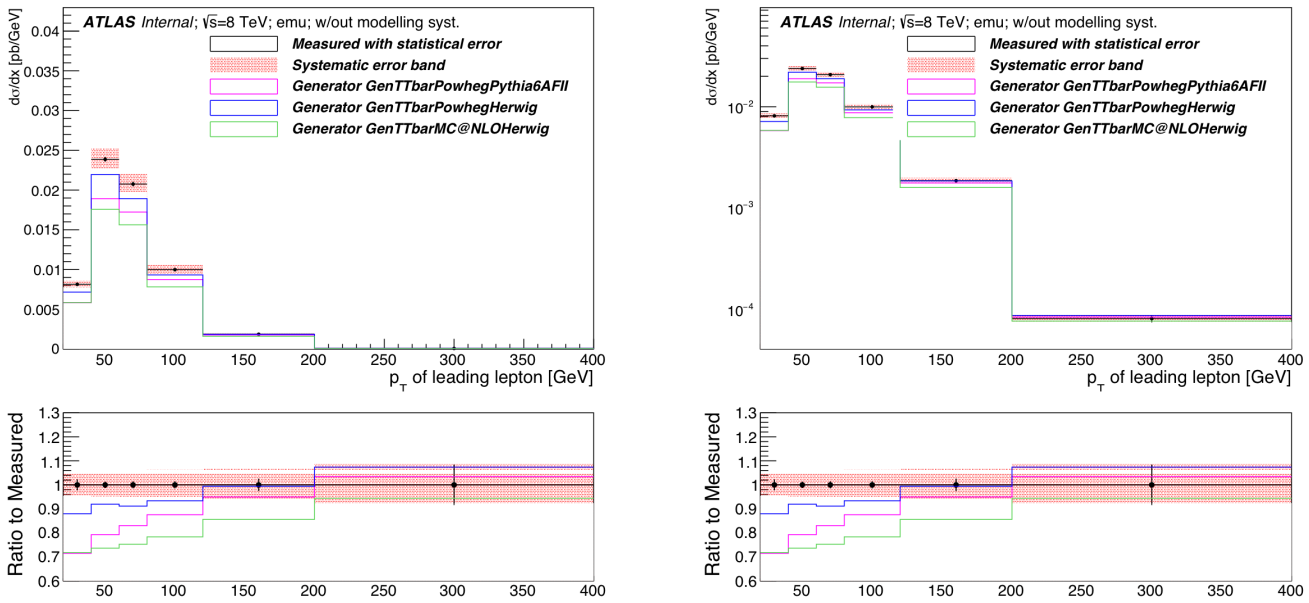

Fig. 8.3 Fiducial differential distribution as a function of the leading lepton p_T. The left hand side plot is linear while the right hand side is semi-log, all the detector modelling systematics have been shown by the systematic error band.

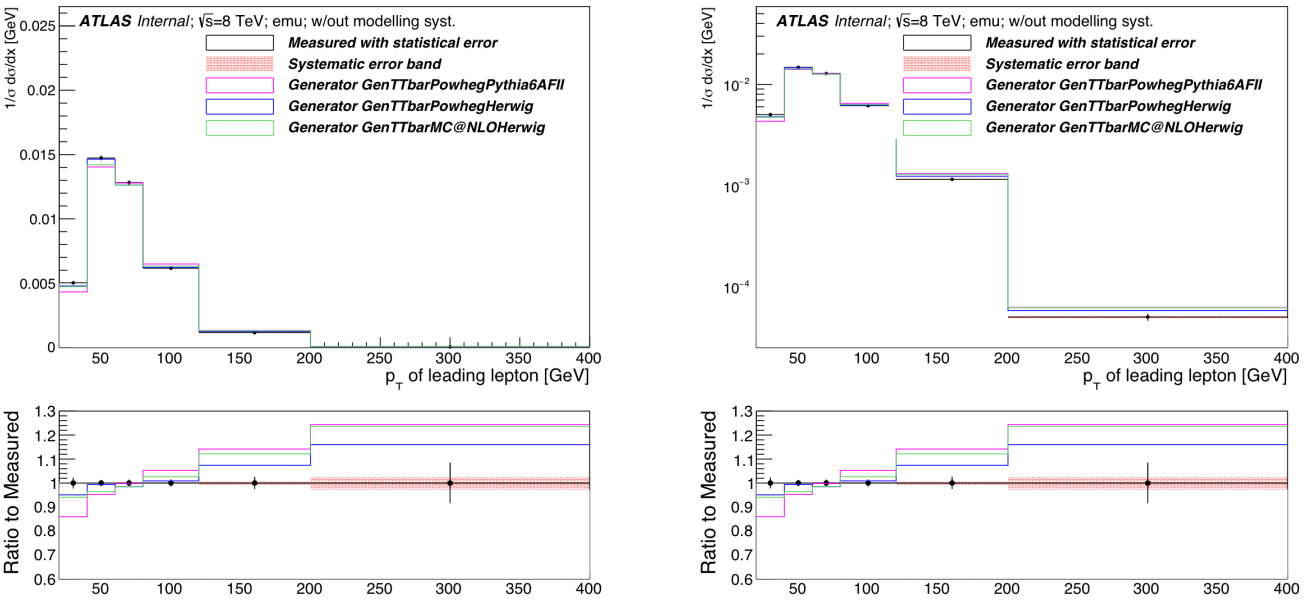

Fig. 8.4 Comparison of the measured fiducial differential cross-section with different predictions as a function of the leading lepton p_T. Only the detector modelling systematics have been shown by the systematic error band. The normalised differential cross-section has been shown on the linear scale while the right hand side plot is on the semi-log scale. The y-axis has been normalised to the unit area to make a direct comparison with particle level predictions.

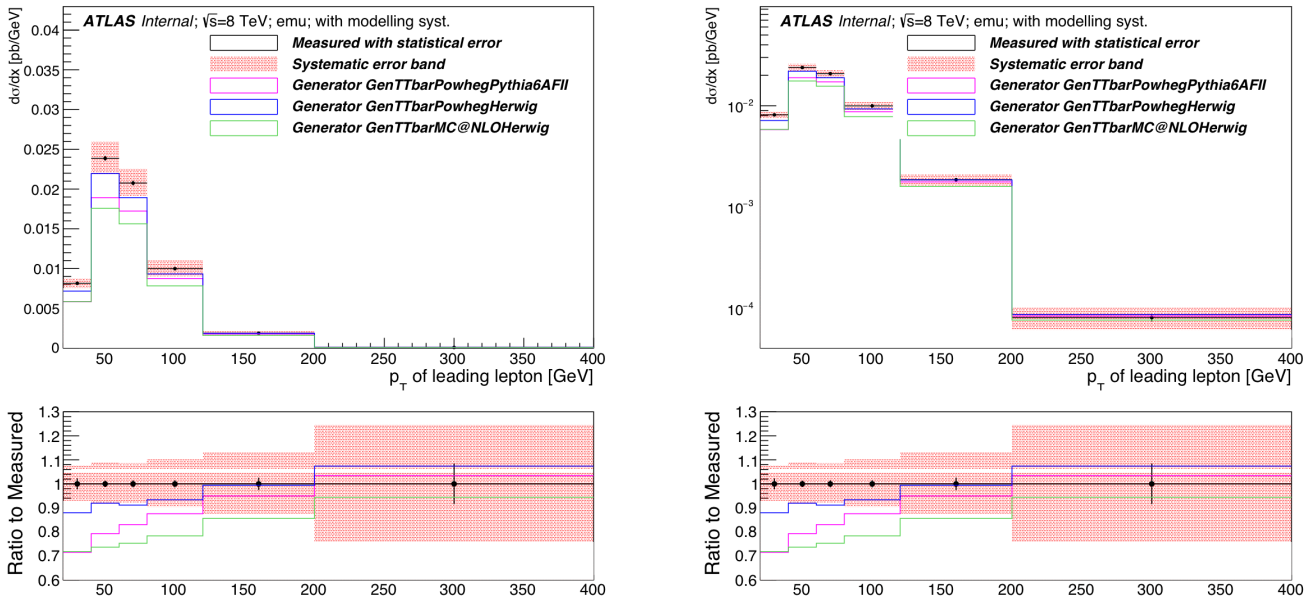

Fig. 8.5 Fiducial differential distribution as a function of the leading lepton p_T. The left hand side plot is linear while the right hand side is semi-log, all the detector modelling, signal modelling and background modelling systematics have been shown by the systematic error band.

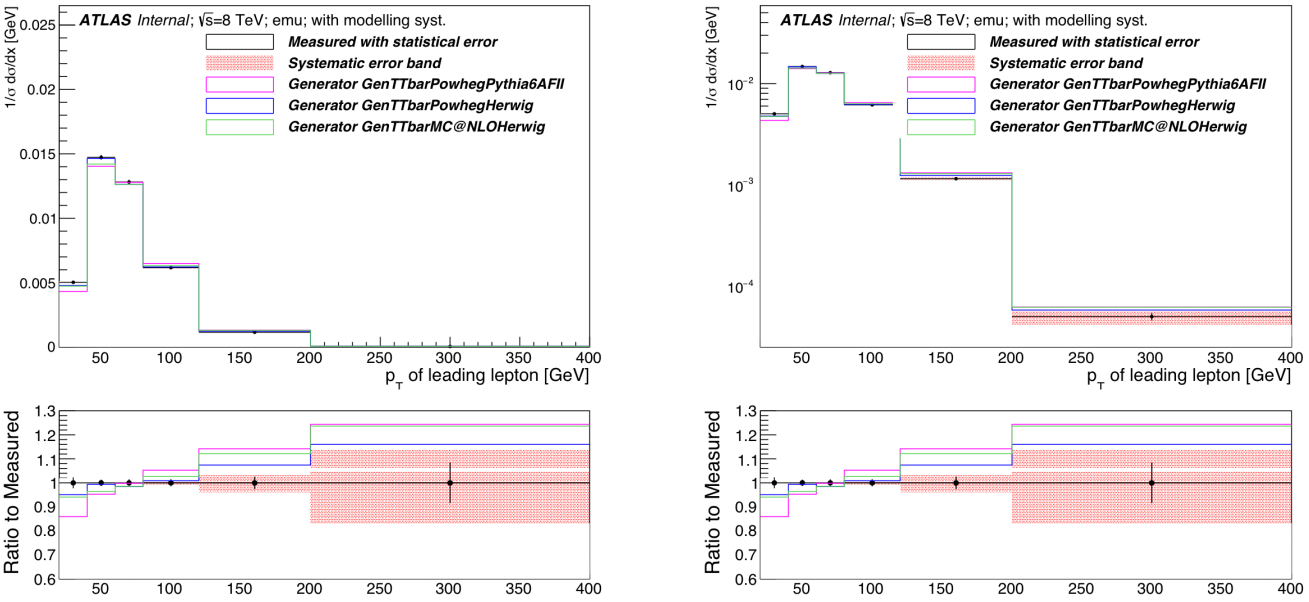

Fig. 8.6 Comparison of the measured fiducial differential cross-section with different predictions as a function of the leading lepton p_T. All the modelling systematics have been shown by the systematic band. The left hand side plot is on the linear scale while the right hand side plot is on the semi-log scale. The plots have been normalized to the unit area to make a direct comparison with particle level predictions. The reduction of the systematic uncertainties for the normalised case have been depicted on the systematic error band.

Uncertainty	[20,40]	[40,60]	[60,80]	[80,120]	[120,200]	[200,400]
StatisticalData	[-2.25,2.25]	[-1.31,1.31]	[-1.42,1.42]	[-1.48,1.48]	[-2.55,2.55]	[-8.42,8.42]
StatisticalBkg	[-0.57,0.57]	[-0.37,0.37]	[-0.34,0.34]	[-0.35,0.35]	[-0.78,0.78]	[-3.13,3.13]
StatisticalSig	[-0.50,0.51]	[-0.27,0.28]	[-0.30,0.30]	[-0.30,0.30]	[-0.50,0.51]	[-1.41,1.45]
BTag	[-4.33,5.29]	[-4.63,5.65]	[-4.82,5.86]	[-5.00,6.07]	[-5.50,6.61]	[-6.46,7.70]
Jeff	[-0.01,0.01]	[-0.02,0.02]	[-0.01,0.01]	[-0.03,0.03]	[-0.01,0.01]	[-0.03,0.03]
Jer	[-0.30,0.30]	[-0.23,0.23]	[-0.43,0.43]	[-0.70,0.70]	[-0.57,0.57]	[-2.95,2.95]
MuidRes	[-0.01,0.01]	[-0.02,0.02]	[-0.01,0.01]	[-0.03,0.03]	[-0.03,0.03]	[-0.15,0.15]
MumsRes	[-0.11,0.11]	[-0.03,0.03]	[-0.04,0.04]	[-0.10,0.10]	[-0.08,0.08]	[-1.14,1.14]
BJesUnc	[-0.43,0.58]	[-0.37,0.37]	[-0.34,0.48]	[-0.45,0.50]	[-0.37,0.60]	[-0.59,0.11]
JesEffectiveStat1	[-0.28,0.39]	[-0.28,0.34]	[-0.27,0.39]	[-0.33,0.37]	[-0.38,0.40]	[-0.23,0.24]
JesEffectiveStat2	[-0.03,0.01]	[-0.03,0.02]	[-0.00,0.02]	[-0.04,0.03]	[-0.06,0.03]	[-0.09,0.09]
JesEffectiveStat3	[-0.03,0.03]	[-0.01,0.00]	[-0.02,0.02]	[-0.02,0.01]	[-0.00,0.01]	[-0.01,0.08]
JesEffectiveStat4	[-0.02,0.03]	[-0.05,0.04]	[-0.04,0.07]	[-0.09,0.03]	[-0.06,0.07]	[-0.05,0.08]
JesEffectiveModel1	[-0.84,0.98]	[-0.81,0.79]	[-0.78,1.03]	[-0.88,0.97]	[-0.97,1.16]	[-1.11,0.43]
JesEffectiveModel2	[-0.01,0.00]	[-0.03,0.02]	[-0.01,0.02]	[-0.03,0.03]	[-0.05,0.03]	[-0.02,0.09]
JesEffectiveModel3	[-0.02,0.04]	[-0.05,0.04]	[-0.04,0.05]	[-0.08,0.03]	[-0.07,0.07]	[-0.05,0.11]
JesEffectiveModel4	[-0.01,0.01]	[-0.01,0.00]	[-0.02,0.02]	[-0.01,0.00]	[-0.01,0.01]	[-0.08,0.08]
JesEffectiveDet1	[-0.03,0.07]	[-0.06,0.05]	[-0.04,0.10]	[-0.09,0.05]	[-0.09,0.06]	[-0.09,0.04]
JesEffectiveDet2	[-0.04,0.04]	[-0.06,0.06]	[-0.05,0.10]	[-0.10,0.05]	[-0.09,0.07]	[-0.11,0.09]
JesEffectiveDet3	[-0.00,0.00]	[-0.01,0.01]	[-0.00,0.02]	[-0.01,0.01]	[-0.01,0.02]	[-0.08,0.08]
JesEffectiveMix1	[-0.09,0.11]	[-0.09,0.08]	[-0.08,0.14]	[-0.14,0.09]	[-0.16,0.13]	[-0.12,0.06]
JesEffectiveMix2	[-0.13,0.16]	[-0.12,0.11]	[-0.12,0.17]	[-0.17,0.11]	[-0.18,0.16]	[-0.12,0.14]
JesEffectiveMix3	[-0.02,0.02]	[-0.05,0.03]	[-0.03,0.05]	[-0.07,0.04]	[-0.07,0.05]	[-0.02,0.10]
JesEffectiveMix4	[-0.00,0.00]	[-0.00,0.00]	[-0.00,0.00]	[-0.00,0.00]	[-0.01,0.01]	[-0.04,0.04]
EtaIntercalibrationModel	[-0.08,0.24]	[-0.13,0.15]	[-0.12,0.17]	[-0.14,0.17]	[-0.18,0.20]	[-0.09,0.09]
EtaIntercalibrationTotalStat	[-0.19,0.24]	[-0.19,0.19]	[-0.19,0.25]	[-0.23,0.22]	[-0.25,0.25]	[-0.22,0.05]
PileupOffsetMu	[-0.04,0.04]	[-0.06,0.06]	[-0.03,0.11]	[-0.08,0.05]	[-0.06,0.03]	[-0.07,0.04]
PileupOffsetNPV	[-0.12,0.12]	[-0.12,0.11]	[-0.01,0.14]	[-0.08,0.12]	[-0.03,0.18]	[-0.16,0.16]
PileupRho	[-0.53,0.77]	[-0.56,0.59]	[-0.57,0.75]	[-0.64,0.72]	[-0.71,0.84]	[-0.82,0.44]
PunchThrough	[-0.00,0.00]	[-0.00,0.00]	[-0.00,0.00]	[-0.00,0.00]	[-0.00,0.00]	[-0.00,0.00]
CTauTag	[-0.02,0.02]	[-0.03,0.03]	[-0.03,0.03]	[-0.04,0.04]	[-0.03,0.03]	[-0.08,0.08]
ElectronEnergyResolution	[-0.07,0.04]	[-0.03,0.03]	[-0.01,0.03]	[-0.03,0.03]	[-0.15,0.15]	[-0.25,0.25]
ElectronEnergyScale	[-0.22,0.05]	[-0.02,0.05]	[-0.03,0.03]	[-0.14,0.24]	[-0.30,0.30]	[-0.98,1.59]
ElectronIdSF	[-0.17,0.17]	[-0.19,0.19]	[-0.20,0.20]	[-0.27,0.26]	[-0.47,0.47]	[-1.09,1.09]
ElectronRecoSF	[-0.02,0.02]	[-0.01,0.01]	[-0.02,0.02]	[-0.04,0.03]	[-0.07,0.07]	[-0.16,0.16]
ElectronTriggerSF	[-0.01,0.01]	[-0.01,0.01]	[-0.01,0.01]	[-0.01,0.01]	[-0.03,0.03]	[-0.07,0.07]
FlavorComp	[-0.16,0.29]	[-0.33,0.26]	[-0.27,0.34]	[-0.28,0.29]	[-0.48,0.34]	[-0.48,0.13]
FlavorResponse	[-0.13,0.23]	[-0.16,0.18]	[-0.17,0.22]	[-0.17,0.19]	[-0.32,0.19]	[-0.24,0.17]
JetVertexFraction	[-0.19,0.22]	[-0.27,0.30]	[-0.22,0.33]	[-0.26,0.29]	[-0.27,0.27]	[-0.14,0.09]
Mistag	[-0.06,0.06]	[-0.08,0.08]	[-0.08,0.08]	[-0.08,0.09]	[-0.10,0.10]	[-0.18,0.18]
MuonIdSF	[-0.04,0.04]	[-0.04,0.04]	[-0.05,0.04]	[-0.06,0.06]	[-0.10,0.10]	[-0.22,0.22]
MuonRecoSF	[-0.02,0.02]	[-0.02,0.02]	[-0.02,0.02]	[-0.03,0.02]	[-0.05,0.05]	[-0.13,0.13]
MuonTriggerSF	[-0.00,0.01]	[-0.00,0.00]	[-0.00,0.00]	[-0.00,0.00]	[-0.01,0.01]	[-0.01,0.01]
Musc	[-0.02,0.02]	[-0.01,0.01]	[-0.01,0.01]	[-0.02,0.02]	[-0.00,0.07]	[-0.08,0.04]
ModellingGenerator	[-0.49,0.49]	[-0.51,0.51]	[-0.60,0.60]	[-0.83,0.83]	[-0.95,0.95]	[-0.64,0.64]
ModellingParton	[-0.90,0.90]	[-0.56,0.56]	[-0.92,0.92]	[-0.98,0.98]	[-1.20,1.20]	[-0.47,0.47]
ModellingRadiation	[-4.08,4.08]	[-5.02,5.02]	[-4.05,4.05]	[-5.85,5.85]	[-4.86,4.86]	[-4.11,4.11]
ModellingSingleTopWtNormalisation	[-0.45,0.45]	[-0.56,0.56]	[-0.57,0.57]	[-0.70,0.70]	[-1.31,1.31]	[-3.00,3.00]
ModellingSingleTopWtInterference	[-3.32,3.32]	[-4.17,4.17]	[-4.28,4.28]	[-5.20,5.20]	[-9.74,9.74]	[-22.37,22.37]

Table 8.4 Per-bin individual statistical and systematic uncertainties for the leading lepton p_T.

8.3 Measurement of $\frac{d\sigma_{t\bar{t}}}{dm_{ll}}$

This section describes the fiducial differential cross-section of $t\bar{t}$ decaying to dilepton as a function of the invariant mass of two oppositely charged leptons in the $e\mu$ channel. The statistical uncertainty, systematic uncertainty, signal modelling systematics, background modelling systematics, MC statistical uncertainty and all detector modelling systematics have been evaluated in each bin of the observable.

Bin [GeV]	Measured $d\sigma/dx$ [pb/GeV]	Statistical Data [%]	Statistical MC Bkg [%]	Statistical MC Sig [%]	Systematic [%]
[20,40]	0.0056	+/- 2.7	+/- 0.6	+/- 0.6	+5.9/-4.9
[40,60]	0.0082	+/- 2.2	+/- 0.8	+/- 0.5	+5.9/-4.8
[60,80]	0.0115	+/- 1.9	+/- 0.5	+/- 0.4	+5.8/-4.8
[80,100]	0.0125	+/- 1.8	+/- 0.4	+/- 0.4	+5.8/-4.8
[100,130]	0.0100	+/- 1.7	+/- 0.3	+/- 0.3	+6.1/-5.0
[130,160]	0.0069	+/- 2.1	+/- 0.4	+/- 0.4	+6.4/-5.2
[160,200]	0.0041	+/- 2.3	+/- 0.5	+/- 0.5	+6.4/-5.4
[200,260]	0.0019	+/- 2.9	+/- 0.7	+/- 0.6	+6.5/-5.4
[260,340]	0.0006	+/- 4.3	+/- 1.2	+/- 0.9	+6.6/-5.5
[340,500]	0.0002	+/- 6.1	+/- 1.6	+/- 1.4	+6.6/-6.1

Table 8.5 Per-bin total statistical and systematic uncertainties in $e\mu$ for the dilepton mass, m_{ll}, without modelling systematic uncertainties.

Bin [GeV]	Measured $d\sigma/dx$ [pb/GeV]	Statistical Data [%]	Statistical MC Bkg [%]	Statistical MC Sig [%]	Systematic [%]
[20,40]	0.0056	+/- 2.7	+/- 0.6	+/- 0.6	+9.7/-9.1
[40,60]	0.0082	+/- 2.2	+/- 0.8	+/- 0.5	+8.9/-8.2
[60,80]	0.0115	+/- 1.9	+/- 0.5	+/- 0.4	+9.2/-8.6
[80,100]	0.0125	+/- 1.8	+/- 0.4	+/- 0.4	+8.4/-7.7
[100,130]	0.0100	+/- 1.7	+/- 0.3	+/- 0.3	+9.4/-8.7
[130,160]	0.0069	+/- 2.1	+/- 0.4	+/- 0.4	+9.3/-8.6
[160,200]	0.0041	+/- 2.3	+/- 0.5	+/- 0.5	+10.0/-9.4
[200,260]	0.0019	+/- 2.9	+/- 0.7	+/- 0.6	+10.7/-10.1
[260,340]	0.0006	+/- 4.3	+/- 1.2	+/- 0.9	+14.0/-13.5
[340,500]	0.0002	+/- 6.1	+/- 1.6	+/- 1.4	+11.4/-11.1

Table 8.6 Per-bin total statistical and systematic uncertainties in $e\mu$ for the dilepton mass, m_{ll}, with detector modelling, signal modelling and background modelling.

The individual components in each bin have been shown in Table 8.7 but the final numbers are shown in summary Tables 8.5 and 8.6. The measured fiducial differential cross-section has been normalised to the unit area in order to be able to make a direct comparison between different particle level predictions. The unfolded cross-section agrees well in shape with the predictions. The systematic uncertainties in the normalised case are certainly reduced and it is obvious from the bottom pad (ratio plot) in Figure 8.12. The most significant contribution arises due to b-tag and Jet Energy Scales. Alternative signal samples have been used to evaluate the systematic uncertainties due to generator, parton showering, and initial and final

state radiation background. Modelling systematics have also been evaluated according to the recommendations of the top working group. The most significant contribution comes from the modelling of signal and backgrounds.

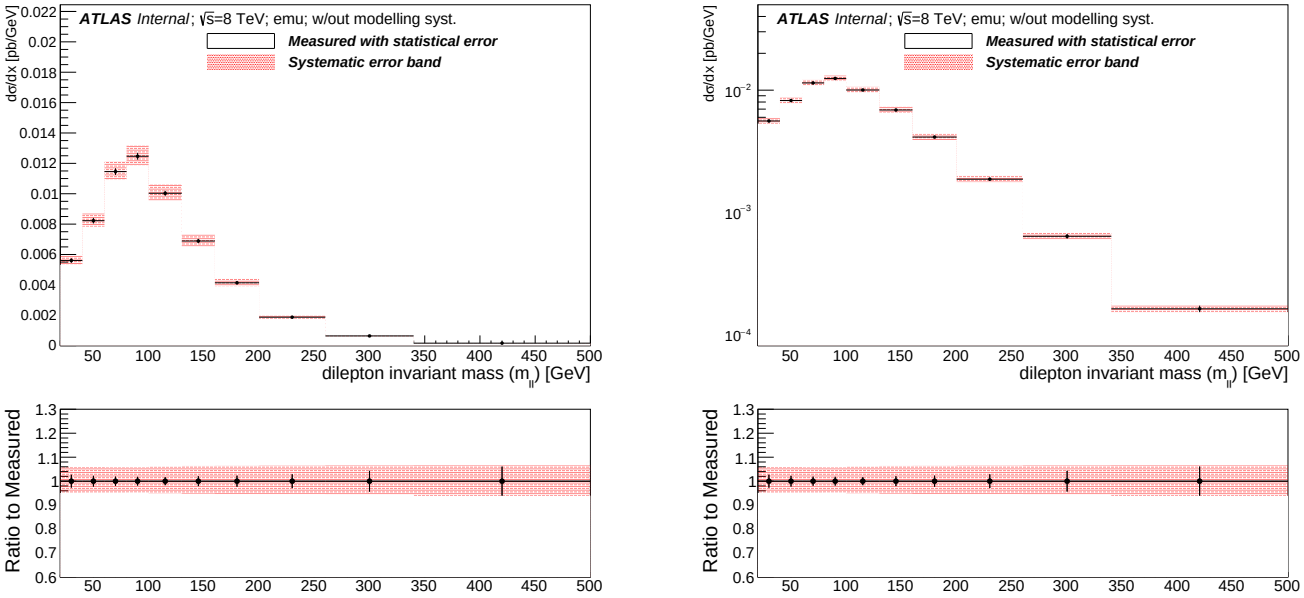

Fig. 8.7 Fiducial differential distribution as a function of the dilepton mass on the linear and semi-log scale. All the detector modelling systematics have been included on the systematic error band.

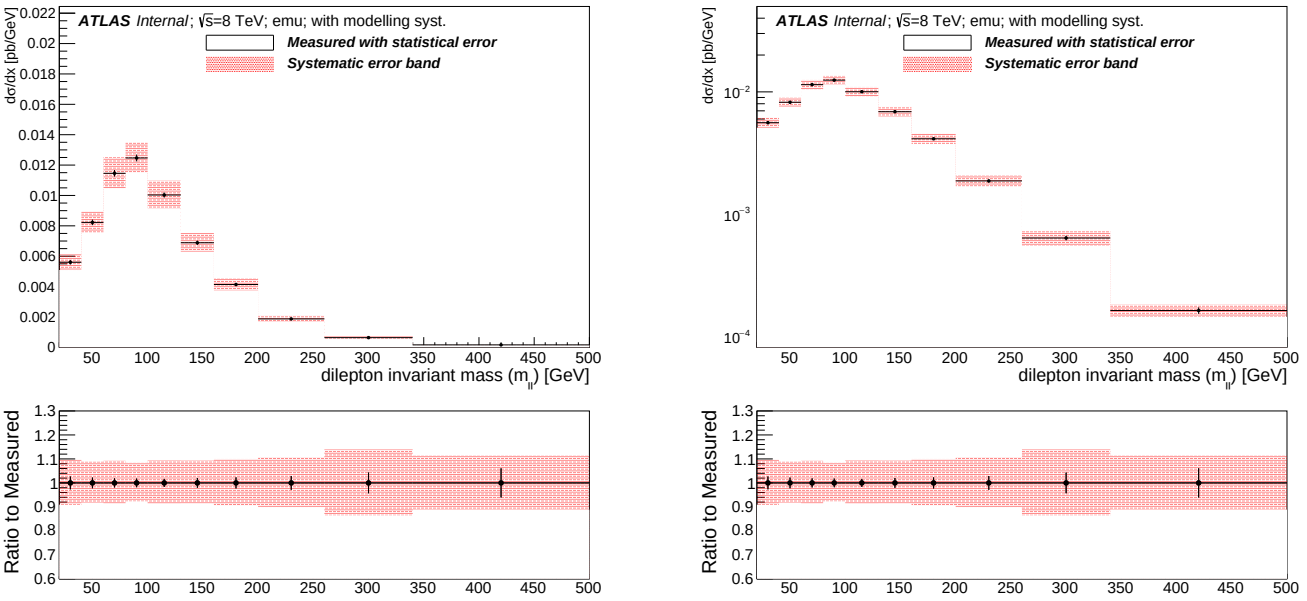

Fig. 8.8 Fiducial differential distribution as a function of the dilepton mass on the linear (left) and semi-log scale (right). All the detector modelling, signal modelling and background modelling systematics are included on the systematic error band.

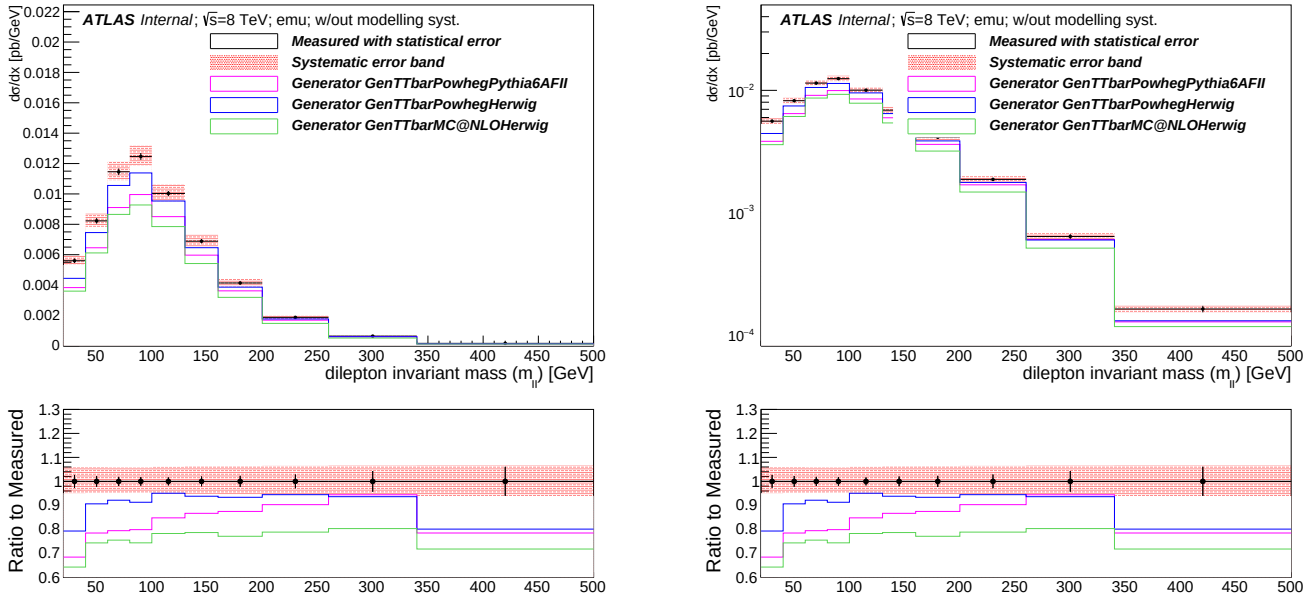

Fig. 8.9 Fiducial differential distribution as a function of the dilepton mass. The left hand side plot is linear while the right hand side is semi-log, all the detector modelling systematics have been included on the systematic error band.

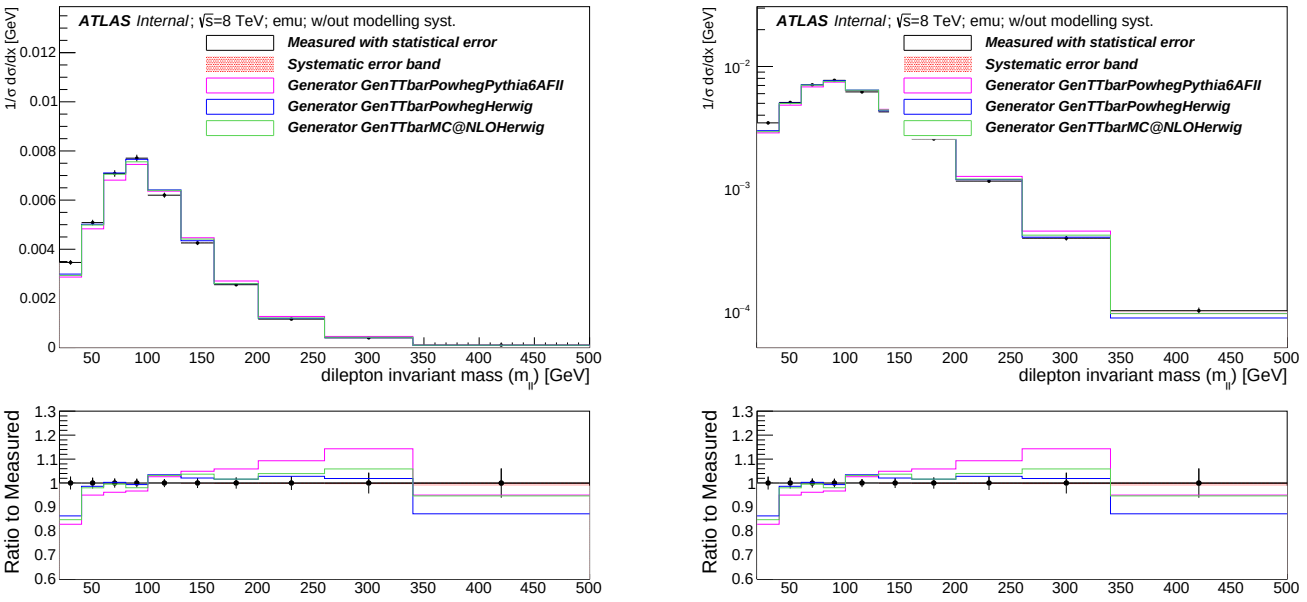

Fig. 8.10 Comparison of the measured fiducial differential cross-section with different predictions as a function of the dilepton mass. Only the detector modelling systematics have been included on the systematic error band. The normalised differential cross-section has been shown on the linear scale while the right hand side plot is on the semi-log scale. The y-axis has been normalised to the unit area to make a direct comparison with particle level predictions.

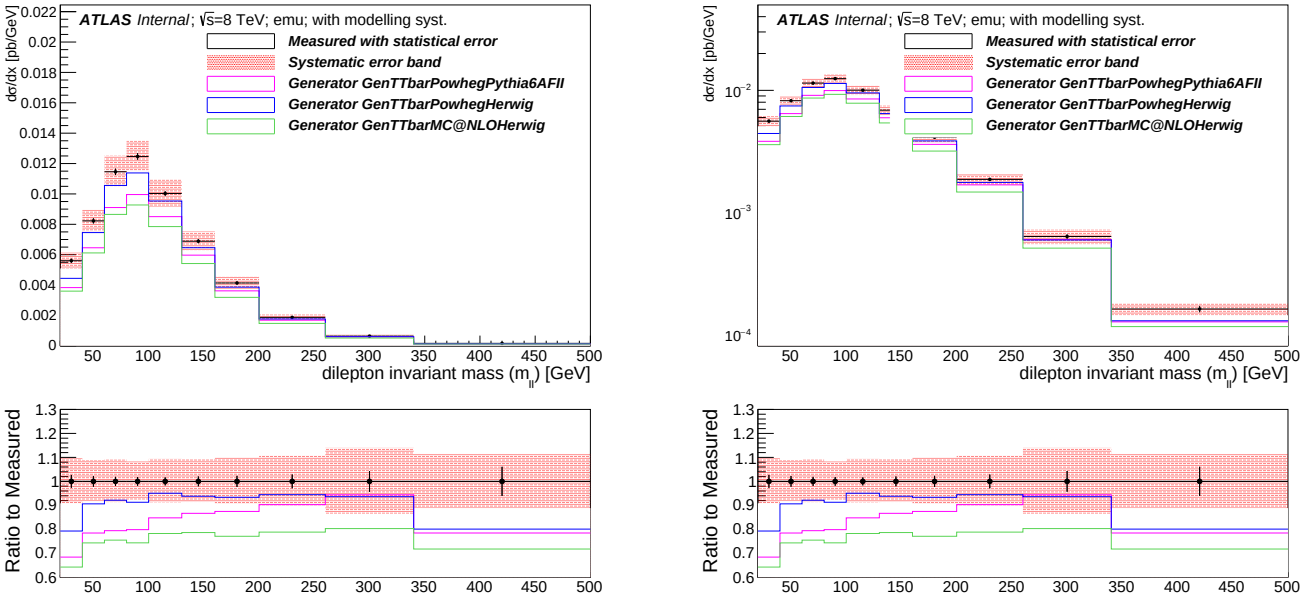

Fig. 8.11 Fiducial differential distribution as a function of the dilepton mass. The left hand side plot is linear while the right hand side is semi-log, all the detector modelling, signal modelling and background modelling systematics are included on the systematic error band.

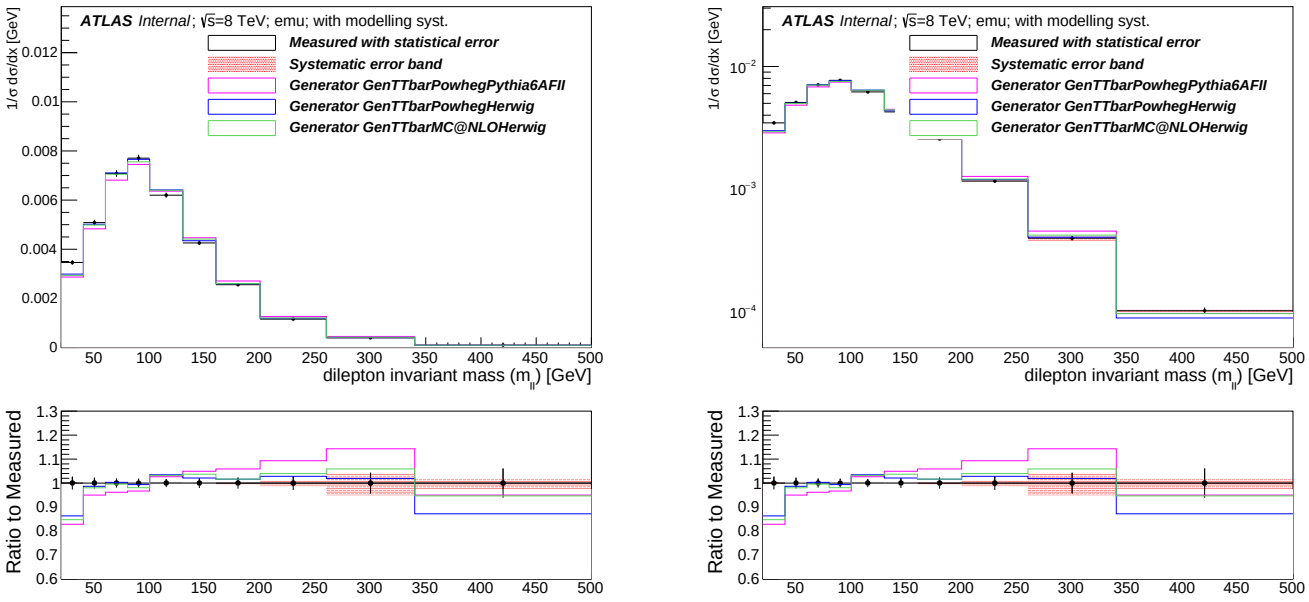

Fig. 8.12 Comparison of the measured fiducial differential cross-section with different predictions as a function of the dilepton mass. All the modelling systematics are included on the systematic error band. The left hand side plot is on the linear scale while the right hand side is on the semi-log scale. The plots have been normalized to the unit area to make a direct comparison with particle level predictions. The reduction of systematic uncertainties for the normalised case have been seen by the size of the systematic error band.

Uncertainty	[20,40]	[40,60]	[60,80]	[80,100]	[100,130]	[130,160]	[160,200]	[200,260]	[260,340]	[340,500]
StatisticalData	[-2.68,2.68]	[-2.24,2.24]	[-1.89,1.89]	[-1.82,1.82]	[-1.68,1.68]	[-2.05,2.05]	[-2.31,2.31]	[-2.88,2.88]	[-4.33,4.33]	[-6.09,6.09]
StatisticalBkg	[-0.60,0.60]	[-0.85,0.85]	[-0.49,0.49]	[-0.38,0.38]	[-0.35,0.35]	[-0.42,0.42]	[-0.50,0.50]	[-0.67,0.67]	[-1.15,1.15]	[-1.56,1.56]
StatisticalSig	[-0.60,0.60]	[-0.46,0.47]	[-0.39,0.39]	[-0.38,0.39]	[-0.35,0.35]	[-0.42,0.43]	[-0.48,0.48]	[-0.58,0.59]	[-0.87,0.88]	[-1.35,1.39]
BTag	[-4.67,5.70]	[-4.70,5.73]	[-4.66,5.68]	[-4.66,5.66]	[-4.83,5.87]	[-4.99,6.05]	[-5.07,6.16]	[-5.16,6.27]	[-5.19,6.26]	[-5.11,6.18]
Jeff	[-0.00,0.00]	[-0.03,0.03]	[-0.00,0.00]	[-0.02,0.02]	[-0.01,0.01]	[-0.04,0.04]	[-0.02,0.02]	[-0.02,0.02]	[-0.02,0.02]	[-0.02,0.02]
Jer	[-0.24,0.24]	[-0.26,0.26]	[-0.04,0.04]	[-0.36,0.36]	[-0.68,0.68]	[-0.95,0.95]	[-0.39,0.39]	[-0.66,0.66]	[-0.60,0.60]	[-0.55,0.55]
MuidRes	[-0.01,0.01]	[-0.06,0.06]	[-0.04,0.04]	[-0.01,0.01]	[-0.03,0.03]	[-0.05,0.05]	[-0.05,0.05]	[-0.04,0.04]	[-0.15,0.15]	[-0.16,0.16]
MumsRes	[-0.01,0.01]	[-0.03,0.03]	[-0.02,0.02]	[-0.03,0.03]	[-0.08,0.08]	[-0.06,0.06]	[-0.06,0.06]	[-0.08,0.08]	[-0.12,0.12]	[-0.12,0.12]
BJesUnc	[-0.46,0.44]	[-0.39,0.48]	[-0.39,0.41]	[-0.30,0.46]	[-0.34,0.50]	[-0.34,0.48]	[-0.56,0.50]	[-0.39,0.41]	[-0.37,0.63]	[-1.08,0.62]
JesEffectiveStat1	[-0.35,0.45]	[-0.30,0.43]	[-0.28,0.30]	[-0.19,0.31]	[-0.28,0.39]	[-0.23,0.44]	[-0.41,0.32]	[-0.29,0.30]	[-0.46,0.52]	[-0.86,0.41]
JesEffectiveStat2	[-0.05,0.02]	[-0.01,0.04]	[-0.02,0.01]	[-0.01,0.02]	[-0.01,0.04]	[-0.03,0.03]	[-0.07,0.01]	[-0.04,0.00]	[-0.02,0.01]	[-0.03,0.02]
JesEffectiveStat3	[-0.02,0.02]	[-0.00,0.05]	[-0.01,0.01]	[-0.00,0.02]	[-0.01,0.01]	[-0.01,0.01]	[-0.01,0.01]	[-0.01,0.01]	[-0.01,0.01]	[-0.03,0.03]
JesEffectiveStat4	[-0.09,0.04]	[-0.04,0.05]	[-0.02,0.05]	[-0.04,0.04]	[-0.04,0.06]	[-0.06,0.06]	[-0.09,0.03]	[-0.09,0.02]	[-0.05,0.04]	[-0.37,0.05]
JesEffectiveModel1	[-0.95,1.07]	[-0.77,0.93]	[-0.87,0.84]	[-0.65,0.82]	[-0.76,0.92]	[-0.83,1.03]	[-1.10,1.09]	[-0.85,0.95]	[-0.87,1.09]	[-1.74,1.37]
JesEffectiveModel2	[-0.03,0.00]	[-0.02,0.04]	[-0.02,0.01]	[-0.01,0.02]	[-0.01,0.03]	[-0.03,0.03]	[-0.07,0.02]	[-0.03,0.00]	[-0.02,0.01]	[-0.07,0.02]
JesEffectiveModel3	[-0.08,0.04]	[-0.04,0.05]	[-0.03,0.02]	[-0.03,0.04]	[-0.04,0.06]	[-0.06,0.05]	[-0.07,0.03]	[-0.09,0.02]	[-0.06,0.04]	[-0.36,0.04]
JesEffectiveModel4	[-0.01,0.01]	[-0.00,0.03]	[-0.01,0.01]	[-0.00,0.02]	[-0.01,0.01]	[-0.00,0.00]	[-0.01,0.01]	[-0.01,0.01]	[-0.00,0.00]	[-0.04,0.04]
JesEffectiveDet1	[-0.11,0.04]	[-0.03,0.08]	[-0.03,0.07]	[-0.03,0.05]	[-0.05,0.08]	[-0.07,0.11]	[-0.11,0.02]	[-0.08,0.02]	[-0.10,0.07]	[-0.42,0.02]
JesEffectiveDet2	[-0.09,0.05]	[-0.05,0.07]	[-0.03,0.07]	[-0.04,0.04]	[-0.04,0.09]	[-0.07,0.13]	[-0.11,0.04]	[-0.09,0.04]	[-0.07,0.05]	[-0.37,0.03]
JesEffectiveDet3	[-0.01,0.01]	[-0.01,0.03]	[-0.01,0.01]	[-0.01,0.02]	[-0.00,0.02]	[-0.01,0.01]	[-0.02,0.01]	[-0.02,0.01]	[-0.00,0.00]	[-0.01,0.01]
JesEffectiveMix1	[-0.17,0.07]	[-0.05,0.14]	[-0.10,0.10]	[-0.07,0.05]	[-0.05,0.13]	[-0.09,0.15]	[-0.18,0.09]	[-0.17,0.07]	[-0.23,0.15]	[-0.48,0.03]
JesEffectiveMix2	[-0.20,0.14]	[-0.08,0.19]	[-0.12,0.11]	[-0.09,0.07]	[-0.10,0.16]	[-0.11,0.18]	[-0.20,0.11]	[-0.16,0.12]	[-0.31,0.13]	[-0.47,0.11]
JesEffectiveMix3	[-0.09,0.02]	[-0.03,0.05]	[-0.03,0.02]	[-0.02,0.04]	[-0.03,0.06]	[-0.05,0.07]	[-0.07,0.02]	[-0.08,0.02]	[-0.01,0.05]	[-0.36,0.03]
JesEffectiveMix4	[-0.00,0.00]	[-0.00,0.00]	[-0.00,0.00]	[-0.00,0.00]	[-0.00,0.00]	[-0.00,0.00]	[-0.00,0.00]	[-0.01,0.01]	[-0.00,0.00]	[-0.00,0.00]
EtaIntercalibrationModel	[-0.19,0.25]	[-0.13,0.21]	[-0.16,0.11]	[-0.10,0.16]	[-0.11,0.17]	[-0.14,0.20]	[-0.12,0.17]	[-0.15,0.13]	[-0.15,0.29]	[-0.24,0.12]
EtaIntercalibrationTotalStat	[-0.26,0.25]	[-0.19,0.29]	[-0.22,0.15]	[-0.15,0.14]	[-0.17,0.25]	[-0.16,0.31]	[-0.24,0.20]	[-0.23,0.23]	[-0.36,0.26]	[-0.71,0.11]
PileupOffsetMu	[-0.03,0.03]	[-0.03,0.11]	[-0.12,0.03]	[-0.02,0.04]	[-0.12,0.12]	[-0.05,0.09]	[-0.05,0.01]	[-0.08,0.06]	[-0.08,0.04]	[-0.48,0.15]
PileupOffsetNPV	[-0.05,0.09]	[-0.02,0.14]	[-0.09,0.11]	[-0.06,0.07]	[-0.01,0.19]	[-0.01,0.16]	[-0.17,0.11]	[-0.08,0.08]	[-0.14,0.06]	[-0.60,0.31]
PileupRho	[-0.71,0.79]	[-0.55,0.64]	[-0.56,0.64]	[-0.43,0.61]	[-0.60,0.72]	[-0.55,0.79]	[-0.80,0.77]	[-0.59,0.62]	[-0.61,0.92]	[-1.44,0.91]
PunchThrough	[-0.00,0.00]	[-0.00,0.00]	[-0.00,0.00]	[-0.00,0.00]	[-0.00,0.00]	[-0.00,0.00]	[-0.00,0.00]	[-0.00,0.00]	[-0.00,0.00]	[-0.00,0.00]
CTauTag	[-0.01,0.01]	[-0.07,0.07]	[-0.02,0.02]	[-0.03,0.03]	[-0.02,0.02]	[-0.02,0.02]	[-0.03,0.03]	[-0.05,0.05]	[-0.02,0.03]	[-0.03,0.03]
ElectronEnergyResolution	[-0.05,0.05]	[-0.01,0.09]	[-0.05,0.00]	[-0.01,0.01]	[-0.06,0.06]	[-0.10,0.07]	[-0.10,0.10]	[-0.18,0.12]	[-0.29,0.14]	[-0.10,0.10]
ElectronEnergyScale	[-0.07,0.14]	[-0.05,0.19]	[-0.10,0.10]	[-0.01,0.01]	[-0.05,0.14]	[-0.13,0.13]	[-0.05,0.16]	[-0.17,0.17]	[-0.68,0.16]	[-0.61,0.83]
ElectronIdSF	[-0.18,0.18]	[-0.24,0.24]	[-0.21,0.21]	[-0.20,0.21]	[-0.22,0.22]	[-0.25,0.25]	[-0.27,0.27]	[-0.34,0.34]	[-0.42,0.42]	[-0.42,0.42]
ElectronRecoSF	[-0.02,0.02]	[-0.02,0.02]	[-0.02,0.02]	[-0.02,0.02]	[-0.02,0.02]	[-0.03,0.03]	[-0.03,0.03]	[-0.05,0.05]	[-0.06,0.06]	[-0.08,0.08]
ElectronTriggerSF	[-0.01,0.01]	[-0.02,0.02]	[-0.01,0.01]	[-0.01,0.01]	[-0.01,0.01]	[-0.01,0.01]	[-0.01,0.01]	[-0.02,0.02]	[-0.03,0.03]	[-0.03,0.03]
FlavorComp	[-0.25,0.39]	[-0.23,0.27]	[-0.36,0.26]	[-0.23,0.21]	[-0.33,0.26]	[-0.32,0.36]	[-0.28,0.39]	[-0.25,0.22]	[-0.53,0.38]	[-0.49,0.73]
FlavorResponse	[-0.20,0.28]	[-0.15,0.17]	[-0.16,0.20]	[-0.12,0.12]	[-0.22,0.21]	[-0.17,0.26]	[-0.21,0.19]	[-0.14,0.12]	[-0.30,0.24]	[-0.40,0.41]
JetVertexFraction	[-0.34,0.18]	[-0.22,0.20]	[-0.24,0.27]	[-0.24,0.25]	[-0.24,0.31]	[-0.23,0.38]	[-0.22,0.36]	[-0.28,0.34]	[-0.24,0.33]	[-0.28,0.18]
Mistag	[-0.09,0.09]	[-0.07,0.07]	[-0.10,0.10]	[-0.07,0.07]	[-0.07,0.07]	[-0.07,0.06]	[-0.11,0.11]	[-0.09,0.09]	[-0.14,0.14]	[-0.10,0.10]
MuonIdSF	[-0.04,0.04]	[-0.05,0.05]	[-0.05,0.05]	[-0.05,0.05]	[-0.05,0.05]	[-0.06,0.05]	[-0.06,0.06]	[-0.07,0.07]	[-0.08,0.08]	[-0.08,0.08]
MuonRecoSF	[-0.02,0.02]	[-0.03,0.03]	[-0.02,0.02]	[-0.02,0.02]	[-0.02,0.02]	[-0.03,0.03]	[-0.03,0.03]	[-0.03,0.03]	[-0.04,0.05]	[-0.05,0.05]
MuonTriggerSF	[-0.00,0.00]	[-0.00,0.00]	[-0.00,0.00]	[-0.00,0.00]	[-0.00,0.00]	[-0.00,0.00]	[-0.00,0.00]	[-0.00,0.00]	[-0.00,0.00]	[-0.00,0.00]
Musc	[-0.03,0.03]	[-0.05,0.01]	[-0.05,0.00]	[-0.01,0.01]	[-0.01,0.01]	[-0.01,0.01]	[-0.00,0.04]	[-0.02,0.02]	[-0.00,0.02]	[-0.01,0.03]
ModellingGenerator	[-2.38,2.38]	[-0.90,0.90]	[-0.66,0.66]	[-0.66,0.66]	[-1.41,1.41]	[-0.54,0.54]	[-0.17,0.17]	[-1.10,1.10]	[-3.83,3.83]	[-0.01,0.01]
ModellingParton	[-1.14,1.14]	[-0.20,0.20]	[-0.42,0.42]	[-0.70,0.70]	[-1.81,1.81]	[-0.17,0.17]	[-0.21,0.21]	[-0.68,0.68]	[-4.06,4.06]	[-0.22,0.22]
ModellingRadiation	[-5.89,5.89]	[-4.63,4.63]	[-5.59,5.59]	[-3.79,3.79]	[-4.99,4.99]	[-4.21,4.21]	[-5.14,5.14]	[-4.60,4.60]	[-6.45,6.45]	[-5.79,5.79]
ModellingSingleTopWtNormalisation	[-0.55,0.55]	[-0.63,0.63]	[-0.58,0.58]	[-0.61,0.61]	[-0.60,0.60]	[-0.71,0.71]	[-0.76,0.76]	[-0.94,0.94]	[-1.19,1.19]	[-0.97,0.97]
ModellingSingleTopWtInterference	[-4.12,4.12]	[-4.67,4.67]	[-4.36,4.36]	[-4.57,4.57]	[-4.49,4.49]	[-5.30,5.30]	[-5.64,5.64]	[-6.99,6.99]	[-8.85,8.85]	[-7.25,7.25]

Table 8.7 Per-bin individual statistical and systematic uncertainties for the dilepton mass, m_{ll}.

8.4 Measurement of $\frac{d\sigma_{t\bar{t}}}{\Delta\eta_{ll}}$

This section describes the fiducial differential cross-section of $t\bar{t}$ decaying to dilepton as a function of the absolute difference of pseudorapidity of two oppositely charged leptons in the $e\mu$ channel. The statistical uncertainty, systematic uncertainty, signal modelling systematics, background modelling systematics, MC statistical uncertainty and all the detector modelling systematics have been evaluated in each bin of the observable.

Bin [unit]	Measured $d\sigma/dx$ [pb/unit]	Statistical Data [%]	Statistical MC Bkg [%]	Statistical MC Sig [%]	Systematic [%]
[-4.0,-3.5]	0.0097	+/- 13.9	+/- 2.1	+/- 4.5	+10.3/-12.3
[-3.5,-3.0]	0.0205	+/- 9.2	+/- 1.6	+/- 2.0	+6.0/-5.0
[-3.0,-2.5]	0.0599	+/- 5.4	+/- 1.1	+/- 1.2	+6.4/-5.3
[-2.5,-2.0]	0.1203	+/- 3.8	+/- 0.8	+/- 0.8	+6.5/-5.3
[-2.0,-1.5]	0.2030	+/- 2.9	+/- 0.7	+/- 0.6	+6.1/-5.1
[-1.5,-1.0]	0.3419	+/- 2.2	+/- 0.5	+/- 0.5	+5.9/-4.9
[-1.0,-0.5]	0.4261	+/- 2.0	+/- 0.5	+/- 0.4	+6.3/-5.2
[-0.5,0.0]	0.4664	+/- 1.9	+/- 0.6	+/- 0.4	+6.0/-5.0
[0.0,0.5]	0.4179	+/- 2.0	+/- 0.6	+/- 0.4	+6.1/-5.1
[0.5,1.0]	0.4092	+/- 2.1	+/- 0.5	+/- 0.4	+6.3/-5.2
[1.0,1.5]	0.3273	+/- 2.3	+/- 0.6	+/- 0.5	+6.0/-5.1
[1.5,2.0]	0.2183	+/- 2.8	+/- 0.5	+/- 0.6	+6.1/-5.0
[2.0,2.5]	0.1329	+/- 3.6	+/- 0.7	+/- 0.8	+5.9/-4.8
[2.5,3.0]	0.0600	+/- 5.3	+/- 1.0	+/- 1.2	+6.0/-5.0
[3.0,3.5]	0.0243	+/- 8.3	+/- 1.1	+/- 2.0	+6.0/-4.9
[3.5,4.0]	0.0081	+/- 14.8	+/- 1.1	+/- 4.1	+8.2/-6.9

Table 8.8 Per-bin total statistical and systematic uncertainties in $e\mu$ for the dilepton absolute $\Delta\eta_{ll}$, without modelling systematic uncertainties.

Bin [unit]	Measured $d\sigma/dx$ [pb/unit]	Statistical Data [%]	Statistical MC Bkg [%]	Statistical MC Sig [%]	Systematic [%]
[-4.0,-3.5]	0.0097	+/- 13.9	+/- 2.1	+/- 4.5	+15.3/-16.6
[-3.5,-3.0]	0.0205	+/- 9.2	+/- 1.6	+/- 2.0	+9.6/-9.0
[-3.0,-2.5]	0.0599	+/- 5.4	+/- 1.1	+/- 1.2	+13.3/-12.9
[-2.5,-2.0]	0.1203	+/- 3.8	+/- 0.8	+/- 0.8	+9.4/-8.6
[-2.0,-1.5]	0.2030	+/- 2.9	+/- 0.7	+/- 0.6	+11.8/-11.3
[-1.5,-1.0]	0.3419	+/- 2.2	+/- 0.5	+/- 0.5	+8.6/-7.9
[-1.0,-0.5]	0.4261	+/- 2.0	+/- 0.5	+/- 0.4	+8.9/-8.2
[-0.5,0.0]	0.4664	+/- 1.9	+/- 0.6	+/- 0.4	+8.9/-8.3
[0.0,0.5]	0.4179	+/- 2.0	+/- 0.6	+/- 0.4	+10.1/-9.5
[0.5,1.0]	0.4092	+/- 2.1	+/- 0.5	+/- 0.4	+10.1/-9.4
[1.0,1.5]	0.3273	+/- 2.3	+/- 0.6	+/- 0.5	+9.8/-9.2
[1.5,2.0]	0.2183	+/- 2.8	+/- 0.5	+/- 0.6	+8.9/-8.2
[2.0,2.5]	0.1329	+/- 3.6	+/- 0.7	+/- 0.8	+8.4/-7.7
[2.5,3.0]	0.0600	+/- 5.3	+/- 1.0	+/- 1.2	+7.9/-7.2
[3.0,3.5]	0.0243	+/- 8.3	+/- 1.1	+/- 2.0	+7.0/-6.1
[3.5,4.0]	0.0081	+/- 14.8	+/- 1.1	+/- 4.1	+20.7/-20.2

Table 8.9 Per-bin total statistical and systematic uncertainties in $e\mu$ for the dilepton absolute $\Delta\eta_{ll}$, with detector modelling, signal modelling and background modelling.

The individual components in each bin are described in Table 8.10 but final numbers are shown in Tables 8.8 and 8.9. The measured fiducial differential cross-section has been normalised to the unit area in order to be able to make a direct comparison between different particle level predictions. The unfolded cross-section agrees well in shape with the predictions. The systematic uncertainties in the normalised case are certainly reduced and it is obvious from the bottom pad (ratio plot) shown in Figure 8.18. The absolute $\Delta\eta$ has almost twice the number of entries in each bin than the raw $\Delta\eta$. The analysis was started with the raw value of the difference of pseudorapidity but it was not a good choice of lepton kinematic variable because $\Delta\eta$ of two leptons = η (lepton1) - η (lepton2) specifies both the magnitude of the angular separation and the direction of each of them. But in the detector it is symmetric in the z-direction, and in pp collisions it is well known that the outcoming particles are also symmetric in the z-direction. It makes more sense to look at the absolute $\Delta\eta$ (magnitude of the angular separation).

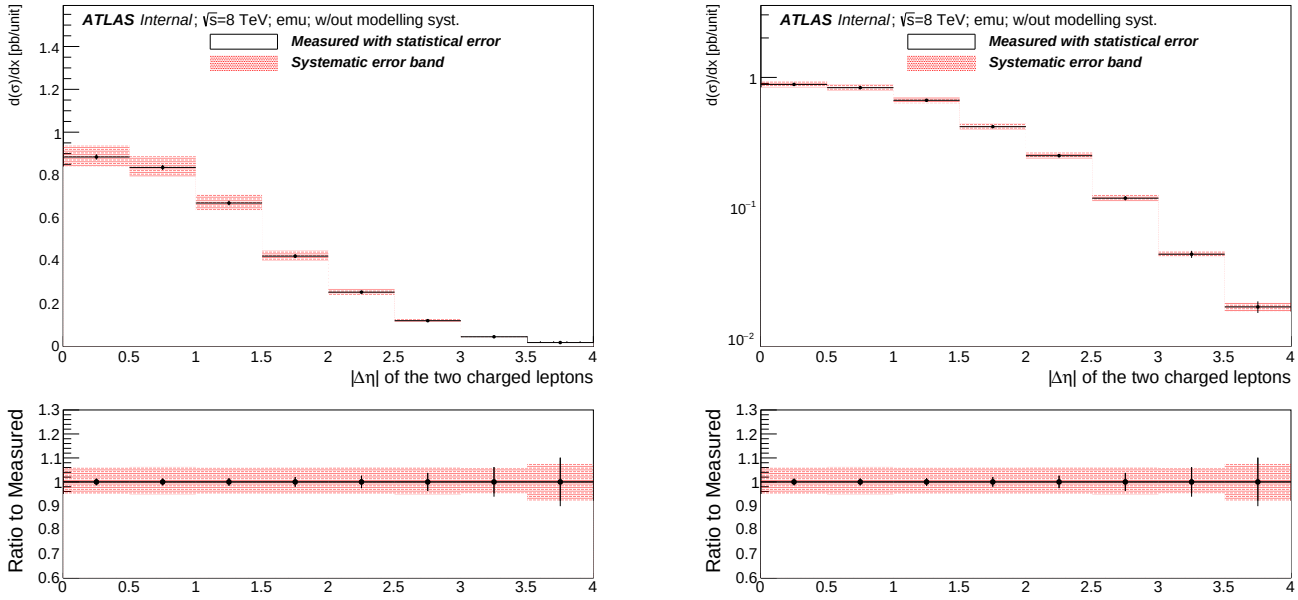

Fig. 8.13 Fiducial differential distribution as a function of the absolute difference of pseudo-rapidity of the dilepton, $|\Delta\eta_{ll}|$ plotted on the linear (left) and semi-log (right) scale. Only the detector modelling systematics are included on the systematic error band.

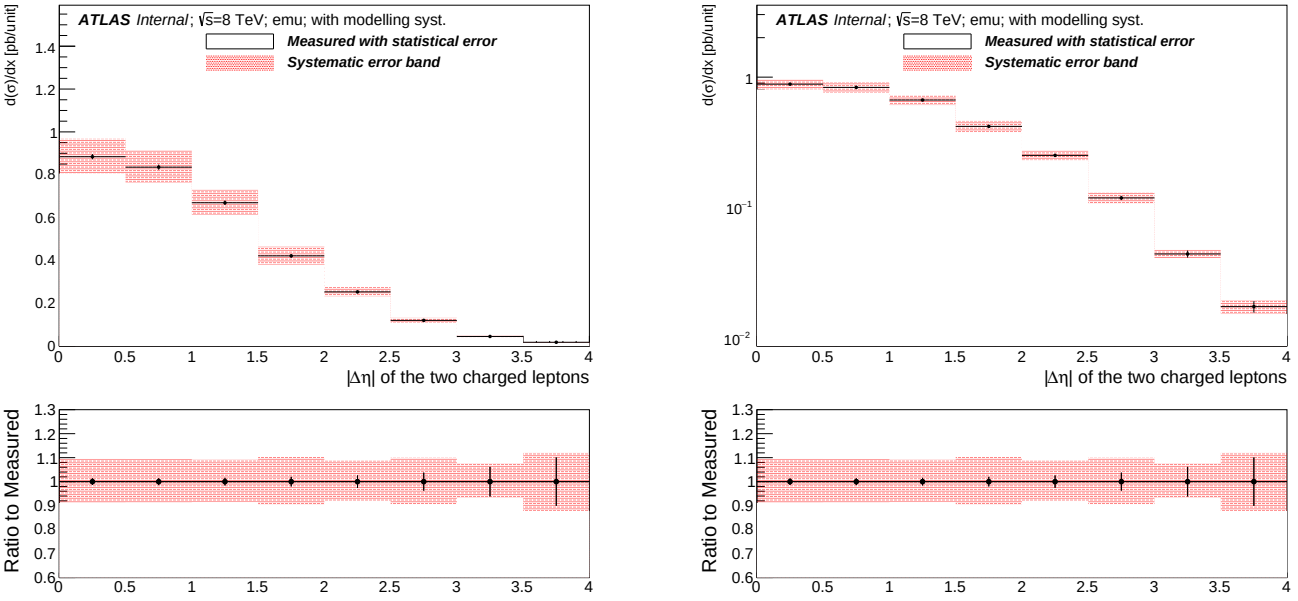

Fig. 8.14 Fiducial differential distribution as a function of the absolute difference of pseudorapidity of the dilepton, $|\Delta\eta_{ll}|$ plotted on a linear (left) and semi-log (right) scale. The detector modelling, signal modelling and background modelling systematics are included on the systematic error band.

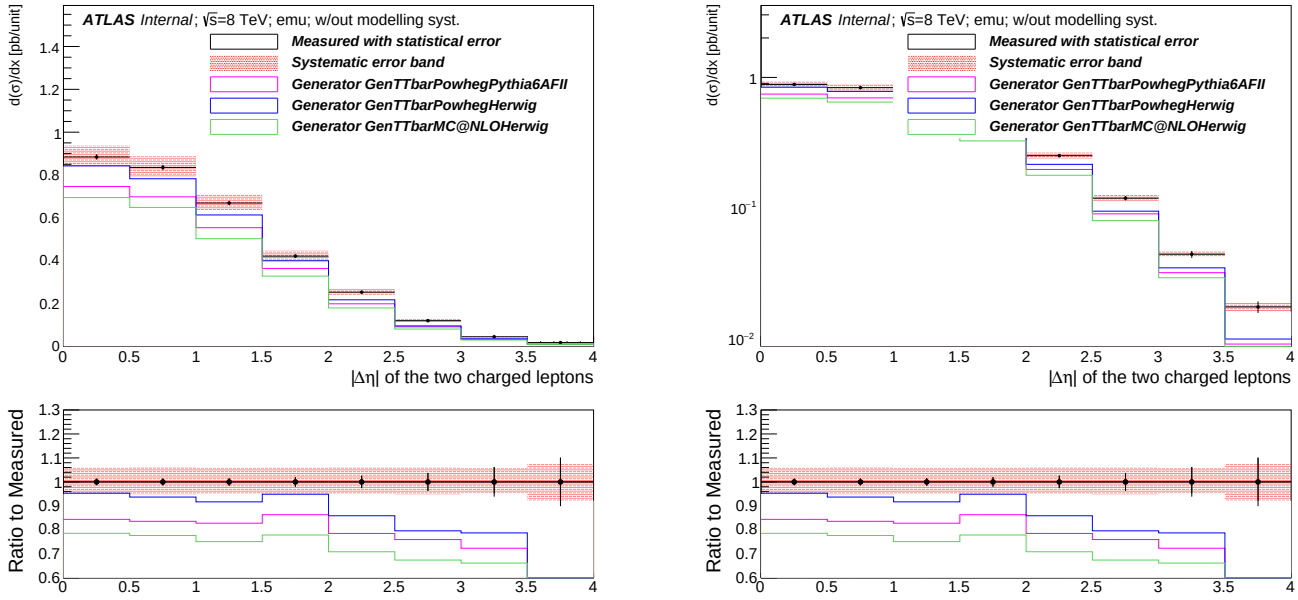

Fig. 8.15 Fiducial differential distribution as a function of the absolute difference of pseudo-rapidity of the dilepton, $\Delta\eta_{ll}$ plotted on a linear (left) and semi-log (right) scale. Only the detector modelling systematics are included on the systematic error band.

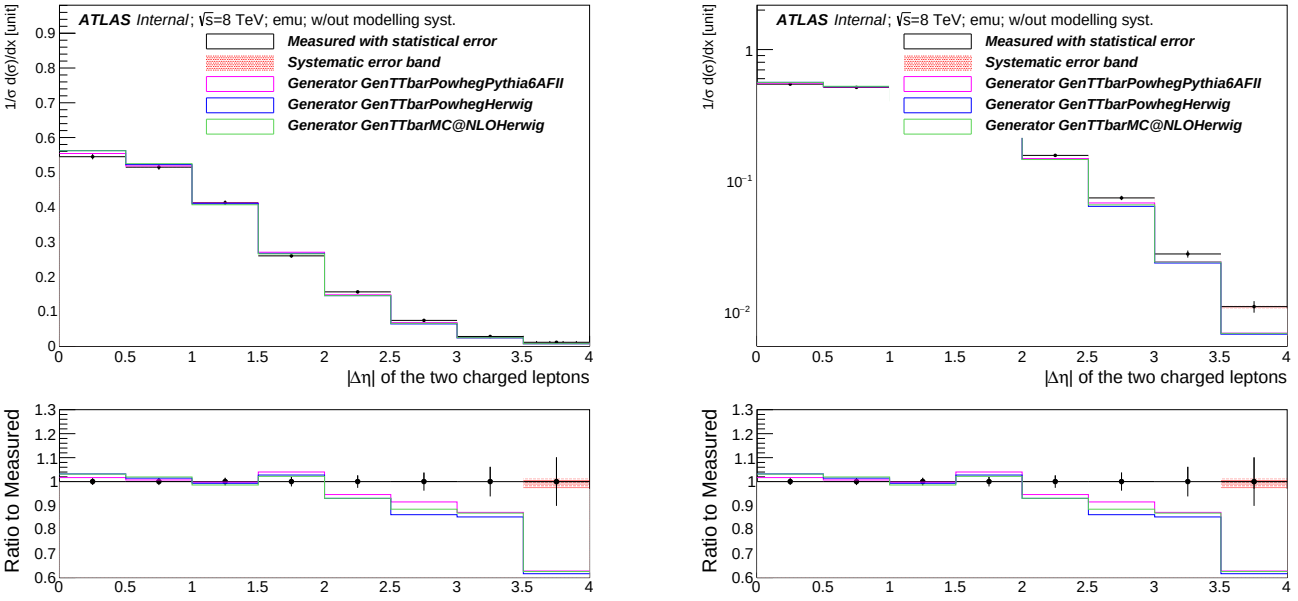

Fig. 8.16 Comparison of the measured fiducial differential distribution as a function of the absolute difference of pseudorapidity of the dilepton, $|\Delta\eta_{ll}|$ plotted on a linear (left) and semi-log (right) scale. Only the detector modelling systematics are included on the systematic error band.

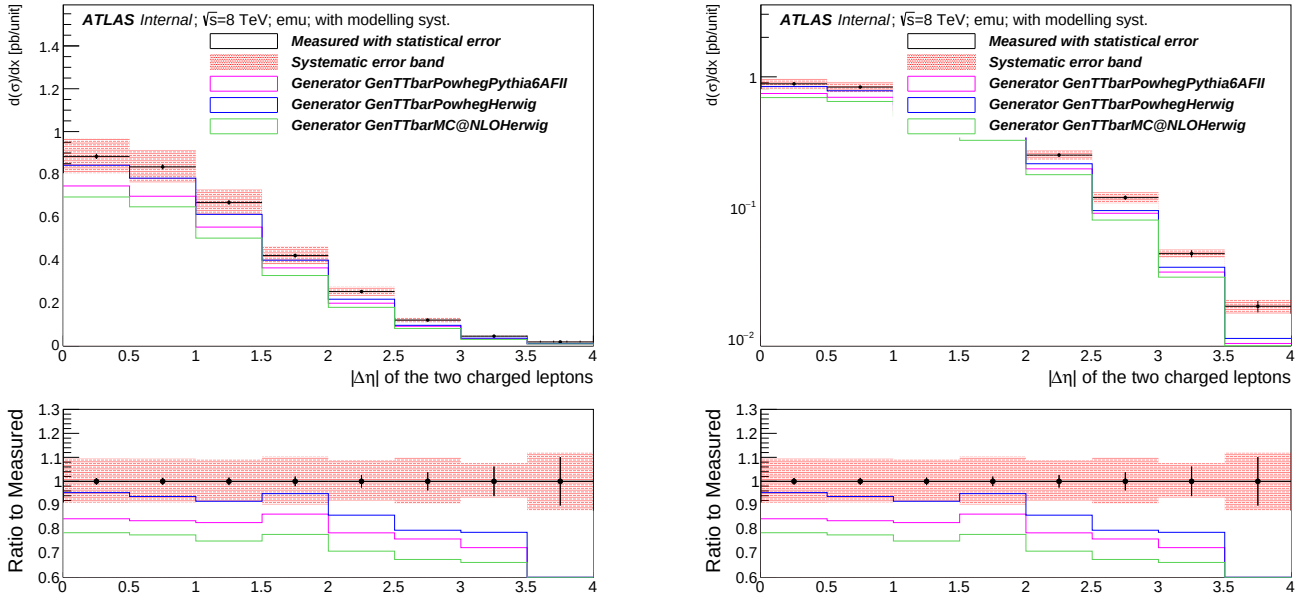

Fig. 8.17 Fiducial differential distribution as a function of the absolute difference of pseudorapidity of the dilepton, $\Delta\eta_{ll}$ plotted on a linear (left) and semi-log (right) scale. All the detector modelling, signal modelling and background modelling systematics are included on the systematic error band.

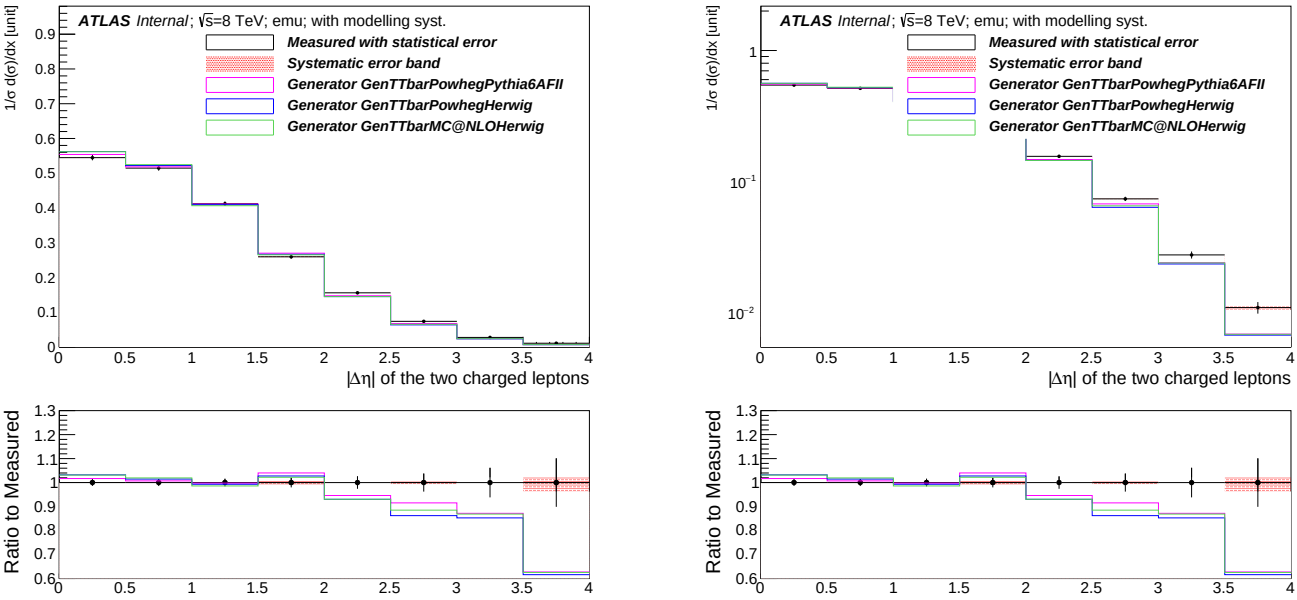

Fig. 8.18 Comparison of the measured fiducial differential cross-section with different predictions as a function of the absolute difference of pseudorapidity of the dilepton, $|\Delta\eta_{ll}|$ plotted on a linear (left) and semi-log (right) scale. All the modelling systematics are included on the systematic error band. The left hand side plot is on the linear scale while the right hand side is on the semi-log scale. The plots have been normalized to the unit area to make a direct comparison with particle level predictions. The reduction of systematic uncertainties for the normalised case are seen from the systematic error band.

Uncertainty	[-4.0,-3.5]	[-3.5,-3.0]	[-3.0,-2.5]	[-2.5,-2.0]	[-2.0,-1.5]	[-1.5,-1.0]	[-1.0,-0.5]	[-0.5,0.0]	[0.0,0.5]	[0.5,1.0]	[1.0,1.5]	[1.5,2.0]	[2.0,2.5]	[2.5,3.0]	[3.0,3.5]	[3.5,4.0]
StatisticalData	[-13.88,13.88]	[-9.18,9.18]	[-5.37,5.37]	[-3.76,3.76]	[-2.89,2.89]	[-2.22,2.22]	[-2.01,2.01]	[-1.92,1.92]	[-2.03,2.03]	[-2.05,2.05]	[-2.28,2.28]	[-2.77,2.77]	[-3.56,3.56]	[-5.27,5.27]	[-8.32,8.32]	[-14.75,14.75]
StatisticalBkg	[-2.06,2.06]	[-1.60,1.60]	[-1.14,1.14]	[-0.81,0.81]	[-0.67,0.67]	[-0.49,0.49]	[-0.54,0.54]	[-0.65,0.65]	[-0.57,0.57]	[-0.53,0.53]	[-0.61,0.61]	[-0.50,0.50]	[-0.69,0.69]	[-1.04,1.04]	[-1.10,1.10]	[-1.12,1.12]
StatisticalSig	[-4.12,4.49]	[-1.93,2.00]	[-1.16,1.19]	[-0.78,0.80]	[-0.57,0.58]	[-0.47,0.47]	[-0.42,0.42]	[-0.41,0.41]	[-0.41,0.41]	[-0.42,0.43]	[-0.47,0.47]	[-0.57,0.58]	[-0.79,0.80]	[-1.15,1.17]	[-1.95,2.03]	[-3.80,4.11]
BTag	[-6.59,8.24]	[-4.54,5.50]	[-5.06,6.14]	[-4.95,6.03]	[-4.87,5.91]	[-4.70,5.74]	[-5.00,6.06]	[-4.75,5.78]	[-4.88,5.92]	[-4.95,6.00]	[-4.76,5.80]	[-4.83,5.88]	[-4.68,5.70]	[-4.80,5.79]	[-4.66,5.73]	[-4.62,5.67]
Jeff	[-0.00,0.00]	[-0.00,0.00]	[-0.00,0.00]	[-0.02,0.02]	[-0.04,0.04]	[-0.03,0.03]	[-0.00,0.00]	[-0.02,0.02]	[-0.02,0.02]	[-0.01,0.01]	[-0.01,0.01]	[-0.02,0.02]	[-0.01,0.01]	[-0.01,0.01]	[-0.00,0.00]	[-0.11,0.11]
Jer	[-5.55,5.55]	[-1.77,1.77]	[-0.25,0.25]	[-1.12,1.12]	[-0.62,0.62]	[-0.49,0.49]	[-0.45,0.45]	[-0.48,0.48]	[-0.58,0.58]	[-0.43,0.43]	[-0.87,0.87]	[-0.41,0.41]	[-0.17,0.17]	[-0.62,0.62]	[-0.19,0.19]	[-4.45,4.45]
MuidRes	[-0.13,0.13]	[-0.02,0.02]	[-0.03,0.03]	[-0.03,0.03]	[-0.06,0.06]	[-0.00,0.00]	[-0.05,0.05]	[-0.02,0.02]	[-0.02,0.02]	[-0.00,0.00]	[-0.06,0.06]	[-0.07,0.07]	[-0.03,0.03]	[-0.00,0.00]	[-0.01,0.01]	[-0.01,0.01]
MumsRes	[-0.11,0.11]	[-0.30,0.30]	[-0.24,0.24]	[-0.03,0.03]	[-0.00,0.00]	[-0.03,0.03]	[-0.00,0.00]	[-0.02,0.02]	[-0.00,0.00]	[-0.02,0.02]	[-0.01,0.01]	[-0.02,0.02]	[-0.00,0.00]	[-0.17,0.17]	[-0.91,0.91]	[-0.22,0.22]
BJesUnc	[-3.41,0.49]	[-0.18,0.29]	[-0.41,0.54]	[-0.44,0.64]	[-0.40,0.39]	[-0.45,0.52]	[-0.39,0.45]	[-0.35,0.46]	[-0.36,0.42]	[-0.42,0.56]	[-0.42,0.48]	[-0.26,0.50]	[-0.37,0.36]	[-0.41,0.30]	[-0.43,0.21]	[-0.71,0.71]
JesEffectiveStat1	[-2.68,0.07]	[-0.14,0.33]	[-0.37,0.54]	[-0.26,0.52]	[-0.30,0.28]	[-0.20,0.33]	[-0.26,0.43]	[-0.34,0.37]	[-0.30,0.33]	[-0.35,0.44]	[-0.32,0.38]	[-0.23,0.34]	[-0.24,0.30]	[-0.31,0.23]	[-0.40,0.19]	[-0.72,0.50]
JesEffectiveStat2	[-0.00,0.19]	[-0.01,0.02]	[-0.01,0.01]	[-0.04,0.03]	[-0.02,0.01]	[-0.03,0.03]	[-0.03,0.01]	[-0.04,0.02]	[-0.04,0.04]	[-0.04,0.07]	[-0.01,0.00]	[-0.00,0.03]	[-0.05,0.00]	[-0.05,0.05]	[-0.15,0.01]	[-0.34,0.00]
JesEffectiveStat3	[-0.23,0.23]	[-0.00,0.01]	[-0.00,0.01]	[-0.00,0.01]	[-0.01,0.02]	[-0.01,0.01]	[-0.01,0.02]	[-0.01,0.02]	[-0.00,0.01]	[-0.02,0.03]	[-0.01,0.00]	[-0.01,0.00]	[-0.02,0.02]	[-0.01,0.01]	[-0.02,0.02]	[-0.01,0.01]
JesEffectiveStat4	[-1.55,0.18]	[-0.01,0.02]	[-0.03,0.01]	[-0.09,0.11]	[-0.04,0.03]	[-0.03,0.06]	[-0.06,0.02]	[-0.08,0.04]	[-0.05,0.11]	[-0.04,0.10]	[-0.05,0.00]	[-0.04,0.02]	[-0.06,0.06]	[-0.05,0.05]	[-0.14,0.02]	[-0.63,0.63]
JesEffectiveModel1	[-3.38,0.51]	[-0.73,0.91]	[-1.10,0.89]	[-0.89,1.35]	[-0.89,0.83]	[-0.74,0.93]	[-0.73,0.92]	[-0.89,0.94]	[-0.80,0.93]	[-0.91,1.07]	[-0.96,0.91]	[-0.76,0.91]	[-0.77,0.88]	[-0.88,0.92]	[-0.53,1.21]	[-0.17,1.50]
JesEffectiveModel2	[-0.00,0.19]	[-0.00,0.02]	[-0.01,0.02]	[-0.04,0.03]	[-0.01,0.01]	[-0.01,0.02]	[-0.03,0.01]	[-0.04,0.03]	[-0.03,0.03]	[-0.05,0.06]	[-0.02,0.02]	[-0.01,0.03]	[-0.04,0.00]	[-0.04,0.04]	[-0.15,0.01]	[-0.33,0.33]
JesEffectiveModel3	[-1.42,0.04]	[-0.00,0.02]	[-0.01,0.01]	[-0.10,0.09]	[-0.04,0.01]	[-0.02,0.05]	[-0.06,0.03]	[-0.08,0.03]	[-0.04,0.08]	[-0.04,0.11]	[-0.05,0.01]	[-0.04,0.02]	[-0.08,0.00]	[-0.07,0.07]	[-0.15,0.02]	[-0.65,0.65]
JesEffectiveModel4	[-0.19,0.19]	[-0.01,0.00]	[-0.00,0.02]	[-0.01,0.01]	[-0.01,0.01]	[-0.01,0.01]	[-0.00,0.00]	[-0.01,0.02]	[-0.00,0.01]	[-0.01,0.03]	[-0.01,0.00]	[-0.00,0.00]	[-0.03,0.00]	[-0.00,0.00]	[-0.01,0.01]	[-0.01,0.00]
JesEffectiveDet1	[-1.58,0.15]	[-0.08,0.08]	[-0.10,0.10]	[-0.13,0.14]	[-0.06,0.04]	[-0.03,0.09]	[-0.05,0.06]	[-0.09,0.03]	[-0.07,0.11]	[-0.05,0.11]	[-0.05,0.06]	[-0.02,0.02]	[-0.07,0.01]	[-0.06,0.06]	[-0.11,0.11]	[-0.64,0.64]
JesEffectiveDet2	[-1.60,1.60]	[-0.00,0.03]	[-0.02,0.02]	[-0.11,0.13]	[-0.04,0.04]	[-0.04,0.08]	[-0.05,0.04]	[-0.09,0.05]	[-0.06,0.12]	[-0.06,0.11]	[-0.06,0.07]	[-0.05,0.04]	[-0.08,0.02]	[-0.05,0.05]	[-0.15,0.15]	[-0.63,0.63]
JesEffectiveDet3	[-0.19,0.19]	[-0.00,0.00]	[-0.02,0.02]	[-0.00,0.02]	[-0.01,0.01]	[-0.00,0.01]	[-0.01,0.01]	[-0.02,0.02]	[-0.01,0.01]	[-0.02,0.03]	[-0.01,0.01]	[-0.00,0.01]	[-0.03,0.00]	[-0.00,0.00]	[-0.06,0.01]	[-0.01,0.00]
JesEffectiveMix1	[-1.59,0.13]	[-0.01,0.01]	[-0.19,0.19]	[-0.14,0.22]	[-0.06,0.06]	[-0.05,0.10]	[-0.12,0.13]	[-0.12,0.08]	[-0.10,0.14]	[-0.11,0.15]	[-0.11,0.09]	[-0.09,0.05]	[-0.10,0.06]	[-0.23,0.23]	[-0.23,0.01]	[-0.64,0.64]
JesEffectiveMix2	[-1.60,1.60]	[-0.04,0.02]	[-0.24,0.03]	[-0.17,0.27]	[-0.10,0.12]	[-0.06,0.11]	[-0.15,0.16]	[-0.14,0.12]	[-0.12,0.17]	[-0.16,0.17]	[-0.14,0.12]	[-0.11,0.08]	[-0.11,0.09]	[-0.23,0.00]	[-0.36,0.02]	[-0.63,0.63]
JesEffectiveMix3	[-1.42,0.05]	[-0.00,0.01]	[-0.00,0.01]	[-0.08,0.07]	[-0.02,0.03]	[-0.02,0.05]	[-0.05,0.02]	[-0.07,0.03]	[-0.02,0.07]	[-0.05,0.11]	[-0.04,0.01]	[-0.02,0.02]	[-0.07,0.01]	[-0.06,0.06]	[-0.15,0.03]	[-0.34,0.00]
JesEffectiveMix4	[-0.00,0.00]	[-0.00,0.00]	[-0.00,0.00]	[-0.00,0.00]	[-0.00,0.00]	[-0.00,0.00]	[-0.00,0.00]	[-0.00,0.00]	[-0.00,0.00]	[-0.00,0.00]	[-0.00,0.00]	[-0.00,0.00]	[-0.01,0.01]	[-0.00,0.00]	[-0.01,0.00]	[-0.00,0.00]
EtaIntercalibrationModel	[-0.18,0.18]	[-0.03,0.25]	[-0.10,0.18]	[-0.14,0.26]	[-0.09,0.21]	[-0.11,0.16]	[-0.09,0.22]	[-0.17,0.14]	[-0.14,0.17]	[-0.18,0.21]	[-0.19,0.11]	[-0.10,0.16]	[-0.06,0.22]	[-0.01,0.01]	[-0.12,0.12]	[-0.30,0.64]
EtaIntercalibrationTotalStat	[-1.93,0.15]	[-0.05,0.08]	[-0.28,0.28]	[-0.19,0.33]	[-0.20,0.18]	[-0.14,0.16]	[-0.20,0.24]	[-0.24,0.22]	[-0.20,0.23]	[-0.23,0.30]	[-0.24,0.21]	[-0.15,0.20]	[-0.12,0.23]	[-0.21,0.05]	[-0.30,0.09]	[-0.66,0.66]
PileupOffsetMu	[-1.97,0.18]	[-0.04,0.04]	[-0.08,0.08]	[-0.15,0.15]	[-0.09,0.06]	[-0.01,0.11]	[-0.04,0.05]	[-0.07,0.02]	[-0.02,0.04]	[-0.08,0.13]	[-0.09,0.08]	[-0.01,0.06]	[-0.04,0.04]	[-0.03,0.03]	[-0.04,0.02]	[-0.62,0.62]
PileupOffsetNPV	[-3.02,0.20]	[-0.41,0.10]	[-0.16,0.16]	[-0.34,0.34]	[-0.15,0.12]	[-0.01,0.17]	[-0.11,0.11]	[-0.08,0.06]	[-0.02,0.10]	[-0.12,0.17]	[-0.19,0.11]	[-0.11,0.11]	[-0.08,0.04]	[-0.04,0.09]	[-0.04,0.04]	[-0.30,0.56]
PileupRho	[-3.41,0.39]	[-0.51,0.68]	[-0.76,0.75]	[-0.60,1.08]	[-0.58,0.61]	[-0.61,0.71]	[-0.55,0.70]	[-0.62,0.69]	[-0.55,0.64]	[-0.65,0.83]	[-0.69,0.67]	[-0.46,0.72]	[-0.44,0.63]	[-0.61,0.36]	[-0.46,0.70]	[-0.49,1.57]
PunchThrough	[-0.00,0.00]	[-0.00,0.00]	[-0.00,0.00]	[-0.00,0.00]	[-0.00,0.00]	[-0.00,0.00]	[-0.00,0.00]	[-0.00,0.00]	[-0.00,0.00]	[-0.00,0.00]	[-0.00,0.00]	[-0.00,0.00]	[-0.00,0.00]	[-0.00,0.00]	[0.00,0.00]	[-0.00,0.00]
CTauTag	[-0.03,0.03]	[-0.01,0.01]	[-0.05,0.05]	[-0.02,0.02]	[-0.03,0.03]	[-0.03,0.03]	[-0.05,0.05]	[-0.04,0.04]	[-0.03,0.03]	[-0.02,0.02]	[-0.03,0.03]	[-0.03,0.03]	[-0.02,0.02]	[-0.03,0.03]	[-0.00,0.00]	[-0.00,0.00]
ElectronEnergyResolution	[-0.13,0.35]	[-0.25,0.25]	[-0.14,0.14]	[-0.02,0.22]	[-0.10,0.10]	[-0.07,0.04]	[-0.04,0.04]	[-0.04,0.13]	[-0.11,0.00]	[-0.04,0.02]	[-0.02,0.06]	[-0.07,0.07]	[-0.18,0.18]	[-0.15,0.15]	[-0.16,0.16]	[-0.13,0.47]
ElectronEnergyScale	[-0.77,0.77]	[-0.05,0.55]	[-0.11,0.30]	[-0.30,0.30]	[-0.13,0.19]	[-0.04,0.04]	[-0.01,0.11]	[-0.07,0.15]	[-0.07,0.07]	[-0.06,0.03]	[-0.13,0.08]	[-0.08,0.05]	[-0.29,0.29]	[-0.28,0.01]	[-0.42,0.13]	[-0.63,1.83]
ElectronIdSF	[-0.15,0.15]	[-0.22,0.22]	[-0.24,0.24]	[-0.24,0.24]	[-0.26,0.26]	[-0.21,0.22]	[-0.25,0.25]	[-0.24,0.24]	[-0.27,0.27]	[-0.26,0.26]	[-0.24,0.24]	[-0.21,0.20]	[-0.19,0.19]	[-0.21,0.21]	[-0.17,0.17]	[-0.17,0.17]
ElectronRecoSF	[-0.02,0.02]	[-0.03,0.03]	[-0.03,0.03]	[-0.03,0.03]	[-0.03,0.03]	[-0.02,0.02]	[-0.02,0.02]	[-0.02,0.02]	[-0.03,0.03]	[-0.02,0.03]	[-0.02,0.02]	[-0.02,0.02]	[-0.02,0.02]	[-0.02,0.02]	[-0.02,0.02]	[-0.03,0.03]
ElectronTriggerSF	[-0.03,0.03]	[-0.03,0.03]	[-0.02,0.02]	[-0.02,0.02]	[-0.02,0.02]	[-0.01,0.01]	[-0.01,0.01]	[-0.01,0.01]	[-0.01,0.01]	[-0.01,0.01]	[-0.01,0.01]	[-0.01,0.01]	[-0.01,0.01]	[-0.02,0.02]	[-0.02,0.01]	[-0.02,0.02]
FlavorComp	[-0.18,0.18]	[-0.24,0.33]	[-0.52,0.35]	[-0.30,0.54]	[-0.28,0.36]	[-0.23,0.24]	[-0.19,0.35]	[-0.41,0.29]	[-0.26,0.25]	[-0.34,0.26]	[-0.42,0.24]	[-0.27,0.30]	[-0.26,0.35]	[-0.29,0.38]	[-0.16,0.34]	[-0.12,0.83]
FlavorResponse	[-0.08,0.02]	[-0.31,0.25]	[-0.31,0.15]	[-0.19,0.40]	[-0.18,0.17]	[-0.12,0.16]	[-0.12,0.22]	[-0.24,0.18]	[-0.17,0.20]	[-0.21,0.22]	[-0.23,0.14]	[-0.16,0.21]	[-0.06,0.25]	[-0.22,0.05]	[-0.34,0.34]	[-0.53,0.84]
JetVertexFraction	[-0.00,0.83]	[-0.08,0.33]	[-0.23,0.16]	[-0.25,0.48]	[-0.18,0.35]	[-0.30,0.28]	[-0.29,0.26]	[-0.25,0.26]	[-0.29,0.24]	[-0.24,0.27]	[-0.16,0.27]	[-0.22,0.34]	[-0.15,0.41]	[-0.30,0.45]	[-0.22,0.18]	[-0.78,0.47]
Mistag	[-0.03,0.03]	[-0.04,0.04]	[-0.18,0.18]	[-0.15,0.15]	[-0.04,0.04]	[-0.05,0.05]	[-0.07,0.07]	[-0.12,0.12]	[-0.10,0.10]	[-0.06,0.06]	[-0.08,0.08]	[-0.10,0.10]	[-0.11,0.11]	[-0.06,0.06]	[-0.03,0.03]	[-0.02,0.02]
MuonIdSF	[-0.03,0.03]	[-0.05,0.05]	[-0.05,0.05]	[-0.05,0.05]	[-0.06,0.06]	[-0.05,0.05]	[-0.05,0.05]	[-0.05,0.05]	[-0.06,0.06]	[-0.06,0.06]	[-0.05,0.05]	[-0.04,0.04]	[-0.04,0.04]	[-0.04,0.04]	[-0.04,0.04]	[-0.03,0.03]
MuonRecoSF	[-0.02,0.02]	[-0.02,0.02]	[-0.02,0.02]	[-0.02,0.02]	[-0.03,0.03]	[-0.02,0.02]	[-0.03,0.03]	[-0.03,0.02]	[-0.03,0.03]	[-0.03,0.03]	[-0.02,0.02]	[-0.02,0.02]	[-0.02,0.02]	[-0.02,0.02]	[-0.02,0.02]	[-0.02,0.02]
MuonTriggerSF	[-0.01,0.01]	[-0.01,0.01]	[-0.01,0.01]	[-0.00,0.01]	[-0.01,0.01]	[-0.00,0.00]	[-0.00,0.00]	[-0.00,0.00]	[-0.00,0.00]	[-0.00,0.00]	[-0.00,0.00]	[-0.00,0.00]	[-0.00,0.00]	[-0.00,0.00]	[-0.01,0.01]	[-0.01,0.01]
Musc	[0.00,0.00]	[-0.20,0.20]	[-0.05,0.05]	[-0.01,0.00]	[-0.04,0.03]	[-0.01,0.01]	[-0.01,0.01]	[-0.01,0.01]	[-0.00,0.00]	[-0.01,0.01]	[-0.05,0.01]	[-0.03,0.02]	[-0.02,0.01]	[-0.04,0.04]	[-0.21,0.21]	[-0.06,0.00]
ModellingGenerator	[-5.20,5.20]	[-4.99,4.99]	[-5.84,5.84]	[-1.62,1.62]	[-2.67,2.67]	[-0.74,0.74]	[-0.09,0.09]	[-0.34,0.34]	[-0.76,0.76]	[-0.34,0.34]	[-0.25,0.25]	[-1.48,1.48]	[-1.31,1.31]	[-0.45,0.45]	[-1.61,1.61]	[-14.90,14.90]
ModellingParton	[-1.43,1.43]	[-1.79,1.79]	[-1.50,1.50]	[-1.87,1.87]	[-0.77,0.77]	[-1.50,1.50]	[-0.61,0.61]	[-0.97,0.97]	[-1.05,1.05]	[-0.93,0.93]	[-0.08,0.08]	[-1.25,1.25]	[-1.73,1.73]	[-2.03,2.03]	[-1.55,1.55]	[-11.33,11.33]
ModellingRadiation	[-9.44,9.44]	[-2.84,2.84]	[-8.64,8.64]	[-3.55,3.55]	[-7.67,7.67]	[-4.29,4.29]	[-3.50,3.50]	[-4.01,4.01]	[-5.63,5.63]	[-5.42,5.42]	[-5.64,5.64]	[-4.91,4.91]	[-3.88,3.88]	[-2.15,2.15]	[-0.80,0.80]	[-3.40,3.40]
ModellingSingleTopWtNormalisation	[-0.39,0.39]	[-0.59,0.59]	[-0.69,0.69]	[-0.70,0.70]	[-0.80,0.80]	[-0.57,0.57]	[-0.70,0.70]	[-0.69,0.69]	[-0.75,0.75]	[-0.75,0.75]	[-0.69,0.69]	[-0.52,0.52]	[-0.53,0.53]	[-0.56,0.56]	[-0.36,0.36]	[-0.00,0.00]
ModellingSingleTopWtInterference	[-2.91,2.91]	[-4.39,4.39]	[-5.12,5.12]	[-5.21,5.21]	[-5.95,5.95]	[-4.22,4.22]	[-5.19,5.19]	[-5.14,5.14]	[-5.59,5.59]	[-5.61,5.61]	[-5.17,5.17]	[-3.84,3.84]	[-3.92,3.92]	[-4.18,4.18]	[-2.72,2.72]	[-0.00,0.00]

Table 8.10 Per-bin individual statistical and systematic uncertainties for the dilepton absolute $\Delta\eta_{ll}$.

8.5 Measurement of $\frac{d\sigma_{t\bar{t}}}{\Delta\phi_{ll}}$

This section describes the fiducial differential cross -section of $t\bar{t}$ decaying to dilepton as a function of the absolute difference of azimuthal angle of two oppositely charged leptons in the $e\mu$ channel. The statistical uncertainty, systematic uncertainty, signal modelling systematics, background modelling systematics, MC statistical uncertainty and all detector modelling systematics have been evaluated in each bin of the observable.

Bin [radian]	Measured $d\sigma/dx$ [pb/radian]	Statistical Data [%]	Statistical MC Bkg [%]	Statistical MC Sig [%]	Systematic [%]
[-3.142,-3.0]	0.1389	+/- 9.5	+/- 2.1	+/- 2.8	+6.2/-5.5
[-3.0,-2.5]	0.1196	+/- 5.4	+/- 1.7	+/- 1.5	+7.5/-6.7
[-2.5,-2.0]	0.1079	+/- 5.7	+/- 1.3	+/- 1.6	+6.3/-5.3
[-2.0,-1.5]	0.0884	+/- 6.6	+/- 1.2	+/- 1.9	+6.8/-5.7
[-1.5,-1.0]	0.0731	+/- 7.1	+/- 2.0	+/- 2.0	+6.5/-5.7
[-1.0,-0.5]	0.0546	+/- 7.9	+/- 2.4	+/- 2.1	+6.4/-6.0
[-0.5,0.0]	0.0515	+/- 8.5	+/- 3.1	+/- 2.4	+7.1/-6.7
[0.0,0.5]	0.0606	+/- 7.7	+/- 1.8	+/- 2.3	+7.0/-5.9
[0.5,1.0]	0.0670	+/- 7.1	+/- 1.3	+/- 2.1	+7.0/-5.7
[1.0,1.5]	0.0707	+/- 7.3	+/- 2.7	+/- 2.0	+6.6/-5.3
[1.5,2.0]	0.0778	+/- 7.0	+/- 2.1	+/- 1.8	+7.0/-6.2
[2.0,2.5]	0.1099	+/- 5.8	+/- 1.3	+/- 1.6	+7.0/-6.5
[2.5,3.0]	0.1024	+/- 6.1	+/- 6.1	+/- 1.5	+11.7/-6.1
[3.0,3.142]	0.1287	+/- 9.7	+/- 1.2	+/- 2.8	+6.0/-6.0

Table 8.11 Per-bin total statistical and systematic uncertainties in $e\mu$ for the dilepton absolute $\Delta\phi_{ll}$, without modelling systematic uncertainties.

Bin [radian]	Measured $d\sigma/dx$ [pb/radian]	Statistical Data [%]	Statistical MC Bkg [%]	Statistical MC Sig [%]	Systematic [%]
[-3.142,-3.0]	0.1389	+/- 9.5	+/- 2.1	+/- 2.8	+19.1/-18.9
[-3.0,-2.5]	0.1196	+/- 5.4	+/- 1.7	+/- 1.5	+13.3/-12.8
[-2.5,-2.0]	0.1079	+/- 5.7	+/- 1.3	+/- 1.6	+12.0/-11.5
[-2.0,-1.5]	0.0884	+/- 6.6	+/- 1.2	+/- 1.9	+10.8/-10.1
[-1.5,-1.0]	0.0731	+/- 7.1	+/- 2.0	+/- 2.0	+10.8/-10.4
[-1.0,-0.5]	0.0546	+/- 7.9	+/- 2.4	+/- 2.1	+11.1/-10.9
[-0.5,0.0]	0.0515	+/- 8.5	+/- 3.1	+/- 2.4	+12.8/-12.6
[0.0,0.5]	0.0606	+/- 7.7	+/- 1.8	+/- 2.3	+11.8/-11.2
[0.5,1.0]	0.0670	+/- 7.1	+/- 1.3	+/- 2.1	+9.8/-8.9
[1.0,1.5]	0.0707	+/- 7.3	+/- 2.7	+/- 2.0	+13.9/-13.3
[1.5,2.0]	0.0778	+/- 7.0	+/- 2.1	+/- 1.8	+15.8/-15.5
[2.0,2.5]	0.1099	+/- 5.8	+/- 1.3	+/- 1.6	+11.1/-10.7
[2.5,3.0]	0.1024	+/- 6.1	+/- 6.1	+/- 1.5	+18.4/-15.4
[3.0,3.142]	0.1287	+/- 9.7	+/- 1.2	+/- 2.8	+8.7/-8.7

Table 8.12 Per-bin total statistical and systematic uncertainties in $e\mu$ for the dilepton absolute $\Delta\phi_{ll}$, with detector modelling, signal modelling and background modelling.

The individual statistical and systematic components in each bin have been shown in Table 8.13 but only the final numbers are shown in Tables 8.11 and 8.12. The measured fiducial differential cross-section has been normalised to the unit area in order to be able

to make a direct comparison between different particle level predictions. The unfolded cross-section agrees well in shape with the predictions. The systematic uncertainties in the normalized case are certainly reduced and it is obvious from the bottom pad (ratio plot) shown in Figure 8.24. The absolute $\Delta\phi$ has almost twice the number of entries in each bin than the raw $\Delta\phi$. The analysis was started with the raw value of the difference of azimuthal but it was decided to look at the absolute $\Delta\phi$ (magnitude of the angular separation) instead. Compared to the other variables, good agreement is seen for the absolute $\Delta\phi$.

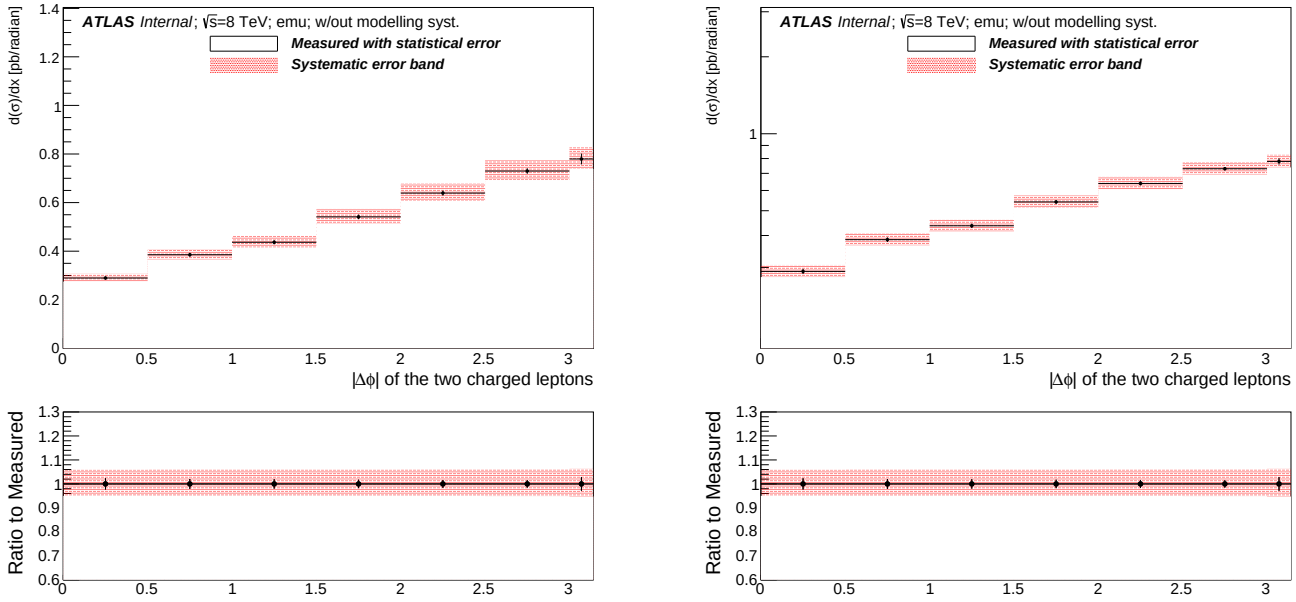

Fig. 8.19 Fiducial differential distribution as a function of the absolute difference of azimuthal angle of the dilepton $\Delta\phi_{ll}$. The left hand side plot is linear while the right hand side is semi-log, only the detector modelling systematics are included on the systematic error band.

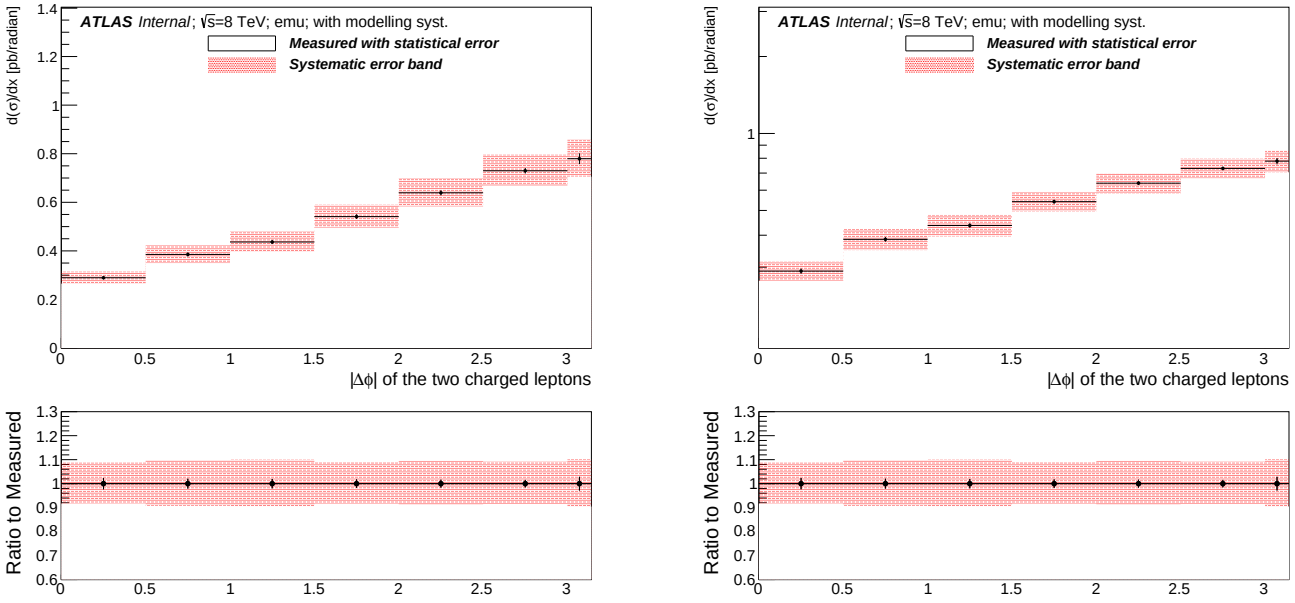

Fig. 8.20 Fiducial differential distribution as a function of the absolute difference of azimuthal angle of the dilepton $\Delta\phi_{ll}$. The left hand side plot is linear while the right hand side is semi-log, the detector modelling, signal modelling and background modelling systematics are included on the systematic error band.

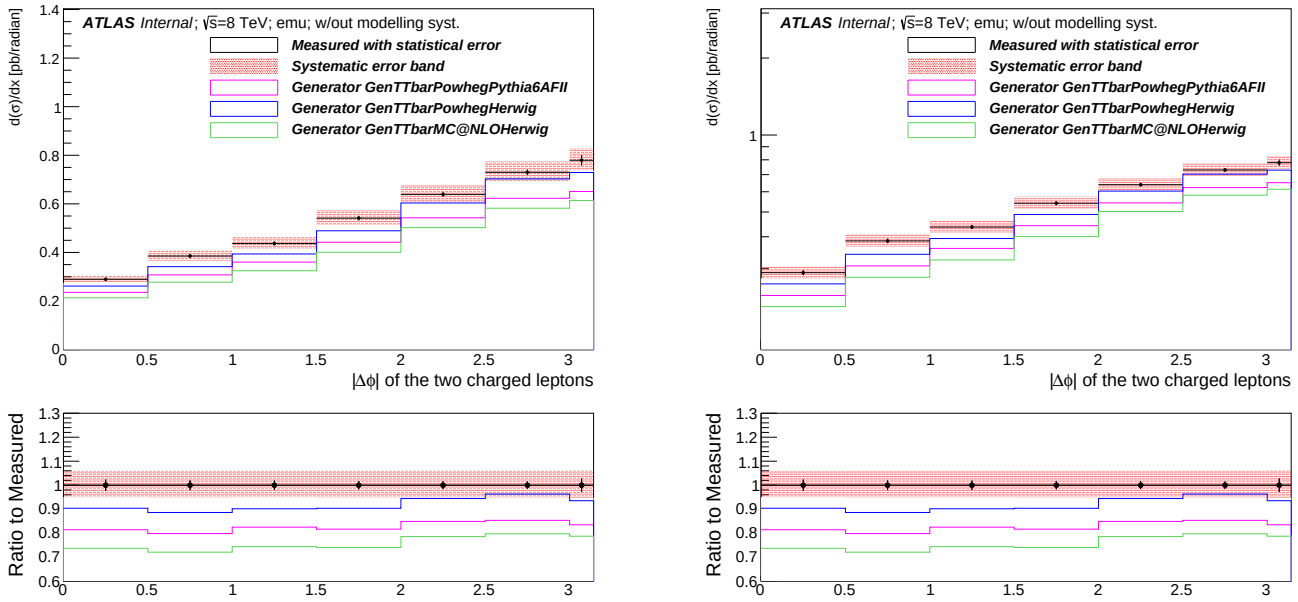

Fig. 8.21 Fiducial differential distribution as a function of the absolute difference of azimuthal angle of the dilepton $\Delta\phi_{ll}$. The left hand side plot is linear while the right hand side is semi-log, the systematic band includes all the detector modelling systematics.

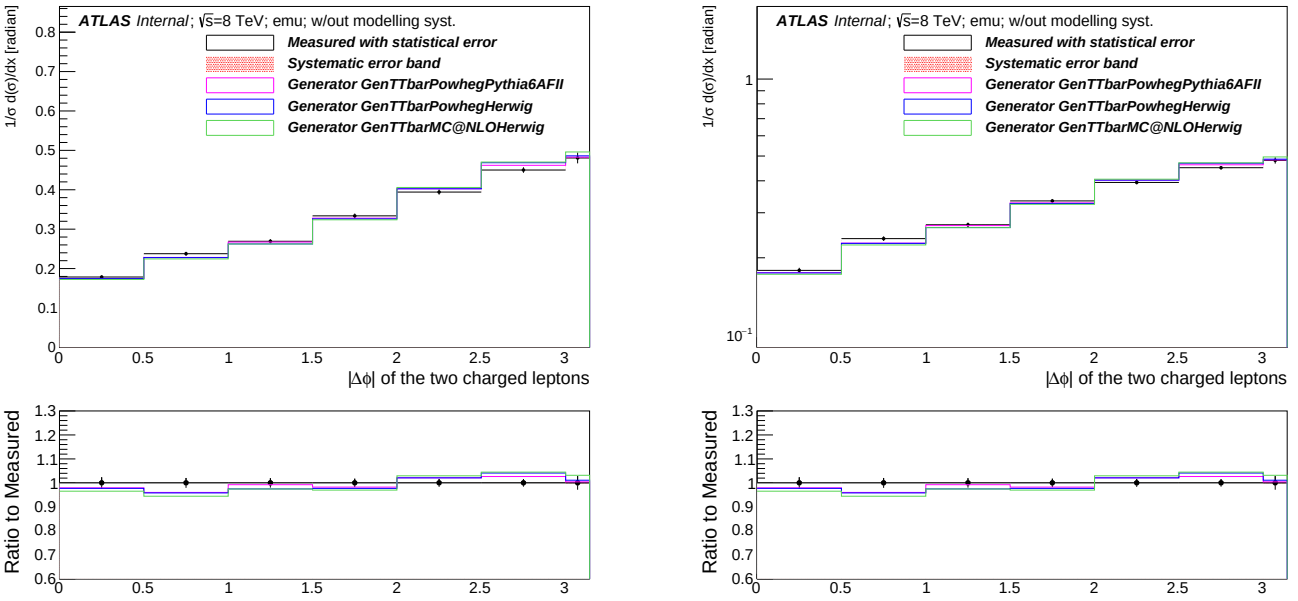

Fig. 8.22 Normalised fiducial differential distribution as a function of the absolute difference of azimuthal angle of the dilepton $\Delta\phi_{ll}$. The left hand side plot is linear while the right hand side is semi-log, the systematic error band includes all the detector modelling systematics.

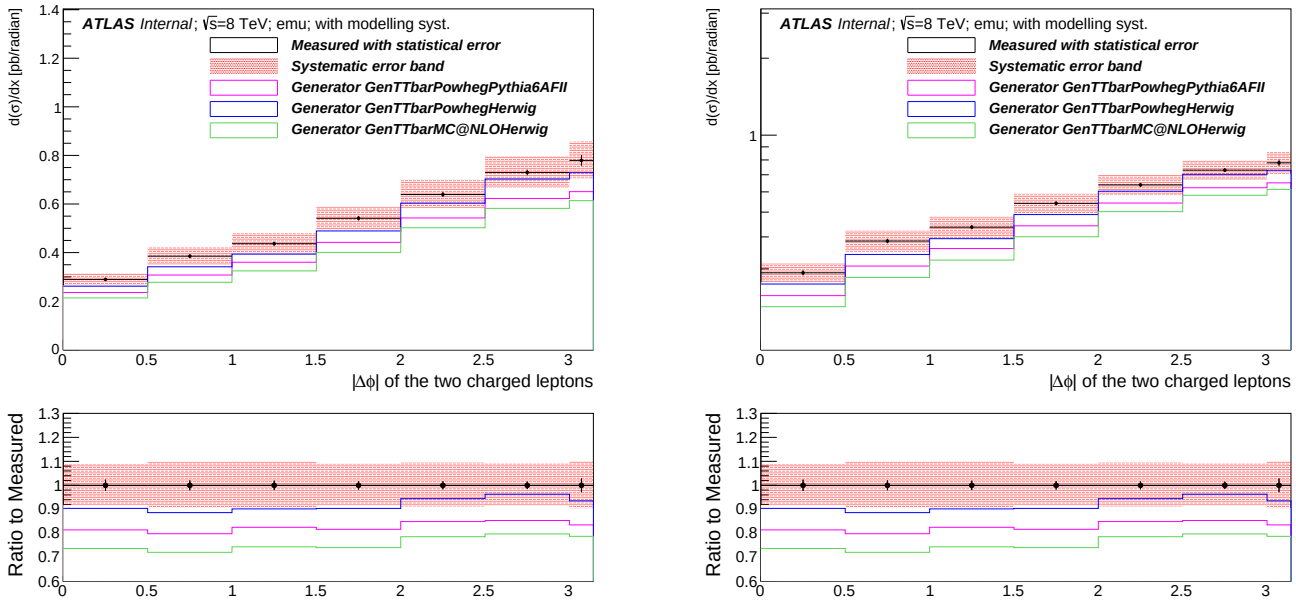

Fig. 8.23 Fiducial differential distribution as a function of the absolute difference of azimuthal angle of the dilepton $\Delta\phi_{ll}$. The left hand side plot is linear while the right hand side is semi-log, the systematic error band includes all the detector modelling, signal modelling and background systematics.

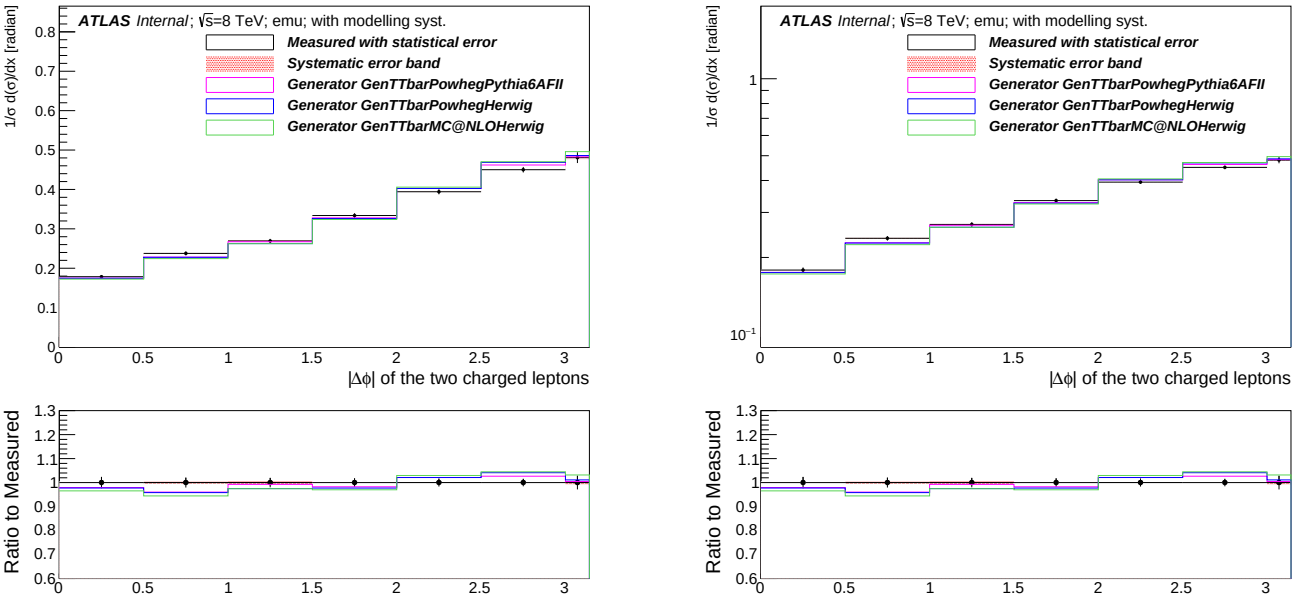

Fig. 8.24 Normalised fiducial differential distribution as a function of the absolute difference of azimuthal angle of the dilepton $\Delta\phi_{ll}$. The systematic error band includes all the detector modelling, signal modelling and background modelling systematics. The left hand side plot is on the linear scale while the right hand side is on the semi-log scale. The plots have been normalized to the unit area to make a direct comparison with particle level predictions. The reduction of systematic uncertainties for the normalised case are clearly seen from the systematic band.

Uncertainty	[-3.142,-3.0]	[-3.0,-2.5]	[-2.5,-2.0]	[-2.0,-1.5]	[-1.5,-1.0]	[-1.0,-0.5]	[-0.5,0.0]	[0.0,0.5]	[0.5,1.0]	[1.0,1.5]	[1.5,2.0]	[2.0,2.5]	[2.5,3.0]	[3.0,3.142]
StatisticalData	[-4.02,4.02]	[-2.18,2.18]	[-2.33,2.33]	[-2.52,2.52]	[-2.78,2.78]	[-2.94,2.94]	[-3.34,3.34]	[-3.34,3.34]	[-2.88,2.88]	[-2.76,2.76]	[-2.47,2.47]	[-2.34,2.34]	[-2.23,2.23]	[-4.03,4.03]
StatisticalBkg	[-0.82,0.82]	[-0.50,0.50]	[-0.48,0.48]	[-0.51,0.51]	[-0.77,0.77]	[-0.91,0.91]	[-0.88,0.88]	[-0.79,0.79]	[-0.84,0.84]	[-1.02,1.02]	[-0.56,0.56]	[-0.64,0.64]	[-0.49,0.49]	[-0.91,0.91]
StatisticalSig	[-0.86,0.88]	[-0.46,0.47]	[-0.48,0.49]	[-0.52,0.52]	[-0.56,0.57]	[-0.59,0.60]	[-0.66,0.67]	[-0.67,0.68]	[-0.59,0.60]	[-0.56,0.57]	[-0.53,0.53]	[-0.49,0.49]	[-0.47,0.47]	[-0.86,0.88]
BTag	[-4.85,5.88]	[-4.81,5.86]	[-4.91,5.96]	[-4.72,5.75]	[-4.83,5.87]	[-5.02,6.12]	[-4.82,5.86]	[-4.76,5.80]	[-4.72,5.74]	[-4.87,5.90]	[-4.88,5.93]	[-4.81,5.85]	[-4.89,5.91]	[-4.92,6.06]
Jeff	[-0.01,0.01]	[-0.01,0.01]	[-0.02,0.02]	[-0.01,0.01]	[-0.02,0.02]	[-0.01,0.01]	[-0.01,0.01]	[-0.00,0.00]	[-0.02,0.02]	[-0.00,0.00]	[-0.03,0.03]	[-0.01,0.01]	[-0.03,0.03]	[-0.01,0.01]
Jer	[-1.68,1.68]	[-0.24,0.24]	[-0.42,0.42]	[-0.48,0.48]	[-0.81,0.81]	[-0.13,0.13]	[-0.28,0.28]	[-0.30,0.30]	[-0.36,0.36]	[-0.09,0.09]	[-0.52,0.52]	[-0.25,0.25]	[-0.88,0.88]	[-0.44,0.44]
MuidRes	[-0.05,0.05]	[-0.05,0.05]	[-0.02,0.02]	[-0.03,0.03]	[-0.02,0.02]	[-0.04,0.04]	[-0.09,0.09]	[-0.12,0.12]	[-0.04,0.04]	[-0.07,0.07]	[-0.03,0.03]	[-0.02,0.02]	[-0.03,0.03]	[-0.04,0.04]
MumsRes	[-0.07,0.07]	[-0.06,0.06]	[-0.05,0.05]	[-0.01,0.01]	[-0.01,0.01]	[-0.03,0.03]	[-0.03,0.03]	[-0.17,0.17]	[-0.07,0.07]	[-0.00,0.00]	[-0.07,0.07]	[-0.05,0.05]	[-0.06,0.06]	[-0.04,0.04]
BJesUnc	[-0.45,0.62]	[-0.33,0.58]	[-0.31,0.46]	[-0.48,0.46]	[-0.35,0.43]	[-0.24,0.44]	[-0.45,0.35]	[-0.39,0.47]	[-0.40,0.40]	[-0.35,0.43]	[-0.39,0.43]	[-0.36,0.52]	[-0.53,0.45]	[-0.52,0.56]
JesEffectiveStat1	[-0.34,0.46]	[-0.28,0.51]	[-0.29,0.29]	[-0.40,0.32]	[-0.24,0.34]	[-0.22,0.36]	[-0.30,0.30]	[-0.30,0.42]	[-0.29,0.36]	[-0.23,0.36]	[-0.31,0.36]	[-0.29,0.40]	[-0.35,0.35]	[-0.37,0.35]
JesEffectiveStat2	[-0.02,0.04]	[-0.05,0.05]	[-0.02,0.02]	[-0.03,0.01]	[-0.02,0.05]	[-0.00,0.01]	[-0.05,0.01]	[-0.02,0.01]	[-0.02,0.02]	[-0.04,0.04]	[-0.03,0.01]	[-0.05,0.02]	[-0.03,0.01]	[-0.02,0.05]
JesEffectiveStat3	[-0.00,0.00]	[-0.00,0.03]	[-0.01,0.01]	[-0.02,0.00]	[-0.02,0.02]	[-0.01,0.01]	[-0.01,0.01]	[-0.00,0.01]	[-0.01,0.02]	[-0.02,0.02]	[-0.04,0.02]	[-0.01,0.01]	[-0.00,0.01]	[-0.01,0.03]
JesEffectiveStat4	[-0.07,0.08]	[-0.04,0.08]	[-0.04,0.03]	[-0.10,0.04]	[-0.11,0.11]	[-0.02,0.04]	[-0.04,0.04]	[-0.05,0.05]	[-0.05,0.05]	[-0.04,0.04]	[-0.09,0.03]	[-0.07,0.02]	[-0.06,0.05]	[-0.06,0.11]
JesEffectiveModel1	[-0.91,1.18]	[-0.81,1.21]	[-0.81,1.05]	[-0.92,0.92]	[-0.74,0.91]	[-0.76,0.83]	[-0.86,0.70]	[-0.82,0.91]	[-0.92,0.80]	[-0.73,0.85]	[-0.79,0.94]	[-0.80,0.97]	[-0.94,0.93]	[-1.22,0.88]
JesEffectiveModel2	[-0.03,0.01]	[-0.04,0.05]	[-0.01,0.01]	[-0.04,0.01]	[-0.01,0.06]	[-0.01,0.01]	[-0.03,0.01]	[-0.02,0.01]	[-0.03,0.03]	[-0.03,0.03]	[-0.03,0.01]	[-0.03,0.02]	[-0.03,0.01]	[-0.02,0.03]
JesEffectiveModel3	[-0.05,0.10]	[-0.05,0.07]	[-0.04,0.04]	[-0.09,0.03]	[-0.10,0.05]	[-0.03,0.02]	[-0.04,0.04]	[-0.08,0.08]	[-0.05,0.05]	[-0.00,0.05]	[-0.08,0.02]	[-0.04,0.03]	[-0.07,0.04]	[-0.04,0.11]
JesEffectiveModel4	[-0.01,0.01]	[-0.00,0.02]	[-0.01,0.01]	[-0.01,0.00]	[-0.02,0.02]	[-0.01,0.01]	[-0.00,0.00]	[-0.00,0.02]	[-0.00,0.01]	[-0.02,0.02]	[-0.02,0.02]	[-0.00,0.01]	[-0.00,0.01]	[-0.00,0.02]
JesEffectiveDet1	[-0.09,0.06]	[-0.07,0.13]	[-0.02,0.05]	[-0.11,0.05]	[-0.11,0.11]	[-0.01,0.05]	[-0.06,0.04]	[-0.08,0.03]	[-0.03,0.05]	[-0.06,0.06]	[-0.11,0.08]	[-0.08,0.02]	[-0.08,0.06]	[-0.05,0.11]
JesEffectiveDet2	[-0.08,0.09]	[-0.05,0.15]	[-0.03,0.05]	[-0.11,0.06]	[-0.12,0.13]	[-0.02,0.05]	[-0.04,0.05]	[-0.08,0.04]	[-0.05,0.06]	[-0.06,0.06]	[-0.10,0.05]	[-0.08,0.03]	[-0.09,0.05]	[-0.06,0.12]
JesEffectiveDet3	[-0.00,0.01]	[-0.01,0.03]	[-0.01,0.01]	[-0.02,0.00]	[-0.01,0.03]	[-0.01,0.00]	[-0.00,0.01]	[-0.01,0.02]	[-0.01,0.01]	[-0.02,0.02]	[-0.03,0.01]	[-0.01,0.01]	[-0.01,0.00]	[-0.00,0.02]
JesEffectiveMix1	[-0.15,0.10]	[-0.11,0.19]	[-0.10,0.11]	[-0.18,0.09]	[-0.10,0.12]	[-0.06,0.08]	[-0.09,0.04]	[-0.07,0.03]	[-0.09,0.10]	[-0.03,0.10]	[-0.15,0.10]	[-0.13,0.08]	[-0.10,0.10]	[-0.13,0.15]
JesEffectiveMix2	[-0.17,0.15]	[-0.14,0.22]	[-0.13,0.15]	[-0.20,0.14]	[-0.13,0.12]	[-0.08,0.09]	[-0.16,0.04]	[-0.10,0.10]	[-0.10,0.17]	[-0.06,0.12]	[-0.17,0.14]	[-0.18,0.10]	[-0.13,0.11]	[-0.15,0.21]
JesEffectiveMix3	[-0.05,0.09]	[-0.04,0.07]	[-0.03,0.03]	[-0.07,0.03]	[-0.08,0.06]	[-0.02,0.01]	[-0.05,0.05]	[-0.07,0.00]	[-0.06,0.04]	[-0.01,0.05]	[-0.06,0.02]	[-0.04,0.02]	[-0.05,0.04]	[-0.04,0.12]
JesEffectiveMix4	[-0.01,0.00]	[-0.00,0.00]	[-0.01,0.01]	[-0.00,0.00]	[-0.01,0.01]	[-0.00,0.00]	[-0.00,0.00]	[-0.00,0.00]	[-0.00,0.00]	[-0.00,0.00]	[-0.00,0.00]	[-0.00,0.00]	[-0.00,0.00]	[-0.00,0.00]
EtaIntercalibrationModel	[-0.12,0.18]	[-0.11,0.22]	[-0.11,0.15]	[-0.24,0.19]	[-0.09,0.21]	[-0.09,0.14]	[-0.07,0.15]	[-0.18,0.18]	[-0.17,0.16]	[-0.09,0.15]	[-0.13,0.17]	[-0.17,0.14]	[-0.13,0.20]	[-0.12,0.14]
EtaIntercalibrationTotalStat	[-0.25,0.28]	[-0.18,0.37]	[-0.20,0.17]	[-0.32,0.21]	[-0.18,0.21]	[-0.18,0.16]	[-0.20,0.13]	[-0.13,0.21]	[-0.25,0.24]	[-0.12,0.20]	[-0.23,0.23]	[-0.22,0.24]	[-0.19,0.19]	[-0.30,0.18]
PileupOffsetMu	[-0.07,0.07]	[-0.06,0.13]	[-0.02,0.06]	[-0.12,0.12]	[-0.12,0.08]	[-0.06,0.08]	[-0.00,0.06]	[-0.04,0.07]	[-0.04,0.04]	[-0.05,0.05]	[-0.12,0.04]	[-0.09,0.07]	[-0.01,0.01]	[-0.07,0.11]
PileupOffsetNPV	[-0.12,0.11]	[-0.28,0.28]	[-0.09,0.07]	[-0.17,0.06]	[-0.05,0.19]	[-0.07,0.07]	[-0.06,0.06]	[-0.20,0.18]	[-0.08,0.04]	[-0.02,0.27]	[-0.05,0.09]	[-0.03,0.19]	[-0.12,0.05]	[-0.40,0.18]
PileupRho	[-0.70,0.81]	[-0.52,0.90]	[-0.56,0.75]	[-0.71,0.67]	[-0.50,0.64]	[-0.46,0.63]	[-0.65,0.54]	[-0.64,0.65]	[-0.65,0.59]	[-0.54,0.66]	[-0.57,0.68]	[-0.54,0.72]	[-0.71,0.72]	[-0.80,0.82]
PunchThrough	[-0.00,0.00]	[-0.00,0.00]	[-0.00,0.00]	[-0.00,0.00]	[-0.00,0.00]	[-0.00,0.00]	[-0.00,0.00]	[-0.00,0.00]	[-0.00,0.00]	[-0.00,0.00]	[-0.00,0.00]	[-0.00,0.00]	[-0.00,0.00]	[-0.00,0.00]
CTauTag	[-0.03,0.03]	[-0.03,0.03]	[-0.04,0.04]	[-0.03,0.03]	[-0.02,0.02]	[-0.02,0.02]	[-0.02,0.02]	[-0.06,0.06]	[-0.03,0.03]	[-0.06,0.06]	[-0.02,0.02]	[-0.03,0.03]	[-0.03,0.03]	[-0.02,0.02]
ElectronEnergyResolution	[-0.11,0.02]	[-0.08,0.08]	[-0.04,0.04]	[-0.01,0.07]	[-0.09,0.08]	[-0.07,0.07]	[-0.01,0.02]	[-0.04,0.03]	[-0.09,0.09]	[-0.10,0.04]	[-0.00,0.07]	[-0.06,0.06]	[-0.10,0.10]	[-0.03,0.12]
ElectronEnergyScale	[-0.09,0.13]	[-0.08,0.08]	[-0.10,0.07]	[-0.00,0.08]	[-0.11,0.05]	[-0.04,0.24]	[-0.10,0.30]	[-0.07,0.07]	[-0.21,0.21]	[-0.08,0.08]	[-0.06,0.06]	[-0.04,0.03]	[-0.13,0.13]	[-0.05,0.07]
ElectronIdSF	[-0.24,0.24]	[-0.23,0.23]	[-0.25,0.25]	[-0.22,0.22]	[-0.26,0.25]	[-0.24,0.24]	[-0.25,0.25]	[-0.21,0.21]	[-0.22,0.22]	[-0.26,0.26]	[-0.22,0.22]	[-0.26,0.26]	[-0.24,0.24]	[-0.25,0.25]
ElectronRecoSF	[-0.02,0.02]	[-0.02,0.02]	[-0.03,0.03]	[-0.02,0.02]	[-0.03,0.03]	[-0.02,0.02]	[-0.02,0.02]	[-0.02,0.02]	[-0.02,0.02]	[-0.03,0.03]	[-0.02,0.02]	[-0.03,0.03]	[-0.03,0.02]	[-0.03,0.03]
ElectronTriggerSF	[-0.01,0.01]	[-0.01,0.01]	[-0.02,0.02]	[-0.01,0.01]	[-0.02,0.02]	[-0.02,0.02]	[-0.01,0.01]	[-0.01,0.01]	[-0.02,0.02]	[-0.01,0.02]	[-0.01,0.01]	[-0.01,0.01]	[-0.01,0.01]	[-0.02,0.02]
FlavorComp	[-0.11,0.29]	[-0.37,0.34]	[-0.30,0.39]	[-0.32,0.34]	[-0.29,0.25]	[-0.24,0.18]	[-0.24,0.28]	[-0.44,0.17]	[-0.29,0.26]	[-0.34,0.29]	[-0.34,0.34]	[-0.29,0.29]	[-0.25,0.36]	[-0.35,0.19]
FlavorResponse	[-0.14,0.16]	[-0.19,0.27]	[-0.22,0.24]	[-0.21,0.21]	[-0.13,0.19]	[-0.15,0.15]	[-0.15,0.19]	[-0.24,0.12]	[-0.21,0.10]	[-0.19,0.19]	[-0.16,0.27]	[-0.17,0.17]	[-0.16,0.22]	[-0.18,0.14]
JetVertexFraction	[-0.19,0.54]	[-0.27,0.29]	[-0.20,0.37]	[-0.24,0.28]	[-0.24,0.32]	[-0.21,0.17]	[-0.32,0.23]	[-0.18,0.21]	[-0.19,0.24]	[-0.18,0.25]	[-0.29,0.34]	[-0.27,0.32]	[-0.28,0.26]	[-0.35,0.24]
Mistag	[-0.05,0.05]	[-0.06,0.06]	[-0.10,0.10]	[-0.08,0.09]	[-0.09,0.09]	[-0.12,0.12]	[-0.06,0.07]	[-0.06,0.06]	[-0.12,0.12]	[-0.06,0.06]	[-0.07,0.07]	[-0.12,0.12]	[-0.08,0.08]	[-0.07,0.07]
MuonIdSF	[-0.05,0.05]	[-0.05,0.05]	[-0.05,0.05]	[-0.05,0.05]	[-0.06,0.06]	[-0.05,0.05]	[-0.06,0.06]	[-0.05,0.05]	[-0.05,0.05]	[-0.06,0.06]	[-0.05,0.05]	[-0.06,0.06]	[-0.05,0.05]	[-0.06,0.05]
MuonRecoSF	[-0.02,0.02]	[-0.02,0.02]	[-0.03,0.03]	[-0.02,0.02]	[-0.02,0.02]	[-0.03,0.03]	[-0.03,0.03]	[-0.02,0.02]	[-0.02,0.02]	[-0.03,0.03]	[-0.02,0.02]	[-0.03,0.03]	[-0.03,0.02]	[-0.02,0.02]
MuonTriggerSF	[-0.00,0.00]	[-0.00,0.00]	[-0.00,0.00]	[-0.00,0.00]	[-0.00,0.00]	[-0.00,0.00]	[-0.00,0.00]	[-0.00,0.00]	[-0.00,0.00]	[-0.00,0.00]	[-0.00,0.00]	[-0.00,0.00]	[-0.00,0.00]	[-0.00,0.00]
Musc	[-0.04,0.04]	[-0.02,0.00]	[-0.00,0.02]	[-0.03,0.03]	[-0.01,0.01]	[-0.03,0.03]	[-0.02,0.02]	[-0.01,0.01]	[-0.02,0.02]	[-0.09,0.01]	[-0.03,0.01]	[-0.02,0.02]	[-0.00,0.01]	[-0.02,0.02]
ModellingGenerator	[-1.31,1.31]	[-2.07,2.07]	[-1.70,1.70]	[-0.80,0.80]	[-1.71,1.71]	[-1.01,1.01]	[-0.09,0.09]	[-0.31,0.31]	[-1.64,1.64]	[-1.89,1.89]	[-0.53,0.53]	[-0.67,0.67]	[-1.13,1.13]	[-0.50,0.50]
ModellingParton	[-2.27,2.27]	[-1.69,1.69]	[-1.41,1.41]	[-1.14,1.14]	[-1.17,1.17]	[-0.62,0.62]	[-1.01,1.01]	[-0.49,0.49]	[-0.13,0.13]	[-0.50,0.50]	[-0.14,0.14]	[-1.10,1.10]	[-0.91,0.91]	[-0.17,0.17]
ModellingRadiation	[-8.10,8.10]	[-4.46,4.46]	[-4.21,4.21]	[-5.07,5.07]	[-5.49,5.49]	[-5.08,5.08]	[-4.76,4.76]	[-4.21,4.21]	[-6.46,6.46]	[-6.03,6.03]	[-4.64,4.64]	[-5.03,5.03]	[-4.21,4.21]	[-2.95,2.95]
ModellingSingleTopWtNormalisation	[-0.71,0.71]	[-0.68,0.68]	[-0.68,0.68]	[-0.58,0.58]	[-0.73,0.73]	[-0.71,0.71]	[-0.73,0.73]	[-0.54,0.54]	[-0.62,0.62]	[-0.71,0.71]	[-0.63,0.63]	[-0.73,0.73]	[-0.67,0.67]	[-0.76,0.76]
ModellingSingleTopWtInterference	[-5.32,5.32]	[-5.09,5.09]	[-5.06,5.06]	[-4.29,4.29]	[-5.46,5.46]	[-5.27,5.27]	[-5.47,5.47]	[-4.03,4.03]	[-4.64,4.64]	[-5.26,5.26]	[-4.73,4.73]	[-5.46,5.46]	[-4.96,4.96]	[-5.64,5.64]

Table 8.13 Per-bin individual statistical and systematic uncertainties for the dilepton absolute $\Delta\phi_{ll}$.

8.6 Integrated fiducial cross-section

The integrated fiducial differential cross-section of all four lepton kinematic variables has been evaluated in this section. To calculate the integrated fiducial cross-section, ${\sigma_{fid}}^{integral}$ from all the bins, the sum of the products of the central value and bin width for all the variables has been computed as:

$$\sigma_{fid}^{integrated} = \sum_{i=1}^{n} \sigma_i \Delta x_i \tag{8.4}$$

The integrated fiducial cross-section can be determined by applying the above formula but a more reliable way to extract the cross-section numbers is to collapse all the bins into a single bin histogram. In order to be able to evaluate the integrated fiducial cross-section, a fake observable has been defined such that when an event passes the dilepton event-selection cut, it falls into this one bin histogram. The details of the contribution of all the detector modelling, signal modelling, background modelling, and data statistics for the $e\mu$ channel are given in Table 8.14. This value is also a cross check of the measured fiducial cross-section obtained from the knowledge of all differential bins.

8.6.1 Integrated fiducial differential cross-section for the $e\mu$ channel

After collapsing all the bins into a single bin (inclusive bin), the integrated fiducial differential cross-section along with systematic and statistical uncertainties are extracted, as given below:
$\sigma_{t\bar{t}_{int}} = 1.62 \pm 0.7\,(stat.) \pm^{9.4}_{8.7}\,(syst.)\,\text{pb}$

In order to be able to compare the results with the predictions and other measurements, the fiducial differential cross-section has been corrected by dividing it with the fiducial acceptance of $e\mu$ events. The acceptance represents the fraction of $t\bar{t}$ events which have a true $e\mu$ event within the detector acceptance (with the fiducial cuts on leptons: $|\eta| < 2.5$ and $p_T > 25$ GeV). The acceptance of $t\bar{t}$ going into the fiducial region times the probability of $t\bar{t}$ going to $e\mu$ is:

$$A_{e\mu} = \frac{N_{e\mu}^{fid}}{N_{e\mu}^{total}} \times \frac{N_{e\mu}^{total}}{N_{t\bar{t}}} = \frac{N_{e\mu}^{fid}}{N_{t\bar{t}}} \tag{8.5}$$

where $N_{e\mu}^{fid}$ is the number of true $e\mu$ events from the MC truth record with fiducial cuts on two lepton kinematic variables $|\eta|$ and p_T ($|\eta| < 2.5$ and $p_T > 25$ GeV) and $N_{t\bar{t}}$ is the total number of events in the MC sample. The value of the fiducial acceptance is:

$N_{t\bar{t}}$	$N_{e\mu}^{fid}$ ($\lvert\eta\rvert < 2.5$ and $p_T > 25$ GeV)	$A_{e\mu}$
1103646	12398	0.0112

Because the MC signal sample used includes only the semileptonic dilepton final states, the acceptance needs to be corrected by taking into account the corresponding branching ratio $B(t\bar{t} \rightarrow \text{not fully hadronic})$ = 1- (1 - (3×0.108))^2 =1 - 0.457 = 0.543.
Then the corrected $e\mu$ fiducial acceptance is:

$$A_{e\mu} = \frac{N_{e\mu}^{fid}}{N_{t\bar{t}} \times \frac{1}{0.543}} = \frac{N_{e\mu}^{fid}}{N_{t\bar{t}}} \times 0.543 = 0.0112 \times 0.543 = 0.0061 \tag{8.6}$$

The systematic uncertainty associated with the fiducial acceptance has not been estimated.

8.6.2 Inclusive cross-section for the $e\mu$ channel

The fiducial cross-section can be defined as:

$$\sigma_{fid} = A_{e\mu} \times \sigma_{t\bar{t}} \tag{8.7}$$

$\sigma_{t\bar{t}} = \frac{1.62}{0.0061} = 265 \pm 0.7\,(stat.) \pm^{9.4}_{8.7}\,(syst.)$pb
To validate the cross-section the analysis has been repeated for ee and $\mu\mu$, the plots and results have been put into the Appendix B. The inclusive cross-section numbers are just to validate the values obtained for the integrated fiducial cross-section so no attempt has been made to evaluate the systematic uncertainties for the full space.

8.7 Summary

The $t\bar{t}$ cross-section is presented as a function of the leading lepton p_T, invariant mass of the dilepton m_{ll}, absolute difference of the azimuthal angle between the leptons $\Delta\phi_{ll}$ and absolute value of separation of the pseudorapidity $\Delta\eta_{ll}$. This analysis has been completed by the cut and count methodology. The fiducial differential cross-section, statistical uncertainties and systematic uncertainties, as a function of these variables, have been calculated. Bin-by-bin values have been shown in Tables 8.3, 8.6, 8.9 and 8.12, and the breakdown of all individual systematic components have been shown in Tables 8.4, 8.7, 8.10 and 8.13. The integrated fiducial cross-section along with systematic and statistical uncertainties have been extracted by collapsing all the bins into one bin. In order to be able to compare the results with the SM prediction, the measured cross-section has been corrected by dividing it with the fiducial acceptance of the detector. The measured cross-sections are consistent with similar measurements in other differential analyses, and with the theoretically predicted values. The main focus was to complete the analysis with the $e\mu$ channel but results have also been produced for the ee and $\mu\mu$ channels and they are included in Appendix B. Generically, the b-tagging, I/FSR, and generator uncertainties are the largest contributors to the total

Uncertainty	[0,1]
StatisticalData	[-0.73,0.73]
StatisticalBkg	[-0.20,0.20]
StatisticalSig	[-0.15,0.15]
BTag	[-4.84,5.89]
Jeff	[-0.02,0.02]
Jer	[-0.46,0.46]
MuidRes	[-0.01,0.01]
MumsRes	[-0.01,0.01]
BJesUnc	[-0.39,0.47]
JesEffectiveStat1	[-0.30,0.37]
JesEffectiveStat2	[-0.03,0.02]
JesEffectiveStat3	[-0.01,0.01]
JesEffectiveStat4	[-0.06,0.05]
JesEffectiveModel1	[-0.84,0.95]
JesEffectiveModel2	[-0.02,0.02]
JesEffectiveModel3	[-0.06,0.04]
JesEffectiveModel4	[-0.00,0.01]
JesEffectiveDet1	[-0.06,0.06]
JesEffectiveDet2	[-0.07,0.07]
JesEffectiveDet3	[-0.01,0.01]
JesEffectiveMix1	[-0.11,0.10]
JesEffectiveMix2	[-0.14,0.14]
JesEffectiveMix3	[-0.05,0.04]
JesEffectiveMix4	[-0.00,0.00]
EtaIntercalibrationModel	[-0.13,0.17]
EtaIntercalibrationTotalStat	[-0.21,0.22]
PileupOffsetMu	[-0.05,0.07]
PileupOffsetNPV	[-0.06,0.12]
PileupRho	[-0.60,0.71]
PunchThrough	[-0.00,0.00]
CTauTag	[-0.03,0.03]
ElectronEnergyResolution	[-0.01,0.01]
ElectronEnergyScale	[-0.04,0.05]
ElectronIdSF	[-0.24,0.24]
ElectronRecoSF	[-0.02,0.02]
ElectronTriggerSF	[-0.01,0.01]
FlavorComp	[-0.30,0.30]
FlavorResponse	[-0.18,0.20]
JetVertexFraction	[-0.24,0.29]
Mistag	[-0.08,0.08]
MuonIdSF	[-0.05,0.05]
MuonRecoSF	[-0.02,0.02]
MuonTriggerSF	[-0.00,0.00]
Musc	[-0.01,0.00]
ModellingGenerator	[-0.60,0.60]
ModellingParton	[-0.92,0.92]
ModellingRadiation	[-4.85,4.85]
ModellingSingleTopWtNormalisation	[-0.67,0.67]
ModellingSingleTopWtInterference	[-5.03,5.03]

Table 8.14 The details of the contribution of all the detector modelling, signal modelling, background modelling systematics and data statistics for the $e\mu$ channel inclusive bin have been shown here.

systematic uncertainty. The analysis, being differential, has been normalised to the unit area (the integral under each curve has been set to 1.0) to retrieve and compare the shapes. The normalised differential distributions have been shown in Figures 8.6, 8.12, 8.18 and 8.24. These normalised plots agree very well in shape but not in normalisation. A dramatic reduction in the total systematic uncertainty for the normalised cross-section is expected and has been seen. A slope is seen in the lepton p_T distribution for the data compared to most of the MCs, which is also seen by similar analyses. Most of the MC models are seen consistent with the measurement, except the tails, which is a common issue that has been seen for other analyses as well.

Chapter 9

Conclusion

The successful operation of the LHC since 2010 has created a huge amount of data which has allowed particle physicists to test and prove their theories at the highest energy regimes. This is most evident by the long awaited discovery of the Higgs Boson which was confirmed by the ATLAS and CMS experiments in 2012. Many new searches and sophisticated experimental techniques are under way to search for possible evidence of new phenomena or make precise measurements of standard processes.

The aim of the analysis presented in this thesis was to perform the measurement of the fiducial differential cross-section of top quark pair production in the dilepton final state at 8 TeV. The cross-section measurements were made in the fiducial phase space, where the electron and muon were required to have opposite charge signs, come from W decays and have a $p_T > 25$ GeV and $\eta < 2.5$. The work presented in this thesis focusses on the measurement of the differential distributions as a function of the kinematics of the dilepton system. Four differential cross-section distributions are measured: the invariant mass of the two leptons (m_{ll}), p_T of the leading lepton, the absolute value of the difference of the azimuthal angle ($|\Delta\phi|$) and pseudorapidity ($|\Delta\eta|$).

The choice of the variables used for this analysis closely follows the ones used for the differential distributions of the mass, transverse momentum and pseudorapidity of the $t\bar{t}$ system. A top quark exclusively decays into a W and a b-quark and the information of the top is carried over to the decay products. This analysis studies the cross-section of $t\bar{t}$ decaying into three decay channels, however, the main channel of interest is the $e\mu$ channel. The $e\mu$ channel has almost twice the number of events compared to individual ee and $\mu\mu$ channels and it also has no contamination from Z boson decaying to $ee/\mu\mu$ + jets. The results of the absolute and normalised kinematic distributions of the $e\mu$ decay channel are given in Chapter 8 while the results for the ee and $\mu\mu$ channels are given in Appendix B. The requirements of

the event selection and analysis object reconstruction criteria have been described in Chapter 5.

The standard top-quark working group recommendation has been followed for the object selection and the final state signatures contain two leptons, two neutrinos, and two jets. One of these two jets has been tagged as a b-jet. By applying one b-tag requirement, a signal purity of 88.5% is achieved. Any measurement based on this purity definitely helps to better compare different predictions in terms of MC simulations. The measurement in this analysis falls within the SM prediction and agrees very well with the theoretically predicted values. The results obtained have been compared with several models, currently in use by the ATLAS experiment, to describe $t\bar{t}$ pairs. By comparing the differential distributions with different models, it has been seen that no single one of these models produced all the features of the distributions, which clearly emphasizes the need to better understand the tuning of the modelling parameters and possibly to improve the underlying physics models.

The POWHEG+PYTHIA $t\bar{t}$ sample describes the production very well. The significant systematics in this analysis come from the modelling of the signals so the discrepancies in the models can be used to tune the MC. As well as being very useful for testing the predictions of perturbative QCD and for modelling the top quark for other physics processes, top production is intrinsically an important background for many new physics searches. Based on this differential measurement, a better description of top production can reduce the modelling systematics.

9.1 Future Work

This analysis can be extended to be tested for almost all known $t\bar{t}$ modelling samples. Then the differential distributions can be compared with the theory and also with each other. This will help establishing which modelling distributions are modelled well. This work may be taken in various directions in "RUN-2" that started in 2015 with a pp collision energy of 13 TeV and targeted integrated luminosity of 100 fb^{-1}. By the end of 2018, it will correspond to one order of magnitude more top quarks than have been collected so far. The large dataset will allow more measurements to test the theoretical predictions and different MC generators for dilepton final states. The differential distributions for one b-tag and two b-tags can be studied separately. Furthermore, if the analysis is done with two b-tagged jets then the purity of the signal reaches 97%, therefore the same analysis can be carried out at 13 TeV or even higher. The two b-tag cuts would eliminate most of the backgrounds except the single top.

Having a higher amount of data at 13 TeV setting compared to 8 TeV, the measurement of the double differential cross-sections using the same variables can also be repeated. The

techniques presented in this analysis can also be used and extended for 13 TeV data and will continue to broaden our understanding of the top quark for the next several years.

References

[1] R. D. Peccei et al. Non-standard couplings of the top quark and precision measurements of the electroweak theory. *Nuclear Physics B*, 349(2):305–322, 1991.

[2] S. Abachi et al. Observation of the top quark. *Physical Review Letters*, 74(14):2632, 1995.

[3] A. Yagil. Observation of top quark production in $p\bar{p}$ collisions with the collider detector at Fermilab. 1995.

[4] M. Peskin and D. Schroeder. *An Introduction to Quantum Field Theory. Advanced book classics*. Addison-Wesley Publishing Company, 1995.

[5] F. Halzen and A. D. Martin. *Quarks and Leptons: An Introductory Course in Modern Particle Physics.* John Wiley & Sons, New York, USA, 1984.

[6] D. J. Griesmayerths. *Introduction to Elementary Particles.* John Wiley & Sons, New York, USA, 1987.

[7] V. D. Barger and R. J. N. Phillips. *Collider Physics.* Addison-Wesley Reading, 1987.

[8] J. Beringer et al. Review of particle physics. *Physical Review D Particles, Fields, Gravitation and Cosmology*, 86(1), 2012.

[9] S. Eidelman et al. Review of particle physics. *Physics Letters B*, 592(1-4):1–5, 2004.

[10] K. A. Olive et al. Review of particle physics. *Chinese Physics C*, 38(9):090001, 2014.

[11] S. L. Glashow. Partial-symmetries of weak interactions. *Nuclear Physics*, 22(4): 579–588, 1961.

[12] A. Salam and J. Ward. Electromagnetic and weak interactions. *Physics Letters*, 13: 168, 1964.

[13] S. Weinberg. A model of leptons. *Physical Review Letters*, 19:1264–1266, 1967.

[14] P. W. Higgs. Broken symmetries, massless particles and gauge fields. *Physics Letters*, 12(2):132–133, 1964.

[15] ATLAS Collaboration. Observation of a new particle in the search for the Standard Model Higgs boson with the ATLAS detector at the LHC. *Physics Letters B*, 716(1): 1–29, 2012.

[16] The CMS Collaboration. Observation of a new boson at a mass of 125 GeV with the CMS experiment at the LHC. *Physics Letters B*, 716(1):30–61, 2012.

[17] N. Cabibbo. Unitary symmetry and leptonic decays. *Physical Review Letters*, 10:531, 1963.

[18] S. L. Glashow et al. Weak interactions with lepton-hadron symmetry. *Physical Review D*, 2:1285, 1970.

[19] R. Turlay et al. Evidence for the 2π decay of the k_2^0 meson. *Physical Review Letters*, 13:138, 1964.

[20] M. Kobayashi and T. Maskawa. CP violation in the renormalizable theory of weak interaction. *Progress of Theoretical Physics*, 49:652–657, 1973.

[21] E. D. Bloom, et al. High-Energy Inelastic *e-p* Scattering at 6° and 10°. *Physical Review Letters*, 23(16):930, 1969.

[22] M. Breidenbach et al. Observed behavior of highly inelastic electron-proton scattering. *Physical Review Letters*, 23(16):935, 1969.

[23] S. L. Glashow et al. Weak interactions with lepton-hadron symmetry. *Physical Review D*, 2(7):1285, 1970.

[24] L. Hoddeson. *The rise of the standard model: A history of particle physics from 1964 to 1979*. Cambridge University Press, 1997.

[25] J. J. Aubert et al. Experimental observation of a heavy particle *J*. *Physical Review Letters*, 33(23):1404, 1974.

[26] J. Augustin et al. Discovery of a narrow resonance in e^+e$^-$ annihilation. *Physical Review Letters*, 33(23):1406, 1974.

[27] M. L. Perl et al. Evidence for anomalous lepton production in $e^+ - e^-$ annihilation. *Physical Review Letters*, 35(22):1489, 1975.

[28] S. Herb et al. Observation of a dimuon resonance at 9.5 GeV in 400-GeV proton-nucleus collisions. *Physical Review Letters*, 39(5):252, 1977.

[29] W. R. Innes et al. Observation of structure in the upsilon region. *Physical Review Letters*, 39(20):1240, 1977.

[30] H. Behrend et al. Search for new heavy quarks in e^+e^- collisions up to 46.78 GeV CM energy. *Physics Letters B*, 144(3-4):297–301, 1984.

[31] M. Althoff et al. Measurement of *R* and search for the top quark in e^+e^- annihilation between 39.8 and 45.2 GeV. *Physics Letters B*, 138(5-6):441–448, 1984.

[32] K. Abe et al. Measurement of *R* and search for new quark flavors decaying into multi-jet final states in e^+e^- collisions between 54.0 and 61.4 GeV CM energies. *Physics Letters B*, 234(3):382–388, 1990.

[33] P. Abreu et al. Search for the t and b' quarks in hadronic decays of the Z^0 boson. *Physics Letters B*, 242(3-4):536–546, 1990.

[34] D. Decamp et al. Search for new quarks and leptons from Z^0 decays at LEP. *Physics Letters B*, 236(4):511–522, 1990.

[35] M. Z. Akrawy et al. A search for the t and b' quarks in hadronic Z^0 decays. *Physics Letters B*, 236(3):364–374, 1990.

[36] G. S. Abrams et al. Searches for new quarks and leptons produced in Z-boson decay. *Physical Review Letters*, 63(22):2447, 1989.

[37] G. Arnison et al. Experimental observation of events with large missing transverse energy accompanied by a jet or a photon (S) in pp collisions at $\sqrt{s}$= 540 GeV. *Physics Letters B*, 139(1-2):115–125, 1984.

[38] J. P. C. Revol et al. Search for the top quark at the CERN proton-antiproton collider with UA1. 1986. URL https://cds.cern.ch/record/175004.

[39] C. Albajar et al. Search for new heavy quarks at the CERN proton-antiproton collider. *Zeitschrift für Physik C Particles and Fields*, 37(4):505–525, 1988.

[40] T. Åkesson et al. Search for top quark production at the CERN $p\bar{p}$ collider. *Zeitschrift für Physik C Particles and Fields*, 46(2):179–189, 1990.

[41] F. Abe et al. Evidence for top quark production in $p\bar{p}$ collisions at $\sqrt{s}$= 1.8 TeV. *Physical Review D*, 50(5):2966, 1994.

[42] F. Abe et al. Observation of top quark production in pp collisions with the collider detector at fermilab. *Physical Review Letters*, 74(14):2626, 1995.

[43] S. Abachi et al. Search for high mass top quark production in $p\bar{p}$ collisions at $\sqrt{s}$= 1.8 TeV. *Physical Review Letters*, 74(13):2422, 1995.

[44] C. Quigg. Unanswered questions in the electroweak theory. *Annual Review of Nuclear and Particle Science*, 59:505–555, 2009.

[45] M. Perelstein. Introduction to collider physics. In *Physics of the Large and the Small: TASI 2009*, pages 421–486. World Scientific, 2011.

[46] M. Mangano. Two lectures on QCD and Hadron Collider physics. *PoS*, page 005, 1998.

[47] M. Czakon et al. Total top-quark pair-production cross-section at Hadron Colliders through $\mathcal{O}(\alpha_S^4)$. *Physical Review Letters*, 110:252004, Jun 2013. doi: 10.1103/PhysRevLett.110.252004. URL https://link.aps.org/doi/10.1103/PhysRevLett.110.252004.

[48] M. Czakon and A. Mitov. Top++: a program for the calculation of the top-pair cross-section at hadron colliders. *Computer Physics Communications*, 185(11):2930–2938, 2014.

[49] M. Baak et al. The global electroweak fit at NNLO and prospects for the LHC and ILC. *The European Physical Journal C*, 74(9):3046, 2014.

[50] J. Kieseler. Extraction of the top-quark mass. In *Top-Quark Pair Production Cross-section and Calibration of the Top-Quark MC Mass*, pages 83–102. Springer, 2016.

[51] Y. Abulaiti et al. Measurement of the top quark charge in pp collisions $\sqrt{s}$= 7 TeV with the ATLAS detector. *Journal of High Energy Physics*, (11):031, 2013.

[52] F. Richard. Present and future constraints on top *EW* couplings. *arXiv preprint arXiv:1403.2893*, 2014.

[53] R. Röntsch and M. Schulze. Constraining couplings of the top quarks to the z boson in $t\bar{t}$+Z production at the LHC. *arXiv preprint arXiv:1404.1005*, 2014.

[54] ATLAS Collaboration et al. The coupling of the higgs boson to fermions and bosons as a function of the particles mass. In *ATLAS-CONF-2015-007. ATLAS-PHO-Event-2015-022*, 2015.

[55] V. Khachatryan et al. Search for the associated production of the higgs boson with a top-quark pair. *Journal of High Energy Physics*, 2014(9):87, 2014.

[56] G. Aad et al. Measurement of spin correlation in top-antitop quark events and search for top squark pair production in pp collisions at $\sqrt{s}$= 8 TeV using the ATLAS detector. *Physical Review Letters*, 114(14):142001, 2015.

[57] K. Shaw, ATLAS Collaboration, et al. Top quark charge asymmetry measurement with ATLAS at the LHC. In *Journal of Physics: Conference Series*, volume 452, page 012058. IOP Publishing, 2013.

[58] ATLAS Collaboration et al. First combination of Tevatron and LHC measurements of the top-quark mass. *arXiv preprint arXiv:1403.4427*, 2014.

[59] ATLAS Collaboration. Measurement of the top quark pair cross section with ATLAS in pp collisions at 7 TeV using final states with an electron or a muon and a hadronically decaying τ lepton. *Physics Letters B*, 717(1-3):89–108, 2012.

[60] ATLAS Collaboration. Measurement of the cross section for top-quark pair production in pp collisions at 7 TeV with the ATLAS detector using final states with two high-p_T leptons. *Journal of High Energy Physics*, 05:059, 2012.

[61] ATLAS Collaboration. Measurement of the top quark pair production cross-section with ATLAS in the single lepton channel. *Physics Letters B*, 711(1-3):067, 2012.

[62] CMS Collaboration. Measurement of the $t\bar{t}$ production cross section in the dilepton channel in pp collisions at 7 TeV. *Journal of High Energy Physics*, 11:067, 2012.

[63] CMS Collaboration. Measurement of the $t\bar{t}$ production cross section in pp collisions at 7 TeV in dilepton final state containing a τ. *Physical Review D*, 85:112007, 2012.

[64] CMS Collaboration. Measurement of the $t\bar{t}$ production cross section in pp collisions at 7 TeV in lepton+jets final state. *Physics Letters B*, 720(1-3):83–104, 2013.

[65] CMS Collaboration. Measurement of the $t\bar{t}$ production cross section in the all-jet final state in pp collisions at 7 TeV. *Journal of High Energy Physics*, 05:067, 2013.

[66] ATLAS Collaboration et al. Measurements of top quark pair relative differential cross-sections with ATLAS in pp collisions at $\sqrt{s}$= 7 TeV. *European Physical Journal C-particles and fields*, 73(1):2261, 2013.

[67] CMS Collaboration. Measurement of the $t\bar{t}$ production cross section in pp collisions at $\sqrt{s}$= 8 TeV in dilepton final states containing one τ lepton. *Physics Letters B*, 739: 23–43, 2014.

[68] CMS Collaboration. Measurement of the differential cross section for top quark pair production in pp collisions at $\sqrt{s}$= 8 TeV. *European Physical Journal C*, 75:542, 2015.

[69] ATLAS Collaboration. Measurements of top-quark pair differential cross-sections in the lepton+jets channel in pp collisions at $\sqrt{s}$= 8 TeV. *European Physical Journal C*, 76:538, 2016.

[70] CMS Collaboration. Measurement of differential top-quark pair production cross-sections in pp collisions at 7 TeV. *European Physical Journal C*, 73:2339, 2013.

[71] K. Kawade. Review of top quark production at LHC and Tevatron. Technical Report ATL-PHYS-PROC-2016-267, CERN, Geneva, Dec 2016. URL https://cds.cern.ch/record/2239212.

[72] A. Airapetian et al. *ATLAS detector and physics performance: Technical Design Report, 1*. Technical Design Report ATLAS. CERN, Geneva, 1999. URL https://cds.cern.ch/record/391176.

[73] L. Evans and P. Bryant. LHC machine. *JINST*, 3(08):S08001, 2008. URL http://stacks.iop.org/1748-0221/3/i=08/a=S08001.

[74] CMS Collaboration. The CMS experiment at the CERN LHC. *JINST*, 3:S08004, 2008.

[75] LHCb Collaboration et al. The LHCb detector at the LHC. *JINST*, 3:S08005, 2008.

[76] ALICE Collaboration et al. The ALICE experiment at the CERN LHC. *JINST*, 3: S08002, 2008.

[77] LHCf Collaboration et al. The LHCf detector at the CERN LHC. *JINST*, 3:S08006, 2008.

[78] J. Pinfold et al. Technical Design Report of the MoEDAL Experiment. Technical Report CERN-LHCC-2009-006. MoEDAL-TDR-001, Jun 2009. URL https://cds.cern.ch/record/1181486.

[79] TOTEM Collaboration et al. The TOTEM experiment at the CERN LHC. *JINST*, 3 (08):S08007, 2008.

[80] C. ÓLuanaigh. LHC experiments back in business at record energy. *Accessed at http://home.cern/about/updates/2015/06/lhc-experiments-back-business-record-energy*, 2015.

[81] C. Lefèvre. The CERN accelerator complex. Dec 2008. URL http://cds.cern.ch/record/1260465.

[82] ATLAS Collaboration. ATLAS experiment: Luminosity public results. https://twiki.cern.ch/twiki/bin/view/AtlasPublic/LuminosityPublicResults, 2013.

[83] ATLAS public results. http://atlas.web.cern.ch/Atlas/public/EVTDISPLAY/events.html. Accessed: 2010-03-20.

[84] T. S. Virdee. Physics requirements for the design of the ATLAS and CMS experiments at the Large Hadron Collider. *Phil. Trans. R. Soc. A*, 370:876–891, 2012. URL https://cds.cern.ch/record/1457849.

[85] G. Aad et al. The ATLAS experiment at the CERN Large Hadron Collider. *JINST*, 3: S08003, 2008.

[86] *ATLAS inner detector: Technical Design Report, 1*. Technical Design Report ATLAS. CERN, Geneva, 1997. URL https://cds.cern.ch/record/331063.

[87] A. Abdesselam et al. The barrel modules of the ATLAS semiconductor tracker. *Nucl. Inst. Meth.*, A 568:642–671, 2006.

[88] A. Abdesselam et al. The ATLAS semiconductor tracker end-cap module. *Nucl. Inst. Meth.*, A 575:98–118, 2007.

[89] Aad, G. and others. Electron performance measurements with the ATLAS detector using the 2010 LHC proton-proton collision data. *The European Physical Journal C*, 72(3):1–46, 2012.

[90] ATLAS Collaboration et al. *ATLAS tile calorimeter: Technical Design Report*. CERN, 1996.

[91] *ATLAS liquid Argon calorimeter: Technical Design Report*. Technical Design Report. CERN, Geneva, 1996. URL http://cds.cern.ch/record/331061.

[92] ATLAS Collaboration. Expected performance of the ATLAS experiment-detector, trigger and physics. *Technical Design Report CERN-LHCC-96-041, CERN*, 2009.

[93] *ATLAS calorimeter performance: Technical Design Report*. Technical Design Report ATLAS. CERN, Geneva, 1996. URL https://cds.cern.ch/record/331059.

[94] D. Gingrich. ATLAS-letter of intent for a general-purpose pp experiment at the Large Hadron Collider at CERN. *CERN/LHCC/92-4 LHCC/I2*, 1992.

[95] A. Artamonov et al. The ATLAS forward calorimeter. *JINST*, 3(02):P02010, 2008.

[96] *ATLAS tile calorimeter: Technical Design Report*. Technical Design Report ATLAS. CERN, Geneva, 1996. URL https://cds.cern.ch/record/331062.

[97] *ATLAS calorimeter performance: Technical Design Report*. Technical Design Report ATLAS. CERN, Geneva, 1996. URL https://cds.cern.ch/record/331059.

[98] E. Diehl. Calibration and Performance of the ATLAS Muon Spectrometer. In *Particles and fields. Proceedings, Meeting of the Division of the American Physical Society, DPF 2011, Providence, USA, August 9-13, 2011*, 2011. URL http://inspirehep.net/record/930228/files/arXiv:1109.6933.pdf.

[99] ATLAS Collaboration et al. Preliminary results on the muon reconstruction efficiency, momentum resolution, and momentum scale in ATLAS 2012 pp collision data. ATLAS-CONF-2013-088, 2013.

[100] P. Hansson. *The ATLAS b-Jet Trigger*. arXiv:hep-ex/1111.4190., 2011.

[101] G. Aad et al. Performance of the ATLAS Trigger System in 2010. *The European Physical Journal C*, 72(1):1–61, 2012.

[102] A. Sbrizzi et al. A Cherenkov Detector for Monitoring ATLAS Luminosity. *Nuclear Physics B-Proceedings Supplements*, 215(1):232–234, 2011.

[103] ATLAS Collaboration et al. Luminosity Determination in pp Collisions at $\sqrt{s}$= 7 TeV using the ATLAS Detector at the LHC. *arXiv preprint arXiv:1101.2185*, 2011.

[104] S. Ask et al. The ATLAS central Level-1 trigger logic and TTC system. *JINST*, 3(08): P08002, 2008.

[105] L. S. Azhgirey et al. Methodical study of the machine induced background formation in the IR8 of LHC. Technical Report LHC-PROJECT-NOTE-258, CERN, Geneva, Jun 2001. URL https://cds.cern.ch/record/691834.

[106] I. S. Baishev et al. Proton Losses Upstream of IP8 in LHC. Technical Report LHC-Project-Report-500. CERN-LHC-Project-Report-500, CERN, Geneva, Aug 2001. URL https://cds.cern.ch/record/517572.

[107] ATLAS Collaboration et al. Non-Collision Backgrounds as measured by the ATLAS detector during the 2010 proton-proton run. ATLAS-CONF-2011-137, 2011.

[108] G. Aad. Studies of the performance of the ATLAS detector using cosmic ray muons. *The European Physical Journal C*, 71(3):1–36, 2011.

[109] V. Cindro et al. The ATLAS beam conditions monitor. *JINST*, 3(02):P02004, 2008.

[110] I. Dolenc. *Development of Beam Conditions Monitor for the ATLAS experiment*. PhD thesis, University Of Ljubljana, 2008.

[111] A. Gorišek et al. Commissioning and first operational experience of the ATLAS beam conditions and loss monitors based on pCVD diamond sensors. *Nuclear Instruments and Methods in Physics Research Section A: Accelerators, Spectrometers, Detectors and Associated Equipment*, 617(1):444–448, 2010.

[112] ATLAS Collaboration et al. Characterisation and mitigation of beam-induced backgrounds observed in the ATLAS detector during the 2011 proton-proton run. *arXiv preprint arXiv:1303.0223*, 2013.

[113] R. Assmann et al. Collimation for the LHC high intensity beams. *Proceedings of HB2010*, 2010.

[114] K. Nakamura et al. Review of particle physics. *Journal of Physics G: Nuclear and Particle Physics*, 37(7A):075021, 2010.

[115] R. Szczygiel et al. ABCD3T Chip Specification. Version: 1.2, 24 July 2000.

[116] ATLAS Collaboration. Non-collision background as measured by the ATLAS detector during the 2010 proton-proton run. *ATLAS-CONF-2011-137*, 2011.

[117] G. Aad et al. Operation and performance of the ATLAS semiconductor tracker. Operation and performance of the ATLAS semiconductor tracker. *JINST*, 9(CERN-PH-EP-2014-049. CERN-PH-EP-2014-049):P08009. 80 p, Apr 2014. URL https://cds.cern.ch/record/1698966.

[118] ATLAS Collaboration. ATLAS Run Queries. *Accessed at http://atlas-runquery.cern.230*, 2012.

[119] J. Roberts et al. Beam Induced Backgrounds Measured in the ATLAS Semiconductor Tracker. Technical Report ATL-COM-INDET-2012-032, CERN, Geneva, May 2012. URL https://cds.cern.ch/record/1452627.

[120] ATLAS Collaboration. *ATLAS-COM-2013-088*. 2013.

[121] S. Shrestha. Search for pair produced new heavy quarks in proton-proton collisions with the ATLAS detector at the LHC, Jul 2014. URL https://cds.cern.ch/record/1966640.

[122] S. Frixione and B. Webber. Matching NLO QCD computations and parton shower simulations. *Journal of High Energy Physics*, 2002(06):029, 2002.

[123] S. Frixione et al. Matching NLO QCD computations with parton shower simulations: the POWHEG method. *Journal of High Energy Physics*, 2007(11):070, 2007.

[124] P. Nason. A new method for combining NLO QCD with shower Monte Carlo algorithms. *Journal of High Energy Physics*, 2004(11):040, 2004.

[125] S. Alioli. A general framework for implementing NLO calculations in shower Monte Carlo programs: the POWHEG box. *Journal of High Energy Physics*, 2010(6):1–58, 2010.

[126] M. Gosselink. Radiating top quarks, 2010. URL https://cds.cern.ch/record/1295161. Presented 14 Oct 2010.

[127] R. K. Ellis et al. *QCD and collider physics*. Cambridge University press, 2003.

[128] A. Buckley et al. General-purpose event generators for LHC physics. *Physics Reports*, 504(5):145–233, 2011.

[129] T. Sjöstrand et al. PYTHIA 6.4 physics and manual. *Journal of High Energy Physics*, 2006(05):026, 2006.

[130] G. Corcella et al. HERWIG 6.5 release note. *arXiv preprint hep-ph/0210213*, 2002.

[131] J. M. Butterworth and M. H. Seymour. Jimmy4: Multiparton interactions in HERWIG for the LHC, 2004.

[132] S. Frixione et al. Matching NLO QCD computations and parton shower simulations. *Journal of High Energy Physics*, 2002(06):029, 2002.

[133] M. Mangano. ALPGEN, a generator for hard multiparton processes in hadronic collisions. *Journal of High Energy Physics*, 2003(07):001, 2003.

[134] M. Schoenherr and F. Krauss. Soft photon radiation in particle decays in SHERPA. *Journal of High Energy Physics*, 2008(12):018, 2008.

[135] G. Pasztor et al. Electron trigger performance in 2012 ATLAS data. Technical Report ATL-COM-DAQ-2015-091, CERN, Geneva, July 2015. URL https://cds.cern.ch/record/2032463.

[136] B. Abbott et al. Performance of the ATLAS muon trigger in pp collisions at $\sqrt{s}$= 8 TeV. 2015.

[137] Top groups' MC12 samples for 2012 data analyses. https://twiki.cern.ch/twiki/bin/viewauth/AtlasProtected/TopMC12.

[138] G. Aad et al. The ATLAS simulation infrastructure. *The European Physical Journal C*, 70(3):823–874, 2010.

[139] E. Richter-Was et al. ATLFAST 2.0 a fast simulation package for ATLAS. 1998.

[140] T. Sjöstrand et al. A brief introduction to PYTHIA 8.1. *Computer Physics Communications*, 178(11):852–867, 2008.

[141] ATLASTopDPD production. https://twiki.cern.ch/twiki/bin/viewauth/AtlasProtected/TopD3PDProduction.

[142] ATLAS TopRootCore analysis framework. https://twiki.cern.ch/twiki/bin/viewauth/AtlasProtected/TopRootCore.

[143] P. Z. Skands. Tuning Monte Carlo generators: the Perugia tunes. *Physical Review D*, 82(7):074018, 2010.

[144] H. I. Lai. New parton distributions for collider physics. *Physical Review D*, 82(7): 074024, 2010.

[145] P. Z. Skands. Tuning monte carlo generators: the perugia tunes. *Physical Review D*, 82(7):074018, 2010.

[146] G. Aad et al. Measurement of $t\bar{t}$ production with a veto on additional central jet activity in pp collisions at $\sqrt{s}$ = 7 TeV using the ATLAS detector. *European Physical Journal C*, 72(CERN-PH-EP-2012-062. CERN-PH-EP-2012-062):2043, Mar 2012. URL https://cds.cern.ch/record/1433862.

[147] Comparison of Monte Carlo generator predictions for gap fraction and jet multiplicity observables in top-antitop events. Technical Report ATL-PHYS-PUB-2014-005, CERN, Geneva, May 2014. URL https://cds.cern.ch/record/1703034.

[148] B. Acharya et al. Object selection and calibration, background estimations and MC samples for top quark analyses using the full 2012 data set. Technical Report ATL-COM-PHYS-2013-1016, CERN, Geneva, Jul 2013. URL https://cds.cern.ch/record/1563201.

[149] ATLAS Collaboration. Top Common Objects for 2012 data. https://twiki.cern.ch/twiki/bin/viewauth/AtlasProtected/TopCommonObjects, 2012.

[150] P. Sommer. Measurement of the electron reconstruction and identification efficiencies in ATLAS. Technical Report ATL-PHYS-PROC-2014-035, CERN, Geneva, May 2014. URL https://cds.cern.ch/record/1698057.

[151] ATLAS Collaboration. Electron isolation tool from ATLAS egamma analysis utils package. https://svnweb.cern.ch/trac/atlasoff/browser/Reconstruction/egamma/egammaAnalysis/egammaAnalysisUtils, 2014.

[152] ATLAS Collaboration. Expected photon performance in the ATLAS experiment. Technical Report ATL-PHYS-PUB-2011-007, CERN, Geneva, April 2011. URL https://cds.cern.ch/record/1345329.

[153] G. Aad et al. Measurement of the muon reconstruction performance of the ATLAS detector using 2011 and 2012 LHC proton–proton collision data. *European Physical Journal C*, 74(CERN-PH-EP-2014-151. CERN-PH-EP-2014-151):3130, Jul 2014. URL https://cds.cern.ch/record/1743068.

[154] M. Cacciari et al. The anti-kt jet clustering algorithm. *Journal of High Energy Physics*, 2008(04):063, 2008.

[155] W. Lampl. Calorimeter Clustering Algorithms: Description and Performance. Technical Report ATL-LARG-PUB-2008-002. ATL-COM-LARG-2008-003, CERN, Geneva, Apr 2008. URL https://cds.cern.ch/record/1099735.

[156] ATLAS Collaboration et al. Pile-up subtraction and suppression for jets in ATLAS. ATLAS-CONF-2013-083, 2013.

[157] G. P. Salam. Elements of QCD for hadron colliders. *arXiv preprint arXiv:1011.5131*, 2010.

[158] D. W. Miller. Pile-up jet energy scale corrections using the jet-vertex fraction method. Technical Report ATL-COM-PHYS-2009-180, CERN, Geneva, Apr 2009. URL https://cds.cern.ch/record/1172636.

[159] J. Beringer et al. Review of particle physics particle data group. *Physical Review D (Particles, Fields, Gravitation and Cosmology)*, 86(1), 2012.

[160] ATLAS Collaboration et al. Commissioning of the ATLAS high-performance *b*-tagging algorithms in the 7 TeV collision data. ATLAS-CONF-2011-102, 2011.

[161] ATLAS Collaboration et al. Measurement of the *b*-tag efficiency in a sample of jets containing muons with 5 fb^{-1} of data from the ATLAS detector. ATLAS-CONF-2012-043, 2012.

[162] ATLAS Collaboration et al. Measuring the *b*-tag efficiency in a top-pair sample with 4.7 fb^{-1} of data from the ATLAS detector. Technical Report ATLAS-CONF-2012-097, CERN, Geneva, 2012.

[163] ATLAS Collaboration. ATLAS *b*-tagging supported taggers and operating points. https://twiki.cern.ch/twiki/bin/viewauth/AtlasProtected/BtagAnalysis172Winter2013.

[164] G. Aad et al. Expected performance of the ATLAS experiment-detector, trigger and physics. 2008.

[165] C. Pizio. *Missing transverse energy measurement in ATLAS detector: first LHC data results and importance for physics study*. PhD thesis, INFN, Milan, 2010.

[166] A. Canepa et al. Missing Transverse Energy for Top Physics analyses with early ATLAS data at *sqrts*=7 TeV. Technical Report ATL-COM-PHYS-2010-821, CERN, Geneva, Oct 2010. URL https://cds.cern.ch/record/1297971.

[167] N. Ghodbane et al. Jets, missing transverse energy and taus for top physics analyses in release 16 with the 2010 dataset. Technical report, ATL-COM-PHYS-2011-132, CERN, Geneva, 2011.

[168] ATLAS Collaboration. Expected relative energy resolution as a function of energy for electrons. https://twiki.cern.ch/twiki/pub/AtlasPublic/AtlasTechnicalPaperListOfFigures/elecEresol_vs_Energy_b37_e55.pdf.

[169] ATLAS Collaboration. Expected stand-alone and combined fractional momentum resolution as a function of p_T for single muons with absolute η<1.1. https://twiki.cern.ch/twiki/pub/AtlasPublic/AtlasTechnicalPaperListOfFigures/res_vs_pt_barrel.pdf, .

[170] ATLAS Collaboration. Expected stand-alone and combined fractional momentum resolution as a function of p_T for single muons with absolute η>1.7. https://twiki.cern.ch/twiki/pub/AtlasPublic/AtlasTechnicalPaperListOfFigures/res_vs_pt_barrel.pdf, .

[171] ATLAS Collaboration. Public plots in ATLAS detector paper to compare resolutions. https://twiki.cern.ch/twiki/bin/view/AtlasPublic/AtlasTechnicalPaperListOfFigures.

[172] ATLAS Collaboration et al. Muon reconstruction efficiency in reprocessed 2010 LHC proton-proton collision data recorded with the ATLAS detector. ATLAS-CONF-2011-063, 2011.

[173] ATLAS Collaboration et al. Jet energy measurement and its systematic uncertainty in proton-proton collisions at 7 TeV with the ATLAS detector. *arXiv preprint arXiv:1406.0076*, 2014.

[174] ATLAS Collaboration et al. Jet energy scale and its systematic uncertainty in proton-proton collisions at $\sqrt{s}$= 7 TeV with ATLAS 2011 data. ATLAS-CONF-2013-004, 2013.

[175] B. Acharya et al. Object selection and calibration, background estimations and MC samples for the Winter 2012 Top Quark analyses with 2011 data. Technical Report ATL-COM-PHYS-2012-224, CERN, Geneva, Feb 2012. URL https://cds.cern.ch/record/1427721.

[176] G. Romeo et al. Jet energy resolution from in-situ techniques with the ATLAS detector using proton-proton collisions at a center of mass energy $\sqrt{s}$= 7 TeV. *ATLAS internal note: ATL-COM-PHYS-2011-240*, 2011.

[177] B. Butler and A. Schwartzman. Track-Jet Reconstruction and Performance. Technical Report ATL-PHYS-INT-2010-040, CERN, Geneva, April 2010. URL https://cds.cern.ch/record/1259686.

[178] ATLAS Collaboration et al. Jet energy resolution and selection efficiency relative to track jets from in-situ techniques with the ATLAS detector using proton-proton collisions at a center of mass energy $\sqrt{s}$= 7 TeV. In *Technical Report ATLAS-CONF-2010-054, CERN, Geneva*, 2010.

Appendix A

Detector modelling systematics list

Table A.1 Systematic variations for detector modelling

Systematic	Name of systematic
	BJesUnc_up
	btag_down
	btag_up
	ctautag_down
	ctautag_up
	eer_down
	eer_up
	ees_down
	ees_up
	el_idSF_down
	el_idSF_up
	el_recSF_down
	el_recSF_up
	el_trigSF_down
	el_trigSF_up
	EtaIntercalibrationModel_down
	EtaIntercalibrationModel_up
	EtaIntercalibrationTotalStat_down
	EtaIntercalibrationTotalStat_up
	flavor_comp_down
	flavor_comp_up
	flavor_response$_d$*own*

$flavor\_response\_up$
$jeff$
jer
$JesEffectiveDet1\_down$
$JesEffectiveDet1\_up$
$JesEffectiveDet2\_down$
$JesEffectiveDet2\_up$
$JesEffectiveDet3\_down$
$JesEffectiveDet3\_up$
$JesEffectiveMix1\_down$
$JesEffectiveMix1\_up$
$JesEffectiveMix2\_down$
$JesEffectiveMix2\_up$
$JesEffectiveMix3\_down$
$JesEffectiveMix3\_up$
$JesEffectiveMix4\_down$
$JesEffectiveMix4\_up$
$JesEffectiveModel1\_down$
$JesEffectiveModel1\_up$
$JesEffectiveModel2\_down$
$JesEffectiveModel2\_up$
$JesEffectiveModel3\_down$
$JesEffectiveModel3\_up$
$esEffectiveModel4\_down$
$JesEffectiveModel4\_up$
$JesEffectiveStat1\_down$
$JesEffectiveStat1\_up$
$JesEffectiveStat2\_down$
$JesEffectiveStat2\_up$
$JesEffectiveStat3\_down$
$JesEffectiveStat3\_up$
$JesEffectiveStat4\_down$
$JesEffectiveStat4\_up$
jvf_down
jvf_up
$mistag\_down$

mistag_up
muid_res
mu_idSF_down
mu_idSF_up
mums_res
mu_recSF_down
mu_recSF_up
musc_down
musc_up
mu_trigSF_down
mu_trigSF_up
Nominal
Pileup_OffsetMu_down
Pileup_OffsetNPV_down
Pileup_OffsetNPV_up
Pileup_Pt_down
Pileup_Pt_up
Pileup_Rho_down
Pileup_Rho_up
PunchThrough_down
$PunchThrough_{up}$
res_soft_down
res_soft_up
sc_soft_down
sc_soft_up
SinglePart_down
SinglePart_up

Appendix B

Fiducial differential cross-section results for ee and $\mu\mu$

B.1 Detailed results for the *ee* channel

B.1.1 Variable inclusive in one bin

Bin [GeV]	Measured $d\sigma/dx$ [pb/unit]	Statistical Data [%]	Statistical MC Bkg [%]	Statistical MC Sig [%]	Systematic [%]
[0,1]	0.5299	+/- 1.9	+/- 0.9	+/- 0.5	+6.8/-5.7

Table B.1 Per-bin total statistical and systematic uncertainties in *ee* for inclusive (one bin), without modelling systematic uncertainties.

Bin [GeV]	Measured $d\sigma/dx$ [pb/unit]	Statistical Data [%]	Statistical MC Bkg [%]	Statistical MC Sig [%]	Systematic [%]
[0,1]	0.5299	+/- 1.9	+/- 0.9	+/- 0.5	+11.4/-10.8

Table B.2 Per-bin total statistical and systematic uncertainties in *ee* for inclusive (one bin), with modelling systematic uncertainties.

Bin [GeV]	Measured $d\sigma/dx$ [pb/unit]	Statistical Data [%]	Total Syst Up [%]	Total Syst Down [%]	GenTTbarPowhegPythia6AFII [%]	GenTTbarPowhegHerwig [%]	GenTTbarMC@NLOHerwig [%]
[0,1]	0.5299	+/- 1.9	6.8	-5.7	-15.1	-6.5	-21.9

Table B.3 Per-bin total statistical and systematic uncertainties in *ee* for inclusive (one bin), with generators, without normalisation.

Bin [GeV]	Measured $d\sigma/dx$ [pb/unit]	Statistical Data [%]	Total Syst Up [%]	Total Syst Down [%]	GenTTbarPowhegPythia6AFII [%]	GenTTbarPowhegHerwig [%]	GenTTbarMC@NLOHerwig [%]
[0,1]	1.0000	+/- 1.9	0.0	0.0	0.0	0.0	0.0

Table B.4 Per-bin total stat. and syst. uncertainties in ee for inclusive (one bin), with generators, with all distributions normalised to unit area.

Uncertainty	[0,1]
StatisticalData	[-1.85,1.85]
StatisticalBkg	[-0.87,0.87]
StatisticalSig	[-0.50,0.51]
BTag	[-4.94,6.00]
Jeff	[-0.02,0.02]
Jer	[-0.69,0.69]
MuidRes	[0.00,0.00]
MumsRes	[-0.01,0.01]
BJesUnc	[-0.83,0.75]
JesEffectiveStat1	[-0.52,0.40]
JesEffectiveStat2	[-0.03,0.05]
JesEffectiveStat3	[-0.11,0.08]
JesEffectiveStat4	[-0.18,0.22]
JesEffectiveModel1	[-1.63,2.02]
JesEffectiveModel2	[-0.01,0.01]
JesEffectiveModel3	[-0.04,0.06]
JesEffectiveModel4	[-0.07,0.10]
JesEffectiveDet1	[-0.41,0.52]
JesEffectiveDet2	[-0.05,0.13]
JesEffectiveDet3	[-0.05,0.07]
JesEffectiveMix1	[-0.38,0.47]
JesEffectiveMix2	[-0.25,0.26]
JesEffectiveMix3	[-0.05,0.05]
JesEffectiveMix4	[-0.01,0.01]
EtaIntercalibrationModel	[-0.50,0.40]
EtaIntercalibrationTotalStat	[-0.44,0.41]
PileupOffsetMu	[-0.15,0.17]
PileupOffsetNPV	[-0.23,0.52]
PileupRho	[-1.20,1.03]
PunchThrough	[-0.00,0.00]
CTauTag	[-0.04,0.04]
ElectronEnergyResolution	[-0.01,0.09]
ElectronEnergyScale	[-0.84,0.88]
ElectronIdSF	[-0.60,0.58]
ElectronRecoSF	[-0.07,0.07]
ElectronTriggerSF	[-0.00,0.00]
FlavorComp	[-0.77,1.01]
FlavorResponse	[-0.51,0.43]
JetVertexFraction	[-0.28,0.37]
Mistag	[-0.22,0.22]
MuonIdSF	[-0.00,0.00]
MuonRecoSF	[-0.00,0.00]
MuonTriggerSF	[0.00,0.00]
Musc	[0.00,0.00]
ModellingGenerator	[-0.74,0.74]
ModellingParton	[-0.42,0.42]
ModellingRadiation	[-7.02,7.02]
ModellingSingleTopWtNormalisation	[-0.77,0.77]
ModellingSingleTopWtInterference	[-5.71,5.71]

Table B.5 Per-bin individual statistical and systematic uncertainties in *ee* for inclusive (one bin).

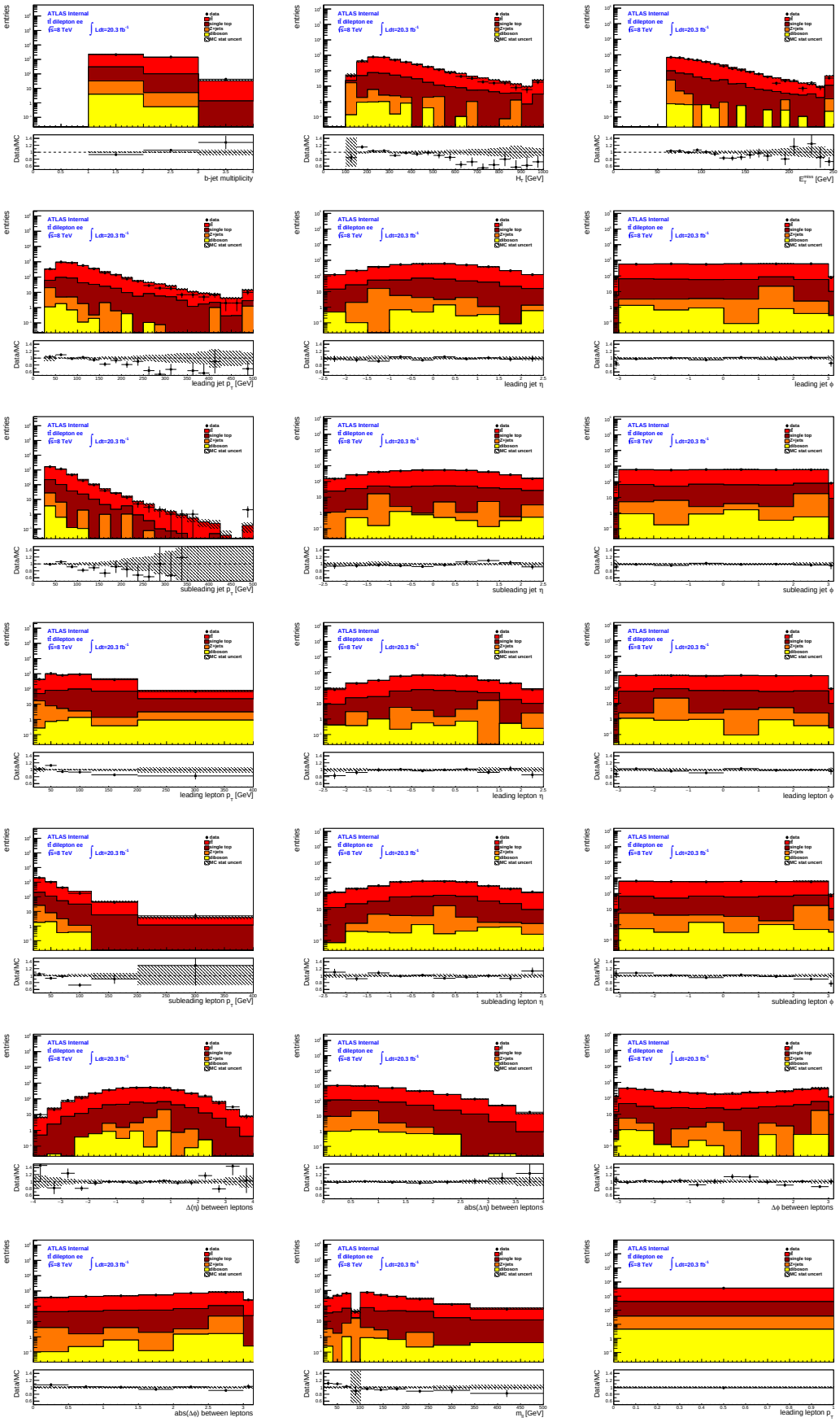

Fig. B.1 Stacked plots per bin (not scaled to density) for channel *ee* for the Nominal MC (no syst).

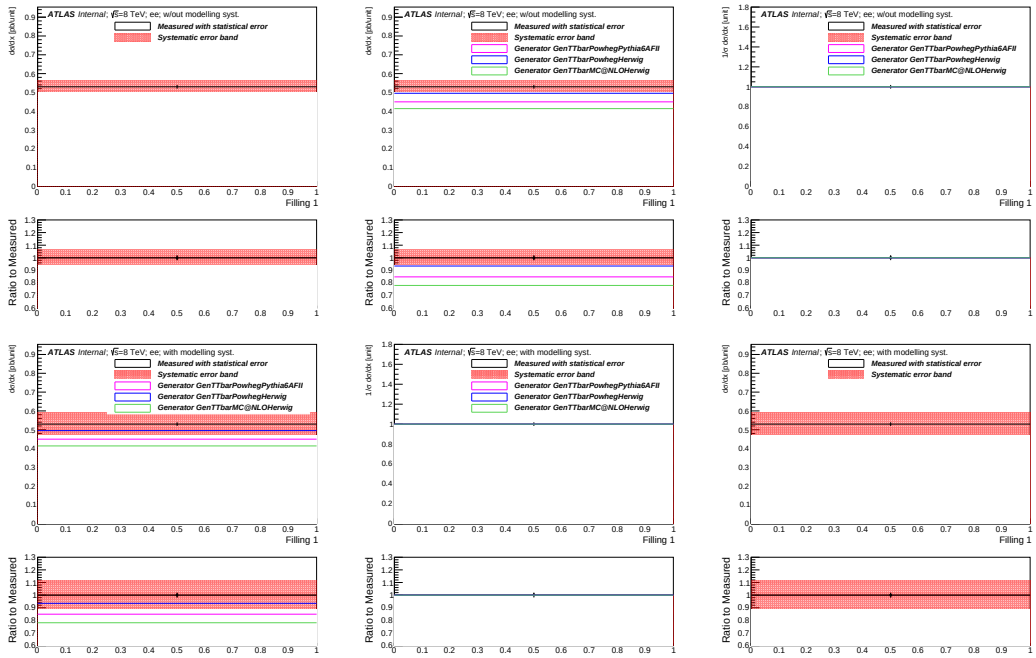

Fig. B.2 Differential cross-section for channel *ee* in the variable of inclusive in one bin.

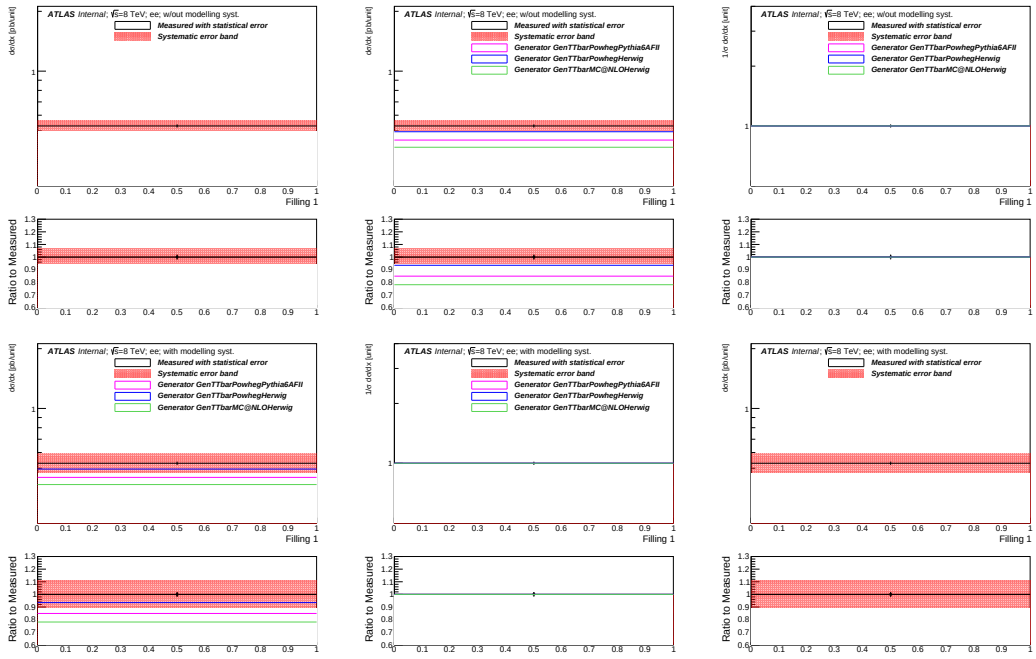

Fig. B.3 Differential cross-section for channel *ee* in the variable of inclusive in one bin (log on y axis).

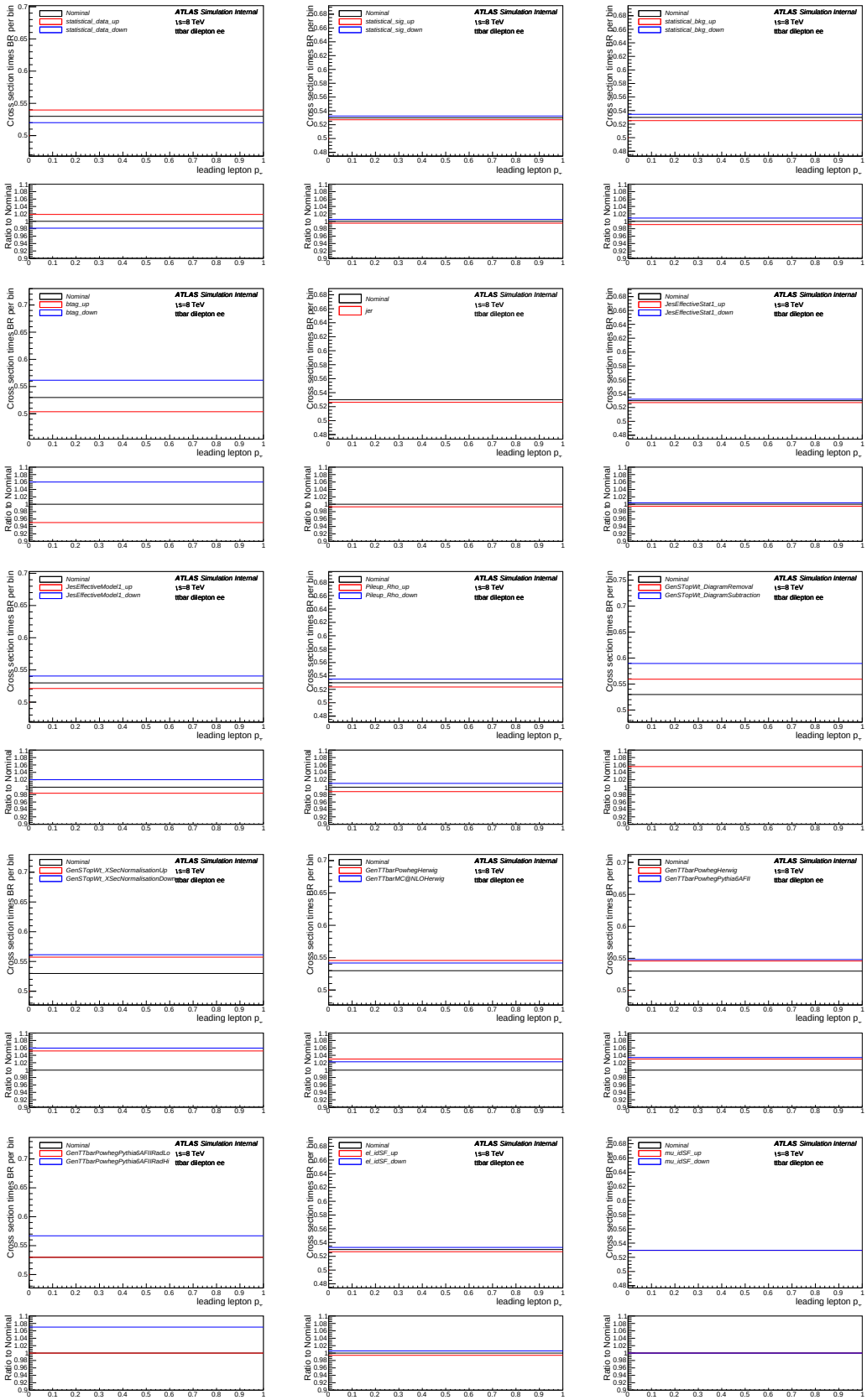

Fig. B.4 Differential cross-section per bin (not scaled to density) for channel *ee* in the variable of inclusive in one bin with measured (with Nominal signal) overlaid with statistical uncertainties on data and MC (signal and background), as well as various systematics.

B.1.2 Variable dilepton invariant mass (m_{ll})

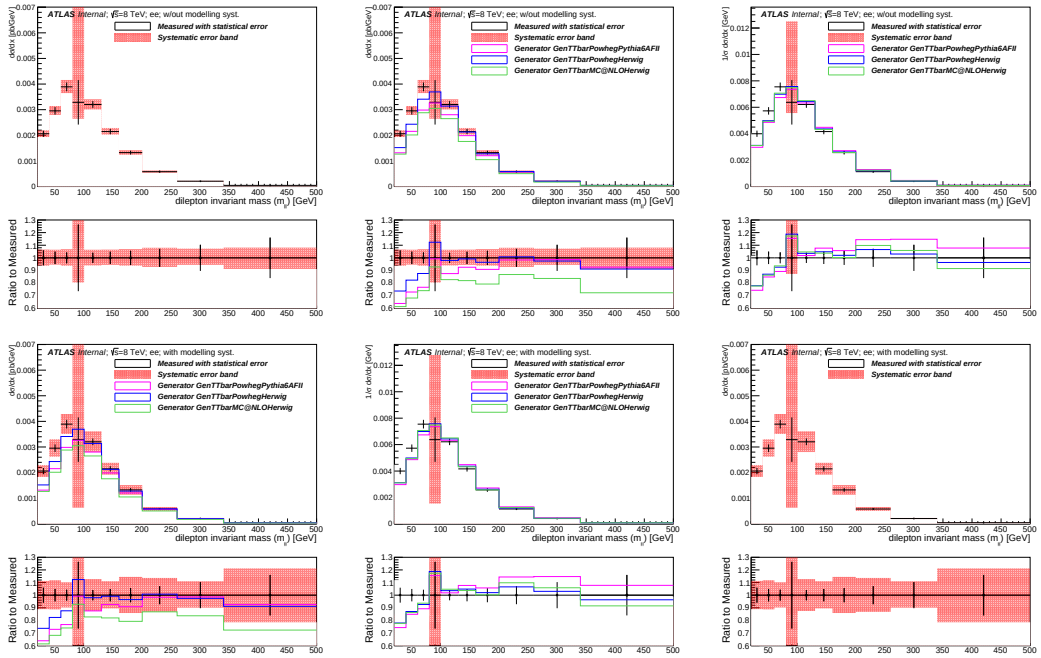

Fig. B.5 Differential cross-section for channel *ee* in the variable of dilepton invariant mass (m_{ll}).

Bin [GeV]	Measured $d\sigma/dx$ [pb/GeV]	Statistical Data [%]	Statistical MC Bkg [%]	Statistical MC Sig [%]	Systematic [%]
[20,40]	0.0021	+/- 5.9	+/- 1.8	+/- 1.8	+6.6/-6.2
[40,60]	0.0030	+/- 4.9	+/- 1.1	+/- 1.4	+6.5/-5.4
[60,80]	0.0039	+/- 4.3	+/- 1.5	+/- 1.2	+6.9/-6.3
[80,100]	0.0033	+/- 26.4	+/- 65.9	+/- 6.7	+143.6/-19.5
[100,130]	0.0032	+/- 4.1	+/- 1.1	+/- 1.1	+6.4/-6.0
[130,160]	0.0021	+/- 4.9	+/- 1.1	+/- 1.3	+6.5/-5.6
[160,200]	0.0013	+/- 5.6	+/- 1.2	+/- 1.5	+7.0/-6.2
[200,260]	0.0006	+/- 7.2	+/- 2.3	+/- 1.8	+8.0/-7.2
[260,340]	0.0002	+/- 10.3	+/- 2.8	+/- 2.7	+7.3/-5.6
[340,500]	0.0000	+/- 16.0	+/- 5.1	+/- 4.0	+8.1/-8.8

Table B.6 Per-bin total statistical and systematic uncertainties in *ee* for the dilepton invariant mass (m_{ll}), without modelling systematic uncertainties.

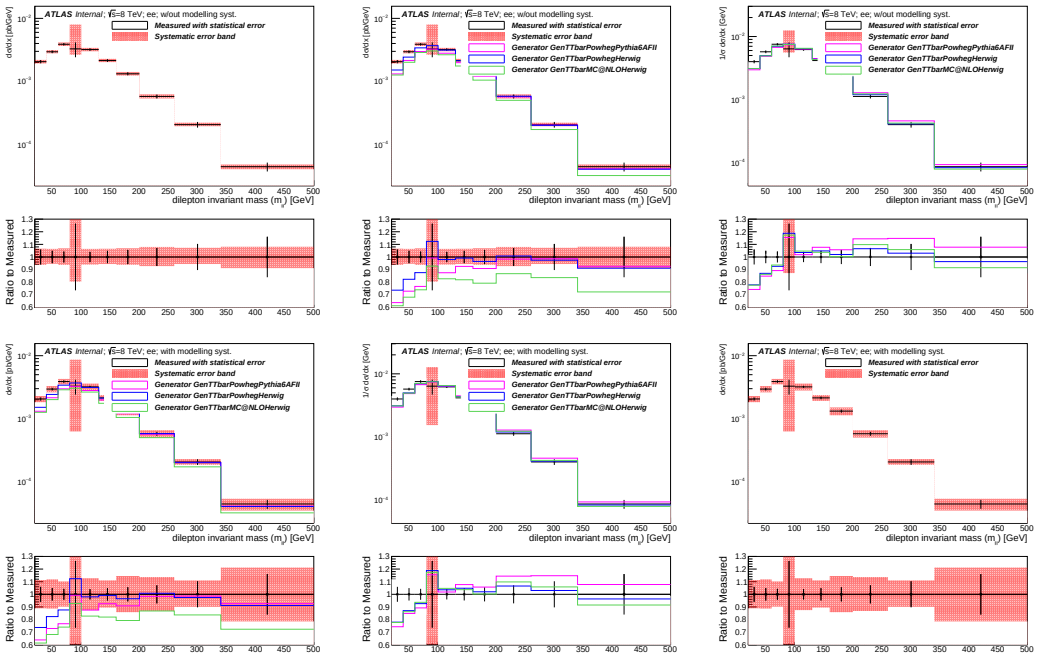

Fig. B.6 Differential cross-section for channel *ee* in the variable of dilepton invariant mass (m_{ll}) (log on y axis).

Bin [GeV]	Measured $d\sigma/dx$ [pb/GeV]	Statistical Data [%]	Statistical MC Bkg [%]	Statistical MC Sig [%]	Systematic [%]
[20,40]	0.0021	+/- 5.9	+/- 1.8	+/- 1.8	+11.3/-11.1
[40,60]	0.0030	+/- 4.9	+/- 1.1	+/- 1.4	+11.8/-11.3
[60,80]	0.0039	+/- 4.3	+/- 1.5	+/- 1.2	+10.2/-9.8
[80,100]	0.0033	+/- 26.4	+/- 65.9	+/- 6.7	+163.6/-80.8
[100,130]	0.0032	+/- 4.1	+/- 1.1	+/- 1.1	+12.7/-12.5
[130,160]	0.0021	+/- 4.9	+/- 1.1	+/- 1.3	+11.0/-10.5
[160,200]	0.0013	+/- 5.6	+/- 1.2	+/- 1.5	+14.5/-14.1
[200,260]	0.0006	+/- 7.2	+/- 2.3	+/- 1.8	+13.6/-13.2
[260,340]	0.0002	+/- 10.3	+/- 2.8	+/- 2.7	+11.0/-9.9
[340,500]	0.0000	+/- 16.0	+/- 5.1	+/- 4.0	+21.2/-21.5

Table B.7 Per-bin total statistical and systematic uncertainties in *ee* for the dilepton invariant mass (m_{ll}), with modelling systematic uncertainties.

Bin [GeV]	Measured $d\sigma/dx$ [pb/GeV]	Statistical Data [%]	Total Syst Up [%]	Total Syst Down [%]	GenTTbarPowhegPythia6AFII [%]	GenTTbarPowhegHerwig [%]	GenTTbarMC@NLOHerwig [%]
[20,40]	0.0021	+/- 5.9	6.6	-6.2	-36.1	-26.3	-38.6
[40,60]	0.0030	+/- 4.9	6.5	-5.4	-27.1	-17.6	-31.8
[60,80]	0.0039	+/- 4.3	6.9	-6.3	-23.3	-12.4	-26.0
[80,100]	0.0033	+/- 26.4	143.6	-19.5	-0.8	12.4	-7.2
[100,130]	0.0032	+/- 4.1	6.4	-6.0	-12.5	-2.0	-17.2
[130,160]	0.0021	+/- 4.9	6.5	-5.6	-7.4	-0.8	-18.0
[160,200]	0.0013	+/- 5.6	7.0	-6.2	-9.1	-3.5	-20.7
[200,260]	0.0006	+/- 7.2	8.0	-7.2	-1.7	0.8	-13.2
[260,340]	0.0002	+/- 10.3	7.3	-5.6	-1.4	-2.5	-16.3
[340,500]	0.0000	+/- 16.0	8.1	-8.8	-7.4	-8.9	-27.7

Table B.8 Per-bin total statistical and systematic uncertainties in *ee* for the dilepton invariant mass (m_{ll}), with generators, without normalisation.

Bin [GeV]	Measured $d\sigma/dx$ [pb/GeV]	Statistical Data [%]	Total Syst Up [%]	Total Syst Down [%]	GenTTbarPowhegPythia6AFII [%]	GenTTbarPowhegHerwig [%]	GenTTbarMC@NLOHerwig [%]
[20,40]	0.0040	+/- 5.9	-14.2	1.7	-25.7	-22.1	-22.3
[40,60]	0.0057	+/- 4.9	-14.3	2.6	-15.1	-12.9	-13.8
[60,80]	0.0075	+/- 4.3	-14.0	1.7	-10.8	-7.4	-6.3
[80,100]	0.0064	+/- 26.4	96.1	-12.7	15.5	18.8	17.4
[100,130]	0.0062	+/- 4.1	-14.3	1.9	1.8	3.6	4.7
[130,160]	0.0042	+/- 4.9	-14.2	2.4	7.7	4.8	3.7
[160,200]	0.0026	+/- 5.6	-13.9	1.7	5.7	2.0	0.3
[200,260]	0.0011	+/- 7.2	-13.1	0.6	14.4	6.6	9.8
[260,340]	0.0004	+/- 10.3	-13.6	2.4	14.7	3.0	5.9
[340,500]	0.0001	+/- 16.0	-13.0	-1.1	7.8	-3.7	-8.5

Table B.9 Per-bin total statistical and systematic uncertainties in *ee* for the dilepton invariant mass (m_{ll}), with generators, with all distributions normalised to unit area.

Uncertainty	[20,40]	[40,60]	[60,80]	[80,100]	[100,130]	[130,160]	[160,200]	[200,260]	[260,340]	[340,500]
StatisticalData	[-5.93,5.93]	[-4.92,4.92]	[-4.34,4.34]	[-26.41,26.41]	[-4.07,4.07]	[-4.87,4.87]	[-5.61,5.61]	[-7.16,7.16]	[-10.35,10.35]	[-16.04,16.04]
StatisticalBkg	[-1.82,1.82]	[-1.07,1.07]	[-1.46,1.46]	[-65.88,65.88]	[-1.08,1.08]	[-1.07,1.07]	[-1.20,1.20]	[-2.33,2.33]	[-2.78,2.78]	[-5.12,5.12]
StatisticalSig	[-1.74,1.80]	[-1.36,1.40]	[-1.15,1.18]	[-5.91,6.71]	[-1.05,1.08]	[-1.23,1.26]	[-1.43,1.47]	[-1.72,1.78]	[-2.52,2.65]	[-3.68,3.98]
BTag	[-4.79,5.91]	[-4.64,5.65]	[-4.85,5.89]	[-4.34,5.39]	[-5.01,6.08]	[-4.93,5.98]	[-4.89,5.98]	[-5.64,6.75]	[-4.80,5.96]	[-5.61,6.67]
Jeff	[-0.03,0.03]	[-0.07,0.07]	[-0.06,0.06]	[-0.00,0.00]	[-0.00,0.00]	[-0.01,0.01]	[-0.05,0.05]	[-0.10,0.10]	[-0.00,0.00]	[0.00,0.00]
Jer	[-1.66,1.66]	[-1.66,1.66]	[-0.22,0.22]	[-2.93,2.93]	[-0.51,0.51]	[-0.59,0.59]	[-2.01,2.01]	[-2.25,2.25]	[-0.63,0.63]	[-2.88,2.88]
MuidRes	[0.00,0.00]	[0.00,0.00]	[0.00,0.00]	[0.00,0.00]	[0.00,0.00]	[0.00,0.00]	[0.00,0.00]	[0.00,0.00]	[0.00,0.00]	[0.00,0.00]
MumsRes	[-0.01,0.01]	[-0.01,0.01]	[0.00,0.00]	[-0.41,0.41]	[0.00,0.00]	[0.00,0.00]	[0.00,0.00]	[-0.06,0.06]	[0.00,0.00]	[0.00,0.00]
BJesUnc	[-0.93,0.68]	[-0.60,0.93]	[-0.75,0.52]	[-0.87,0.38]	[-0.87,0.53]	[-0.83,0.81]	[-0.91,0.95]	[-1.08,1.31]	[-0.69,0.69]	[-1.26,0.88]
JesEffectiveStat1	[-1.05,0.26]	[-0.42,0.36]	[-0.19,0.56]	[-0.10,0.11]	[-0.68,0.28]	[-0.46,0.42]	[-0.55,0.59]	[-0.56,0.35]	[-0.12,0.12]	[-2.01,0.88]
JesEffectiveStat2	[-0.06,0.06]	[-0.08,0.08]	[-0.14,0.14]	[-0.52,0.52]	[-0.10,0.10]	[-0.04,0.17]	[-0.09,0.02]	[-0.03,0.03]	[-0.09,0.03]	[-0.04,0.11]
JesEffectiveStat3	[-0.13,0.05]	[-0.05,0.16]	[-0.11,0.25]	[-0.41,0.41]	[-0.22,0.07]	[-0.14,0.09]	[-0.20,0.01]	[-0.08,0.08]	[-0.15,0.10]	[-0.14,0.08]
JesEffectiveStat4	[-0.26,0.26]	[-0.11,0.26]	[-0.15,0.50]	[-0.62,0.62]	[-0.29,0.08]	[-0.13,0.28]	[-0.15,0.19]	[-0.20,0.06]	[-0.13,0.09]	[-0.11,0.60]
JesEffectiveModel1	[-1.82,1.29]	[-1.27,1.57]	[-1.23,1.73]	[-1.49,62.64]	[-1.72,1.31]	[-1.60,1.44]	[-1.84,1.59]	[-2.32,1.72]	[-1.49,3.09]	[-2.39,1.58]
JesEffectiveModel2	[-0.09,0.09]	[-0.12,0.12]	[-0.09,0.09]	[-0.58,0.58]	[-0.13,0.03]	[-0.05,0.05]	[-0.06,0.03]	[-0.08,0.10]	[-0.09,0.00]	[-0.52,0.52]
JesEffectiveModel3	[-0.16,0.16]	[-0.05,0.05]	[-0.24,0.24]	[-0.87,0.87]	[-0.12,0.12]	[-0.07,0.13]	[-0.25,0.15]	[-0.03,0.01]	[-0.03,0.01]	[-0.07,0.46]
JesEffectiveModel4	[-0.02,0.02]	[-0.06,0.19]	[-0.08,0.19]	[-0.16,0.16]	[-0.08,0.02]	[-0.08,0.05]	[-0.03,0.14]	[-0.16,0.06]	[-0.14,0.01]	[-0.07,0.61]
JesEffectiveDet1	[-0.43,0.43]	[-0.20,0.47]	[-0.39,0.98]	[-0.55,0.55]	[-0.55,0.26]	[-0.43,0.59]	[-0.48,0.47]	[-0.50,0.70]	[-0.16,0.54]	[-0.22,0.46]
JesEffectiveDet2	[-0.12,0.12]	[-0.13,0.13]	[-0.05,0.35]	[-0.56,0.56]	[-0.21,0.10]	[-0.06,0.17]	[-0.03,0.03]	[-0.12,0.12]	[-0.09,0.09]	[-0.50,0.50]
JesEffectiveDet3	[-0.01,0.01]	[-0.02,0.12]	[-0.03,0.17]	[-0.14,0.14]	[-0.10,0.02]	[-0.06,0.06]	[-0.02,0.01]	[-0.09,0.02]	[-0.12,0.01]	[-0.61,0.61]
JesEffectiveMix1	[-0.49,0.01]	[-0.31,0.58]	[-0.22,0.88]	[-0.62,0.62]	[-0.55,0.27]	[-0.33,0.49]	[-0.46,0.43]	[-0.55,0.51]	[-0.31,0.12]	[-0.08,0.38]
JesEffectiveMix2	[-0.64,0.01]	[-0.22,0.18]	[-0.10,0.44]	[-0.57,0.57]	[-0.40,0.18]	[-0.17,0.35]	[-0.17,0.34]	[-0.19,0.22]	[-0.29,0.04]	[-0.22,0.56]
JesEffectiveMix3	[-0.11,0.11]	[-0.18,0.18]	[-0.26,0.26]	[-0.59,0.59]	[-0.08,0.08]	[-0.14,0.14]	[-0.05,0.08]	[-0.23,0.06]	[-0.01,0.01]	[-0.33,0.33]
JesEffectiveMix4	[-0.00,0.01]	[-0.01,0.01]	[-0.00,0.04]	[-0.10,0.10]	[-0.02,0.02]	[-0.04,0.02]	[-0.01,0.01]	[-0.01,0.01]	[-0.01,0.01]	[-0.00,0.01]
EtaIntercalibrationModel	[-0.47,0.47]	[-0.22,0.37]	[-0.39,0.48]	[-0.14,0.14]	[-0.85,0.23]	[-0.34,0.53]	[-0.56,0.40]	[-0.67,1.06]	[-0.41,0.39]	[-0.24,0.24]
EtaIntercalibrationTotalStat	[-0.80,0.15]	[-0.29,0.29]	[-0.31,0.63]	[-0.55,0.55]	[-0.52,0.27]	[-0.32,0.46]	[-0.43,0.50]	[-0.65,0.53]	[-0.24,0.16]	[-1.80,0.70]
PileupOffsetMu	[-0.65,0.07]	[-0.22,0.19]	[-0.14,0.14]	[-0.70,0.70]	[-0.28,0.28]	[-0.10,0.26]	[-0.06,0.06]	[-0.12,0.70]	[-0.20,1.18]	[-0.62,0.73]
PileupOffsetNPV	[-0.71,0.71]	[-0.03,0.43]	[-0.24,0.23]	[-0.24,61.77]	[-0.36,0.36]	[-0.08,0.08]	[-0.14,0.29]	[-0.50,0.50]	[-1.23,1.23]	[-1.99,0.76]
PileupRho	[-1.59,0.89]	[-0.98,1.13]	[-0.89,1.10]	[-0.62,0.04]	[-1.34,0.69]	[-1.07,1.02]	[-1.29,1.42]	[-1.56,1.46]	[-0.87,0.92]	[-2.86,0.99]
PunchThrough	[-0.03,0.03]	[-0.00,0.02]	[-0.00,0.04]	[-0.00,0.00]	[-0.03,0.03]	[-0.01,0.00]	[-0.02,0.03]	[-0.02,0.02]	[-0.00,0.00]	[-0.03,0.03]
CTauTag	[-0.08,0.08]	[-0.05,0.05]	[-0.04,0.04]	[-0.04,0.04]	[-0.02,0.02]	[-0.03,0.03]	[-0.02,0.02]	[-0.07,0.08]	[-0.11,0.11]	[-0.00,0.00]
ElectronEnergyResolution	[-0.10,0.18]	[-0.38,0.38]	[-2.75,0.19]	[-1.30,58.56]	[-0.36,0.15]	[-0.07,0.04]	[-0.22,0.24]	[-0.52,0.79]	[-0.54,0.54]	[-0.32,0.32]
ElectronEnergyScale	[-0.87,0.71]	[-0.18,0.48]	[-1.89,1.89]	[-4.55,72.73]	[-0.99,0.74]	[-0.51,0.64]	[-1.22,0.73]	[-1.43,0.95]	[-0.87,1.22]	[-1.84,0.82]
ElectronIdSF	[-0.50,0.49]	[-0.42,0.41]	[-0.54,0.52]	[-3.02,2.95]	[-0.53,0.52]	[-0.47,0.45]	[-0.63,0.62]	[-0.93,0.91]	[-0.77,0.74]	[-1.33,1.29]
ElectronRecoSF	[-0.05,0.05]	[-0.04,0.04]	[-0.05,0.05]	[-0.21,0.21]	[-0.05,0.05]	[-0.05,0.05]	[-0.07,0.07]	[-0.13,0.13]	[-0.10,0.10]	[-0.23,0.23]
ElectronTriggerSF	[-0.00,0.01]	[-0.01,0.01]	[-0.00,0.00]	[-0.01,0.01]	[-0.00,0.00]	[-0.00,0.00]	[-0.00,0.00]	[-0.01,0.01]	[-0.00,0.00]	[-0.00,0.00]
FlavorComp	[-0.79,0.69]	[-0.73,0.33]	[-0.55,0.52]	[-0.34,61.64]	[-0.93,0.35]	[-0.74,0.63]	[-0.84,0.75]	[-0.86,0.66]	[-0.19,0.71]	[-1.36,0.90]
FlavorResponse	[-0.80,0.68]	[-0.43,0.33]	[-0.32,0.65]	[-0.36,0.09]	[-0.70,0.16]	[-0.41,0.41]	[-0.59,0.50]	[-0.39,0.55]	[-0.08,0.40]	[-1.67,0.63]
JetVertexFraction	[-0.33,0.15]	[-0.24,0.38]	[-0.35,0.50]	[-0.01,0.19]	[-0.28,0.44]	[-0.17,0.29]	[-0.26,0.23]	[-0.24,0.37]	[-0.44,0.67]	[-0.12,0.15]
Mistag	[-0.18,0.18]	[-0.06,0.06]	[-0.05,0.05]	[-17.74,17.84]	[-0.04,0.05]	[-0.06,0.06]	[-0.13,0.13]	[-0.10,0.10]	[-0.12,0.12]	[-0.20,0.21]
MuonIdSF	[0.00,0.00]	[-0.00,0.00]	[-0.00,0.00]	[-0.00,0.00]	[-0.00,0.00]	[-0.00,0.00]	[-0.00,0.00]	[-0.00,0.00]	[0.00,0.00]	[0.00,0.00]
MuonRecoSF	[0.00,0.00]	[-0.00,0.00]	[-0.00,0.00]	[-0.00,0.00]	[-0.00,0.00]	[-0.00,0.00]	[-0.00,0.00]	[-0.00,0.00]	[0.00,0.00]	[0.00,0.00]
MuonTriggerSF	[0.00,0.00]	[0.00,0.00]	[0.00,0.00]	[0.00,0.00]	[0.00,0.00]	[0.00,0.00]	[0.00,0.00]	[0.00,0.00]	[0.00,0.00]	[0.00,0.00]
Musc	[0.00,0.00]	[0.00,0.00]	[0.00,0.00]	[0.00,0.00]	[0.00,0.00]	[0.00,0.00]	[0.00,0.00]	[0.00,0.00]	[0.00,0.00]	[0.00,0.00]
ModellingGenerator	[-3.07,3.07]	[-2.96,2.96]	[-1.22,1.22]	[-17.85,17.85]	[-1.55,1.55]	[-4.49,4.49]	[-5.05,5.05]	[-3.44,3.44]	[-0.48,0.48]	[-10.28,10.28]
ModellingParton	[-2.59,2.59]	[-0.51,0.51]	[-1.69,1.69]	[-1.67,1.67]	[-4.34,4.34]	[-0.94,0.94]	[-1.40,1.40]	[-1.67,1.67]	[-1.20,1.20]	[-0.76,0.76]
ModellingRadiation	[-5.98,5.98]	[-8.43,8.43]	[-3.81,3.81]	[-76.16,76.16]	[-8.30,8.30]	[-6.69,6.69]	[-9.81,9.81]	[-3.30,3.30]	[-0.64,0.64]	[-10.17,10.17]
ModellingSingleTopWtNormalisation	[-0.75,0.75]	[-0.56,0.56]	[-0.81,0.81]	[-0.71,0.71]	[-0.73,0.73]	[-0.48,0.48]	[-0.82,0.82]	[-1.31,1.31]	[-1.07,1.07]	[-1.75,1.75]
ModellingSingleTopWtInterference	[-5.62,5.62]	[-4.19,4.19]	[-6.07,6.07]	[-5.31,5.31]	[-5.43,5.43]	[-3.58,3.58]	[-6.12,6.12]	[-9.76,9.76]	[-7.99,7.99]	[-13.03,13.03]

Table B.10 Per-bin individual statistical and systematic uncertainties in *ee* for the dilepton invariant mass (m_{ll}).

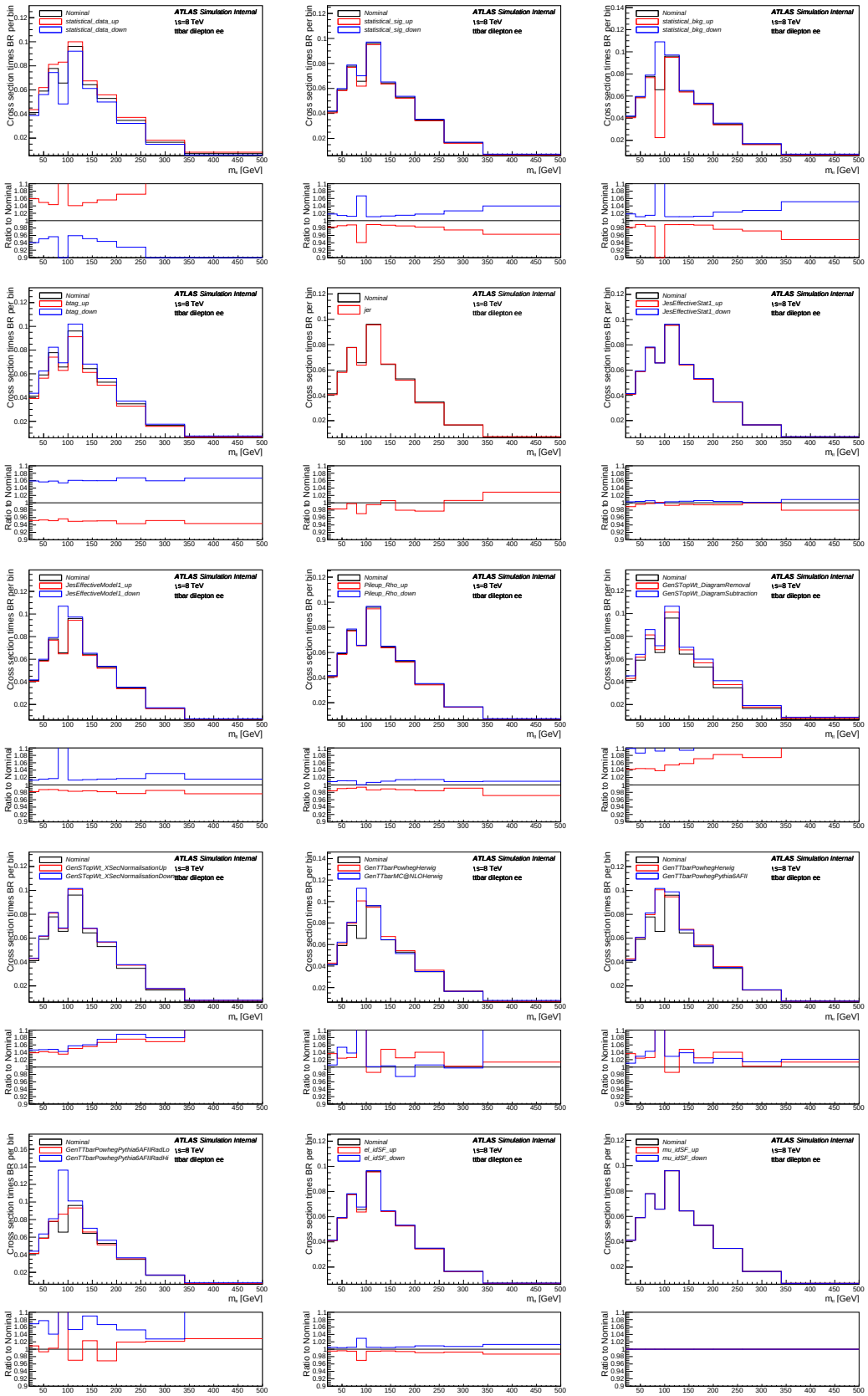

Fig. B.7 Differential cross-section per bin (not scaled to density) for channel *ee* in the variable of dilepton invariant mass (m_{ll}) with measured (with Nominal signal) overlaid with statistical uncertainties on data and MC (signal and background), as well as various systematics.

B.1.3 Variable p_{T} of leading lepton

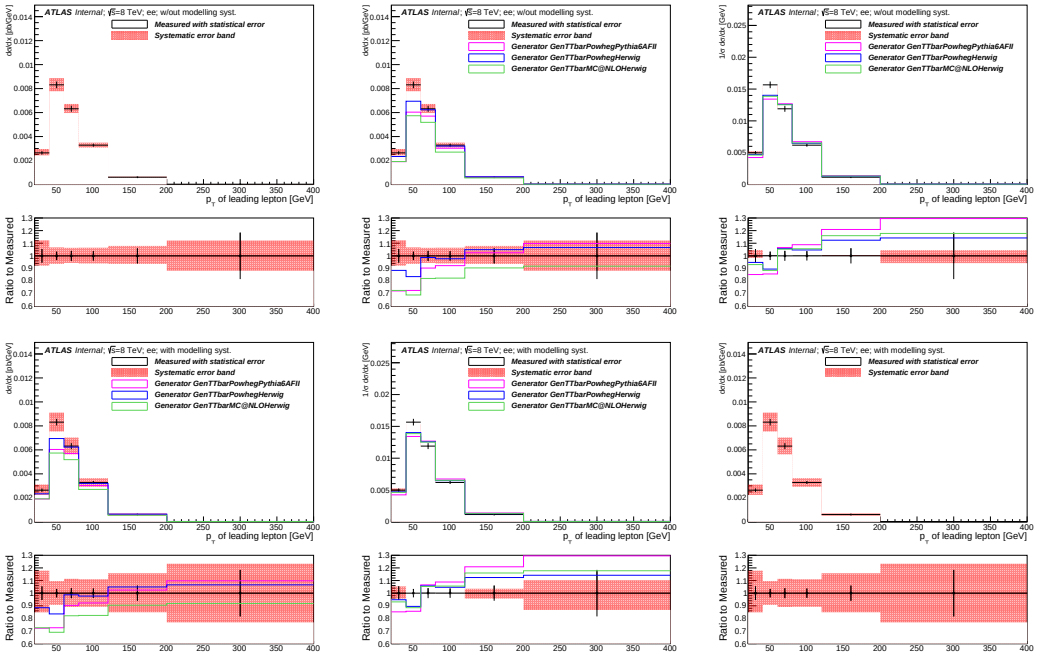

Fig. B.8 Differential cross-section for channel *ee* in the variable of p_{T} of leading lepton.

Bin [GeV]	Measured $d\sigma/dx$ [pb/GeV]	Statistical Data [%]	Statistical MC Bkg [%]	Statistical MC Sig [%]	Systematic [%]
[20,40]	0.0026	+/- 5.4	+/- 4.9	+/- 1.5	+12.3/-7.8
[40,60]	0.0083	+/- 3.3	+/- 0.9	+/- 1.0	+6.7/-6.4
[60,80]	0.0063	+/- 3.9	+/- 1.1	+/- 1.1	+6.4/-5.6
[80,120]	0.0033	+/- 3.7	+/- 0.9	+/- 1.0	+6.5/-6.1
[120,200]	0.0006	+/- 6.0	+/- 1.9	+/- 1.4	+7.9/-6.4
[200,400]	0.0000	+/- 18.4	+/- 10.4	+/- 3.8	+12.1/-11.8

Table B.11 Per-bin total statistical and systematic uncertainties in *ee* for the leading lepton p_T, without modelling systematic uncertainties.

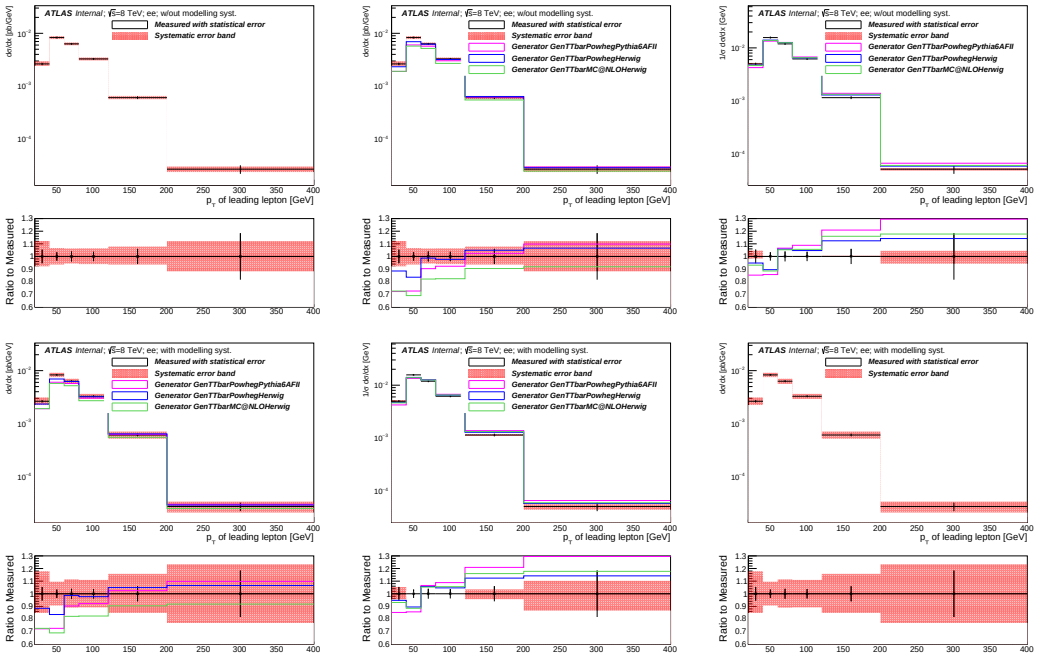

Fig. B.9 Differential cross-section for channel *ee* in the variable of p_{T} of leading lepton (log on y axis).

Bin [GeV]	Measured $d\sigma/dx$ [pb/GeV]	Statistical Data [%]	Statistical MC Bkg [%]	Statistical MC Sig [%]	Systematic [%]
[20,40]	0.0026	+/- 5.4	+/- 4.9	+/- 1.5	+17.9/-15.2
[40,60]	0.0083	+/- 3.3	+/- 0.9	+/- 1.0	+9.5/-9.3
[60,80]	0.0063	+/- 3.9	+/- 1.1	+/- 1.1	+11.3/-10.9
[80,120]	0.0033	+/- 3.7	+/- 0.9	+/- 1.0	+11.0/-10.8
[120,200]	0.0006	+/- 6.0	+/- 1.9	+/- 1.4	+15.8/-15.1
[200,400]	0.0000	+/- 18.4	+/- 10.4	+/- 3.8	+23.3/-23.1

Table B.12 Per-bin total statistical and systematic uncertainties in *ee* for the leading lepton p_T, with modelling systematic uncertainties.

Bin [GeV]	Measured $d\sigma/dx$ [pb/GeV]	Statistical Data [%]	Total Syst Up [%]	Total Syst Down [%]	GenTTbarPowhegPythia6AFII [%]	GenTTbarPowhegHerwig [%]	GenTTbarMC@NLOHerwig [%]
[20,40]	0.0026	+/- 5.4	12.3	-7.8	-27.8	-11.5	-27.4
[40,60]	0.0083	+/- 3.3	6.7	-6.4	-27.4	-16.4	-31.0
[60,80]	0.0063	+/- 3.9	6.4	-5.6	-9.7	-1.3	-17.9
[80,120]	0.0033	+/- 3.7	6.5	-6.1	-7.8	-2.3	-17.6
[120,200]	0.0006	+/- 6.0	7.9	-6.4	2.5	4.9	-9.6
[200,400]	0.0000	+/- 18.4	12.1	-11.8	9.8	6.6	-8.2

Table B.13 Per-bin total statistical and systematic uncertainties in *ee* for the leading lepton p_T, with generators, without normalisation.

Bin [GeV]	Measured $d\sigma/dx$ [pb/GeV]	Statistical Data [%]	Total Syst Up [%]	Total Syst Down [%]	GenTTbarPowhegPythia6AFII [%]	GenTTbarPowhegHerwig [%]	GenTTbarMC@NLOHerwig [%]
[20,40]	0.0050	+/- 5.4	4.6	-1.6	-14.8	-5.2	-6.9
[40,60]	0.0157	+/- 3.3	-0.5	-0.1	-14.3	-10.5	-11.5
[60,80]	0.0119	+/- 3.9	-0.8	0.8	6.6	5.7	5.3
[80,120]	0.0062	+/- 3.7	-0.8	0.3	8.8	4.7	5.6
[120,200]	0.0011	+/- 6.0	0.6	-0.1	20.9	12.4	16.0
[200,400]	0.0001	+/- 18.4	4.5	-5.8	29.5	14.2	17.8

Table B.14 Per-bin total statistical and systematic uncertainties in *ee* for the leading lepton p_T, with generators, with all distributions normalised to unit area.

Uncertainty	[20,40]	[40,60]	[60,80]	[80,120]	[120,200]	[200,400]
StatisticalData	[-5.41,5.41]	[-3.34,3.34]	[-3.95,3.95]	[-3.72,3.72]	[-6.01,6.01]	[-18.41,18.41]
StatisticalBkg	[-4.94,4.94]	[-0.87,0.87]	[-1.15,1.15]	[-0.92,0.92]	[-1.91,1.91]	[-10.42,10.42]
StatisticalSig	[-1.48,1.53]	[-0.99,1.01]	[-1.05,1.07]	[-0.97,0.99]	[-1.40,1.44]	[-3.55,3.82]
BTag	[-4.69,5.68]	[-4.79,5.82]	[-4.74,5.79]	[-5.01,6.10]	[-5.70,6.83]	[-6.33,7.49]
Jeff	[-0.02,0.02]	[-0.04,0.04]	[-0.02,0.02]	[-0.05,0.05]	[-0.00,0.00]	[-0.00,0.00]
Jer	[-0.99,0.99]	[-1.08,1.08]	[-0.41,0.41]	[-0.32,0.32]	[-0.02,0.02]	[-7.11,7.11]
MuidRes	[0.00,0.00]	[0.00,0.00]	[0.00,0.00]	[0.00,0.00]	[0.00,0.00]	[0.00,0.00]
MumsRes	[0.00,0.00]	[-0.01,0.01]	[0.00,0.00]	[-0.00,0.00]	[-0.04,0.04]	[0.00,0.00]
BJesUnc	[-0.62,0.89]	[-0.85,0.78]	[-0.74,0.71]	[-0.95,0.53]	[-0.83,1.38]	[-1.24,1.24]
JesEffectiveStat1	[-0.39,0.47]	[-0.48,0.49]	[-0.57,0.27]	[-0.60,0.23]	[-0.43,0.79]	[-0.56,0.56]
JesEffectiveStat2	[-0.13,0.13]	[-0.02,0.14]	[-0.03,0.03]	[-0.09,0.09]	[-0.10,0.01]	[-0.03,0.03]
JesEffectiveStat3	[-0.01,0.13]	[-0.15,0.18]	[-0.10,0.13]	[-0.14,0.14]	[-0.06,0.03]	[-1.38,1.38]
JesEffectiveStat4	[-0.14,0.38]	[-0.22,0.36]	[-0.13,0.15]	[-0.21,0.09]	[-0.17,0.17]	[-0.09,0.09]
JesEffectiveModel1	[-1.20,6.12]	[-1.56,1.71]	[-1.48,1.46]	[-2.00,1.24]	[-1.64,1.97]	[-1.94,1.94]
JesEffectiveModel2	[-0.13,0.13]	[-0.00,0.06]	[-0.04,0.01]	[-0.03,0.03]	[-0.11,0.10]	[-0.29,0.29]
JesEffectiveModel3	[-0.04,0.19]	[-0.01,0.14]	[-0.01,0.04]	[-0.07,0.07]	[-0.08,0.05]	[-1.38,1.38]
JesEffectiveModel4	[-0.01,0.24]	[-0.08,0.13]	[-0.03,0.04]	[-0.09,0.06]	[-0.17,0.11]	[-0.06,0.01]
JesEffectiveDet1	[-0.15,0.65]	[-0.49,0.51]	[-0.46,0.50]	[-0.42,0.30]	[-0.30,1.14]	[-1.45,1.45]
JesEffectiveDet2	[-0.23,0.23]	[-0.10,0.27]	[-0.07,0.08]	[-0.07,0.00]	[-0.09,0.09]	[-0.05,0.05]
JesEffectiveDet3	[-0.17,0.17]	[-0.07,0.10]	[-0.03,0.02]	[-0.06,0.01]	[-0.11,0.11]	[-0.07,0.01]
JesEffectiveMix1	[-0.19,0.47]	[-0.44,0.56]	[-0.40,0.55]	[-0.37,0.28]	[-0.42,0.75]	[-1.57,1.57]
JesEffectiveMix2	[-0.11,0.28]	[-0.26,0.38]	[-0.33,0.14]	[-0.23,0.16]	[-0.24,0.47]	[-0.26,0.26]
JesEffectiveMix3	[-0.15,0.15]	[-0.16,0.16]	[-0.02,0.02]	[-0.12,0.05]	[-0.07,0.11]	[-0.17,0.17]
JesEffectiveMix4	[-0.00,0.00]	[-0.02,0.03]	[-0.02,0.02]	[-0.03,0.01]	[-0.03,0.03]	[-0.01,0.01]
EtaIntercalibrationModel	[-0.25,0.44]	[-0.48,0.46]	[-0.60,0.31]	[-0.61,0.22]	[-0.26,0.84]	[-0.94,0.94]
EtaIntercalibrationTotalStat	[-0.30,0.44]	[-0.37,0.46]	[-0.55,0.34]	[-0.49,0.26]	[-0.45,0.80]	[-0.45,0.45]
PileupOffsetMu	[-0.07,0.13]	[-0.13,0.21]	[-0.35,0.25]	[-0.06,0.06]	[-0.08,0.42]	[-0.41,0.41]
PileupOffsetNPV	[-0.35,4.11]	[-0.06,0.18]	[-0.20,0.12]	[-0.43,0.43]	[-0.10,0.10]	[-0.47,0.47]
PileupRho	[-0.76,1.30]	[-1.23,1.23]	[-1.07,0.75]	[-1.43,0.81]	[-1.21,1.62]	[-1.44,1.44]
PunchThrough	[-0.04,0.04]	[-0.01,0.01]	[-0.02,0.02]	[-0.00,0.01]	[-0.00,0.00]	[-0.00,0.00]
CTauTag	[-0.02,0.02]	[-0.06,0.06]	[-0.04,0.04]	[-0.02,0.02]	[-0.05,0.05]	[-0.12,0.13]
ElectronEnergyResolution	[-4.24,4.24]	[-1.43,1.43]	[-0.10,0.60]	[-0.30,0.30]	[-0.28,0.28]	[-0.52,0.52]
ElectronEnergyScale	[-3.89,3.89]	[-2.83,0.76]	[-1.18,1.18]	[-1.18,0.49]	[-1.11,0.80]	[-4.26,3.22]
ElectronIdSF	[-0.58,0.57]	[-0.39,0.38]	[-0.53,0.51]	[-0.59,0.58]	[-1.05,1.02]	[-2.49,2.42]
ElectronRecoSF	[-0.06,0.06]	[-0.04,0.04]	[-0.05,0.05]	[-0.08,0.07]	[-0.14,0.14]	[-0.35,0.34]
ElectronTriggerSF	[-0.01,0.01]	[-0.00,0.00]	[-0.00,0.00]	[-0.00,0.00]	[-0.00,0.00]	[-0.01,0.01]
FlavorComp	[-0.24,4.81]	[-0.59,0.51]	[-1.01,0.40]	[-0.98,0.58]	[-0.59,0.65]	[-1.96,1.96]
FlavorResponse	[-0.01,0.61]	[-0.47,0.41]	[-0.77,0.47]	[-0.58,0.36]	[-0.35,0.52]	[-0.66,0.66]
JetVertexFraction	[-0.35,0.25]	[-0.36,0.20]	[-0.22,0.58]	[-0.22,0.39]	[-0.22,0.39]	[-0.51,0.98]
Mistag	[-1.19,1.20]	[-0.05,0.05]	[-0.06,0.06]	[-0.09,0.09]	[-0.19,0.19]	[-0.60,0.61]
MuonIdSF	[-0.00,0.00]	[-0.00,0.00]	[-0.00,0.00]	[-0.00,0.00]	[-0.00,0.00]	[0.00,0.00]
MuonRecoSF	[-0.00,0.00]	[-0.00,0.00]	[-0.00,0.00]	[-0.00,0.00]	[-0.00,0.00]	[0.00,0.00]
MuonTriggerSF	[0.00,0.00]	[0.00,0.00]	[0.00,0.00]	[0.00,0.00]	[0.00,0.00]	[0.00,0.00]
Musc	[0.00,0.00]	[0.00,0.00]	[0.00,0.00]	[0.00,0.00]	[0.00,0.00]	[0.00,0.00]
ModellingGenerator	[-2.13,2.13]	[-1.51,1.51]	[-0.09,0.09]	[-2.12,2.12]	[-0.69,0.69]	[-3.33,3.33]
ModellingParton	[-0.46,0.46]	[-0.62,0.62]	[-0.55,0.55]	[-0.50,0.50]	[-0.57,0.57]	[-0.02,0.02]
ModellingRadiation	[-11.95,11.95]	[-5.32,5.32]	[-7.51,7.51]	[-6.54,6.54]	[-7.39,7.39]	[-2.64,2.64]
ModellingSingleTopWtNormalisation	[-0.62,0.62]	[-0.51,0.51]	[-0.75,0.75]	[-0.74,0.74]	[-1.53,1.53]	[-2.59,2.59]
ModellingSingleTopWtInterference	[-4.62,4.62]	[-3.82,3.82]	[-5.56,5.56]	[-5.54,5.54]	[-11.41,11.41]	[-19.28,19.28]

Table B.15 Per-bin individual statistical and systematic uncertainties in *ee* for the leading lepton p_T.

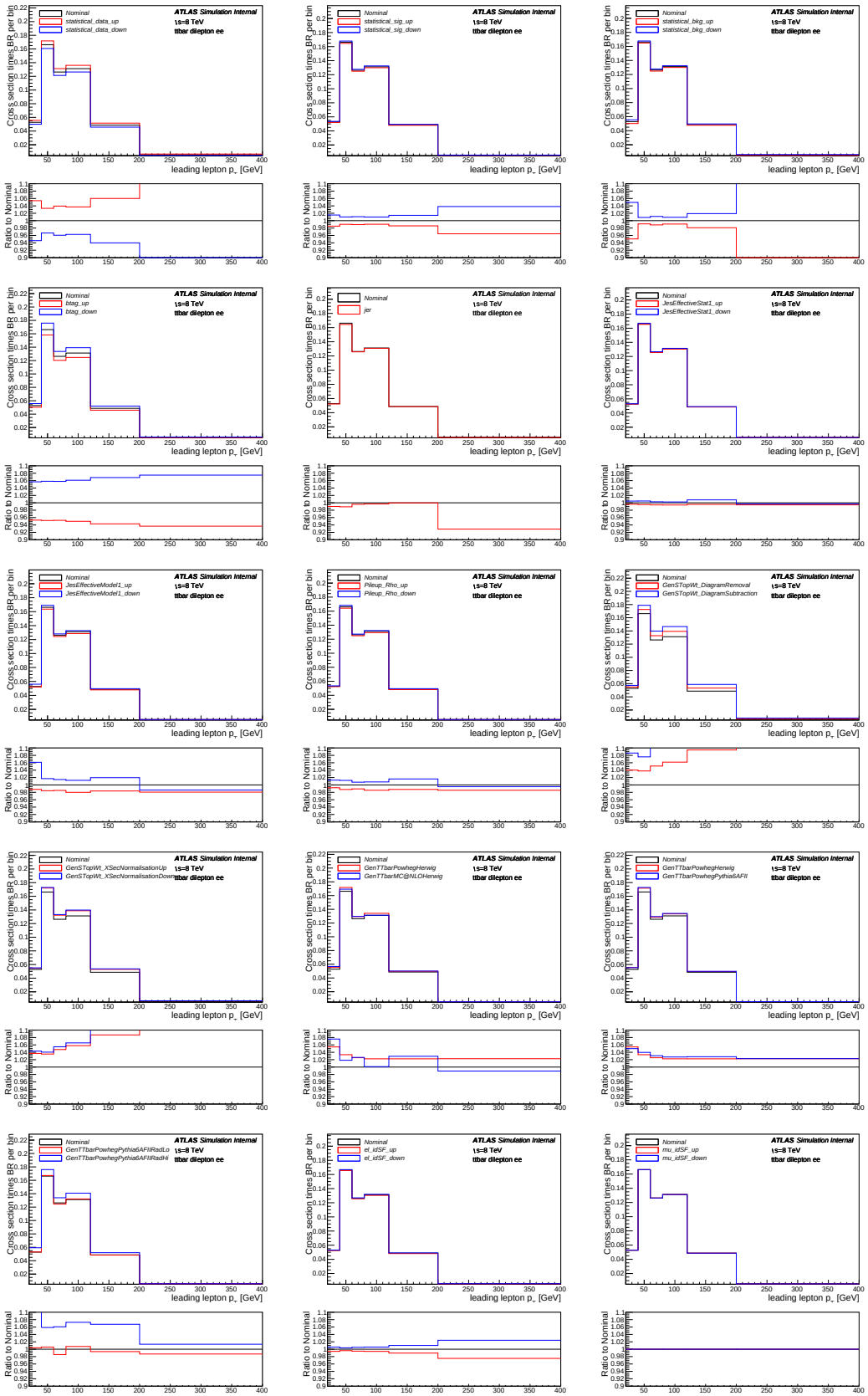

Fig. B.10 Differential cross-section per bin (not scaled to density) for channel *ee* in the variable of p_{T} of leading lepton with measured (with Nominal signal) overlaid with statistical uncertainties on data and MC (signal and background), as well as various systematics.

B.1.4 Variable dilepton $\Delta\eta$

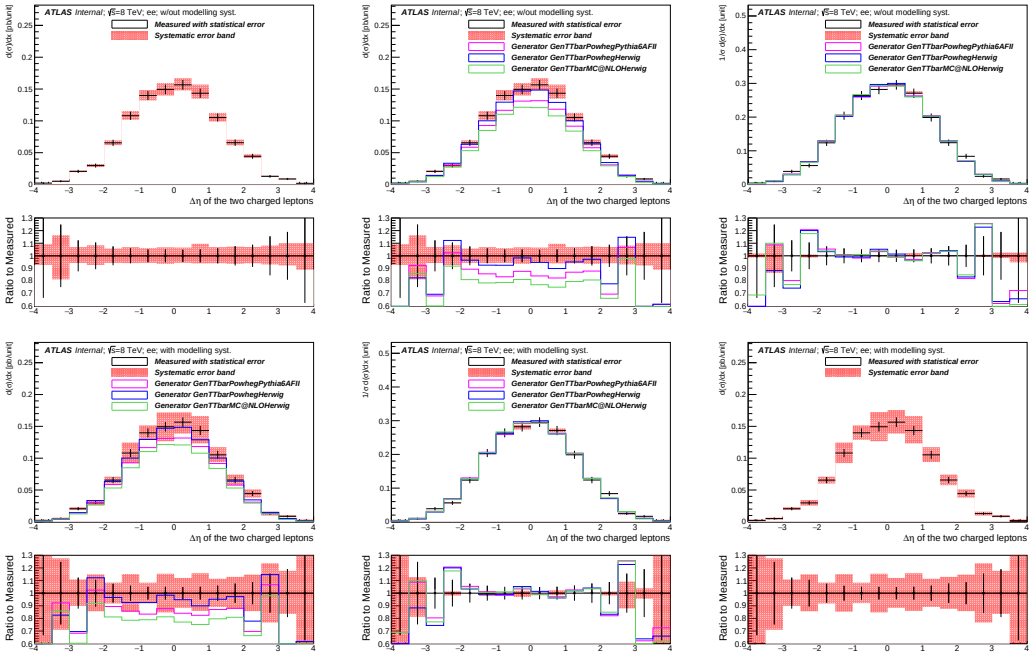

Fig. B.11 Differential cross-section for channel *ee* in the variable of dilepton $\Delta\eta$.

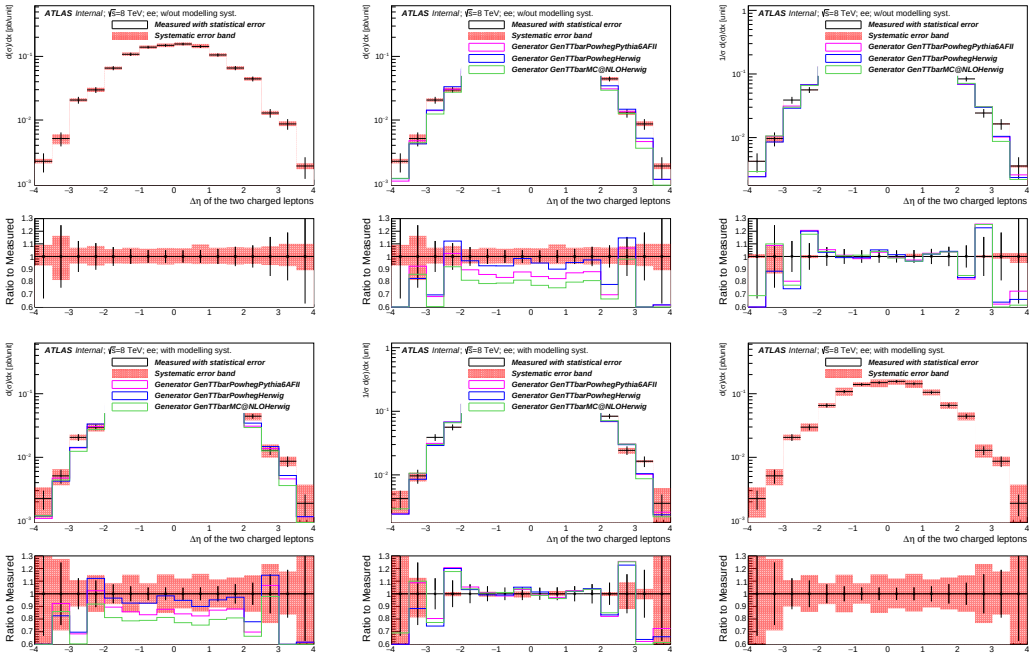

Fig. B.12 Differential cross-section for channel *ee* in the variable of dilepton $\Delta\eta$ (log on y axis).

Bin [unit]	Measured $d\sigma/dx$ [pb/unit]	Statistical Data [%]	Statistical MC Bkg [%]	Statistical MC Sig [%]	Systematic [%]
[-4.0,-3.5]	0.0022	+/- 33.3	+/- 2.2	+/- 13.0	+9.2/-7.1
[-3.5,-3.0]	0.0051	+/- 24.8	+/- 8.1	+/- 6.3	+16.4/-18.7
[-3.0,-2.5]	0.0206	+/- 12.3	+/- 2.4	+/- 3.9	+6.9/-5.7
[-2.5,-2.0]	0.0298	+/- 10.6	+/- 2.7	+/- 2.6	+8.4/-7.2
[-2.0,-1.5]	0.0655	+/- 7.5	+/- 1.6	+/- 2.0	+5.8/-5.6
[-1.5,-1.0]	0.1081	+/- 5.9	+/- 1.7	+/- 1.6	+6.9/-5.8
[-1.0,-0.5]	0.1398	+/- 5.0	+/- 1.1	+/- 1.4	+6.1/-5.6
[-0.5,0.0]	0.1494	+/- 5.0	+/- 1.5	+/- 1.3	+6.8/-6.4
[0.0,0.5]	0.1566	+/- 4.8	+/- 1.5	+/- 1.3	+6.6/-5.5
[0.5,1.0]	0.1434	+/- 5.1	+/- 4.4	+/- 1.4	+9.5/-6.0
[1.0,1.5]	0.1053	+/- 6.0	+/- 1.6	+/- 1.6	+6.9/-5.9
[1.5,2.0]	0.0657	+/- 7.7	+/- 2.1	+/- 2.1	+7.3/-6.3
[2.0,2.5]	0.0443	+/- 8.8	+/- 1.6	+/- 2.8	+7.0/-5.9
[2.5,3.0]	0.0129	+/- 15.5	+/- 3.5	+/- 3.7	+8.1/-6.8
[3.0,3.5]	0.0087	+/- 19.0	+/- 2.5	+/- 6.8	+10.0/-7.6
[3.5,4.0]	0.0019	+/- 37.3	+/- 3.8	+/- 13.3	+10.0/-10.9

Table B.16 Per-bin total statistical and systematic uncertainties in *ee* for the dilepton $\Delta\eta$, without modelling systematic uncertainties.

Bin [unit]	Measured $d\sigma/dx$ [pb/unit]	Statistical Data [%]	Statistical MC Bkg [%]	Statistical MC Sig [%]	Systematic [%]
[-4.0,-3.5]	0.0022	+/- 33.3	+/- 2.2	+/- 13.0	+50.0/-49.7
[-3.5,-3.0]	0.0051	+/- 24.8	+/- 8.1	+/- 6.3	+27.6/-29.0
[-3.0,-2.5]	0.0206	+/- 12.3	+/- 2.4	+/- 3.9	+10.8/-10.0
[-2.5,-2.0]	0.0298	+/- 10.6	+/- 2.7	+/- 2.6	+14.9/-14.3
[-2.0,-1.5]	0.0655	+/- 7.5	+/- 1.6	+/- 2.0	+8.4/-8.2
[-1.5,-1.0]	0.1081	+/- 5.9	+/- 1.7	+/- 1.6	+15.1/-14.7
[-1.0,-0.5]	0.1398	+/- 5.0	+/- 1.1	+/- 1.4	+8.3/-7.9
[-0.5,0.0]	0.1494	+/- 5.0	+/- 1.5	+/- 1.3	+15.4/-15.2
[0.0,0.5]	0.1566	+/- 4.8	+/- 1.5	+/- 1.3	+12.1/-11.5
[0.5,1.0]	0.1434	+/- 5.1	+/- 4.4	+/- 1.4	+15.8/-14.0
[1.0,1.5]	0.1053	+/- 6.0	+/- 1.6	+/- 1.6	+11.4/-10.8
[1.5,2.0]	0.0657	+/- 7.7	+/- 2.1	+/- 2.1	+12.9/-12.4
[2.0,2.5]	0.0443	+/- 8.8	+/- 1.6	+/- 2.8	+14.7/-14.2
[2.5,3.0]	0.0129	+/- 15.5	+/- 3.5	+/- 3.7	+23.6/-23.2
[3.0,3.5]	0.0087	+/- 19.0	+/- 2.5	+/- 6.8	+17.7/-16.5
[3.5,4.0]	0.0019	+/- 37.3	+/- 3.8	+/- 13.3	+96.7/-96.8

Table B.17 Per-bin total stattistical and systematic uncertainties in *ee* for the dilepton $\Delta\eta$, with modelling systematic uncertainties.

Bin [unit]	Measured $d\sigma/dx$ [pb/unit]	Statistical Data [%]	Total Syst Up [%]	Total Syst Down [%]	GenTTbarPowhegPythia6AFII [%]	GenTTbarPowhegHerwig [%]	GenTTbarMC@NLOHerwig [%
[-4.0,-3.5]	0.0022	+/- 33.3	9.2	-7.1	-51.2	-46.6	-46.1
[-3.5,-3.0]	0.0051	+/- 24.8	16.4	-18.7	-7.7	-17.4	-14.1
[-3.0,-2.5]	0.0206	+/- 12.3	6.9	-5.7	-31.7	-30.4	-39.7
[-2.5,-2.0]	0.0298	+/- 10.6	8.4	-7.2	2.4	12.2	-8.1
[-2.0,-1.5]	0.0655	+/- 7.5	5.8	-5.6	-10.6	-3.4	-18.8
[-1.5,-1.0]	0.1081	+/- 5.9	6.9	-5.8	-14.3	-7.4	-21.4
[-1.0,-0.5]	0.1398	+/- 5.0	6.1	-5.6	-16.6	-7.4	-21.1
[-0.5,0.0]	0.1494	+/- 5.0	6.8	-6.4	-12.3	-1.6	-18.7
[0.0,0.5]	0.1566	+/- 4.8	6.6	-5.5	-15.9	-5.2	-22.9
[0.5,1.0]	0.1434	+/- 5.1	9.5	-6.0	-17.5	-10.0	-24.8
[1.0,1.5]	0.1053	+/- 6.0	6.9	-5.9	-12.9	-4.8	-20.3
[1.5,2.0]	0.0657	+/- 7.7	7.3	-6.3	-12.1	-2.7	-19.1
[2.0,2.5]	0.0443	+/- 8.8	7.0	-5.9	-30.3	-22.1	-33.7
[2.5,3.0]	0.0129	+/- 15.5	8.1	-6.8	6.7	14.7	-2.1
[3.0,3.5]	0.0087	+/- 19.0	10.0	-7.6	-47.2	-40.3	-58.5
[3.5,4.0]	0.0019	+/- 37.3	10.0	-10.9	-38.4	-38.3	-52.0

Table B.18 Per-bin total statistical and systematic uncertainties in *ee* for the dilepton $\Delta\eta$, with generators, without normalisation.

Bin [unit]	Measured $d\sigma/dx$ [pb/unit]	Statistical Data [%]	Total Syst Up [%]	Total Syst Down [%]	GenTTbarPowhegPythia6AFII [%]	GenTTbarPowhegHerwig [%]	GenTTbarMC@NLOHerwig [%]
[-4.0,-3.5]	0.0042	+/- 33.3	1.9	-1.2	-42.5	-42.9	-31.0
[-3.5,-3.0]	0.0097	+/- 24.8	8.6	-13.5	8.7	-11.7	10.0
[-3.0,-2.5]	0.0389	+/- 12.3	-0.2	0.4	-19.6	-25.6	-22.7
[-2.5,-2.0]	0.0562	+/- 10.6	1.1	-1.3	20.7	20.0	17.6
[-2.0,-1.5]	0.1237	+/- 7.5	-1.3	0.4	5.4	3.3	3.9
[-1.5,-1.0]	0.2041	+/- 5.9	-0.3	0.3	1.0	-0.9	0.6
[-1.0,-0.5]	0.2640	+/- 5.0	-1.0	0.5	-1.7	-1.0	1.1
[-0.5,0.0]	0.2821	+/- 5.0	-0.4	-0.4	3.4	5.2	4.0
[0.0,0.5]	0.2957	+/- 4.8	-0.6	0.5	-0.9	1.4	-1.3
[0.5,1.0]	0.2708	+/- 5.1	2.2	-0.0	-2.8	-3.8	-3.7
[1.0,1.5]	0.1988	+/- 6.0	-0.3	0.1	2.6	1.8	2.0
[1.5,2.0]	0.1240	+/- 7.7	0.1	-0.3	3.6	4.1	3.6
[2.0,2.5]	0.0837	+/- 8.8	-0.1	0.1	-17.9	-16.7	-15.1
[2.5,3.0]	0.0243	+/- 15.5	0.9	-0.8	25.7	22.7	25.3
[3.0,3.5]	0.0164	+/- 19.0	2.6	-1.7	-37.7	-36.2	-46.9
[3.5,4.0]	0.0036	+/- 37.3	2.6	-5.2	-27.5	-34.0	-38.6

Table B.19 Per-bin total statistical and systematic uncertainties in *ee* for the dilepton $\Delta\eta$, with generators, with all distributions normalised to unit area.

Uncertainty	[-4.0,-3.5]	[-3.5,-3.0]	[-3.0,-2.5]	[-2.5,-2.0]	[-2.0,-1.5]	[-1.5,-1.0]	[-1.0,-0.5]	[-0.5,0.0]	[0.0,0.5]	[0.5,1.0]	[1.0,1.5]	[1.5,2.0]	[2.0,2.5]	[2.5,3.0]	[3.0,3.5]	[3.5,4.0]
StatisticalData	[-33.29,33.29]	[-24.76,24.76]	[-12.28,12.28]	[-10.57,10.57]	[-7.46,7.46]	[-5.90,5.90]	[-5.04,5.04]	[-5.02,5.02]	[-4.83,4.83]	[-5.10,5.10]	[-6.00,6.00]	[-7.67,7.67]	[-8.78,8.78]	[-15.47,15.47]	[-18.96,18.96]	[-37.28,37.28]
StatisticalBkg	[-2.16,2.16]	[-8.13,8.13]	[-2.43,2.43]	[-2.65,2.65]	[-1.56,1.56]	[-1.71,1.71]	[-1.12,1.12]	[-1.50,1.50]	[-1.46,1.46]	[-4.44,4.44]	[-1.57,1.57]	[-2.15,2.15]	[-1.59,1.59]	[-3.49,3.49]	[-2.48,2.48]	[-3.79,3.79]
StatisticalSig	[-10.30,12.97]	[-5.60,6.31]	[-3.59,3.87]	[-2.46,2.59]	[-1.95,2.03]	[-1.59,1.64]	[-1.36,1.40]	[-1.31,1.35]	[-1.31,1.35]	[-1.38,1.42]	[-1.59,1.64]	[-2.01,2.09]	[-2.61,2.75]	[-3.46,3.72]	[-5.96,6.77]	[-10.51,13.31]
BTag	[-3.51,4.37]	[-3.09,4.28]	[-4.26,5.27]	[-5.57,6.63]	[-4.39,5.42]	[-4.80,5.89]	[-4.75,5.78]	[-5.07,6.13]	[-5.01,6.04]	[-4.84,5.86]	[-5.23,6.36]	[-5.11,6.24]	[-5.15,6.24]	[-5.36,6.65]	[-6.14,7.35]	[-3.60,4.54]
Jetf	[0.00,0.00]	[-0.00,0.00]	[-0.22,0.22]	[-0.06,0.06]	[-0.01,0.01]	[-0.02,0.02]	[-0.03,0.03]	[-0.09,0.09]	[-0.04,0.04]	[-0.04,0.04]	[-0.00,0.00]	[-0.09,0.09]	[-0.03,0.03]	[0.00,0.00]	[0.00,0.00]	[0.00,0.00]
Jer	[-4.87,4.87]	[-7.48,7.48]	[-0.91,0.91]	[-1.40,1.40]	[-1.05,1.05]	[-2.05,2.05]	[-0.39,0.39]	[-0.63,0.63]	[-1.09,1.09]	[-0.94,0.94]	[-0.00,0.00]	[-0.23,0.23]	[-0.00,0.00]	[-2.43,2.43]	[-3.35,3.35]	[-8.14,8.14]
MuoIdRes	[0.00,0.00]	[0.00,0.00]	[0.00,0.00]	[0.00,0.00]	[0.00,0.00]	[0.00,0.00]	[0.00,0.00]	[0.00,0.00]	[0.00,0.00]	[0.00,0.00]	[0.00,0.00]	[0.00,0.00]	[0.00,0.00]	[0.00,0.00]	[0.00,0.00]	[0.00,0.00]
MuonsRes	[0.00,0.00]	[0.00,0.00]	[0.00,0.00]	[0.00,0.00]	[0.00,0.00]	[0.00,0.00]	[0.00,0.00]	[0.00,0.00]	[-0.01,0.01]	[0.00,0.00]	[-0.08,0.08]	[0.00,0.00]	[0.00,0.00]	[0.00,0.00]	[0.00,0.00]	[0.00,0.00]
BJetsUnc	[-0.15,0.15]	[-0.36,0.40]	[-0.70,1.45]	[-0.57,0.63]	[-0.58,0.56]	[-0.63,1.04]	[-0.85,0.66]	[-0.95,0.72]	[-0.79,0.69]	[-0.95,0.76]	[-0.76,0.56]	[-1.34,0.75]	[-1.03,0.89]	[-0.42,1.09]	[-0.43,0.73]	[-0.65,0.65]
JesEffectiveStat1	[-0.03,0.03]	[-4.79,0.79]	[-0.28,0.58]	[-0.34,1.10]	[-0.45,0.06]	[-0.37,0.47]	[-0.66,0.30]	[-0.58,0.50]	[-0.34,0.26]	[-0.59,0.44]	[-0.46,0.26]	[-1.04,0.60]	[-0.18,0.26]	[-0.44,0.44]	[-0.06,0.57]	[-1.76,1.76]
JesEffectiveStat2	[-0.00,0.00]	[-0.00,0.00]	[-0.13,0.13]	[-0.85,0.85]	[-0.10,0.10]	[-0.02,0.07]	[-0.11,0.11]	[-0.11,0.19]	[-0.03,0.07]	[-0.05,0.05]	[-0.11,0.02]	[-0.04,0.04]	[-0.01,0.01]	[-0.05,0.01]	[-0.01,0.26]	[-0.00,0.00]
JesEffectiveStat3	[-0.13,0.13]	[-0.22,0.22]	[-0.00,0.01]	[-0.04,0.14]	[-0.16,0.11]	[-0.08,0.10]	[-0.19,0.14]	[-0.19,0.10]	[-0.14,0.04]	[-0.13,0.03]	[-0.10,0.07]	[-0.01,0.01]	[-0.01,0.01]	[-0.00,0.11]	[-0.45,0.45]	[-0.02,0.02]
JesEffectiveStat4	[-0.11,0.11]	[-0.23,0.23]	[-0.26,0.07]	[-0.04,0.94]	[-0.18,0.13]	[-0.12,0.25]	[-0.20,0.08]	[-0.35,0.25]	[-0.11,0.09]	[-0.22,0.22]	[-0.18,0.09]	[-0.10,0.53]	[-0.14,0.55]	[-0.02,0.07]	[-0.01,0.23]	[-0.03,0.03]
JesEffectiveMode1	[-1.51,1.51]	[-9.08,8.39]	[-1.12,3.07]	[-1.43,2.13]	[-1.80,1.10]	[-1.31,1.50]	[-1.65,1.09]	[-1.84,1.42]	[-1.20,1.36]	[-1.94,5.05]	[-1.50,1.72]	[-2.15,2.05]	[-1.52,1.34]	[-0.78,1.82]	[-0.27,2.76]	[-4.85,0.91]
JesEffectiveMode2	[-0.00,0.01]	[-0.00,0.29]	[-0.11,0.11]	[-0.00,0.08]	[-0.08,0.01]	[-0.04,0.10]	[-0.02,0.02]	[-0.10,0.14]	[-0.05,0.06]	[-0.08,0.08]	[-0.02,0.02]	[-0.09,0.09]	[-0.59,0.59]	[-0.04,0.07]	[-0.01,0.26]	[-0.03,0.03]
JesEffectiveMode3	[-0.08,0.08]	[-0.22,0.22]	[-0.12,0.06]	[-0.85,0.85]	[-0.19,0.11]	[-0.03,0.03]	[-0.16,0.16]	[-0.28,0.09]	[-0.09,0.06]	[-0.08,0.09]	[-0.04,0.02]	[-0.04,0.46]	[-0.11,0.27]	[-0.05,0.02]	[-1.01,1.01]	[-0.02,0.01]
JesEffectiveMode4	[-0.00,0.00]	[-0.29,0.29]	[-0.08,0.01]	[-0.01,0.14]	[-0.10,0.07]	[-0.01,0.01]	[-0.11,0.10]	[-0.13,0.18]	[-0.07,0.01]	[-0.11,0.07]	[-0.06,0.06]	[-0.03,0.17]	[-0.50,0.50]	[-0.04,0.07]	[-0.24,0.24]	[-0.00,0.03]
JesEffectiveDet1	[-0.18,0.18]	[-0.25,0.25]	[-0.37,0.44]	[-0.45,1.10]	[-0.48,0.21]	[-0.39,0.63]	[-0.28,0.58]	[-0.60,0.59]	[-0.24,0.51]	[-0.43,0.40]	[-0.46,0.39]	[-0.47,0.59]	[-0.53,0.71]	[-0.16,0.05]	[-0.69,0.81]	[-0.01,0.04]
JesEffectiveDet2	[-0.00,0.01]	[-0.30,0.30]	[-0.19,0.08]	[-0.86,0.86]	[-0.04,0.04]	[-0.06,0.14]	[-0.16,0.01]	[-0.24,0.28]	[-0.05,0.05]	[-0.02,0.15]	[-0.04,0.04]	[-0.09,0.26]	[-0.02,0.46]	[-0.03,0.03]	[-1.02,1.02]	[-0.02,0.02]
JesEffectiveDet3	[-0.00,0.00]	[-0.01,0.00]	[-0.01,0.01]	[-0.00,0.15]	[-0.10,0.06]	[-0.00,0.04]	[-0.09,0.04]	[-0.14,0.17]	[-0.00,0.00]	[-0.04,0.04]	[-0.05,0.05]	[-0.06,0.11]	[-0.24,0.24]	[-0.04,0.01]	[-0.24,0.24]	[-0.00,0.00]
JesEffectiveMix1	[-0.16,0.16]	[-0.56,0.75]	[-0.47,0.21]	[-0.39,1.01]	[-0.39,0.15]	[-0.29,0.55]	[-0.35,0.37]	[-0.55,0.56]	[-0.23,0.51]	[-0.49,0.37]	[-0.44,0.31]	[-0.27,0.70]	[-0.50,0.66]	[-0.06,0.06]	[-0.81,1.63]	[-0.01,0.04]
JesEffectiveMix2	[-0.00,0.03]	[-0.28,0.28]	[-0.31,0.28]	[-0.11,0.96]	[-0.21,0.21]	[-0.21,0.38]	[-0.33,0.03]	[-0.56,0.41]	[-0.10,0.31]	[-0.34,0.28]	[-0.23,0.06]	[-0.05,0.50]	[-0.22,0.22]	[-0.00,0.00]	[-0.11,0.58]	[-0.02,0.02]
JesEffectiveMix3	[-0.09,0.09]	[-0.23,0.23]	[-0.14,0.04]	[-0.82,0.82]	[-0.16,0.06]	[-0.13,0.13]	[-0.07,0.03]	[-0.01,0.07]	[-0.13,0.08]	[-0.06,0.06]	[-0.02,0.02]	[-0.29,0.29]	[-0.08,0.51]	[-0.06,0.09]	[-0.44,0.44]	[-0.00,0.02]
JesEffectiveMix4	[-0.00,0.00]	[-0.00,0.00]	[-0.01,0.01]	[-0.00,0.00]	[-0.12,0.01]	[-0.01,0.02]	[-0.01,0.01]	[-0.03,0.03]	[-0.01,0.01]	[-0.01,0.04]	[-0.01,0.01]	[-0.00,0.06]	[-0.01,0.00]	[-0.03,0.01]	[-0.01,0.00]	[-0.00,0.00]
EtaIntercalibrationModel	[-0.08,0.08]	[-0.79,0.44]	[-0.24,0.29]	[-0.97,1.12]	[-0.55,0.13]	[-0.53,0.56]	[-0.65,0.17]	[-0.64,0.49]	[-0.40,0.03]	[-0.27,0.66]	[-0.56,0.35]	[-0.70,0.81]	[-0.15,0.18]	[-0.33,0.33]	[-1.15,1.15]	[-0.05,1.10]
EtaIntercalibrationTotalStat	[-0.11,0.11]	[-4.77,1.24]	[-0.30,0.42]	[-0.31,1.11]	[-0.44,0.05]	[-0.39,0.65]	[-0.46,0.14]	[-0.80,0.51]	[-0.21,0.37]	[-0.47,0.45]	[-0.47,0.24]	[-0.44,0.62]	[-0.28,0.28]	[-0.32,0.32]	[-0.15,0.57]	[-1.74,0.94]
PileupOffsetMu	[-0.10,0.10]	[-0.24,7.73]	[-0.31,0.25]	[-0.05,0.96]	[-0.33,0.03]	[-0.22,0.14]	[-0.32,0.32]	[-0.23,0.23]	[-0.06,0.12]	[-0.05,0.28]	[-0.18,0.28]	[-0.36,0.59]	[-0.11,0.19]	[-0.04,0.41]	[-0.05,0.40]	[-0.05,0.05]
PileupOffsetNPV	[-2.11,2.11]	[-4.35,7.26]	[-0.06,0.84]	[-0.86,0.86]	[-0.73,0.73]	[-0.02,0.05]	[-0.35,0.35]	[-0.27,0.27]	[-0.39,0.69]	[-0.14,3.03]	[-0.29,0.12]	[-0.25,0.25]	[-0.24,0.24]	[-0.64,0.64]	[-0.57,0.50]	[-1.86,1.86]
PileupRho	[-1.50,1.50]	[-8.54,0.85]	[-0.41,1.47]	[-0.91,1.70]	[-1.30,0.60]	[-0.96,1.36]	[-1.16,0.76]	[-1.45,1.14]	[-0.82,0.80]	[-1.42,1.05]	[-1.11,0.94]	[-1.84,1.19]	[-1.11,1.10]	[-0.15,1.66]	[-0.57,1.38]	[-1.66,0.52]
PunchThrough	[0.00,0.00]	[0.00,0.00]	[-0.03,0.03]	[-0.05,0.05]	[-0.00,0.00]	[-0.03,0.03]	[-0.02,0.02]	[-0.04,0.01]	[-0.03,0.00]	[-0.00,0.01]	[-0.02,0.02]	[-0.00,0.00]	[-0.13,0.13]	[-0.00,0.00]	[0.00,0.00]	[0.00,0.00]
CTauTag	[-0.12,0.12]	[-0.06,0.06]	[-0.02,0.02]	[-0.14,0.14]	[-0.05,0.05]	[-0.04,0.04]	[-0.00,0.00]	[-0.04,0.05]	[-0.09,0.09]	[-0.04,0.04]	[-0.01,0.01]	[-0.03,0.03]	[-0.04,0.04]	[-0.01,0.01]	[-0.09,0.10]	[-0.01,0.01]
ElectronEnergyResolution	[-0.99,2.47]	[-1.73,1.73]	[-0.79,0.92]	[-0.47,0.47]	[-0.27,0.28]	[-0.35,0.36]	[-0.13,0.13]	[-0.39,0.29]	[-0.26,0.08]	[-0.31,0.31]	[-0.45,0.45]	[-0.36,0.10]	[-0.43,1.04]	[-0.39,0.39]	[-0.80,0.01]	[-0.45,0.76]
ElectronEnergyScale	[-1.67,4.72]	[-0.33,0.33]	[-2.91,0.95]	[-2.98,0.37]	[-1.49,0.27]	[-1.03,0.57]	[-0.51,0.77]	[-1.59,0.84]	[-0.25,0.84]	[-0.27,0.98]	[-0.31,1.02]	[-0.51,1.50]	[-1.27,1.42]	[-2.52,2.52]	[-1.39,0.57]	[-0.45,1.37]
ElectronIdSF	[-0.02,0.00]	[-0.69,0.67]	[-0.49,0.47]	[-0.56,0.54]	[-0.59,0.58]	[-0.64,0.62]	[-0.49,0.48]	[-0.64,0.63]	[-0.54,0.53]	[-0.70,0.69]	[-0.65,0.64]	[-0.70,0.69]	[-0.45,0.44]	[-0.60,0.58]	[-0.25,0.24]	[-0.33,0.33]
ElectronRecoSF	[-0.05,0.05]	[-0.09,0.09]	[-0.05,0.05]	[-0.06,0.06]	[-0.08,0.08]	[-0.09,0.09]	[-0.05,0.05]	[-0.07,0.07]	[-0.07,0.07]	[-0.08,0.08]	[-0.09,0.09]	[-0.10,0.10]	[-0.07,0.06]	[-0.06,0.06]	[-0.02,0.02]	[-0.05,0.05]
ElectronTriggerSF	[-0.02,0.02]	[-0.02,0.02]	[-0.01,0.01]	[-0.00,0.00]	[-0.00,0.00]	[-0.01,0.00]	[-0.00,0.00]	[-0.00,0.00]	[-0.00,0.00]	[-0.01,0.01]	[-0.00,0.00]	[-0.01,0.01]	[-0.00,0.00]	[-0.01,0.01]	[-0.00,0.00]	[-0.03,0.03]
FlavorComp	[-1.41,1.41]	[-6.02,1.33]	[-0.24,1.17]	[-0.96,1.10]	[-0.79,0.17]	[-0.38,0.61]	[-0.90,0.25]	[-1.26,0.36]	[-0.42,0.41]	[-1.05,3.76]	[-0.80,0.60]	[-0.65,1.20]	[-0.16,0.79]	[-0.53,0.53]	[-0.05,3.44]	[-0.81,0.81]
FlavorResponse	[-4.00,1.41]	[-4.59,1.20]	[-0.37,0.93]	[-0.62,1.24]	[-0.55,0.55]	[-0.16,0.48]	[-0.46,0.19]	[-0.72,0.52]	[-0.21,0.16]	[-0.91,0.26]	[-0.56,0.77]	[-0.59,0.87]	[-0.23,0.41]	[-0.30,0.30]	[-0.29,1.88]	[-1.03,0.58]
JetVertexFraction	[-0.31,0.31]	[-0.09,0.00]	[-0.77,0.09]	[-0.06,0.51]	[-0.03,0.21]	[-0.26,0.15]	[-0.35,0.36]	[-0.18,0.47]	[-0.41,0.37]	[-0.29,0.68]	[-0.36,0.30]	[-0.25,0.22]	[-0.20,0.21]	[-0.00,0.64]	[-0.82,0.08]	[-0.00,0.00]
Mistag	[-0.09,0.09]	[-0.26,0.26]	[-0.05,0.05]	[-0.11,0.11]	[-0.14,0.14]	[-0.12,0.12]	[-0.04,0.04]	[-0.12,0.12]	[-0.05,0.05]	[-1.14,1.15]	[-0.03,0.03]	[-0.11,0.11]	[-0.04,0.04]	[-0.01,0.01]	[-0.17,0.17]	[-0.28,0.28]
MuonIdSF	[0.00,0.00]	[0.00,0.00]	[0.00,0.00]	[-0.00,0.00]	[0.00,0.00]	[-0.00,0.00]	[-0.00,0.00]	[-0.00,0.00]	[-0.00,0.00]	[0.00,0.00]	[-0.00,0.00]	[0.00,0.00]	[-0.00,0.00]	[-0.00,0.00]	[0.00,0.00]	[0.00,0.00]
MuonRecoSF	[0.00,0.00]	[0.00,0.00]	[0.00,0.00]	[0.00,0.00]	[-0.00,0.00]	[-0.00,0.00]	[-0.00,0.00]	[-0.00,0.00]	[-0.00,0.00]	[0.00,0.00]	[-0.00,0.00]	[0.00,0.00]	[-0.00,0.00]	[0.00,0.00]	[0.00,0.00]	[0.00,0.00]
MuonTriggerSF	[0.00,0.00]	[0.00,0.00]	[0.00,0.00]	[0.00,0.00]	[0.00,0.00]	[0.00,0.00]	[0.00,0.00]	[0.00,0.00]	[0.00,0.00]	[0.00,0.00]	[0.00,0.00]	[0.00,0.00]	[0.00,0.00]	[0.00,0.00]	[0.00,0.00]	[0.00,0.00]
Musc	[0.00,0.00]	[0.00,0.00]	[0.00,0.00]	[0.00,0.00]	[0.00,0.00]	[0.00,0.00]	[0.00,0.00]	[0.00,0.00]	[0.00,0.00]	[0.00,0.00]	[0.00,0.00]	[0.00,0.00]	[0.00,0.00]	[0.00,0.00]	[0.00,0.00]	[0.00,0.00]
ModellingGenerator	[-34.69,34.69]	[-9.63,9.63]	[-2.26,2.26]	[-4.69,4.69]	[-0.91,0.91]	[-3.22,3.22]	[-0.27,0.27]	[-0.03,0.03]	[-1.70,1.70]	[-4.64,4.64]	[-4.83,4.83]	[-6.20,6.20]	[-9.83,9.83]	[-2.54,2.54]	[-0.78,0.78]	[-73.75,73.75]
ModellingParton	[-30.61,30.61]	[-4.94,4.94]	[-4.36,4.36]	[-9.21,9.21]	[-0.15,0.15]	[-2.48,2.48]	[-2.08,2.08]	[-3.24,3.24]	[-1.26,1.26]	[-2.12,2.12]	[-0.17,0.17]	[-0.28,0.28]	[-4.89,4.89]	[-0.45,0.45]	[-0.86,0.86]	[-61.56,61.56]
ModellingRadiation	[-16.68,16.68]	[-16.29,16.29]	[-3.62,3.62]	[-2.47,2.47]	[-2.66,2.66]	[-11.12,11.12]	[-1.72,1.72]	[-11.43,11.43]	[-8.56,8.56]	[-10.72,10.72]	[-2.55,2.55]	[-4.20,4.20]	[-5.53,5.53]	[-20.67,20.67]	[-14.40,14.40]	[-3.55,3.55]
ModellingSingleTopWtNormalisation	[-0.00,0.00]	[-1.41,1.41]	[-0.75,0.75]	[-0.85,0.85]	[-0.70,0.70]	[-0.85,0.85]	[-0.65,0.65]	[-0.94,0.94]	[-0.66,0.66]	[-0.58,0.58]	[-0.96,0.96]	[-1.00,1.00]	[-0.54,0.54]	[-1.01,1.01]	[-0.31,0.31]	[-0.49,0.49]
ModellingSingleTopWtInterference	[-0.00,0.00]	[-10.49,10.49]	[-5.56,5.56]	[-6.30,6.30]	[-5.25,5.25]	[-6.37,6.37]	[-4.87,4.87]	[-7.03,7.03]	[-4.96,4.96]	[-4.34,4.34]	[-7.19,7.19]	[-7.47,7.47]	[-4.01,4.01]	[-7.55,7.55]	[-2.33,2.33]	[-3.64,3.64]

Table B.20 Per-bin individual statistical and systematic uncertainties in ee for the dilepton $\Delta\eta$.

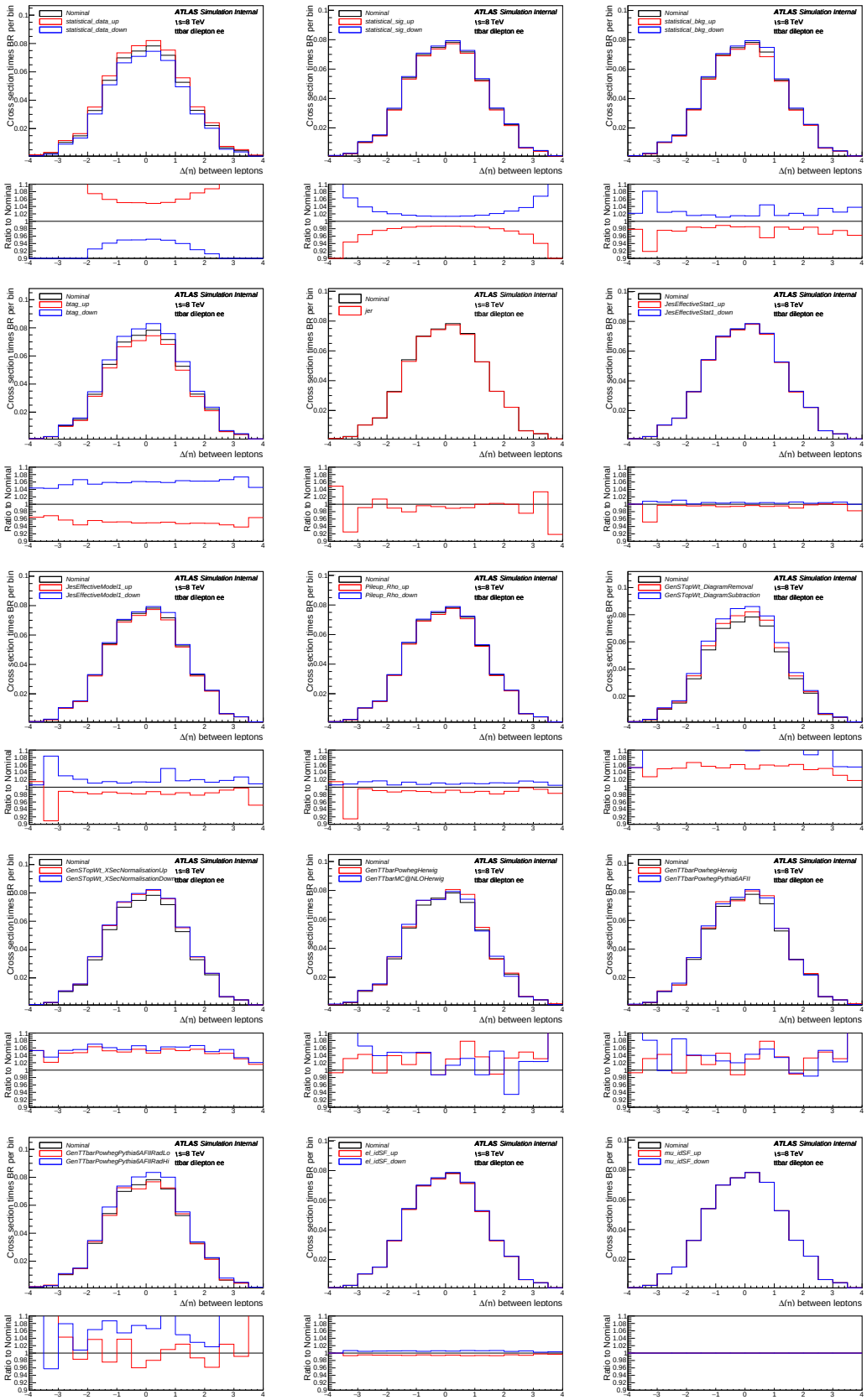

Fig. B.13 Differential cross-section per bin (not scaled to density) for channel *ee* in the variable of dilepton $\Delta\eta$ with measured (with Nominal signal) overlaid with statistical uncertainties on data and MC (signal and background), as well as various systematics.

B.1.5 Variable dilepton $|\Delta\eta|$

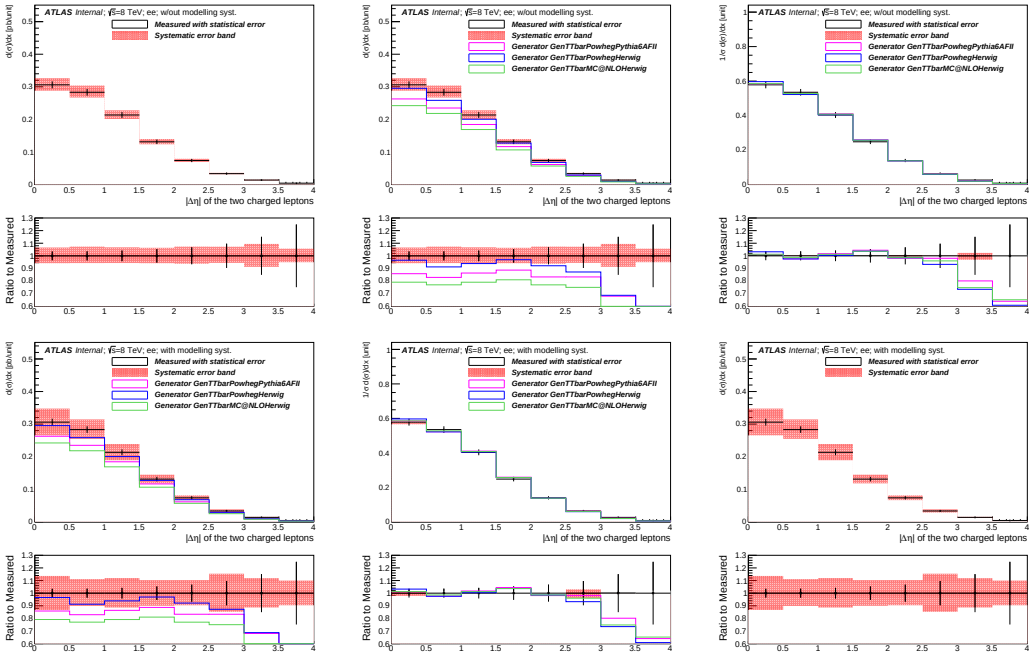

Fig. B.14 Differential cross-section for channel *ee* in the variable of dilepton $|\Delta\eta|$.

Bin [unit]	Measured $d\sigma/dx$ [pb/unit]	Statistical Data [%]	Statistical MC Bkg [%]	Statistical MC Sig [%]	Systematic [%]
[0.0,0.5]	0.3060	+/- 3.5	+/- 1.1	+/- 0.9	+6.6/-5.8
[0.5,1.0]	0.2832	+/- 3.6	+/- 2.4	+/- 1.0	+7.4/-5.7
[1.0,1.5]	0.2134	+/- 4.2	+/- 1.2	+/- 1.2	+6.8/-5.7
[1.5,2.0]	0.1311	+/- 5.3	+/- 1.4	+/- 1.4	+6.4/-5.8
[2.0,2.5]	0.0737	+/- 6.8	+/- 1.4	+/- 1.9	+7.4/-6.3
[2.5,3.0]	0.0334	+/- 9.6	+/- 2.0	+/- 2.7	+7.3/-5.6
[3.0,3.5]	0.0137	+/- 15.1	+/- 3.5	+/- 4.5	+9.5/-8.7
[3.5,4.0]	0.0042	+/- 24.8	+/- 2.1	+/- 9.0	+5.7/-5.0

Table B.21 Per-bin total statistical and systematic uncertainties in *ee* for the dilepton $|\Delta\eta|$, without modelling systematic uncertainties.

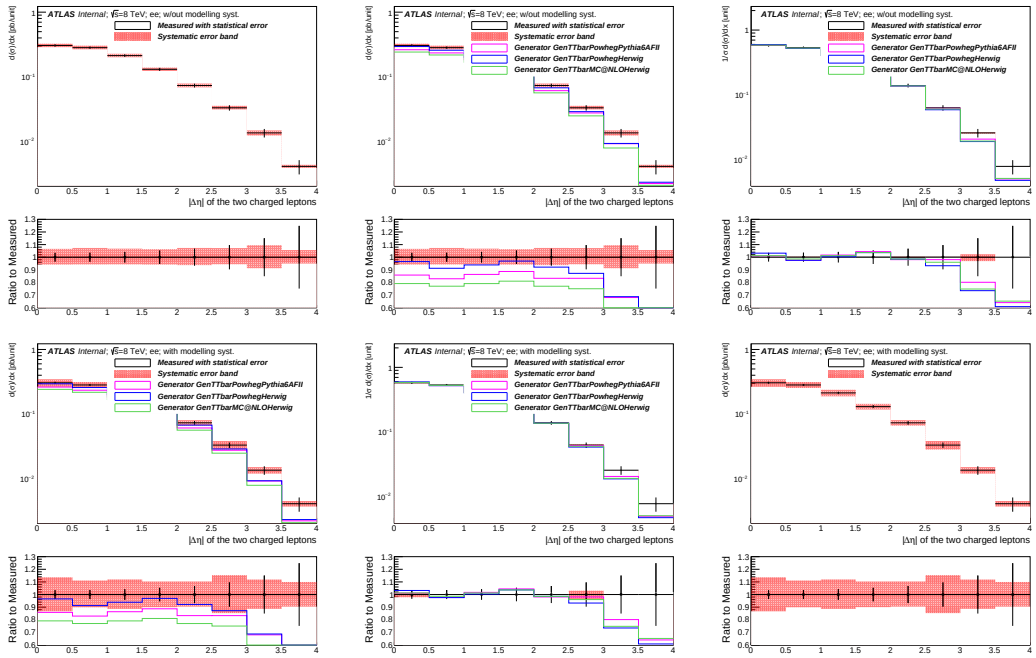

Fig. B.15 Differential cross-section for channel *ee* in the variable of dilepton $|\Delta\eta|$ (log on y axis).

Bin [unit]	Measured $d\sigma/dx$ [pb/unit]	Statistical Data [%]	Statistical MC Bkg [%]	Statistical MC Sig [%]	Systematic [%]
[0.0,0.5]	0.3060	+/- 3.5	+/- 1.1	+/- 0.9	+13.6/-13.3
[0.5,1.0]	0.2832	+/- 3.6	+/- 2.4	+/- 1.0	+11.1/-10.1
[1.0,1.5]	0.2134	+/- 4.2	+/- 1.2	+/- 1.2	+11.9/-11.3
[1.5,2.0]	0.1311	+/- 5.3	+/- 1.4	+/- 1.4	+10.3/-10.0
[2.0,2.5]	0.0737	+/- 6.8	+/- 1.4	+/- 1.9	+10.3/-9.6
[2.5,3.0]	0.0334	+/- 9.6	+/- 2.0	+/- 2.7	+15.4/-14.7
[3.0,3.5]	0.0137	+/- 15.1	+/- 3.5	+/- 4.5	+11.9/-11.3
[3.5,4.0]	0.0042	+/- 24.8	+/- 2.1	+/- 9.0	+10.0/-9.6

Table B.22 Per-bin total statistical and systematic uncertainties in *ee* for the dilepton $|\Delta\eta|$, with modelling systematic uncertainties.

Bin [unit]	Measured $d\sigma/dx$ [pb/unit]	Statistical Data [%]	Total Syst Up [%]	Total Syst Down [%]	GenTTbarPowhegPythia6AFII [%]	GenTTbarPowhegHerwig [%]	GenTTbarMC@NLOHerwig [%
[0.0,0.5]	0.3060	+/- 3.5	6.6	-5.8	-14.1	-3.5	-20.9
[0.5,1.0]	0.2832	+/- 3.6	7.4	-5.7	-17.1	-8.8	-23.0
[1.0,1.5]	0.2134	+/- 4.2	6.8	-5.7	-13.6	-6.1	-20.9
[1.5,2.0]	0.1311	+/- 5.3	6.4	-5.8	-11.3	-3.1	-19.0
[2.0,2.5]	0.0737	+/- 6.8	7.4	-6.3	-16.7	-7.8	-23.0
[2.5,3.0]	0.0334	+/- 9.6	7.3	-5.6	-16.7	-12.8	-25.0
[3.0,3.5]	0.0137	+/- 15.1	9.5	-8.7	-31.9	-31.3	-41.5
[3.5,4.0]	0.0042	+/- 24.8	5.7	-5.0	-45.6	-43.1	-49.0

Table B.23 Per-bin total statistical and systematic uncertainties in *ee* for the dilepton $|\Delta\eta|$, with generators, without normalisation.

Bin [unit]	Measured $d\sigma/dx$ [pb/unit]	Statistical Data [%]	Total Syst Up [%]	Total Syst Down [%]	GenTTbarPowhegPythia6AFII [%]	GenTTbarPowhegHerwig [%]	GenTTbarMC@NLOHerwig [%]
[0.0,0.5]	0.5781	+/- 3.5	-0.3	0.0	1.1	3.2	1.3
[0.5,1.0]	0.5350	+/- 3.6	0.4	0.1	-2.3	-2.4	-1.4
[1.0,1.5]	0.4032	+/- 4.2	-0.1	0.2	1.7	0.4	1.2
[1.5,2.0]	0.2478	+/- 5.3	-0.5	0.0	4.5	3.7	3.7
[2.0,2.5]	0.1392	+/- 6.8	0.4	-0.4	-1.9	-1.5	-1.4
[2.5,3.0]	0.0631	+/- 9.6	0.3	0.3	-1.9	-6.7	-4.0
[3.0,3.5]	0.0258	+/- 15.1	2.4	-3.1	-19.9	-26.5	-25.2
[3.5,4.0]	0.0079	+/- 24.8	-1.1	0.8	-36.0	-39.1	-34.8

Table B.24 Per-bin total statistical and systematic uncertainties in *ee* for the dilepton $|\Delta\eta|$, with generators, with all distributions normalised to unit area.

Uncertainty	[0.0,0.5]	[0.5,1.0]	[1.0,1.5]	[1.5,2.0]	[2.0,2.5]	[2.5,3.0]	[3.0,3.5]	[3.5,4.0]
StatisticalData	[-3.48,3.48]	[-3.58,3.58]	[-4.21,4.21]	[-5.35,5.35]	[-6.75,6.75]	[-9.62,9.62]	[-15.06,15.06]	[-24.83,24.83]
StatisticalBkg	[-1.07,1.07]	[-2.42,2.42]	[-1.19,1.19]	[-1.40,1.40]	[-1.44,1.44]	[-2.01,2.01]	[-3.50,3.50]	[-2.06,2.06]
StatisticalSig	[-0.93,0.95]	[-0.97,0.99]	[-1.13,1.15]	[-1.41,1.45]	[-1.80,1.87]	[-2.52,2.65]	[-4.16,4.53]	[-7.61,8.97]
BTag	[-5.04,6.08]	[-4.80,5.82]	[-5.02,6.12]	[-4.75,5.82]	[-5.34,6.41]	[-4.89,5.94]	[-4.69,5.83]	[-3.54,4.44]
Jeff	[-0.07,0.07]	[-0.01,0.01]	[-0.01,0.01]	[-0.03,0.03]	[-0.05,0.05]	[-0.11,0.11]	[-0.00,0.00]	[0.00,0.00]
Jer	[-0.87,0.87]	[-0.66,0.66]	[-1.04,1.04]	[-0.44,0.44]	[-0.86,0.86]	[-1.45,1.45]	[-1.38,1.38]	[-2.36,2.36]
MuidRes	[0.00,0.00]	[0.00,0.00]	[0.00,0.00]	[0.00,0.00]	[0.00,0.00]	[0.00,0.00]	[0.00,0.00]	[0.00,0.00]
MumsRes	[-0.01,0.01]	[0.00,0.00]	[-0.04,0.04]	[0.00,0.00]	[0.00,0.00]	[0.00,0.00]	[0.00,0.00]	[0.00,0.00]
BJesUnc	[-0.87,0.71]	[-0.90,0.71]	[-0.70,0.80]	[-0.95,0.66]	[-0.78,0.77]	[-0.59,1.34]	[-0.42,0.56]	[-0.28,0.28]
JesEffectiveStat1	[-0.46,0.38]	[-0.63,0.37]	[-0.41,0.37]	[-0.74,0.33]	[-0.27,0.62]	[-0.10,0.52]	[-1.93,0.69]	[-0.93,0.02]
JesEffectiveStat2	[-0.02,0.08]	[-0.04,0.01]	[-0.07,0.05]	[-0.07,0.02]	[-0.36,0.36]	[-0.09,0.00]	[-0.01,0.13]	[-0.00,0.00]
JesEffectiveStat3	[-0.16,0.07]	[-0.16,0.09]	[-0.09,0.09]	[-0.08,0.06]	[-0.07,0.07]	[-0.00,0.06]	[-0.27,0.27]	[-0.06,0.06]
JesEffectiveStat4	[-0.23,0.17]	[-0.21,0.15]	[-0.15,0.17]	[-0.14,0.33]	[-0.09,0.70]	[-0.11,0.02]	[-0.00,0.24]	[-0.07,0.07]
JesEffectiveModel1	[-1.52,1.39]	[-1.80,3.09]	[-1.41,1.61]	[-1.97,1.57]	[-1.47,1.68]	[-0.98,2.48]	[-3.90,4.73]	[-1.91,0.79]
JesEffectiveModel2	[-0.02,0.04]	[-0.05,0.04]	[-0.03,0.05]	[-0.05,0.05]	[-0.31,0.31]	[-0.07,0.07]	[-0.15,0.15]	[-0.02,0.02]
JesEffectiveModel3	[-0.11,0.11]	[-0.04,0.04]	[-0.02,0.03]	[-0.13,0.13]	[-0.02,0.52]	[-0.08,0.04]	[-0.49,0.49]	[-0.05,0.05]
JesEffectiveModel4	[-0.10,0.09]	[-0.11,0.09]	[-0.03,0.03]	[-0.07,0.12]	[-0.00,0.34]	[-0.02,0.02]	[-0.27,0.27]	[-0.01,0.01]
JesEffectiveDet1	[-0.42,0.55]	[-0.36,0.49]	[-0.42,0.51]	[-0.47,0.40]	[-0.47,0.86]	[-0.28,0.25]	[-0.32,0.53]	[-0.08,0.08]
JesEffectiveDet2	[-0.10,0.16]	[-0.09,0.08]	[-0.05,0.07]	[-0.06,0.12]	[-0.36,0.36]	[-0.09,0.05]	[-0.49,0.49]	[-0.01,0.01]
JesEffectiveDet3	[-0.07,0.08]	[-0.06,0.04]	[-0.03,0.05]	[-0.08,0.08]	[-0.00,0.20]	[-0.02,0.01]	[-0.12,0.12]	[-0.00,0.00]
JesEffectiveMix1	[-0.39,0.53]	[-0.42,0.37]	[-0.37,0.43]	[-0.33,0.42]	[-0.43,0.79]	[-0.22,0.13]	[-0.70,1.18]	[-0.08,0.08]
JesEffectiveMix2	[-0.32,0.36]	[-0.34,0.15]	[-0.22,0.22]	[-0.14,0.23]	[-0.01,0.52]	[-0.15,0.14]	[-0.21,0.29]	[-0.02,0.02]
JesEffectiveMix3	[-0.03,0.03]	[-0.02,0.05]	[-0.06,0.06]	[-0.06,0.06]	[-0.31,0.31]	[-0.10,0.06]	[-0.33,0.33]	[-0.05,0.05]
JesEffectiveMix4	[-0.01,0.01]	[-0.01,0.03]	[-0.01,0.01]	[-0.06,0.03]	[-0.00,0.00]	[-0.01,0.00]	[-0.01,0.00]	[-0.00,0.00]
EtaIntercalibrationModel	[-0.52,0.26]	[-0.46,0.42]	[-0.54,0.45]	[-0.62,0.46]	[-0.52,0.59]	[-0.10,0.32]	[-0.50,0.50]	[-0.58,0.58]
EtaIntercalibrationTotalStat	[-0.50,0.44]	[-0.46,0.30]	[-0.43,0.44]	[-0.44,0.33]	[-0.11,0.63]	[-0.06,0.37]	[-1.97,0.92]	[-0.88,0.03]
PileupOffsetMu	[-0.15,0.03]	[-0.18,0.06]	[-0.20,0.21]	[-0.16,0.12]	[-0.04,0.50]	[-0.09,0.09]	[-0.15,3.22]	[-0.07,0.07]
PileupOffsetNPV	[-0.33,0.29]	[-0.24,1.47]	[-0.16,0.09]	[-0.49,0.49]	[-0.03,0.25]	[-0.72,0.72]	[-1.42,2.51]	[-0.38,0.01]
PileupRho	[-1.13,0.97]	[-1.29,0.91]	[-1.04,1.15]	[-1.56,0.89]	[-1.01,1.35]	[-0.31,1.56]	[-3.76,1.11]	[-0.18,0.59]
PunchThrough	[-0.02,0.02]	[-0.01,0.01]	[-0.00,0.00]	[-0.00,0.00]	[-0.06,0.06]	[-0.02,0.02]	[0.00,0.00]	[0.00,0.00]
CTauTag	[-0.07,0.07]	[-0.02,0.02]	[-0.02,0.02]	[-0.04,0.04]	[-0.08,0.08]	[-0.01,0.01]	[-0.02,0.02]	[-0.05,0.05]
ElectronEnergyResolution	[-0.15,0.01]	[-0.05,0.22]	[-0.33,0.33]	[-0.09,0.09]	[-0.23,0.43]	[-0.48,0.26]	[-0.57,0.57]	[-0.05,0.93]
ElectronEnergyScale	[-0.92,0.84]	[-0.39,0.87]	[-0.67,0.80]	[-1.01,0.87]	[-2.03,0.90]	[-1.30,1.60]	[-0.60,0.48]	[-0.04,1.96]
ElectronIdSF	[-0.59,0.58]	[-0.59,0.58]	[-0.65,0.63]	[-0.64,0.63]	[-0.50,0.48]	[-0.53,0.51]	[-0.42,0.41]	[-0.19,0.18]
ElectronRecoSF	[-0.07,0.07]	[-0.06,0.06]	[-0.09,0.09]	[-0.09,0.09]	[-0.06,0.06]	[-0.05,0.05]	[-0.05,0.05]	[-0.00,0.00]
ElectronTriggerSF	[-0.00,0.00]	[-0.00,0.00]	[-0.00,0.01]	[-0.00,0.00]	[-0.00,0.00]	[-0.01,0.01]	[-0.01,0.01]	[-0.01,0.01]
FlavorComp	[-0.83,0.49]	[-0.98,2.02]	[-0.59,0.60]	[-0.73,0.67]	[-0.56,0.87]	[-0.81,0.81]	[-2.57,2.35]	[-1.10,1.10]
FlavorResponse	[-0.46,0.34]	[-0.69,0.23]	[-0.36,0.62]	[-0.57,0.41]	[-0.41,0.76]	[-0.12,0.61]	[-1.92,1.54]	[-0.33,0.33]
JetVertexFraction	[-0.30,0.42]	[-0.32,0.53]	[-0.31,0.22]	[-0.13,0.21]	[-0.13,0.36]	[-0.41,0.39]	[-0.43,0.04]	[-0.15,0.15]
Mistag	[-0.09,0.09]	[-0.59,0.60]	[-0.07,0.07]	[-0.12,0.13]	[-0.07,0.07]	[-0.04,0.04]	[-0.22,0.22]	[-0.19,0.19]
MuonIdSF	[-0.00,0.00]	[-0.00,0.00]	[-0.00,0.00]	[0.00,0.00]	[-0.00,0.00]	[-0.00,0.00]	[0.00,0.00]	[0.00,0.00]
MuonRecoSF	[-0.00,0.00]	[-0.00,0.00]	[-0.00,0.00]	[0.00,0.00]	[-0.00,0.00]	[-0.00,0.00]	[0.00,0.00]	[0.00,0.00]
MuonTriggerSF	[0.00,0.00]	[0.00,0.00]	[0.00,0.00]	[0.00,0.00]	[0.00,0.00]	[0.00,0.00]	[0.00,0.00]	[0.00,0.00]
Musc	[0.00,0.00]	[0.00,0.00]	[0.00,0.00]	[0.00,0.00]	[0.00,0.00]	[0.00,0.00]	[0.00,0.00]	[0.00,0.00]
ModellingGenerator	[-0.85,0.85]	[-2.17,2.17]	[-0.86,0.86]	[-3.57,3.57]	[-2.79,2.79]	[-0.22,0.22]	[-4.16,4.16]	[-2.89,2.89]
ModellingParton	[-2.27,2.27]	[-2.10,2.10]	[-1.17,1.17]	[-0.22,0.22]	[-2.05,2.05]	[-1.99,1.99]	[-1.70,1.70]	[-0.90,0.90]
ModellingRadiation	[-10.00,10.00]	[-6.18,6.18]	[-6.89,6.89]	[-3.45,3.45]	[-3.94,3.94]	[-11.85,11.85]	[-0.94,0.94]	[-7.38,7.38]
ModellingSingleTopWtNormalisation	[-0.80,0.80]	[-0.62,0.62]	[-0.91,0.91]	[-0.85,0.85]	[-0.67,0.67]	[-0.85,0.85]	[-0.74,0.74]	[-0.22,0.22]
ModellingSingleTopWtInterference	[-5.97,5.97]	[-4.60,4.60]	[-6.77,6.77]	[-6.34,6.34]	[-4.96,4.96]	[-6.34,6.34]	[-5.48,5.48]	[-1.62,1.62]

Table B.25 Per-bin individual statistical and systematic uncertainties in *ee* for the dilepton $|\Delta\eta|$.

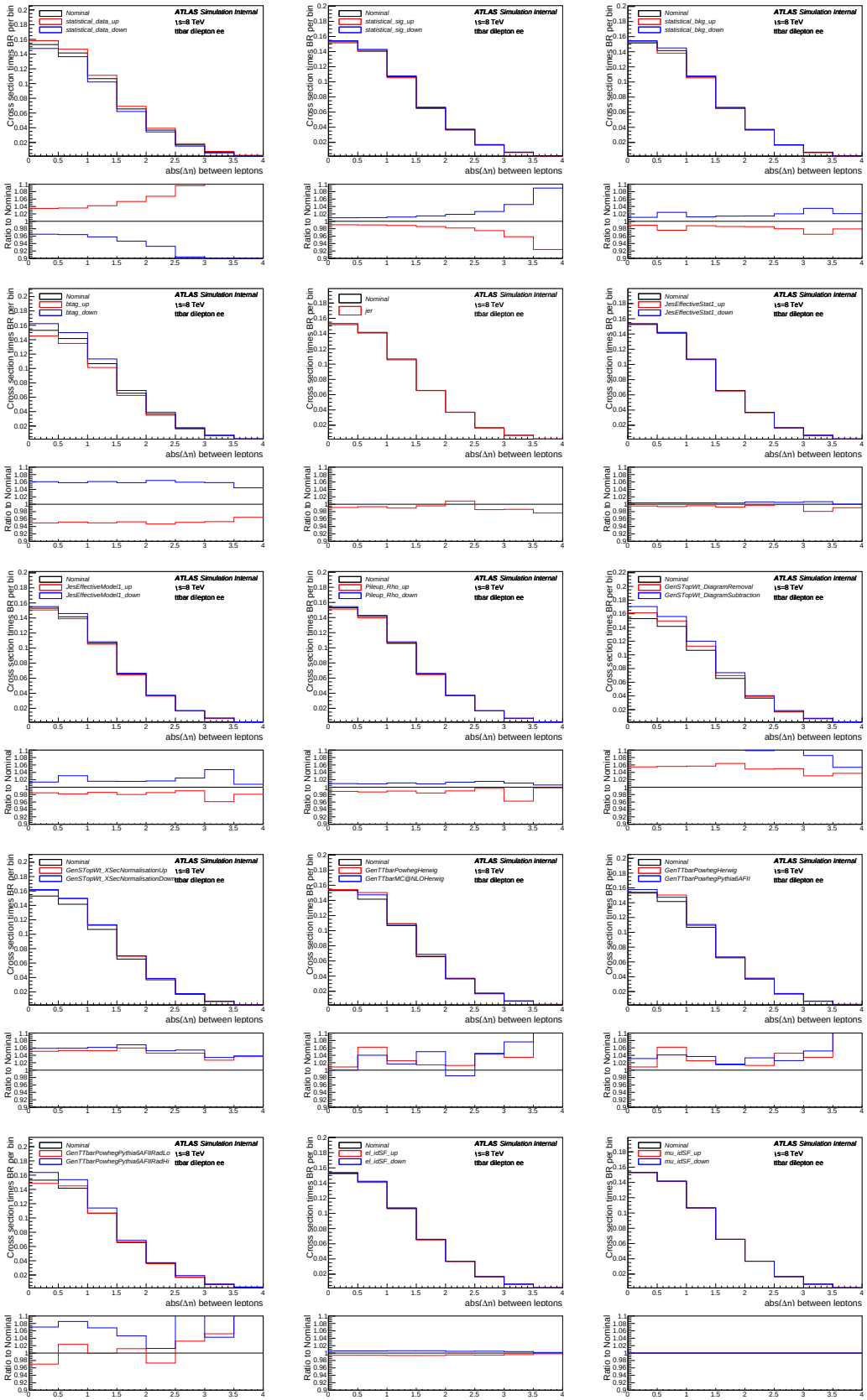

Fig. B.16 Differential cross-section per bin (not scaled to density) for channel *ee* in the variable of dilepton $|\Delta\eta|$ with measured (with Nominal signal) overlaid with statistical uncertainties on data and MC (signal and background), as well as various systematics.

B.1.6 Variable dilepton $\Delta\phi$

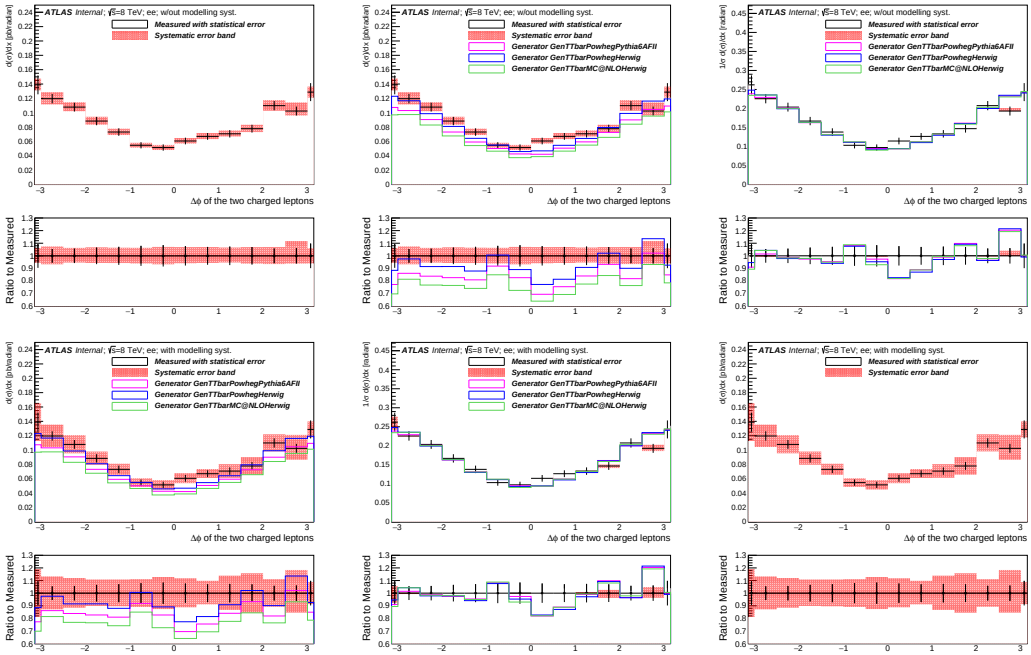

Fig. B.17 Differential cross-section for channel *ee* in the variable of dilepton $\Delta\phi$.

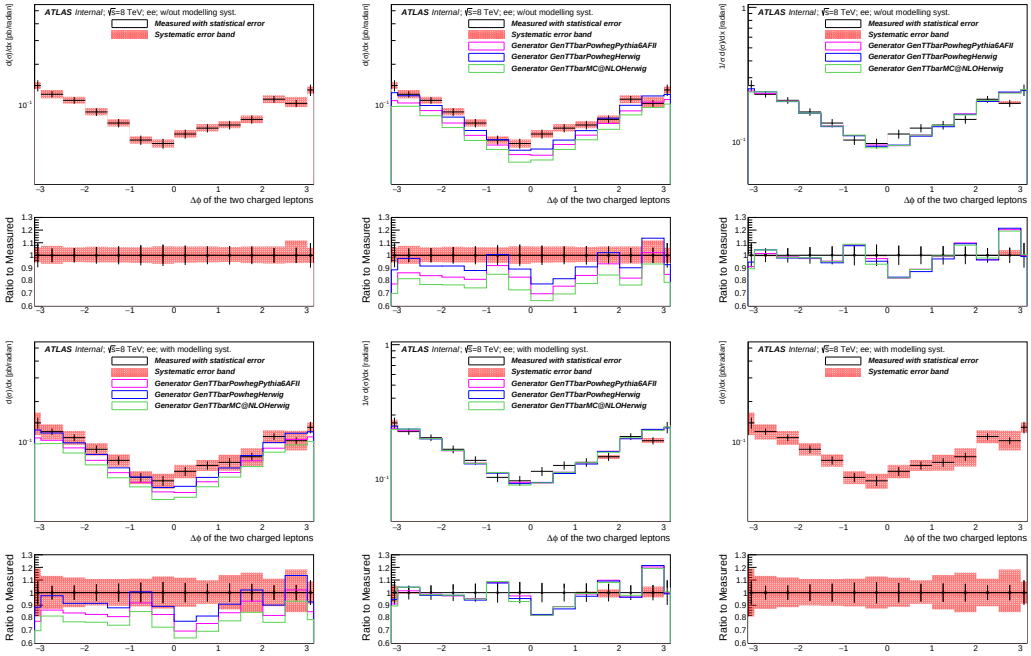

Fig. B.18 Differential cross-section for channel *ee* in the variable of dilepton $\Delta\phi$ (log on y axis).

Bin [radian]	Measured $d\sigma/dx$ [pb/radian]	Statistical Data [%]	Statistical MC Bkg [%]	Statistical MC Sig [%]	Systematic [%]
[-3.142,-3.0]	0.1389	+/- 9.5	+/- 2.1	+/- 2.8	+6.2/-5.5
[-3.0,-2.5]	0.1196	+/- 5.4	+/- 1.7	+/- 1.5	+7.5/-6.7
[-2.5,-2.0]	0.1079	+/- 5.7	+/- 1.3	+/- 1.6	+6.3/-5.3
[-2.0,-1.5]	0.0884	+/- 6.6	+/- 1.2	+/- 1.9	+6.8/-5.7
[-1.5,-1.0]	0.0731	+/- 7.1	+/- 2.0	+/- 2.0	+6.5/-5.7
[-1.0,-0.5]	0.0546	+/- 7.9	+/- 2.4	+/- 2.1	+6.4/-6.0
[-0.5,0.0]	0.0515	+/- 8.5	+/- 3.1	+/- 2.4	+7.1/-6.7
[0.0,0.5]	0.0606	+/- 7.7	+/- 1.8	+/- 2.3	+7.0/-5.9
[0.5,1.0]	0.0670	+/- 7.1	+/- 1.3	+/- 2.1	+7.0/-5.7
[1.0,1.5]	0.0707	+/- 7.3	+/- 2.7	+/- 2.0	+6.6/-5.3
[1.5,2.0]	0.0778	+/- 7.0	+/- 2.1	+/- 1.8	+7.0/-6.2
[2.0,2.5]	0.1099	+/- 5.8	+/- 1.3	+/- 1.6	+7.0/-6.5
[2.5,3.0]	0.1024	+/- 6.1	+/- 6.1	+/- 1.5	+11.7/-6.1
[3.0,3.142]	0.1287	+/- 9.7	+/- 1.2	+/- 2.8	+6.0/-6.0

Table B.26 Per-bin total statistical and systematic uncertainties in *ee* for the dilepton $\Delta\phi$, without modelling systematic uncertainties.

Bin [radian]	Measured $d\sigma/dx$ [pb/radian]	Statistical Data [%]	Statistical MC Bkg [%]	Statistical MC Sig [%]	Systematic [%]
[-3.142,-3.0]	0.1389	+/- 9.5	+/- 2.1	+/- 2.8	+19.1/-18.9
[-3.0,-2.5]	0.1196	+/- 5.4	+/- 1.7	+/- 1.5	+13.3/-12.8
[-2.5,-2.0]	0.1079	+/- 5.7	+/- 1.3	+/- 1.6	+12.0/-11.5
[-2.0,-1.5]	0.0884	+/- 6.6	+/- 1.2	+/- 1.9	+10.8/-10.1
[-1.5,-1.0]	0.0731	+/- 7.1	+/- 2.0	+/- 2.0	+10.8/-10.4
[-1.0,-0.5]	0.0546	+/- 7.9	+/- 2.4	+/- 2.1	+11.1/-10.9
[-0.5,0.0]	0.0515	+/- 8.5	+/- 3.1	+/- 2.4	+12.8/-12.6
[0.0,0.5]	0.0606	+/- 7.7	+/- 1.8	+/- 2.3	+11.8/-11.2
[0.5,1.0]	0.0670	+/- 7.1	+/- 1.3	+/- 2.1	+9.8/-8.9
[1.0,1.5]	0.0707	+/- 7.3	+/- 2.7	+/- 2.0	+13.9/-13.3
[1.5,2.0]	0.0778	+/- 7.0	+/- 2.1	+/- 1.8	+15.8/-15.5
[2.0,2.5]	0.1099	+/- 5.8	+/- 1.3	+/- 1.6	+11.1/-10.7
[2.5,3.0]	0.1024	+/- 6.1	+/- 6.1	+/- 1.5	+18.4/-15.4
[3.0,3.142]	0.1287	+/- 9.7	+/- 1.2	+/- 2.8	+8.7/-8.7

Table B.27 Per-bin total statistical and systematic uncertainties in *ee* for the dilepton $\Delta\phi$, with modelling systematic uncertainties.

Bin [radian]	Measured $d\sigma/dx$ [pb/radian]	Statistical Data [%]	Total Syst Up [%]	Total Syst Down [%]	GenTTbarPowhegPythia6AFII [%]	GenTTbarPowhegHerwig [%]	GenTTbarMC@NLOHerwig [%]
[-3.142,-3.0]	0.1389	+/- 9.5	6.2	-5.5	-22.7	-11.5	-30.1
[-3.0,-2.5]	0.1196	+/- 5.4	7.5	-6.7	-13.8	-2.4	-18.5
[-2.5,-2.0]	0.1079	+/- 5.7	6.3	-5.3	-16.1	-8.5	-23.1
[-2.0,-1.5]	0.0884	+/- 6.6	6.8	-5.7	-17.3	-8.5	-23.4
[-1.5,-1.0]	0.0731	+/- 7.1	6.5	-5.7	-19.0	-12.0	-25.8
[-1.0,-0.5]	0.0546	+/- 7.9	6.4	-6.0	-8.1	0.6	-15.0
[-0.5,0.0]	0.0515	+/- 8.5	7.1	-6.7	-17.3	-10.9	-27.4
[0.0,0.5]	0.0606	+/- 7.7	7.0	-5.9	-30.4	-22.6	-35.9
[0.5,1.0]	0.0670	+/- 7.1	7.0	-5.7	-24.4	-18.5	-30.6
[1.0,1.5]	0.0707	+/- 7.3	6.6	-5.3	-15.9	-9.2	-22.3
[1.5,2.0]	0.0778	+/- 7.0	7.0	-6.2	-6.7	2.1	-15.6
[2.0,2.5]	0.1099	+/- 5.8	7.0	-6.5	-18.1	-9.9	-23.5
[2.5,3.0]	0.1024	+/- 6.1	11.7	-6.1	2.2	13.6	-6.9
[3.0,3.142]	0.1287	+/- 9.7	6.0	-6.0	-15.1	-7.4	-21.4

Table B.28 Per-bin total statistical and systematic uncertainties in *ee* for the dilepton $\Delta\phi$, with generators, without normalisation.

Bin [radian]	Measured $d\sigma/dx$ [pb/radian]	Statistical Data [%]	Total Syst Up [%]	Total Syst Down [%]	GenTTbarPowhegPythia6AFII [%]	GenTTbarPowhegHerwig [%]	GenTTbarMC@NLOHerwig [%]
[-3.142,-3.0]	0.2621	+/- 9.5	-1.0	0.5	-8.9	-5.3	-10.6
[-3.0,-2.5]	0.2258	+/- 5.4	0.2	-0.8	1.5	4.3	4.3
[-2.5,-2.0]	0.2036	+/- 5.7	-0.9	0.7	-1.2	-2.1	-1.6
[-2.0,-1.5]	0.1669	+/- 6.6	-0.4	0.3	-2.6	-2.1	-2.0
[-1.5,-1.0]	0.1380	+/- 7.1	-0.8	0.3	-4.6	-5.9	-5.0
[-1.0,-0.5]	0.1031	+/- 7.9	-0.8	-0.1	8.2	7.6	8.8
[-0.5,0.0]	0.0972	+/- 8.5	-0.2	-0.8	-2.6	-4.7	-7.0
[0.0,0.5]	0.1144	+/- 7.7	-0.3	0.1	-18.1	-17.3	-17.9
[0.5,1.0]	0.1265	+/- 7.1	-0.2	0.4	-11.0	-12.9	-11.2
[1.0,1.5]	0.1334	+/- 7.3	-0.6	0.7	-1.0	-2.9	-0.6
[1.5,2.0]	0.1469	+/- 7.0	-0.3	-0.2	9.8	9.2	8.0
[2.0,2.5]	0.2074	+/- 5.8	-0.2	-0.6	-3.5	-3.6	-2.1
[2.5,3.0]	0.1932	+/- 6.1	4.1	-0.2	20.3	21.5	19.2
[3.0,3.142]	0.2430	+/- 9.7	-1.2	-0.0	0.0	-0.9	0.6

Table B.29 Per-bin total statistical and systematic uncertainties in *ee* for the dilepton $\Delta\phi$, with generators, with all distributions normalised to unit area.

Uncertainty	[-3.142,-3.0]	[-3.0,-2.5]	[-2.5,-2.0]	[-2.0,-1.5]	[-1.5,-1.0]	[-1.0,-0.5]	[-0.5,0.0]	[0.0,0.5]	[0.5,1.0]	[1.0,1.5]	[1.5,2.0]	[2.0,2.5]	[2.5,3.0]	[3.0,3.142]
StatisticalData	[-9.50,9.50]	[-5.43,5.43]	[-5.72,5.72]	[-6.57,6.57]	[-7.14,7.14]	[-7.93,7.93]	[-8.46,8.46]	[-7.67,7.67]	[-7.06,7.06]	[-7.34,7.34]	[-7.01,7.01]	[-5.84,5.84]	[-6.10,6.10]	[-9.75,9.75]
StatisticalBkg	[-2.14,2.14]	[-1.75,1.75]	[-1.29,1.29]	[-1.17,1.17]	[-2.00,2.00]	[-2.39,2.39]	[-3.10,3.10]	[-1.85,1.85]	[-1.25,1.25]	[-2.69,2.69]	[-2.05,2.05]	[-1.26,1.26]	[-6.11,6.11]	[-1.18,1.18]
StatisticalSig	[-2.64,2.79]	[-1.44,1.48]	[-1.57,1.62]	[-1.83,1.90]	[-1.97,2.05]	[-1.99,2.08]	[-2.24,2.35]	[-2.24,2.35]	[-1.98,2.06]	[-1.95,2.03]	[-1.77,1.84]	[-1.59,1.64]	[-1.46,1.50]	[-2.64,2.79]
BTag	[-4.60,5.59]	[-5.09,6.14]	[-4.46,5.43]	[-4.81,5.81]	[-4.61,5.65]	[-4.63,5.77]	[-5.17,6.24]	[-4.61,5.65]	[-5.50,6.62]	[-4.82,5.88]	[-5.42,6.51]	[-5.19,6.34]	[-5.07,6.19]	[-4.73,5.72]
Jeff	[-0.11,0.11]	[-0.01,0.01]	[-0.09,0.09]	[-0.01,0.01]	[-0.06,0.06]	[-0.10,0.10]	[-0.07,0.07]	[0.00,0.00]	[-0.09,0.09]	[-0.02,0.02]	[-0.08,0.08]	[-0.03,0.03]	[-0.07,0.07]	[-0.11,0.11]
Jer	[-0.47,0.47]	[-2.97,2.97]	[-0.04,0.04]	[-0.95,0.95]	[-2.05,2.05]	[-0.05,0.05]	[-0.37,0.37]	[-1.22,1.22]	[-0.31,0.31]	[-0.05,0.05]	[-1.16,1.16]	[-1.50,1.50]	[-0.04,0.04]	[-0.13,0.13]
MuidRes	[0.00,0.00]	[0.00,0.00]	[0.00,0.00]	[0.00,0.00]	[0.00,0.00]	[0.00,0.00]	[0.00,0.00]	[0.00,0.00]	[0.00,0.00]	[0.00,0.00]	[0.00,0.00]	[0.00,0.00]	[0.00,0.00]	[0.00,0.00]
MumsRes	[0.00,0.00]	[0.00,0.00]	[0.00,0.00]	[0.00,0.00]	[-0.02,0.02]	[-0.01,0.01]	[0.00,0.00]	[0.00,0.00]	[0.00,0.00]	[0.00,0.00]	[-0.04,0.04]	[0.00,0.00]	[-0.04,0.04]	[0.00,0.00]
BJesUnc	[-0.98,0.86]	[-0.95,0.92]	[-1.03,0.85]	[-0.53,1.12]	[-1.11,0.57]	[-0.84,0.36]	[-0.49,0.60]	[-1.07,0.37]	[-0.30,1.16]	[-0.64,0.97]	[-0.53,0.33]	[-1.08,0.48]	[-0.87,1.08]	[-0.96,0.14]
JesEffectiveStat1	[-0.72,0.40]	[-0.66,0.33]	[-0.47,0.68]	[-0.32,0.32]	[-0.30,0.33]	[-1.17,0.54]	[-1.14,0.59]	[-0.61,0.78]	[-0.05,0.05]	[-0.56,0.69]	[-0.40,0.09]	[-0.57,0.18]	[-0.62,0.52]	[-0.50,0.06]
JesEffectiveStat2	[-0.06,0.06]	[-0.05,0.05]	[-0.43,0.43]	[-0.06,0.06]	[-0.02,0.03]	[-0.08,0.00]	[-0.09,0.00]	[-0.01,0.01]	[-0.10,0.10]	[-0.15,0.14]	[-0.02,0.06]	[-0.16,0.16]	[-0.02,0.09]	[-0.11,0.11]
JesEffectiveStat3	[-0.19,0.02]	[-0.17,0.00]	[-0.06,0.18]	[-0.00,0.00]	[-0.14,0.17]	[-0.12,0.14]	[-0.04,0.00]	[-0.29,0.10]	[-0.22,0.22]	[-0.10,0.18]	[-0.05,0.17]	[-0.14,0.14]	[-0.23,0.06]	[-0.20,0.14]
JesEffectiveStat4	[-0.18,0.18]	[-0.24,0.14]	[-0.04,0.43]	[-0.04,0.20]	[-0.14,0.38]	[-0.10,0.31]	[-0.38,0.05]	[-0.33,0.68]	[-0.16,0.16]	[-0.13,0.21]	[-0.04,0.19]	[-0.30,0.30]	[-0.32,0.20]	[-0.32,0.32]
JesEffectiveModel1	[-1.77,1.58]	[-1.81,2.03]	[-1.54,1.69]	[-1.78,1.91]	[-1.81,1.08]	[-1.71,1.74]	[-1.86,1.77]	[-1.86,1.80]	[-0.30,1.37]	[-1.15,1.50]	[-1.58,0.95]	[-2.09,1.61]	[-1.57,6.12]	[-1.76,0.85]
JesEffectiveModel2	[-0.06,0.06]	[-0.06,0.06]	[-0.17,0.17]	[-0.06,0.25]	[-0.07,0.07]	[-0.17,0.17]	[-0.18,0.10]	[-0.10,0.10]	[-0.09,0.09]	[-0.10,0.16]	[-0.04,0.04]	[-0.16,0.16]	[-0.01,0.06]	[-0.21,0.21]
JesEffectiveModel3	[-0.09,0.09]	[-0.15,0.15]	[-0.04,0.45]	[-0.10,0.10]	[-0.07,0.03]	[-0.16,0.16]	[-0.06,0.06]	[-0.07,0.43]	[-0.11,0.11]	[-0.10,0.08]	[-0.01,0.12]	[-0.42,0.42]	[-0.03,0.05]	[-0.09,0.09]
JesEffectiveModel4	[-0.08,0.01]	[-0.09,0.03]	[-0.06,0.21]	[-0.02,0.20]	[-0.11,0.19]	[-0.04,0.20]	[-0.10,0.10]	[-0.13,0.06]	[-0.08,0.08]	[-0.17,0.17]	[-0.07,0.06]	[-0.11,0.01]	[-0.04,0.05]	[-0.31,0.00]
JesEffectiveDet1	[-0.39,0.34]	[-0.60,0.27]	[-0.41,0.70]	[-0.28,0.43]	[-0.13,0.56]	[-0.42,0.47]	[-0.46,0.23]	[-0.55,0.78]	[-0.11,0.34]	[-0.39,0.41]	[-0.14,0.57]	[-0.52,0.05]	[-0.57,1.40]	[-0.55,0.38]
JesEffectiveDet2	[-0.09,0.09]	[-0.22,0.22]	[-0.41,0.41]	[-0.17,0.17]	[-0.11,0.11]	[-0.13,0.13]	[-0.17,0.17]	[-0.10,0.57]	[-0.09,0.09]	[-0.03,0.15]	[-0.01,0.04]	[-0.31,0.04]	[-0.02,0.32]	[-0.11,0.01]
JesEffectiveDet3	[-0.06,0.00]	[-0.12,0.02]	[-0.04,0.22]	[-0.01,0.05]	[-0.10,0.19]	[-0.00,0.01]	[-0.07,0.10]	[-0.11,0.06]	[-0.05,0.05]	[-0.00,0.16]	[-0.04,0.06]	[-0.03,0.03]	[-0.05,0.04]	[-0.16,0.01]
JesEffectiveMix1	[-0.38,0.15]	[-0.58,0.26]	[-0.33,0.66]	[-0.43,0.43]	[-0.07,0.53]	[-0.68,0.46]	[-0.48,0.19]	[-0.59,0.90]	[-0.45,0.45]	[-0.34,0.62]	[-0.22,0.26]	[-0.50,0.09]	[-0.64,0.99]	[-0.40,0.40]
JesEffectiveMix2	[-0.29,0.29]	[-0.38,0.18]	[-0.24,0.56]	[-0.18,0.18]	[-0.09,0.27]	[-0.30,0.14]	[-0.86,0.05]	[-0.51,0.65]	[-0.10,0.10]	[-0.12,0.26]	[-0.07,0.19]	[-0.34,0.13]	[-0.40,0.59]	[-0.23,0.12]
JesEffectiveMix3	[-0.07,0.02]	[-0.15,0.00]	[-0.00,0.40]	[-0.02,0.29]	[-0.03,0.27]	[-0.01,0.28]	[-0.13,0.11]	[-0.36,0.36]	[-0.12,0.12]	[-0.08,0.18]	[-0.05,0.06]	[-0.12,0.12]	[-0.02,0.02]	[-0.21,0.21]
JesEffectiveMix4	[-0.06,0.00]	[-0.02,0.02]	[-0.03,0.01]	[-0.03,0.03]	[-0.00,0.00]	[-0.11,0.00]	[-0.00,0.02]	[-0.01,0.01]	[-0.02,0.02]	[-0.00,0.04]	[-0.01,0.05]	[-0.00,0.00]	[-0.01,0.01]	[-0.00,0.00]
EtaIntercalibrationModel	[-0.63,0.36]	[-0.54,0.38]	[-0.71,0.62]	[-0.24,1.09]	[-0.33,0.35]	[-0.42,0.29]	[-1.16,1.16]	[-0.31,0.71]	[-0.10,0.20]	[-0.47,0.67]	[-0.38,0.18]	[-0.66,0.35]	[-0.60,0.22]	[-0.63,0.62]
EtaIntercalibrationTotalStat	[-0.49,0.16]	[-0.48,0.34]	[-0.37,0.62]	[-0.35,0.35]	[-0.20,0.56]	[-0.64,0.43]	[-0.91,0.34]	[-0.65,0.69]	[-0.30,0.30]	[-0.37,0.51]	[-0.38,0.24]	[-0.66,0.23]	[-0.74,0.56]	[-0.50,0.16]
PileupOffsetMu	[-0.12,0.12]	[-0.38,0.32]	[-0.02,0.13]	[-0.35,0.35]	[-0.17,0.14]	[-0.26,0.00]	[-0.69,0.04]	[-0.15,0.73]	[-0.03,0.05]	[-0.36,0.36]	[-0.22,0.22]	[-0.17,0.17]	[-0.22,0.14]	[-0.28,0.19]
PileupOffsetNPV	[-0.46,0.09]	[-0.15,0.38]	[-0.15,0.25]	[-0.68,0.36]	[-0.03,0.26]	[-0.47,0.16]	[-1.00,0.25]	[-0.27,0.58]	[-0.01,0.33]	[-0.10,0.10]	[-0.33,0.33]	[-0.37,0.37]	[-0.47,4.92]	[-0.52,0.52]
PileupRho	[-1.28,1.02]	[-1.50,1.20]	[-1.15,1.22]	[-1.16,1.40]	[-1.07,1.14]	[-1.51,1.02]	[-1.53,1.07]	[-1.18,1.20]	[-0.45,0.61]	[-0.96,1.20]	[-0.88,0.27]	[-1.39,1.07]	[-1.27,1.05]	[-1.14,0.53]
PunchThrough	[-0.00,0.00]	[-0.03,0.03]	[-0.00,0.00]	[-0.00,0.04]	[-0.07,0.07]	[0.00,0.04]	[-0.01,0.01]	[-0.00,0.00]	[-0.00,0.00]	[-0.00,0.01]	[-0.03,0.01]	[-0.01,0.01]	[-0.00,0.00]	[0.00,0.00]
CTauTag	[-0.04,0.04]	[-0.03,0.03]	[-0.04,0.04]	[-0.03,0.03]	[-0.10,0.09]	[-0.05,0.05]	[-0.15,0.15]	[-0.04,0.04]	[-0.02,0.02]	[-0.06,0.06]	[-0.03,0.03]	[-0.00,0.00]	[-0.02,0.02]	[-0.04,0.04]
ElectronEnergyResolution	[-0.24,0.24]	[-0.30,0.30]	[-0.19,0.26]	[-0.23,0.56]	[-0.32,0.25]	[-0.39,0.39]	[-0.50,0.87]	[-0.37,0.37]	[-0.42,0.42]	[-0.09,0.26]	[-0.14,0.19]	[-0.02,0.21]	[-0.07,0.09]	[-0.89,0.89]
ElectronEnergyScale	[-0.15,1.41]	[-0.42,0.88]	[-1.17,1.05]	[-0.79,1.16]	[-0.22,0.74]	[-1.27,0.42]	[-1.36,1.39]	[-1.15,0.87]	[-0.30,0.33]	[-0.58,0.30]	[-1.26,1.48]	[-1.25,1.12]	[-0.38,0.67]	[-1.74,0.51]
ElectronIdSF	[-0.57,0.56]	[-0.61,0.59]	[-0.47,0.46]	[-0.45,0.44]	[-0.54,0.53]	[-0.60,0.59]	[-0.74,0.72]	[-0.47,0.46]	[-0.50,0.49]	[-0.64,0.62]	[-0.67,0.65]	[-0.59,0.58]	[-0.92,0.90]	[-0.45,0.44]
ElectronRecoSF	[-0.08,0.08]	[-0.08,0.08]	[-0.07,0.07]	[-0.05,0.05]	[-0.05,0.05]	[-0.06,0.06]	[-0.08,0.08]	[-0.05,0.05]	[-0.05,0.05]	[-0.06,0.06]	[-0.08,0.08]	[-0.08,0.08]	[-0.11,0.11]	[-0.07,0.07]
ElectronTriggerSF	[-0.00,0.00]	[-0.00,0.00]	[-0.00,0.00]	[-0.00,0.00]	[-0.01,0.01]	[-0.01,0.01]	[-0.01,0.01]	[-0.00,0.00]	[-0.00,0.00]	[-0.01,0.01]	[-0.00,0.01]	[-0.00,0.00]	[-0.00,0.00]	[-0.00,0.00]
FlavorComp	[-0.68,0.38]	[-0.64,0.89]	[-0.66,0.39]	[-0.93,0.56]	[-0.57,0.40]	[-1.43,0.64]	[-1.19,0.99]	[-1.30,1.28]	[-0.48,0.48]	[-0.15,0.53]	[-0.80,0.24]	[-1.05,0.56]	[-0.88,5.25]	[-1.12,0.09]
FlavorResponse	[-0.27,0.09]	[-0.58,0.64]	[-0.34,0.27]	[-0.33,0.45]	[-0.30,0.36]	[-1.32,0.79]	[-1.20,0.75]	[-0.59,1.50]	[-0.08,0.34]	[-0.07,0.46]	[-0.68,0.05]	[-0.43,0.42]	[-0.68,0.29]	[-0.80,0.26]
JetVertexFraction	[-0.20,0.18]	[-0.26,0.21]	[-0.23,0.47]	[-0.30,0.13]	[-0.37,0.24]	[-0.39,0.29]	[-0.28,0.12]	[-0.19,0.14]	[-0.14,0.34]	[-0.10,1.24]	[-0.26,0.46]	[-0.40,0.49]	[-0.32,0.43]	[-0.38,0.16]
Mistag	[-0.10,0.10]	[-0.11,0.11]	[-0.11,0.11]	[-0.05,0.05]	[-0.04,0.04]	[-0.12,0.12]	[-0.15,0.16]	[-0.15,0.15]	[-0.06,0.06]	[-0.17,0.17]	[-0.03,0.03]	[-0.03,0.02]	[-1.46,1.48]	[-0.12,0.12]
MuonIdSF	[-0.00,0.00]	[-0.00,0.00]	[-0.00,0.00]	[-0.00,0.00]	[0.00,0.00]	[-0.00,0.00]	[0.00,0.00]	[0.00,0.00]	[-0.00,0.00]	[0.00,0.00]	[-0.00,0.00]	[-0.00,0.00]	[-0.00,0.00]	[-0.00,0.00]
MuonRecoSF	[-0.00,0.00]	[-0.00,0.00]	[-0.00,0.00]	[-0.00,0.00]	[0.00,0.00]	[-0.00,0.00]	[0.00,0.00]	[0.00,0.00]	[-0.00,0.00]	[0.00,0.00]	[-0.00,0.00]	[-0.00,0.00]	[-0.00,0.00]	[-0.00,0.00]
MuonTriggerSF	[0.00,0.00]	[0.00,0.00]	[0.00,0.00]	[0.00,0.00]	[0.00,0.00]	[0.00,0.00]	[0.00,0.00]	[0.00,0.00]	[0.00,0.00]	[0.00,0.00]	[0.00,0.00]	[0.00,0.00]	[0.00,0.00]	[0.00,0.00]
Musc	[0.00,0.00]	[0.00,0.00]	[0.00,0.00]	[0.00,0.00]	[0.00,0.00]	[0.00,0.00]	[0.00,0.00]	[0.00,0.00]	[0.00,0.00]	[0.00,0.00]	[0.00,0.00]	[0.00,0.00]	[0.00,0.00]	[0.00,0.00]
ModellingGenerator	[-1.53,1.53]	[-4.58,4.58]	[-6.41,6.41]	[-3.65,3.65]	[-3.75,3.75]	[-3.12,3.12]	[-0.78,0.78]	[-7.12,7.12]	[-0.32,0.32]	[-4.26,4.26]	[-3.52,3.52]	[-1.14,1.14]	[-0.05,0.05]	[-5.56,5.56]
ModellingParton	[-4.29,4.29]	[-2.68,2.68]	[-1.66,1.66]	[-2.56,2.56]	[-3.76,3.76]	[-3.50,3.50]	[-2.31,2.31]	[-2.70,2.70]	[-2.42,2.42]	[-0.91,0.91]	[-0.75,0.75]	[-2.44,2.44]	[-2.41,2.41]	[-0.76,0.76]
ModellingRadiation	[-16.35,16.35]	[-7.81,7.81]	[-7.14,7.14]	[-5.72,5.72]	[-2.01,2.01]	[-4.15,4.15]	[-6.99,6.99]	[-1.80,1.80]	[-2.24,2.24]	[-8.74,8.74]	[-11.83,11.83]	[-5.45,5.45]	[-11.95,11.95]	[-1.66,1.66]
ModellingSingleTopWtNormalisation	[-0.82,0.82]	[-0.73,0.73]	[-0.40,0.40]	[-0.56,0.56]	[-0.87,0.87]	[-0.87,0.87]	[-1.02,1.02]	[-0.72,0.72]	[-0.80,0.80]	[-0.96,0.96]	[-0.93,0.93]	[-0.79,0.79]	[-0.96,0.96]	[-0.31,0.31]
ModellingSingleTopWtInterference	[-6.15,6.15]	[-5.44,5.44]	[-3.01,3.01]	[-4.20,4.20]	[-6.51,6.51]	[-6.47,6.47]	[-7.59,7.59]	[-5.35,5.35]	[-5.94,5.94]	[-7.18,7.18]	[-6.93,6.93]	[-5.93,5.93]	[-7.13,7.13]	[-2.33,2.33]

Table B.30 Per-bin individual statistical and systematic uncertainties in *ee* for the dilepton $\Delta\phi$.

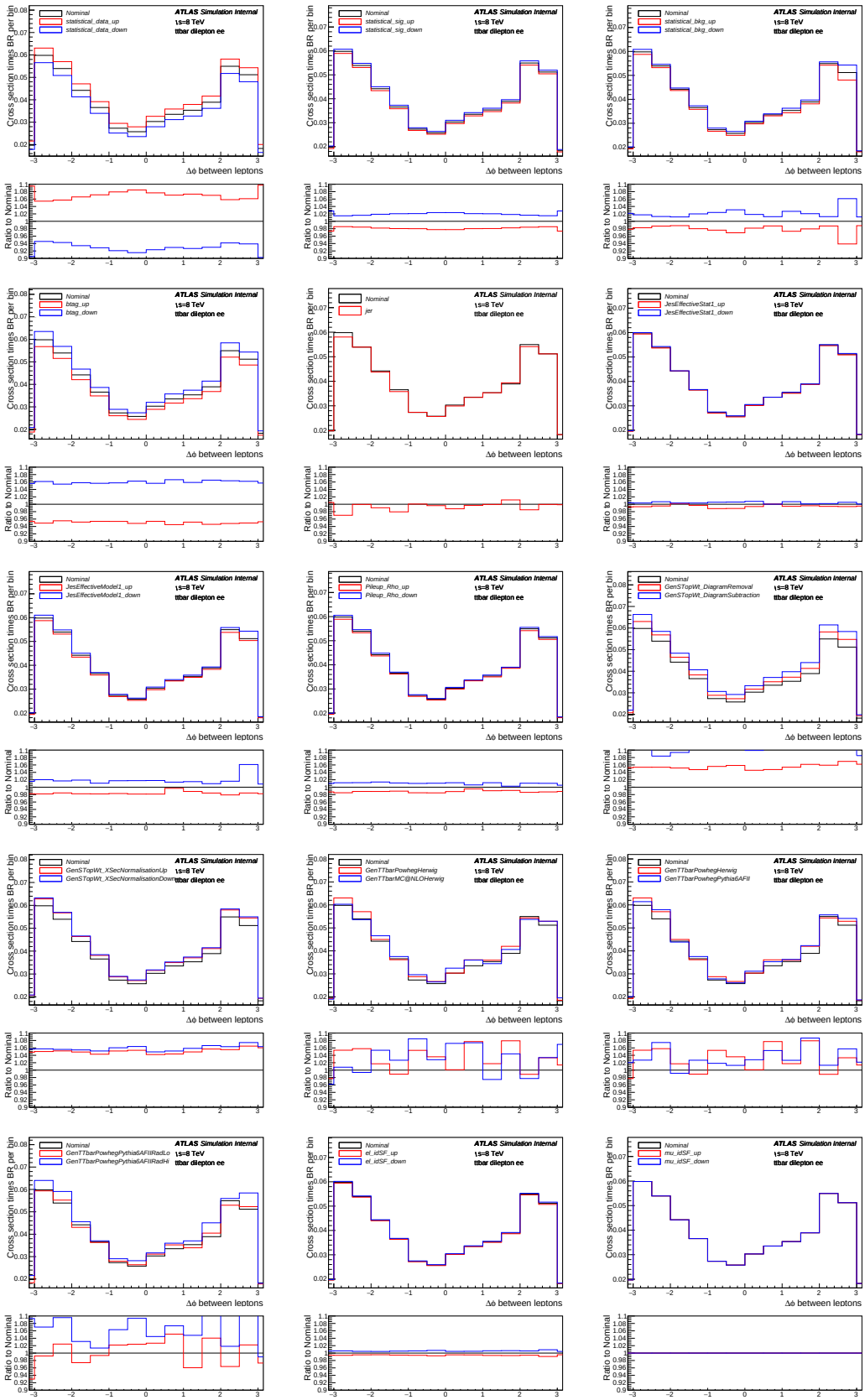

Fig. B.19 Differential cross-section per bin (not scaled to density) for channel *ee* in the variable of dilepton $\Delta\phi$ with measured (with Nominal signal) overlaid with statistical uncertainties on data and MC (signal and background), as well as various systematics.

B.1.7 Variable dilepton $|\Delta\phi|$

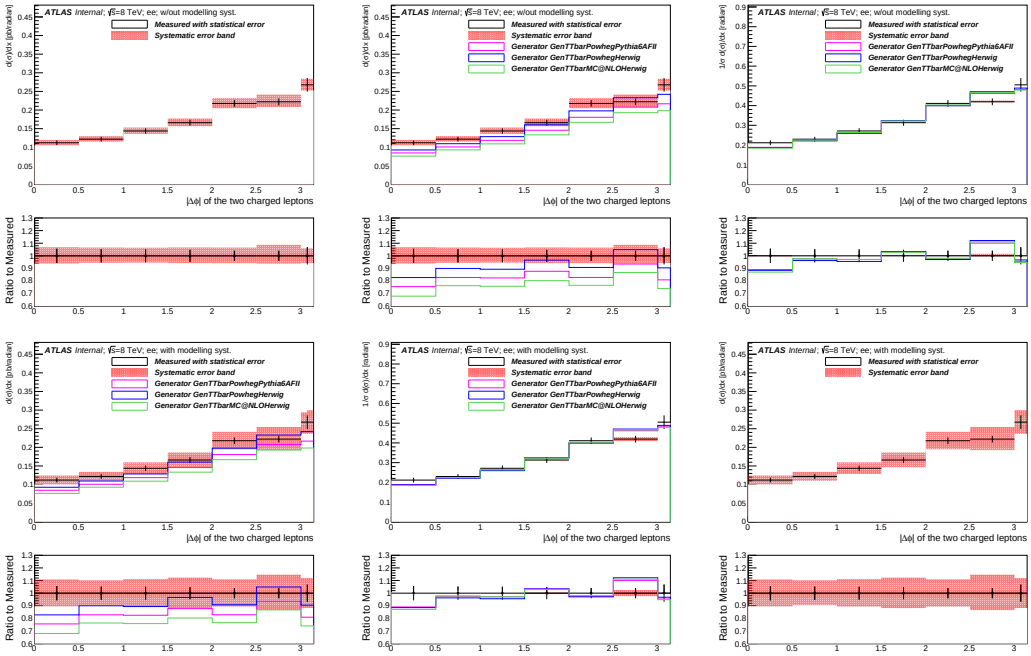

Fig. B.20 Differential cross-section for channel *ee* in the variable of dilepton $|\Delta\phi|$.

Bin [radian]	Measured $d\sigma/dx$ [pb/radian]	Statistical Data [%]	Statistical MC Bkg [%]	Statistical MC Sig [%]	Systematic [%]
[0.0,0.5]	0.1121	+/- 5.7	+/- 1.8	+/- 1.7	+6.9/-6.2
[0.5,1.0]	0.1217	+/- 5.3	+/- 1.3	+/- 1.5	+6.6/-5.5
[1.0,1.5]	0.1438	+/- 5.1	+/- 1.7	+/- 1.4	+6.4/-5.4
[1.5,2.0]	0.1660	+/- 4.8	+/- 1.2	+/- 1.3	+6.7/-5.8
[2.0,2.5]	0.2178	+/- 4.1	+/- 1.0	+/- 1.1	+6.6/-5.9
[2.5,3.0]	0.2221	+/- 4.1	+/- 3.1	+/- 1.1	+8.7/-6.2
[3.0,3.142]	0.2676	+/- 6.8	+/- 1.3	+/- 2.0	+6.0/-5.6

Table B.31 Per-bin total statistical and systematic uncertainties in *ee* for the dilepton $|\Delta\phi|$, without modelling systematic uncertainties.

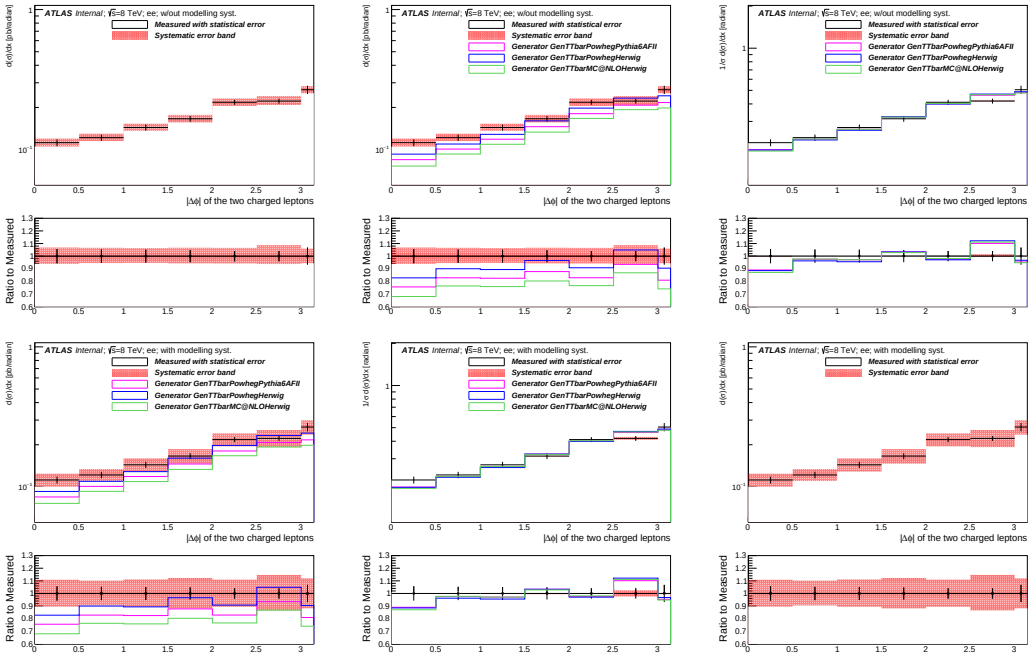

Fig. B.21 Differential cross-section for channel *ee* in the variable of dilepton $|\Delta\phi|$ (log on y axis).

Bin [radian]	Measured $d\sigma/dx$ [pb/radian]	Statistical Data [%]	Statistical MC Bkg [%]	Statistical MC Sig [%]	Systematic [%]
[0.0,0.5]	0.1121	+/- 5.7	+/- 1.8	+/- 1.7	+10.9/-10.4
[0.5,1.0]	0.1217	+/- 5.3	+/- 1.3	+/- 1.5	+10.2/-9.5
[1.0,1.5]	0.1438	+/- 5.1	+/- 1.7	+/- 1.4	+11.1/-10.5
[1.5,2.0]	0.1660	+/- 4.8	+/- 1.2	+/- 1.3	+12.3/-11.8
[2.0,2.5]	0.2178	+/- 4.1	+/- 1.0	+/- 1.1	+11.0/-10.6
[2.5,3.0]	0.2221	+/- 4.1	+/- 3.1	+/- 1.1	+14.7/-13.4
[3.0,3.142]	0.2676	+/- 6.8	+/- 1.3	+/- 2.0	+12.0/-11.8

Table B.32 Per-bin total statistical and systematic uncertainties in *ee* for the dilepton $|\Delta\phi|$, with modelling systematic uncertainties.

Bin [radian]	Measured $d\sigma/dx$ [pb/radian]	Statistical Data [%]	Total Syst Up [%]	Total Syst Down [%]	GenTTbarPowhegPythia6AFII [%]	GenTTbarPowhegHerwig [%]	GenTTbarMC@NLOHerwig [%]
[0.0,0.5]	0.1121	+/- 5.7	6.9	-6.2	-24.4	-17.2	-31.9
[0.5,1.0]	0.1217	+/- 5.3	6.6	-5.5	-17.1	-10.0	-23.6
[1.0,1.5]	0.1438	+/- 5.1	6.4	-5.4	-17.5	-10.6	-24.1
[1.5,2.0]	0.1660	+/- 4.8	6.7	-5.8	-12.2	-3.4	-19.7
[2.0,2.5]	0.2178	+/- 4.1	6.6	-5.9	-17.1	-9.2	-23.3
[2.5,3.0]	0.2221	+/- 4.1	8.7	-6.2	-6.5	4.9	-13.2
[3.0,3.142]	0.2676	+/- 6.8	6.0	-5.6	-19.0	-9.5	-25.9

Table B.33 Per-bin total statistical and systematic uncertainties in *ee* for the dilepton $|\Delta\phi|$, with generators, without normalisation.

Bin [radian]	Measured $d\sigma/dx$ [pb/radian]	Statistical Data [%]	Total Syst Up [%]	Total Syst Down [%]	GenTTbarPowhegPythia6AFII [%]	GenTTbarPowhegHerwig [%]	GenTTbarMC@NLOHerwig [%]
[0.0,0.5]	0.2116	+/- 5.7	-0.1	-0.4	-10.9	-11.5	-12.9
[0.5,1.0]	0.2298	+/- 5.3	-0.4	0.4	-2.4	-3.7	-2.3
[1.0,1.5]	0.2714	+/- 5.1	-0.5	0.5	-2.8	-4.4	-2.9
[1.5,2.0]	0.3134	+/- 4.8	-0.3	0.1	3.4	3.3	2.8
[2.0,2.5]	0.4111	+/- 4.1	-0.4	-0.0	-2.4	-2.9	-1.9
[2.5,3.0]	0.4193	+/- 4.1	1.6	-0.4	10.1	12.2	11.1
[3.0,3.142]	0.5052	+/- 6.8	-0.9	0.2	-4.6	-3.2	-5.2

Table B.34 Per-bin total statistical and systematic uncertainties in *ee* for the dilepton $|\Delta\phi|$, with generators, with all distributions normalised to unit area.

Uncertainty	[0.0,0.5]	[0.5,1.0]	[1.0,1.5]	[1.5,2.0]	[2.0,2.5]	[2.5,3.0]	[3.0,3.142]
StatisticalData	[-5.69,5.69]	[-5.27,5.27]	[-5.12,5.12]	[-4.80,4.80]	[-4.09,4.09]	[-4.06,4.06]	[-6.80,6.80]
StatisticalBkg	[-1.76,1.76]	[-1.33,1.33]	[-1.70,1.70]	[-1.21,1.21]	[-0.97,0.97]	[-3.08,3.08]	[-1.26,1.26]
StatisticalSig	[-1.60,1.65]	[-1.41,1.46]	[-1.39,1.43]	[-1.28,1.31]	[-1.12,1.15]	[-1.03,1.05]	[-1.88,1.96]
BTag	[-4.87,5.93]	[-5.08,6.20]	[-4.71,5.76]	[-5.11,6.15]	[-4.83,5.89]	[-5.09,6.17]	[-4.67,5.66]
Jeff	[-0.04,0.04]	[-0.09,0.09]	[-0.02,0.02]	[-0.05,0.05]	[-0.03,0.03]	[-0.04,0.04]	[-0.00,0.00]
Jer	[-0.78,0.78]	[-0.16,0.16]	[-1.06,1.06]	[-0.15,0.15]	[-0.78,0.78]	[-1.61,1.61]	[-0.16,0.16]
MuidRes	[0.00,0.00]	[0.00,0.00]	[0.00,0.00]	[0.00,0.00]	[0.00,0.00]	[0.00,0.00]	[0.00,0.00]
MumsRes	[0.00,0.00]	[-0.01,0.01]	[-0.01,0.01]	[-0.02,0.02]	[0.00,0.00]	[-0.02,0.02]	[0.00,0.00]
BJesUnc	[-0.78,0.48]	[-0.57,0.76]	[-0.88,0.77]	[-0.53,0.74]	[-1.05,0.67]	[-0.91,0.99]	[-0.98,0.50]
JesEffectiveStat1	[-0.86,0.70]	[-0.55,0.28]	[-0.43,0.51]	[-0.11,0.20]	[-0.52,0.43]	[-0.64,0.42]	[-0.62,0.23]
JesEffectiveStat2	[-0.05,0.05]	[-0.01,0.01]	[-0.09,0.09]	[-0.01,0.01]	[-0.06,0.22]	[-0.04,0.03]	[-0.02,0.03]
JesEffectiveStat3	[-0.17,0.05]	[-0.03,0.18]	[-0.12,0.17]	[-0.02,0.09]	[-0.07,0.02]	[-0.20,0.03]	[-0.20,0.08]
JesEffectiveStat4	[-0.35,0.38]	[-0.04,0.23]	[-0.13,0.29]	[-0.04,0.20]	[-0.17,0.21]	[-0.28,0.17]	[-0.25,0.25]
JesEffectiveModel1	[-1.84,1.80]	[-1.00,1.55]	[-1.48,1.29]	[-1.69,1.42]	[-1.82,1.65]	[-1.71,3.89]	[-1.77,1.21]
JesEffectiveModel2	[-0.09,0.09]	[-0.12,0.12]	[-0.01,0.10]	[-0.05,0.12]	[-0.03,0.07]	[-0.03,0.01]	[-0.13,0.13]
JesEffectiveModel3	[-0.06,0.20]	[-0.13,0.13]	[-0.04,0.01]	[-0.06,0.06]	[-0.23,0.19]	[-0.05,0.05]	[-0.09,0.09]
JesEffectiveModel4	[-0.11,0.08]	[-0.01,0.13]	[-0.05,0.18]	[-0.05,0.13]	[-0.09,0.11]	[-0.07,0.04]	[-0.20,0.00]
JesEffectiveDet1	[-0.51,0.53]	[-0.26,0.39]	[-0.26,0.48]	[-0.21,0.49]	[-0.46,0.38]	[-0.58,0.80]	[-0.47,0.36]
JesEffectiveDet2	[-0.14,0.27]	[-0.10,0.10]	[-0.11,0.11]	[-0.08,0.08]	[-0.15,0.23]	[-0.12,0.12]	[-0.07,0.07]
JesEffectiveDet3	[-0.09,0.08]	[-0.02,0.02]	[-0.05,0.17]	[-0.03,0.06]	[-0.03,0.10]	[-0.09,0.03]	[-0.11,0.01]
JesEffectiveMix1	[-0.54,0.56]	[-0.31,0.44]	[-0.21,0.57]	[-0.11,0.34]	[-0.42,0.38]	[-0.61,0.60]	[-0.39,0.27]
JesEffectiveMix2	[-0.67,0.37]	[-0.10,0.11]	[-0.11,0.27]	[-0.13,0.13]	[-0.29,0.35]	[-0.39,0.37]	[-0.26,0.26]
JesEffectiveMix3	[-0.13,0.13]	[-0.19,0.19]	[-0.09,0.09]	[-0.04,0.17]	[-0.06,0.15]	[-0.07,0.01]	[-0.14,0.14]
JesEffectiveMix4	[-0.01,0.01]	[-0.04,0.00]	[-0.00,0.02]	[-0.02,0.03]	[-0.02,0.01]	[-0.01,0.01]	[-0.03,0.03]
EtaIntercalibrationModel	[-0.71,0.24]	[-0.11,0.09]	[-0.40,0.51]	[-0.31,0.63]	[-0.68,0.48]	[-0.57,0.30]	[-0.63,0.49]
EtaIntercalibrationTotalStat	[-0.76,0.53]	[-0.30,0.36]	[-0.28,0.53]	[-0.12,0.29]	[-0.51,0.43]	[-0.61,0.44]	[-0.50,0.16]
PileupOffsetMu	[-0.40,0.40]	[-0.15,0.03]	[-0.05,0.25]	[-0.14,0.14]	[-0.09,0.03]	[-0.30,0.24]	[-0.11,0.15]
PileupOffsetNPV	[-0.62,0.43]	[-0.23,0.24]	[-0.02,0.08]	[-0.52,0.09]	[-0.26,0.02]	[-0.31,2.46]	[-0.38,0.38]
PileupRho	[-1.34,1.13]	[-0.97,0.80]	[-1.01,1.17]	[-1.03,0.84]	[-1.27,1.15]	[-1.40,1.12]	[-1.21,0.77]
PunchThrough	[-0.01,0.01]	[-0.02,0.02]	[-0.04,0.04]	[-0.00,0.00]	[-0.01,0.01]	[-0.01,0.01]	[-0.00,0.00]
CTauTag	[-0.09,0.09]	[-0.03,0.03]	[-0.08,0.08]	[-0.03,0.03]	[-0.02,0.02]	[-0.03,0.03]	[-0.04,0.04]
ElectronEnergyResolution	[-0.25,0.24]	[-0.14,0.10]	[-0.21,0.26]	[-0.02,0.20]	[-0.12,0.12]	[-0.02,0.20]	[-0.29,0.10]
ElectronEnergyScale	[-1.27,1.13]	[-0.77,0.35]	[-0.41,0.52]	[-1.04,1.30]	[-1.21,1.08]	[-0.40,0.78]	[-0.91,0.95]
ElectronIdSF	[-0.60,0.58]	[-0.55,0.53]	[-0.59,0.58]	[-0.55,0.54]	[-0.53,0.52]	[-0.75,0.73]	[-0.52,0.50]
ElectronRecoSF	[-0.07,0.06]	[-0.06,0.05]	[-0.06,0.06]	[-0.07,0.06]	[-0.07,0.08]	[-0.10,0.10]	[-0.08,0.08]
ElectronTriggerSF	[-0.01,0.01]	[-0.01,0.01]	[-0.01,0.01]	[-0.00,0.00]	[-0.00,0.00]	[-0.00,0.00]	[-0.00,0.00]
FlavorComp	[-1.22,1.15]	[-0.48,0.32]	[-0.36,0.46]	[-0.87,0.39]	[-0.85,0.48]	[-0.76,2.88]	[-0.90,0.23]
FlavorResponse	[-0.87,1.14]	[-0.49,0.34]	[-0.18,0.41]	[-0.52,0.24]	[-0.39,0.35]	[-0.63,0.46]	[-0.53,0.17]
JetVertexFraction	[-0.24,0.13]	[-0.25,0.32]	[-0.24,0.73]	[-0.28,0.30]	[-0.31,0.48]	[-0.29,0.31]	[-0.29,0.17]
Mistag	[-0.15,0.15]	[-0.09,0.09]	[-0.11,0.11]	[-0.04,0.04]	[-0.07,0.07]	[-0.73,0.73]	[-0.11,0.11]
MuonIdSF	[0.00,0.00]	[-0.00,0.00]	[0.00,0.00]	[-0.00,0.00]	[-0.00,0.00]	[-0.00,0.00]	[-0.00,0.00]
MuonRecoSF	[0.00,0.00]	[-0.00,0.00]	[0.00,0.00]	[-0.00,0.00]	[-0.00,0.00]	[-0.00,0.00]	[-0.00,0.00]
MuonTriggerSF	[0.00,0.00]	[0.00,0.00]	[0.00,0.00]	[0.00,0.00]	[0.00,0.00]	[-0.00,0.00]	[0.00,0.00]
Musc	[0.00,0.00]	[0.00,0.00]	[0.00,0.00]	[0.00,0.00]	[0.00,0.00]	[0.00,0.00]	[0.00,0.00]
ModellingGenerator	[-3.19,3.19]	[-1.41,1.41]	[-0.31,0.31]	[-0.13,0.13]	[-3.70,3.70]	[-2.23,2.23]	[-1.90,1.90]
ModellingParton	[-0.21,0.21]	[-2.97,2.97]	[-2.35,2.35]	[-1.00,1.00]	[-2.08,2.08]	[-0.11,0.11]	[-2.60,2.60]
ModellingRadiation	[-4.37,4.37]	[-3.23,3.23]	[-5.35,5.35]	[-8.64,8.64]	[-6.25,6.25]	[-9.81,9.81]	[-8.79,8.79]
ModellingSingleTopWtNormalisation	[-0.86,0.86]	[-0.83,0.83]	[-0.92,0.92]	[-0.74,0.74]	[-0.60,0.60]	[-0.83,0.83]	[-0.58,0.58]
ModellingSingleTopWtInterference	[-6.39,6.39]	[-6.18,6.18]	[-6.84,6.84]	[-5.51,5.51]	[-4.46,4.46]	[-6.22,6.22]	[-4.32,4.32]

Table B.35 Per-bin individual statistical and systematic uncertainties in *ee* for the dilepton $|\Delta\phi|$.

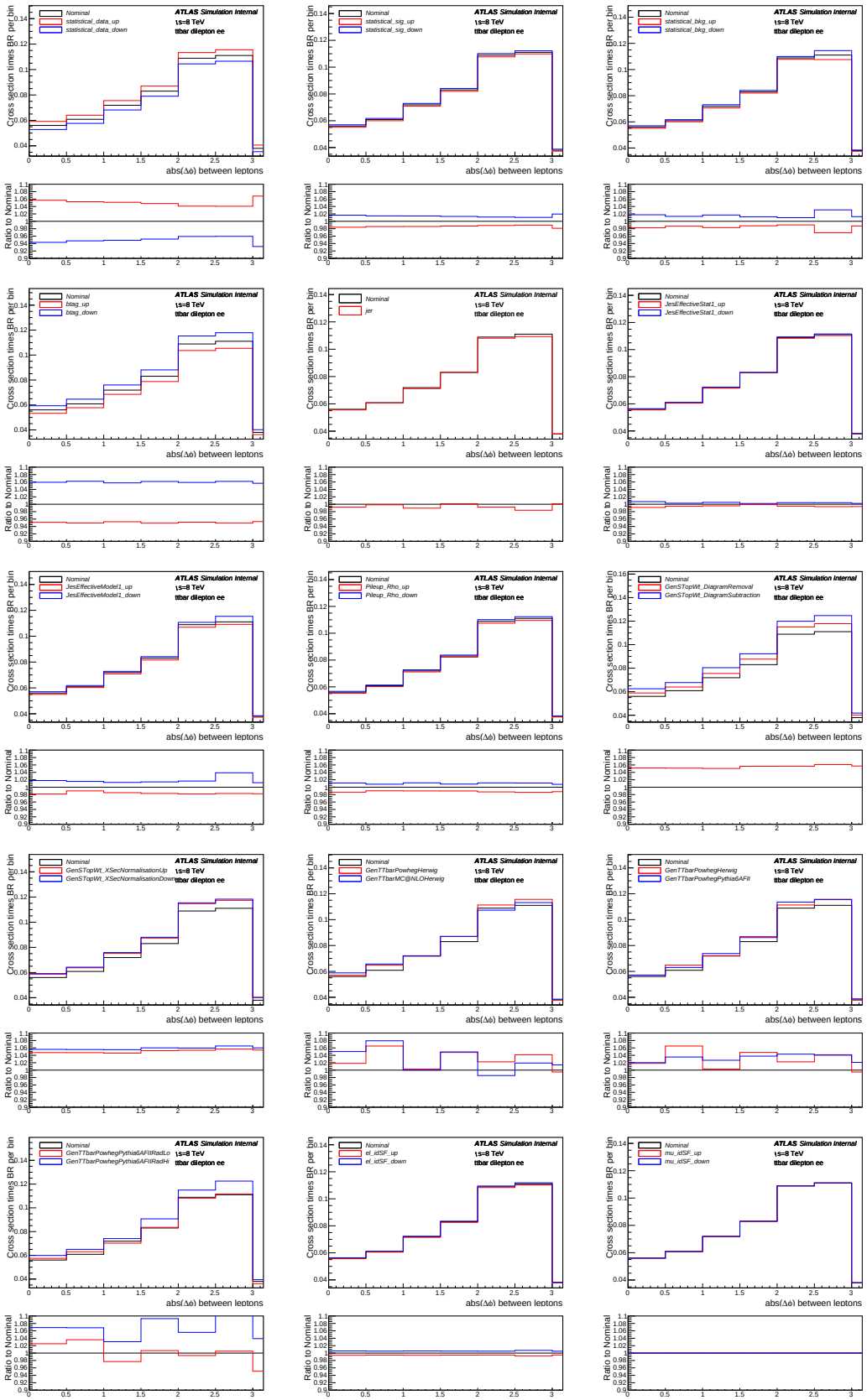

Fig. B.22 Differential cross-section per bin (not scaled to density) for channel *ee* in the variable of dilepton $|\Delta\phi|$ with measured (with Nominal signal) overlaid with statistical uncertainties on data and MC (signal and background), as well as various systematics.

B.2 Detailed results for the $\mu\mu$ channel

B.2.1 Variable inclusive in one bin

Bin [GeV]	Measured $d\sigma/dx$ [pb/unit]	Statistical Data [%]	Statistical MC Bkg [%]	Statistical MC Sig [%]	Systematic [%]
[0,1]	1.1956	+/- 1.2	+/- 0.4	+/- 0.3	+6.4/-5.6

Table B.36 Per-bin total statistical and systematic uncertainties in $\mu\mu$ for inclusive (one bin), without modelling systematic uncertainties.

Bin [GeV]	Measured $d\sigma/dx$ [pb/unit]	Statistical Data [%]	Statistical MC Bkg [%]	Statistical MC Sig [%]	Systematic [%]
[0,1]	1.1956	+/- 1.2	+/- 0.4	+/- 0.3	+9.2/-8.7

Table B.37 Per-bin total statistical and systematic uncertainties in $\mu\mu$ for inclusive (one bin), with modelling systematic uncertainties.

Bin [GeV]	Measured $d\sigma/dx$ [pb/unit]	Statistical Data [%]	Total Syst Up [%]	Total Syst Down [%]	GenTTbarPowhegPythia6AFII [%]	GenTTbarPowhegHerwig [%]	GenTTbarMC@NLOHerwig [%]
[0,1]	1.1956	+/- 1.2	6.4	-5.6	-17.9	-8.4	-24.5

Table B.38 Per-bin total statistical and systematic uncertainties in $\mu\mu$ for inclusive (one bin), with generators, without normalisation.

Bin [GeV]	Measured $d\sigma/dx$ [pb/unit]	Statistical Data [%]	Total Syst Up [%]	Total Syst Down [%]	GenTTbarPowhegPythia6AFII [%]	GenTTbarPowhegHerwig [%]	GenTTbarMC@NLOHerwig [%]
[0,1]	1.0000	+/- 1.2	0.0	0.0	0.0	0.0	0.0

Table B.39 Per-bin total statistical and systematic uncertainties in $\mu\mu$ for inclusive (one bin), with generators, with all distributions normalised to unit area.

Uncertainty	[0,1]
StatisticalData	[-1.21,1.21]
StatisticalBkg	[-0.45,0.45]
StatisticalSig	[-0.34,0.35]
BTag	[-4.90,5.94]
Jeff	[-0.01,0.01]
Jer	[-0.22,0.22]
MuidRes	[-0.03,0.03]
MumsRes	[-0.05,0.05]
BJesUnc	[-0.67,0.76]
JesEffectiveStat1	[-0.51,0.43]
JesEffectiveStat2	[-0.02,0.02]
JesEffectiveStat3	[-0.10,0.13]
JesEffectiveStat4	[-0.15,0.15]
JesEffectiveModel1	[-1.74,1.42]
JesEffectiveModel2	[-0.01,0.01]
JesEffectiveModel3	[-0.00,0.00]
JesEffectiveModel4	[-0.05,0.08]
JesEffectiveDet1	[-0.34,0.35]
JesEffectiveDet2	[-0.11,0.09]
JesEffectiveDet3	[-0.04,0.05]
JesEffectiveMix1	[-0.32,0.34]
JesEffectiveMix2	[-0.19,0.22]
JesEffectiveMix3	[-0.01,0.01]
JesEffectiveMix4	[-0.02,0.03]
EtaIntercalibrationModel	[-0.29,0.33]
EtaIntercalibrationTotalStat	[-0.38,0.38]
PileupOffsetMu	[-0.14,0.11]
PileupOffsetNPV	[-0.15,0.15]
PileupRho	[-1.28,1.05]
PunchThrough	[-0.00,0.00]
CTauTag	[-0.04,0.04]
ElectronEnergyResolution	[-0.00,0.00]
ElectronEnergyScale	[-0.04,0.00]
ElectronIdSF	[-0.00,0.00]
ElectronRecoSF	[0.00,0.00]
ElectronTriggerSF	[-0.00,0.00]
FlavorComp	[-1.00,0.69]
FlavorResponse	[-0.64,0.40]
JetVertexFraction	[-0.31,0.33]
Mistag	[-0.10,0.10]
MuonIdSF	[-0.11,0.11]
MuonRecoSF	[-0.05,0.05]
MuonTriggerSF	[-0.06,0.06]
Musc	[-0.06,0.01]
ModellingGenerator	[-0.09,0.09]
ModellingParton	[-0.56,0.56]
ModellingRadiation	[-4.20,4.20]
ModellingSingleTopWtNormalisation	[-0.69,0.69]
ModellingSingleTopWtInterference	[-5.14,5.14]

Table B.40 Per-bin individual statistical and systematic uncertainties in $\mu\mu$ for inclusive (one bin).

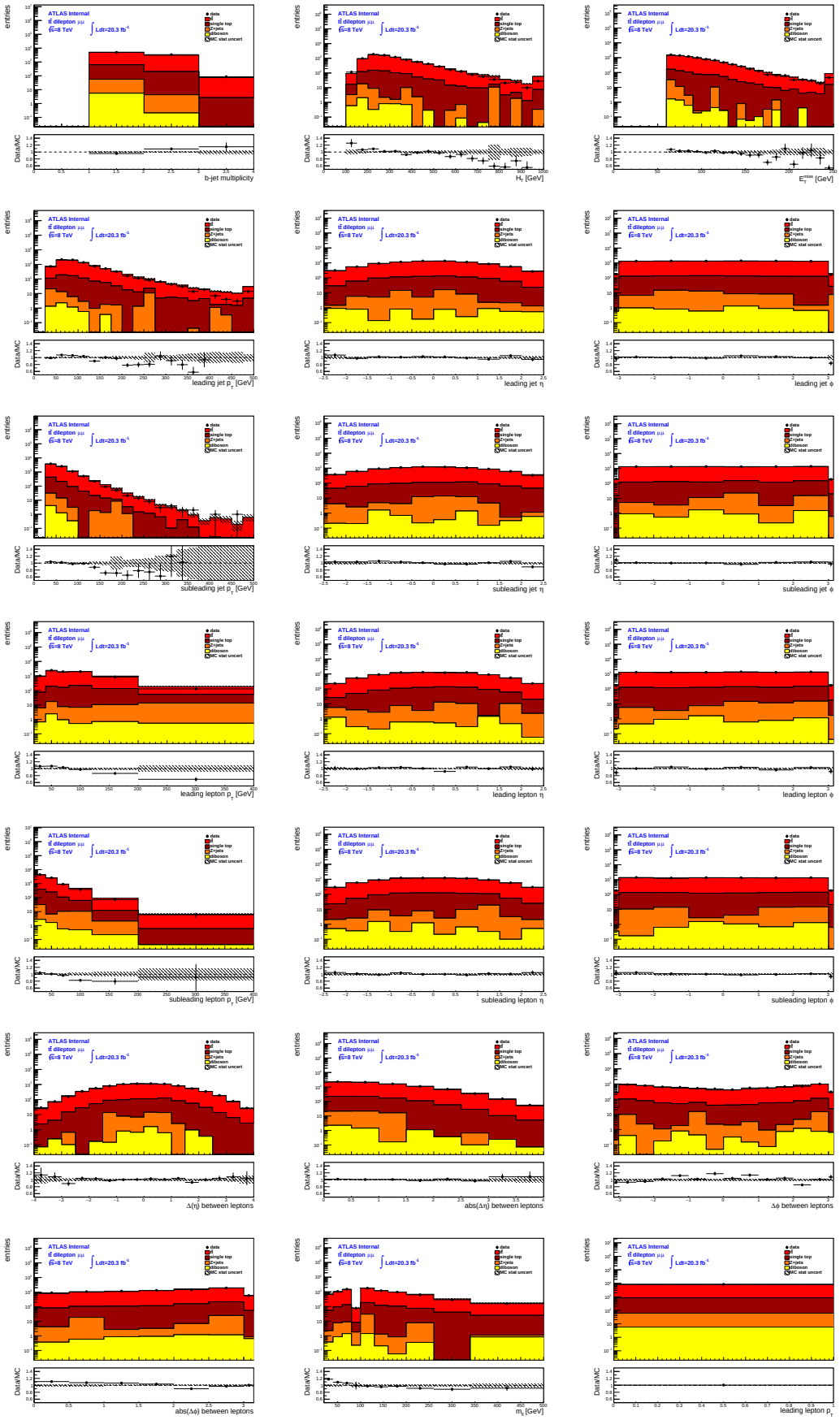

Fig. B.23 Stacked plots per bin (not scaled to density) for channel $\mu\mu$ for the Nominal MC (no syst).

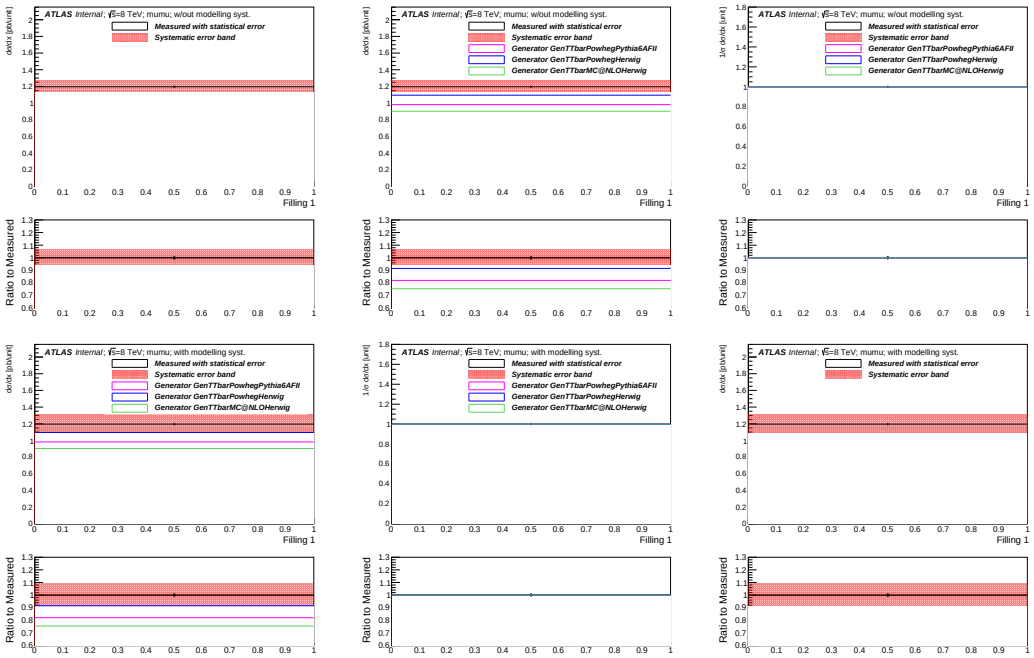

Fig. B.24 Differential cross-section for channel $\mu\mu$ in the variable of inclusive in one bin.

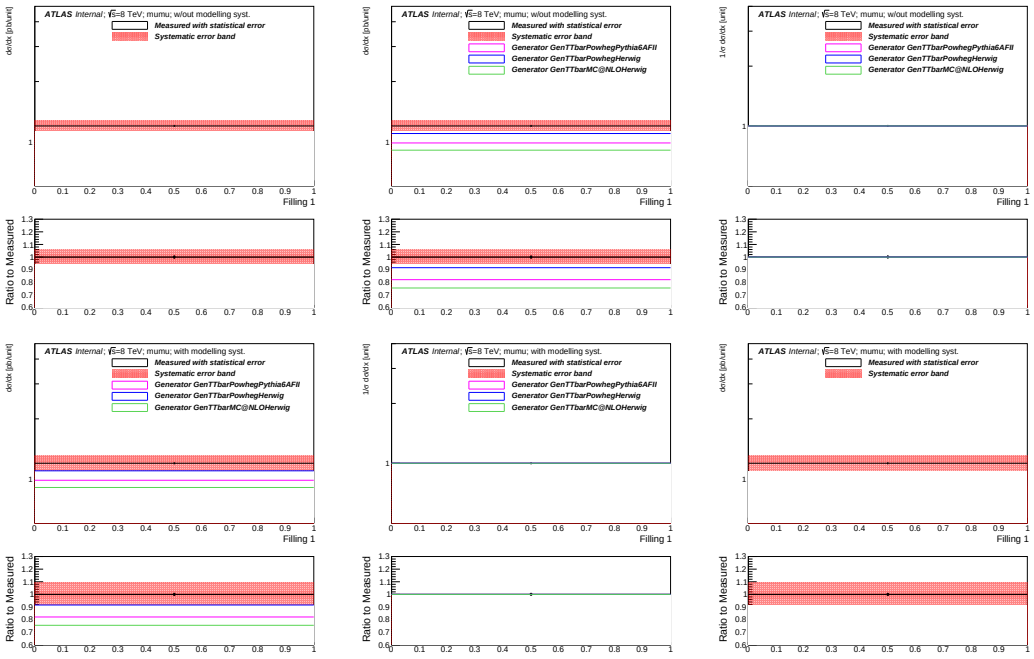

Fig. B.25 Differential cross-section for channel $\mu\mu$ in the variable of inclusive in one bin (log on y axis).

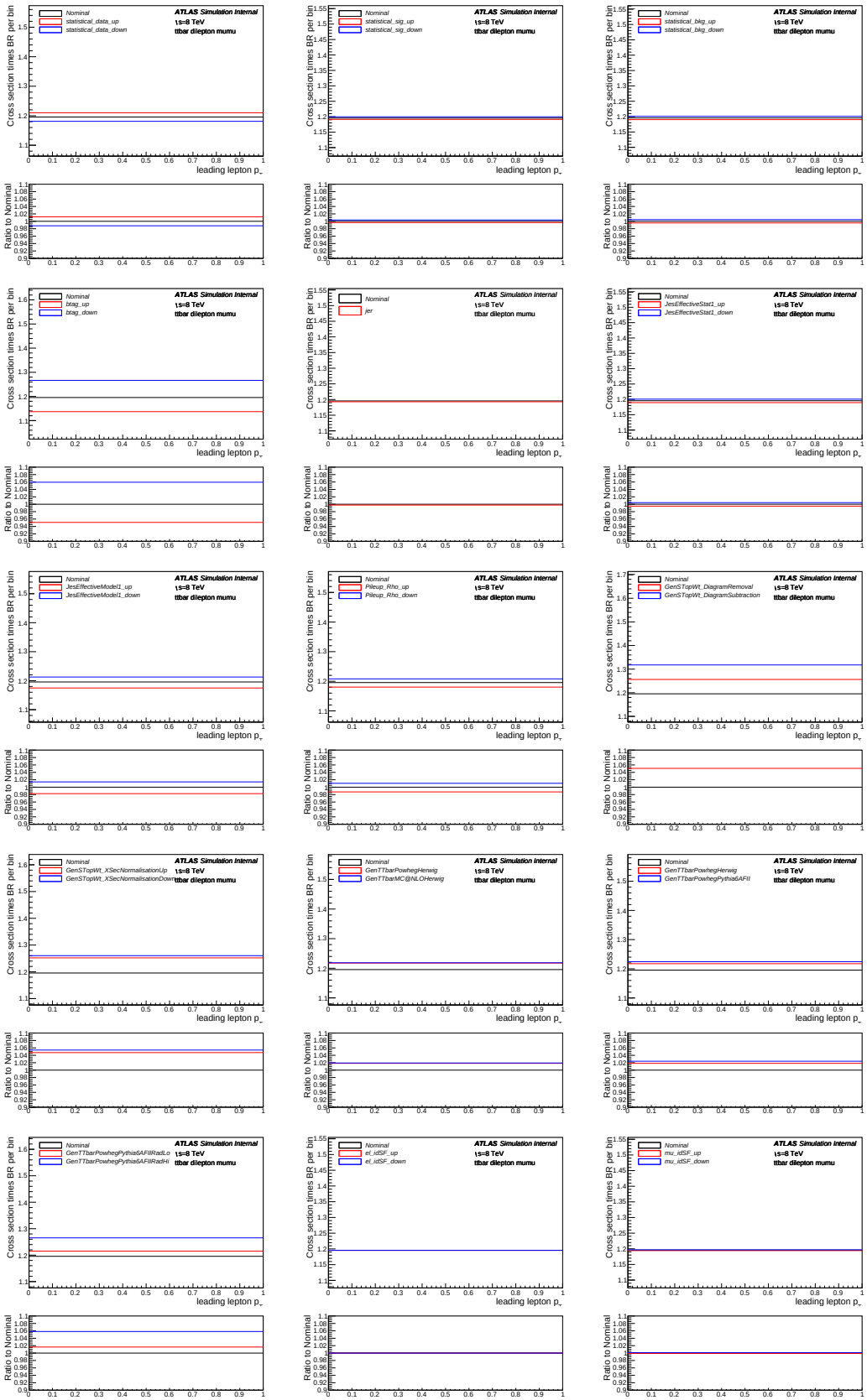

Fig. B.26 Differential cross-section per bin (not scaled to density) for channel $\mu\mu$ in the variable of inclusive in one bin with measured (with Nominal signal) overlaid with statistical uncertainties on data and MC (signal and background), as well as various systematics.

B.2.2 Variable dilepton invariant mass (m_{ll})

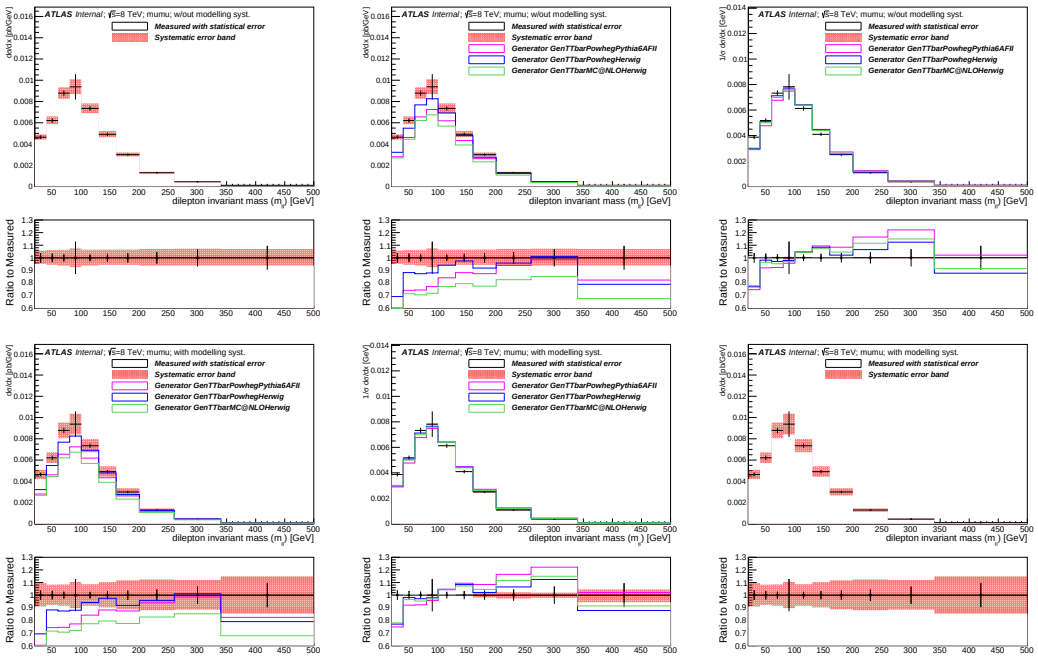

Fig. B.27 Differential cross-section for channel $\mu\mu$ in the variable of dilepton invariant mass (m_{ll}).

Bin [GeV]	Measured $d\sigma/dx$ [pb/GeV]	Statistical Data [%]	Statistical MC Bkg [%]	Statistical MC Sig [%]	Systematic [%]
[20,40]	0.0046	+/- 3.8	+/- 0.8	+/- 1.2	+5.8/-4.8
[40,60]	0.0062	+/- 3.4	+/- 1.0	+/- 1.0	+6.3/-5.5
[60,80]	0.0088	+/- 2.8	+/- 0.7	+/- 0.8	+6.4/-6.2
[80,100]	0.0094	+/- 12.8	+/- 4.4	+/- 4.6	+7.6/-7.3
[100,130]	0.0073	+/- 2.7	+/- 1.3	+/- 0.7	+6.5/-6.1
[130,160]	0.0049	+/- 3.2	+/- 0.7	+/- 0.9	+6.5/-5.5
[160,200]	0.0030	+/- 3.6	+/- 0.9	+/- 1.0	+6.6/-5.6
[200,260]	0.0013	+/- 4.6	+/- 2.2	+/- 1.2	+7.1/-6.2
[260,340]	0.0004	+/- 6.9	+/- 1.7	+/- 1.7	+7.3/-6.1
[340,500]	0.0001	+/- 9.5	+/- 3.0	+/- 2.6	+7.0/-6.1

Table B.41 Per-bin total statistical and systematic uncertainties in $\mu\mu$ for the dilepton invariant mass (m_{ll}), without modelling systematic uncertainties.

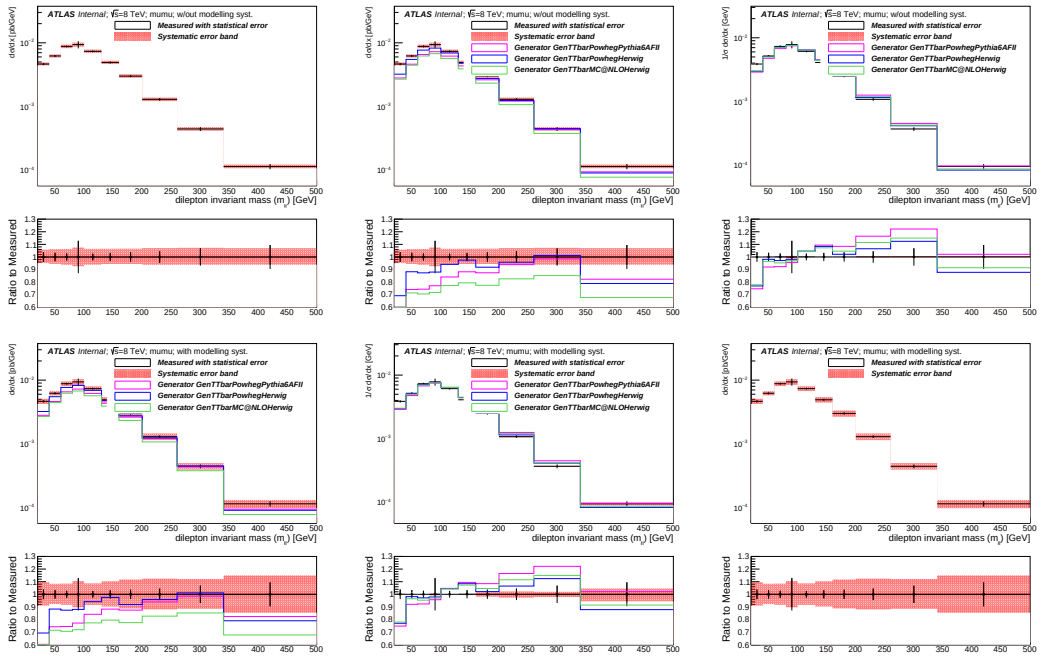

Fig. B.28 Differential cross-section for channel $\mu\mu$ in the variable of dilepton invariant mass (m_{ll}) (log on y axis).

Bin [GeV]	Measured $d\sigma/dx$ [pb/GeV]	Statistical Data [%]	Statistical MC Bkg [%]	Statistical MC Sig [%]	Systematic [%]
[20,40]	0.0046	+/- 3.8	+/- 0.8	+/- 1.2	+9.6/-9.0
[40,60]	0.0062	+/- 3.4	+/- 1.0	+/- 1.0	+8.3/-7.8
[60,80]	0.0088	+/- 2.8	+/- 0.7	+/- 0.8	+8.5/-8.4
[80,100]	0.0094	+/- 12.8	+/- 4.4	+/- 4.6	+10.5/-10.3
[100,130]	0.0073	+/- 2.7	+/- 1.3	+/- 0.7	+8.7/-8.4
[130,160]	0.0049	+/- 3.2	+/- 0.7	+/- 0.9	+10.3/-9.7
[160,200]	0.0030	+/- 3.6	+/- 0.9	+/- 1.0	+11.7/-11.2
[200,260]	0.0013	+/- 4.6	+/- 2.2	+/- 1.2	+12.4/-11.9
[260,340]	0.0004	+/- 6.9	+/- 1.7	+/- 1.7	+12.1/-11.4
[340,500]	0.0001	+/- 9.5	+/- 3.0	+/- 2.6	+15.0/-14.6

Table B.42 Per-bin total statistical and systematic uncertainties in $\mu\mu$ for the dilepton invariant mass (m_{ll}), with modelling systematic uncertainties.

Bin [GeV]	Measured $d\sigma/dx$ [pb/GeV]	Statistical Data [%]	Total Syst Up [%]	Total Syst Down [%]	GenTTbarPowhegPythia6AFII [%]	GenTTbarPowhegHerwig [%]	GenTTbarMC@NLOHerwig [%]
[20,40]	0.0046	+/- 3.8	5.8	-4.8	-39.6	-30.7	-42.1
[40,60]	0.0062	+/- 3.4	6.3	-5.5	-25.7	-11.7	-28.4
[60,80]	0.0088	+/- 2.8	6.4	-6.2	-25.5	-12.6	-29.3
[80,100]	0.0094	+/- 12.8	7.6	-7.3	-22.8	-11.9	-28.1
[100,130]	0.0073	+/- 2.7	6.5	-6.1	-15.8	-5.8	-22.6
[130,160]	0.0049	+/- 3.2	6.5	-5.5	-11.7	-2.5	-20.5
[160,200]	0.0030	+/- 3.6	6.6	-5.6	-12.5	-8.1	-22.4
[200,260]	0.0013	+/- 4.6	7.1	-6.2	-6.0	-4.2	-17.3
[260,340]	0.0004	+/- 6.9	7.3	-6.1	-1.4	1.2	-14.8
[340,500]	0.0001	+/- 9.5	7.0	-6.1	-17.6	-21.0	-32.2

Table B.43 Per-bin total statistical and systematic uncertainties in $\mu\mu$ for the dilepton invariant mass (m_{ll}), with generators, without normalisation.

Bin [GeV]	Measured $d\sigma/dx$ [pb/GeV]	Statistical Data [%]	Total Syst Up [%]	Total Syst Down [%]	GenTTbarPowhegPythia6AFII [%]	GenTTbarPowhegHerwig [%]	GenTTbarMC@NLOHerwig [%]
[20,40]	0.0039	+/- 3.8	-0.8	1.3	-25.2	-22.9	-22.0
[40,60]	0.0052	+/- 3.4	-0.3	0.6	-7.9	-1.8	-3.5
[60,80]	0.0073	+/- 2.8	-0.3	-0.2	-7.6	-2.8	-4.7
[80,100]	0.0078	+/- 12.8	0.9	-1.4	-4.3	-2.1	-3.0
[100,130]	0.0061	+/- 2.7	-0.2	-0.1	4.3	4.7	4.3
[130,160]	0.0041	+/- 3.2	-0.1	0.5	9.4	8.4	7.3
[160,200]	0.0025	+/- 3.6	-0.0	0.5	8.4	2.2	4.6
[200,260]	0.0011	+/- 4.6	0.4	-0.2	16.5	6.5	11.5
[260,340]	0.0004	+/- 6.9	0.6	-0.1	22.2	12.4	15.0
[340,500]	0.0001	+/- 9.5	0.3	-0.1	2.1	-12.1	-8.5

Table B.44 Per-bin total statistical and systematic uncertainties in $\mu\mu$ for the dilepton invariant mass (m_{ll}), with generators, with all distributions normalised to unit area.

Uncertainty	[20,40]	[40,60]	[60,80]	[80,100]	[100,130]	[130,160]	[160,200]	[200,260]	[260,340]	[340,500]
StatisticalData	[-3.85,3.85]	[-3.37,3.37]	[-2.82,2.82]	[-12.82,12.82]	[-2.65,2.65]	[-3.23,3.23]	[-3.65,3.65]	[-4.55,4.55]	[-6.88,6.88]	[-9.50,9.50]
StatisticalBkg	[-0.76,0.76]	[-0.96,0.96]	[-0.73,0.73]	[-4.42,4.42]	[-1.33,1.33]	[-0.71,0.71]	[-0.87,0.87]	[-2.18,2.18]	[-1.68,1.68]	[-3.01,3.01]
StatisticalSig	[-1.22,1.25]	[-0.95,0.97]	[-0.80,0.81]	[-4.22,4.61]	[-0.72,0.73]	[-0.86,0.87]	[-0.97,0.99]	[-1.15,1.18]	[-1.67,1.73]	[-2.48,2.61]
BTag	[-4.60,5.60]	[-4.91,5.95]	[-4.55,5.55]	[-4.17,5.24]	[-4.88,5.91]	[-4.95,5.99]	[-5.13,6.21]	[-5.56,6.65]	[-5.39,6.56]	[-5.28,6.40]
Jeff	[-0.11,0.11]	[-0.03,0.03]	[-0.02,0.02]	[-0.32,0.32]	[-0.05,0.05]	[-0.00,0.00]	[-0.01,0.01]	[-0.02,0.02]	[-0.01,0.01]	[-0.14,0.14]
Jer	[-0.13,0.13]	[-0.53,0.53]	[-0.83,0.83]	[-2.41,2.41]	[-0.53,0.53]	[-0.49,0.49]	[-0.26,0.26]	[-0.09,0.09]	[-0.34,0.34]	[-0.12,0.12]
MuidRes	[-0.07,0.07]	[-0.01,0.01]	[-0.03,0.03]	[-1.46,1.46]	[-0.03,0.03]	[-0.09,0.09]	[-0.03,0.03]	[-0.05,0.05]	[-0.01,0.01]	[-0.21,0.21]
MumsRes	[-0.06,0.06]	[-0.26,0.26]	[-0.04,0.04]	[-3.29,3.29]	[-0.22,0.22]	[-0.45,0.45]	[-0.02,0.02]	[-0.06,0.06]	[-1.14,1.14]	[-1.58,1.58]
BJesUnc	[-0.17,0.47]	[-0.65,0.58]	[-0.79,0.99]	[-1.08,0.36]	[-0.80,0.66]	[-0.64,0.80]	[-0.67,0.82]	[-1.09,0.70]	[-1.06,1.06]	[-0.60,0.49]
JesEffectiveStat1	[-0.17,0.19]	[-0.59,0.21]	[-0.59,0.58]	[-0.52,0.81]	[-0.58,0.50]	[-0.56,0.46]	[-0.61,0.47]	[-0.44,0.40]	[-0.11,0.44]	[-1.00,0.42]
JesEffectiveStat2	[-0.06,0.06]	[-0.01,0.06]	[-0.07,0.00]	[-0.05,0.25]	[-0.02,0.02]	[-0.03,0.01]	[-0.05,0.11]	[-0.03,0.03]	[-0.03,0.03]	[-0.11,0.11]
JesEffectiveStat3	[-0.03,0.03]	[-0.22,0.14]	[-0.09,0.16]	[-0.23,0.23]	[-0.07,0.09]	[-0.13,0.13]	[-0.12,0.16]	[-0.06,0.11]	[-0.11,0.28]	[-0.21,0.00]
JesEffectiveStat4	[-0.00,0.11]	[-0.18,0.14]	[-0.31,0.17]	[-0.33,0.49]	[-0.09,0.12]	[-0.15,0.12]	[-0.13,0.23]	[-0.02,0.17]	[-0.17,0.05]	[-0.31,0.21]
JesEffectiveModel1	[-0.99,1.00]	[-1.27,0.93]	[-2.28,1.76]	[-2.11,0.70]	[-2.42,1.46]	[-1.54,1.67]	[-1.21,1.34]	[-1.66,1.30]	[-1.64,1.71]	[-1.09,1.15]
JesEffectiveModel2	[-0.06,0.06]	[-0.01,0.07]	[-0.06,0.06]	[-0.25,0.25]	[-0.05,0.00]	[-0.03,0.03]	[-0.06,0.12]	[-0.04,0.04]	[-0.05,0.00]	[-0.02,0.01]
JesEffectiveModel3	[-0.04,0.04]	[-0.03,0.03]	[-0.13,0.13]	[-0.11,0.31]	[-0.03,0.06]	[-0.08,0.03]	[-0.03,0.15]	[-0.06,0.03]	[-0.03,0.21]	[-0.20,0.20]
JesEffectiveModel4	[-0.03,0.03]	[-0.04,0.07]	[-0.07,0.07]	[-0.20,0.40]	[-0.04,0.04]	[-0.08,0.12]	[-0.08,0.17]	[-0.04,0.04]	[-0.08,0.08]	[-0.07,0.07]
JesEffectiveDet1	[-0.08,0.22]	[-0.45,0.40]	[-0.41,0.39]	[-0.32,0.52]	[-0.26,0.28]	[-0.47,0.32]	[-0.30,0.38]	[-0.38,0.39]	[-0.17,0.41]	[-0.45,0.37]
JesEffectiveDet2	[-0.09,0.09]	[-0.18,0.11]	[-0.32,0.14]	[-0.11,0.28]	[-0.04,0.05]	[-0.10,0.01]	[-0.12,0.16]	[-0.07,0.07]	[-0.11,0.11]	[-0.13,0.18]
JesEffectiveDet3	[-0.06,0.06]	[-0.01,0.06]	[-0.05,0.04]	[-0.01,0.21]	[-0.04,0.01]	[-0.08,0.08]	[-0.07,0.16]	[-0.00,0.02]	[-0.07,0.02]	[-0.09,0.09]
JesEffectiveMix1	[-0.09,0.19]	[-0.36,0.28]	[-0.40,0.40]	[-0.33,0.72]	[-0.29,0.31]	[-0.50,0.32]	[-0.27,0.39]	[-0.21,0.43]	[-0.12,0.43]	[-0.57,0.29]
JesEffectiveMix2	[-0.11,0.17]	[-0.24,0.14]	[-0.31,0.30]	[-0.31,0.34]	[-0.12,0.18]	[-0.31,0.19]	[-0.15,0.22]	[-0.12,0.29]	[-0.01,0.27]	[-0.40,0.30]
JesEffectiveMix3	[-0.07,0.07]	[-0.00,0.01]	[-0.12,0.02]	[-0.16,0.16]	[-0.05,0.01]	[-0.08,0.06]	[-0.03,0.09]	[-0.06,0.06]	[-0.10,0.10]	[-0.02,0.05]
JesEffectiveMix4	[-0.06,0.06]	[-0.03,0.03]	[-0.01,0.01]	[-0.00,0.00]	[-0.03,0.01]	[-0.06,0.04]	[-0.01,0.09]	[-0.02,0.02]	[-0.00,0.01]	[-0.00,0.00]
EtaIntercalibrationModel	[-0.00,0.22]	[-0.52,0.14]	[-0.59,0.46]	[-0.28,0.18]	[-0.40,0.45]	[-0.40,0.34]	[-0.42,0.33]	[-1.06,1.06]	[-0.02,0.30]	[-0.46,0.50]
EtaIntercalibrationTotalStat	[-0.19,0.17]	[-0.46,0.27]	[-0.53,0.44]	[-0.40,1.01]	[-0.42,0.43]	[-0.50,0.42]	[-0.26,0.34]	[-0.16,0.41]	[-0.27,0.42]	[-0.53,0.46]
PileupOffsetMu	[-0.25,0.25]	[-0.12,0.12]	[-0.26,0.17]	[-0.32,0.33]	[-0.15,0.21]	[-0.15,0.02]	[-0.09,0.27]	[-0.21,0.21]	[-0.18,0.17]	[-0.08,0.22]
PileupOffsetNPV	[-0.02,0.12]	[-0.23,0.23]	[-0.64,0.64]	[-0.48,0.48]	[-0.34,0.34]	[-0.22,0.18]	[-0.21,0.24]	[-0.38,0.21]	[-0.81,0.81]	[-0.50,0.50]
PileupRho	[-0.57,0.62]	[-0.96,0.80]	[-1.98,1.38]	[-1.46,0.80]	[-1.59,1.08]	[-0.98,1.11]	[-1.07,1.00]	[-1.16,1.07]	[-1.11,0.88]	[-1.43,1.09]
PunchThrough	[-0.04,0.04]	[-0.02,0.00]	[-0.01,0.01]	[-0.01,0.01]	[-0.01,0.01]	[-0.01,0.01]	[-0.01,0.01]	[-0.00,0.00]	[-0.05,0.05]	[-0.05,0.00]
CTauTag	[-0.04,0.04]	[-0.04,0.04]	[-0.07,0.07]	[-0.00,0.00]	[-0.05,0.05]	[-0.03,0.03]	[-0.03,0.03]	[-0.02,0.02]	[-0.04,0.04]	[-0.07,0.07]
ElectronEnergyResolution	[0.00,0.00]	[0.00,0.02]	[0.00,0.00]	[0.00,0.00]	[0.00,0.00]	[0.00,0.00]	[-0.00,0.00]	[0.00,0.00]	[0.00,0.00]	[0.00,0.00]
ElectronEnergyScale	[-0.01,0.01]	[-0.01,0.02]	[-0.01,0.00]	[0.00,0.00]	[-0.18,0.01]	[0.00,0.00]	[-0.00,0.00]	[-0.00,0.00]	[-0.01,0.00]	[-0.00,0.00]
ElectronIdSF	[-0.00,0.00]	[-0.00,0.00]	[-0.00,0.00]	[-0.00,0.00]	[-0.00,0.00]	[0.00,0.00]	[0.00,0.00]	[0.00,0.00]	[0.00,0.00]	[0.00,0.00]
ElectronRecoSF	[-0.00,0.00]	[-0.00,0.00]	[-0.00,0.00]	[0.00,0.00]	[0.00,0.00]	[0.00,0.00]	[0.00,0.00]	[0.00,0.00]	[0.00,0.00]	[0.00,0.00]
ElectronTriggerSF	[-0.00,0.00]	[-0.00,0.00]	[-0.00,0.00]	[0.00,0.00]	[0.00,0.00]	[0.00,0.00]	[0.00,0.00]	[0.00,0.00]	[0.00,0.00]	[0.00,0.00]
FlavorComp	[-0.57,0.58]	[-0.90,0.90]	[-1.89,0.95]	[-1.41,0.48]	[-1.46,1.22]	[-0.53,0.66]	[-0.50,0.38]	[-0.37,0.25]	[-0.74,1.16]	[-0.29,0.92]
FlavorResponse	[-0.28,0.42]	[-0.62,0.62]	[-1.22,0.62]	[-0.82,0.45]	[-0.86,0.44]	[-0.34,0.53]	[-0.40,0.23]	[-0.16,0.28]	[-0.69,0.99]	[-0.67,0.55]
JetVertexFraction	[-0.26,0.19]	[-0.22,0.29]	[-0.25,0.26]	[-0.47,0.47]	[-0.33,0.37]	[-0.28,0.35]	[-0.30,0.41]	[-0.53,0.47]	[-0.35,0.23]	[-0.51,0.62]
Mistag	[-0.08,0.08]	[-0.08,0.08]	[-0.04,0.04]	[-0.07,0.07]	[-0.18,0.18]	[-0.08,0.08]	[-0.09,0.09]	[-0.24,0.24]	[-0.07,0.07]	[-0.09,0.09]
MuonIdSF	[-0.07,0.07]	[-0.10,0.10]	[-0.10,0.09]	[-0.12,0.12]	[-0.12,0.12]	[-0.11,0.11]	[-0.12,0.12]	[-0.14,0.14]	[-0.17,0.16]	[-0.19,0.19]
MuonRecoSF	[-0.03,0.03]	[-0.05,0.05]	[-0.04,0.04]	[-0.03,0.03]	[-0.05,0.05]	[-0.05,0.05]	[-0.06,0.06]	[-0.07,0.07]	[-0.09,0.09]	[-0.11,0.11]
MuonTriggerSF	[-0.04,0.04]	[-0.06,0.06]	[-0.06,0.06]	[-0.07,0.07]	[-0.07,0.07]	[-0.07,0.07]	[-0.07,0.07]	[-0.09,0.09]	[-0.09,0.09]	[-0.09,0.09]
Musc	[-0.02,0.07]	[-0.02,0.02]	[-0.08,0.01]	[-2.32,2.32]	[-0.13,0.01]	[-0.03,0.04]	[-0.14,0.08]	[-0.14,0.14]	[-0.14,0.04]	[-0.15,0.15]
ModellingGenerator	[-1.38,1.38]	[-0.48,0.48]	[-2.11,2.11]	[-4.15,4.15]	[-0.09,0.09]	[-0.87,0.87]	[-2.86,2.86]	[-1.36,1.36]	[-1.44,1.44]	[-4.58,4.58]
ModellingParton	[-0.32,0.32]	[-0.74,0.74]	[-0.14,0.14]	[-2.99,2.99]	[-0.35,0.35]	[-1.72,1.72]	[-2.70,2.70]	[-1.92,1.92]	[-4.18,4.18]	[-3.50,3.50]
ModellingRadiation	[-6.75,6.75]	[-2.42,2.42]	[-2.20,2.20]	[-3.53,3.53]	[-3.18,3.18]	[-5.28,5.28]	[-6.04,6.04]	[-8.12,8.12]	[-1.01,1.01]	[-6.26,6.26]
ModellingSingleTopWtNormalisation	[-0.43,0.43]	[-0.64,0.64]	[-0.62,0.62]	[-0.48,0.48]	[-0.63,0.63]	[-0.74,0.74]	[-0.86,0.86]	[-0.75,0.75]	[-1.13,1.13]	[-1.35,1.35]
ModellingSingleTopWtInterference	[-3.21,3.21]	[-4.81,4.81]	[-4.65,4.65]	[-3.61,3.61]	[-4.73,4.73]	[-5.52,5.52]	[-6.39,6.39]	[-5.61,5.61]	[-8.42,8.42]	[-10.06,10.06]

Table B.45 Per-bin individual statistical and systematic uncertainties in $\mu\mu$ for the dilepton invariant mass (m_{ll}).

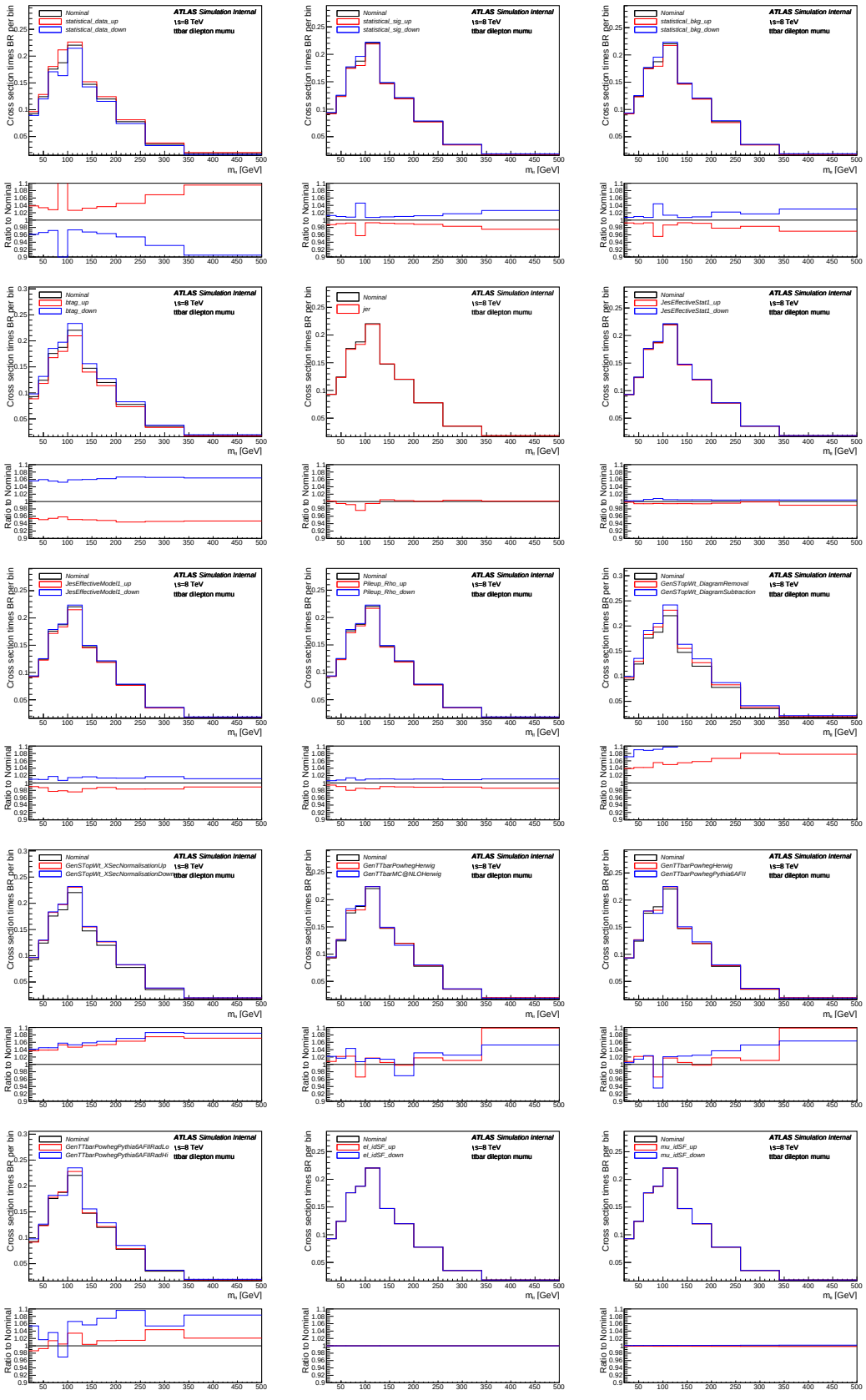

Fig. B.29 Differential cross-section per bin (not scaled to density) for channel $\mu\mu$ in the variable of dilepton invariant mass (m_{ll}) with measured (with Nominal signal) overlaid with statistical uncertainties on data and MC (signal and background), as well as various systematics.

B.2.3 Variable p_{T} of leading lepton

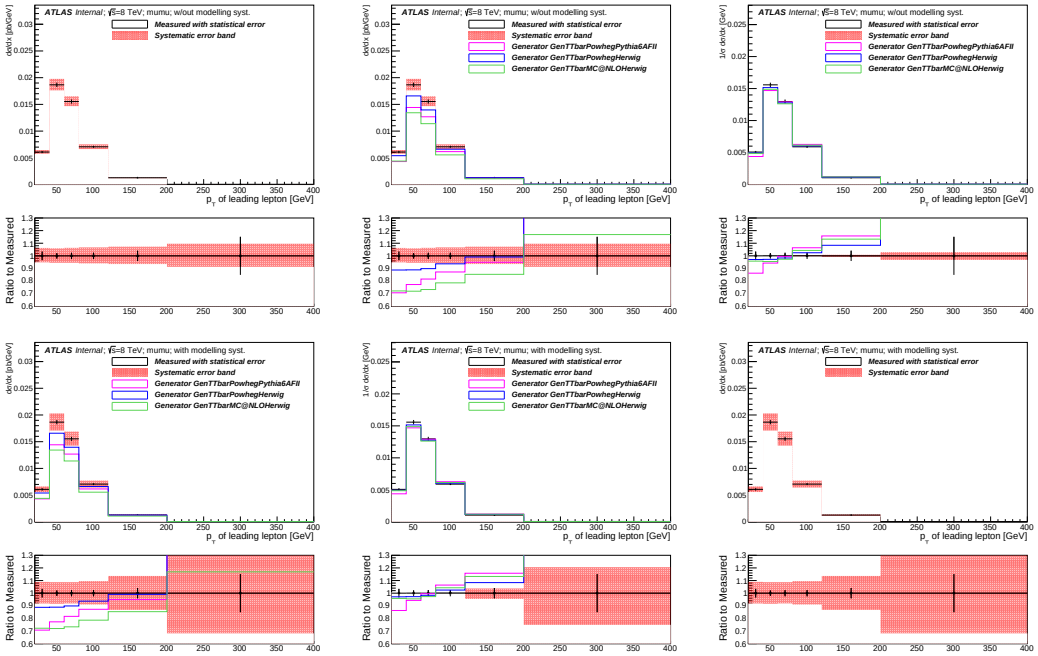

Fig. B.30 Differential cross-section for channel $\mu\mu$ in the variable of p_{T} of leading lepton.

Bin [GeV]	Measured $d\sigma/dx$ [pb/GeV]	Statistical Data [%]	Statistical MC Bkg [%]	Statistical MC Sig [%]	Systematic [%]
[20,40]	0.0061	+/- 3.4	+/- 0.8	+/- 1.0	+6.3/-5.2
[40,60]	0.0187	+/- 2.2	+/- 0.8	+/- 0.7	+6.0/-5.5
[60,80]	0.0155	+/- 2.5	+/- 0.6	+/- 0.7	+6.4/-5.5
[80,120]	0.0071	+/- 2.5	+/- 0.7	+/- 0.7	+6.7/-6.0
[120,200]	0.0013	+/- 4.1	+/- 2.0	+/- 1.0	+7.3/-6.5
[200,400]	0.0000	+/- 15.1	+/- 17.7	+/- 2.6	+9.6/-8.7

Table B.46 Per-bin total statistical and systematic uncertainties in $\mu\mu$ for the leading lepton p_T, without modelling systematic uncertainties.

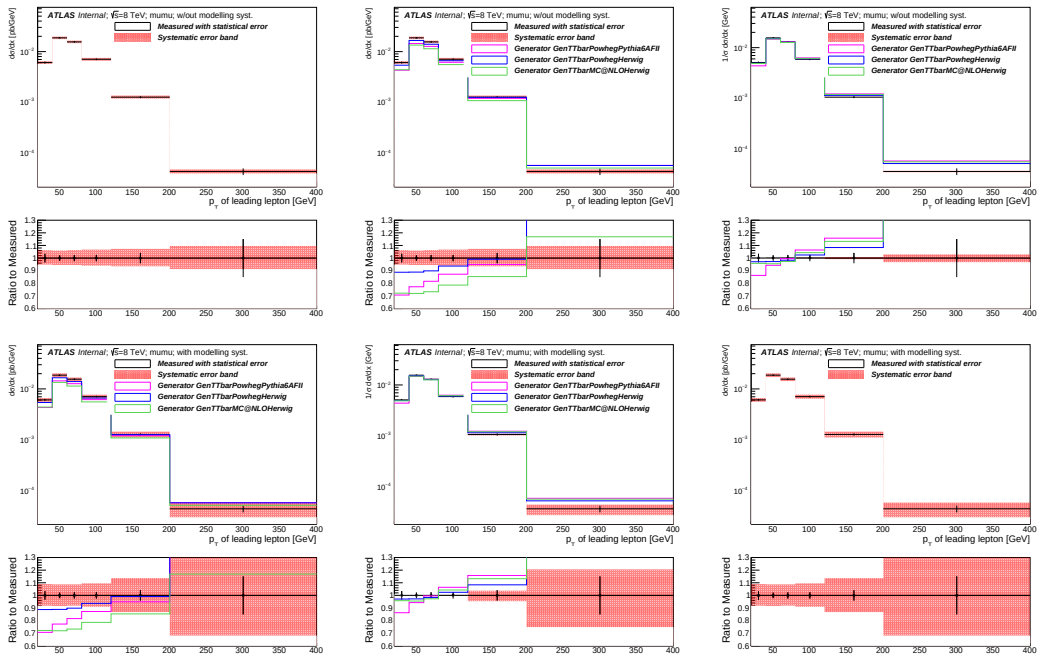

Fig. B.31 Differential cross-section for channel $\mu\mu$ in the variable of p_{T} of leading lepton (log on y axis).

Bin [GeV]	Measured $d\sigma/dx$ [pb/GeV]	Statistical Data [%]	Statistical MC Bkg [%]	Statistical MC Sig [%]	Systematic [%]
[20,40]	0.0061	+/- 3.4	+/- 0.8	+/- 1.0	+8.9/-8.2
[40,60]	0.0187	+/- 2.2	+/- 0.8	+/- 0.7	+8.7/-8.4
[60,80]	0.0155	+/- 2.5	+/- 0.6	+/- 0.7	+8.7/-8.1
[80,120]	0.0071	+/- 2.5	+/- 0.7	+/- 0.7	+9.5/-9.0
[120,200]	0.0013	+/- 4.1	+/- 2.0	+/- 1.0	+13.6/-13.2
[200,400]	0.0000	+/- 15.1	+/- 17.7	+/- 2.6	+32.1/-31.8

Table B.47 Per-bin total statistical and systematic uncertainties in $\mu\mu$ for the leading lepton p_T, with modelling systematic uncertainties.

Bin [GeV]	Measured $d\sigma/dx$ [pb/GeV]	Statistical Data [%]	Total Syst Up [%]	Total Syst Down [%]	GenTTbarPowhegPythia6AFII [%]	GenTTbarPowhegHerwig [%]	GenTTbarMC@NLOHerwig [%]
[20,40]	0.0061	+/- 3.4	6.3	-5.2	-29.3	-11.2	-27.8
[40,60]	0.0187	+/- 2.2	6.0	-5.5	-22.7	-11.1	-28.0
[60,80]	0.0155	+/- 2.5	6.4	-5.5	-18.4	-10.1	-26.7
[80,120]	0.0071	+/- 2.5	6.7	-6.0	-12.8	-6.3	-21.4
[120,200]	0.0013	+/- 4.1	7.3	-6.5	-5.1	-0.9	-14.6
[200,400]	0.0000	+/- 15.1	9.6	-8.7	31.9	31.1	16.9

Table B.48 Per-bin total statistical and systematic uncertainties in $\mu\mu$ for the leading lepton p_T, with generators, without normalisation.

Bin [GeV]	Measured $d\sigma/dx$ [pb/GeV]	Statistical Data [%]	Total Syst Up [%]	Total Syst Down [%]	GenTTbarPowhegPythia6AFII [%]	GenTTbarPowhegHerwig [%]	GenTTbarMC@NLOHerwig [%]
[20,40]	0.0051	+/- 3.4	-0.1	0.6	-13.7	-2.9	-4.2
[40,60]	0.0156	+/- 2.2	-0.4	0.2	-5.7	-2.8	-4.5
[60,80]	0.0130	+/- 2.5	-0.1	0.2	-0.4	-1.7	-2.7
[80,120]	0.0059	+/- 2.5	0.3	-0.3	6.4	2.5	4.3
[120,200]	0.0011	+/- 4.1	0.8	-0.8	15.8	8.4	13.2
[200,400]	0.0000	+/- 15.1	3.0	-3.2	60.9	43.4	55.0

Table B.49 Per-bin total statistical and systematic uncertainties in $\mu\mu$ for the leading lepton p_T, with generators, with all distributions normalised to unit area.

Uncertainty	[20,40]	[40,60]	[60,80]	[80,120]	[120,200]	[200,400]
StatisticalData	[-3.41,3.41]	[-2.19,2.19]	[-2.46,2.46]	[-2.50,2.50]	[-4.09,4.09]	[-15.08,15.08]
StatisticalBkg	[-0.82,0.82]	[-0.82,0.82]	[-0.57,0.57]	[-0.69,0.69]	[-1.98,1.98]	[-17.70,17.70]
StatisticalSig	[-1.00,1.02]	[-0.66,0.67]	[-0.72,0.73]	[-0.68,0.69]	[-1.00,1.02]	[-2.46,2.58]
BTag	[-4.43,5.40]	[-4.44,5.44]	[-4.83,5.87]	[-5.20,6.29]	[-5.92,7.05]	[-7.44,8.79]
Jeff	[-0.11,0.11]	[-0.01,0.01]	[-0.04,0.04]	[-0.00,0.00]	[-0.00,0.00]	[-0.03,0.03]
Jer	[-1.64,1.64]	[-0.11,0.11]	[-0.27,0.27]	[-0.13,0.13]	[-1.18,1.18]	[-0.53,0.53]
MuidRes	[-0.00,0.00]	[-0.13,0.13]	[-0.11,0.11]	[-0.07,0.07]	[-0.22,0.22]	[-0.98,0.98]
MumsRes	[-0.06,0.06]	[-0.00,0.00]	[-0.06,0.06]	[-0.25,0.25]	[-0.09,0.09]	[-2.53,2.53]
BJesUnc	[-0.57,1.01]	[-0.79,0.86]	[-0.64,0.71]	[-0.67,0.73]	[-0.55,0.49]	[-0.75,0.75]
JesEffectiveStat1	[-0.29,0.41]	[-0.52,0.43]	[-0.52,0.52]	[-0.60,0.44]	[-0.41,0.27]	[-1.29,0.42]
JesEffectiveStat2	[-0.01,0.07]	[-0.04,0.03]	[-0.03,0.03]	[-0.02,0.04]	[-0.08,0.08]	[-0.00,0.04]
JesEffectiveStat3	[-0.04,0.13]	[-0.11,0.19]	[-0.07,0.12]	[-0.12,0.11]	[-0.13,0.09]	[-0.21,0.09]
JesEffectiveStat4	[-0.17,0.13]	[-0.18,0.19]	[-0.16,0.14]	[-0.11,0.16]	[-0.12,0.11]	[-0.11,0.07]
JesEffectiveModel1	[-1.18,1.76]	[-1.95,1.45]	[-1.78,1.46]	[-1.88,1.49]	[-1.47,0.88]	[-1.20,0.79]
JesEffectiveModel2	[-0.01,0.10]	[-0.02,0.04]	[-0.01,0.03]	[-0.02,0.02]	[-0.06,0.06]	[-0.08,0.08]
JesEffectiveModel3	[-0.04,0.09]	[-0.01,0.02]	[-0.00,0.06]	[-0.03,0.02]	[-0.06,0.06]	[-0.20,0.09]
JesEffectiveModel4	[-0.02,0.08]	[-0.03,0.07]	[-0.05,0.08]	[-0.09,0.09]	[-0.05,0.06]	[-0.18,0.17]
JesEffectiveDet1	[-0.26,0.42]	[-0.32,0.38]	[-0.39,0.33]	[-0.41,0.36]	[-0.17,0.31]	[-0.37,0.37]
JesEffectiveDet2	[-0.17,0.11]	[-0.16,0.15]	[-0.10,0.07]	[-0.06,0.06]	[-0.05,0.05]	[-0.07,0.07]
JesEffectiveDet3	[-0.01,0.06]	[-0.03,0.06]	[-0.03,0.06]	[-0.06,0.06]	[-0.07,0.01]	[-0.01,0.06]
JesEffectiveMix1	[-0.26,0.30]	[-0.32,0.37]	[-0.39,0.40]	[-0.35,0.36]	[-0.14,0.24]	[-0.33,0.33]
JesEffectiveMix2	[-0.20,0.16]	[-0.23,0.26]	[-0.22,0.23]	[-0.16,0.20]	[-0.09,0.18]	[-0.24,0.17]
JesEffectiveMix3	[-0.07,0.04]	[-0.02,0.02]	[-0.03,0.05]	[-0.02,0.02]	[-0.07,0.01]	[-0.17,0.19]
JesEffectiveMix4	[-0.01,0.01]	[-0.01,0.04]	[-0.03,0.06]	[-0.02,0.01]	[-0.02,0.01]	[-0.01,0.00]
EtaIntercalibrationModel	[-0.22,0.40]	[-0.53,0.34]	[-0.35,0.40]	[-0.39,0.35]	[-0.73,0.73]	[-0.29,0.07]
EtaIntercalibrationTotalStat	[-0.25,0.38]	[-0.42,0.37]	[-0.43,0.47]	[-0.39,0.39]	[-0.31,0.27]	[-0.23,0.11]
PileupOffsetMu	[-0.14,0.08]	[-0.18,0.14]	[-0.15,0.19]	[-0.12,0.09]	[-0.06,0.06]	[-0.17,0.17]
PileupOffsetNPV	[-0.15,0.44]	[-0.40,0.40]	[-0.30,0.30]	[-0.26,0.13]	[-0.07,0.01]	[-0.91,0.91]
PileupRho	[-0.78,1.35]	[-1.58,1.07]	[-1.06,1.10]	[-1.47,1.08]	[-1.08,0.57]	[-1.44,0.85]
PunchThrough	[-0.02,0.02]	[-0.00,0.00]	[-0.01,0.01]	[-0.00,0.00]	[-0.02,0.02]	[-0.00,0.00]
CTauTag	[-0.06,0.06]	[-0.02,0.02]	[-0.05,0.05]	[-0.03,0.03]	[-0.07,0.07]	[-0.28,0.28]
ElectronEnergyResolution	[-0.01,0.00]	[-0.00,0.02]	[0.00,0.00]	[0.00,0.00]	[-0.01,0.00]	[0.00,0.00]
ElectronEnergyScale	[-0.01,0.00]	[-0.00,0.01]	[-0.01,0.00]	[-0.00,0.00]	[-0.38,0.01]	[0.00,0.00]
ElectronIdSF	[0.00,0.00]	[-0.00,0.00]	[-0.00,0.00]	[-0.00,0.00]	[0.00,0.00]	[0.00,0.00]
ElectronRecoSF	[0.00,0.00]	[-0.00,0.00]	[0.00,0.00]	[0.00,0.00]	[0.00,0.00]	[0.00,0.00]
ElectronTriggerSF	[0.00,0.00]	[-0.00,0.00]	[0.00,0.00]	[0.00,0.00]	[0.00,0.00]	[0.00,0.00]
FlavorComp	[-1.20,0.59]	[-1.23,0.94]	[-0.96,0.71]	[-0.89,0.71]	[-0.74,0.04]	[-1.37,1.37]
FlavorResponse	[-0.18,0.42]	[-0.91,0.25]	[-0.44,0.49]	[-0.77,0.60]	[-0.52,0.21]	[-0.80,0.28]
JetVertexFraction	[-0.29,0.21]	[-0.24,0.26]	[-0.35,0.36]	[-0.29,0.39]	[-0.32,0.38]	[-1.61,0.89]
Mistag	[-0.09,0.09]	[-0.08,0.08]	[-0.09,0.09]	[-0.09,0.09]	[-0.20,0.20]	[-0.35,0.35]
MuonIdSF	[-0.08,0.08]	[-0.09,0.09]	[-0.09,0.09]	[-0.12,0.12]	[-0.19,0.19]	[-0.71,0.70]
MuonRecoSF	[-0.03,0.03]	[-0.04,0.04]	[-0.04,0.04]	[-0.06,0.06]	[-0.10,0.10]	[-0.42,0.42]
MuonTriggerSF	[-0.04,0.04]	[-0.05,0.05]	[-0.05,0.05]	[-0.07,0.07]	[-0.12,0.12]	[-0.43,0.43]
Musc	[-0.03,0.02]	[-0.08,0.08]	[-0.07,0.01]	[-0.01,0.02]	[-0.11,0.11]	[-0.23,0.11]
ModellingGenerator	[-0.41,0.41]	[-1.16,1.16]	[-1.99,1.99]	[-0.51,0.51]	[-1.04,1.04]	[-2.96,2.96]
ModellingParton	[-0.71,0.71]	[-1.18,1.18]	[-1.16,1.16]	[-1.07,1.07]	[-2.76,2.76]	[-7.15,7.15]
ModellingRadiation	[-4.96,4.96]	[-4.63,4.63]	[-3.77,3.77]	[-2.31,2.31]	[-7.02,7.02]	[-7.79,7.79]
ModellingSingleTopWtNormalisation	[-0.52,0.52]	[-0.53,0.53]	[-0.53,0.53]	[-0.82,0.82]	[-1.15,1.15]	[-3.80,3.80]
ModellingSingleTopWtInterference	[-3.85,3.85]	[-3.99,3.99]	[-3.98,3.98]	[-6.12,6.12]	[-8.55,8.55]	[-28.34,28.34]

Table B.50 Per-bin individual statistical and systematic uncertainties in $\mu\mu$ for leading lepton p_T.

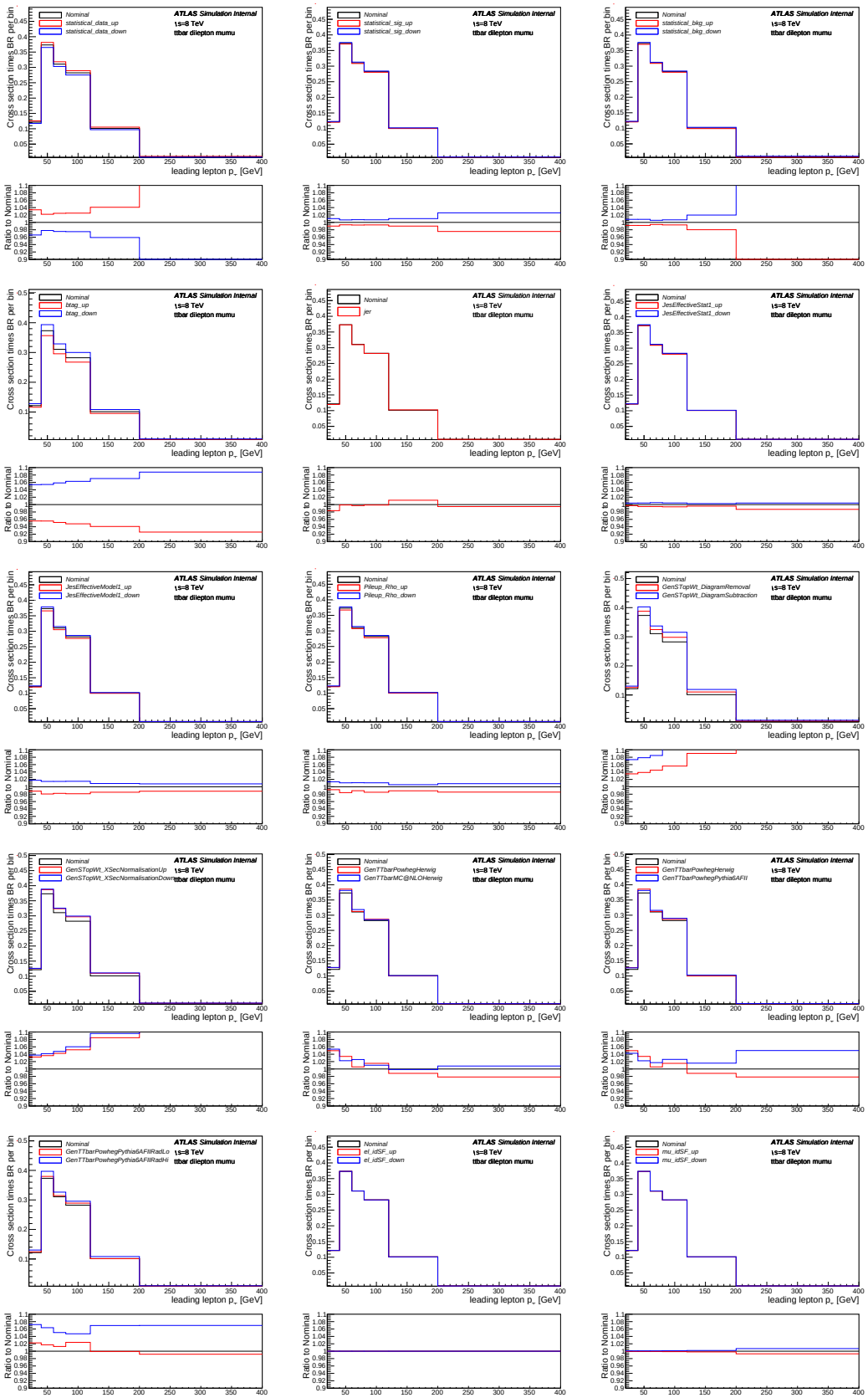

Fig. B.32 Differential cross-section per bin (not scaled to density) for channel $\mu\mu$ in the variable of p_{T} of leading lepton with measured (with Nominal signal) overlaid with statistical uncertainties on data and MC (signal and background), as well as various systematics.

B.2.4 Variable dilepton $\Delta\eta$

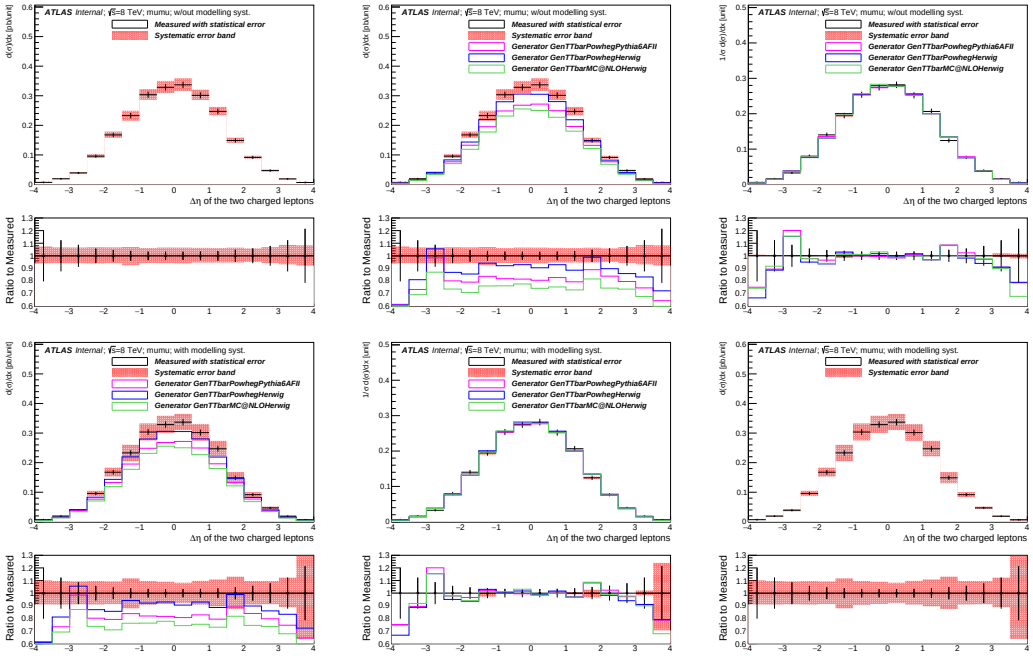

Fig. B.33 Differential cross-section for channel $\mu\mu$ in the variable of dilepton $\Delta\eta$.

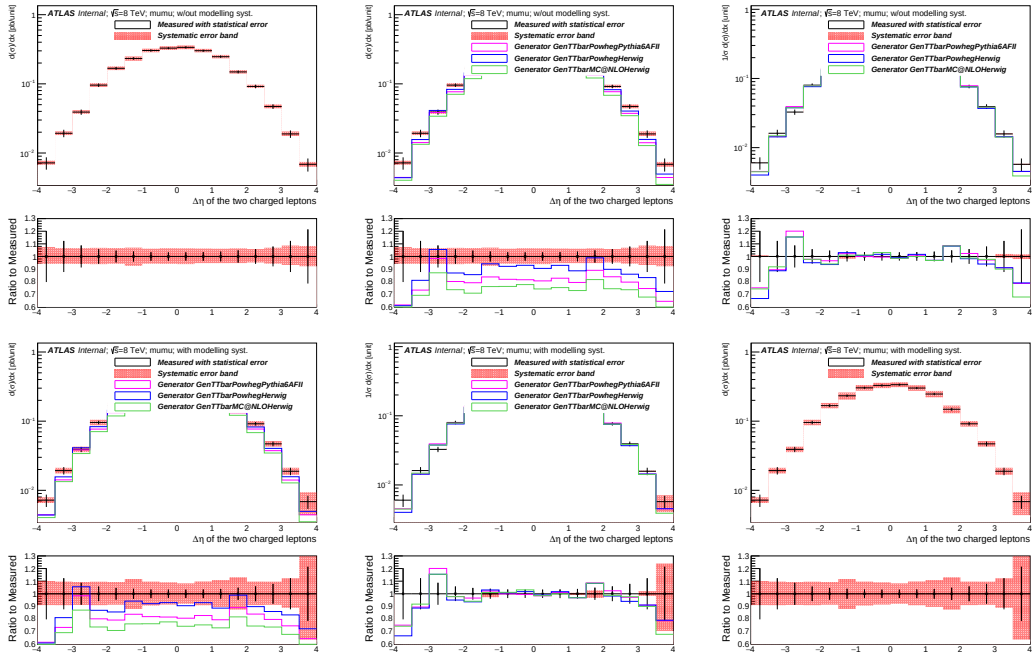

Fig. B.34 Differential cross-section for channel $\mu\mu$ in the variable of dilepton $\Delta\eta$ (log on y axis).

Bin [unit]	Measured $d\sigma/dx$ [pb/unit]	Statistical Data [%]	Statistical MC Bkg [%]	Statistical MC Sig [%]	Systematic [%]
[-4.0,-3.5]	0.0072	+/- 20.3	+/- 3.5	+/- 7.3	+7.5/-5.9
[-3.5,-3.0]	0.0193	+/- 12.3	+/- 1.9	+/- 3.8	+6.7/-5.8
[-3.0,-2.5]	0.0391	+/- 8.7	+/- 1.8	+/- 2.3	+6.6/-5.9
[-2.5,-2.0]	0.0958	+/- 5.8	+/- 1.0	+/- 1.7	+6.8/-6.1
[-2.0,-1.5]	0.1677	+/- 4.7	+/- 1.0	+/- 1.4	+6.7/-5.8
[-1.5,-1.0]	0.2330	+/- 4.0	+/- 2.1	+/- 1.1	+7.0/-7.5
[-1.0,-0.5]	0.3035	+/- 3.4	+/- 1.0	+/- 1.0	+6.2/-5.7
[-0.5,0.0]	0.3286	+/- 3.3	+/- 0.8	+/- 1.0	+6.6/-5.8
[0.0,0.5]	0.3369	+/- 3.3	+/- 1.3	+/- 1.0	+6.5/-6.0
[0.5,1.0]	0.3014	+/- 3.4	+/- 1.7	+/- 1.0	+6.3/-5.3
[1.0,1.5]	0.2469	+/- 3.9	+/- 1.0	+/- 1.1	+6.2/-5.3
[1.5,2.0]	0.1487	+/- 4.8	+/- 1.1	+/- 1.3	+6.5/-5.3
[2.0,2.5]	0.0917	+/- 5.9	+/- 1.1	+/- 1.7	+5.9/-4.8
[2.5,3.0]	0.0470	+/- 7.8	+/- 1.3	+/- 2.3	+6.9/-5.7
[3.0,3.5]	0.0189	+/- 12.3	+/- 2.2	+/- 3.7	+8.6/-6.7
[3.5,4.0]	0.0069	+/- 21.4	+/- 5.1	+/- 7.4	+8.3/-7.7

Table B.51 Per-bin total statistical and systematic uncertainties in $\mu\mu$ for the dilepton $\Delta\eta$, without modelling systematic uncertainties.

Bin [unit]	Measured $d\sigma/dx$ [pb/unit]	Statistical Data [%]	Statistical MC Bkg [%]	Statistical MC Sig [%]	Systematic [%]
[-4.0,-3.5]	0.0072	+/- 20.3	+/- 3.5	+/- 7.3	+10.1/-9.0
[-3.5,-3.0]	0.0193	+/- 12.3	+/- 1.9	+/- 3.8	+9.6/-9.0
[-3.0,-2.5]	0.0391	+/- 8.7	+/- 1.8	+/- 2.3	+9.3/-8.8
[-2.5,-2.0]	0.0958	+/- 5.8	+/- 1.0	+/- 1.7	+9.6/-9.0
[-2.0,-1.5]	0.1677	+/- 4.7	+/- 1.0	+/- 1.4	+9.3/-8.7
[-1.5,-1.0]	0.2330	+/- 4.0	+/- 2.1	+/- 1.1	+11.7/-12.0
[-1.0,-0.5]	0.3035	+/- 3.4	+/- 1.0	+/- 1.0	+9.6/-9.3
[-0.5,0.0]	0.3286	+/- 3.3	+/- 0.8	+/- 1.0	+9.1/-8.6
[0.0,0.5]	0.3369	+/- 3.3	+/- 1.3	+/- 1.0	+8.3/-7.9
[0.5,1.0]	0.3014	+/- 3.4	+/- 1.7	+/- 1.0	+9.7/-9.1
[1.0,1.5]	0.2469	+/- 3.9	+/- 1.0	+/- 1.1	+10.8/-10.4
[1.5,2.0]	0.1487	+/- 4.8	+/- 1.1	+/- 1.3	+13.1/-12.5
[2.0,2.5]	0.0917	+/- 5.9	+/- 1.1	+/- 1.7	+9.6/-9.0
[2.5,3.0]	0.0470	+/- 7.8	+/- 1.3	+/- 2.3	+9.6/-8.7
[3.0,3.5]	0.0189	+/- 12.3	+/- 2.2	+/- 3.7	+12.3/-11.0
[3.5,4.0]	0.0069	+/- 21.4	+/- 5.1	+/- 7.4	+36.4/-36.2

Table B.52 Per-bin total statistical and systematic uncertainties in $\mu\mu$ for the dilepton $\Delta\eta$, with modelling systematic uncertainties.

Bin [unit]	Measured $d\sigma/dx$ [pb/unit]	Statistical Data [%]	Total Syst Up [%]	Total Syst Down [%]	GenTTbarPowhegPythia6AFII [%]	GenTTbarPowhegHerwig [%]	GenTTbarMC@NLOHerwig [%]
[-4.0,-3.5]	0.0072	+/- 20.3	7.5	-5.9	-38.4	-39.0	-44.0
[-3.5,-3.0]	0.0193	+/- 12.3	6.7	-5.8	-26.6	-18.9	-30.8
[-3.0,-2.5]	0.0391	+/- 8.7	6.6	-5.9	-1.6	5.6	-12.9
[-2.5,-2.0]	0.0958	+/- 5.8	6.8	-6.1	-19.8	-13.1	-26.3
[-2.0,-1.5]	0.1677	+/- 4.7	6.7	-5.8	-20.8	-14.4	-29.1
[-1.5,-1.0]	0.2330	+/- 4.0	7.0	-7.5	-16.2	-5.8	-23.8
[-1.0,-0.5]	0.3035	+/- 3.4	6.2	-5.7	-18.1	-7.8	-23.7
[-0.5,0.0]	0.3286	+/- 3.3	6.6	-5.8	-18.4	-7.0	-22.3
[0.0,0.5]	0.3369	+/- 3.3	6.5	-6.0	-19.3	-9.4	-25.7
[0.5,1.0]	0.3014	+/- 3.4	6.3	-5.3	-17.2	-7.0	-24.6
[1.0,1.5]	0.2469	+/- 3.9	6.2	-5.3	-20.6	-11.4	-27.0
[1.5,2.0]	0.1487	+/- 4.8	6.5	-5.3	-11.0	-1.1	-18.3
[2.0,2.5]	0.0917	+/- 5.9	5.9	-4.8	-16.1	-10.2	-25.5
[2.5,3.0]	0.0470	+/- 7.8	6.9	-5.7	-20.3	-14.0	-26.3
[3.0,3.5]	0.0189	+/- 12.3	8.6	-6.7	-25.4	-16.7	-32.2
[3.5,4.0]	0.0069	+/- 21.4	8.3	-7.7	-35.5	-27.7	-48.8

Table B.53 Per-bin total statistical and systematic uncertainties in $\mu\mu$ for the dilepton $\Delta\eta$, with generators, without normalisation.

Bin [unit]	Measured $d\sigma/dx$ [pb/unit]	Statistical Data [%]	Total Syst Up [%]	Total Syst Down [%]	GenTTbarPowhegPythia6AFII [%]	GenTTbarPowhegHerwig [%]	GenTTbarMC@NLOHerwig [%]
[-4.0,-3.5]	0.0060	+/- 20.3	1.0	-0.1	-24.9	-33.3	-25.7
[-3.5,-3.0]	0.0161	+/- 12.3	0.2	-0.0	-10.5	-11.3	-8.2
[-3.0,-2.5]	0.0327	+/- 8.7	0.1	-0.1	20.1	15.4	15.5
[-2.5,-2.0]	0.0801	+/- 5.8	0.3	-0.3	-2.2	-4.9	-2.2
[-2.0,-1.5]	0.1402	+/- 4.7	0.2	0.0	-3.4	-6.4	-5.9
[-1.5,-1.0]	0.1948	+/- 4.0	0.5	-1.7	2.2	3.0	1.0
[-1.0,-0.5]	0.2537	+/- 3.4	-0.3	0.1	-0.1	0.8	1.2
[-0.5,0.0]	0.2747	+/- 3.3	0.1	-0.0	-0.5	1.7	3.1
[0.0,0.5]	0.2816	+/- 3.3	-0.0	-0.2	-1.6	-1.0	-1.5
[0.5,1.0]	0.2520	+/- 3.4	-0.2	0.6	1.0	1.7	-0.0
[1.0,1.5]	0.2064	+/- 3.9	-0.3	0.6	-3.1	-3.1	-3.1
[1.5,2.0]	0.1243	+/- 4.8	-0.0	0.6	8.6	8.2	8.4
[2.0,2.5]	0.0767	+/- 5.9	-0.5	1.1	2.4	-1.8	-1.2
[2.5,3.0]	0.0393	+/- 7.8	0.4	0.1	-2.8	-6.0	-2.3
[3.0,3.5]	0.0158	+/- 12.3	2.0	-1.0	-9.0	-8.9	-10.0
[3.5,4.0]	0.0057	+/- 21.4	1.7	-2.0	-21.3	-20.9	-32.1

Table B.54 Per-bin total statistical and systematic uncertainties in $\mu\mu$ for the dilepton $\Delta\eta$, with generators, with all distributions normalised to unit area.

Uncertainty	[-4.0,-3.5]	[-3.5,-3.0]	[-3.0,-2.5]	[-2.5,-2.0]	[-2.0,-1.5]	[-1.5,-1.0]	[-1.0,-0.5]	[-0.5,0.0]	[0.0,0.5]	[0.5,1.0]	[1.0,1.5]	[1.5,2.0]	[2.0,2.5]	[2.5,3.0]	[3.0,3.5]	[3.5,4.0]
StatisticalData	[-20.26,20.26]	[-12.32,12.32]	[-8.73,8.73]	[-5.76,5.76]	[-4.65,4.65]	[-3.99,3.99]	[-3.40,3.40]	[-3.30,3.30]	[-3.29,3.29]	[-3.44,3.44]	[-3.85,3.85]	[-4.84,4.84]	[-5.86,5.86]	[-7.85,7.85]	[-12.32,12.32]	[-21.43,21.43]
StatisticalBkg	[-3.47,3.47]	[-1.86,1.86]	[-1.84,1.84]	[-0.97,0.97]	[-0.97,0.97]	[-2.12,2.12]	[-0.96,0.96]	[-0.83,0.83]	[-1.31,1.31]	[-1.70,1.70]	[-0.98,0.98]	[-1.09,1.09]	[-1.14,1.14]	[-1.34,1.34]	[-2.24,2.24]	[-5.15,5.15]
StatisticalSig	[-6.38,7.31]	[-3.55,3.82]	[-2.17,2.27]	[-1.63,1.68]	[-1.35,1.39]	[-1.11,1.14]	[-0.96,0.98]	[-0.93,0.95]	[-0.95,0.96]	[-0.96,0.98]	[-1.12,1.14]	[-1.29,1.33]	[-1.62,1.67]	[-2.17,2.26]	[-3.43,3.68]	[-6.48,7.44]
BTag	[-5.54,6.73]	[-4.61,5.79]	[-4.47,5.52]	[-5.02,6.11]	[-4.99,6.09]	[-5.29,6.39]	[-4.97,5.98]	[-4.91,5.92]	[-4.89,5.92]	[-4.80,5.86]	[-4.75,5.77]	[-4.86,5.88]	[-4.60,5.53]	[-4.72,5.80]	[-4.58,5.55]	[-5.62,6.60]
Jeff	[0.00,0.00]	[-0.09,0.09]	[-0.04,0.04]	[-0.05,0.05]	[-0.13,0.13]	[-0.00,0.00]	[-0.01,0.01]	[-0.04,0.04]	[-0.05,0.05]	[-0.03,0.03]	[-0.03,0.03]	[-0.02,0.02]	[-0.02,0.02]	[-0.00,0.00]	[-0.00,0.00]	[-0.95,0.95]
Jer	[-0.83,0.83]	[-0.29,0.29]	[-2.89,2.89]	[-2.33,2.33]	[-0.07,0.07]	[-0.74,0.74]	[-0.14,0.14]	[-0.54,0.54]	[-0.47,0.47]	[-0.07,0.07]	[-0.32,0.32]	[-0.42,0.42]	[-0.24,0.24]	[-1.46,1.46]	[-0.46,0.46]	[-2.14,2.14]
MuidRes	[-0.06,0.06]	[-0.28,0.28]	[-0.14,0.14]	[-0.12,0.12]	[-0.57,0.57]	[-0.16,0.16]	[-0.09,0.09]	[-0.03,0.03]	[-0.13,0.13]	[-0.01,0.01]	[-0.28,0.28]	[-0.19,0.19]	[-0.04,0.04]	[-0.05,0.05]	[-0.38,0.38]	[-0.13,0.13]
MumsRes	[-0.29,0.29]	[-0.60,0.60]	[-0.48,0.48]	[-0.27,0.27]	[-0.19,0.19]	[-0.12,0.12]	[-0.05,0.05]	[-0.52,0.52]	[-0.46,0.46]	[-0.13,0.13]	[-0.17,0.17]	[-0.15,0.15]	[-0.09,0.09]	[-1.17,1.17]	[-0.31,0.31]	[-1.59,1.59]
BJesUnc	[-0.37,0.30]	[-1.31,1.10]	[-0.96,0.79]	[-0.83,0.85]	[-1.01,0.95]	[-0.86,0.53]	[-0.65,0.74]	[-0.50,0.85]	[-0.69,0.66]	[-0.63,0.72]	[-0.78,0.64]	[-0.46,0.78]	[-0.47,0.92]	[-0.74,0.74]	[-0.99,1.59]	[-0.70,1.87]
JesEffectiveStat1	[-0.16,0.16]	[-0.75,0.75]	[-0.36,0.80]	[-0.50,0.51]	[-0.70,0.54]	[-0.68,0.20]	[-0.59,0.14]	[-0.38,0.66]	[-0.70,0.40]	[-0.50,0.43]	[-0.48,0.44]	[-0.26,0.42]	[-0.30,0.32]	[-0.25,0.68]	[-0.54,1.50]	[-0.59,0.45]
JesEffectiveStat2	[-0.01,0.01]	[-0.08,0.07]	[-0.04,0.04]	[-0.04,0.05]	[-0.06,0.01]	[-0.02,0.05]	[-0.03,0.03]	[-0.00,0.02]	[-0.05,0.05]	[-0.07,0.07]	[-0.03,0.03]	[-0.03,0.06]	[-0.03,0.03]	[-0.01,0.02]	[-0.01,1.19]	[-0.49,0.00]
JesEffectiveStat3	[-0.03,0.03]	[-0.04,0.15]	[-0.12,0.11]	[-0.03,0.10]	[-0.04,0.11]	[-0.14,0.09]	[-0.09,0.12]	[-0.03,0.17]	[-0.24,0.05]	[-0.00,0.05]	[-0.10,0.18]	[-0.12,0.20]	[-0.15,0.26]	[-0.02,0.21]	[-0.28,1.07]	[-0.58,0.44]
JesEffectiveStat4	[-0.04,0.04]	[-0.03,0.38]	[-0.12,0.12]	[-0.11,0.11]	[-0.13,0.13]	[-0.39,0.13]	[-0.11,0.17]	[-0.08,0.11]	[-0.20,0.16]	[-0.16,0.10]	[-0.14,0.18]	[-0.13,0.31]	[-0.03,0.01]	[-0.21,0.00]	[-1.07,1.07]	[-0.49,0.49]
JesEffectiveModel1	[-0.57,2.02]	[-1.56,1.50]	[-1.60,1.10]	[-1.61,0.93]	[-1.80,1.86]	[-2.77,1.11]	[-1.76,0.94]	[-1.83,1.63]	[-2.18,1.70]	[-1.44,1.49]	[-1.43,1.39]	[-1.28,1.68]	[-0.72,1.25]	[-0.84,1.24]	[-1.50,2.77]	[-2.41,1.86]
JesEffectiveModel2	[-0.06,0.06]	[-0.13,0.00]	[-0.04,0.02]	[-0.02,0.06]	[-0.08,0.04]	[-0.09,0.06]	[-0.02,0.02]	[-0.04,0.04]	[-0.06,0.06]	[-0.01,0.01]	[-0.05,0.05]	[-0.00,0.08]	[-0.01,0.01]	[-0.02,0.02]	[-1.19,1.19]	[-0.05,0.00]
JesEffectiveModel3	[-0.03,0.03]	[-0.22,0.22]	[-0.13,0.13]	[-0.07,0.07]	[-0.00,0.09]	[-0.22,0.22]	[-0.07,0.07]	[-0.05,0.05]	[-0.13,0.13]	[-0.12,0.07]	[-0.00,0.06]	[-0.11,0.11]	[-0.10,0.12]	[-0.04,0.04]	[-0.91,0.91]	[-0.58,0.44]
JesEffectiveModel4	[-0.04,0.00]	[-0.03,0.06]	[-0.03,0.03]	[-0.08,0.08]	[-0.09,0.02]	[-0.02,0.03]	[-0.04,0.05]	[-0.02,0.07]	[-0.08,0.03]	[-0.04,0.05]	[-0.08,0.14]	[-0.03,0.21]	[-0.11,0.09]	[-0.07,0.04]	[-0.92,0.92]	[-0.49,0.49]
JesEffectiveDet1	[-0.19,0.19]	[-0.93,0.93]	[-0.51,0.50]	[-0.29,0.25]	[-0.40,0.42]	[-0.48,0.27]	[-0.42,0.40]	[-0.19,0.42]	[-0.48,0.23]	[-0.27,0.29]	[-0.30,0.27]	[-0.27,0.50]	[-0.22,0.13]	[-0.15,0.38]	[-0.14,1.56]	[-0.21,0.60]
JesEffectiveDet2	[-0.02,0.02]	[-0.13,0.13]	[-0.04,0.23]	[-0.06,0.06]	[-0.02,0.06]	[-0.33,0.07]	[-0.09,0.10]	[-0.05,0.05]	[-0.18,0.06]	[-0.17,0.12]	[-0.09,0.13]	[-0.04,0.17]	[-0.04,0.04]	[-0.12,0.12]	[-1.29,1.29]	[-0.50,0.50]
JesEffectiveDet3	[-0.04,0.00]	[-0.12,0.12]	[-0.04,0.01]	[-0.03,0.03]	[-0.08,0.08]	[-0.05,0.02]	[-0.02,0.04]	[-0.03,0.05]	[-0.06,0.06]	[-0.02,0.02]	[-0.06,0.08]	[-0.04,0.14]	[-0.05,0.13]	[-0.07,0.04]	[-0.99,0.99]	[-0.49,0.00]
JesEffectiveMix1	[-0.01,0.17]	[-0.78,0.78]	[-0.47,0.34]	[-0.31,0.38]	[-0.27,0.40]	[-0.53,0.24]	[-0.31,0.30]	[-0.20,0.39]	[-0.44,0.26]	[-0.29,0.31]	[-0.28,0.27]	[-0.29,0.40]	[-0.17,0.36]	[-0.11,0.56]	[-0.28,1.47]	[-0.59,0.09]
JesEffectiveMix2	[-0.04,0.37]	[-0.75,0.75]	[-0.04,0.39]	[-0.06,0.18]	[-0.12,0.18]	[-0.38,0.13]	[-0.25,0.17]	[-0.11,0.16]	[-0.25,0.13]	[-0.29,0.30]	[-0.14,0.30]	[-0.16,0.26]	[-0.08,0.04]	[-0.10,0.38]	[-1.38,1.38]	[-0.57,0.57]
JesEffectiveMix3	[-0.03,0.00]	[-0.04,0.04]	[-0.05,0.23]	[-0.06,0.06]	[-0.13,0.18]	[-0.21,0.21]	[-0.07,0.07]	[-0.02,0.02]	[-0.05,0.04]	[-0.12,0.05]	[-0.08,0.08]	[-0.04,0.12]	[-0.02,0.05]	[-0.11,0.11]	[-1.20,1.20]	[-0.49,0.49]
JesEffectiveMix4	[-0.01,0.00]	[-0.00,0.00]	[-0.01,0.01]	[-0.08,0.08]	[-0.05,0.00]	[-0.03,0.03]	[-0.01,0.02]	[-0.01,0.03]	[-0.03,0.04]	[-0.00,0.00]	[-0.01,0.02]	[-0.00,0.08]	[-0.04,0.06]	[-0.00,0.01]	[-0.95,0.95]	[-0.00,0.01]
EtaIntercalibrationModel	[-0.38,0.38]	[-0.05,0.74]	[-0.41,0.24]	[-0.03,0.43]	[-0.39,0.47]	[-0.79,0.23]	[-0.49,0.19]	[-0.33,0.40]	[-0.27,0.27]	[-0.33,0.54]	[-0.33,0.30]	[-0.30,0.38]	[-0.28,0.26]	[-0.03,0.32]	[-1.14,1.14]	[-1.04,1.99]
EtaIntercalibrationTotalStat	[-0.10,0.10]	[-0.17,0.70]	[-0.37,0.40]	[-0.10,0.53]	[-0.48,0.60]	[-0.73,0.31]	[-0.39,0.17]	[-0.30,0.49]	[-0.64,0.30]	[-0.32,0.39]	[-0.27,0.43]	[-0.13,0.39]	[-0.29,0.23]	[-0.13,0.40]	[-1.46,1.46]	[-1.02,0.93]
PileupOffsetMu	[-0.78,0.78]	[-0.77,0.77]	[-0.17,0.24]	[-0.11,0.11]	[-0.34,0.07]	[-0.47,0.17]	[-0.07,0.01]	[-0.01,0.15]	[-0.13,0.13]	[-0.11,0.16]	[-0.19,0.14]	[-0.00,0.16]	[-0.17,0.15]	[-0.35,0.11]	[-0.96,0.96]	[-0.05,0.05]
PileupOffsetNPV	[-0.60,0.60]	[-1.18,0.38]	[-0.21,0.14]	[-0.13,0.23]	[-0.06,0.16]	[-1.53,1.53]	[-0.32,0.32]	[-0.33,0.33]	[-0.82,0.82]	[-0.02,0.05]	[-0.09,0.19]	[-0.40,0.40]	[-0.42,0.42]	[-0.03,1.15]	[-0.97,1.54]	[-1.28,1.04]
PileupRho	[-0.52,1.31]	[-1.67,1.52]	[-1.08,0.89]	[-1.02,0.78]	[-1.38,1.12]	[-2.50,0.69]	[-1.27,0.78]	[-1.43,1.26]	[-1.32,1.17]	[-0.99,1.19]	[-1.07,0.95]	[-0.91,1.18]	[-0.28,1.04]	[-0.67,1.25]	[-1.37,2.26]	[-2.34,1.30]
PunchThrough	[0.00,0.01]	[-0.17,0.17]	[-0.08,0.08]	[-0.00,0.00]	[-0.00,0.00]	[-0.02,0.02]	[-0.01,0.01]	[-0.01,0.00]	[-0.01,0.01]	[-0.01,0.01]	[-0.00,0.00]	[-0.00,0.00]	[-0.02,0.02]	[-0.00,0.00]	[-0.00,0.00]	[-0.01,0.00]
CTauTag	[-0.01,0.01]	[-0.02,0.02]	[-0.01,0.01]	[-0.02,0.02]	[-0.02,0.02]	[-0.05,0.05]	[-0.07,0.07]	[-0.03,0.03]	[-0.07,0.07]	[-0.06,0.06]	[-0.05,0.06]	[-0.02,0.02]	[-0.01,0.01]	[-0.01,0.01]	[-0.03,0.03]	[-0.01,0.01]
ElectronEnergyResolution	[0.00,0.00]	[-0.00,0.00]	[0.00,0.00]	[0.00,0.00]	[0.00,0.00]	[0.00,0.01]	[0.00,0.00]	[-0.01,0.00]	[0.00,0.01]	[0.00,0.02]	[0.00,0.00]	[-0.01,0.00]	[0.00,0.00]	[0.00,0.00]	[0.00,0.00]	[0.00,0.00]
ElectronEnergyScale	[0.00,0.00]	[-0.00,0.00]	[0.00,0.00]	[0.00,0.00]	[0.00,0.00]	[-0.01,0.00]	[-0.01,0.00]	[-0.26,0.26]	[0.00,0.01]	[-0.02,0.02]	[0.00,0.00]	[-0.01,0.00]	[-0.01,0.00]	[-0.00,0.00]	[0.00,0.00]	[0.00,0.00]
ElectronIdSF	[0.00,0.00]	[0.00,0.00]	[0.00,0.00]	[0.00,0.00]	[0.00,0.00]	[-0.00,0.00]	[0.00,0.00]	[-0.00,0.00]	[0.00,0.00]	[0.00,0.00]	[0.00,0.00]	[0.00,0.00]	[0.00,0.00]	[0.00,0.00]	[0.00,0.00]	[0.00,0.00]
ElectronRecoSF	[0.00,0.00]	[0.00,0.00]	[0.00,0.00]	[0.00,0.00]	[0.00,0.00]	[-0.00,0.00]	[0.00,0.00]	[-0.00,0.00]	[0.00,0.00]	[0.00,0.00]	[0.00,0.00]	[0.00,0.00]	[0.00,0.00]	[0.00,0.00]	[0.00,0.00]	[0.00,0.00]
ElectronTriggerSF	[0.00,0.00]	[0.00,0.00]	[0.00,0.00]	[0.00,0.00]	[0.00,0.00]	[-0.00,0.00]	[0.00,0.00]	[0.00,0.00]	[0.00,0.00]	[0.00,0.00]	[0.00,0.00]	[0.00,0.00]	[0.00,0.00]	[0.00,0.00]	[0.00,0.00]	[0.00,0.00]
FlavorComp	[-0.39,1.48]	[-0.03,0.33]	[-0.58,0.62]	[-1.08,0.55]	[-0.65,0.60]	[-1.89,1.62]	[-1.06,0.19]	[-1.45,0.80]	[-1.55,0.79]	[-0.64,0.56]	[-0.59,0.48]	[-0.49,0.64]	[-0.02,0.41]	[-1.51,1.51]	[-1.26,0.45]	[-0.55,0.03]
FlavorResponse	[-0.28,0.99]	[-0.09,0.19]	[-0.37,0.03]	[-0.38,0.39]	[-0.49,0.44]	[-1.79,0.14]	[-0.78,0.07]	[-0.92,0.58]	[-0.64,0.43]	[-0.36,0.50]	[-0.40,0.60]	[-0.35,0.52]	[-0.10,0.10]	[-1.47,1.47]	[-0.33,0.57]	[-1.02,1.02]
JetVertexFraction	[-0.94,0.43]	[-0.69,0.01]	[-0.44,0.42]	[-0.22,0.22]	[-0.33,0.28]	[-0.44,0.32]	[-0.30,0.33]	[-0.28,0.44]	[-0.29,0.32]	[-0.18,0.30]	[-0.47,0.34]	[-0.27,0.31]	[-0.19,0.40]	[-0.28,0.25]	[-0.38,0.50]	[-0.02,0.02]
Mistag	[-0.10,0.10]	[-0.03,0.03]	[-0.03,0.03]	[-0.00,0.00]	[-0.03,0.02]	[-0.29,0.29]	[-0.11,0.12]	[-0.08,0.08]	[-0.15,0.15]	[-0.03,0.03]	[-0.08,0.08]	[-0.10,0.10]	[-0.14,0.14]	[-0.04,0.04]	[-0.10,0.10]	[-0.06,0.06]
MuonIdSF	[-0.09,0.09]	[-0.06,0.06]	[-0.10,0.10]	[-0.09,0.09]	[-0.11,0.10]	[-0.13,0.13]	[-0.10,0.10]	[-0.11,0.11]	[-0.11,0.11]	[-0.13,0.13]	[-0.11,0.11]	[-0.12,0.12]	[-0.09,0.09]	[-0.08,0.08]	[-0.09,0.09]	[-0.11,0.11]
MuonRecoSF	[-0.05,0.05]	[-0.02,0.02]	[-0.04,0.04]	[-0.04,0.04]	[-0.05,0.05]	[-0.07,0.07]	[-0.05,0.05]	[-0.05,0.05]	[-0.05,0.05]	[-0.07,0.07]	[-0.06,0.06]	[-0.06,0.05]	[-0.04,0.04]	[-0.03,0.03]	[-0.03,0.03]	[-0.06,0.06]
MuonTriggerSF	[-0.05,0.05]	[-0.01,0.01]	[-0.04,0.04]	[-0.05,0.05]	[-0.07,0.06]	[-0.07,0.07]	[-0.07,0.06]	[-0.07,0.07]	[-0.07,0.07]	[-0.08,0.08]	[-0.07,0.07]	[-0.08,0.08]	[-0.04,0.04]	[-0.04,0.04]	[-0.02,0.02]	[-0.00,0.00]
Musc	[-0.07,0.00]	[-0.16,0.17]	[-0.08,0.08]	[-0.04,0.14]	[-0.07,0.07]	[-0.09,0.07]	[-0.01,0.01]	[-0.12,0.12]	[-0.08,0.05]	[-0.16,0.16]	[-0.04,0.08]	[-0.05,0.05]	[-0.04,0.24]	[-0.05,0.13]	[-0.22,0.22]	[-0.49,0.00]
ModellingGenerator	[-0.13,0.13]	[-2.26,2.26]	[-1.63,1.63]	[-2.90,2.90]	[-1.16,1.16]	[-4.80,4.80]	[-3.38,3.38]	[-0.56,0.56]	[-0.58,0.58]	[-1.66,1.66]	[-1.12,1.12]	[-0.79,0.79]	[-0.76,0.76]	[-2.45,2.45]	[-1.50,1.50]	[-18.32,18.32]
ModellingParton	[-3.70,3.70]	[-4.75,4.75]	[-4.54,4.54]	[-0.62,0.62]	[-1.27,1.27]	[-1.74,1.74]	[-2.33,2.33]	[-0.53,0.53]	[-0.24,0.24]	[-0.10,0.10]	[-0.43,0.43]	[-3.13,3.13]	[-0.03,0.03]	[-2.53,2.53]	[-2.24,2.24]	[-6.40,6.40]
ModellingRadiation	[-2.34,2.34]	[-4.18,4.18]	[-0.97,0.97]	[-4.41,4.41]	[-3.18,3.18]	[-5.51,5.51]	[-3.90,3.90]	[-3.70,3.70]	[-2.41,2.41]	[-3.08,3.08]	[-6.44,6.44]	[-9.11,9.11]	[-5.99,5.99]	[-4.69,4.69]	[-6.63,6.63]	[-28.44,28.44]
ModellingSingleTopWtNormalisation	[-0.69,0.69]	[-0.22,0.22]	[-0.58,0.58]	[-0.54,0.54]	[-0.71,0.71]	[-0.75,0.75]	[-0.62,0.62]	[-0.66,0.66]	[-0.59,0.59]	[-0.87,0.87]	[-0.80,0.80]	[-0.79,0.79]	[-0.61,0.61]	[-0.42,0.42]	[-0.66,0.66]	[-1.09,1.09]
ModellingSingleTopWtInterference	[-5.12,5.12]	[-1.62,1.62]	[-4.31,4.31]	[-4.02,4.02]	[-5.31,5.31]	[-5.59,5.59]	[-4.65,4.65]	[-4.95,4.95]	[-4.43,4.43]	[-6.46,6.46]	[-5.97,5.97]	[-5.87,5.87]	[-4.57,4.57]	[-3.10,3.10]	[-4.96,4.96]	[-8.12,8.12]

Table B.55 Per-bin individual statistical and systematic uncertainties in $\mu\mu$ for the dilepton $\Delta\eta$.

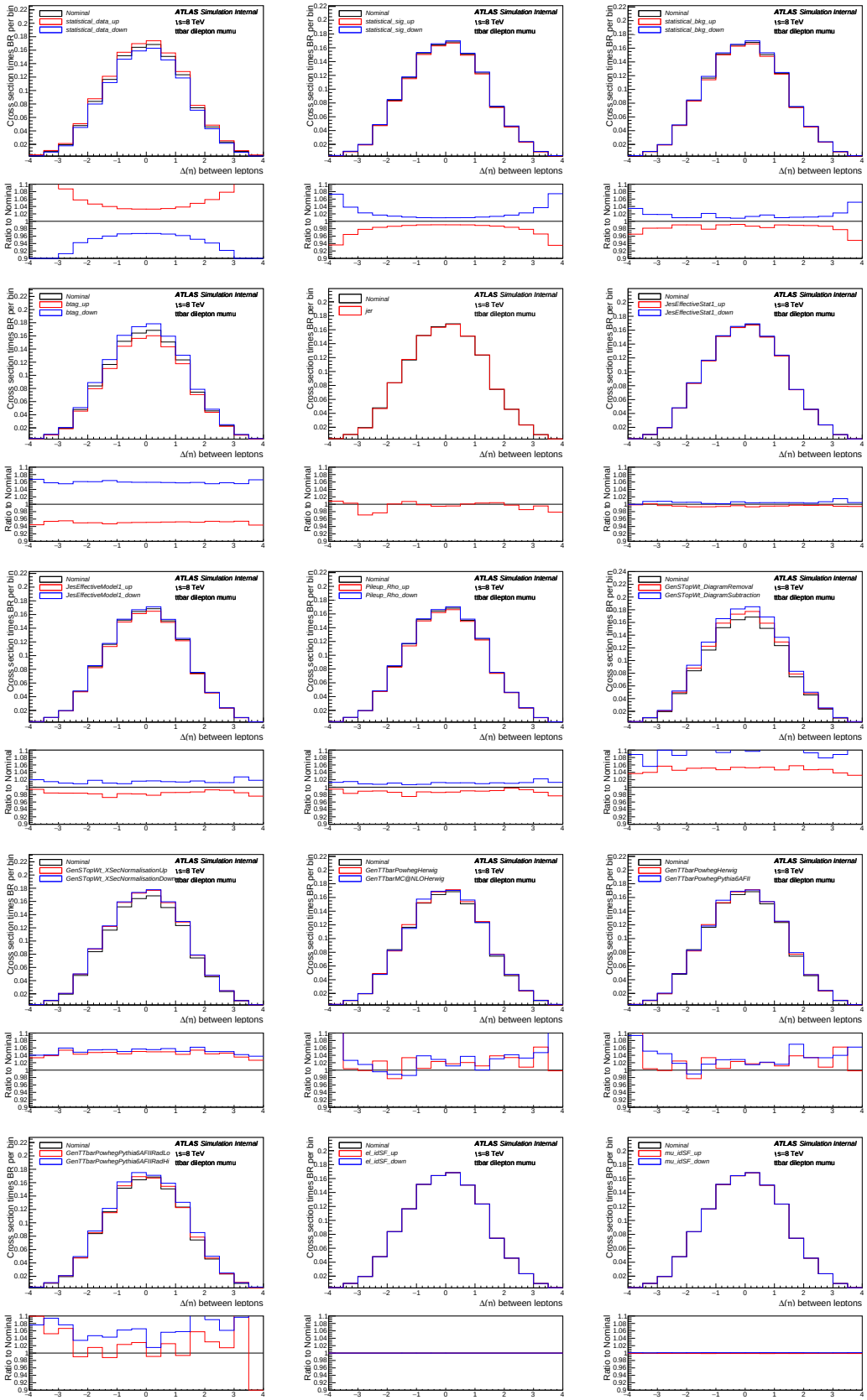

Fig. B.35 Differential cross-section per bin (not scaled to density) for channel $\mu\mu$ in the variable of dilepton $\Delta\eta$ with measured (with Nominal signal) overlaid with statistical uncertainties on data and MC (signal and background), as well as various systematics.

B.2.5 Variable dilepton $|\Delta\eta|$

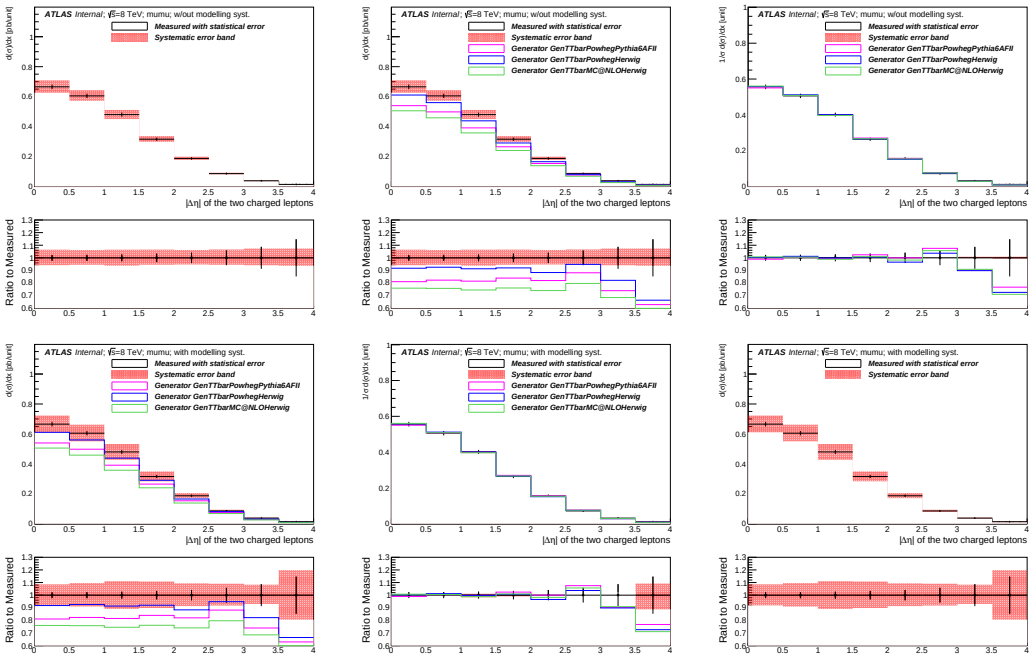

Fig. B.36 Differential cross-section for channel $\mu\mu$ in the variable of dilepton $|\Delta\eta|$.

Bin [unit]	Measured $d\sigma/dx$ [pb/unit]	Statistical Data [%]	Statistical MC Bkg [%]	Statistical MC Sig [%]	Systematic [%]
[0.0,0.5]	0.6654	+/- 2.3	+/- 0.8	+/- 0.7	+6.5/-5.9
[0.5,1.0]	0.6049	+/- 2.4	+/- 1.0	+/- 0.7	+6.3/-5.5
[1.0,1.5]	0.4799	+/- 2.8	+/- 1.2	+/- 0.8	+6.5/-6.2
[1.5,2.0]	0.3158	+/- 3.4	+/- 0.7	+/- 1.0	+6.6/-5.5
[2.0,2.5]	0.1874	+/- 4.1	+/- 0.8	+/- 1.2	+6.3/-5.3
[2.5,3.0]	0.0861	+/- 5.8	+/- 1.2	+/- 1.6	+6.6/-5.5
[3.0,3.5]	0.0382	+/- 8.7	+/- 1.5	+/- 2.6	+7.4/-5.9
[3.5,4.0]	0.0141	+/- 14.7	+/- 3.1	+/- 5.1	+7.4/-6.3

Table B.56 Per-bin total statistical and systematic uncertainties in $\mu\mu$ for the dilepton $|\Delta\eta|$, without modelling systematic uncertainties.

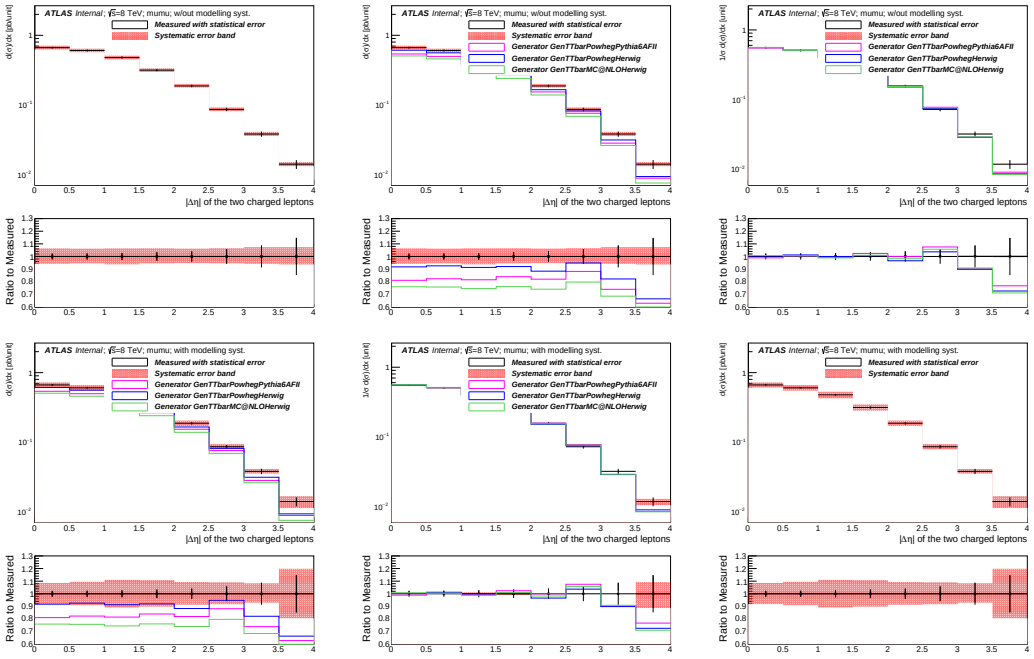

Fig. B.37 Differential cross-section for channel $\mu\mu$ in the variable of dilepton $|\Delta\eta|$ (log on y axis).

Bin [unit]	Measured $d\sigma/dx$ [pb/unit]	Statistical Data [%]	Statistical MC Bkg [%]	Statistical MC Sig [%]	Systematic [%]
[0.0,0.5]	0.6654	+/- 2.3	+/- 0.8	+/- 0.7	+8.6/-8.1
[0.5,1.0]	0.6049	+/- 2.4	+/- 1.0	+/- 0.7	+9.5/-9.0
[1.0,1.5]	0.4799	+/- 2.8	+/- 1.2	+/- 0.8	+11.0/-10.8
[1.5,2.0]	0.3158	+/- 3.4	+/- 0.7	+/- 1.0	+10.8/-10.2
[2.0,2.5]	0.1874	+/- 4.1	+/- 0.8	+/- 1.2	+9.3/-8.7
[2.5,3.0]	0.0861	+/- 5.8	+/- 1.2	+/- 1.6	+9.1/-8.3
[3.0,3.5]	0.0382	+/- 8.7	+/- 1.5	+/- 2.6	+8.3/-7.0
[3.5,4.0]	0.0141	+/- 14.7	+/- 3.1	+/- 5.1	+19.8/-19.4

Table B.57 Per-bin total statistical and systematic uncertainties in $\mu\mu$ for the dilepton $|\Delta\eta|$, with modelling systematic uncertainties.

Bin [unit]	Measured $d\sigma/dx$ [pb/unit]	Statistical Data [%]	Total Syst Up [%]	Total Syst Down [%]	GenTTbarPowhegPythia6AFII [%]	GenTTbarPowhegHerwig [%]	GenTTbarMC@NLOHerwig [%]
[0.0,0.5]	0.6654	+/- 2.3	6.5	-5.9	-18.9	-8.2	-24.0
[0.5,1.0]	0.6049	+/- 2.4	6.3	-5.5	-17.7	-7.4	-24.2
[1.0,1.5]	0.4799	+/- 2.8	6.5	-6.2	-18.5	-8.6	-25.4
[1.5,2.0]	0.3158	+/- 3.4	6.6	-5.5	-16.0	-8.0	-23.9
[2.0,2.5]	0.1874	+/- 4.1	6.3	-5.3	-18.0	-11.6	-25.9
[2.5,3.0]	0.0861	+/- 5.8	6.6	-5.5	-11.8	-5.2	-20.3
[3.0,3.5]	0.0382	+/- 8.7	7.4	-5.9	-26.0	-17.8	-31.4
[3.5,4.0]	0.0141	+/- 14.7	7.4	-6.3	-37.0	-33.5	-46.4

Table B.58 Per-bin total statistical and systematic uncertainties in $\mu\mu$ for the dilepton $|\Delta\eta|$, with generators, without normalisation.

Bin [unit]	Measured $d\sigma/dx$ [pb/unit]	Statistical Data [%]	Total Syst Up [%]	Total Syst Down [%]	GenTTbarPowhegPythia6AFII [%]	GenTTbarPowhegHerwig [%]	GenTTbarMC@NLOHerwig [%]
[0.0,0.5]	0.5564	+/- 2.3	0.0	-0.1	-1.1	0.3	0.8
[0.5,1.0]	0.5058	+/- 2.4	-0.2	0.2	0.4	1.2	0.5
[1.0,1.5]	0.4013	+/- 2.8	0.0	-0.5	-0.5	-0.1	-1.1
[1.5,2.0]	0.2641	+/- 3.4	0.1	0.3	2.4	0.6	1.0
[2.0,2.5]	0.1567	+/- 4.1	-0.2	0.5	0.0	-3.4	-1.8
[2.5,3.0]	0.0720	+/- 5.8	0.2	0.3	7.5	3.7	5.7
[3.0,3.5]	0.0319	+/- 8.7	0.9	-0.2	-9.8	-10.1	-9.1
[3.5,4.0]	0.0118	+/- 14.7	0.9	-0.6	-23.2	-27.3	-28.9

Table B.59 Per-bin total statistical and systematic uncertainties in $\mu\mu$ for the dilepton $|\Delta\eta|$, with generators, with all distributions normalised to unit area.

Uncertainty	[0.0,0.5]	[0.5,1.0]	[1.0,1.5]	[1.5,2.0]	[2.0,2.5]	[2.5,3.0]	[3.0,3.5]	[3.5,4.0]
StatisticalData	[-2.33,2.33]	[-2.42,2.42]	[-2.77,2.77]	[-3.36,3.36]	[-4.11,4.11]	[-5.84,5.84]	[-8.71,8.71]	[-14.72,14.72]
StatisticalBkg	[-0.80,0.80]	[-1.00,1.00]	[-1.22,1.22]	[-0.74,0.74]	[-0.76,0.76]	[-1.15,1.15]	[-1.52,1.52]	[-3.11,3.11]
StatisticalSig	[-0.67,0.68]	[-0.68,0.69]	[-0.79,0.80]	[-0.94,0.96]	[-1.15,1.18]	[-1.54,1.59]	[-2.49,2.62]	[-4.63,5.11]
BTag	[-4.90,5.92]	[-4.89,5.92]	[-5.02,6.08]	[-4.92,5.97]	[-4.81,5.82]	[-4.59,5.65]	[-4.59,5.67]	[-5.57,6.66]
Jeff	[-0.01,0.01]	[-0.01,0.01]	[-0.02,0.02]	[-0.06,0.06]	[-0.02,0.02]	[-0.02,0.02]	[-0.04,0.04]	[-0.47,0.47]
Jer	[-0.50,0.50]	[-0.04,0.04]	[-0.53,0.53]	[-0.25,0.25]	[-1.28,1.28]	[-2.15,2.15]	[-0.09,0.09]	[-0.66,0.66]
MuidRes	[-0.05,0.05]	[-0.05,0.05]	[-0.06,0.06]	[-0.19,0.19]	[-0.08,0.08]	[-0.09,0.09]	[-0.06,0.06]	[-0.04,0.04]
MumsRes	[-0.03,0.03]	[-0.09,0.09]	[-0.15,0.15]	[-0.16,0.16]	[-0.09,0.09]	[-0.85,0.85]	[-0.43,0.43]	[-0.65,0.65]
BJesUnc	[-0.59,0.76]	[-0.64,0.73]	[-0.82,0.58]	[-0.73,0.87]	[-0.65,0.88]	[-0.39,0.76]	[-1.15,1.35]	[-0.54,1.07]
JesEffectiveStat1	[-0.54,0.53]	[-0.55,0.29]	[-0.58,0.31]	[-0.47,0.48]	[-0.40,0.41]	[-0.30,0.74]	[-0.23,1.14]	[-0.36,0.21]
JesEffectiveStat2	[-0.03,0.01]	[-0.04,0.04]	[-0.04,0.04]	[-0.01,0.00]	[-0.02,0.01]	[-0.03,0.03]	[-0.05,0.64]	[-0.24,0.24]
JesEffectiveStat3	[-0.13,0.11]	[-0.05,0.09]	[-0.12,0.13]	[-0.08,0.16]	[-0.09,0.18]	[-0.07,0.16]	[-0.07,0.52]	[-0.30,0.20]
JesEffectiveStat4	[-0.14,0.13]	[-0.14,0.14]	[-0.26,0.15]	[-0.13,0.22]	[-0.06,0.06]	[-0.17,0.06]	[-0.01,0.73]	[-0.25,0.25]
JesEffectiveModel1	[-2.00,1.67]	[-1.60,1.21]	[-2.08,1.25]	[-1.54,1.77]	[-1.17,1.09]	[-1.22,1.17]	[-1.53,2.15]	[-1.49,1.96]
JesEffectiveModel2	[-0.02,0.02]	[-0.02,0.02]	[-0.04,0.05]	[-0.04,0.07]	[-0.01,0.03]	[-0.03,0.00]	[-0.54,0.54]	[-0.03,0.03]
JesEffectiveModel3	[-0.04,0.01]	[-0.02,0.05]	[-0.08,0.08]	[-0.10,0.10]	[-0.02,0.08]	[-0.01,0.08]	[-0.57,0.57]	[-0.30,0.20]
JesEffectiveModel4	[-0.05,0.05]	[-0.04,0.05]	[-0.05,0.08]	[-0.06,0.12]	[-0.05,0.09]	[-0.05,0.02]	[-0.01,0.50]	[-0.24,0.24]
JesEffectiveDet1	[-0.34,0.32]	[-0.35,0.35]	[-0.39,0.27]	[-0.34,0.46]	[-0.26,0.19]	[-0.33,0.43]	[-0.04,1.25]	[-0.21,0.24]
JesEffectiveDet2	[-0.11,0.06]	[-0.13,0.11]	[-0.21,0.10]	[-0.03,0.12]	[-0.03,0.03]	[-0.08,0.11]	[-0.69,0.69]	[-0.25,0.25]
JesEffectiveDet3	[-0.04,0.05]	[-0.02,0.02]	[-0.05,0.05]	[-0.06,0.06]	[-0.04,0.08]	[-0.05,0.02]	[-0.45,0.45]	[-0.24,0.24]
JesEffectiveMix1	[-0.32,0.33]	[-0.30,0.31]	[-0.40,0.26]	[-0.28,0.40]	[-0.24,0.36]	[-0.29,0.44]	[-0.14,1.13]	[-0.21,0.04]
JesEffectiveMix2	[-0.18,0.15]	[-0.27,0.24]	[-0.26,0.21]	[-0.14,0.22]	[-0.07,0.11]	[-0.07,0.38]	[-1.07,1.07]	[-0.30,0.30]
JesEffectiveMix3	[-0.02,0.03]	[-0.06,0.06]	[-0.06,0.06]	[-0.08,0.15]	[-0.04,0.04]	[-0.08,0.06]	[-0.63,0.63]	[-0.24,0.24]
JesEffectiveMix4	[-0.02,0.04]	[-0.00,0.01]	[-0.01,0.01]	[-0.03,0.04]	[-0.06,0.03]	[-0.00,0.01]	[-0.48,0.48]	[-0.00,0.00]
EtaIntercalibrationModel	[-0.03,0.26]	[-0.41,0.36]	[-0.56,0.27]	[-0.35,0.42]	[-0.16,0.35]	[-0.22,0.28]	[-0.95,0.95]	[-0.71,0.96]
EtaIntercalibrationTotalStat	[-0.47,0.40]	[-0.36,0.28]	[-0.50,0.36]	[-0.30,0.49]	[-0.20,0.38]	[-0.26,0.40]	[-1.09,1.09]	[-0.56,0.45]
PileupOffsetMu	[-0.07,0.07]	[-0.09,0.09]	[-0.33,0.15]	[-0.18,0.11]	[-0.09,0.13]	[-0.26,0.17]	[-0.76,0.76]	[-0.39,0.01]
PileupOffsetNPV	[-0.25,0.25]	[-0.17,0.17]	[-0.65,0.65]	[-0.29,0.29]	[-0.33,0.33]	[-0.11,0.68]	[-1.08,0.97]	[-0.34,0.73]
PileupRho	[-1.37,1.21]	[-1.13,0.98]	[-1.77,0.81]	[-1.15,1.16]	[-0.65,0.91]	[-0.88,1.07]	[-1.52,1.90]	[-1.42,1.31]
PunchThrough	[-0.00,0.00]	[-0.01,0.01]	[-0.01,0.01]	[-0.00,0.00]	[-0.01,0.01]	[-0.04,0.04]	[-0.08,0.08]	[-0.00,0.00]
CTauTag	[-0.05,0.05]	[-0.06,0.06]	[-0.05,0.05]	[-0.02,0.02]	[-0.02,0.02]	[-0.01,0.01]	[-0.02,0.02]	[-0.00,0.00]
ElectronEnergyResolution	[0.00,0.00]	[0.00,0.01]	[0.00,0.01]	[-0.00,0.00]	[0.00,0.00]	[0.00,0.00]	[-0.00,0.00]	[0.00,0.00]
ElectronEnergyScale	[-0.13,0.00]	[-0.01,0.01]	[-0.01,0.00]	[-0.00,0.00]	[-0.01,0.00]	[-0.00,0.00]	[-0.00,0.00]	[0.00,0.00]
ElectronIdSF	[-0.00,0.00]	[0.00,0.00]	[-0.00,0.00]	[0.00,0.00]	[0.00,0.00]	[0.00,0.00]	[0.00,0.00]	[0.00,0.00]
ElectronRecoSF	[0.00,0.00]	[0.00,0.00]	[-0.00,0.00]	[0.00,0.00]	[0.00,0.00]	[0.00,0.00]	[0.00,0.00]	[0.00,0.00]
ElectronTriggerSF	[0.00,0.00]	[0.00,0.00]	[-0.00,0.00]	[0.00,0.00]	[0.00,0.00]	[0.00,0.00]	[0.00,0.00]	[0.00,0.00]
FlavorComp	[-1.50,0.80]	[-0.85,0.38]	[-1.22,1.03]	[-0.57,0.62]	[-0.55,0.48]	[-0.16,1.11]	[-0.49,0.22]	[-0.47,0.76]
FlavorResponse	[-0.78,0.50]	[-0.57,0.28]	[-1.08,0.36]	[-0.42,0.48]	[-0.15,0.25]	[-0.78,0.78]	[-0.07,0.25]	[-0.65,0.38]
JetVertexFraction	[-0.28,0.38]	[-0.24,0.32]	[-0.45,0.33]	[-0.30,0.29]	[-0.20,0.31]	[-0.36,0.34]	[-0.53,0.26]	[-0.47,0.23]
Mistag	[-0.11,0.11]	[-0.07,0.07]	[-0.18,0.18]	[-0.06,0.06]	[-0.07,0.07]	[-0.03,0.04]	[-0.06,0.06]	[-0.02,0.02]
MuonIdSF	[-0.11,0.11]	[-0.12,0.12]	[-0.12,0.12]	[-0.11,0.11]	[-0.09,0.09]	[-0.09,0.09]	[-0.07,0.07]	[-0.10,0.10]
MuonRecoSF	[-0.05,0.05]	[-0.06,0.06]	[-0.06,0.06]	[-0.05,0.05]	[-0.04,0.04]	[-0.04,0.04]	[-0.03,0.03]	[-0.05,0.05]
MuonTriggerSF	[-0.07,0.07]	[-0.07,0.07]	[-0.07,0.07]	[-0.07,0.07]	[-0.05,0.05]	[-0.04,0.04]	[-0.01,0.01]	[-0.03,0.03]
Musc	[-0.10,0.00]	[-0.08,0.08]	[-0.07,0.07]	[-0.06,0.01]	[-0.09,0.09]	[-0.10,0.10]	[-0.13,0.13]	[-0.28,0.00]
ModellingGenerator	[-0.01,0.01]	[-2.53,2.53]	[-2.95,2.95]	[-0.20,0.20]	[-1.13,1.13]	[-2.05,2.05]	[-0.43,0.43]	[-9.16,9.16]
ModellingParton	[-0.15,0.15]	[-1.21,1.21]	[-0.65,0.65]	[-2.16,2.16]	[-0.33,0.33]	[-3.55,3.55]	[-1.26,1.26]	[-1.89,1.89]
ModellingRadiation	[-3.05,3.05]	[-3.49,3.49]	[-5.97,5.97]	[-6.06,6.06]	[-5.22,5.22]	[-2.80,2.80]	[-1.13,1.13]	[-14.38,14.38]
ModellingSingleTopWtNormalisation	[-0.63,0.63]	[-0.74,0.74]	[-0.78,0.78]	[-0.75,0.75]	[-0.58,0.58]	[-0.49,0.49]	[-0.44,0.44]	[-0.88,0.88]
ModellingSingleTopWtInterference	[-4.69,4.69]	[-5.56,5.56]	[-5.78,5.78]	[-5.58,5.58]	[-4.29,4.29]	[-3.65,3.65]	[-3.31,3.31]	[-6.56,6.56]

Table B.60 Per-bin individual statistical and systematic uncertainties in $\mu\mu$ for the dilepton $|\Delta\eta|$.

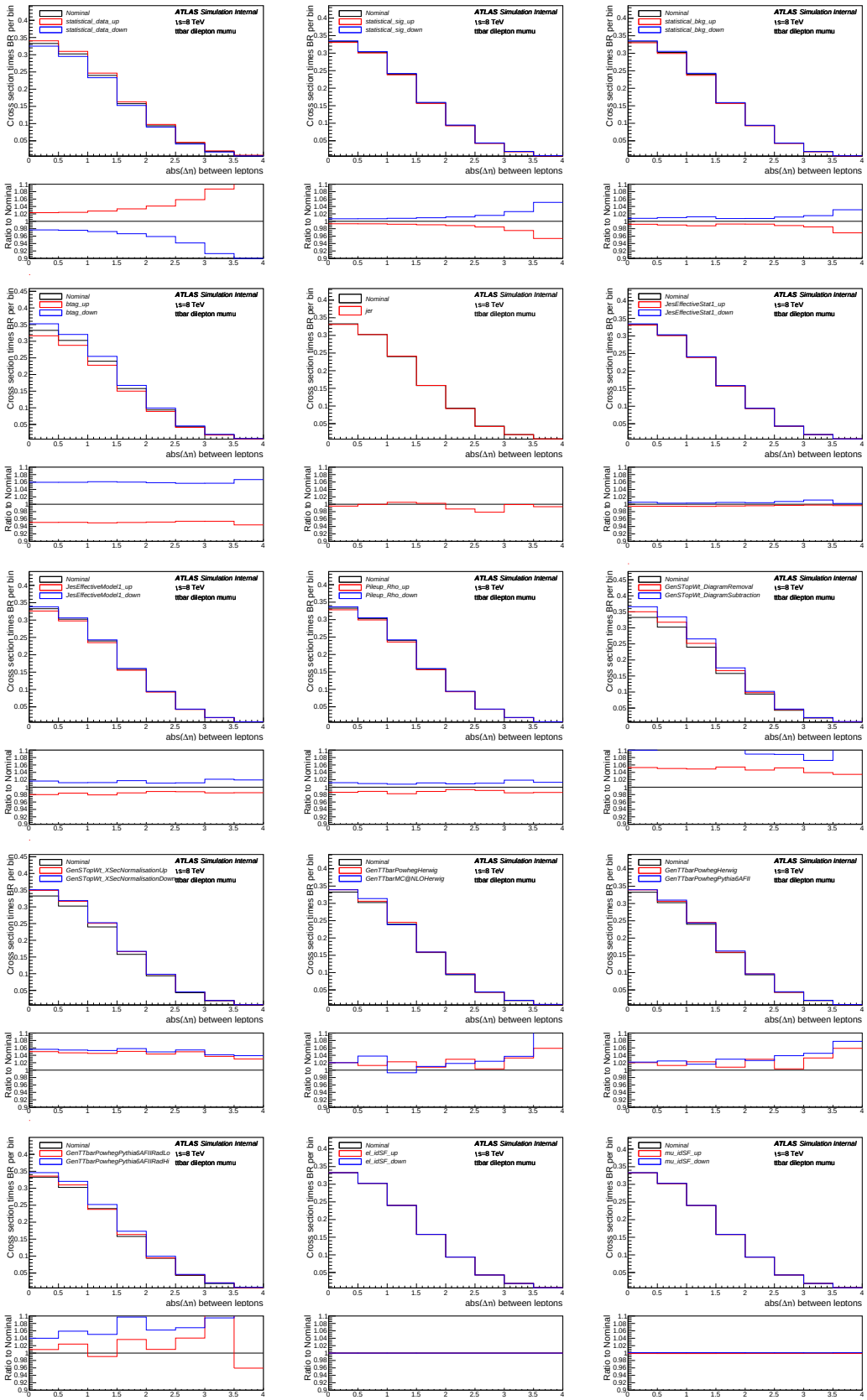

Fig. B.38 Differential cross-section per bin (not scaled to density) for channel $\mu\mu$ in the variable of dilepton $|\Delta\eta|$ with measured (with Nominal signal) overlaid with statistical uncertainties on data and MC (signal and background), as well as various systematics.

B.2.6 Variable dilepton $\Delta\phi$

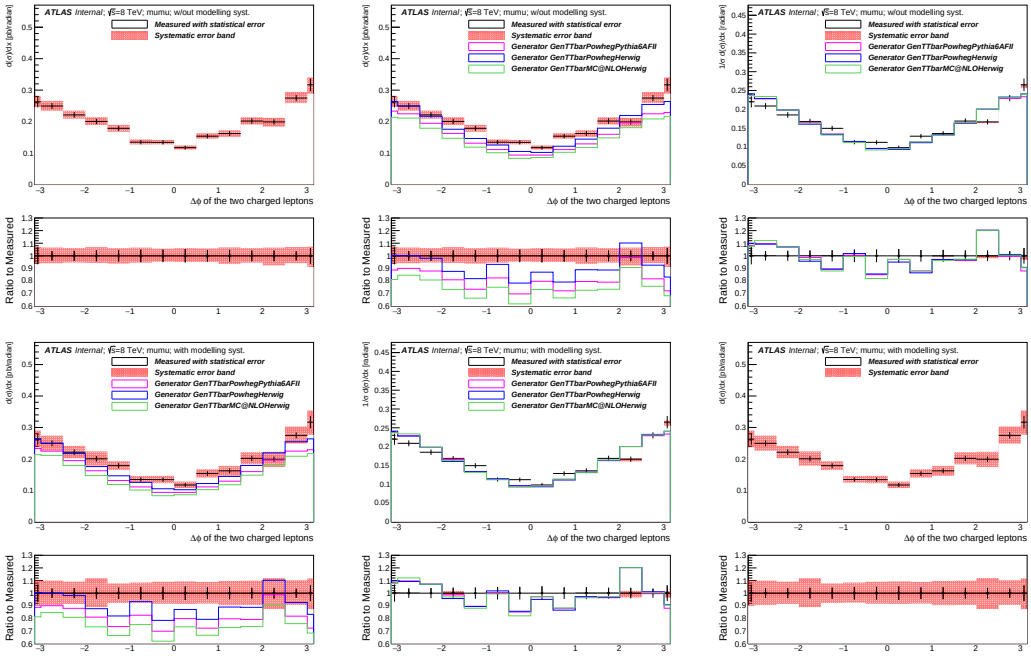

Fig. B.39 Differential cross-section for channel $\mu\mu$ in the variable of dilepton $\Delta\phi$.

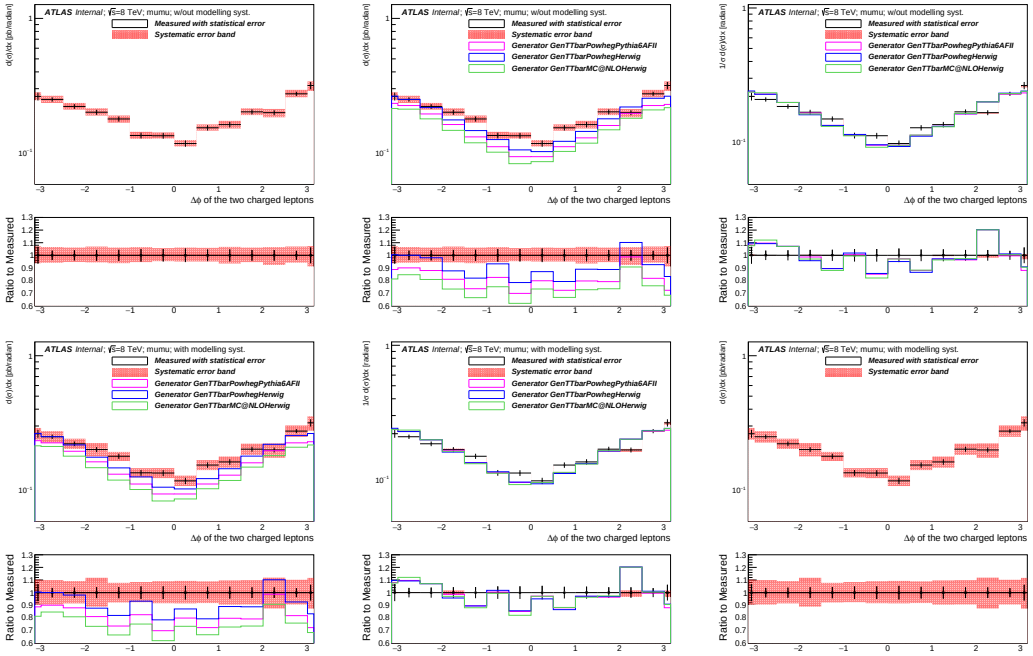

Fig. B.40 Differential cross-section for channel $\mu\mu$ in the variable of dilepton $\Delta\phi$ (log on y axis).

Bin [radian]	Measured $d\sigma/dx$ [pb/radian]	Statistical Data [%]	Statistical MC Bkg [%]	Statistical MC Sig [%]	Systematic [%]
[-3.142,-3.0]	0.2629	+/- 6.7	+/- 1.5	+/- 1.8	+7.2/-6.3
[-3.0,-2.5]	0.2495	+/- 3.7	+/- 1.6	+/- 1.0	+6.6/-5.9
[-2.5,-2.0]	0.2212	+/- 4.0	+/- 1.0	+/- 1.1	+6.2/-5.3
[-2.0,-1.5]	0.2004	+/- 4.3	+/- 0.9	+/- 1.3	+6.9/-5.6
[-1.5,-1.0]	0.1786	+/- 4.4	+/- 1.1	+/- 1.4	+6.2/-6.2
[-1.0,-0.5]	0.1345	+/- 5.0	+/- 2.9	+/- 1.4	+6.5/-5.4
[-0.5,0.0]	0.1340	+/- 5.0	+/- 1.3	+/- 1.6	+5.8/-4.6
[0.0,0.5]	0.1172	+/- 5.4	+/- 1.5	+/- 1.6	+6.2/-4.9
[0.5,1.0]	0.1536	+/- 4.6	+/- 1.2	+/- 1.4	+6.0/-4.9
[1.0,1.5]	0.1621	+/- 4.7	+/- 1.1	+/- 1.4	+6.7/-6.5
[1.5,2.0]	0.2017	+/- 4.3	+/- 1.0	+/- 1.3	+6.2/-5.4
[2.0,2.5]	0.1990	+/- 4.2	+/- 1.1	+/- 1.1	+6.5/-7.6
[2.5,3.0]	0.2748	+/- 3.6	+/- 1.8	+/- 1.0	+7.0/-5.8
[3.0,3.142]	0.3168	+/- 6.2	+/- 1.1	+/- 1.9	+7.4/-8.8

Table B.61 Per-bin total statistical and systematic uncertainties in $\mu\mu$ for the dilepton $\Delta\phi$, without modelling systematic uncertainties.

Bin [radian]	Measured $d\sigma/dx$ [pb/radian]	Statistical Data [%]	Statistical MC Bkg [%]	Statistical MC Sig [%]	Systematic [%]
[-3.142,-3.0]	0.2629	+/- 6.7	+/- 1.5	+/- 1.8	+10.4/-9.8
[-3.0,-2.5]	0.2495	+/- 3.7	+/- 1.6	+/- 1.0	+9.9/-9.5
[-2.5,-2.0]	0.2212	+/- 4.0	+/- 1.0	+/- 1.1	+9.1/-8.5
[-2.0,-1.5]	0.2004	+/- 4.3	+/- 0.9	+/- 1.3	+11.8/-11.0
[-1.5,-1.0]	0.1786	+/- 4.4	+/- 1.1	+/- 1.4	+7.8/-7.8
[-1.0,-0.5]	0.1345	+/- 5.0	+/- 2.9	+/- 1.4	+8.4/-7.6
[-0.5,0.0]	0.1340	+/- 5.0	+/- 1.3	+/- 1.6	+9.1/-8.4
[0.0,0.5]	0.1172	+/- 5.4	+/- 1.5	+/- 1.6	+9.3/-8.5
[0.5,1.0]	0.1536	+/- 4.6	+/- 1.2	+/- 1.4	+8.9/-8.3
[1.0,1.5]	0.1621	+/- 4.7	+/- 1.1	+/- 1.4	+9.7/-9.5
[1.5,2.0]	0.2017	+/- 4.3	+/- 1.0	+/- 1.3	+9.9/-9.4
[2.0,2.5]	0.1990	+/- 4.2	+/- 1.1	+/- 1.1	+11.9/-12.5
[2.5,3.0]	0.2748	+/- 3.6	+/- 1.8	+/- 1.0	+10.2/-9.4
[3.0,3.142]	0.3168	+/- 6.2	+/- 1.1	+/- 1.9	+11.7/-12.6

Table B.62 Per-bin total statistical and systematic uncertainties in $\mu\mu$ for the dilepton $\Delta\phi$, with modelling systematic uncertainties.

Bin [radian]	Measured $d\sigma/dx$ [pb/radian]	Statistical Data [%]	Total Syst Up [%]	Total Syst Down [%]	GenTTbarPowhegPythia6AFII [%]	GenTTbarPowhegHerwig [%]	GenTTbarMC@NLOHerwig [%]
[-3.142,-3.0]	0.2629	+/- 6.7	7.2	-6.3	-11.2	0.5	-18.7
[-3.0,-2.5]	0.2495	+/- 3.7	6.6	-5.9	-9.9	0.1	-15.4
[-2.5,-2.0]	0.2212	+/- 4.0	6.2	-5.3	-12.0	-1.9	-19.1
[-2.0,-1.5]	0.2004	+/- 4.3	6.9	-5.6	-19.0	-12.3	-26.7
[-1.5,-1.0]	0.1786	+/- 4.4	6.2	-6.2	-26.4	-18.1	-33.5
[-1.0,-0.5]	0.1345	+/- 5.0	6.5	-5.4	-17.5	-6.7	-24.9
[-0.5,0.0]	0.1340	+/- 5.0	5.8	-4.6	-30.1	-21.6	-38.0
[0.0,0.5]	0.1172	+/- 5.4	6.2	-4.9	-20.1	-12.9	-26.7
[0.5,1.0]	0.1536	+/- 4.6	6.0	-4.9	-27.7	-20.7	-33.3
[1.0,1.5]	0.1621	+/- 4.7	6.7	-6.5	-20.3	-11.0	-27.2
[1.5,2.0]	0.2017	+/- 4.3	6.2	-5.4	-20.8	-11.2	-26.5
[2.0,2.5]	0.1990	+/- 4.2	6.5	-7.6	-1.3	10.2	-9.2
[2.5,3.0]	0.2748	+/- 3.6	7.0	-5.8	-18.2	-7.4	-24.1
[3.0,3.142]	0.3168	+/- 6.2	7.4	-8.8	-27.7	-16.8	-31.6

Table B.63 Per-bin total statistical and systematic uncertainties in $\mu\mu$ for the dilepton $\Delta\phi$, with generators, without normalisation.

Bin [radian]	Measured $d\sigma/dx$ [pb/radian]	Statistical Data [%]	Total Syst Up [%]	Total Syst Down [%]	GenTTbarPowhegPythia6AFII [%]	GenTTbarPowhegHerwig [%]	GenTTbarMC@NLOHerwig [%]
[-3.142,-3.0]	0.2199	+/- 6.7	0.6	-0.4	8.1	9.7	7.6
[-3.0,-2.5]	0.2087	+/- 3.7	0.1	0.0	9.7	9.3	12.1
[-2.5,-2.0]	0.1850	+/- 4.0	-0.3	0.6	7.1	7.1	7.1
[-2.0,-1.5]	0.1676	+/- 4.3	0.4	0.3	-1.3	-4.3	-2.9
[-1.5,-1.0]	0.1494	+/- 4.4	-0.3	-0.3	-10.4	-10.5	-12.0
[-1.0,-0.5]	0.1125	+/- 5.0	0.0	0.5	0.5	1.8	-0.5
[-0.5,0.0]	0.1121	+/- 5.0	-0.7	1.3	-14.9	-14.4	-18.0
[0.0,0.5]	0.0980	+/- 5.4	-0.3	1.0	-2.8	-4.9	-2.9
[0.5,1.0]	0.1285	+/- 4.6	-0.5	1.0	-12.0	-13.5	-11.7
[1.0,1.5]	0.1356	+/- 4.7	0.2	-0.6	-2.9	-2.8	-3.6
[1.5,2.0]	0.1687	+/- 4.3	-0.3	0.5	-3.6	-3.1	-2.6
[2.0,2.5]	0.1664	+/- 4.2	0.0	-1.9	20.2	20.3	20.2
[2.5,3.0]	0.2298	+/- 3.6	0.5	0.1	-0.4	1.1	0.5
[3.0,3.142]	0.2650	+/- 6.2	0.8	-3.1	-12.0	-9.1	-9.4

Table B.64 Per-bin total statistical and systematic uncertainties in $\mu\mu$ for the dilepton $\Delta\phi$, with generators, with all distributions normalised to unit area.

Uncertainty	[-3.142,-3.0]	[-3.0,-2.5]	[-2.5,-2.0]	[-2.0,-1.5]	[-1.5,-1.0]	[-1.0,-0.5]	[-0.5,0.0]	[0.0,0.5]	[0.5,1.0]	[1.0,1.5]	[1.5,2.0]	[2.0,2.5]	[2.5,3.0]	[3.0,3.142]
StatisticalData	[-6.74,6.74]	[-3.74,3.74]	[-4.02,4.02]	[-4.32,4.32]	[-4.43,4.43]	[-4.96,4.96]	[-5.01,5.01]	[-5.39,5.39]	[-4.63,4.63]	[-4.74,4.74]	[-4.26,4.26]	[-4.24,4.24]	[-3.57,3.57]	[-6.24,6.24]
StatisticalBkg	[-1.52,1.52]	[-1.64,1.64]	[-0.97,0.97]	[-0.95,0.95]	[-1.08,1.08]	[-2.89,2.89]	[-1.29,1.29]	[-1.47,1.47]	[-1.18,1.18]	[-1.13,1.13]	[-1.04,1.04]	[-1.14,1.14]	[-1.82,1.82]	[-1.15,1.15]
StatisticalSig	[-1.77,1.83]	[-1.00,1.02]	[-1.10,1.12]	[-1.25,1.28]	[-1.34,1.38]	[-1.35,1.39]	[-1.53,1.58]	[-1.53,1.58]	[-1.40,1.44]	[-1.35,1.39]	[-1.24,1.27]	[-1.09,1.11]	[-1.00,1.02]	[-1.87,1.94]
BTag	[-5.31,6.32]	[-4.99,6.05]	[-4.86,5.88]	[-4.93,5.97]	[-4.93,5.98]	[-5.17,6.24]	[-4.47,5.47]	[-4.53,5.49]	[-4.45,5.50]	[-5.15,6.22]	[-4.75,5.79]	[-4.75,5.81]	[-5.27,6.31]	[-4.81,5.83]
Jeff	[-0.07,0.07]	[-0.05,0.05]	[-0.05,0.05]	[-0.06,0.06]	[-0.08,0.08]	[-0.01,0.01]	[-0.20,0.20]	[-0.03,0.03]	[-0.03,0.03]	[-0.00,0.00]	[-0.05,0.05]	[-0.05,0.05]	[-0.02,0.02]	[-0.09,0.09]
Jer	[-2.38,2.38]	[-0.03,0.03]	[-0.12,0.12]	[-0.44,0.44]	[-0.13,0.13]	[-0.87,0.87]	[-0.00,0.00]	[-1.13,1.13]	[-0.04,0.04]	[-0.61,0.61]	[-0.23,0.23]	[-0.23,0.23]	[-0.15,0.15]	[-3.23,3.23]
MuidRes	[-0.10,0.10]	[-0.10,0.10]	[-0.06,0.06]	[-0.15,0.15]	[-0.10,0.10]	[-0.30,0.30]	[-0.08,0.08]	[-0.18,0.18]	[-0.12,0.12]	[-0.57,0.57]	[-0.25,0.25]	[-0.16,0.16]	[-0.15,0.15]	[-0.30,0.30]
MumsRes	[-0.13,0.13]	[-0.01,0.01]	[-0.07,0.07]	[-0.07,0.07]	[-0.10,0.10]	[-0.15,0.15]	[-0.26,0.26]	[-0.06,0.06]	[-1.08,1.08]	[-0.01,0.01]	[-0.33,0.33]	[-0.17,0.17]	[-0.05,0.05]	[-0.08,0.08]
BJesUnc	[-0.61,0.60]	[-0.65,0.81]	[-0.89,0.68]	[-0.78,1.29]	[-0.51,0.50]	[-0.21,0.34]	[-0.28,0.80]	[-0.11,0.80]	[-0.60,0.68]	[-0.90,0.76]	[-0.72,0.74]	[-0.88,1.07]	[-0.76,0.60]	[-1.23,0.69]
JesEffectiveStat1	[-0.34,0.52]	[-0.69,0.50]	[-0.36,0.27]	[-0.82,0.65]	[-0.38,0.23]	[-0.22,0.31]	[-0.42,0.42]	[-0.27,0.31]	[-0.25,0.41]	[-0.83,0.52]	[-0.40,0.41]	[-0.79,0.55]	[-0.50,0.38]	[-1.27,0.68]
JesEffectiveStat2	[-0.02,0.02]	[-0.02,0.02]	[-0.01,0.04]	[-0.05,0.05]	[-0.09,0.00]	[-0.03,0.02]	[-0.00,0.02]	[-0.03,0.20]	[-0.11,0.11]	[-0.01,0.05]	[-0.01,0.13]	[-0.08,0.01]	[-0.04,0.04]	[-0.11,0.11]
JesEffectiveStat3	[-0.01,0.03]	[-0.05,0.12]	[-0.07,0.20]	[-0.21,0.08]	[-0.04,0.04]	[-0.03,0.13]	[-0.10,0.10]	[-0.40,0.40]	[-0.00,0.05]	[-0.38,0.19]	[-0.15,0.17]	[-0.11,0.18]	[-0.10,0.10]	[-0.15,0.15]
JesEffectiveStat4	[-0.17,0.17]	[-0.20,0.11]	[-0.28,0.21]	[-0.19,0.14]	[-0.16,0.07]	[-0.06,0.11]	[-0.10,0.10]	[-0.35,0.35]	[-0.15,0.15]	[-0.36,0.26]	[-0.08,0.12]	[-0.12,0.11]	[-0.26,0.14]	[-0.19,0.16]
JesEffectiveModel1	[-1.60,1.65]	[-1.92,1.59]	[-1.33,1.31]	[-1.46,2.29]	[-2.14,0.92]	[-0.70,0.91]	[-0.70,0.75]	[-0.63,1.27]	[-1.16,1.06]	[-2.17,1.39]	[-1.71,1.39]	[-3.29,1.75]	[-1.45,1.56]	[-4.45,1.62]
JesEffectiveModel2	[-0.04,0.04]	[-0.01,0.04]	[-0.01,0.03]	[-0.02,0.02]	[-0.04,0.01]	[-0.02,0.02]	[-0.04,0.04]	[-0.25,0.25]	[-0.06,0.10]	[-0.01,0.01]	[-0.05,0.10]	[-0.15,0.15]	[-0.02,0.02]	[-0.02,0.02]
JesEffectiveModel3	[-0.14,0.14]	[-0.03,0.03]	[-0.04,0.02]	[-0.15,0.15]	[-0.09,0.01]	[-0.06,0.06]	[-0.05,0.05]	[-0.29,0.29]	[-0.14,0.14]	[-0.00,0.03]	[-0.01,0.04]	[-0.10,0.13]	[-0.14,0.00]	[-0.16,0.16]
JesEffectiveModel4	[-0.03,0.03]	[-0.00,0.09]	[-0.03,0.10]	[-0.13,0.00]	[-0.05,0.05]	[-0.01,0.08]	[-0.02,0.02]	[-0.27,0.27]	[-0.06,0.09]	[-0.09,0.08]	[-0.06,0.09]	[-0.09,0.08]	[-0.10,0.08]	[-0.01,0.05]
JesEffectiveDet1	[-0.03,0.28]	[-0.42,0.29]	[-0.48,0.43]	[-0.42,0.40]	[-0.28,0.29]	[-0.11,0.21]	[-0.10,0.32]	[-0.01,0.56]	[-0.21,0.36]	[-0.63,0.53]	[-0.25,0.22]	[-0.30,0.35]	[-0.48,0.37]	[-0.55,0.21]
JesEffectiveDet2	[-0.01,0.10]	[-0.06,0.06]	[-0.18,0.11]	[-0.07,0.06]	[-0.11,0.04]	[-0.07,0.10]	[-0.09,0.09]	[-0.26,0.26]	[-0.07,0.13]	[-0.35,0.15]	[-0.07,0.13]	[-0.11,0.06]	[-0.23,0.04]	[-0.15,0.06]
JesEffectiveDet3	[-0.04,0.01]	[-0.01,0.06]	[-0.05,0.09]	[-0.09,0.03]	[-0.05,0.05]	[-0.01,0.03]	[-0.06,0.06]	[-0.22,0.22]	[-0.02,0.10]	[-0.04,0.03]	[-0.07,0.07]	[-0.07,0.02]	[-0.10,0.06]	[-0.03,0.03]
JesEffectiveMix1	[-0.07,0.22]	[-0.38,0.30]	[-0.37,0.36]	[-0.49,0.54]	[-0.23,0.28]	[-0.07,0.23]	[-0.14,0.29]	[-0.53,0.53]	[-0.06,0.33]	[-0.59,0.36]	[-0.36,0.23]	[-0.31,0.39]	[-0.46,0.38]	[-0.55,0.21]
JesEffectiveMix2	[-0.09,0.20]	[-0.21,0.18]	[-0.22,0.12]	[-0.23,0.39]	[-0.13,0.15]	[-0.07,0.27]	[-0.16,0.16]	[-0.02,0.40]	[-0.02,0.17]	[-0.49,0.29]	[-0.22,0.17]	[-0.12,0.17]	[-0.33,0.21]	[-0.45,0.24]
JesEffectiveMix3	[-0.09,0.09]	[-0.06,0.05]	[-0.10,0.10]	[-0.07,0.03]	[-0.14,0.01]	[-0.00,0.07]	[-0.07,0.10]	[-0.30,0.30]	[-0.14,0.14]	[-0.09,0.09]	[-0.08,0.08]	[-0.13,0.03]	[-0.16,0.16]	[-0.01,0.00]
JesEffectiveMix4	[-0.00,0.00]	[-0.00,0.01]	[-0.01,0.01]	[-0.04,0.02]	[-0.03,0.03]	[-0.01,0.02]	[-0.02,0.03]	[-0.18,0.18]	[-0.00,0.05]	[-0.02,0.01]	[-0.02,0.04]	[-0.03,0.02]	[-0.02,0.05]	[-0.00,0.00]
EtaIntercalibrationModel	[-0.19,0.24]	[-0.46,0.46]	[-0.28,0.25]	[-0.49,0.39]	[-0.43,0.37]	[-0.30,0.46]	[-0.28,0.28]	[-0.16,0.47]	[-0.24,0.51]	[-0.51,0.09]	[-0.44,0.35]	[-0.60,0.33]	[-0.50,0.25]	[-0.51,0.46]
EtaIntercalibrationTotalStat	[-0.21,0.24]	[-0.34,0.42]	[-0.36,0.33]	[-0.58,0.67]	[-0.29,0.15]	[-0.14,0.34]	[-0.00,0.33]	[-0.10,0.45]	[-0.19,0.33]	[-0.76,0.38]	[-0.38,0.38]	[-0.48,0.41]	[-0.47,0.40]	[-0.97,0.53]
PileupOffsetMu	[-0.11,0.11]	[-0.20,0.09]	[-0.19,0.02]	[-0.28,0.10]	[-0.09,0.13]	[-0.07,0.07]	[-0.12,0.07]	[-0.00,0.50]	[-0.17,0.17]	[-0.22,0.22]	[-0.11,0.26]	[-0.34,0.10]	[-0.28,0.26]	[-0.24,0.24]
PileupOffsetNPV	[-0.20,0.20]	[-0.54,0.28]	[-0.18,0.18]	[-0.37,0.46]	[-0.18,0.18]	[-0.00,0.17]	[-0.11,0.49]	[-0.39,0.39]	[-0.06,0.18]	[-0.39,0.39]	[-0.19,0.19]	[-1.34,1.34]	[-0.24,0.05]	[-2.01,2.01]
PileupRho	[-1.15,1.03]	[-1.57,1.22]	[-0.88,0.85]	[-1.15,1.67]	[-1.94,0.76]	[-0.60,0.67]	[-0.06,0.90]	[-0.35,1.08]	[-0.74,0.82]	[-1.72,1.08]	[-1.17,0.90]	[-2.98,1.23]	[-0.99,1.09]	[-1.94,1.19]
PunchThrough	[-0.00,0.00]	[-0.01,0.01]	[-0.00,0.01]	[-0.02,0.02]	[-0.01,0.01]	[-0.01,0.01]	[-0.02,0.00]	[-0.00,0.00]	[-0.06,0.06]	[-0.00,0.00]	[-0.01,0.00]	[-0.01,0.00]	[-0.00,0.00]	[-0.00,0.00]
CTauTag	[-0.03,0.03]	[-0.04,0.04]	[-0.04,0.04]	[-0.03,0.03]	[-0.04,0.04]	[-0.06,0.06]	[-0.02,0.02]	[-0.05,0.06]	[-0.06,0.06]	[-0.04,0.04]	[-0.07,0.07]	[-0.06,0.06]	[-0.04,0.04]	[-0.03,0.03]
ElectronEnergyResolution	[0.00,0.00]	[0.00,0.01]	[0.00,0.00]	[-0.00,0.00]	[0.00,0.00]	[-0.01,0.00]	[0.00,0.00]	[0.00,0.05]	[0.00,0.02]	[0.00,0.00]	[0.00,0.00]	[-0.01,0.00]	[0.00,0.00]	[0.00,0.00]
ElectronEnergyScale	[0.00,0.00]	[0.00,0.01]	[-0.02,0.02]	[-0.00,0.00]	[-0.01,0.00]	[-0.01,0.00]	[0.00,0.01]	[0.00,0.05]	[0.00,0.01]	[-0.03,0.00]	[0.00,0.00]	[-0.43,0.00]	[-0.02,0.01]	[0.00,0.00]
ElectronIdSF	[0.00,0.00]	[0.00,0.00]	[-0.00,0.00]	[0.00,0.00]	[-0.00,0.00]	[-0.00,0.00]	[0.00,0.00]	[-0.00,0.00]	[0.00,0.00]	[-0.00,0.00]	[0.00,0.00]	[0.00,0.00]	[-0.00,0.00]	[0.00,0.00]
ElectronRecoSF	[0.00,0.00]	[0.00,0.00]	[0.00,0.00]	[0.00,0.00]	[-0.00,0.00]	[-0.00,0.00]	[0.00,0.00]	[0.00,0.00]	[0.00,0.00]	[-0.00,0.00]	[0.00,0.00]	[0.00,0.00]	[0.00,0.00]	[0.00,0.00]
ElectronTriggerSF	[0.00,0.00]	[0.00,0.00]	[0.00,0.00]	[0.00,0.00]	[0.00,0.00]	[0.00,0.00]	[0.00,0.00]	[0.00,0.00]	[0.00,0.00]	[-0.00,0.00]	[0.00,0.00]	[0.00,0.00]	[0.00,0.00]	[0.00,0.00]
FlavorComp	[-0.62,0.82]	[-0.91,0.74]	[-0.37,0.37]	[-0.64,0.71]	[-1.68,0.41]	[-0.44,0.41]	[-0.52,0.52]	[-0.46,0.78]	[-0.54,0.77]	[-1.42,0.52]	[-0.66,0.50]	[-2.50,0.46]	[-0.70,1.90]	[-3.17,0.36]
FlavorResponse	[-0.35,0.35]	[-0.73,0.68]	[-0.11,0.16]	[-0.48,0.37]	[-1.44,0.31]	[-0.13,0.49]	[-0.25,0.20]	[-0.19,0.53]	[-0.40,0.48]	[-1.06,0.42]	[-0.29,0.33]	[-2.33,0.36]	[-0.21,0.48]	[-0.57,0.39]
JetVertexFraction	[-0.37,0.35]	[-0.41,0.42]	[-0.42,0.42]	[-0.50,0.19]	[-0.18,0.31]	[-0.23,0.44]	[-0.25,0.12]	[-0.15,0.18]	[-0.20,0.32]	[-0.31,0.26]	[-0.16,0.26]	[-0.19,0.25]	[-0.26,0.57]	[-0.86,0.26]
Mistag	[-0.16,0.16]	[-0.20,0.20]	[-0.08,0.09]	[-0.01,0.01]	[-0.04,0.04]	[-0.07,0.07]	[-0.09,0.09]	[-0.11,0.11]	[-0.07,0.07]	[-0.03,0.03]	[-0.08,0.08]	[-0.08,0.08]	[-0.25,0.25]	[-0.01,0.01]
MuonIdSF	[-0.12,0.12]	[-0.13,0.13]	[-0.11,0.11]	[-0.10,0.10]	[-0.09,0.09]	[-0.13,0.13]	[-0.09,0.09]	[-0.11,0.11]	[-0.09,0.09]	[-0.12,0.12]	[-0.10,0.10]	[-0.12,0.12]	[-0.13,0.13]	[-0.09,0.09]
MuonRecoSF	[-0.07,0.07]	[-0.07,0.07]	[-0.05,0.05]	[-0.04,0.04]	[-0.04,0.04]	[-0.06,0.06]	[-0.05,0.05]	[-0.05,0.05]	[-0.04,0.04]	[-0.05,0.05]	[-0.05,0.05]	[-0.06,0.06]	[-0.06,0.06]	[-0.04,0.04]
MuonTriggerSF	[-0.08,0.08]	[-0.08,0.08]	[-0.08,0.08]	[-0.05,0.05]	[-0.05,0.05]	[-0.06,0.06]	[-0.06,0.06]	[-0.06,0.06]	[-0.03,0.03]	[-0.06,0.06]	[-0.06,0.06]	[-0.08,0.08]	[-0.08,0.08]	[-0.06,0.06]
Musc	[-0.02,0.16]	[-0.06,0.03]	[-0.07,0.24]	[-0.11,0.11]	[-0.12,0.12]	[-0.00,0.03]	[-0.14,0.16]	[-0.07,0.07]	[-0.05,0.05]	[-0.09,0.09]	[-0.11,0.04]	[-0.09,0.09]	[-0.12,0.12]	[-0.16,0.16]
ModellingGenerator	[-2.94,2.94]	[-0.23,0.23]	[-0.19,0.19]	[-0.43,0.43]	[-0.58,0.58]	[-0.89,0.89]	[-0.10,0.10]	[-2.95,2.95]	[-3.19,3.19]	[-0.18,0.18]	[-0.50,0.50]	[-2.18,2.18]	[-0.06,0.06]	[-1.70,1.70]
ModellingParton	[-1.98,1.98]	[-2.87,2.87]	[-1.26,1.26]	[-0.18,0.18]	[-0.09,0.09]	[-1.17,1.17]	[-2.74,2.74]	[-0.94,0.94]	[-0.80,0.80]	[-1.43,1.43]	[-1.14,1.14]	[-0.95,0.95]	[-0.67,0.67]	[-4.08,4.08]
ModellingRadiation	[-0.58,0.58]	[-3.72,3.72]	[-3.14,3.14]	[-8.19,8.19]	[-0.07,0.07]	[-1.22,1.22]	[-4.88,4.88]	[-3.27,3.27]	[-4.73,4.73]	[-2.22,2.22]	[-5.85,5.85]	[-7.93,7.93]	[-4.41,4.41]	[-6.96,6.96]
ModellingSingleTopWtNormalisation	[-0.87,0.87]	[-0.76,0.76]	[-0.76,0.76]	[-0.64,0.64]	[-0.62,0.62]	[-0.66,0.66]	[-0.56,0.56]	[-0.70,0.70]	[-0.44,0.44]	[-0.86,0.86]	[-0.64,0.64]	[-0.72,0.72]	[-0.78,0.78]	[-0.49,0.49]
ModellingSingleTopWtInterference	[-6.52,6.52]	[-5.68,5.68]	[-5.69,5.69]	[-4.76,4.76]	[-4.64,4.64]	[-4.95,4.95]	[-4.15,4.15]	[-5.24,5.24]	[-3.28,3.28]	[-6.40,6.40]	[-4.79,4.79]	[-5.40,5.40]	[-5.84,5.84]	[-3.68,3.68]

Table B.65 Per-bin individual statistical and systematic uncertainties in $\mu\mu$ for the dilepton $\Delta\phi$.

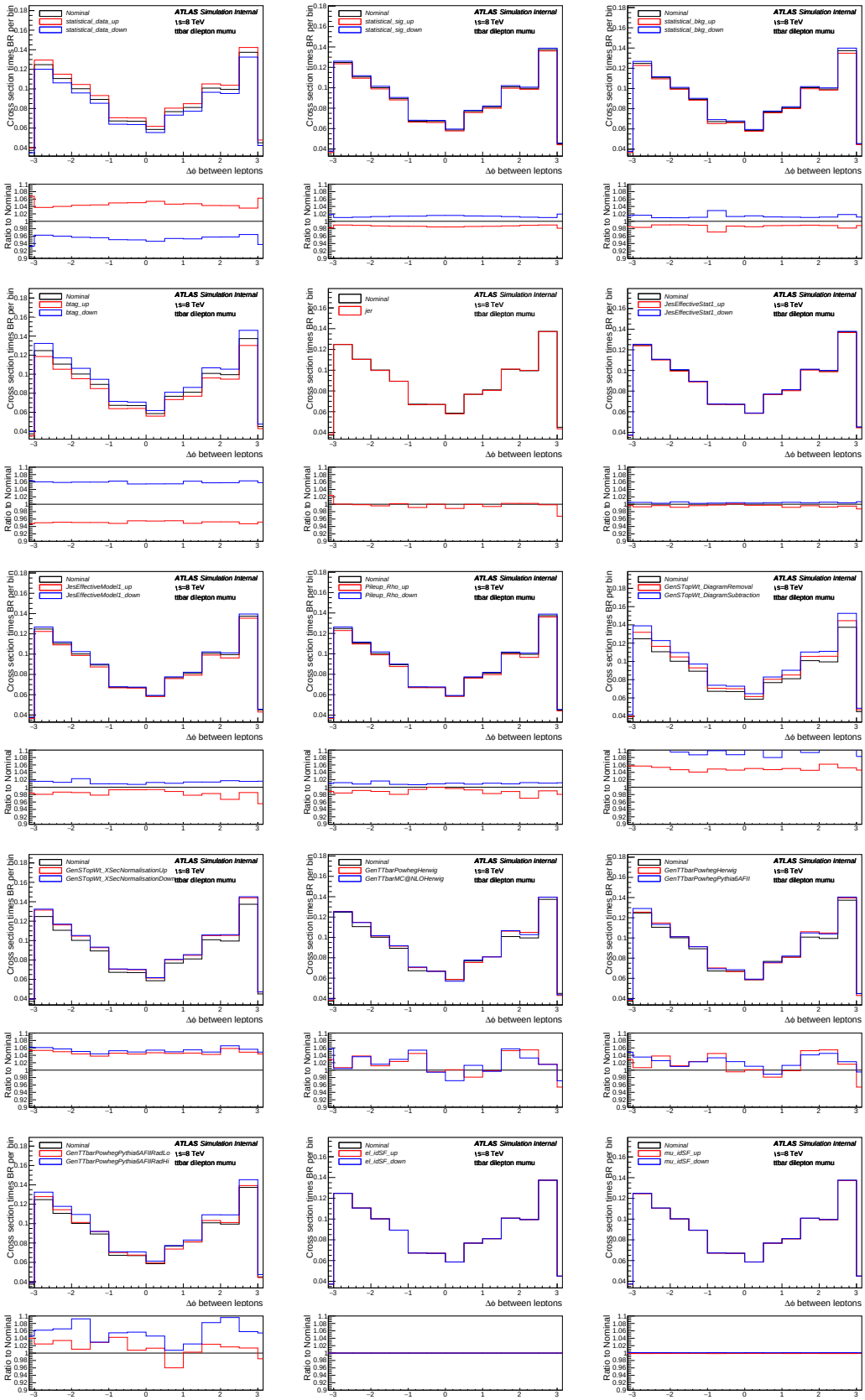

Fig. B.41 Differential cross-section per bin (not scaled to density) for channel $\mu\mu$ in the variable of dilepton $\Delta\phi$ with measured (with Nominal signal) overlaid with statistical uncertainties on data and MC (signal and background), as well as various systematics.

B.2.7 Variable dilepton $|\Delta\phi|$

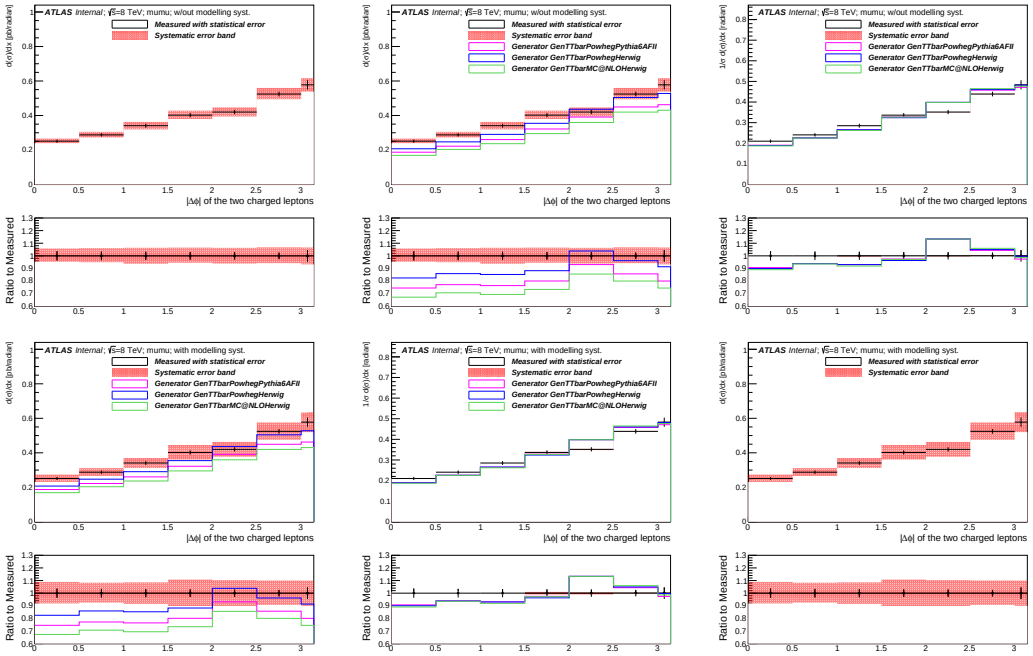

Fig. B.42 Differential cross-section for channel $\mu\mu$ in the variable of dilepton $|\Delta\phi|$.

Bin [radian]	Measured $d\sigma/dx$ [pb/radian]	Statistical Data [%]	Statistical MC Bkg [%]	Statistical MC Sig [%]	Systematic [%]
[0.0,0.5]	0.2512	+/- 3.7	+/- 1.0	+/- 1.1	+5.9/-4.7
[0.5,1.0]	0.2877	+/- 3.4	+/- 1.6	+/- 1.0	+6.2/-5.1
[1.0,1.5]	0.3408	+/- 3.2	+/- 0.8	+/- 1.0	+6.4/-6.3
[1.5,2.0]	0.4020	+/- 3.0	+/- 0.7	+/- 0.9	+6.5/-5.5
[2.0,2.5]	0.4201	+/- 2.9	+/- 0.8	+/- 0.8	+6.3/-6.1
[2.5,3.0]	0.5243	+/- 2.6	+/- 1.2	+/- 0.7	+6.8/-5.8
[3.0,3.142]	0.5777	+/- 4.6	+/- 1.0	+/- 1.3	+6.6/-6.7

Table B.66 Per-bin total statistical and systematic uncertainties in $\mu\mu$ for the dilepton $|\Delta\phi|$, without modelling systematic uncertainties.

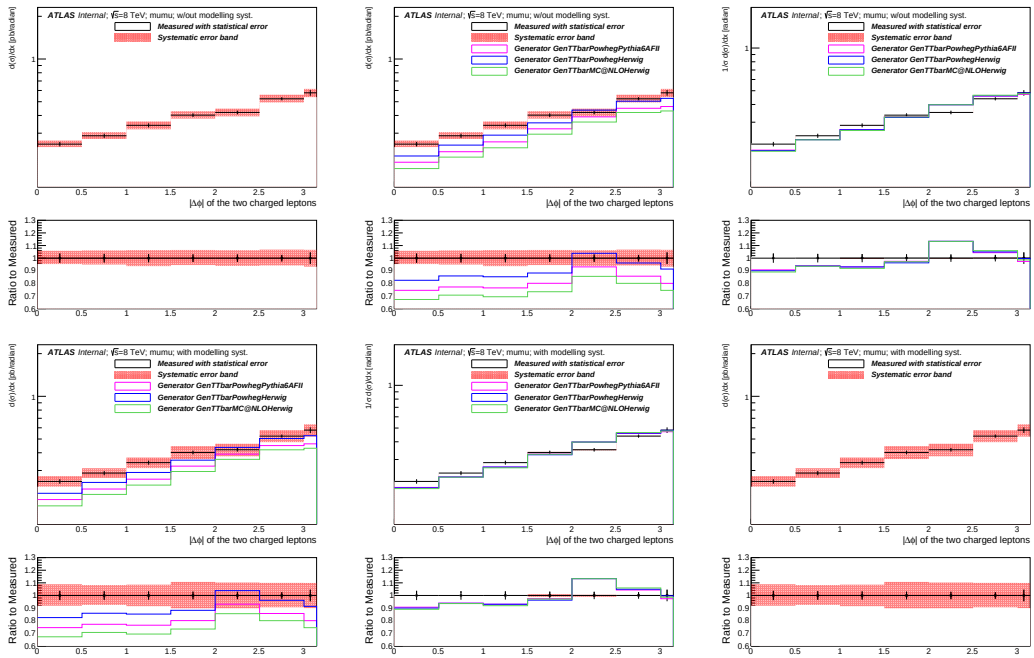

Fig. B.43 Differential cross-section for channel $\mu\mu$ in the variable of dilepton $|\Delta\phi|$ (log on y axis).

Bin [radian]	Measured $d\sigma/dx$ [pb/radian]	Statistical Data [%]	Statistical MC Bkg [%]	Statistical MC Sig [%]	Systematic [%]
[0.0,0.5]	0.2512	+/- 3.7	+/- 1.0	+/- 1.1	+8.9/-8.1
[0.5,1.0]	0.2877	+/- 3.4	+/- 1.6	+/- 1.0	+8.3/-7.5
[1.0,1.5]	0.3408	+/- 3.2	+/- 0.8	+/- 1.0	+8.6/-8.5
[1.5,2.0]	0.4020	+/- 3.0	+/- 0.7	+/- 0.9	+10.7/-10.1
[2.0,2.5]	0.4201	+/- 2.9	+/- 0.8	+/- 0.8	+10.2/-10.1
[2.5,3.0]	0.5243	+/- 2.6	+/- 1.2	+/- 0.7	+10.0/-9.3
[3.0,3.142]	0.5777	+/- 4.6	+/- 1.0	+/- 1.3	+9.9/-10.0

Table B.67 Per-bin total statistical and systematic uncertainties in $\mu\mu$ for the dilepton $|\Delta\phi|$, with modelling systematic uncertainties.

Bin [radian]	Measured $d\sigma/dx$ [pb/radian]	Statistical Data [%]	Total Syst Up [%]	Total Syst Down [%]	GenTTbarPowhegPythia6AFII [%]	GenTTbarPowhegHerwig [%]	GenTTbarMC@NLOHerwig [%]
[0.0,0.5]	0.2512	+/- 3.7	5.9	-4.7	-25.5	-17.5	-32.7
[0.5,1.0]	0.2877	+/- 3.4	6.2	-5.1	-22.8	-14.1	-29.3
[1.0,1.5]	0.3408	+/- 3.2	6.4	-6.3	-23.6	-14.7	-30.6
[1.5,2.0]	0.4020	+/- 3.0	6.5	-5.5	-19.9	-11.8	-26.6
[2.0,2.5]	0.4201	+/- 2.9	6.3	-6.1	-6.9	3.8	-14.4
[2.5,3.0]	0.5243	+/- 2.6	6.8	-5.8	-14.3	-3.8	-20.0
[3.0,3.142]	0.5777	+/- 4.6	6.6	-6.7	-20.0	-8.6	-25.5

Table B.68 Per-bin total statistical and systematic uncertainties in $\mu\mu$ for the dilepton $|\Delta\phi|$, with generators, without normalisation.

Bin [radian]	Measured $d\sigma/dx$ [pb/radian]	Statistical Data [%]	Total Syst Up [%]	Total Syst Down [%]	GenTTbarPowhegPythia6AFII [%]	GenTTbarPowhegHerwig [%]	GenTTbarMC@NLOHerwig [%]
[0.0,0.5]	0.2102	+/- 3.7	-0.5	1.1	-9.3	-10.0	-11.0
[0.5,1.0]	0.2407	+/- 3.4	-0.2	0.7	-6.1	-6.2	-6.4
[1.0,1.5]	0.2852	+/- 3.2	-0.0	-0.6	-6.9	-7.0	-8.1
[1.5,2.0]	0.3364	+/- 3.0	0.1	0.3	-2.5	-3.7	-2.8
[2.0,2.5]	0.3515	+/- 2.9	-0.1	-0.4	13.3	13.3	13.3
[2.5,3.0]	0.4387	+/- 2.6	0.3	-0.1	4.3	5.0	6.0
[3.0,3.142]	0.4834	+/- 4.6	0.2	-1.1	-2.6	-0.3	-1.4

Table B.69 Per-bin total statistical and systematic uncertainties in $\mu\mu$ for the dilepton $|\Delta\phi|$, with generators, with all distributions normalised to unit area.

Uncertainty	[0.0,0.5]	[0.5,1.0]	[1.0,1.5]	[1.5,2.0]	[2.0,2.5]	[2.5,3.0]	[3.0,3.142]
StatisticalData	[-3.67,3.67]	[-3.39,3.39]	[-3.24,3.24]	[-3.03,3.03]	[-2.91,2.91]	[-2.58,2.58]	[-4.58,4.58]
StatisticalBkg	[-0.98,0.98]	[-1.55,1.55]	[-0.80,0.80]	[-0.71,0.71]	[-0.76,0.76]	[-1.24,1.24]	[-0.97,0.97]
StatisticalSig	[-1.09,1.11]	[-0.97,0.99]	[-0.96,0.97]	[-0.88,0.90]	[-0.77,0.79]	[-0.71,0.72]	[-1.29,1.33]
BTag	[-4.49,5.48]	[-4.80,5.86]	[-5.04,6.10]	[-4.84,5.88]	[-4.80,5.85]	[-5.13,6.18]	[-5.05,6.07]
Jeff	[-0.12,0.12]	[-0.01,0.01]	[-0.04,0.04]	[-0.05,0.05]	[-0.05,0.05]	[-0.03,0.03]	[-0.08,0.08]
Jer	[-0.56,0.56]	[-0.39,0.39]	[-0.25,0.25]	[-0.10,0.10]	[-0.05,0.05]	[-0.08,0.08]	[-0.53,0.53]
MuidRes	[-0.13,0.13]	[-0.09,0.09]	[-0.22,0.22]	[-0.05,0.05]	[-0.11,0.11]	[-0.13,0.13]	[-0.09,0.09]
MumsRes	[-0.15,0.15]	[-0.47,0.47]	[-0.06,0.06]	[-0.13,0.13]	[-0.11,0.11]	[-0.02,0.02]	[-0.11,0.11]
BJesUnc	[-0.20,0.79]	[-0.40,0.51]	[-0.70,0.63]	[-0.75,1.01]	[-0.88,0.87]	[-0.72,0.70]	[-0.93,0.64]
JesEffectiveStat1	[-0.10,0.36]	[-0.24,0.36]	[-0.60,0.37]	[-0.61,0.53]	[-0.57,0.41]	[-0.60,0.44]	[-0.81,0.59]
JesEffectiveStat2	[-0.01,0.09]	[-0.00,0.07]	[-0.05,0.03]	[-0.03,0.05]	[-0.02,0.00]	[-0.02,0.02]	[-0.04,0.04]
JesEffectiveStat3	[-0.25,0.25]	[-0.02,0.09]	[-0.20,0.12]	[-0.18,0.13]	[-0.09,0.19]	[-0.07,0.11]	[-0.08,0.08]
JesEffectiveStat4	[-0.22,0.22]	[-0.03,0.13]	[-0.25,0.16]	[-0.13,0.13]	[-0.20,0.16]	[-0.23,0.13]	[-0.09,0.16]
JesEffectiveModel1	[-0.67,1.00]	[-0.92,0.98]	[-2.17,1.16]	[-1.58,1.83]	[-2.27,1.53]	[-1.68,1.57]	[-3.10,1.62]
JesEffectiveModel2	[-0.10,0.10]	[-0.02,0.05]	[-0.01,0.01]	[-0.04,0.04]	[-0.06,0.06]	[-0.01,0.01]	[-0.00,0.01]
JesEffectiveModel3	[-0.15,0.15]	[-0.08,0.08]	[-0.03,0.00]	[-0.08,0.00]	[-0.04,0.04]	[-0.08,0.08]	[-0.00,0.03]
JesEffectiveModel4	[-0.14,0.14]	[-0.04,0.09]	[-0.07,0.03]	[-0.09,0.05]	[-0.06,0.09]	[-0.05,0.09]	[-0.00,0.04]
JesEffectiveDet1	[-0.06,0.43]	[-0.16,0.28]	[-0.45,0.41]	[-0.34,0.31]	[-0.40,0.39]	[-0.45,0.33]	[-0.28,0.25]
JesEffectiveDet2	[-0.17,0.17]	[-0.07,0.11]	[-0.22,0.09]	[-0.07,0.10]	[-0.15,0.08]	[-0.15,0.05]	[-0.08,0.08]
JesEffectiveDet3	[-0.14,0.14]	[-0.02,0.06]	[-0.04,0.01]	[-0.08,0.05]	[-0.06,0.05]	[-0.06,0.06]	[-0.03,0.03]
JesEffectiveMix1	[-0.05,0.41]	[-0.07,0.27]	[-0.40,0.32]	[-0.42,0.38]	[-0.34,0.37]	[-0.42,0.34]	[-0.30,0.21]
JesEffectiveMix2	[-0.27,0.27]	[-0.05,0.22]	[-0.30,0.22]	[-0.22,0.28]	[-0.17,0.15]	[-0.28,0.20]	[-0.26,0.22]
JesEffectiveMix3	[-0.11,0.11]	[-0.07,0.07]	[-0.03,0.02]	[-0.03,0.03]	[-0.07,0.07]	[-0.07,0.07]	[-0.04,0.04]
JesEffectiveMix4	[-0.01,0.10]	[-0.00,0.04]	[-0.03,0.00]	[-0.03,0.03]	[-0.02,0.01]	[-0.01,0.03]	[-0.00,0.00]
EtaIntercalibrationModel	[-0.04,0.36]	[-0.27,0.48]	[-0.47,0.23]	[-0.46,0.37]	[-0.44,0.29]	[-0.05,0.29]	[-0.34,0.34]
EtaIntercalibrationTotalStat	[-0.06,0.38]	[-0.16,0.34]	[-0.52,0.26]	[-0.48,0.52]	[-0.42,0.37]	[-0.41,0.41]	[-0.58,0.38]
PileupOffsetMu	[-0.06,0.28]	[-0.12,0.12]	[-0.16,0.05]	[-0.19,0.18]	[-0.16,0.16]	[-0.25,0.18]	[-0.09,0.05]
PileupOffsetNPV	[-0.37,0.37]	[-0.03,0.18]	[-0.27,0.27]	[-0.28,0.17]	[-0.72,0.72]	[-0.38,0.16]	[-0.97,0.97]
PileupRho	[-0.21,0.98]	[-0.66,0.74]	[-1.85,0.91]	[-1.16,1.28]	[-1.90,1.04]	[-1.27,1.16]	[-1.54,1.10]
PunchThrough	[-0.01,0.00]	[-0.00,0.02]	[-0.00,0.00]	[-0.01,0.01]	[-0.01,0.01]	[-0.00,0.01]	[-0.00,0.00]
CTauTag	[-0.04,0.04]	[-0.06,0.06]	[-0.04,0.04]	[-0.05,0.05]	[-0.05,0.05]	[-0.04,0.04]	[-0.03,0.03]
ElectronEnergyResolution	[0.00,0.03]	[0.00,0.01]	[0.00,0.00]	[-0.00,0.00]	[-0.00,0.00]	[0.00,0.00]	[0.00,0.00]
ElectronEnergyScale	[-0.03,0.03]	[-0.00,0.00]	[-0.01,0.01]	[-0.00,0.00]	[-0.20,0.01]	[-0.01,0.01]	[0.00,0.00]
ElectronIdSF	[-0.00,0.00]	[-0.00,0.00]	[-0.00,0.00]	[0.00,0.00]	[-0.00,0.00]	[-0.00,0.00]	[0.00,0.00]
ElectronRecoSF	[0.00,0.00]	[-0.00,0.00]	[-0.00,0.00]	[0.00,0.00]	[-0.00,0.00]	[0.00,0.00]	[0.00,0.00]
ElectronTriggerSF	[0.00,0.00]	[0.00,0.00]	[-0.00,0.00]	[0.00,0.00]	[0.00,0.00]	[0.00,0.00]	[0.00,0.00]
FlavorComp	[-0.50,0.37]	[-0.49,0.58]	[-1.57,0.47]	[-0.65,0.60]	[-1.40,0.42]	[-0.81,1.34]	[-1.95,0.59]
FlavorResponse	[-0.23,0.36]	[-0.26,0.48]	[-1.27,0.36]	[-0.38,0.35]	[-1.18,0.26]	[-0.46,0.58]	[-0.45,0.36]
JetVertexFraction	[-0.20,0.15]	[-0.22,0.38]	[-0.24,0.29]	[-0.33,0.23]	[-0.30,0.34]	[-0.33,0.49]	[-0.62,0.31]
Mistag	[-0.10,0.10]	[-0.07,0.07]	[-0.04,0.04]	[-0.04,0.03]	[-0.08,0.08]	[-0.22,0.22]	[-0.07,0.07]
MuonIdSF	[-0.10,0.10]	[-0.11,0.11]	[-0.10,0.10]	[-0.10,0.10]	[-0.12,0.12]	[-0.13,0.13]	[-0.10,0.10]
MuonRecoSF	[-0.05,0.05]	[-0.05,0.05]	[-0.05,0.05]	[-0.04,0.04]	[-0.05,0.06]	[-0.07,0.07]	[-0.05,0.05]
MuonTriggerSF	[-0.06,0.06]	[-0.05,0.05]	[-0.06,0.06]	[-0.05,0.05]	[-0.08,0.08]	[-0.08,0.08]	[-0.07,0.07]
Musc	[-0.04,0.08]	[-0.03,0.01]	[-0.11,0.11]	[-0.08,0.08]	[-0.08,0.16]	[-0.05,0.05]	[-0.08,0.04]
ModellingGenerator	[-1.56,1.56]	[-2.06,2.06]	[-0.19,0.19]	[-0.46,0.46]	[-1.19,1.19]	[-0.15,0.15]	[-2.29,2.29]
ModellingParton	[-1.84,1.84]	[-0.18,0.18]	[-0.67,0.67]	[-0.66,0.66]	[-1.10,1.10]	[-1.76,1.76]	[-3.05,3.05]
ModellingRadiation	[-4.07,4.07]	[-3.05,3.05]	[-1.15,1.15]	[-7.01,7.01]	[-5.51,5.51]	[-4.07,4.07]	[-3.80,3.80]
ModellingSingleTopWtNormalisation	[-0.62,0.62]	[-0.55,0.55]	[-0.73,0.73]	[-0.64,0.64]	[-0.74,0.74]	[-0.77,0.77]	[-0.67,0.67]
ModellingSingleTopWtInterference	[-4.66,4.66]	[-4.07,4.07]	[-5.47,5.47]	[-4.78,4.78]	[-5.55,5.55]	[-5.77,5.77]	[-5.01,5.01]

Table B.70 Per-bin individual statistical and systematic uncertainties in $\mu\mu$ for the dilepton $|\Delta\phi|$.

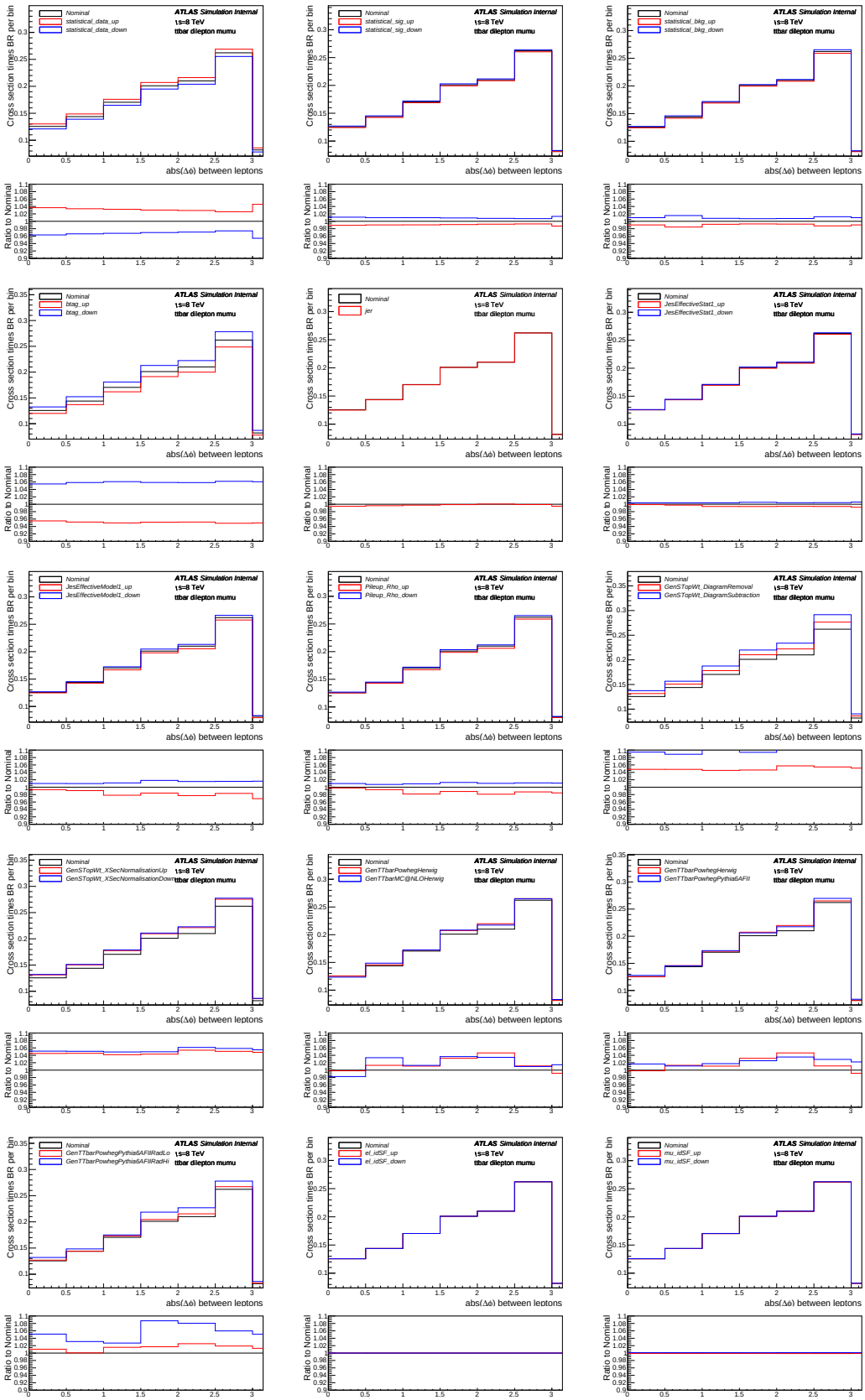

Fig. B.44 Differential cross-section per bin (not scaled to density) for channel $\mu\mu$ in the variable of dilepton $|\Delta\phi|$ with measured (with Nominal signal) overlaid with statistical uncertainties on data and MC (signal and background), as well as various systematics.